UNRAVELING THE BIOLOGY, GENETICS, AND HOST/ENVIRONMENTAL INTERACTIONS OF ACINETOBACTER

EDITED BY: Maria Alejandra Mussi and Maria Soledad Ramirez
PUBLISHED IN: Frontiers in Microbiology

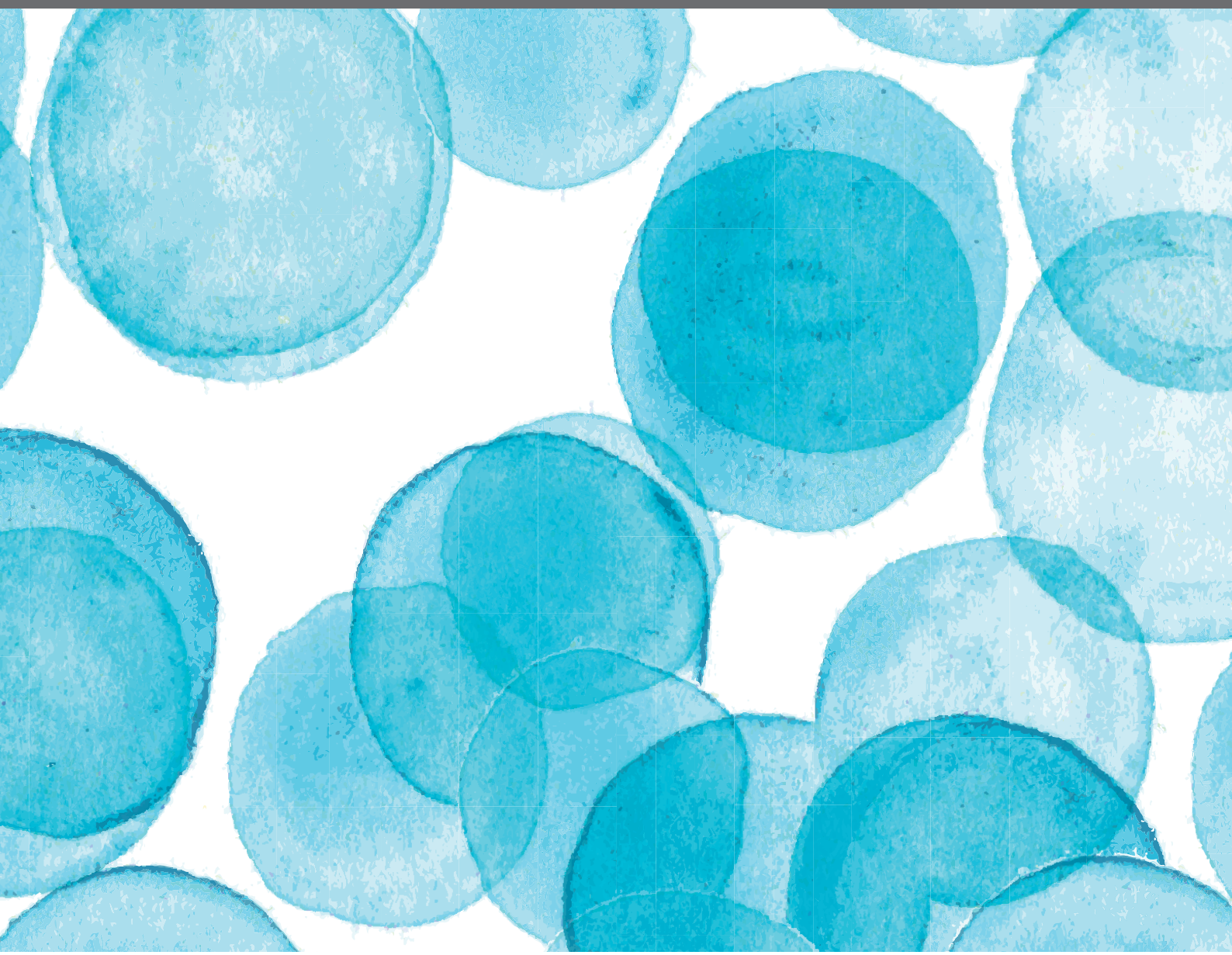

frontiers Research Topics

ISSN 1664-8714
ISBN 978-2-88963-946-5
DOI 10.3389/978-2-88963-946-5

About Frontiers

Frontiers is more than just an open-access publisher of scholarly articles: it is a pioneering approach to the world of academia, radically improving the way scholarly research is managed. The grand vision of Frontiers is a world where all people have an equal opportunity to seek, share and generate knowledge. Frontiers provides immediate and permanent online open access to all its publications, but this alone is not enough to realize our grand goals.

Frontiers Journal Series

The Frontiers Journal Series is a multi-tier and interdisciplinary set of open-access, online journals, promising a paradigm shift from the current review, selection and dissemination processes in academic publishing. All Frontiers journals are driven by researchers for researchers; therefore, they constitute a service to the scholarly community. At the same time, the Frontiers Journal Series operates on a revolutionary invention, the tiered publishing system, initially addressing specific communities of scholars, and gradually climbing up to broader public understanding, thus serving the interests of the lay society, too.

Dedication to Quality

Each Frontiers article is a landmark of the highest quality, thanks to genuinely collaborative interactions between authors and review editors, who include some of the world's best academicians. Research must be certified by peers before entering a stream of knowledge that may eventually reach the public - and shape society; therefore, Frontiers only applies the most rigorous and unbiased reviews.
Frontiers revolutionizes research publishing by freely delivering the most outstanding research, evaluated with no bias from both the academic and social point of view. By applying the most advanced information technologies, Frontiers is catapulting scholarly publishing into a new generation.

What are Frontiers Research Topics?

Frontiers Research Topics are very popular trademarks of the Frontiers Journals Series: they are collections of at least ten articles, all centered on a particular subject. With their unique mix of varied contributions from Original Research to Review Articles, Frontiers Research Topics unify the most influential researchers, the latest key findings and historical advances in a hot research area! Find out more on how to host your own Frontiers Research Topic or contribute to one as an author by contacting the Frontiers Editorial Office: researchtopics@frontiersin.org

UNRAVELING THE BIOLOGY, GENETICS, AND HOST/ENVIRONMENTAL INTERACTIONS OF ACINETOBACTER

Topic Editors:
Maria Alejandra Mussi, Consejo Nacional de Investigaciones Científicas y Técnicas (CONICET), Argentina
Maria Soledad Ramirez, California State University, Fullerton, United States

Despite not being a disease in and of itself, antibiotic resistance could be considered the global epidemic of modern times, since it produces the failure to prevent and treat many infectious diseases. This can ultimately lead to untreatable microbial infections becoming more widespread and this will significantly increase morbidity and mortality. This worldwide problem is estimated to cause millions of deaths per year and could become an even more significant menace to humanity than established illnesses, such as cancer.

In February 2017, the World Health Organization (WHO) published a list of antibiotic-resistant "priority pathogens" – a catalogue of 12 families of bacteria which pose the greatest threat to human health - and Acinetobacter baumannii is leading the list. The most critical group includes multidrug-resistant bacteria, which pose a particular threat in hospitals, nursing homes, and among patients whose care requires devices such as ventilators and blood catheters. This group includes Acinetobacter, Pseudomonas, and various Enterobacteriaceae and they are often associated with deadly infections, such as bloodstream infections and pneumonia. Furthermore, these bacteria have become resistant to a large number of antibiotics, including carbapenems and third generation cephalosporins – the best available antibiotics for treating multidrug-resistant bacteria.

A. baumannii is a particularly worrisome example and demands attention: This pathogen turned into a menace to humans during the late 70s, likely as a result of intense antibiotic use in hospital settings, and became one of the microorganisms that are challenging the antibiotic era. Its extreme genome plasticity, combined with mechanisms of horizontal genetic transfer, have played a key role in the evolution of this microorganism, as well as its adaptability to unfavorable environments. However, its pathophysiology, as well as the mechanisms leading to its success as a pathogen, are not that simple to unveil. However, what is clear is that the triad of host-pathogen-environment is crucial in selection and establishment of multidrug-resistant clones and outbreaks.

Indeed, there are still many aspects of this pathogen that require a deeper understanding - not only regarding mechanisms of resistance but also its global pathophysiology. For example, basic understanding of transmission mechanisms; knowledge of 'external' factors modulating persistence of the pathogen; genetic effects on host susceptibility and infectiousness; mechanisms of pathogenicity and their dynamics; and genetic variation of the pathogen affecting virulence and transmissibility are some aspects that would require further study.

Furthermore, the importance of other members of the genus as important nosocomial pathogens, such as Acinetobacter nosocomialis, has been increasingly recognized during the last few years.

Citation: Mussi, M. A., Ramirez, M. S., eds. (2020). Unraveling the Biology, Genetics, and Host/Environmental Interactions of Acinetobacter. Lausanne: Frontiers Media SA. doi: 10.3389/978-2-88963-946-5

Table of Contents

frontiers in Microbiology

ORIGINAL RESEARCH
published: 16 November 2018
doi: 10.3389/fmicb.2018.02776

Metabolic Analyses Revealed Time-Dependent Synergistic Killing by Colistin and Aztreonam Combination Against Multidrug-Resistant *Acinetobacter baumannii*

Mei-Ling Han[1,2†], Xiaofen Liu[2†], Tony Velkov[3], Yu-Wei Lin[1], Yan Zhu[1], Mengyao Li[1], Heidi H. Yu[1], Zhihui Zhou[4], Darren J. Creek[5], Jing Zhang[2‡] and Jian Li[1,2‡]*

[1] Biomedicine Discovery Institute, Infection and Immunity Program, Department of Microbiology, Monash University, Clayton, VIC, Australia, [2] Institute of Antibiotics, Huashan Hospital, Fudan University, Shanghai, China, [3] Department of Pharmacology & Therapeutics, School of Biomedical Sciences, Faculty of Medicine, Dentistry and Health Sciences, The University of Melbourne, Parkville, VIC, Australia, [4] Department of Infectious Diseases, Sir Run Run Shaw Hospital, Zhejiang University School of Medicine, Hangzhou, China, [5] Drug Delivery, Disposition and Dynamics, Monash Institute of Pharmaceutical Sciences, Monash University, Parkville, VIC, Australia

Background: Polymyxins are a last-line class of antibiotics against multidrug-resistant *Acinetobacter baumannii*; however, polymyxin resistance can emerge with monotherapy. Therefore, synergistic combination therapy is a crucial strategy to reduce polymyxin resistance.

Methods: This study conducted untargeted metabolomics to investigate metabolic responses of a multidrug-resistant (MDR) *A. baumannii* clinical isolate, AB090342, to colistin and aztreonam alone, and their combination at 1, 4, and 24 h. Metabolomics data were analyzed using univariate and multivariate statistics; metabolites showing ≥ 2-fold changes were subjected to bioinformatics analysis.

Results: The synergistic action of colistin-aztreonam combination was initially driven by colistin via significant disruption of bacterial cell envelope, with decreased phospholipid and fatty acid levels at 1 h. Cell wall biosynthesis was inhibited at 4 and 24 h by aztreonam alone and the combination as shown by the decreased levels of two amino sugars, UDP-*N*-acetylglucosamine and UDP-*N*-acetylmuramate; these results suggested that aztreonam was primarily responsible for the synergistic killing at later time points. Moreover, aztreonam alone and the combination significantly depleted pentose phosphate pathway, amino acid, peptide and nucleotide metabolism, but elevated fatty acid and key phospholipid levels. Collectively, the combination synergy between colistin and aztreonam was mainly due to the inhibition of cell envelope biosynthesis via different metabolic perturbations.

OPEN ACCESS

Edited by:
Maria Alejandra Mussi, Consejo Nacional de Investigaciones Científicas y Técnicas (CONICET), Argentina

Reviewed by:
Ziad Daoud, University of Balamand, Lebanon
Ilya R. Akberdin, San Diego State University, United States

***Correspondence:**
Jing Zhang
zhangj_fudan@aliyun.com

[†] *These authors have contributed equally to this work*

[‡] *Joint senior authors*

Specialty section:
This article was submitted to Infectious Diseases, a section of the journal Frontiers in Microbiology

Received: *03 September 2018*
Accepted: *30 October 2018*
Published: *16 November 2018*

Citation:
Han M-L, Liu X, Velkov T, Lin Y-W, Zhu Y, Li M, Yu HH, Zhou Z, Creek DJ, Zhang J and Li J (2018) Metabolic Analyses Revealed Time-Dependent Synergistic Killing by Colistin and Aztreonam Combination Against Multidrug-Resistant Acinetobacter baumannii. Front. Microbiol. 9:2776. doi: 10.3389/fmicb.2018.02776

Conclusion: This metabolomics study is the first to elucidate multiple cellular pathways associated with the time-dependent synergistic action of colistin-aztreonam combination against MDR *A. baumannii*. Our results provide important mechanistic insights into optimizing synergistic colistin combinations in patients.

Keywords: polymyxin, beta-lactam, combination therapy, lipopolysaccharide, peptidoglycan, metabolomics

INTRODUCTION

Multidrug-resistant (MDR) *Acinetobacter baumannii* is an important nosocomial pathogen and can cause ventilator-related pneumonia, bloodstream infections, urinary tract infections and meningitis (Dijkshoorn et al., 2007; Fishbain and Peleg, 2010). It has become very problematic due to rapid development of resistance to all currently available antibiotics, including β-lactams (Perez et al., 2007; Mak et al., 2008; Boucher et al., 2009). Without novel classes of antibiotics in the near future, polymyxins (i.e., polymyxin B and colistin) have resurged as a last-resort therapy against MDR *A. baumannii* (Zavascki et al., 2007; Lim et al., 2010; Sampson et al., 2012). Polymyxins kill bacterial cells via an initial electrostatic interaction between the positively charged L-α,γ-diaminobutyric acid (Dab) residues of polymyxins and the negatively charged phosphate groups of lipopolysaccharide (LPS) in Gram-negative outer membrane (OM) (Velkov et al., 2010). This is followed by non-polar interactions which allow the hydrophobic moieties (*N*-terminal fatty acyl tail and D-Phe^6-L-Leu^7) of polymyxins to penetrate into the OM, disorganize the cell envelope, and result in cell death (Velkov et al., 2010, 2013; Yu et al., 2015; Rabanal and Cajal, 2017). However, the exact mechanism of polymyxin killing is still not clear.

Unfortunately, *A. baumannii* can develop resistance to polymyxins through covalent modifications of lipid A phosphate groups with positively charged moieties [e.g., phosphoethanolamine (pEtN) and galatosamine (GalN)] or by the complete loss of LPS (Moffatt et al., 2010; Arroyo et al., 2011; Henry et al., 2011; Boll et al., 2015). These modifications significantly reduce the net negative charge on the bacterial membrane and repel the binding to polymyxins. Therefore, to reduce the emergence of polymyxin resistance, combination therapies of polymyxins with other antibiotics are strongly recommended (Karageorgopoulos and Falagas, 2008; Cai et al., 2012; Henry et al., 2015; Nation et al., 2015; Maifiah et al., 2017). A number of *in vitro* and *in vivo* studies and clinical case reports have proposed synergistic colistin combination therapies against heteroresistant *A. baumannii* isolates to prevent the development of colistin resistance (Montero et al., 2002; Yoon et al., 2004; Vidaillac et al., 2012; Bae et al., 2016). Aztreonam was approved by FDA in 1986 and is the only clinically available monobactam against aerobic Gram-negative bacteria. In the context of the global spread of MDR Gram-negatives, the pharmacokinetics and pharmacodynamics of aztreonam have been re-investigated recently (Eliopoulos and Bush, 2001; Ramsey and MacGowan, 2016). However, aztreonam monotherapy can be problematic due to the degradation by β-lactamases including extended-spectrum β-lactamases (ESBLs), AmpC type β-lactamase and *Klebsiella pneumonia* carbapenemases (KPCs) in Gram-negative bacteria, which has promoted interest in combination therapies (Gutmann et al., 1988; Ramsey and MacGowan, 2016). In a recent study, using a multiple-combination bactericidal test, the combination of colistin and aztreonam showed synergistic effect against a number of colistin-resistant *A. baumannii* clinical strains (Bae et al., 2016). However, the mechanism that underlies the synergistic killing of the colistin-aztreonam combination has not been fully investigated.

Systems pharmacology has been extensively used for understanding bacterial physiology and mechanisms of antibiotic killing and resistance (Henry et al., 2015; Maifiah et al., 2017; Zampieri et al., 2017; Zhu et al., 2018). In particular, metabolomics provides a powerful systems tool to identify and quantify key intracellular metabolites at the network level in responses to antibiotics (Kaddurah-Daouk et al., 2008; Maifiah et al., 2017; Zampieri et al., 2017). In the present study, comparative metabolomics was conducted to elucidate the mechanism of the synergistic colistin-aztreonam combination against *A. baumannii*. Our findings provide important insights into the optimization of this important combination for the treatment of MDR *A. baumannii* infections.

MATERIALS AND METHODS

Strain, Antibiotics and Reagents

Acinetobacter baumannii AB090342 was collected in a clinical study approved by the institutional review board of Sir Run Run Shaw Hospital, Zhejiang, China. Written informed consent was obtained from a 60-year-old male patient who was given intravenous colistimethate sodium (150 mg colistin base activity every 12 h for 10 days) for the treatment of ventilator-associated pneumonia. The patient showed clinical and microbiological failure and *A. baumannii* AB090342 was isolated from the sputum. The isolate was identified using 16S ribosomal DNA sequencing and multilocus sequence typing (MLST). *A. baumannii* AB090342 was colistin susceptible (MIC = 0.5 mg/L), while aztreonam resistant (MIC > 128 mg/L.)

Colistin (sulfate, CAS# 1264-72-8) and aztreonam (CAS# 78110-38-0) were purchased from Sigma-Aldrich (Saint Louis, United States). Antibiotic solutions were prepared before the metabolomics study using Milli-Q water (Millipore Australia, North Ryde, NSW, Australia) and filtered through 0.22-μm syringe filters (Sartorius, Melbourne, VIC, Australia).

Genome Sequencing

The genomic DNA was extracted using a Genomic DNA Purification Kit (Tiangen, Beijing, China) according to the producer instruction and stored at −80°C before sequencing. A 300-bp paired-end library was constructed with the purified DNA sample following the standard Illumina paired-end protocol. Cluster generation was performed in C-bot and sequencing was performed on Illumina Hiseq2500 (Illumina, San Diego, CL, United States) with 150 cycles. Draft genome was assembled using Velvet (Ver 1.0.15) (Delcher et al., 2007; Zerbino and Birney, 2008). Raw data of AB090342 was aligned to the AB307-0294 genome (Genbank Accession: NC_011595) and single nucleotide polymorphisms (SNPs) determined by Velvet (Langmead and Salzberg, 2012).

Bacterial Culture for Metabolomic Experiments

Prior to experiments, *A. baumannii* AB090342 was subcultured on nutrient agar plates and incubated for 16–18 h at 37°C. A single colony was then inoculated into 10 mL of cation-adjusted Mueller-Hinton broth (CaMHB, Oxoid) and incubated in a shaking water bath at 180 rpm and 37°C for 18 h. The overnight culture was then diluted by 1:100 into four different reservoirs with 100 mL fresh CaMHB and grown to an optical density at 600 nm (OD_{600}) of 0.50 ± 0.02 to achieve the starting inoculum at $\sim 10^8$ cfu/mL at early logarithmic growth phase. The bacterial culture was treated with colistin (1 mg/L), aztreonam (128 mg/L), and the combination of colistin and aztreonam (1 mg/L and 128 mg/L, respectively) for 1, 4 and 24 h; concentrations of colistin and aztreonam were chosen based on their MICs, pharmacokinetics in patients, and *in vitro* static time-kill results to ensure sufficient bacterial cells for the metabolomics study. The untreated bacterial culture was served as the control and five biological replicates were prepared independently from different colonies of AB090342 on different days.

Preparation of Metabolite Samples

Cellular metabolites of AB090342 were extracted based on a previously reported method (Han et al., 2018). In brief, both treated and untreated bacterial culture (20 mL) were collected at 0, 1, 4, and 24 h and immediately quenched in a dry ice-ethanol bath for 30 s to stop metabolic processes. The culture was then normalized according to OD_{600} at 0.50 ± 0.02, 15 mL of which was centrifuged at 3,220 × *g* and 4°C for 10 min to obtain bacterial cell pellets. After washed twice with 2 mL 0.9% sodium chloride, cell pellets were resuspended in 0.5 mL extraction solvent ($CHCl_3$/MeOH/H_2O, 1:3:1, v/v) containing 1 μM generic internal standards (CHAPS, CAPS, PIPES, and TRIS), which was followed by three freeze-thaw cycles in liquid nitrogen to lyse cells and release cellular metabolites. The supernatants (0.3 mL) containing extracted metabolites were collected after centrifugation at 3,220 × *g* and 4°C for 10 min, then further centrifuged at 14,000 × *g* for 10 min to achieve particle-free samples (0.2 mL) for LC-MS analysis.

LC-MS Analysis of Metabolites

Based on a published method (Han et al., 2018), metabolite samples were analyzed on a Q-Exactive Orbitrap mass spectrometer (Thermo Fisher) coupled to a Dionex U3000 high-performance liquid chromatography (HPLC) with a ZIC-pHILIC column (5 μm, polymeric, 150 × 4.6 mm; SeQuant, Merck). The MS system was operated in both positive and negative electro-spray ionisation (ESI) mode with a resolution at 35,000 and a detection range of 85 to 1,275 *m/z*. The samples were maintained at 4°C and 10 μL of which were eluted by a multi-step gradient system which started from 20% mobile phase A (20 mM ammonium carbonate) to 80% mobile phase B (acetonitrile) to 50% A and 50% B over 15 min by a linear gradient at 0.3 mL/min. This was followed by another gradient to 5% B at 18 min and continued for 3 min before a re-equilibration with 20% A and 80% B over the next 8 min. All metabolomics samples containing internal standards were analyzed within the same LC-MS batch to minimize any potential variations. A pooled biological quality control (PBQC) sample containing an aliquot of 10 μL of each sample was analyzed periodically through the batch to monitor the chromatographic peaks, signal reproducibility and analyte stability. Eight mixtures consisting of more than 300 authentic standards were also analyzed within the batch for assisting the identification of metabolites.

Data Processing, Statistics and Pathway Analysis

Metabolomics raw data were initially converted to mzXML files and split into both positive and negative polarity and followed by feature detection with XCMS; data from all samples were then combined and annotated using mzMatch (Smith et al., 2006; Kessner et al., 2008; Scheltema et al., 2011). The mzMatch data were filtered, identified, quantified and visualized in IDEOM using default values[1] (Creek et al., 2012). The dataset of relative intensity (peak height) was normalized according to the median height of all putatively identified peaks, and log transformed in MetaboAnalyst 3.0 before further analysis (Xia et al., 2015). Multivariate statistics using unsupervised principle component analysis (PCA) was applied to visualize the global metabolic profiles of the samples with antibiotic treatments at each time point. Univariate statistical analysis using one-way analysis of variance (ANOVA) for multiple comparison and *post hoc* analysis using Tukey's honestly significant difference (HSD) were conducted for the identification of significant metabolic perturbations (FDR < 0.05, $p < 0.05$, $\log_2$(fold change) ≥ 1 or ≤ -1) between treated and untreated groups at each time point. Metabolites with an IDEOM confidence score of 6 or greater (identified by the accurate mass and standard, or predicted, retention time, corresponding to MSI level 1 or 2 based on Metabolomics Standards Initiative Guidelines), and a ≥ 2-fold change were further analyzed and subjected to pathway analysis using Kyoto Encyclopedia of Genes and Genomes (KEGG) pathway (Kanehisa and Goto, 2000), Biocyc (Karp et al., 2005) and iPath 3 (Letunic et al., 2008).

[1] http://mzmatch.sourceforge.net/ideom.php

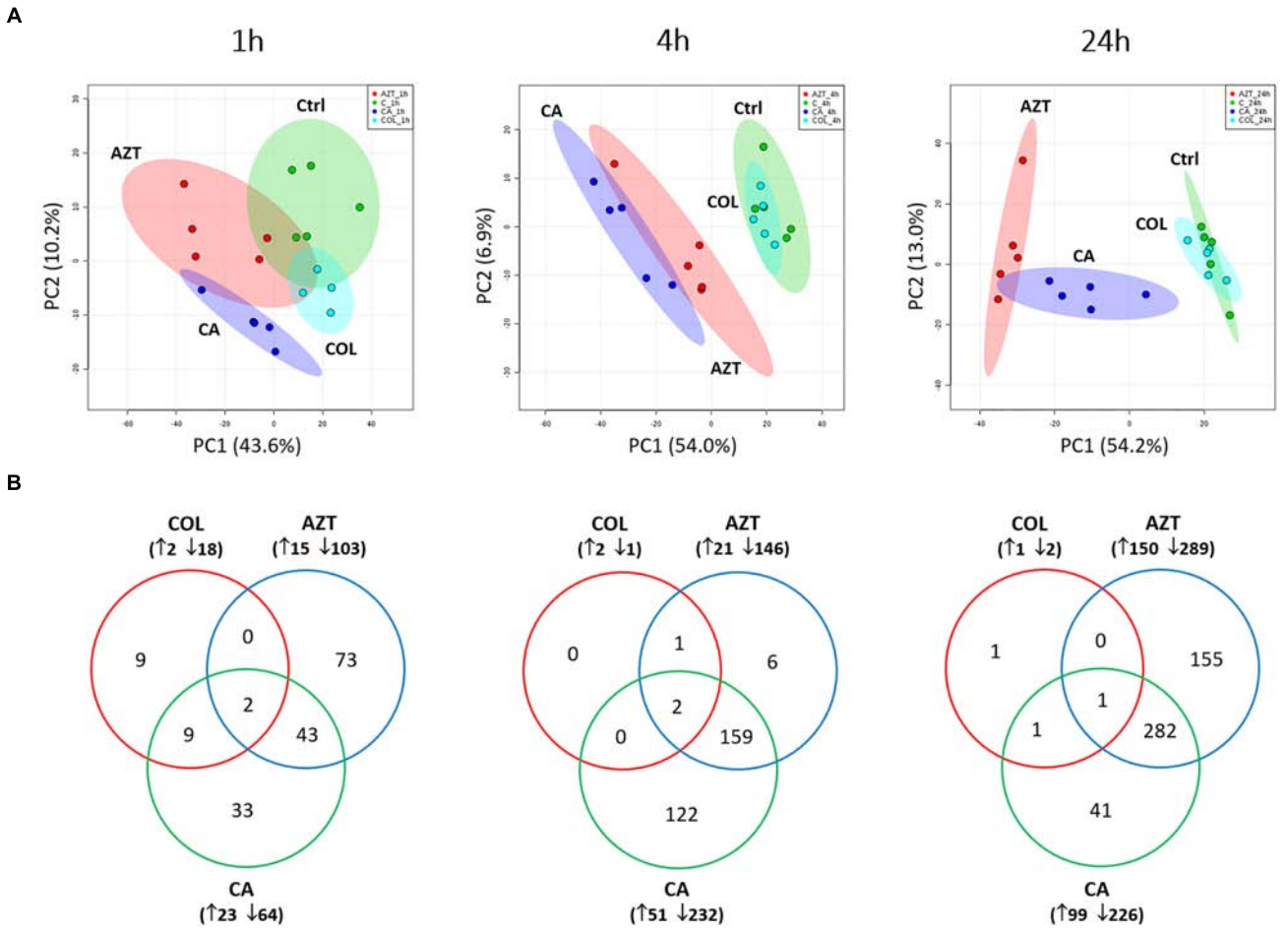

FIGURE 1 | Multivariate and univariate analyses of global metabolic changes. **(A)** PCA score plots of the first two principle components for metabolite levels in *A. baumannii* AB090342 after treatments with colistin, aztreonam alone and the combination at 1, 4, and 24 h. Each dataset represents a total of 20 samples of 5 biological replicates under each condition. Green, untreated control (C); cyan, colistin alone (COL); red, aztreonam (AZT) alone; blue, combination (CA). **(B)** Venn diagrams show the number of significantly affected metabolites by each treatment at 1, 4, and 24 h. Significant metabolites were selected based on FDR < 0.05, $p < 0.05$ and FC ≥ 2 (one-way ANOVA).

RESULTS

Genomic Analysis of the Clinical Isolate *A. baumannii* AB090342

The genome sequencing produced 3,246,666 pairs of 300-bp reads for *A. baumannii* AB090342. Assembly of the genome resulted in 60 contigs larger than 500 bp, representing a 3.91 Mb draft genome. Totally, 3,683 putative coding sequences were predicted for AB090342. Our data showed that AB090342 shared 98.0% sequence similarity to colistin-susceptible *A. baumannii* AB307-0294 (Genbank Accession No: NC_011595). The genome annotation revealed that AB090342 contains multiple antibiotic resistance genes encoding OXA-51, OXA-23, metallo-beta-lactamase; aminoglycoside phosphotransferase; DNA gyrase and DNA topoisomerase IV; and TetR family transcriptional regulator responsible for tetracycline resistance. The MIC results showed consistent results with imipenem and meropenem $\geq$ 16 mg/L, amikacin $>$ 128 mg/L and ciprofloxacin $>$ 32 mg/L. Furthermore, a comparison of AB090342 and AB307-0294 revealed 1,441 variations of non-synonymous single nucleotide polymorphisms (SNPs), among which, a missense mutation of A138V and A444T in *pmrB* gene was identified. Nevertheless, the MIC results showed that AB090342 was susceptible to colistin with an MIC of 0.5 mg/L.

Global Metabolic Variations in Response to Colistin and Aztreonam Alone and Their Combination

A total number of 1,060 putatively identified metabolites were obtained, involving in a wide range of pathways, including metabolism of amino acids, carbohydrates, lipids, nucleotides (**Supplementary Dataset S1**). The median relative standard deviation (RSD) value of the pooled quality control samples was 14.2%, showing minimal technical variation which was well within the acceptable limits for metabolomics (**Supplementary Figure S1**) (Kirwan et al., 2014). The median RSD value for

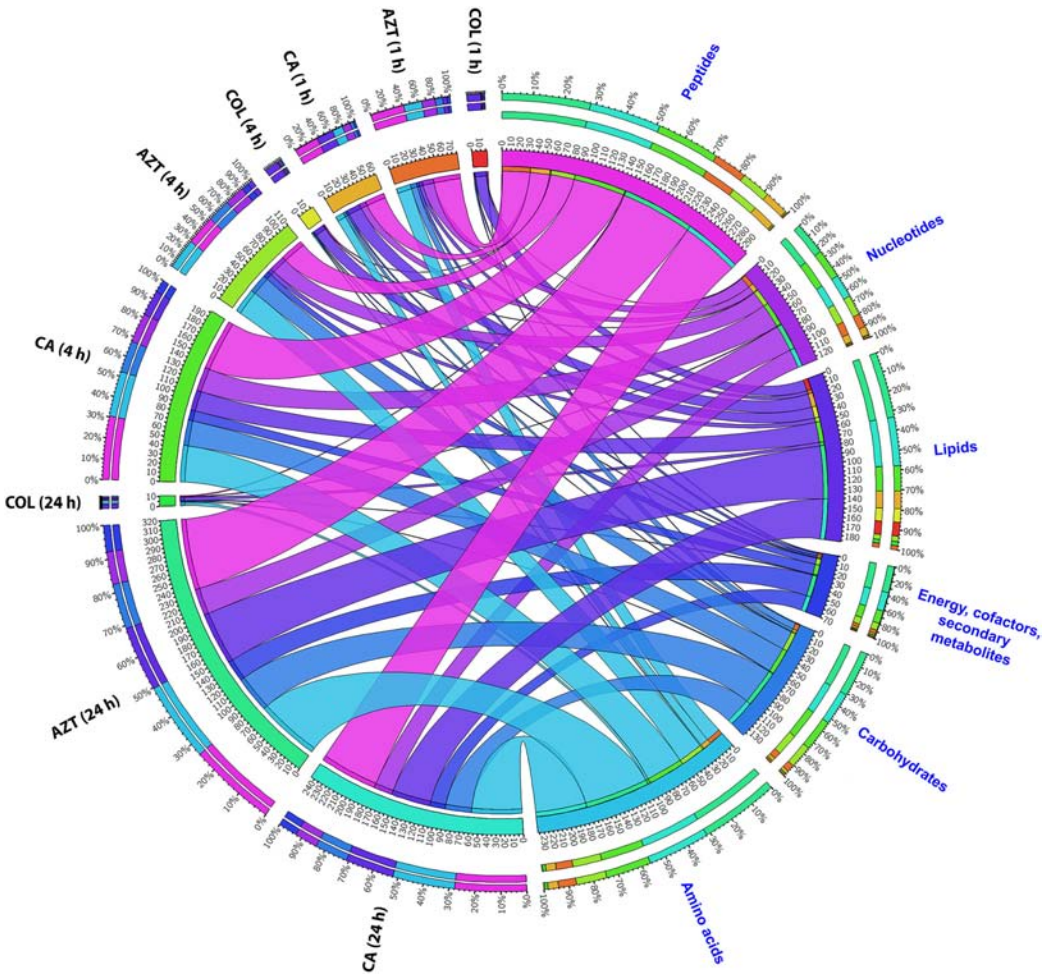

FIGURE 2 | Metabolomic responses of *A. baumannii* AB090342 after the treatment with colistin (COL), aztreonam (AZT) and the combination (CA) at 1, 4, and 24 h. Bipartite graph shows the correlations of the total number and percentage of significantly affected metabolites (FDR < 0.05, $p < 0.05$ and FC > 2) in different major classes and all conditions (treatments and time points).

each sample group (15–35%) indicated the dynamics of bacterial metabolism during *in vitro* culture (**Supplementary Figure S1**). As shown in the principle component analysis (PCA) score plots, the colistin and aztreonam combination induced significant metabolic changes as early as 1 h (PC1 = 43.6%), and lasted at least till 24 h (PC1 = 54.2%; **Figure 1A**). However, the metabolic changes induced by colistin monotherapy were only observed at 1 h. In contrast, significant metabolic perturbations caused by aztreonam monotherapy were detected at 4 and 24 h, which was even more dramatic according to the PCA analysis than the combination treatment at 24 h (**Figure 1A**). With regards to the number of significantly changed metabolites [FDR < 0.05, $p < 0.05$, and fold change (FC) ≥ 2, one-way analysis of variance (ANOVA)], the combination therapy resulted in 8.2% (87), 26.7% (283) and 30.7% (325) metabolic changes at 1, 4, and 24 h, respectively. Similarly, aztreonam monotherapy induced 11.1% (118), 15.8% (167) and 41.4% (439) metabolic variations across all three time points, respectively (**Figures 1B**, **2** and **Supplementary Figure S2**). However, only 1.9% (20) metabolic changes were induced by colistin alone at 1 h, and metabolism was not significantly altered at 4 or 24 h (**Figures 1B**, **2** and **Supplementary Figure S2**). In general, a large number of metabolites were shared between aztreonam monotherapy and the combination at 4 and 24 h, indicating that the synergistic killing of colistin-aztreonam combination was largely driven by aztreonam at both time points (**Figure 1B**).

The metabolite enrichment analysis revealed that multiple key biochemical pathways, including nucleotide, amino acid and lipid metabolism and pentose phosphate pathway (PPP) were significantly affected in AB090342 following the treatments with colistin and aztreonam alone and the combination over 24 h (**Supplementary Figure S3**). In detail, both aztreonam alone and the combination significantly decreased metabolic levels in amino acid, peptide, nucleotide, pentose phosphate and amino sugar metabolism at all three time points (**Figures 2**, **3**, **Supplementary Figure S2** and **Supplementary Dataset S2**). On the contrary, lipid metabolism, in particular, fatty acids and glycerophospholipids (GPLs) were significantly enriched

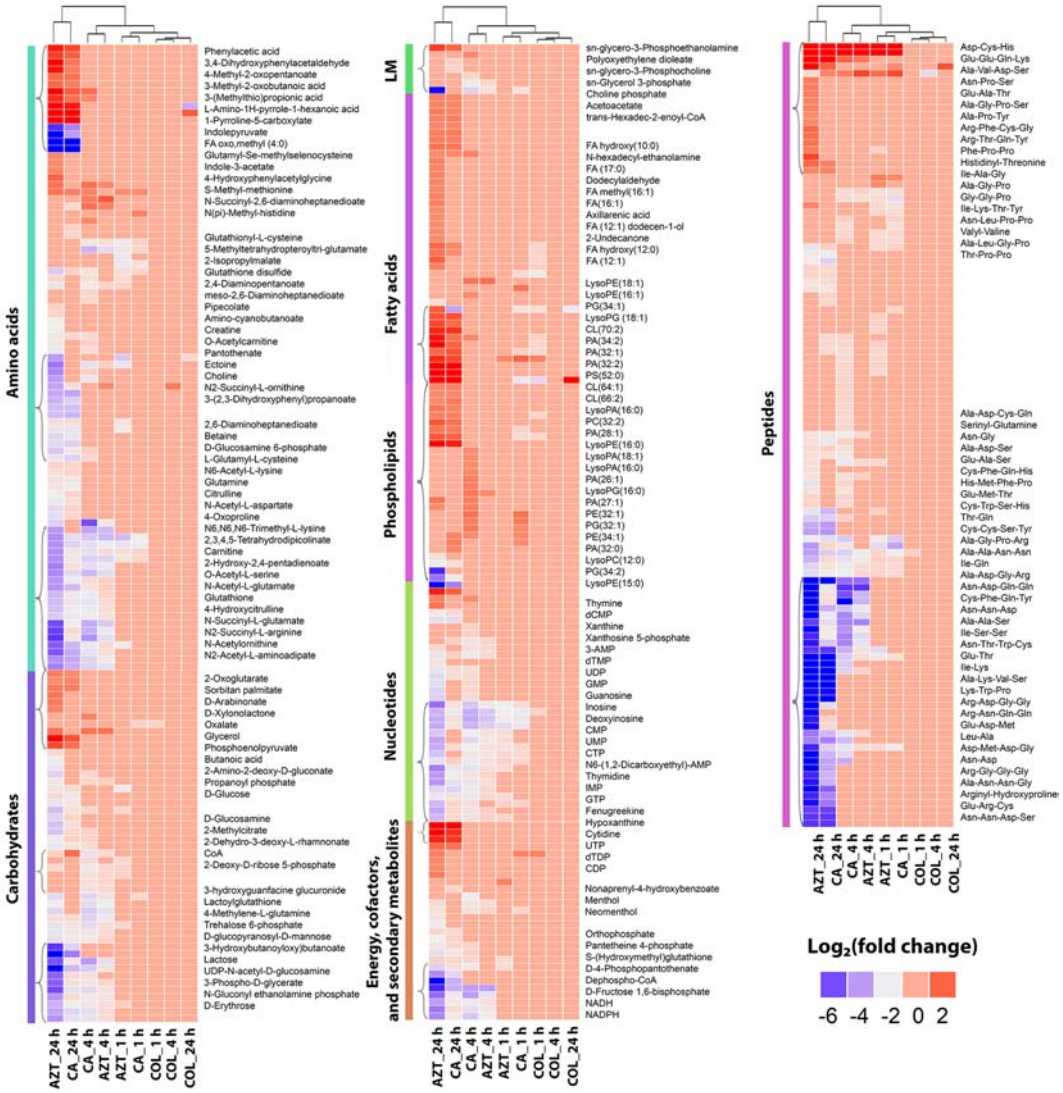

FIGURE 3 | Clustered heatmap profiles of the relative abundance for significantly affected metabolites in *A. baumannii* AB090342. Metabolites are grouped into different classes: amino acids, carbohydrates, lipids (lipid metabolism [LM], fatty acids and phospholipids), nucleotides, energy, secondary metabolites and peptides. The colors indicate the relative abundance of significantly affected metabolites by all three treatments (colistin alone, aztreonam alone and the combination) at 1, 4, and 24 h compared to the untreated control samples. Metabolite names were only labeled for top-significant metabolites as shown in single brackets. Blue and gray, significantly decrease ($\log_2$ FC ≤ -1); red, significantly increase ($\log_2$ FC ≥ 1); and pink, not significant.

by aztreonam alone and the combination at 24 h (**Figure 3** and **Supplementary Dataset S2**); whereas, colistin alone and the combination caused a dramatic decrease in lipid levels at 1 h (**Figures 3** and **Supplementary Figure S2**). Furthermore, despite the significant changes caused by both aztreonam and the combination, it is notable that the combination exclusively induced significant accumulations of fatty acids and GPLs at 1 and 4 h.

Amino Acid and Short-Chain Peptide Metabolism

Treatment with aztreonam alone and the combination showed considerable changes in the levels of amino acids and peptides, especially at 4 and 24 h (**Figures 2**, **3** and **Supplementary Dataset S2**). In particular, the pathways related to arginine and proline (e.g., *N*-acetyl-L-glutamate, L-citrulline, 4-oxoproline and N_2-succinyl-L-arginine), alanine, aspartate and glutamate (e.g., *N*-acetyl-L-aspartate and *O*-acetylcarnitine), glutathione (e.g., glutathione and glutathione disulfide), and lysine (e.g., N_2-acetyl-L-aminoadipate and *N*-succinyl-2,6-diaminoheptanedioate) metabolism were all significantly decreased due to aztreonam monotherapy and the combination treatment at 4 and 24 h ($\log_2$FC ≤ -1) (**Figures 3**, **4** and **Supplementary Dataset S2**). In contrast, the levels of phenylacetic acid, 4-methyl-2-oxopentanoate, and 3-(methylthio)propionic acid were dramatically increased in response to both aztreonam

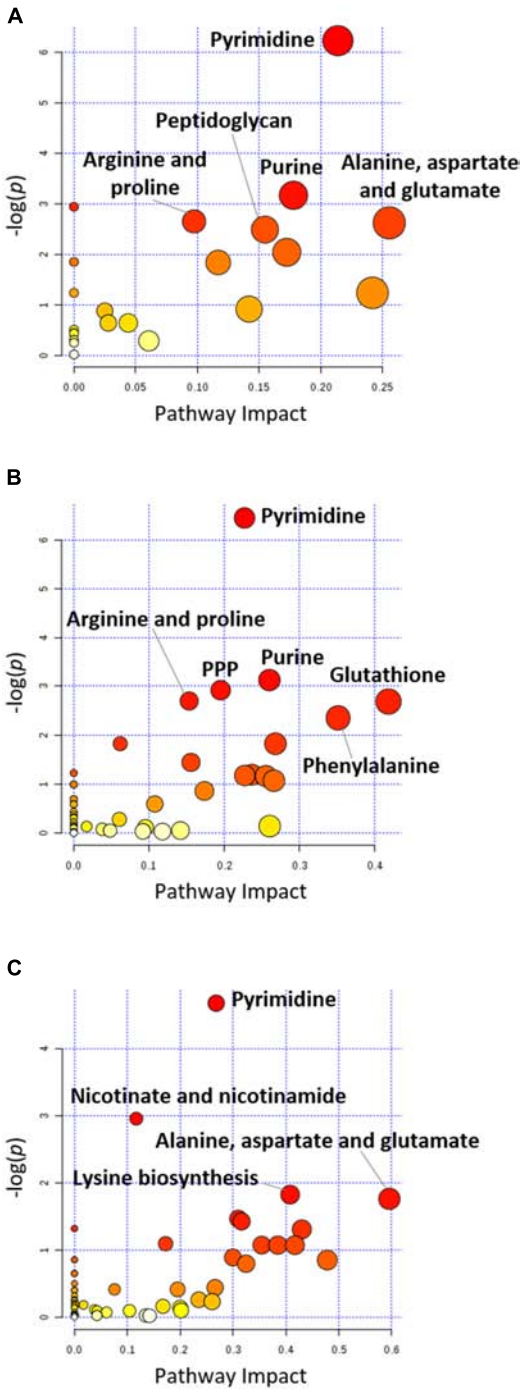

FIGURE 4 | Pathway analysis of significantly affected metabolites in *A. baumannii* AB090342 following the treatments with colistin, aztreonam alone and the combination at **(A)** 1 h, **(B)** 4 h, and **(C)** 24 h (FDR < 0.05, $p < 0.05$ and FC ≥ 2, one-way ANOVA). The pathway enrichment analysis was based on KEGG Pathway (http://www.genome.jp/kegg/pathway.html) with reference to *Escherichia coli* K-12. The figure was generated by MetaboAnalyst 4.0 (https://www.metaboanalyst.ca/).

alone and the combination treatments ($\log_2$FC > 1) at 24 h. Interestingly, the abundance of several metabolites associated with tryptophan metabolism (e.g., indole-3-acetate, indolepyruvate and isophenoxazine) was elevated following treatment with aztreonam alone or the combination over 24 h. Consistently, a substantial perturbation in the levels of short-chain peptides was also observed due to aztreonam alone and the combination treatments. Apparently, aztreonam monotherapy induced more metabolic changes in amino acid and peptide levels at 24 h compared to the combination treatment (**Figures 2**, **3**).

Pentose Phosphate Pathway and Amino Sugar Metabolism

Central carbon metabolism was significantly decreased by aztreonam alone and the combination, with major changes observed for the metabolites associated with bacterial anabolic metabolism of the PPP at 1, 4, and 24 h. A number of key metabolites (e.g., gluconate 6-phosphate, D-sedoheptulose 7-phosphate, glyceraldehyde 3-phosphate and D-glucono-1,5-lactone 6-phosphate) were significantly decreased ($\log_2$FC ≤ -1) in their abundance in response to aztreonam alone and the combination (**Figure 5A**). Moreover, the levels of sedoheptulose ($\log_2$FC $= -1.3$ to -2.0) and D-fructose 1,6-biphosphate ($\log_2$FC $= -1.4$ to -3.9) related to carbon fixation and PPP metabolism were also significantly decreased at 4 and 24 h (**Figure 5B**). In addition, a significant perturbation in the amino sugar metabolism was also observed after the treatments of aztreonam alone and the combination at all three time points (**Figure 5C**). In detail, the decreased relative abundance of three metabolites (i.e., D-glucosamine, D-glucosamine 6-phosphate and *N*-acetyl-D-glucosamine 6-phosphate) was observed ($\log_2$FC < -1), which resulted in the decreased level of uridine diphosphate-*N*-acetylglucosamine (UDP-GlcNAc), an important precursor for the synthesis of lipopolysaccharide and peptidoglycan. The decreased metabolite level in this pathway resulted in the accumulation of *N*-acetyl-D-glucosamine (GlcNAc) at 4 and 24 h under aztreonam alone ($\log_2$FC $= 1.1$ and 1.6, respectively) and the combination ($\log_2$FC $= 1.7$ and 0.8, respectively). Moreover, at 1 h aztreonam monotherapy significantly decreased the level of UDP-*N*-acetylmuramate (UDP-MurNAc, $\log_2$FC $= -2.1$), another key metabolite associated with peptidoglycan synthesis (**Figures 4**, **5C**).

Perturbations in Fatty Acid and Phospholipid Levels

Treatments with colistin alone and the combination with aztreonam significantly disrupted bacterial lipids at 1 h; in particular, the medium-chain fatty acids [FA (12:1) and FA hydroxyl (10:0)] and glycerophosphates [PA (32:0) and PA (32:2)] were depleted significantly ($\log_2$FC < -1) (**Figure 6A**). Interestingly, the combination treatment significantly enriched a number of GPLs, in particular, phosphatidylethanolamine [PE (32:1)], phophatidylglycerol [PG (32:1)] and cardiolipin [CL (64:1 and 66:2)] over 24 h ($\log_2$FC > 1). Obviously, aztreonam monotherapy elevated fatty acid levels more dramatically compared to the combination treatment, whereas, long-chain GPLs, including PA (26:1 and 32:1), PE (32:0, 32:1, and 34:1) and PG (32:1 and 34:1) were more significantly enriched by the

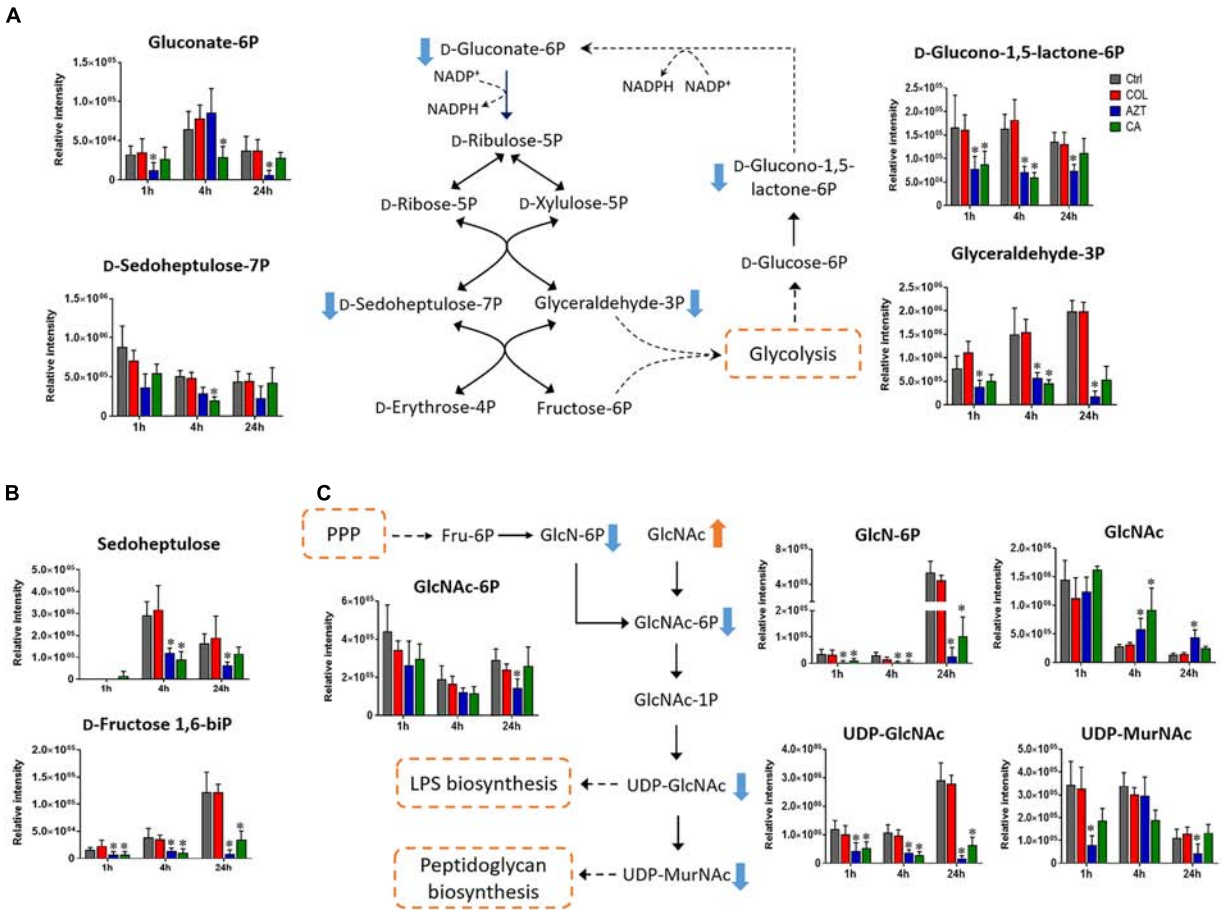

FIGURE 5 | Metabolic changes in **(A)** pentose phosphate pathway (PPP), **(B)** metabolites associated with PPP and carbon fixation, and **(C)** amino sugar metabolism in *A. baumannii* AB090342 after the treatment with colistin (COL, red), aztreonam (AZT, blue) and the combination (CA, green) compared to untreated control (Ctrl, gray) at 1, 4, and 24 h. The pathway flow charts were adapted from KEGG Pathway (http://www.genome.jp/kegg/pathway.html) with reference to *Escherichia coli* K-12. Orange and blue arrows indicate that the metabolites were significantly increased and decreased, respectively. *FDR < 0.05, $p < 0.05$ and $\log_2$ FC ≥ 1 or ≤ -1 (one-way ANOVA).

combination at 24 h (**Figure 6A** and **Supplementary Dataset S2**). In addition, our results also showed that significant perturbations of metabolites related to fatty acid elongation and degradation (hexadec-2-enoyl-CoA) and GPLs biosynthesis and degradation (*sn*-glycero-3-phosphate, *sn*-glycero-3-phosphocholine and *sn*-glycero-3-phosphoethanolamine) were induced by either aztreonam alone or the combination over 24 h (**Figure 6B**).

Purine and Pyrimidine Metabolism

Metabolite levels related to purine and pyrimidine metabolism were significantly decreased by either aztreonam alone or the combination across all three time points (**Figures 4**, **7A**). However, adenosine and uracil were significantly enriched at 24 h by aztreonam monotherapy ($\log_2$FC = 3.2 and 1.6, respectively) and the combination treatment ($\log_2$FC = 2.1 and 0.8, respectively). Notably, compared to aztreonam alone, the combination induced more dramatic changes in nucleotide metabolism at 4 h, but less at 24 h (**Figure 7A**). Specifically, two important energy sources, adenosine diphosphate (ADP) and adenosine triphosphate (ATP) ($\log_2$FC = −1.1 to −2.0) at 24 h, and three nucleotide-derived metabolites related to redox status, nicotinamide adenine dinucleotide phosphate ($NADP^+$), NADPH and NADH at 4 and 24 h ($\log_2$FC = −1.0 to −4.9) were all dramatically depleted after the treatments of aztreonam alone and the combination at 24 h (**Figure 7B**).

DISCUSSION

Polymyxin combination therapies with other antibiotics have been demonstrated synergistic against MDR *A. baumannii* by increasing bacterial kill and reducing emergence of resistance (Cai et al., 2012; Vidaillac et al., 2012; Bae et al., 2016). In the present study, we investigated the metabolic responses of an *A. baumannii* clinical isolate under the treatments with colistin and aztreonam alone and in combination over 24 h. Significantly, our metabolomics results revealed that at the tested concentrations: (1) colistin-facilitated while aztreonam-dominated metabolic perturbations; (2) time-dependent pathway

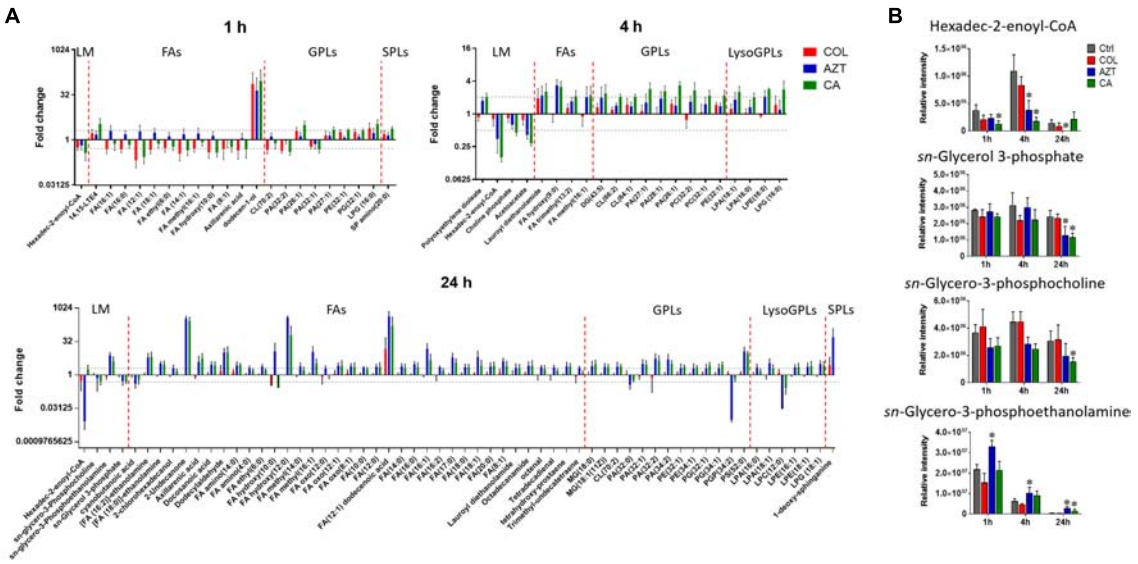

FIGURE 6 | Perturbations of lipids and the related metabolites in *A. baumannii* AB090342. **(A)** Significantly perturbed major lipid classes following the treatment with colistin (COL, red), aztreonam (AZT, blue), and the combination (CA, green) at 1, 4, and 24 h. Lipid names were putatively identified based on the accurate mass. LM: lipid metabolism; FAs: fatty acids; GPLs: glycerophospholipids; SPLs: sphingolipids. **(B)** Significantly perturbed metabolites related to fatty acid and phospholipid synthesis and degradation after treated by colistin, aztreonam and the combination across all three time points. *FDR < 0.05, $p < 0.05$ and $\log_2$ FC ≥ 1 or ≤ -1 (one-way ANOVA).

alterations; (3) changes in PPP and the downstream lipid, amino acid and nucleotide metabolism; and (4) synergistic inhibition of cell envelope synthesis and alterations in the membrane phospholipid composition by the combination.

Our genome sequencing data for AB090342 revealed a mutation of two bases, an in-frame mutation of A138V and A444T, in *pmrB* which has not been characterized before. It is known that polymyxin resistance in *A. baumannii* can be associated with mutations in *pmrB* which upregulate the phosphoethanolamine transferase, EptA, and subsequently result in lipid A modification (Moffatt et al., 2010; Arroyo et al., 2011). Although both mutations in *pmrB* did not cause lipid A modification or polymyxin resistance in AB090342 (colistin MIC = 0.5 mg/L), the constant exposure to colistin in the clinic may have resulted in resistance in clinical isolates. Therefore, colistin combination therapies with other antibiotics are strongly recommended to increase the killing effect and minimize the emergence of resistance.

Our metabolomics results showed that the synergistic action of colistin-aztreonam combination resulted in metabolic alterations in lipid, carbohydrate, nucleotide, amino acid and peptide metabolism. The initial metabolic perturbations following colistin monotherapy and the combination at 1 h mainly involved lipid metabolism (13 out of 20 significant metabolites), in particular the significantly decreased levels of fatty acids and increased phospholipids (**Figures 3**, **6A**). Colistin displays its antimicrobial activity through the initial target LPS on the Gram-negative OM, which results in the increased OM permeability and phospholipid exchange (Velkov et al., 2013; Rabanal and Cajal, 2017). Notably, the significantly perturbed lipid levels by the combination at 1 h were consistent with those observed for colistin alone, suggesting the membrane-targeted killing mechanism. Our results are consistent with previous transcriptomics and metabolomics findings in *A. baumannii* that colistin significantly disturbed OM asymmetry and up-regulated expression of the Mla system which is responsible for phospholipid transfer (Henry et al., 2015; Maifiah et al., 2017). On the contrary, aztreonam alone did not produce any significant alterations in lipid levels at 1 h, but considerably depleted metabolites in amino acid, central carbon and nucleotide metabolism. The mode of action of aztreonam is through interaction with penicillin binding protein 3 (PBP3) which leads to the inhibition of bacterial cell wall synthesis (Ramsey and MacGowan, 2016). Consistent with this primary mechanism, aztreonam monotherapy for 1 h resulted in dramatic decrease in the intracellular level of UDP-MurNAc which is an important precursor for peptidoglycan synthesis (**Figures 3**, **4**, **5C**).

The metabolic responses of *A. baumannii* AB090342 to colistin and aztreonam monotherapy and the combination indicated time-dependent metabolic alterations over 24 h (**Figures 2**, **3**, **Supplementary Figure S2** and **Supplementary Dataset S2**). Aztreonam alone and the combination at 4 and 24 h significantly decreased metabolic levels in amino acid, carbohydrate and nucleotide metabolism, but increased lipid levels. However, colistin alone failed to produce any significant metabolic alterations at 4 or 24 h. The largely shared metabolic changes between aztreonam monotherapy and the combination demonstrated that the synergistic killing by colistin-aztreonam combination was mainly driven by aztreonam at 4 and 24 h. The treatments of aztreonam alone and the combination significantly perturbed metabolite levels in the synthesis of amino sugars at 4 and 24 h, in particular, UDP-GlcNAc and UDP-MurNAc which

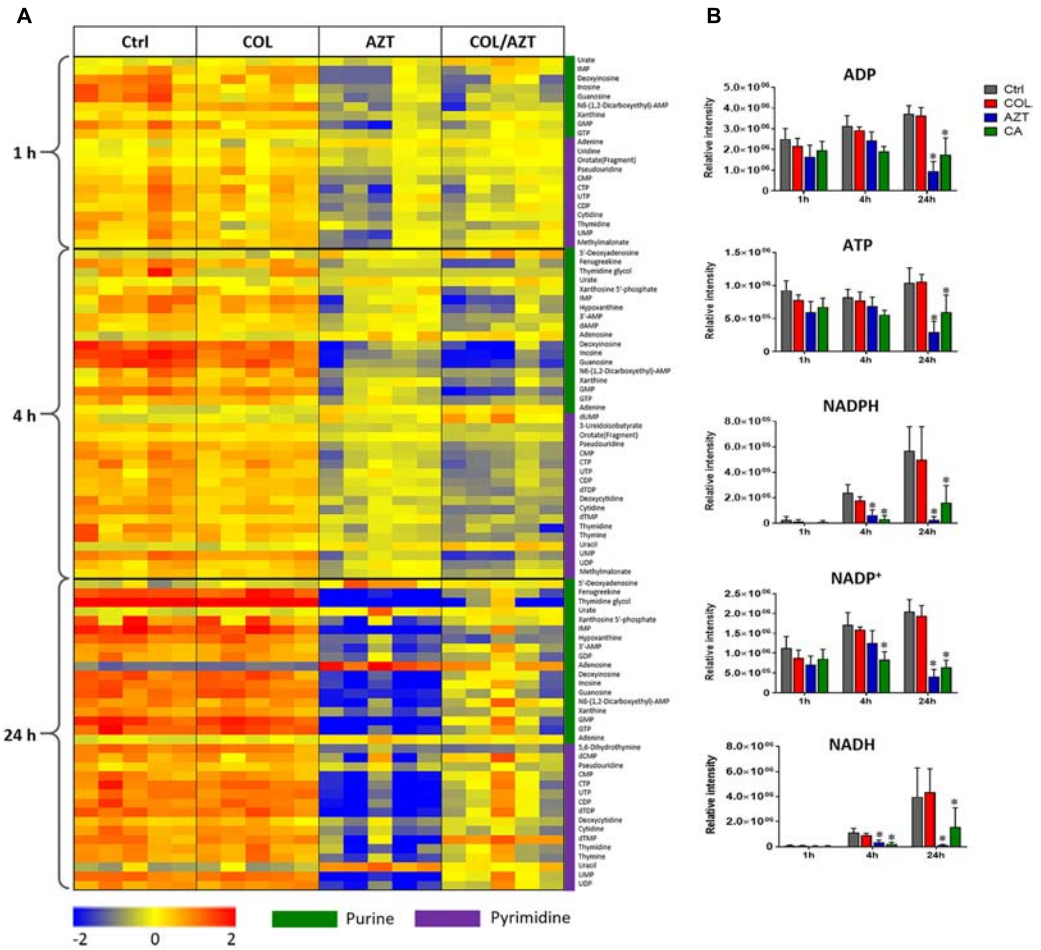

FIGURE 7 | Perturbations of nucleotide metabolism. **(A)** Heatmap profiles of the relative abundance of nucleotide metabolites after treated with colistin (COL), aztreonam (AZT) and the combination (COL/AZT) at 1, 4, and 24 h. **(B)** Significantly altered metabolites associated with nucleotide metabolism due to aztreonam alone and the combination of colistin and aztreonam at 1, 4, and 24 h in *A. baumannii* AB090342. *$\log_2$ FC ≥ 1 or ≤ -1, $p < 0.05$, FDR < 0.05 (one-way ANOVA). Metabolomics data were collected from five biological replicates per condition.

are important precursors for LPS and cell wall biosynthesis, consistent with the antibacterial activity of aztreonam (targeting cell wall) and colistin (targeting cell envelope) (Cho et al., 2014; Ramsey and MacGowan, 2016; Maifiah et al., 2017; Han et al., 2018). In addition to disturbing cell wall biosynthesis, aztreonam also severely depleted the levels of metabolites related to amino acid and nucleotide metabolism which is consistent with the substantially decreased peptide levels (**Figures 3**, **7A**). Moreover, the decreased metabolite levels in PPP coupled to the lower levels of NAD metabolites suggested an imbalanced redox state within bacterial cells treated by aztreonam alone and the combination (Ying, 2008). In contrast, the fatty acid and phospholipid levels were significantly elevated by aztreonam monotherapy and the combination at 4 and 24 h, which was possibly due to the reduced utilization as an energy source, decreased cell turn over and/or membrane remodeling (**Figures 3**, **6**; Lobritz et al., 2015).

Notably, despite the largely shared metabolic perturbations with colistin monotherapy at 1 h and aztreonam monotherapy at 4 and 24 h, the combination displayed the greatest metabolic changes at 4 h and a number of unique metabolic alterations at each time point (**Figures 1**, **3** and **Supplementary Figure S2**). In particular, the combination displayed synergy as early as 1 h and lasted for at least 24 h, which was shown by the significant changes in the membrane phospholipid composition that PA, PE, PG and cardiolipin were more dramatically enriched by the combination compared to either monotherapy over 24 h (**Figures 3**, **6**). It is also evident that the combination synergistically inhibited the LPS and cell wall synthesis (**Figure 5C**). Interestingly, lipid A modification pathways were not affected at any time point under neither of the conditions investigated here, which was also reported for the combination of polymyxin B and doripenem against *A. baumannii* (Maifiah et al., 2017). Collectively, these results show that the combination synergy between polymyxins and β-lactams is mainly due to the inhibition of cell envelope, but not the prevention of lipid A modification mediated polymyxin resistance.

Taken together, our metabolomic results demonstrated, for the first time, that the time-dependent synergistic killing against *A. baumannii* by colistin-aztreonam combination was initially driven by colistin and subsequently by aztreonam through inhibiting multiple key biochemical pathways. This study provides important mechanistic information for optimizing colistin-aztreonam combination therapy in patients using pharmacokinetics/pharmacodynamics.

AUTHOR CONTRIBUTIONS

JZ and JL conceived the project. M-LH and XL performed the experiments, and M-LH, XL, TV, Y-WL, ML, YZ, and DC analyzed the results. All authors involved in the design of the experiments and reviewed the manuscript.

FUNDING

This research was supported by a research grant from the National Natural Science Foundation of China (NSFC 81628015). JL, TV, and DC are supported by the National Institute of Allergy and Infectious Diseases of the National Institutes of Health (R01 AI111965). The content is solely the responsibility of the authors and does not necessarily represent the official views of the National Institutes of Health or the National Natural Science Foundation of China. M-LH and Y-WL are recipients of the 2018 Faculty Bridging Fellowship, Monash University. JL is an Australian National Health and Medical Research Council (NHMRC) Senior Research Fellow. TV and DC are Australian NHMRC Career Development Research Fellows.

ACKNOWLEDGMENTS

The authors are grateful to Monash Biomedical Proteomics Facility (MBPF) for technical assistance with the metabolomics study.

SUPPLEMENTARY MATERIAL

The Supplementary Material for this article can be found online at: https://www.frontiersin.org/articles/10.3389/fmicb.2018.02776/full#supplementary-material

REFERENCES

Arroyo, L. A., Herrera, C. M., Fernandez, L., Hankins, J. V., Trent, M. S., and Hancock, R. E. (2011). The *pmrCAB* operon mediates polymyxin resistance in *Acinetobacter baumannii* ATCC 17978 and clinical isolates through phosphoethanolamine modification of Lipid A. *Antimicrob. Agents Chemother.* 5, 3743–3751. doi: 10.1128/AAC.00256-11

Bae, S., Kim, M.-C., Park, S.-J., Kim, H. S., Sung, H., Kim, M.-N., et al. (2016). *In vitro* synergistic activity of antimicrobial agents in combination against clinical isolates of colistin-resistant *Acinetobacter baumannii*. *Antimicrob. Aents Cemother.* 60, 6774–6779. doi: 10.1128/AAC.00839-16

Boll, J. M., Tucker, A. T., Klein, D. R., Beltran, A. M., Brodbelt, J. S., Davies, B. W., et al. (2015). Reinforcing lipid A acylation on the cell surface of *Acinetobacter baumannii* promotes cationic antimicrobial peptide resistance and desiccation survival. *mBio* 6:e478-15. doi: 10.1128/mBio.00478-15

Boucher, H. W., Talbot, G. H., Bradley, J. S., Edwards, J. E., Gilbert, D., Rice, L. B., et al. (2009). Bad bugs, no drugs: no ESKAPE! an update from the infectious diseases society of america. *Clin. Infect. Dis.* 48, 1–12. doi: 10.1086/595011

Cai, Y., Chai, D., Wang, R., Liang, B., and Bai, N. (2012). Colistin resistance of *Acinetobacter baumannii*: clinical reports, mechanisms and antimicrobial strategies. *J. Antimicrob. Cemother.* 67, 1607–1615. doi: 10.1093/jac/dks084

Cho, H., Uehara, T., and Bernhardt, T. G. (2014). Beta-lactam antibiotics induce a lethal malfunctioning of the bacterial cell wall synthesis machinery. *Cell* 159, 1300–1311. doi: 10.1016/j.cell.2014.11.017

Creek, D. J., Jankevics, A., Burgess, K. E., Breitling, R., and Barrett, M. P. (2012). IDEOM: an excel interface for analysis of LC–MS-based metabolomics data. *Bioinformatics* 28, 1048–1049. doi: 10.1093/bioinformatics/bts069

Delcher, A. L., Bratke, K. A., Powers, E. C., and Salzberg, S. L. (2007). Identifying bacterial genes and endosymbiont DNA with glimmer. *Bioinformatics* 23, 673–679. doi: 10.1093/bioinformatics/btm009

Dijkshoorn, L., Nemec, A., and Seifert, H. (2007). An increasing threat in hospitals: multidrug-resistant *Acinetobacter baumannii*. *Nat. Rev. Microbiol.* 5, 939–951. doi: 10.1038/nrmicro1789

Eliopoulos, G. M., and Bush, K. (2001). New β-lactamases in gram-negative bacteria: diversity and impact on the selection of antimicrobial therapy. *Clin. Infect. Dis.* 32, 1085–1089. doi: 10.1086/319610

Fishbain, J., and Peleg, A. Y. (2010). Treatment of acinetobacter infections. *Clin. Infect. Dis.* 51, 79–84. doi: 10.1086/653120

Gutmann, L., Kitzis, M., Billot-Klein, D., Goldstein, F., Van Nhieu, G. T., Lu, T., et al. (1988). Plasmid-mediated β-lactamase (TEM-7) involved in resistance to ceftazidime and aztreonam. *Clin. Infect. Dis.* 10, 860–866. doi: 10.1093/clinids/10.4.860

Han, M.-L., Zhu, Y., Creek, D. J., Lin, Y.-W., Anderson, D., Shen, H.-H., et al. (2018). Alterations of metabolic and lipid profiles in polymyxin-resistant *Pseudomonas aeruginosa*. *Antimicrob. Agents Chemother.* 62, e2656–e2617. doi: 10.1128/AAC.02656-17

Henry, R., Crane, B., Powell, D., Deveson Lucas, D., Li, Z., Aranda, J., et al. (2015). The transcriptomic response of *Acinetobacter baumannii* to colistin and doripenem alone and in combination in an *in vitro* pharmacokinetics/pharmacodynamics model. *J. Antimicrobial. Chemother.* 70, 1303–1313. doi: 10.1093/jac/dku536

Henry, R., Vithanage, N., Harrison, P., Seemann, T., Coutts, S., Moffatt, J. H., et al. (2011). Colistin-resistant, lipopolysaccharide-deficient *Acinetobacter baumannii* responds to lipopolysaccharide loss through increased expression of genes involved in the synthesis and transport of lipoproteins, phospholipids and poly-β-1, 6-N-acetylglucosamine. *Antimicrob. Agents Chemother.* 56, 59–69. doi: 10.1128/AAC.05191-11

Kaddurah-Daouk, R., Kristal, B. S., and Weinshilboum, R. M. (2008). Metabolomics: a global biochemical approach to drug response and disease. *Annu. Rev. Pharmacol. Toxicol.* 48, 653–683. doi: 10.1146/annurev.pharmtox.48.113006.094715

Kanehisa, M., and Goto, S. (2000). KEGG: kyoto encyclopedia of genes and genomes. *Nucleic Acids Res.* 28, 27–30. doi: 10.1093/nar/28.1.27

Karageorgopoulos, D. E., and Falagas, M. E. (2008). Current control and treatment of multidrug-resistant *Acinetobacter baumannii* infections. *Lancet Infect. Dis.* 8, 751–762. doi: 10.1016/S1473-3099(08)70279-2

Karp, P. D., Ouzounis, C. A., Moore-Kochlacs, C., Goldovsky, L., Kaipa, P., Ahrén, D., et al. (2005). Expansion of the biocyc collection of pathway/genome databases to 160 genomes. *Nucleic Acids Res.* 33, 6083–6089. doi: 10.1093/nar/gki892

Kessner, D., Chambers, M., Burke, R., Agus, D., and Mallick, P. (2008). ProteoWizard: open source software for rapid proteomics tools development. *Bioinformatics* 24, 2534–2536. doi: 10.1093/bioinformatics/btn323

Kirwan, J. A., Weber, R. J., Broadhurst, D. I., and Viant, M. R. (2014). Direct infusion mass spectrometry metabolomics dataset: a benchmark for data processing and quality control. *Sci. Data* 1:140012. doi: 10.1038/sdata.2014.12

Langmead, B., and Salzberg, S. L. (2012). Fast gapped-read alignment with bowtie 2. *Nat. Methods* 9, 357–359. doi: 10.1038/nmeth.1923

Letunic, I., Yamada, T., Kanehisa, M., and Bork, P. (2008). iPath: interactive exploration of biochemical pathways and networks. *Trends Biochem. Sci.* 33, 101–103. doi: 10.1016/j.tibs.2008.01.001

Lim, L. M., Ly, N., Anderson, D., Yang, J. C., Macander, L., Jarkowski, A., et al. (2010). Resurgence of colistin: a review of resistance, toxicity, pharmacodynamics, and dosing. *Pharmacotherapy* 30, 1279–1291. doi: 10.1592/phco.30.12.1279

Lobritz, M. A., Belenky, P., Porter, C. B., Gutierrez, A., Yang, J. H., Schwarz, E. G., et al. (2015). Antibiotic efficacy is linked to bacterial cellular respiration. *Proc. Natl. Acad. Sci. U.S.A.* 112, 8173–8180. doi: 10.1073/pnas.1509743112

Maifiah, M. H. M., Creek, D. J., Nation, R. L., Forrest, A., Tsuji, B. T., Velkov, T., et al. (2017). Untargeted metabolomics analysis reveals key pathways responsible for the synergistic killing of colistin and doripenem combination against *Acinetobacter baumannii*. *Sci. Rep.* 7:45527. doi: 10.1038/srep45527

Mak, J. K., Kim, M.-J., Pham, J., Tapsall, J., and White, P. A. (2008). Antibiotic resistance determinants in nosocomial strains of multidrug-resistant *Acinetobacter baumannii*. *J. Antimicrobl. Chemother.* 63, 47–54. doi: 10.1093/jac/dkn454

Moffatt, J. H., Harper, M., Harrison, P., Hale, J. D., Vinogradov, E., Seemann, T., et al. (2010). Colistin resistance in *Acinetobacter baumannii* is mediated by complete loss of lipopolysaccharide production. *Antimicrob. Agents Chemother.* 54, 4971–4977. doi: 10.1128/AAC.00834-10

Montero, A., Ariza, J., Corbella, X., Doménech, A., Cabellos, C., Ayats, J., et al. (2002). Efficacy of colistin versus β-lactams, aminoglycosides, and rifampin as monotherapy in a mouse model of pneumonia caused by multiresistant *Acinetobacter baumannii*. *Antimicrob. Agents Chemother.* 46, 1946–1952. doi: 10.1128/AAC.46.6.1946-1952.2002

Nation, R. L., Li, J., Cars, O., Couet, W., Dudley, M. N., Kaye, K. S., et al. (2015). Framework for optimisation of the clinical use of colistin and polymyxin b: the prato polymyxin consensus. *Lancet Infect. Dis.* 15, 225–234. doi: 10.1016/S1473-3099(14)70850-3

Perez, F., Hujer, A. M., Hujer, K. M., Decker, B. K., Rather, P. N., and Bonomo, R. A. (2007). Global challenge of multidrug-resistant *Acinetobacter baumannii*. *Antimicrob. Agents Chemother.* 51, 3471–3484. doi: 10.1128/AAC.01464-06

Rabanal, F., and Cajal, Y. (2017). Recent advances and perspectives in the design and development of polymyxins. *Nat. Prod. Rep.* 34, 886–908. doi: 10.1039/c7np00023e

Ramsey, C., and MacGowan, A. P. (2016). A review of the pharmacokinetics and pharmacodynamics of aztreonam. *J. Antimicrob. Chemother.* 71, 2704–2712. doi: 10.1093/jac/dkw231

Sampson, T. R., Liu, X., Schroeder, M. R., Kraft, C. S., Burd, E. M., and Weiss, D. S. (2012). Rapid killing of *Acinetobacter baumannii* by polymyxins is mediated by a hydroxyl radical death pathway. *Antimicrob. Agents Chemother.* 56, 5642–5649. doi: 10.1128/AAC.00756-12

Scheltema, R. A., Jankevics, A., Jansen, R. C., Swertz, M. A., and Breitling, R. (2011). PeakML/mzMatch: a file format, Java library, R library, and tool-chain for mass spectrometry data analysis. *Anal. Chem.* 83, 2786–2793. doi: 10.1021/ac2000994

Smith, C. A., Want, E. J., O'maille, G., Abagyan, R., and Siuzdak, G. (2006). XCMS: processing mass spectrometry data for metabolite profiling using nonlinear peak alignment, matching, and identification. *Anal. Chem.* 78, 779–787. doi: 10.1021/ac051437y

Velkov, T., Roberts, K. D., Nation, R. L., Thompson, P. E., and Li, J. (2013). Pharmacology of polymyxins: new insights into an 'old'class of antibiotics. *Future Microbiol.* 8, 711–724. doi: 10.2217/fmb.13.39

Velkov, T., Thompson, P. E., Nation, R. L., and Li, J. (2010). Structure-activity relationships of polymyxin antibiotics. *J. Med. Chem.* 53, 1898–1916. doi: 10.1021/jm900999h

Vidaillac, C., Benichou, L., and Duval, R. E. (2012). In-vitro synergy of colistin combinations against colistin-resistant *Acinetobacter baumannii*, *Pseudomonas aeruginosa* and *Klebsiella pneumoniae* isolates. *Antimicrob. Agents Chemother.* 56, 4856–4861. doi: 10.1128/AAC.05996-11

Xia, J., Sinelnikov, I. V., Han, B., and Wishart, D. S. (2015). Metaboanalyst 3.0-making metabolomics more meaningful. *Nucleic Acids Res.* 43, W251–W257. doi: 10.1093/nar/gkv380

Ying, W. (2008). NAD+/NADH and NADP+/NADPH in cellular functions and cell death: regulation and biological consequences. *Antioxid. Redox Signal.* 10, 179–206. doi: 10.1089/ars.2007.1672

Yoon, J., Urban, C., Terzian, C., Mariano, N., and Rahal, J. J. (2004). In vitro double and triple synergistic activities of polymyxin B, imipenem, and rifampin against multidrug-resistant *Acinetobacter baumannii*. *Antimicrob. Agents Chemother.* 48, 753–757. doi: 10.1128/AAC.48.3.753-757.2004

Yu, Z., Qin, W., Lin, J., Fang, S., and Qiu, J. (2015). Antibacterial mechanisms of polymyxin and bacterial resistance. *Biomed. Res. Int.* 2015:697019. doi: 10.1155/2015/679109

Zampieri, M., Zimmermann, M., Claassen, M., and Sauer, U. (2017). Nontargeted metabolomics reveals the multilevel response to antibiotic perturbations. *Cell Rep.* 19, 1214–1228. doi: 10.1016/j.celrep.2017.04.002

Zavascki, A. P., Goldani, L. Z., Li, J., and Nation, R. L. (2007). Polymyxin B for the treatment of multidrug-resistant pathogens: a critical review. *J. Antimicrob. Chemother.* 60, 1206–1215. doi: 10.1093/jac/dkm357

Zerbino, D., and Birney, E. (2008). Velvet: algorithms for de novo short read assembly using de Bruijn graphs. *Genome Res.* 18, 821–829. doi: 10.1101/gr.074492.107

Zhu, Y., Czauderna, T., Zhao, J., Klapperstueck, M., Maifiah, M. H. M., Han, M.-L., et al. (2018). Genome-scale metabolic modelling of responses to polymyxins in *Pseudomonas aeruginosa*. *Gigascience* 7:giy021. doi: 10.1093/gigascience/giy021

Conflict of Interest Statement: The authors declare that the research was conducted in the absence of any commercial or financial relationships that could be construed as a potential conflict of interest.

frontiers in Microbiology

ORIGINAL RESEARCH
published: 17 December 2018
doi: 10.3389/fmicb.2018.03105

Relationship Between the Quorum Network (Sensing/Quenching) and Clinical Features of Pneumonia and Bacteraemia Caused by *A. baumannii*

*Laura Fernandez-Garcia[1†], Antón Ambroa[1†], Lucia Blasco[1], Ines Bleriot[1], Maria López[1], Rocio Alvarez-Marin[2], Felipe Fernández-Cuenca[3], Luis Martinez-Martinez[4], Jordi Vila[5], Jesús Rodríguez-Baño[3], Jose Garnacho-Montero[6], Jose Miguel Cisneros[2], Alvaro Pascual[3], Jeronimo Pachón[2,7], German Bou[1], Younes Smani[2] and Maria Tomás[1]**

[1] Microbiology Department-Biomedical Research Institute A Coruña (INIBIC), Hospital A Coruña (CHUAC), University of A Coruña (UDC), A Coruña, Spain, [2] Clinical Unit for Infectious Diseases, Microbiology and Preventive Medicine, Institute of Biomedicine of Seville (IBIS), University Hospital Virgen del Rocío/CSIC/University Seville, Seville, Spain, [3] Clinical Unit for Infectious Diseases, Microbiology and Preventive Medicine, Department of Microbiology and Medicine, Biomedicine Institute of Seville, Hospital Universitario Virgen Macarena, University of Seville, Seville, Spain, [4] Unit of Microbiology, Department of Microbiology, Maimonides Biomedical Research Institute of Cordoba, University Hospital Reina Sofía, University of Córdoba, Córdoba, Spain, [5] Institute of Global Health of Barcelona (ISGlobal), Hospital Clínic - Universitat de Barcelona, Barcelona, Spain, [6] Intensive Care Clinical Unit-Institute of Biomedicine of Seville (IBIS), Hospital Virgen Macarena, Seville, Spain, [7] Department of Medicine, University of Seville, Seville, Spain

Acinetobacter baumannii (Ab) is one of the most important pathogens associated with nosocomial infections, especially pneumonia. Interest in the Quorum network, i.e., Quorum Sensing (QS)/Quorum Quenching (QQ), in this pathogen has grown in recent years. The Quorum network plays an important role in regulating diverse virulence factors such as surface motility and bacterial competition through the type VI secretion system (T6SS), which is associated with bacterial invasiveness. In the present study, we investigated 30 clinical strains of *A. baumannii* isolated in the "II Spanish Study of *A. baumannii* GEIH-REIPI 2000-2010" (*Genbank Umbrella Bioproject* PRJNA422585), a multicentre study describing the relationship between the Quorum network in *A. baumannii* and the development of pneumonia and associated bacteraemia. Expression of the *aidA* gene (encoding the AidA protein, QQ enzyme) was lower ($P < 0.001$) in strains of *A. baumannii* isolated from patients with bacteraemic pneumonia than in strains isolated from patients with non-bacteraemic pneumonia. Moreover, *aidA* expression in the first type of strain was not regulated in the presence of environmental stress factors such as the 3-oxo-C12-HSL molecule (substrate of AidA protein, QQ activation) or H_2O_2 (inhibitor of AidA protein, QS activation). However, in the *A. baumannii* strains isolated from patients with non-bacteraemic pneumonia, *aidA* gene expression was regulated by stressors such as 3-oxo-C12-HSL and H_2O_2. In an *in vivo Galleria mellonella* model of *A. baumannii* infection, the *A. baumannii* ATCC 17978 strain was associated with higher mortality (100% at 24 h) than the mutant, *abaI*-deficient, strain

OPEN ACCESS

Edited by:
Maria Soledad Ramirez, California State University, Fullerton, United States

Reviewed by:
Adriana S. Limansky, CONICET Instituto de Biología Molecular y Celular de Rosario (IBR), Argentina
Vishvanath Tiwari, Central University of Rajasthan, India

***Correspondence:**
Maria Tomás
ma.del.mar.tomas.carmona@sergas.es

[†]These authors have contributed equally to this work

Specialty section:
This article was submitted to Infectious Diseases, a section of the journal Frontiers in Microbiology

Received: *22 September 2018*
Accepted: *30 November 2018*
Published: *17 December 2018*

Citation:
Fernandez-Garcia L, Ambroa A, Blasco L, Bleriot I, López M, Alvarez-Marin R, Fernández-Cuenca F, Martinez-Martinez L, Vila J, Rodríguez-Baño J, Garnacho-Montero J, Cisneros JM, Pascual A, Pachón J, Bou G, Smani Y and Tomás M (2018) Relationship Between the Quorum Network (Sensing/Quenching) and Clinical Features of Pneumonia and Bacteraemia Caused by A. baumannii. Front. Microbiol. 9:3105. doi: 10.3389/fmicb.2018.03105

(carrying a synthetase enzyme of Acyl homoserine lactone molecules) (70% at 24 h). These data suggest that the QS (*abaR* and *abaI* genes)/QQ (*aidA* gene) network affects the development of secondary bacteraemia in pneumonia patients and also the virulence of *A. baumannii*.

Keywords: quorum, sensing/quenching, pneumonia, bacteraemia, *Acinetobacter*

INTRODUCTION

Acinetobacter baumannii is a major cause of hospital-acquired infections associated with high mortality rates (Fuchs, 2016),s usually affecting patients in Intensive Care Units (ICU) (del Mar Tomas et al., 2005; Lee et al., 2017). In these patients, *A. baumannii* causes infections such as pneumonia or, to a lesser extent, serious infections of the bloodstream (around 10% of clinical isolates of *A. baumannii* cause bacteraemia) (Cisneros and Rodríguez-Baño, 2002; El Kettani et al., 2017).

The success of this bacterium as a nosocomial pathogen, has been attributed to the following factors, amongst others: (i) high genetic versatility, facilitating rapid adaptation to stressful or unfavorable situations (Gayoso et al., 2014; Trastoy et al., 2018); (ii) ability to acquire new genes horizontally by the acquisition of plasmids and phages (López et al., 2018); (iii) ability to persist for a long time on animate and inanimate surfaces (resistance to desiccation) (Gayoso et al., 2014), which is generally attributed to biofilm formation; (iv) resistance to antimicrobial agents, including broad-spectrum antibiotics such as carbapenems, colistin, and tigecycline (Fernández-Cuenca et al., 2015), as well as to disinfectants and biocides (Fernández-García et al., 2018); and (v) high virulence (colonization, invasiveness, and cytotoxicity) (Rumbo et al., 2014; Wong et al., 2017). These characteristics contribute to the fact that nosocomial outbreaks caused by *A. baumannii* are difficult to control and that therapeutic options to treat infections are scarce or non-existent (Fernández-Cuenca et al., 2013). In February, 2017, the World Health Organization (WHO) published a list of "priority pathogens." The list includes antibiotic resistant bacteria, considered a serious threat to human health and for which new antibiotics are urgently needed, and is headed by carbapenem-resistant *A. baumannii* (Tacconelli et al., 2018).

The Quorum Sensing (QS) network is generally used by Gram-negative bacterial pathogens to regulate biological processes such as virulence, conjugation, resistance, biofilm formation (which also depends on other factors such as the lytic enzymes responsible for peptidoglycan recycling: Vijayakumar et al., 2016), motility and bacterial competition, via secretion systems (T6SS), which are associated with greater invasiveness (LaSarre and Federle, 2013; López et al., 2017a,b). Two proteins (AbaI /AbaR) identified in *A. baumannii* have been described as homologs of the LuxI/LuxR system found in *Vibrio fischeri*. This system comprises a signal or autoinducer molecule (acyl-homoserine lactone, AHL), an enzyme that synthesizes signaling molecules (AbaI) and a receptor protein activator of the QS (AbaR), which forms a complex with N-(3-hydroxydodecanoil)-L-homoserine lactone (3-OH-C12-HSL) to regulate virulence factors, biofilm formation, surface motility, and bacterial competence (T6SS) (Stacy et al., 2012). When a threshold concentration is reached, the AHL molecules present inside the cell are transported to its receptor (AbaR), putatively joining the lux-box, which is located 67 bp upstream of the ATG of AbaI, resulting in the synthesis of more AHL molecules (López et al., 2017b). The QS mechanism, on the other hand, acts naturally under environmental stress conditions such as the presence of bile salts in the gastrointestinal tract and H_2O_2 (ROS response) in the respiratory tract (López et al., 2017b).

A new enzyme (AidA) has recently been cloned in *E. coli* BL21 (DE3) and functionally characterized in clinical strains of *A. baumannii* capable of inhibiting their own QS (by Quorum Quenching) (López et al., 2017b). This enzyme acts by degrading signaling molecules such as N-(3-Oxo-dodecanoyl), L-homoserine lactone (3-Oxo-C12-HSL), and N-dodecanoyl-L-homoserine lactone (C12-HSL), as confirmed by observation of inhibition of motility, biofilm formation and other virulence factors associated with activation of the Quorum Sensing system (López et al., 2017b; Mayer et al., 2018). Other QQ enzymes have also recently been described in *A. baumannii* ATCC17978 (A1S_0383, A1S_2662, A1S_1876) (Mayer et al., 2018). Multiple QQ enzymes have been analyzed in diverse pathogens such as *Pseudomonas aeruginosa* (Zhang et al., 2011), *Deinococcus radiodurans*, *Hyphomonas neptunium*, *Photorhabdus luminicencens,* and *Rhizobium* spp. (Kalia et al., 2011; Krysciak et al., 2011).

Based on these findings, in the present study, we examined the relationship between the global Quorum regulatory network (QS/QQ) mediated by the *abaR* (QS) and *aidA* (QQ) genes and the development of pneumonia and bacteraemia in clinical strains of *A. baumannii* isolated in the "II Spanish Study of *A. baumannii* GEIH-REIPI 2000-2010," a multicentre study involving 45 Spanish hospitals and 246 patients. In addition, we used an *in vivo* infection model consisting of larvae of the wax moth *Galleria mellonella* to examine the relationship between the global QS/QQ and the development of mortality by a mutant *abaI* (QS)-deficient strain of *A. baumannii* (*A. baumannii* ATCC17978Δ*abaI*) relative to that of the wild-type *A. baumannii* ATCC17978 strain.

MATERIALS AND METHODS

Bacteria and Samples

To carry out this study, we analyzed 30 clinical strains of *A. baumannii* from the 465 strains isolated in the "II Spanish Study of *A. baumannii* GEIH-REIPI 2000-2010" multicentre

study (Genbank Umbrella Bioproject PRJNA422585). The multicentre study included 45 hospitals in Spain, in which new cases of colonization or infection by *A. baumannii* were analyzed between February and March 2010 (Villar et al., 2014). The 30 *A. baumannii* strains were all isolated from respiratory samples from patients with nosocomial pneumonia ($n = 13$: 6 with and 7 without bacteraemia) or *A. baumannii* colonization of the lower respiratory tract ($n = 17$) (Sánchez-Encinales et al., 2017). Molecular typing was performed by Multilocus Sequence Typing (MLST) (Mosqueda et al., 2014). In addition, we used a killing assay with the *Galleria mellonella* infection model and an *A. baumannii* ATCC17978Δ*abaI* mutant strain (identified by Castañeda-Tamez et al., 2018).

The main clinical study variables included demographics, underlying diseases, mechanical ventilation, tracheostomy, colonization of lower respiratory airways, bacteraemic pneumonia (Pn-B), non-bacteraemic pneumonia (Pn-NB) (Horan et al., 2008) and any cause of death during hospitalization.

To design the primers and probes of the QS genes and QQ enzymes, we analyzed the presence of QS genes (*abaR* and *abaI*) and the QQ enzyme (*aidA*) in *A. baumannii* ATCC 17978 (Genbank genome accession numbers CP000521.1 [CP018664.1]) and in 1000 *A. baumannii* genomes by consulting the "Integrated Microbial Genomes and Microbiomes" web page (https://img.jgi.doe.gov) and using nucleotide BLAST. The gene sequences used in the search were selected from the *Acinetobacter baumannii* ATCC 17978 genome. A threshold of 1e-50 was used as the limit for analysis of the nucleotide sequence, where the e-value was defined as the probability of random alignments with the same score. We also calculated the percentage presence of these genes in the genomes (**Figure S1**).

RNA Extraction

RNA Extraction to Analyze the Quorum Regulatory Network (QS/QQ)

All clinical strains of *A. baumannii* were cultured on solid Luria-Bertani (LB) plates and incubated at 37° C for 24 h. One colony was removed and inoculated in liquid LB medium and incubated overnight at 37° C under stirring at 180 rpm. The inoculum was diluted (1:100) and allowed to grow until an optical density (OD_{600} nm) of 0.4–0.6 (corresponding to the logarithmic growth phase) was reached. The RNA was then extracted using the High Pure RNA Isolation kit (Roche, Germany) and the extract was treated with Dnase (Roche, Germany). The extracted RNA was subsequently quantified in a NanoDrop ND-1000 spectrophotometer (NanoDrop Technologies), and the concentration was adjusted to 50 ng/μl in order to yield efficiencies of 90-110% (Rumbo et al., 2013). All extractions were carried out in duplicate.

RNA Extraction to Analyze the Quorum Regulatory Network (QS/QQ) Under Stress Conditions (3-Oxo-C12-HSL and H_2O_2)

The 13 strains of *A. baumannii*, isolated from patients with pneumonia, were cultured on solid Luria-Bertani (LB) plates and incubated at 37°C for 24 h. One colony was then removed, inoculated in liquid LB medium and incubated overnight at 37°C under stirring at 180 rpm. The preinoculum was diluted (1:100) and allowed to grow until an optical density (OD600 nm) of 0.3 was reached. Aliquots of 10 μM of 3-Oxo-C12-HSL (QS-inactivating molecule by expression of the AidA protein) (Stacy et al., 2012; López et al., 2017b) and (10 μl) H_2O_2 were then added for 5 min (QS-activator by ROS response) (López et al., 2018). All controls were prepared by adding the same volumes of DMSO (dimethyl sulfoxide), 3-Oxo-C12-HSL and of sample, but with no H_2O_2. After incubation of the samples for 4 and 5 h in the presence of 3-Oxo-C12-HSL, to study the regulatory QS/QQ genes (*abaR* and *aidA*), as well as 5 min under H_2O_2 in static at 37°C, RNA was extracted using the High Pure RNA Isolation kit (Roche, Germany) and treated with Dnase. The extracted RNA was subsequently quantified as described above (Rumbo et al., 2013).

RT-qPCR

The studies were carried out with a Lightcycler 480 RNA MasterHydrolysis Probe (Roche, Germany), under the following conditions: reverse transcription at 63°C for 3 min, denaturation at 95°C for 30 s, followed by 45 cycles of 15 s at 95°C and 45 s at 60°C and, finally, cooling at 40°C for 30 s. The UPL primers and probes from conserved DNA regions identified by PCR (Universal Probe Library-Roche, Germany) used in the analysis are shown in **Table 1**.

All of the experiments were carried out in a final volume of 20 μl per well (18 μl of master mix and 2 μl of RNA). Each experiment was carried out in duplicate with two RNA extracts (50 ng/μl). For each strain, the expression of all genes, primers, and probes was normalized relative to the reference or housekeeping gene, *rpoB*, for RT-qPCR studies of Quorum sensing Primer sequences (5′-3′) with Taqman probes (Rumbo et al., 2013; López et al., 2017b). Analysis of the controls without reverse transcriptase confirmed the absence of DNA contamination.

Galleria mellonella Infection Model

The *Galleria mellonella* model was an adapted version of that developed by Peleg et al. (2009), Yang et al. (2015). The procedure was as follows: twelve *G. mellonella* larvae, acquired from TruLarvTM (Biosystems Technology, Exeter, Devon, UK), were each injected with 10 μl of a suspension of *A. baumannii* ATCC17978, or its isogenic deficient mutant *A. baumannii* ATCC17978Δ*abaI*, diluted in sterile phosphate buffer saline (PBS) and containing 8×10^4 CFU ($\pm$ 0. 5 log). The injection was performed with a Hamilton syringe (volume 100 μl) (Hamilton, Shanghai, China). In addition, a control group of twelve larvae were injected with 10 μl of sterile PBS. After being injected, the groups of larvae were placed in Petri dishes and incubated in darkness at 37°C. The number of dead larvae was recorded twice a day (morning and afternoon) for 6 days. The larvae were considered dead when they showed no movement in response to touch (Peleg et al., 2009).

TABLE 1 | Primers and Probes used in this study.

		Sequence (5′-3′)	Probe	Reference
QUORUM SENSING				
abaR	Forw	TGGCAAGAAGATTTATTATCAGCA	119/TTGGTGGT	This study
	Rev	TGCGGTAGATTTAACGATCTCA		
	Forw	AGAGGCGTTACGTTGGACTG	155/GAAGGCAA	This study
	Rev	CCAAGAATCTGAGCTATTGC		
QUORUM QUENCHING				
aidA	Forw	GGGAACTTCTTTCGGTGGAG	145/CAGCGACC	López et al., 2017b
	Rev	AACAGCAGCAAGTCGATTATCA		
	Forw	CCTAACCTTGCATTAGGGCTATTA	53/TGGCAGAG	López et al., 2017b
	Rev	CGGTAAACCACAGGTCGGTA		
HOUSEKEEPING				
rpoB	Forw	CGTGTATCTGCGCTTGG	131/CTGGTGGT	Rumbo et al., 2014
	Rev	CGTACTTCGAAGCCTGCAC		

Statistical Analysis

The gene expression studies were carried out in duplicate, and the data obtained were analyzed by Student's *t*-test, implemented with GraphPad Prism v.6 software (GraphPad Software Inc. San Diego, CA). The graphs were constructed using the GraphPad program, and the results were represented as means and their respective standard deviations.

The mortality curves corresponding to the *in vivo Galleria mellonella* infection model were constructed using GraphPad Prism v.6 and the data were analyzed using the Log-rank test (Mantel-Cox). In both cases, p-values < 0.05 were considered statistically significant, and the data were expressed as mean values.

The statistical analyses were applied to the following categorical variables: age, sex, immunosuppressive treatment, surgery, ICU stay, mechanical ventilation, tracheostomy, severe sepsis, septic shock, and expression of the Quorum genes in *A. baumannii* clinical strains (Bone et al., 1992). In addition, the severity of co-morbidities was assessed using the Charlson score (Charlson et al., 1987) and the McCabe score (McCabe and Jackson, 1962). Chi-square and Fisher tests were used in the univariate analysis of categorical variables. Continuous variables were analyzed using two-sample *t*-test or Mann Whitney, as appropriate. A logistic regression analysis was performed to identify factors independently associated with pneumonia and bacteraemia. Differences were considered significant at $p < 0.05$. All statistical analyses were performed using SPSS v.16.0 (SPSS Inc., Chicago, IL).

RESULTS

Study of the Gene Expression of the *abaR* and *aidA* Genes of the Quorum Network (QS/QQ)

The Relative Expression (RE) of the *abaR* and *aidA* genes of the Quorum network (QS/QQ) was quantified by RT-qPCR analysis of the 17 isolates of *A. baumannii* from colonized patients and of the 13 isolates of *A. baumannii* from patients with pneumonia (**Figure 1A**). The mean values (of two biological replicates) are presented in **Tables 2**, **3**. These values were first used to determine any significant differences between the two types of strains in terms of gene expression in the Quorum network.

The results did not reveal any significant differences in the RE of the Quorum network genes (*abaR*, *aidA*) between clinical strains of *A. baumannii* isolated from colonized patients and strains of *A. baumannii* isolated from patients with pneumonia (0.086/0.094 vs. 0.071/0.095, $p > 0.05$).

We then proceeded to study the RE of the *abaR* and *aidA* genes in strains of *A. baumannii* from patients with pneumonia, differentiating the strains isolated from patients with bacteraemia (Pn-B) from those isolated from patients without bacteraemia (Pn-NB). The resulting graphs are shown below (**Figure 1B**). The findings reveal significant differences in the expression of the *abaR* and *aidA* genes between clinical strains of *A. baumannii* from patients with bacteraemic pneumonia (Pn-B) and those with non-bacteraemic pneumonia (Pn-NB). We observed that *abaR* gene was overexpressed in *A. baumannii* isolates from Pn-B patients relative to Pn-NB patients (0.047 vs. 0.097, $p < 0.05$). By contrast, the *aidA* gene was overexpressed in *A. baumannii* clinical strains in Pn-NB patients relative to Pn-B patients (0.173 vs. 0.0045, $p < 0.001$) (**Figure 1B**). Only one strain, Ab 148_GEIH-2010 (ST-2), isolated from Pn-B patients, showed an *aidA* gene profile different from the other isolates of this group, although the RE of this gene was lower (0.022) than that of isolates from Pn-NB patients.

Study of *abaR*/*aidA* Genes (QS/QQ) Under Stress Conditions (3-Oxo-C12-HSL and H_2O_2)

The values of the RE of the *abaR* and *aidA* genes (Quorum network) in the presence of 3-Oxo-C12-HSL (Inhibition of the QS) and H_2O_2 (Activation of the QS), obtained by RT-qPCR of the 13 isolates of *A. baumannii* from patients with pneumonia (differentiated from Pn-NB) are shown in **Table 3**, expressed as

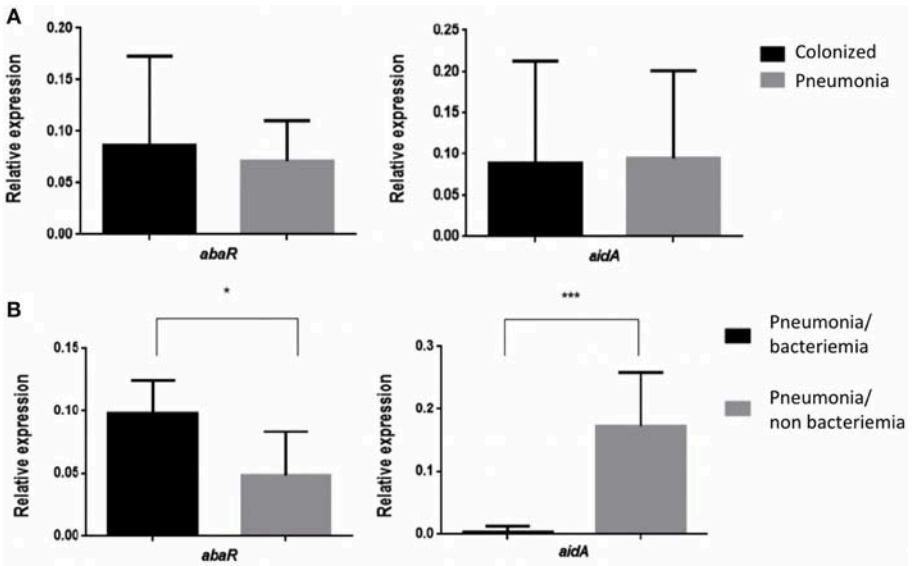

FIGURE 1 | (A) Relative Expression of the *abaR* and *aidA* genes in strains of *A. baumannii* from patients colonized with *A. baumannii* and patients with pneumonia caused by *A. baumannii*. No significant differences ($p > 0.05$) were detected in either case. **(B)** Relative expression of the *abaR* and *aidA* genes in isolates of *A. baumannii* from patients with bacteraemic and non-bacteraemic pneumonia. *p-value < 0.05 and ***p-value < 0.001.

TABLE 2 | Results of RT-qPCR analysis of the Relative Expression (RE) of the *abaR* and *aidA* genes (Quorum network genes) in the *A. baumannii* isolates from colonized patients.

Strain (MLST[a])	*abaR* (RE)	*aidA* (RE)
STRAINS OF *A. baumannii* ISOLATED FROM COLONIZED PATIENTS		
Ab 22_GEIH-2010 (ST-52)	0.043	0.042
Ab 38_GEIH-2010 (ST-2)	0.078	0.146
Ab 59_GEIH-2010 (ST-269)	0.081	0.003
Ab 64_GEIH-2010 (ST-2)	0.076	0.213
Ab 77_GEIH-2010 (ST-261)	0.018	0.112
Ab 112_GEIH-2010 (ST-263)	0.112	0.038
Ab 141_GEIH-2010 (ST-264)	**0.001**	0.010
Ab 177_GEIH-2010 (ST-2)	**0.001**	0.067
Ab 205_GEIH-2010 (ST-2)	0.131	0.126
Ab 288_GEIH-2010 (ST-263)	0.067	0.199
Ab 290_GEIH-2010 (ST-264)	0.141	0.006
Ab 294_GEIH-2010 (ST-2)	0.123	0.481
Ab 326_GEIH-2010 (ST-2)	0.123	0.015
Ab 354_GEIH-2010 (ST79)	0.052	0.020
Ab 364_GEIH-2010 (ST-79)	**0.001**	0.081
Ab 399_GEIH-2010 (ST-79)	0.061	0.050
Ab 456_GEIH-2010 (ST-269)	0.368	**0.001**

The results are expressed as the mean value of the two biological replicates. [a]MLST (Mutilocus Sequence Typing by Pasteur database, https://pubmlst.org/) (Villar et al., 2014). In bold, RE ≤0.001 not detected by RT-PCR.

the mean value of the two biological replicates. These values were then analyzed to determine any significant differences in the RE of the *abaR/aidA* (QS/QQ) genes between the different clinical isolates (**Figures 2**, **3**).

In the clinical strains of *A. baumannii* isolated from Pn-NB (**Figure 2**), we observed regulation of expression of the *aidA* gene in the presence of 3-Oxo-C12-HSL (overexpression, RE $\geq$ 1.5) (**Figure 2A**) and of H_2O_2 [underexpression, RE $\leq$ 0.5 (**Figure 2B**)]. Expression of the *abaR* gene decreased significantly in the presence of the 3-Oxo-C12-HSL molecule (RE $\leq$ 0.5, **Figure 2A**).

In the clinical strains *A. baumannii* isolated from Pn-B (**Figure 3**), expression of the *aidA* gene was not regulated in the presence of 3-Oxo-C12-HSL or H_2O_2. However, the *abaR* gene was overexpressed in the presence of H_2O_2 (RE $\geq$ 1.5, **Figure 3B**).

These results indicate that the isolates of *A. baumannii* from Pn-NB may harbor a functional AidA protein (QQ enzyme), in contrast to the isolates of *A. baumannii* from Pn-B, which did not have this functional protein. Therefore, in the *A. baumannii* strains isolated from Pn-B, overexpression of the *abaR* gene (activation of the QS) in the presence of H_2O_2 (ROS response) would enable the development of the virulence factors favoring invasiveness, such as type VI secretion system (T6SS) and motility.

Quorum Network (QS/QQ) Genes and Clinical Variables

Analysis of the risk factors associated with the development of pneumonia vs. colonization by clinical strains of *A. baumannii* revealed only one statistically significant variable, i.e., diabetes mellitus (**Table 4**).

However, analysis of the risk factors associated with the development of bacteraemia in pneumonia caused by *A. baumannii* revealed underexpression of the *aidA* gene as the only statistically significant variable ($p < 0.05$) (**Table 5**).

TABLE 3 | Results of RT-qPCR analysis of the Relative Expression (RE) of the *abaR* and *aidA* genes (Quorum network genes) in the *A. baumannii* isolates from patients with bacteraemic pneumonia (Pn-B) or non-bacteraemic pneumonia (Pn-NB).

***A. baumannii* strains from Pn-NB patients**			***A. baumannii* strains from Pn-B patients**		
Strain (MLST[a])	***abaR* (RE)**	***aidA* (RE)**	**Strain (MLST[a])**	***abaR* (RE)**	***aidA* (RE)**
Ab 8_GEIH-2010 (ST-2)	0.035	0.108	Ab 148_GEIH-2010 (ST-2)	0.094	0.022
	0.592*	1.545*		1.032*	1.204*
	0.940**	0.873**		1.407**	0.598**
Ab 73_GEIH-2010 (ST-2)	0.036	0.361	Ab 215_GEIH-2010 (ST-2)	0.085	**0.001**
	0.564*	1.695*		0.883*	**0.001***
	0.763**	0.450**		1.376**	**0.001****
Ab 125_GEIH-2010 (ST-257)	0.047	0.156	Ab 232_GEIH-2010 (ST-2)	0.139	**0.001**
	0.431*	1.582*		0.692*	**0.001***
	1.366**	1.076**		0.845**	**0.001****
Ab 157_GEIH-2010 (ST-2)	**0.001**	0.172	Ab 275_GEIH-2010 (ST-181)	0.110	**0.001**
	0.329*	2.308*		0.638*	**0.001***
	1.272**	0.685**		1.430**	**0.001****
Ab 240_GEIH-2010 (ST-2)	0.078	0.150	Ab 371_GEIH-2010 (ST-79)	0.059	**0.001**
	0.561*	0.858*		0.503*	**0.001***
	0.553**	0.703**		1.233**	**0.001****
Ab 268_GEIH-2010 (ST-181)	0.034	0.139	Ab 461_GEIH-2010 (ST-2)	0.099	**0.001**
	0.683*	1.530*		1.221*	**0.001***
	0.845**	0.717**		2.713**	**0.001****
Ab 276_GEIH-2010 (ST-181)	0.108	0.126			
	0.553*	1.007*			
	0.586**	0.722**			

*The results are expressed as the mean values of the two biological replicates. [a]MLST (Mutilocus Sequence Typing by Pasteur database, https://pubmlst.org/) (Villar et al., 2014). In bold, RE ≤0.001, not detected by RT-PCR. * Results of RT-qPCR analysis of the Relative Expression (RE) of the abaR/aidA genes (Quorum network genes) in the presence of 3-Oxo-C12-HSL in strains of A. baumannii from patients with bacteraemic pneumonia (Pn-B) or non-bacteraemic pneumonia (Pn-NB). ** Results of RT-qPCR analysis of the Relative Expression (RE) of the abaR/aidA genes (Quorum network genes) in the presence of H_2O_2 in strains of A. baumannii from patients with bacteraemic pneumonia (Pn-B) or non-bacteraemic pneumonia (Pn-NB).*

Mortality in the *in vivo Galleria mellonella* Model

Injection of *G. mellonella* larvae with *A. baumannii* ATCC17978 at a concentration of 8 x 10^4 CFU/larva (± 0.5 log) caused 100% mortality after 24 h, whereas injection of the larvae with the same concentration of *A. baumannii* ATCC17978Δ*abaI* resulted in 70% mortality after 24 h (**Figure 4**; $p < 0.05$, Mantel-Cox analysis).

DISCUSSION

In this study, we analyzed the expression of Quorum network (QS/QQ) genes that differed between genomes of clinical isolates of *A. baumannii*, *abaR* and *abaI* (QS system) and *aidA* (QQ mechanism) in relation to clinical features of pneumonia and bacteraemia. Although other QQ enzymes have been described in *A. baumannii* ATCC 17978 (Mayer et al., 2018), these were not analyzed in the present study due to the lack of any differences between *A. baumannii* genomes.

In clinical strains of *A. baumannii* isolated from patients with bacteraemic pneumonia (Pn-B), the *abaR* gene was overexpressed ($p < 0.05$). The AbaR protein was the receptor activator of the Quorum Sensing system (QS), and the *aidA* gene was not expressed. Moreover, we observed regulation of *aidA* gene expression in clinical strains of pneumonia-causing *A. baumannii* (non-bacteraemic pneumonia, Pn-NB) by the 3-Oxo-C12-HSL molecule (which is an AidA enzyme substrate in QQ activity) and H_2O_2 (an activator of the QS system). However, there was no difference in the expression of Quorum network genes between colonized and pneumonia patients, as previously described (Stones and Krachler, 2016).

On the other hand, clinical analysis of the risk factors associated with pneumonia caused by *A. baumannii* revealed diabetes mellitus as only statistically significant risk factor (Kim et al., 2014). In relation to bacteraemia in *A. baumannii* pneumonia ($P < 0.05$), underexpression of the *aidA* gene was also the only statistically significant variable ($P < 0.05$).

In several pathogens, such as *Yersinia pseudotuberculosis*, *Proteus mirabilis,* and *Vibrio cholerae*, the QS system is the main regulatory mechanism of bacterial competence via T6SS, which is involved in the invasiveness and motility that favor the development of bacteraemia (Zhang et al., 2011; Debnath et al., 2018; Jaskólska et al., 2018; Trastoy et al., 2018). Moreover, in 86% of ICU patients, gastrointestinal tract colonization by a clinical strain of *A. baumannii* led to development of bacteraemia caused by genetically similar strains (Thom et al., 2010). This implies that clinical isolates of *A. baumannii* most capable of

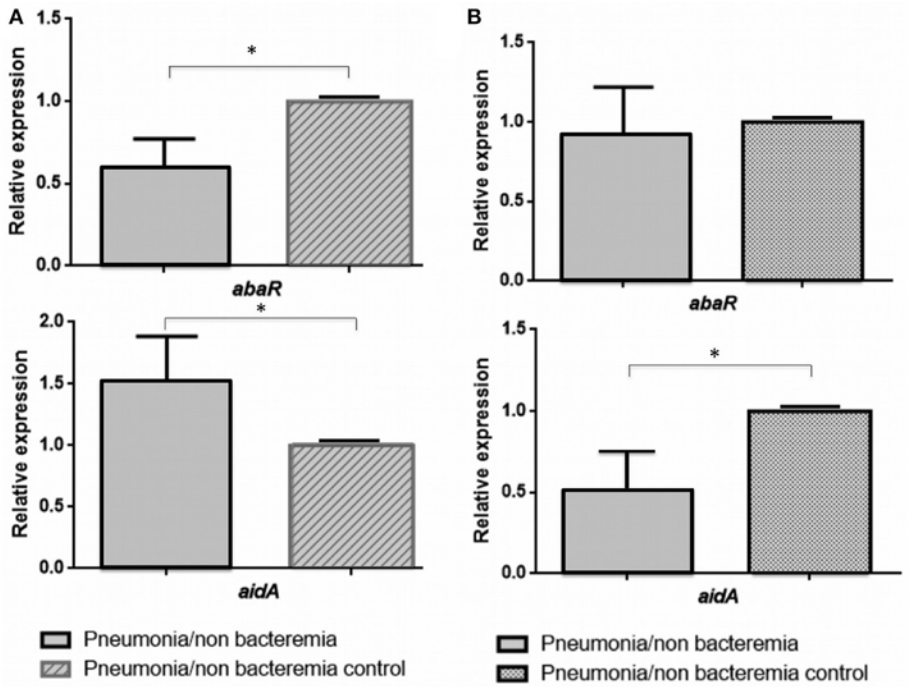

FIGURE 2 | Relative expression of the *abaR* and *aidA* genes under 3-oxo-C12-HSL **(A)** and H_2O_2 **(B)** in isolates of *A. baumannii* from patients with non-bacteraemic pneumonia (Pn-NB). **p*-value < 0.05.

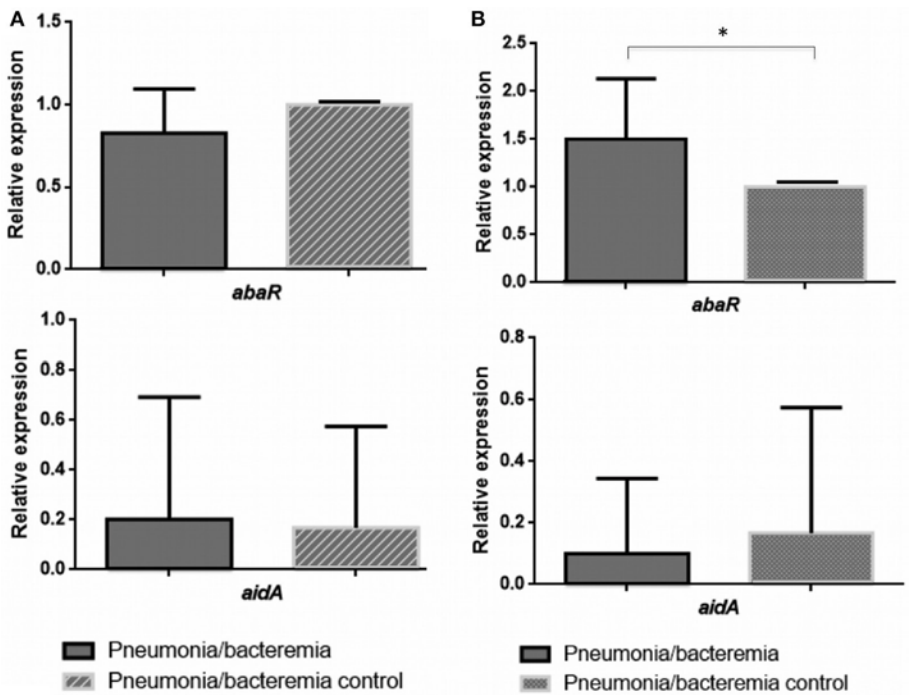

FIGURE 3 | Relative expression of the *abaR* and *aidA* genes under 3-oxo-C12-HSL **(A)** and H_2O_2 **(B)** in isolates of *A. baumannii* from patients with bacteraemic pneumonia (Pn-B). **p*-value < 0.05.

TABLE 4 | Univariate analysis of risk factors associated with development of pneumonia relative to colonization by clinical strains of *A. baumannii*.

Variable	Colonized patients (*n* = 17)	Patients with pneumonia (*n* = 13)	*P*-value
Age, Med ± SEM	55.06 ± 5.12	59.31 ± 5.90	0.590
Female sex	5 (29.41)	6 (46.15)	0.287
Charlson score, Med ± SEM	2.12 ± 0.67	2.46 ± 0.69	0.729
Comorbity condition, no. (%)			
McCabe score, ultimately or rapidly	8 (47.06)	5 (38.46)	0.840
Cancer	1 (5.88)	2 (15.38)	0.397
Diabetes	**3 (17.65)**	**7 (53.85)**	**0.045**
Cirrhosis	0 (0)	0 (0)	NA
AIDS	0 (0)	1 (7.69)	0.433
Chronic lung disease	2 (11.67)	4 (30.78)	0.204
CRF	0 (0)	1 (7.69)	0.433
Immunosuppression	1 (5.88)	2 (15.38)	0.397
Surgery, No. (%)	5 (29.41)	4 (30.78)	0.623
ICU stay, No. (%)	15 (88.23)	11 (84.61)	0.591
Tracheostomy	4 (23.53)	2 (15.38)	0.469
Mechanical ventilation	10 (58.82)	7 (53.85)	0.538
Death	3 (17.65)	3 (23.08)	0.531
abaR	0.09 ± 0.02	0.07 ± 0.04	0.547
aidA	0.09 ± 0.03	0.09 ± 0.03	0.919

In bold and highlighted the variables that showed a $p < 0.05$.

TABLE 5 | Univariate analysis of risk factors associated with the development of bacteraemia in pneumonia caused by *A. baumannii* relative to the non-bacteraemic pneumonia control.

Variable	Pn-NB patients (*N* = 7)	Pn-B patients (*N* = 6)	*P*-value
Age, Med ± SEM	58.43 ± 10.13	60.33 ± 6.08	0.880
Female sex	4 (57.14)	2 (33.33)	0.383
Charlson score, Med ± SEM	2.00 ± 0.79	3.20 ± 1.24	0.497
Comorbity condition, no. (%)			
McCabe score, ultimately or rapidly	3 (42.86)	2 (33.33)	0.380
Cancer	1 (14.28)	1 (20)	0.731
Diabetes	2 (28.57)	5 (83.33)	0.078
Cirrhosis	0 (0)	0 (0)	NA
AIDS	0 (0)	1 (20)	0.462
Chronic lung disease	3 (42.86)	1 (20)	0.343
CRF	1 (14.28)	0 (0)	0.538
Immunosuppression	2 (28.57)	0 (0)	0.269
Surgery, No. (%)	3 (42.86)	1 (20)	0.343
ICU stay, No. (%)	5 (71.43)	6 (100)	0.269
Tracheostomy	0 (0)	2 (33.33)	0.192
Mechanical ventilation	3 (42.86)	4 (66.67)	0.383
Severe sepsis and septic shock, No. (%)	2 (28.57)	3 (50)	0.565
Death	3 (42.86)	0 (0)	0.122
abaR	0.78 ± 0.015	0.06 ± 0.02	0.522
aidA	**0.15 ± 0.04**	**0.03 ± 0.03**	**0.045**

In bold and highlighted the variables that showed a $p < 0.05$.

surviving under stress conditions (such as the presence of bile salts in the gastrointestinal tract or H_2O_2 in the respiratory tract) (Zheng et al., 2018) may have a higher invasive capacity due to virulence factors, such as the type VI secretion system (T6SS), previously activated under stressful conditions. Motility is also a crucial virulence factor, allowing penetration of the bacteria into the host's body and subsequent colonization (Gellatly and Hancock, 2013). Previous studies have demonstrated the existence of a relationship between motility and the origin of the isolates. Indeed, blood isolates of *A. baumannii* have been found to be more mobile than sputum isolates (Vijayakumar et al., 2016). Interestingly, 67% of the clinical isolates of *A. baumannii* were non-mobile and all of them had the AidA protein and were of respiratory origin (López et al., 2017a,b). In addition, the *aidA* gene was not located in the genome of the only mobile strain (clone ST79/PFGE-HUI-1) isolated from blood and which was the origin of a bacteraemic outbreak (López et al., 2017a,b).

Finally, multiple studies carried out with the *abaI* mutant of the M2 strain of *Acinetobacter nosocomialis* have analyzed the role of the *abaI* gene (responsible for the synthesis of quorum sensing synthesizing molecules) in various virulence factors such as biofilm formation and motility. In both cases, *abaI* deficiency led to a decrease in biofilm production and motility (Niu et al., 2008; Bhargava et al., 2012). The mutant lacking *abaI* is believed to be less virulent than the wild strain. This result was confirmed in our study in which injection of *G. mellonella* larvae with the reference *A. baumannii* ATCC17978 strain caused higher mortality than injection with the mutant *A. baumannii* ATCC17978Δ*abaI*. Regarding the mortality of the reference strain (*A. baumannii* ATCC17978), similar effects have been observed in other studies, in which injection of *G. mellonella* larvae with the reference strain *A. baumannii* ATCC17978 resulted in rapid death. Mortality was significantly dependent on the number of cells injected. More than 75% of the larvae died in the first 48 h of injection with at least 3.7×10^5 CFU / larva, while very few of the larvae died after being injected with a concentration equal to or lower than 3.7×10^4 CFU/larva ($p < 0.01$) (Clemmer et al., 2011). The results regarding the mutant *A. baumannii* ATCC17978Δ*abaI* are consistent with those obtained in a study of *Pseudomonas aeruginosa* (Steindler et al., 2009) in which a mutant Δ*rhLI* Δ*lasI* (QS systems homologous to *abaI*) was obtained, demonstrating that inactivation of both QS systems leads to a significant reduction in pathogenicity ($p < 0.01$) when virulence factors are not activated, such as the type VI secretion system (T6SS) and motility (Jaskólska et al., 2018).

In conclusion, our findings suggest that the QS (*abaR* and *abaI* genes)/QQ (*aidA* gene) network plays a role in the development of bacteraemia in patients with pneumonia caused by *A. baumannii*. This is the first study reporting a relationship between reduced expression of this bacterial QQ enzyme gene (AidA protein) and bacteraemia. Further studies

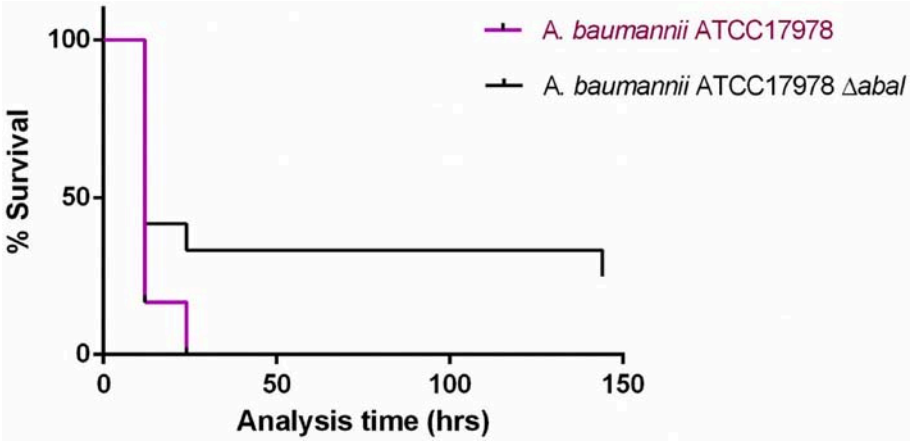

FIGURE 4 | Survival curves for *G. mellonella* larvae injected with *A. baumannii* ATCC17978 reference strain and its isogenic derivative *A. baumannii* ATCC17978 Δ*abaI*. Data from a single representative assay. For simplicity, the control group is not included in this figure.

of this relationship in the same and other bacterial QQ enzymes would be of great interest.

AUTHOR CONTRIBUTIONS

LF-G, AA, LB, IB, ML and RA-M developed the experiments. FF-C, LM-M, JV, JR-B, JG-M, JMC, AP, JP, GB, and YS wrote the manuscript and provided the strains. MT led the experiments and manuscript redaction.

ACKNOWLEDGMENTS

This study was funded by grant PI16/01163 awarded to MT within the State Plan for R+D+I 2013-2016 (National Plan for Scientific Research, Technological Development and Innovation 2008-2011) and co-financed by the ISCIII-Deputy General Directorate for Evaluation and Promotion of Research—European Regional Development Fund A way of Making Europe and Instituto de Salud Carlos III FEDER, Spanish Network for the Research in Infectious Diseases (REIPI, RD16/0016/0001, RD16/0016/0006, RD16/0016/0008, RD16/0016/0009, and RD16/0016/0010) and by the Study Group on Mechanisms of Action and Resistance to Antimicrobials, GEMARA (SEIMC, http://www.seimc.org/). MT was financially supported by the Miguel Servet Research Programme (SERGAS and ISCIII). LF-G was financially supported by a predoctoral fellowship from the Xunta de Galicia (GAIN, Axencia de Innovación).

SUPPLEMENTARY MATERIAL

The Supplementary Material for this article can be found online at: https://www.frontiersin.org/articles/10.3389/fmicb.2018.03105/full#supplementary-material

REFERENCES

Bhargava, N., Sharma, P., and Capalash, N. (2012). N-acyl homoserine lactone mediated interspecies interactions between *A. baumannii* and *P. aeruginosa*. *Biofouling*. 28, 813–822. doi: 10.1080/08927014.2012.714372

Bone, R. C., Balk, R. A., Cerra, F. B., Dellinger, R. P., Fein, A. M., Knaus, W. A., et al. (1992). Definitions for sepsis and organ failure and guidelines for the use of innovative therapies in sepsis. The ACCP/SCCM Consensus Conference Committee. American College of Chest Physicians/Society of Critical Care Medicine. *Chest* H101, 1644–1655. doi: 10.1378/chest.101.6.1644

Castañeda-Tamez, P., Ramírez-Peris, J., Pérez-Velázquez, J., Kuttler, C., Jalalimanesh, A., Saucedo-Mora, M. Á., et al. (2018). Pyocyanin restricts social cheating in Pseudomonas aeruginosa. *Front. Microbiol.* 9:1348. doi: 10.3389/fmicb.2018.01348

Charlson, M. E., Pompei, P., Ales, K. L., and MacKenzie, C. R. (1987). A new method of classifying prognostic comorbidity in longitudinal studies: development and validation. *J. Chronic Dis.* 40, 373–383. doi: 10.1016/0021-9681(87)90171-8

Cisneros, J. M., and Rodríguez-Baño, J. (2002). Nosocomial bacteremia due to Acinetobacter baumannii: epidemiology, clinical features and treatment. *Clin. Microbiol. Infect.* 8, 687–693. doi: 10.1046/j.1469-0691.2002.00487.x

Clemmer, K. M., Bonomo, R. A., and Rather, P. N. (2011). Genetic analysis of surface motility in *Acinetobacter baumannii*. *Microbiology* 157, 2534–2544. doi: 10.1099/mic.0.049791-0

Debnath, I., Stringer, A. M., Smith, S. N., Bae, E., Mobley, H. L. T., Wade, J. T., et al. (2018). MrpJ directly regulates proteus mirabilis virulence factors, including fimbriae and type VI secretion, during urinary tract infection. *Infect Immun.* 86, e00388–18. doi: 10.1128/IAI.00388-18

del Mar Tomas, M., Cartelle, M., Pertega, S., Beceiro, A., Llinares, P., Canle, D., et al. (2005). Hospital outbreak caused by a carbapenem-resistant strain of Acinetobacter baumannii: patient prognosis and risk-factors for colonisation and infection. *Clin. Microbiol. Infect.* 11, 540–546. doi: 10.1111/j.1469-0691.2005.01184.x

El Kettani, A., Maaloum, F., Diawara, I., Katfy, K., Harrar, N., Zerouali, K., et al. (2017). Prevalence of *Acinetobacter baumannii* bacteremia in intensive care units of Ibn Rochd University Hospital, Casablanca. *Iran J Microbiol.* 9, 318–323.

Fernández-Cuenca, F., Tomás, M., Caballero-Moyano, F. J., Bou, G., Martínez-Martínez, L., Vila, J., et al. (2015). Reduced susceptibility to biocides in *Acinetobacter baumannii*: association with resistance to antimicrobials, epidemiological behaviour, biological cost and effect on the expression of genes

encoding porins and efflux pumps. *J. Antimicrob. Chemother.* 70, 3222–3229. doi: 10.1093/jac/dkv262

Fernández-Cuenca, F., Tomás-Carmona, M., Caballero-Moyano, F., Bou, G., Martínez-Martínez, L., Vila, J., et al. (2013). [*In vitro* activity of 18 antimicrobial agents against clinical isolates of Acinetobacter spp.: multicenter national study GEIH-REIPI-Ab 2010]. *Enferm. Infecc. Microbiol. Clin.* 31, 4–9. doi: 10.1016/j.eimc.2012.06.010

Fernández-García, L., Fernandez-Cuenca, F., Blasco, L., Lopez-Rojas, R., Ambroa, A., Lopez, M., et al. (2018). Relationship between tolerance and persistence mechanisms in Acinetobacter baumannii strains with AbkAB Toxin-Antitoxin system. *Antimicrob Agents Chemother.* 62, e00250–18. doi: 10.1128/AAC.00250-18

Fuchs, R. P. (2016). Tolerance of lesions in E. coli: Chronological competition between Translesion Synthesis and Damage Avoidance. *DNA Repair* 44, 51–58. doi: 10.1016/j.dnarep.2016.05.006

Gayoso, C. M., Mateos, J., Méndez, J. A., Fernández-Puente, P., Rumbo, C., Tomás, M., et al. (2014). Molecular mechanisms involved in the response to desiccation stress and persistence in *Acinetobacter baumannii*. *J. Proteome Res.* 13, 460–476. doi: 10.1021/pr400603f

Gellatly, S. L., and Hancock, R. E. (2013) Pseudomonas aeruginosa: new insights into pathogenesis and host defenses. *Pathog. Dis.* 67, 1590–173. doi: 10.1111/2049-632x.12033

Horan, T. C., Andrus, M., and Dudeck, M. A. (2008). CDC/NHSN surveillance definition of health care-associated infection and criteria for specific types of infections in the acute care setting. *Am. J. Infect. Control.* 36, 309–332. doi: 10.1016/j.ajic.2008.03.002

Jaskólska, M., Stutzmann, S., Stoudmann, C., and Blokesch, M. (2018). QstR-dependent regulation of natural competence and type VI secretion in *Vibrio cholerae*. *Nucleic Acids Res.* 46, 10619–10634. doi: 10.1093/nar/gky717

Kalia, V. C., Raju, S. C., and Purohit, H. J. (2011). Genomic analysis reveals versatile organisms for quorum quenching enzymes: acyl-homoserine lactone-acylase and -lactonase. *Open Microbiol. J.* 5, 1–13. doi: 10.2174/18742858011050 10001

Kim, T., Chong, Y. P., Park, S. Y., Jeon, M. H., Choo, E. J., Chung, J. W., et al. (2014). Risk factors for hospital-acquired pneumonia caused by carbapenem-resistant Gram-negative bacteria in critically ill patients: a multicenter study in Korea. *Diagn. Microbiol. Infect. Dis.* 78, 457–461. doi: 10.1016/j.diagmicrobio.2013.08.011

Krysciak, D., Schmeisser, C., Preuss, S., Riethausen, J., Quitschau, M., Grond, S., et al. (2011). Involvement of multiple loci in quorum quenching of autoinducer I molecules in the nitrogen-fixing symbiont Rhizobium (Sinorhizobium) sp. strain NGR234. *Appl. Environ. Microbiol.* 77, 5089–5099. doi: 10.1128/AEM.00112-11

LaSarre, B., and Federle, M. J. (2013). Exploiting quorum sensing to confuse bacterial pathogens. *Microbiol. Mol. Biol. Rev.* 77, 73–111. doi: 10.1128/MMBR.00046-12

Lee, C. R., Lee, J. H., Park, M., Park, K. S., Bae, I. K., Kim, Y. B., et al. (2017). Biology of *Acinetobacter baumannii*: pathogenesis, antibiotic resistance mechanisms, and prospective treatment options. *Front. Cell. Infect. Microbiol.* 7:55. doi: 10.3389/fcimb.2017.00055

López, M., Blasco, L., Gato, E., Perez, A., Fernandez-Garcia, L., Martinez-Martinez, L., et al. (2017a). Response to bile salts in clinical strains of *Acinetobacter baumannii* lacking the AdeABC efflux pump: virulence associated with quorum sensing. *Front. Cell. Infect. Microbiol.* 7:143. doi: 10.3389/fcimb.2017.00143

López, M., Mayer, C., Fernandez-Garcia, L., Blasco, L., Muras, A., Ruiz, F. M., et al. (2017b). Quorum sensing network in clinical strains of *A. baumannii*: AidA is a new quorum quenching enzyme. *PLoS ONE* 12:e0174454. doi: 10.1371/journal.pone.0174454

López, M., Rueda, A., Florido, J. P., Blasco, L., Fernandez-Garcia, L., Trastoy, R., et al. (2018). Evolution of the Quorum network and the mobilome (plasmids and bacteriophages) in clinical strains of *Acinetobacter baumannii* during a decade. *Sci. Rep.* 8:2523. doi: 10.1038/s41598-018-20847-7

Mayer, C., Muras A., Romero, M., López, M., Tomás, M., and Otero, A. (2018). Multiple quorum quenching enzymes are active in the nosocomial pathogen Acinetobacter baumannii ATCC17978. *Front. Cell Infect. Microbiol.* 8:310. doi: 10.3389/fcimb.2018.00310

McCabe, W. R., and Jackson, G. G. (1962). Gram-negative bacteremia. I. Etiology and ecology. *Arch Int Med.* 110, 847–855.

Mosqueda, N., Gato, E., Roca, I., Lopez, M., de Alegria, C. R., Fernandez Cuenca, F., et al. (2014). Characterization of plasmids carrying the blaOXA-24/40 carbapenemase gene and the genes encoding the AbkA/AbkB proteins of a toxin/antitoxin system. *J. Antimicrob. Chemother.* 69, 2629–2633. doi: 10.1093/jac/dku179

Niu, C., Clemmer, K. M., Bonomo, R. A., and Rather, P. N. (2008). Isolation and characterization of an autoinducer synthase from *Acinetobacter baumannii*. *J. Bacteriol.* 190, 3386–3392. doi: 10.1128/JB.01929-07

Peleg, A. Y., Jara, S., Monga, D., Eliopoulos, G. M., Moellering, R. C., and Mylonakis, E. (2009). Galleria mellonella as a model system to study *Acinetobacter baumannii* pathogenesis and therapeutics. *Antimicrob. Agents Chemother.* 53, 2605–2609. doi: 10.1128/AAC.01533-08

Rumbo, C., Gato, E., López, M., Ruiz de Alegría, C., Fernández-Cuenca, F., Martínez-Martínez, L., et al. (2013). Contribution of efflux pumps, porins, and β-lactamases to multidrug resistance in clinical isolates of Acinetobacter baumannii. *Antimicrob. Agents Chemother.* 57, 5247–5257. doi: 10.1128/AAC.00730-13

Rumbo, C., Tomás, M., Fernández Moreira, E., Soares, N. C., Carvajal, M., Santillana, E., et al. (2014). The Acinetobacter baumannii Omp33-36 porin is a virulence factor that induces apoptosis and modulates autophagy in human cells. *Infect. Immun.* 82, 4666–4680. doi: 10.1128/IAI.02034-14

Sánchez-Encinales, V., Álvarez-Marín, R., Pachón-Ibá-ez, M. E., Fernández-Cuenca, F., Pascual, A., Garnacho-Montero, J., et al. (2017). Overproduction of Outer Membrane Protein A by Acinetobacter baumannii as a risk factor for nosocomial pneumonia, bacteremia, and mortality rate increase. *J. Infect. Dis.* 215, 966–974. doi: 10.1093/infdis/jix010

Stacy, D. M., Welsh, M. A., Rather, P. N., and Blackwell, H. E. (2012). Attenuation of quorum sensing in the pathogen Acinetobacter baumannii using non-native N-Acyl homoserine lactones. *ACS Chem. Biol.*. 7, 1719–1728. doi: 10.1021/cb300351x

Steindler, L., Bertani, I., De Sordi, L., Schwager, S., Eberl, L., and Venturi, V. (2009). LasI/R and RhlI/R quorum sensing in a strain of Pseudomonas aeruginosa beneficial to plants. *Appl. Environ. Microbiol.*. 75, 5131–5140. doi: 10.1128/AEM.02914-08

Stones, D. H., and Krachler, A. M. (2016). Against the tide: the role of bacterial adhesion in host colonization. *Biochem. Soc. Trans.*. 44, 1571–1580. doi: 10.1042/BST20160186

Tacconelli, E., Carrara, E., Savoldi, A., Harbarth, S., Mendelson, M., Monnet, D. L., et al. (2018). Discovery, research, and development of new antibiotics: the WHO priority list of antibiotic-resistant bacteria and tuberculosis. *Lancet Infect. Dis.*. 18, 318–327. doi: 10.1016/S1473-3099(17)30753-3

Thom, K. A., Hsiao, W. W., Harris, A. D., Stine, O. C., Rasko, D. A., and Johnson, J. K. (2010). Patients with *Acinetobacter baumannii* bloodstream infections are colonized in the gastrointestinal tract with identical strains. *Am. J. Infect. Control.* 38, 751–753. doi: 10.1016/j.ajic.2010.03.005

Trastoy, R., Manso, T., Fernández-García, L., Blasco, L., Ambroa, A., Pérez Del Molino, M. L., et al. (2018). Mechanisms of bacterial tolerance and persistence in the gastrointestinal and respiratory environments. *Clin. Microbiol. Rev.* 31:e00023–18. doi: 10.1128/CMR.00023-18

Vijayakumar, S., Rajenderan, S., Laishram, S., Anandan, S., Balaji, V., and Biswas, I. (2016). Biofilm formation and motility depend on the nature of the *Acinetobacter baumannii* clinical isolates. *Front Public Health.* 4:105. doi: 10.3389/fpubh.2016.00105

Villar, M., Cano, M. E., Gato, E., Garnacho-Montero, J., Miguel Cisneros, J., Ruíz de Alegría, C., et al. (2014). Epidemiologic and clinical impact of Acinetobacter baumannii colonization and infection: a reappraisal. *Medicine* 93, 202–210. doi: 10.1097/MD.0000000000000036

Wong, D., Nielsen, T. B., Bonomo, R. A., Pantapalangkoor, P., Luna, B., and Spellberg, B. (2017). Clinical and pathophysiological overview of acinetobacter infections: a century of challenges. *Clin. Microbiol. Rev.* 30, 409–447. doi: 10.1128/CMR.00058-16

Yang, H., Chen, G., Hu, L., Liu, Y., Cheng, J., Li, H., et al. (2015). *In vivo* activity of daptomycin/colistin combination therapy in a Galleria mellonella model of *Acinetobacter baumannii* infection. *Int. J. Antimicrob. Agents* 45, 188–191. doi: 10.1016/j.ijantimicag.2014.10.012

Zhang, W., Xu, S., Li, J., Shen, X., Wang, Y., and Yuan, Z. (2011). Modulation of a thermoregulated type VI secretion system by AHL-dependent quorum sensing in *Yersinia pseudotuberculosis*. *Arch. Microbiol.* 193, 351–363. doi: 10.1007/s00203-011-0680-2

Zheng, Y., Li, Y., Long, H., Zhao, X., Jia, K., Li, J., et al. (2018). *bifA* regulates biofilm development of *Pseudomonas putida* MnB1 as a primary response to H_2O_2 and Mn^2. *Front. Microbiol.* 9:1490. doi: 10.3389/fmicb.2018.01490

Conflict of Interest Statement: The authors declare that the research was conducted in the absence of any commercial or financial relationships that could be construed as a potential conflict of interest.

frontiers in Microbiology

ORIGINAL RESEARCH
published: 04 January 2019
doi: 10.3389/fmicb.2018.02898

Emergence and Persistence of High-Risk Clones Among MDR and XDR *A. baumannii* at a Brazilian Teaching Hospital

Laís Calissi Brisolla Tavares[1,2], *Francielli Mahnic de Vasconcellos*[2], *William Vaz de Sousa*[2], *Taisa Trevizani Rocchetti*[3], *Alessandro Lia Mondelli*[2], *Adriano Martison Ferreira*[3], *Augusto Cezar Montelli*[3], *Terue Sadatsune*[3], *Monique Ribeiro Tiba-Casas*[2] and *Carlos Henrique Camargo*[1,2]*

[1] Faculdade de Medicina da Universidade de São Paulo, São Paulo, Brazil, [2] Centro de Bacteriologia, Instituto Adolfo Lutz, São Paulo, Brazil, [3] Faculdade de Medicina de Botucatu, Botucatu, Brazil

Dissemination of carbapenem-resistant *Acinetobacter baumannii* is currently one of the priority themes discussed around the world, including in Brazil, where this pathogen is considered endemic. A total of 107 carbapenem-resistant *A. baumannii* (CRAB) isolates were collected from patients with bacteraemia attended at a teaching hospital in Brazil from 2008 to 2014. From these samples, 104 (97.2%) carried $bla_{\text{OXA-23-like}}$, all of them associated with IS*Aba1* The $bla_{\text{OXA-231}}$ (1.9%) and $bla_{\text{OXA-72}}$ (0.9%) genes were also detected in low frequencies. All isolates were susceptible to minocycline, and 38.3% of isolates presented intermediate susceptibility to tigecycline (MIC = 4 μg/ml). Molecular typing assessed by multi-locus sequence typing demonstrated that the strains were mainly associated with clonal complexes CC79 (47.4%), followed by CC1 (16.9%), and CC317 (18.6%), belonging to different pulsotypes and in different prevalences over the years. Changes in the clones' prevalence reinforce the need of identifying and controlling CRAB in hospital settings to preserve the already scarce therapeutic options available.

Keywords: ***Acinetobacter baumannii,*** **oxacillinases, resistance epidemiology, healthcare associated infections, clonal complexes, MLST**

OPEN ACCESS

Edited by:
Maria Alejandra Mussi, Consejo Nacional de Investigaciones Científicas y Técnicas (CONICET), Argentina

Reviewed by:
Benjamin Andrew Evans, University of East Anglia, United Kingdom
Guillermo Daniel Repizo, CONICET Instituto de Biología Molecular y Celular de Rosario (IBR), Argentina

***Correspondence:**
Carlos Henrique Camargo
carlos.camargo@ial.sp.gov.br

Specialty section:
This article was submitted to Infectious Diseases, a section of the journal Frontiers in Microbiology

Received: *28 July 2018*
Accepted: *12 November 2018*
Published: *04 January 2019*

Citation:
Tavares LCB, Vasconcellos FM, Sousa WV, Rocchetti TT, Mondelli AL, Ferreira AM, Montelli AC, Sadatsune T, Tiba-Casas MR and Camargo CH (2019) Emergence and Persistence of High-Risk Clones Among MDR and XDR A. baumannii at a Brazilian Teaching Hospital. Front. Microbiol. 9:2898. doi: 10.3389/fmicb.2018.02898

INTRODUCTION

Emergence and dissemination of carbapenem-resistant *Acinetobacter baumannii* (CRAB) is currently one of the priority themes discussed around the world (Higgins et al., 2010; US Centers for Disease Control Prevention. *Antibiotic Resistance Threats in the United States*., 2013; World Health Organization, 2017). In Brazil, a continental country in which healthcare associated infections rates are distinctly high (Fortaleza et al., 2017), CRAB is considered endemic (Rossi, 2011) and *Acinetobacter* infections present the highest mortality rates among ICU patients with bacterial bloodstream infections (Marra et al., 2011). Carbapenem resistance in *Acinetobacter* is usually mediated by carbapenem-hydrolysing class D β-lactamase (CHDL), mainly codified by the $bla_{\text{OXA-23}}$-like, $bla_{\text{OXA-24}}$-like, $bla_{\text{OXA-58}}$-like and $bla_{\text{OXA-143}}$-like genes (Zarrillii et al., 2013).

Molecular epidemiology of CRAB highlights the prevalence of International Clone 1 (Clonal Complex CC1) worldwide, while International Clones 2 (CC2) and 3 (CC3) are prevalent in Europe and in the United States (Zarrilli et al., 2009; Karah et al., 2012; Zarrillii et al., 2013). In Brazil and other Latin American countries (Clímaco et al., 2013; Medeiros and Lincopan, 2013; Stietz et al., 2013; Rodríguez et al., 2016; Escandón-Vargas et al., 2017), clonal complexes CC1, CC15 are

predominant, along with CC79, which has also been identified in Spain and in the United States (Villalón et al., 2011; Mosqueda et al., 2014; Kanamori et al., 2016).

Circulation of a limited number of lineages of multidrug- (MDR) and extensively-drug resistance (XDR) *A. baumannii* underscores the need for surveillance and effective implementation of measures to contain their dissemination.

To determine the occurrence of high-risk clones CRAB circulating in a Brazilian hospital, we evaluated their antimicrobial susceptibility and clonality in isolates recovered from bloodstream infections in patients attended at a teaching hospital in inner Brazil.

MATERIALS AND METHODS

Epidemiological Design

This was an observational retrospective study performed with 107 carbapenem-resistant *A. baumannii* isolates recovered from not-repeated patients with bacteraemia attending at Botucatu Medical School Hospital/UNESP (BMSH/UNESP), from 2008 to 2014. The study was approved as a retrospective study by the Local Research Ethics Committee (Process CAAE 49985115.5.0000.0059). We were granted an exemption from the requirement to obtain written informed-consent from the participants and/or their legal guardians because the isolates included in the study had already been stored, on an ongoing basis, in the Culture Collection of the Department of Microbiology and Immunology, UNESP, Botucatu, São Paulo, Brazil.

Settings and *A. baumannii* Isolates

BMSH/UNESP is a 415-bed (52 intensive care unit beds) tertiary regional reference hospital, located in the inner of the State of Sao Paulo, Brazil. For this study, frozen isolates stocked in deep-freezer were recovered in Brain-Heart Infusion (BHI) broth and streaked onto BHI Agar plates. *Acinetobacter* isolates were initially identified by morphological and biochemical characteristics (Gram stain, oxidase-negative, catalase-positive, glucose oxidation, ability to grow at 42° and 44°C) (Vaneechoutte et al., 2015). *A. baumannii* species was screened by PCR detection of $bla_{\text{OXA-51-like}}$ (Woodford et al., 2006) and *glt*A genes (Wong et al., 2014). A subset of randomly selected isolates was submitted to ITS and/or *rpo*B gene sequencing (Chang et al., 2005; La Scola et al., 2006). As MLST was carried out for each pulsotype (see below), *A. baumannii* identification was also confirmed by this method.

Detection of Oxacillinase Genes and IS*Aba1*

PCR for CHDL oxacillinases-encoding genes ($bla_{\text{OXA-23-like}}$, $bla_{\text{OXA-24/40-like}}$, $bla_{\text{OXA-143-like}}$ and $bla_{\text{OXA-58-like}}$) and other carbapenemases (bla_{KPC}, bla_{NDM}, bla_{SPM}, bla_{IMP}, bla_{VIM}, $bla_{\text{OXA-48}}$) was performed in all isolates as previously described (Woodford et al., 2006; Higgins et al., 2010; Poirel et al., 2011). Full sequencing of the $bla_{\text{OXA-24}}$-like and the $bla_{\text{OXA-143-like}}$ was carried out for allele determination (Héritier et al., 2005; Higgins et al., 2009; Cayô et al., 2014). Presence of the IS*Aba1* upstream the bla_{OXA} genes was also investigated by PCR mapping, employing the IS*Aba1* forward primer (Segal et al., 2005) and the bla_{OXA} reverse primers (Woodford et al., 2006).

Antimicrobial Susceptibility Testing

Minimum inhibitory concentration (MIC) values were determined for ampicillin-sulbactam, minocycline, and tetracycline (broth microdilution method), imipenem, meropenem, tigecycline, and polymyxin B (E-test, BioMeriéux, Marci l'Etoile, France). The susceptibility profile of the isolates was completed by disc-diffusion method to amikacin, cefepime, ceftazidime, cefotaxime, ciprofloxacin, gentamicin, levofloxacin, piperacillin-tazobactam, trimethoprim-sulfamethoxazole, ticarcillin-clavulanate, and tobramycin. Breakpoints employed to define susceptibility, intermediate or resistance followed CLSI recommendations (Clinical Laboratory Standards Institute, 2015), except for tigecycline, for which the US Food and Drug Administration breakpoints were applied (susceptible: $\leq$2 μg ml^{-1}; resistant: $\geq$8 μg ml−1). Isolates were categorized as multidrug- (MDR, non-susceptibility to $\geq$1 agent in $\geq$3 antimicrobial categories among aminoglycosides, antipseudomonal carbapenems, antipseudomonal fluoroquinolones, antipseudomonal penicillins + β-lactamase inhibitors, extended-spectrum cephalosporins, folate pathway inhibitors, penicillins + β-lactamase inhibitors, polymyxins, tetracyclines) or extensively-drug-resistant (XDR, non-susceptibility to $\geq$1 agent in all but $\leq$2 categories, as described earlier) (Magiorakos et al., 2012).

Determination of the Electrophoretic Pattern by PFGE

Genetic diversity among all the 107 *A. baumannii* isolates were investigated by PFGE (Seifert et al., 2005). Macrorestriction was performed with ApaI (Promega) and DNA digested fragments were resolved using a CHEF-DR-III (Bio-Rad). Dendrogram was generated with BioNumerics v.7.6.2 (Applied Maths, Sint-Martens-Latem, Belgium) based on the Dice similarity using the UPGMA method, with tolerance and optimization parameters set at 1.5%. Clusters were defined as isolates with similarity $\geq$87% and named with capital letters (A to K) while pulsotypes were defined as each electrophoretic pattern with 100% similarity (named with capital letters and numbers, from A1 to K4).

MLST Analysis

MLST was performed in a representative isolate of each pulsotype as per the Institute Pasteur protocol (https://pubmlst.org/abaumannii/info/primers_Pasteur.shtml), in order to sequence the internal region of the genes *gltA, fusA, recA, cpn60, pyrG, rplB* and *rpoB*. PCR products were purified with enzyme ExoSAP-IT (Affymetrix) according to manufacturer's instructions. Nucleotide sequences were obtained using an Applied 3730 Automatic Sequencer (Applied Biosystems). The results were analyzed on BioNumerics v.7.6.2 (Applied Maths, Sint-Martens-Latem, Belgium), and compared with the Institute Pasteur database (https://pubmlst.org/abaumannii/); clonal complexes were determined by the eBurst algorithm (http://eburst.mlst.net/).

TABLE 1 | Distribution (frequency and %) of antimicrobial susceptibility (S) and non-susceptibility (NS, intermediate + resistance) among the clones of *A. baumannii*.

Antimicrobial1	CC1 ($n = 11$)				CC15 ($n = 10$)				CC79 ($n = 53$)				ST317 ($n = 28$)				Others (ST25, ST107, ST22) ($n = 5$)			
	S	(%)	NS	(%)	S	(%)	NS	(%)	S	(%)	NS	(%)	S	(%)	NS	(%)	S	(%)	NS	(%)
GN	0	(0)	11	(100)	0	(0)	10	(100)	5	(9.4)	48	(90.6)	17	(60.7)	11	(39.3)	3	(60)	2	(40)
TOB	0	(0)	11	(100)	1	(10)	9	(90)	14	(26.4)	39	(73.6)	15	(53.6)	13	(46.4)	4	(80)	1	(20)
AK	6	(54.5)	5	(45.5)	0	(0)	10	(100)	2	(3.8)	51	(96.2)	0	(0)	28	(100)	2	(40)	3	(60)
IMP	0	(0)	11	(100)	0	(0)	10	(100)	0	(0)	53	(100)	0	(0)	28	(100)	0	(0)	5	(100)
MEM	0	(0)	11	(100)	0	(0)	10	(100)	0	(0)	53	(100)	0	(0)	28	(100)	0	(0)	5	(100)
CIP	0	(0)	11	(100)	0	(0)	10	(100)	0	(0)	53	(100)	0	(0)	28	(100)	0	(0)	5	(100)
LEV	0	(0)	11	(100)	0	(0)	10	(100)	0	(0)	53	(100)	0	(0)	28	(100)	0	(0)	5	(100)
PTZ	0	(0)	11	(100)	0	(0)	10	(100)	0	(0)	53	(100)	0	(0)	28	(100)	0	(0)	5	(100)
TIM	0	(0)	11	(100)	0	(0)	10	(100)	0	(0)	53	(100)	1	(3.6)	27	(96.4)	0	(0)	5	(100)
CTX	0	(0)	11	(100)	0	(0)	10	(100)	0	(0)	53	(100)	0	(0)	28	(100)	0	(0)	5	(100)
CAZ	0	(0)	11	(100)	0	(0)	10	(100)	0	(0)	53	(100)	0	(0)	28	(100)	0	(0)	5	(100)
FEP	0	(0)	11	(100)	0	(0)	10	(100)	0	(0)	53	(100)	0	(0)	28	(100)	0	(0)	5	(100)
SXT	5	(45.5)	6	(54.5)	1	(10)	9	(90)	2	(3.8)	51	(96.2)	26	(92.9)	2	(7.1)	0	(0)	5	(100)
SAM	0	(0)	11	(100)	2	(20)	8	(80)	2	(3.8)	51	(96.2)	15	(53.6)	13	(46.4)	1	(20)	4	(80)
PB	11	(100)	0	(0)	10	(100)	0	(0)	53	(100)	0	(0)	28	(100)	0	(0)	5	(100)	0	(0)
TE	8	(72.7)	3	(27.3)	2	(20)	8	(80)	18	(34)	35	(66)	21	(75)	7	(25)	2	(40)	3	(60)
MIN	11	(100)	0	(0)	10	(100)	0	(0)	53	(100)	0	(0)	28	(100)	0	(0)	5	(100)	0	(0)
TG	0	(0)	11	(100)	7	(70)	3	(30)	5	(9.4)	48	(90.6)	25	(89.3)	3	(10.7)	3	(60)	2	(40)

CC, clonal complex; ST, sequence type. 1 *GN, gentamycin; TOB, tobramycin; AK, amikacin; IMP, imipenem; MEM, meropenem; CIP, ciprofloxacin; LEV, levofloxacin; PTZ, piperacillin-tazobactam; TIM, ticarcillin-clavulanic acid; CTX, cefotaxime; CAZ; ceftazidime; FEP, cefepime; SXT, sulfamethoxazole-trimethoprim; SAM, ampicillin-sulbactam; PB, polymyxin B; TE, tetracycline; MIN, minocycline; TG, tigecycline.*

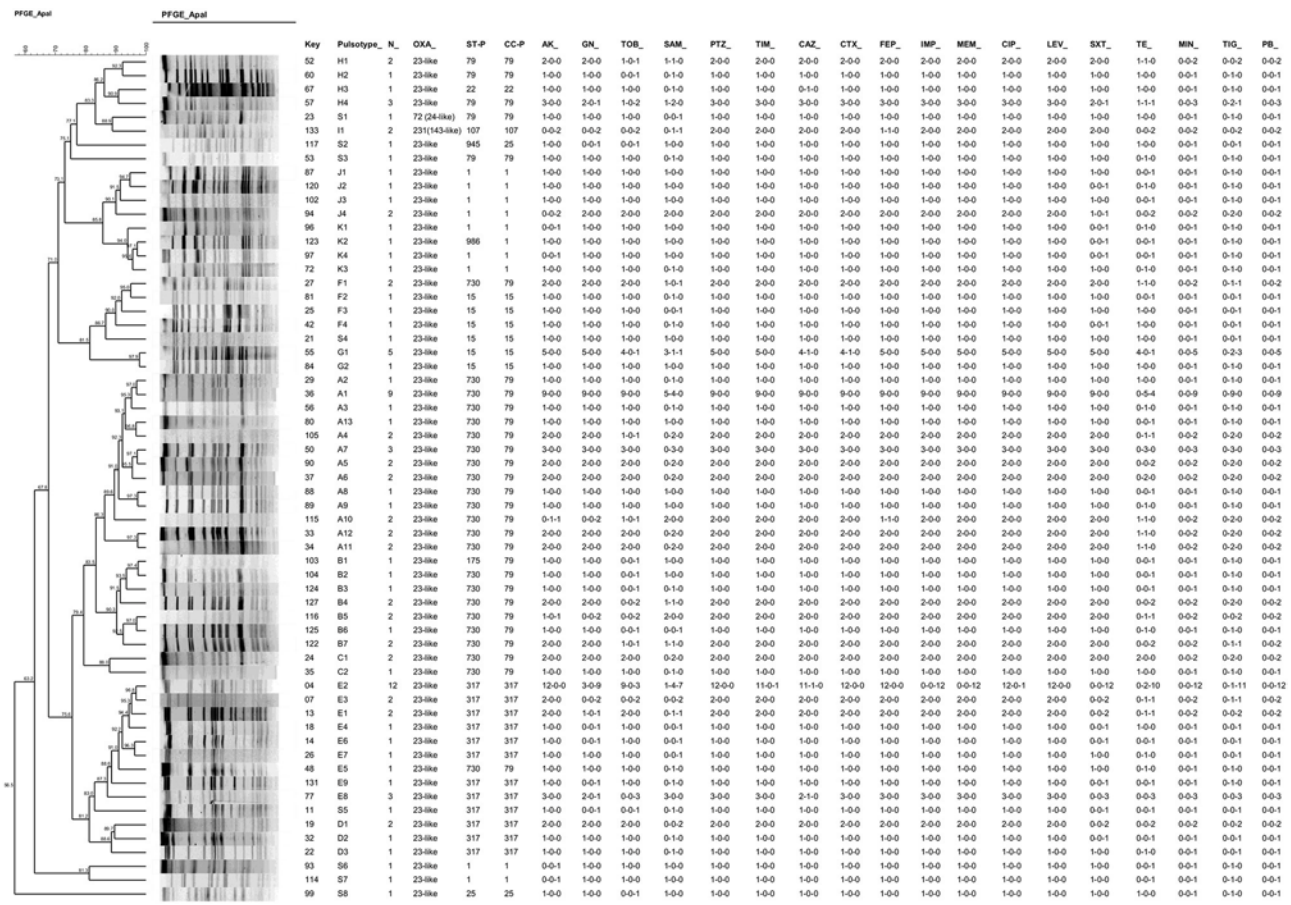

Key	Pulsotype_	N_	OXA_	ST-P	CC-P	AK_	GN_	TOB_	SAM_	PTZ_	TIM_	CAZ_	CTX_	FEP_	IMP_	MEM_	CIP_	LEV_	SXT_	TE_	MIN_	TIG_	PB_
52	H1	2	23-like	79	79	2-0-0	2-0-0	1-0-1	1-1-0	2-0-0	2-0-0	2-0-0	2-0-0	2-0-0	2-0-0	2-0-0	2-0-0	2-0-0	2-0-0	1-1-0	0-0-2	0-0-2	0-0-2
60	H2	1	23-like	79	79	1-0-0	1-0-0	0-0-1	0-1-0	1-0-0	1-0-0	1-0-0	1-0-0	1-0-0	1-0-0	1-0-0	1-0-0	1-0-0	1-0-0	1-0-0	0-0-1	0-1-0	0-0-1
67	H3	1	23-like	22	22	1-0-0	1-0-0	1-0-0	0-1-0	1-0-0	1-0-0	0-1-0	1-0-0	1-0-0	1-0-0	1-0-0	1-0-0	1-0-0	1-0-0	1-0-0	0-0-1	0-1-0	0-0-1
57	H4	3	23-like	79	79	3-0-0	2-0-1	1-0-2	1-2-0	3-0-0	3-0-0	3-0-0	3-0-0	3-0-0	3-0-0	3-0-0	3-0-0	3-0-0	2-0-1	1-1-1	0-0-3	0-2-1	0-0-3
23	S1	1	72 (24-like)	79	79	1-0-0	1-0-0	1-0-0	0-0-1	1-0-0	1-0-0	1-0-0	1-0-0	1-0-0	1-0-0	1-0-0	1-0-0	1-0-0	1-0-0	1-0-0	0-0-1	0-1-0	0-0-1
133	I1	2	231(143-like)	107	107	0-0-2	0-0-2	0-0-2	0-1-1	2-0-0	2-0-0	2-0-0	2-0-0	1-1-0	2-0-0	2-0-0	2-0-0	2-0-0	2-0-0	0-0-2	0-0-2	0-0-2	0-0-2
117	S2	1	23-like	945	25	1-0-0	0-0-1	0-0-1	1-0-0	1-0-0	1-0-0	1-0-0	1-0-0	1-0-0	1-0-0	1-0-0	1-0-0	1-0-0	1-0-0	1-0-0	0-0-1	0-0-1	0-0-1
53	S3	1	23-like	79	79	1-0-0	1-0-0	1-0-0	0-1-0	1-0-0	1-0-0	1-0-0	1-0-0	1-0-0	1-0-0	1-0-0	1-0-0	1-0-0	1-0-0	0-1-0	0-0-1	0-1-0	0-0-1
87	J1	1	23-like	1	1	1-0-0	1-0-0	1-0-0	1-0-0	1-0-0	1-0-0	1-0-0	1-0-0	1-0-0	1-0-0	1-0-0	1-0-0	1-0-0	1-0-0	0-0-1	0-0-1	0-1-0	0-0-1
120	J2	1	23-like	1	1	1-0-0	1-0-0	1-0-0	1-0-0	1-0-0	1-0-0	1-0-0	1-0-0	1-0-0	1-0-0	1-0-0	1-0-0	1-0-0	0-0-1	0-1-0	0-0-1	0-1-0	0-0-1
102	J3	1	23-like	1	1	1-0-0	1-0-0	1-0-0	1-0-0	1-0-0	1-0-0	1-0-0	1-0-0	1-0-0	1-0-0	1-0-0	1-0-0	1-0-0	1-0-0	0-0-1	0-0-1	0-1-0	0-0-1
94	J4	2	23-like	1	1	0-0-2	2-0-0	2-0-0	2-0-0	2-0-0	2-0-0	2-0-0	2-0-0	2-0-0	2-0-0	2-0-0	2-0-0	2-0-0	1-0-1	0-0-2	0-0-2	0-2-0	0-0-2
96	K1	1	23-like	1	1	0-0-1	1-0-0	1-0-0	1-0-0	1-0-0	1-0-0	1-0-0	1-0-0	1-0-0	1-0-0	1-0-0	1-0-0	1-0-0	0-0-1	0-1-0	0-0-1	0-1-0	0-0-1
123	K2	1	23-like	986	1	1-0-0	1-0-0	1-0-0	1-0-0	1-0-0	1-0-0	1-0-0	1-0-0	1-0-0	1-0-0	1-0-0	1-0-0	1-0-0	0-0-1	0-0-1	0-0-1	0-1-0	0-0-1
97	K4	1	23-like	1	1	0-0-1	1-0-0	1-0-0	1-0-0	1-0-0	1-0-0	1-0-0	1-0-0	1-0-0	1-0-0	1-0-0	1-0-0	1-0-0	0-0-1	0-0-1	0-0-1	0-1-0	0-0-1
72	K3	1	23-like	1	1	1-0-0	1-0-0	1-0-0	0-1-0	1-0-0	1-0-0	1-0-0	1-0-0	1-0-0	1-0-0	1-0-0	1-0-0	1-0-0	1-0-0	0-1-0	0-0-1	0-1-0	0-0-1
27	F1	2	23-like	730	79	2-0-0	2-0-0	2-0-0	1-0-1	2-0-0	2-0-0	2-0-0	2-0-0	2-0-0	2-0-0	2-0-0	2-0-0	2-0-0	2-0-0	1-1-0	0-0-2	0-1-1	0-0-2
81	F2	1	23-like	15	15	1-0-0	1-0-0	1-0-0	0-1-0	1-0-0	1-0-0	1-0-0	1-0-0	1-0-0	1-0-0	1-0-0	1-0-0	1-0-0	1-0-0	0-0-1	0-0-1	0-0-1	0-0-1
25	F3	1	23-like	15	15	1-0-0	1-0-0	1-0-0	0-0-1	1-0-0	1-0-0	1-0-0	1-0-0	1-0-0	1-0-0	1-0-0	1-0-0	1-0-0	1-0-0	1-0-0	0-0-1	0-0-1	0-0-1
42	F4	1	23-like	15	15	1-0-0	1-0-0	1-0-0	0-1-0	1-0-0	1-0-0	1-0-0	1-0-0	1-0-0	1-0-0	1-0-0	1-0-0	1-0-0	0-0-1	1-0-0	0-0-1	0-0-1	0-0-1
21	S4	1	23-like	15	15	1-0-0	1-0-0	1-0-0	1-0-0	1-0-0	1-0-0	1-0-0	1-0-0	1-0-0	1-0-0	1-0-0	1-0-0	1-0-0	1-0-0	1-0-0	0-0-1	0-0-1	0-0-1
55	G1	5	23-like	15	15	5-0-0	5-0-0	4-0-1	3-1-1	5-0-0	5-0-0	4-1-0	4-1-0	5-0-0	5-0-0	5-0-0	5-0-0	5-0-0	5-0-0	4-0-1	0-0-5	0-2-3	0-0-5
84	G2	1	23-like	15	15	1-0-0	1-0-0	1-0-0	1-0-0	1-0-0	1-0-0	1-0-0	1-0-0	1-0-0	1-0-0	1-0-0	1-0-0	1-0-0	1-0-0	1-0-0	0-0-1	0-1-0	0-0-1
29	A2	1	23-like	730	79	1-0-0	1-0-0	1-0-0	0-1-0	1-0-0	1-0-0	1-0-0	1-0-0	1-0-0	1-0-0	1-0-0	1-0-0	1-0-0	1-0-0	1-0-0	0-0-1	0-1-0	0-0-1
36	A1	9	23-like	730	79	9-0-0	9-0-0	9-0-0	5-4-0	9-0-0	9-0-0	9-0-0	9-0-0	9-0-0	9-0-0	9-0-0	9-0-0	9-0-0	9-0-0	0-5-4	0-0-9	0-9-0	0-0-9
56	A3	1	23-like	730	79	1-0-0	1-0-0	1-0-0	0-1-0	1-0-0	1-0-0	1-0-0	1-0-0	1-0-0	1-0-0	1-0-0	1-0-0	1-0-0	1-0-0	0-1-0	0-0-1	0-1-0	0-0-1
80	A13	1	23-like	730	79	1-0-0	1-0-0	1-0-0	1-0-0	1-0-0	1-0-0	1-0-0	1-0-0	1-0-0	1-0-0	1-0-0	1-0-0	1-0-0	1-0-0	0-0-1	0-0-1	0-1-0	0-0-1
105	A4	2	23-like	730	79	2-0-0	2-0-0	1-0-1	0-2-0	2-0-0	2-0-0	2-0-0	2-0-0	2-0-0	2-0-0	2-0-0	2-0-0	2-0-0	2-0-0	0-1-1	0-0-2	0-2-0	0-0-2
50	A7	3	23-like	730	79	3-0-0	3-0-0	3-0-0	0-3-0	3-0-0	3-0-0	3-0-0	3-0-0	3-0-0	3-0-0	3-0-0	3-0-0	3-0-0	3-0-0	0-3-0	0-0-3	0-3-0	0-0-3
90	A5	2	23-like	730	79	2-0-0	2-0-0	2-0-0	0-2-0	2-0-0	2-0-0	2-0-0	2-0-0	2-0-0	2-0-0	2-0-0	2-0-0	2-0-0	2-0-0	0-0-2	0-0-2	0-2-0	0-0-2
37	A6	2	23-like	730	79	2-0-0	2-0-0	2-0-0	0-2-0	2-0-0	2-0-0	2-0-0	2-0-0	2-0-0	2-0-0	2-0-0	2-0-0	2-0-0	2-0-0	0-2-0	0-0-2	0-2-0	0-0-2
88	A8	1	23-like	730	79	1-0-0	1-0-0	1-0-0	1-0-0	1-0-0	1-0-0	1-0-0	1-0-0	1-0-0	1-0-0	1-0-0	1-0-0	1-0-0	1-0-0	0-0-1	0-0-1	0-1-0	0-0-1
89	A9	1	23-like	730	79	1-0-0	1-0-0	1-0-0	1-0-0	1-0-0	1-0-0	1-0-0	1-0-0	1-0-0	1-0-0	1-0-0	1-0-0	1-0-0	1-0-0	0-1-0	0-0-1	0-1-0	0-0-1
115	A10	2	23-like	730	79	0-1-1	0-0-2	1-0-1	2-0-0	2-0-0	2-0-0	2-0-0	2-0-0	1-1-0	2-0-0	2-0-0	2-0-0	2-0-0	2-0-0	1-1-0	0-0-2	0-2-0	0-0-2
33	A12	2	23-like	730	79	2-0-0	2-0-0	2-0-0	0-2-0	2-0-0	2-0-0	2-0-0	2-0-0	2-0-0	2-0-0	2-0-0	2-0-0	2-0-0	2-0-0	1-1-0	0-0-2	0-2-0	0-0-2
34	A11	2	23-like	730	79	2-0-0	2-0-0	2-0-0	0-2-0	2-0-0	2-0-0	2-0-0	2-0-0	2-0-0	2-0-0	2-0-0	2-0-0	2-0-0	2-0-0	1-1-0	0-0-2	0-2-0	0-0-2
103	B1	1	23-like	175	79	1-0-0	1-0-0	0-0-1	1-0-0	1-0-0	1-0-0	1-0-0	1-0-0	1-0-0	1-0-0	1-0-0	1-0-0	1-0-0	1-0-0	0-0-1	0-0-1	0-1-0	0-0-1
104	B2	1	23-like	730	79	1-0-0	1-0-0	0-0-1	1-0-0	1-0-0	1-0-0	1-0-0	1-0-0	1-0-0	1-0-0	1-0-0	1-0-0	1-0-0	1-0-0	0-0-1	0-0-1	0-1-0	0-0-1
124	B3	1	23-like	730	79	1-0-0	1-0-0	0-0-1	0-1-0	1-0-0	1-0-0	1-0-0	1-0-0	1-0-0	1-0-0	1-0-0	1-0-0	1-0-0	1-0-0	0-0-1	0-0-1	0-1-0	0-0-1
127	B4	2	23-like	730	79	2-0-0	2-0-0	0-0-2	1-1-0	2-0-0	2-0-0	2-0-0	2-0-0	2-0-0	2-0-0	2-0-0	2-0-0	2-0-0	2-0-0	0-0-2	0-0-2	0-2-0	0-0-2
116	B5	2	23-like	730	79	1-0-1	0-0-2	0-0-2	2-0-0	2-0-0	2-0-0	2-0-0	2-0-0	2-0-0	2-0-0	2-0-0	2-0-0	2-0-0	2-0-0	0-1-1	0-0-2	0-0-2	0-0-2
125	B6	1	23-like	730	79	1-0-0	1-0-0	0-0-1	0-0-1	1-0-0	1-0-0	1-0-0	1-0-0	1-0-0	1-0-0	1-0-0	1-0-0	1-0-0	1-0-0	0-1-0	0-0-1	0-1-0	0-0-1
122	B7	2	23-like	730	79	2-0-0	2-0-0	1-0-1	1-1-0	2-0-0	2-0-0	2-0-0	2-0-0	2-0-0	2-0-0	2-0-0	2-0-0	2-0-0	2-0-0	0-0-2	0-0-2	0-1-1	0-0-2
24	C1	2	23-like	730	79	2-0-0	2-0-0	2-0-0	0-2-0	2-0-0	2-0-0	2-0-0	2-0-0	2-0-0	2-0-0	2-0-0	2-0-0	2-0-0	2-0-0	2-0-0	0-0-2	0-2-0	0-0-2
35	C2	1	23-like	730	79	1-0-0	1-0-0	1-0-0	0-1-0	1-0-0	1-0-0	1-0-0	1-0-0	1-0-0	1-0-0	1-0-0	1-0-0	1-0-0	1-0-0	1-0-0	0-0-1	0-1-0	0-0-1
04	E2	12	23-like	317	317	12-0-0	3-0-9	9-0-3	1-4-7	12-0-0	11-0-1	11-1-0	12-0-0	12-0-0	0-0-12	0-0-12	12-0-1	12-0-0	0-0-12	0-2-10	0-0-12	0-1-11	0-0-12
07	E3	2	23-like	317	317	2-0-0	0-0-2	0-0-2	0-0-2	2-0-0	2-0-0	2-0-0	2-0-0	2-0-0	2-0-0	2-0-0	2-0-0	2-0-0	0-0-2	0-1-1	0-0-2	0-1-1	0-0-2
13	E1	2	23-like	317	317	2-0-0	1-0-1	2-0-0	0-1-1	2-0-0	2-0-0	2-0-0	2-0-0	2-0-0	2-0-0	2-0-0	2-0-0	2-0-0	0-0-2	0-1-1	0-0-2	0-0-2	0-0-2
18	E4	1	23-like	317	317	1-0-0	0-0-1	1-0-0	0-0-1	1-0-0	1-0-0	1-0-0	1-0-0	1-0-0	1-0-0	1-0-0	1-0-0	1-0-0	0-0-1	1-0-0	0-0-1	0-0-1	0-0-1
14	E6	1	23-like	317	317	1-0-0	0-0-1	1-0-0	0-0-1	1-0-0	1-0-0	1-0-0	1-0-0	1-0-0	1-0-0	1-0-0	1-0-0	1-0-0	0-0-1	0-0-1	0-0-1	0-0-1	0-0-1
26	E7	1	23-like	317	317	1-0-0	1-0-0	1-0-0	0-0-1	1-0-0	1-0-0	1-0-0	1-0-0	1-0-0	1-0-0	1-0-0	1-0-0	1-0-0	1-0-0	0-1-0	0-0-1	0-0-1	0-0-1
48	E5	1	23-like	730	79	1-0-0	1-0-0	1-0-0	0-1-0	1-0-0	1-0-0	1-0-0	1-0-0	1-0-0	1-0-0	1-0-0	1-0-0	1-0-0	1-0-0	0-1-0	0-0-1	0-1-0	0-0-1
131	E9	1	23-like	317	317	1-0-0	0-0-1	1-0-0	0-1-0	1-0-0	1-0-0	1-0-0	1-0-0	1-0-0	1-0-0	1-0-0	1-0-0	1-0-0	0-0-1	0-0-1	0-0-1	0-1-0	0-0-1
77	E8	3	23-like	317	317	3-0-0	2-0-1	0-0-3	3-0-0	3-0-0	3-0-0	2-1-0	3-0-0	3-0-0	3-0-0	3-0-0	3-0-0	3-0-0	0-0-3	0-0-3	0-0-3	0-0-3	0-0-3
11	S5	1	23-like	317	317	1-0-0	0-0-1	0-0-1	0-1-0	1-0-0	1-0-0	1-0-0	1-0-0	1-0-0	1-0-0	1-0-0	1-0-0	1-0-0	0-0-1	0-0-1	0-0-1	0-0-1	0-0-1
19	D1	2	23-like	317	317	2-0-0	2-0-0	2-0-0	0-0-2	2-0-0	2-0-0	2-0-0	2-0-0	2-0-0	2-0-0	2-0-0	2-0-0	2-0-0	0-0-2	0-0-2	0-0-2	0-0-2	0-0-2
32	D2	1	23-like	317	317	1-0-0	1-0-0	1-0-0	0-1-0	1-0-0	1-0-0	1-0-0	1-0-0	1-0-0	1-0-0	1-0-0	1-0-0	1-0-0	0-0-1	0-0-1	0-0-1	0-0-1	0-0-1
22	D3	1	23-like	317	317	1-0-0	1-0-0	1-0-0	0-1-0	1-0-0	1-0-0	1-0-0	1-0-0	1-0-0	1-0-0	1-0-0	1-0-0	1-0-0	1-0-0	0-1-0	0-0-1	0-0-1	0-0-1
93	S6	1	23-like	1	1	0-0-1	1-0-0	1-0-0	1-0-0	1-0-0	1-0-0	1-0-0	1-0-0	1-0-0	1-0-0	1-0-0	1-0-0	1-0-0	1-0-0	0-0-1	0-0-1	0-1-0	0-0-1
114	S7	1	23-like	1	1	0-0-1	1-0-0	1-0-0	1-0-0	1-0-0	1-0-0	1-0-0	1-0-0	1-0-0	1-0-0	1-0-0	1-0-0	1-0-0	1-0-0	0-0-1	0-0-1	0-1-0	0-0-1
99	S8	1	23-like	25	25	1-0-0	1-0-0	0-0-1	1-0-0	1-0-0	1-0-0	1-0-0	1-0-0	1-0-0	1-0-0	1-0-0	1-0-0	1-0-0	1-0-0	1-0-0	0-0-1	0-1-0	0-0-1

FIGURE 1 | Dendrogram resulted from PFGE analysis of one representative isolate of each pulsotype ($n = 61$) combined with antimicrobial susceptibility results of each pulsotype. Information on additional OXA-enzymes, PFGE cluster, STs and CCs defined by MLST are shown. The susceptibility results are indicated in occurrences for each pulsotype in the following order: resistant-intermediate-susceptible number of strains (i.e., 1-1-0 for a given antimicrobial means 1 resistant strain; 1 intermediate and zero susceptible). AK, amikacin; GN, gentamycin; TOB, tobramycin; SAM, ampicillin-sulbactam; PTZ, piperacillin-tazobactam; TIM, ticarcillin-clavulanic acid; CAZ; ceftazidime; CTX, cefotaxime; FEP, cefepime; IMP, imipenem; MEM, meropenem; CIP, ciprofloxacin; LEV, levofloxacin; SXT, sulfamethoxazole-trimethoprim; TE, tetracycline; MIN, minocycline; TG, tigecycline; PB, polymyxin B. Key: univocal identification number; ST, sequence type; CC, Clonal Complex.

RESULTS

A. baumannii Isolates and Detection of Oxacillinase Genes

The 107 isolates were recovered from non-repetitive patients with bacteremia attending a teaching hospital in the State of São Paulo, Brazil, between 2008 and 2014. These isolates were recovered from blood (96.3%) or vascular catheter (3.7%).

All isolates were confirmed as *A. baumannii* species by PCR detection of $bla_{\mathrm{OXA-51-like}}$ and/or sequencing of the *rpo*B and ITS genes, as well as by the MLST analysis. Out of these isolates, 104 (97.2%) carried the $bla_{\mathrm{OXA-23-like}}$ with IS*Aba1* upstream; remaining strains carried $bla_{\mathrm{OXA-231}}$ ($bla_{\mathrm{OXA-143-like}}$; $n = 2$; 1.9%) or $bla_{\mathrm{OXA-72}}$ ($bla_{\mathrm{OXA-24-like}}$; $n = 1$; 0.9%). The $bla_{\mathrm{OXA-58-like}}$ gene was not detected, as well as the additional carbapenemases investigated.

Antimicrobial Susceptibility Testing

According to the susceptibility test, 39.3% of isolates were considered MDR, and 60.7% XDR. The entire population evaluated confirmed resistance to imipenem, meropenem, ciprofloxacin, piperacillin-tazobactam and levofloxacin, while susceptibility to minocycline was observed in all the isolates. Resistance rates to other antimicrobials tested by disc-diffusion method were: amikacin (89.7%), cefepime (98.1%), ceftazidime (96.2%), cefotaxime (99.0%), gentamicin (76.6%), trimethoprim-sulfamethoxazole (68.2%), ticarcillin-clavulanate (99.0%), and tobramycin (68.2%). The MIC_{50}/MIC_{90} (μg/ml) values were calculated for each antimicrobial agent, as follows: imipenem (>32/>32), meropenem (>32/>32), tetracycline (8/16), ampicillin-sulbactam (16:8/32:16), minocycline (0.25/0.5) and tigecycline (2/3). Although resistance to tigecycline was not detected, 38.3% of isolates presented intermediate susceptibility to this drug (according to FDA breakpoints).

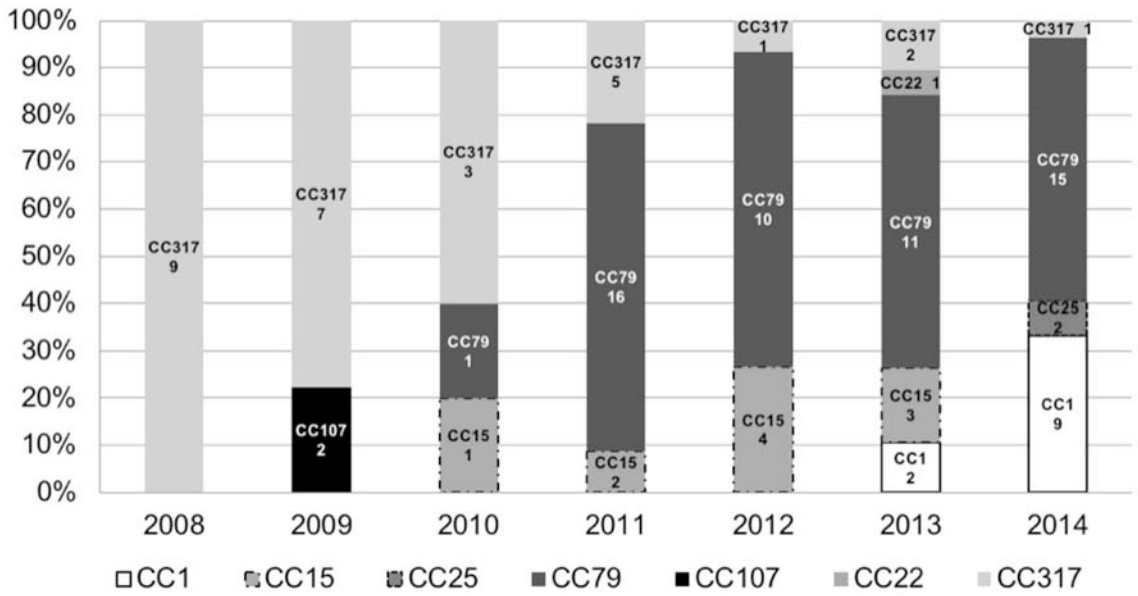

FIGURE 2 | Distribution of Sequence Types (ST) or Clonal Complexes (CC) defined by MLST (Institute Pasteur protocol) over the years. Numbers below the CC or ST indicate number of occurrences ($n = 107$).

Distribution of susceptibility rates among the clones (**Table 1**) evidenced high-rates of non-susceptibility to cephalosporins, carbapenems, quinolones and ticarcillin-clavulanic acid. For the aminoglycosides, the highest susceptibility rate to amikacin was detected for isolates belonging to CC1 (54.5%), while gentamycin and tobramycin were more active against isolates belonging to CC317 (60.7% and 53.6% of susceptibility, respectively). Furthermore, isolates belonging to CC317 presented the highest susceptibility rates to sulfamethoxazole-trimethoprim (92.9%), tigecycline (75%), and ampicillin-sulbactam (53.6%).

Molecular Typing

The 107 CRAB isolates were distributed into 53 PFGE pulsotypes belonging to eleven clusters (A, B, C, D, E, F, G, H, I, J, K) and eight additional pulsotypes with a single isolate (**Figure 1**). By extrapolating the results of MLST to isolates presenting the same pulsotypes, we observed the frequencies of 49.5% of strains belonging to clonal complexes (and sequence types) CC79 (ST79, 8.4%; ST175, 0.9% and ST730, 40.2%); 26.2% for CC317 (ST317, 100%), 10.3% for CC1 (ST1, 9.3%; ST986, 0.9%); 9.3% for CC15 (ST15, 9.3%), 1.9% for CC25 (ST25, 0.9%; ST945, 0.9%), 1.9% for CC107 (ST107, 100%), and 0.9% for CC22 (ST22 0.9%). With the exception of the PFGE cluster I, which presented the $bla_{\text{OXA}-231}$ allele, the $bla_{\text{OXA}-23-\text{like}}$ gene associated with upstream IS*Aba1* was present in all clusters (**Figure 1**).

Distribution of clones over the time evidenced the emergence of *A. baumannii* pulsotypes belonging to clonal complex 79 in 2010, which became endemic in the institution until 2014 (**Figure 2**). The CC79 strains ($n = 53$) were distributed into 29 pulsotypes (**Figure 1**), recovered from 2010 to 2014. Although the pulsotype A1 was the most numerous (9 isolates), it was distributed in 2011 (4 isolates), 2013 (4 isolates) and 2014 (1 isolate). The remaining 28 pulsotypes were represented by 1, 2, or 3 isolates, each, and were recovered from the period comprised between 2010 over 2014. The 2014 isolates (the year with the largest number of isolates (13) belonging to CC79) were represented by 9 different pulsotypes with only 1 or 2 isolates in each electrophoretic pattern.

On the other hand, reduction in the frequency of CC317 was remarkable (**Figure 2**). The CC317 isolates ($n = 28$) were typed into 12 pulsotypes. A major clone (pulsotype E2) was identified comprising 12 isolates recovered from 2008 (6), 2009 (2), 2010 (2), 2011 (1), 2012 (1). Conversely, the remaining 11 pulsotypes were represented by 1, 2, or 3 isolates, each, recovered over the period of 2008–2013.

CC1 strains were detected in 2013 at frequency lower than 10% (2 isolates) but in 2014 this clonal complex represented more than 30% of the CRAB isolated from BSI (9 isolates belonging to 8 different pulsotypes), same year that CC25 strains were firstly detected.

DISCUSSION

In this study, we verified the high prevalence of $bla_{\text{OXA}-23-\text{like}}$ in MDR and XDR strains isolated from patients with bacteraemia caused by carbapenem-resistant *Acinetobacter baumannii* in a teaching hospital in Brazil. In addition, changes in the clonal structure of circulating strains was verified, with predominance of Clonal Complexes CC1, CC15, CC79, and CC317.

The oxacillinase genes are differently distributed around the globe, with the $bla_{\text{OXA}-23}$-like gene being predominant and widespread in several countries (Evans and Amyes, 2014). In this study, the $bla_{\text{OXA}-23-\text{like}}$ gene was identified in most of the isolates belonging to different PFGE restriction patterns and MLST clonal complexes, reinforcing the already known data from this country (Medeiros and Lincopan, 2013). In addition,

we also detected the bla_{OXA-72} and $bla_{OXA-231}$ genes, but in lower frequencies ($n = 2$, 1.9%; and $n = 1$; 0.9%, respectively), consistent with previous reports that detected both genes in this country over the last years (Gionco et al., 2012; Vasconcelos et al., 2015; Camargo et al., 2016; Pagano et al., 2017). Absence of another carbapenemases reinforces the role of oxacillinases among the isolates from Brazil, a country in which CRAB is considered highly prevalent (Rossi, 2011), but we cannot exclude the occurrence of other emergent carbapenemases (such as OXA-235-like or TMB-like), not sought in this study.

Minocycline was active against all the isolates, even if they presented MDR or XDR phenotypes. Although the study performed by Wang and colleagues had demonstrated a higher susceptibility rate to minocycline by microdilution method in CRAB compared to epsilometric method, MIC values identified in the isolates of this study were far below the intermediate value for this drug, confirming their susceptibilities (Wang et al., 2016). This antimicrobial is commonly effective against carbapenem-resistant *Acinetobacter baumannii* (Lashinsky et al., 2017; Poirel et al., 2017), although resistance is already being observed (Cheah et al., 2016; Pournaras et al., 2017; Vasconcellos et al., 2017a). On the other hand, resistance rates to other antimicrobial classes were remarkable. Aminoglycosides, for instance, presented susceptibilities rates ranging from 31.8% to tobramycin to only 9.3% to amikacin. Despite the controversies, tigecycline can be considered one of the few therapeutic options for treatment of MDR infection in skin and soft tissue infections and meningitis (Montravers et al., 2013; Kooli et al., 2016; Lauretti et al., 2017). Still tigecycline is not recommended for the treatment of ventilator-associated pneumonia and BSI (http://www.fda.gov/drugs/drugsafety/ucm224370.htm), we evaluate the tigecycline activity in our BSI isolates with surveillance purposes and no resistance was observed, even this phenotype becomes progressively more common in *A. baumannii* in several countries (Navon-Venezia et al., 2007; Al-Sweih et al., 2011; Montravers et al., 2013; Sun et al., 2013; Provasi Cardoso et al., 2016; Vasconcellos et al., 2017a; Royer et al., 2018).

Among the CRAB isolates from a single hospital, we identified the predominance of CC79 (49.5%), CC1 (10.3%), and CC15 (9.3%), corresponding to 69.2% of all the isolates evaluated over the entire period. This finding is well documented in Brazil as well as the occurrence of isolates belonging to the CC25, which seems to configure an emerging clone in our country (Chagas et al., 2014; Campos et al., 2015; Camargo et al., 2016; Provasi Cardoso et al., 2016; Vasconcellos et al., 2017a,b; Royer et al., 2018), although ST25 has already been detected worldwide (Sahl et al., 2015). ST107 was also identified, corresponding to the two isolates carrying OXA-231, which reinforces the association between ST107 and OXA-231 in Brazil (Camargo et al., 2016; Rodrigues-Costa et al., 2018). Remarkably, we detected a ST barely reported in studies around the world, the ST317, belonging to the still small CC317. CC317 was identified in 26.2% of all isolates (belonging to 11 different pulsotypes) in this study, representing the most frequent ST in BSI over the years 2008 to 2010. According to MLST database, the first ST317 isolate was detected in 2009 from an unknown sample in Rio de Janeiro, Brazil (https://pubmlst.org/abaumannii/). The only other strain deposited at the MLST database was detected in the State of São Paulo, isolated from upper respiratory tract secretion in 2011 (Camargo et al., 2016), likely indicating a limited spread of this clone, only in Brazil. Although very prevalent among the isolates studied herein, CC317 seemed to be replaced by other clones (ST79 and ST730), which belong to CC79. Conversely, analysis of our data indicate that CC317 presented less pronounced antimicrobial resistance to sulfamethoxazole-trimethoprim, tigecycline, and ampicillin-sulbactam, indicating that, at least in parts, antimicrobial resistance can drive changes in prevalence of clones in specific settings under selective pressure.

In the latest years of the study, however, the emergence of strains belonging to CC1 likely indicate that another epidemiologic shift has occurred. Changes in clonal structure of *Acinetobacter* strains were reported in other hospitals (Park et al., 2012; Villalón et al., 2015), but the reasons to explain this shift remain to be totally understood. In our study, a remarkable diversity of pulsotypes identified into each of these clonal complexes suggests that selective pressure, instead of a strict clone spread, plays a more decisive role in the emergence of CRAB.

CONCLUSION

In summary, we observed a change in the prevalence of CRAB clones in a single hospital, despite the persistence of OXA-23-producing isolates with MDR or XDR phenotypes, possibly driven by antimicrobial resistance and selective pressure. Longitudinal studies, as the present, provide this type of temporal observation, making possible to track the dispersion dynamics of successful clones associated with the persistence of well-stablished resistance phenotypes in *Acinetobacter baumannii* and to propose measures to contain its dissemination.

ETHICS STATEMENT

This study was submitted and approved by the Adolfo Lutz Institute Ethics Committee under the register number CAAE 49985115.5.0000.0059.

AUTHOR CONTRIBUTIONS

LT and CC conceived and designed the study, analyzed the data, and wrote the paper. LT, FV, and WS performed the experiments. MT-C, CC, TR, ALM, AF, ACM, and TS contributed reagents, materials, analysis tools.

FUNDING

This study was supported by grants n°. 2015/13179-4 and 2018/23620-8 São Paulo Research Foundation (FAPESP), São Paulo, Brazil.

REFERENCES

Al-Sweih, N. A., Al-Hubail, M. A., and Rotimi, V. O. (2011). Emergence of tigecycline and colistin resistance in *Acinetobacter* species isolated from patients in Kuwait hospitals. *J. Chemother.* 23, 13–16. doi: 10.1179/joc.2011.23.1.13

Camargo, C. H., Tiba, M. R., Saes, M. R., Vasconcellos, F. M., Santos, L. F., Romero, E. C., et al. (2016). Population structure analysis of carbapenem-resistant *Acinetobacter baumannii* clinical isolates from Brazil reveals predominance of clonal complexes 1, 15, and 79. *Antimicrob. Agents Chemother.* 60, 2545–2547. doi: 10.1128/AAC.02186-15

Campos, J., Pereira, M., Yub, E. A., and Sampaio, J. (2015). "First report of NDM-1 producing *Acinetobacter radioresistens* and *Acinetobacter ursingii* from Brazil," in *25th European Congress of Clinical Microbiology and Infectious Disease (ECCMID)* (Copenhagen).

Cayô, R., Merino, M., Ruiz Del Castillo, B., Cano, M. E., Calvo, J., and Bou, G. (2014). OXA-207, a novel OXA-24 variant with reduced catalytic efficiency against carbapenems in *Acinetobacter pittii* from Spain. *Antimicrob. Agents Chemother.* 58, 4944–4948. doi: 10.1128/AAC.02633-13

Chagas, T. P., Carvalho, K. R., de Oliveira Santos, I. C., Carvalho-Assef, A. P., and Asensi, M. D. (2014). Characterization of carbapenem-resistant *Acinetobacter baumannii* in Brazil (2008).-2011): countrywide spread of OXA-23-producing clones (CC15 and CC79). *Diagn. Microbiol. Infect. Dis.* 79, 68–72. doi: 10.1016/j.diagmicrobio.2014.03.006

Chang, H. C., Wei, Y. F., Dijkshoorn, L., Vaneechoutte, M., Tang, C. T., and Chang, T. C. (2005). Species-level identification of isolates of the *Acinetobacter calcoaceticus-Acinetobacter baumannii* complex by sequence analysis of the 16S-23S rRNA gene spacer region. *J. Clin. Microbiol.* 43, 1632–1639. doi: 10.1128/JCM.43.4.1632-1639.2005

Cheah, S. E., Li, J., Tsuji, B. T., Forrest, A., Bulitta, J. B., and Nation, R. L. (2016). Colistin and polymyxin B dosage regimens against *Acinetobacter baumannii*: differences in activity and the emergence of resistance. *Antimicrob. Agents Chemother.* 60, 3921–3933. doi: 10.1128/AAC.02927-15

Clímaco, E. C., Oliveira, M. L., Pitondo-Silva, A., Oliveira, M. G., Medeiros, M., Lincopan, N., et al. (2013). Clonal complexes 104, 109 and 113 playing a major role in the dissemination of OXA-carbapenemase-producing *Acinetobacter baumannii* in Southeast Brazil. *Infect. Genet. Evol.* 19, 127–133. doi: 10.1016/j.meegid.2013.06.024

Clinical and Laboratory Standards Institute (2015). *Performance Standards for Antimicrobial Susceptibility Testing.* Vol. M100-S25. Wayne: Clinical and Laboratory Standards Institute.

Escandón-Vargas, K., Reyes, S., Gutiérrez, S., and Villegas, M. V. (2017). The epidemiology of carbapenemases in Latin America and the Caribbean. *Expert Rev. Anti Infect. Ther.* 15, 277–297. doi: 10.1080/14787210.2017.1268918

Evans, B. A., and Amyes, S. G. (2014). OXA β-lactamases. *Clin. Microbiol. Rev.* 27, 241–263. doi: 10.1128/CMR.00117-13

Fortaleza, C. M. C. B., Padoveze, M. C., Kiffer, C. R. V., Barth, A. L., Carneiro, I. C. D. R. S., Giamberardino, H. I. G., et al. (2017). Multi-state survey of healthcare-associated infections in acute care hospitals in Brazil. *J. Hosp. Infect.* 96, 139–144. doi: 10.1016/j.jhin.2017.03.024

Gionco, B., Pelayo, J. S., Venancio, E. J., Cay,ô, R., Gales, A. C., and Carrara-Marroni, F. E. (2012). Detection of OXA-231, a new variant of $bla_{\mathrm{OXA-143}}$, in *Acinetobacter baumannii* from Brazil: a case report. *J. Antimicrob. Chemother.* 67, 2531–2532. doi: 10.1093/jac/dks223

Héritier, C., Poirel, L., Fournier, P. E., Claverie, J. M., Raoult, D., and Nordmann, P. (2005). Characterization of the naturally occurring oxacillinase of *Acinetobacter baumannii. Antimicrob. Agents Chemother.* 49, 4174–4179. doi: 10.1128/AAC.49.10.4174-4179.2005

Higgins, P. G., Lehmann, M., and Seifert, H. (2010). Inclusion of OXA-143 primers in a multiplex polymerase chain reaction (PCR) for genes encoding prevalent OXA carbapenemases in *Acinetobacter* spp. *Int. J. Antimicrob. Agents* 35:305. doi: 10.1016/j.ijantimicag.2009.10.014

Higgins, P. G., Poirel, L., Lehmann, M., Nordmann, P., and Seifert, H. (2009). OXA-143, a novel carbapenem-hydrolyzing class D beta-lactamase in *Acinetobacter baumannii. Antimicrob. Agents Chemother.* 53, 5035–5038. doi: 10.1128/AAC.00856-09

Kanamori, H., Parobek, C. M., Weber, D. J., van Duin, D., Rutala, W. A., Cairns, B. A., Juliano, J. J., et al. (2016). Next-generation sequencing and comparative analysis of sequential outbreaks caused by multidrug-resistant *Acinetobacter baumannii* at a large academic burn center. *Antimicrob. Agents Chemother.* 60, 1249–1257. doi: 10.1128/AAC.02014-15

Karah, N., Sundsfjord, A., Towner, K., and Samuelsen, Ø. (2012). Insights into the global molecular epidemiology of carbapenem non-susceptible clones of *Acinetobacter baumannii*. *Drug Resist. Updat.* 15, 237–247. doi: 10.1016/j.drup.2012.06.001

Kooli, I., Brahim, H. B., Kilani, M., Gannouni, C., Aouam, A., Toumi, A., et al. (2016). Successful treatment of postoperative multidrug-resistant *Acinetobacter baumannii* meningitis by tigecycline. *J. Glob. Antimicrob. Resist.* 5:62–63. doi: 10.1016/j.jgar.2015.12.003

La Scola, B., Gundi, V. A., Khamis, A., and Raoult, D. (2006). Sequencing of the rpoB gene and flanking spacers for molecular identification of *Acinetobacter* species. *J. Clin. Microbiol.* 44, 827–832. doi: 10.1128/JCM.44.3.827-832.2006

Lashinsky, J. N., Henig, O., and Pogue, J. M., and Kaye, K. S. (2017). Minocycline for the treatment of multidrug and extensively drug-resistant, A. *baumannii*: a review. *Infect. Dis. Ther.* 6, 199–211. doi: 10.1007/s40121-017-0153-2

Lauretti, L., D'Alessandris, Q. G., Fantoni, M., D'Inzeo, T., Fernandez, E., and Pallini, R. (2017). First reported case of intraventricular tigecycline for meningitis from extremely drug-resistant *Acinetobacter baumannii*. *J. Neurosurg.* 127, 370–373. doi: 10.3171/2016.6

Magiorakos, A. P., Srinivasan, A., Carey, R. B., Carmeli, Y., Falagas, M. E., and Giske, C. G. (2012). Multidrug-resistant, extensively drug-resistant and pandrug-resistant bacteria: an international expert proposal for interim standard definitions for acquired resistance. *Clin. Microbiol. Infect.* 18, 268–281. doi: 10.1111/j.1469-0691.2011.03570.x

Marra, A. R., Camargo, L. F., Pignatari, A. C., Sukiennik, T., Behar, P. R., Medeiros, E. A., et al. (2011). Nosocomial bloodstream infections in Brazilian hospitals: analysis of 2,563 cases from a prospective nationwide surveillance study. *J. Clin. Microbiol.* 49, 1866–1871. doi: 10.1128/JCM.00376-11

Medeiros, M., and Lincopan, N. (2013). Oxacillinase (OXA)-producing *Acinetobacter baumannii* in Brazil: clinical and environmental impact and therapeutic options. *J. Bras. Patol. Med. Lab.* 49, 391–405. doi: 10.1590/S1676-24442013000600003

Montravers, P., Bassetti, M., Dupont, H., Eckmann, C., Heizmann, W. R., Guirao, X., et al. (2013). Efficacy of tigecycline for the treatment of complicated skin and soft-tissue infections in real-life clinical practice from five European observational studies. *J. Antimicrob. Chemother.* 68(Suppl. 2):ii15–24. doi: 10.1093/jac/dkt141

Mosqueda, N., Gato, E., Roca, I., López, M., de Alegría, C. R., Fernández Cuenca, F., et al. (2014). Characterization of plasmids carrying the $bla_{\mathrm{OXA-24/40}}$ carbapenemase gene and the genes encoding the AbkA/AbkB proteins of a toxin/antitoxin system. *J. Antimicrob. Chemother.* 69, 2629–2633. doi: 10.1093/jac/dku179

Navon-Venezia, S., , Leavitt, A., and Carmeli, Y. (2007). High tigecycline resistance in multidrug-resistant *Acinetobacter baumannii. J. Antimicrob. Chemother.* 59, 772–774. doi: 10.1093/jac/dkm018

Pagano, M., Rocha, L., Sampaio, J. L., Martins, A. F., and Barth, A. L. (2017). Emergence of OXA-72-producing *Acinetobacter baumannii* Belonging to High-Risk Clones (CC15 and CC79) in Different Brazilian States. *Infect. Control Hosp. Epidemiol.* 38, 252–254. doi: 10.1017/ice.2016.287

Park, Y. K., Jung, S. I., Park, K. H., Kim, D. H., Choi, J. Y., and Kim, S. H. (2012). Changes in antimicrobial susceptibility and major clones of *Acinetobacter calcoaceticus-baumannii* complex isolates from a single hospital in Korea over 7 years. *J. Med. Microbiol.* 61, 71–79. doi: 10.1099/jmm.0.033852-0

Poirel, L., Jayol, A., and Nordmann, P. (2017). Polymyxins: antibacterial activity, susceptibility testing, and resistance mechanisms encoded by plasmids or chromosomes. *Clin. Microbiol. Rev.* 30, 557–596. doi: 10.1128/CMR.00064-16

Poirel, L., Walsh, T. R., Cuvillier, V., and Nordmann, P. (2011). Multiplex PCR for detection of acquired carbapenemase genes. *Diagn. Microbiol. Infect. Dis.* 70, 119–123. doi: 10.1016/j.diagmicrobio.2010.12.002

Pournaras, S., Dafopoulou, K., Del Franco, M., Zarkotou, O., Dimitroulia, E., Protonotariou, E., et al. (2017). Predominance of international clone 2 OXA-23-producing-*Acinetobacter baumannii* clinical isolates in Greece, 2015: results of a nationwide study. *Int. J. Antimicrob. Agents* 49, 749–753. doi: 10.1016/j.ijantimicag.2017.01.028

Provasi Cardoso, J., Cay,ô, R., Girardello, R., and Gales, A. C. (2016). Diversity of mechanisms conferring resistance to β-lactams among OXA-23-producing *Acinetobacter baumannii* clones. *Diagn. Microbiol. Infect. Dis.* 85, 90–97. doi: 10.1016/j.diagmicrobio.2016.01.018

Rodrigues-Costa, F., Cayô, R., Matos, A. P., Girardello, R., Martins, W. M. B. S., Carrara-Marroni, F. E., et al. (2018). Temporal evolution of *Acinetobacter baumannii* ST107 clone: conversion of $bla_{OXA-143}$ into $bla_{OXA-231}$ coupled with mobilization of IS*Aba1* upstream *occAB1*. *Res. Microbiol.* doi: 10.1016/j.resmic.2018.07.001. [Epub ahead of print].

Rodríguez, C. H., Balderrama Yarhui, N., Nastro, M., Nuñez Quezada, T., Castro Cañarte, G., Magne Ventura, R., et al. (2016). Molecular epidemiology of carbapenem-resistant *Acinetobacter baumannii* in South America. *J. Med. Microbiol.* 65, 1088–1091. doi: 10.1099/jmm.0.000328

Rossi, F. (2011). The challenges of antimicrobial resistance in Brazil. *Clin. Infect. Dis.* 9, 1138–1143. doi: 10.1093/cid/cir120

Royer, S., de Campos, P. A., Araújo, B. F., Ferreira, M. L., Gonçalves, I. R., and Batistão, D. W. D. F. (2018). Molecular characterization and clonal dynamics of nosocomial bla_{OXA-23} producing XDR *Acinetobacter baumannii*. *PLoS ONE* 13:e0198643. doi: 10.1371/journal.pone.0198643

Sahl, J. W., Del Franco, M., Pournaras, S., Colman, R. E., Karah, N., Dijkshoorn, L., et al. (2015). Phylogenetic and genomic diversity in isolates from the globally distributed *Acinetobacter baumannii* ST25 lineage. *Sci. Rep.* 5:15188. doi: 10.1038/srep15188

Segal, H., Garny, S., and Elisha, B. G. (2005). Is IS(ABA-1) customized for *Acinetobacter*? *FEMS Microbiol. Lett.* 243, 425–429. doi: 10.1016/j.femsle.2005.01.005

Seifert, H., Dolzani, L., Bressan, R., van der Reijden, T., van Strijen, B., and Stefanik, D. (2005). Standardization and interlaboratory reproducibility assessment of pulsed-field gel electrophoresis-generated fingerprints of *Acinetobacter baumannii*. *J. Clin. Microbiol.* 43, 4328–4335. doi: 10.1128/JCM.43.9.4328-4335.2005

Stietz, M. S., Ramírez, M. S., Vilacoba, E., Merkier, A. K., Limansky, A. S., and Centrón, D. (2013). *Acinetobacter baumannii* extensively drug resistant lineages in Buenos Aires hospitals differ from the international clones I-III. *Infect. Genet. Evol.* 14, 294–301. doi: 10.1016/j.meegid.2012.12.020

Sun, Y., Cai, Y., Liu, X., Bai, N., Liang, B., and Wang, R. (2013). The emergence of clinical resistance to tigecycline. *Int. J. Antimicrob. Agents* 41, 110–116. doi: 10.1016/j.ijantimicag.2012.09.005

US Centers for Disease Control and Prevention. *Antibiotic Resistance Threats in the United States*. (2013). Available online at: http://www.cdc.gov/drugresistance/threat-report-2013/pdf/ar-threats-2013-508.pdf (accessed November 20, 2017).

Vaneechoutte, M., Nemec, A., KÄmpfer, P., Cools, P., and Wauters, G. (2015).). "*Acinetobacter, Chryseobacterium, Moraxella*, and Other Nonfermentative Gram-Negative Rods*," in *Manual of Clinical Microbiology, 11th Edn.*, eds J. Jorgensen, M. Pfaller, K. Carroll, G. Funke, M. Landry, S. Richter, and D. Warnock (Washington, DC: ASM Press), 813–837. doi: 10.1128/9781555817381.ch44

Vasconcellos, F. M., Casas, M. R., Tavares, L. C., Garcia, D. O., and Camargo, C. H. (2017a). *In vitro* activity of antimicrobial agents against multidrug- and extensively drug-resistant *Acinetobacter baumannii*. *J. Med. Microbiol.* 66, 98–102. doi: 10.1099/jmm.0.000422

Vasconcellos, F. M., Tiba-Casas, M. R., Tavares, L. C. B., Souza, W. V., Garcia, D. O., and Camargo, C. H. (2017b). Evaluation of a new trilocus sequence-based multiplex-PCR to detect major *Acinetobacter baumannii* clonal complexes circulating in Brazil. *Infect. Genet. Evol.*. 54, 4–6. doi: 10.1016/j.meegid.2017.06.009

Vasconcelos, A. T., Barth, A. L., Zavascki, A. P., Gales, A. C., Levin, A. S., and Lucarevschi, B. R. (2015). The changing epidemiology of *Acinetobacter* spp. producing OXA carbapenemases causing bloodstream infections in Brazil: a BrasNet report. *Diagn Microbiol. Infect. Dis.* 83, 382–385. doi: 10.1016/j.diagmicrobio.2015.08.006

Villalón, P., Valdezate, S., Cabezas, T., Ortega, M., Garrido, N., and Vindel, A. (2015). Endemic and epidemic *Acinetobacter baumannii* clones: a twelve-year study in a tertiary care hospital. *BMC Microbiol.* 15:47. doi: 10.1186/s12866-015-0383-y

Villalón, P., Valdezate, S., Medina-Pascual, M. J., Rubio, V., Vindel, A., and Saez-Nieto, J. A. (2011). Clonal diversity of nosocomial epidemic *Acinetobacter baumannii* strains isolated in Spain. *J. Clin. Microbiol.* 49, 875–882. doi: 10.1128/JCM.01026-10

Wang, P., Bowler, S. L., Kantz, S. F., Mettus, R. T., Guo, Y., McElheny, C. L., et al. (2016). Comparison of minocycline susceptibility testing methods for carbapenem-resistant *Acinetobacter baumannii*. *J. Clin. Microbiol.* 54, 2937–2941. doi: 10.1128/JCM.01810-16

Wong, Y. P., Chua, K. H., and Thong, K. L. (2014). One-step species-specific high resolution melting analysis for nosocomial bacteria detection. *J. Microbiol. Methods* 107, 133–137. doi: 10.1016/j.mimet.2014.10.001

Woodford, N., Ellington, M. J., Coelho, J. M., Turton, J. F., Ward, M. E., Brown, S., et al. (2006). Multiplex PCR for genes encoding prevalent OXA carbapenemases *in Acinetobacter* spp. *Int. J. Antimicrob. Agents* 27, 351–353. doi: 10.1016/j.ijantimicag.2006.01.004

World Health Organization (2017). *Global Priority List of Antibiotic-Resistant Bacteria to Guide Research, Discovery, and Development of New Antibiotics*. Geneva: World Health Organization.

Zarrilli, R., Giannouli, M., Tomasone, F., Triassi, M., and Tsakris, A. (2009). Carbapenem resistance in *Acinetobacter baumannii*: the molecular epidemic features of an emerging problem in health care facilities. *J. Infect. Dev. Ctries.* 3, 335–341. doi: 10.3855/jidc.240

Zarrillii, R., Pournaras, S., Giannouli, M., and Tsakris, A. (2013). Global evolution of multidrug-resistant *Acinetobacter baumannii* clonal lineages. *Int. J. Antimicrob. Agents* 41, 11–19. doi: 10.1016/j.ijantimicag.2012.09.008

Conflict of Interest Statement: The authors declare that the research was conducted in the absence of any commercial or financial relationships that could be construed as a potential conflict of interest.

frontiers in Microbiology

ORIGINAL RESEARCH
published: 08 January 2019
doi: 10.3389/fmicb.2018.03116

Surface-Related Features and Virulence Among *Acinetobacter baumannii* Clinical Isolates Belonging to International Clones I and II

Jūratė Skerniškytė[1], Renatas Krasauskas[1], Christine Péchoux[2], Saulius Kulakauskas[3], Julija Armalytė[1] and Edita Sužiedėlienė[1]*

[1] Institute of Biosciences, Life Sciences Center, Vilnius University, Vilnius, Lithuania, [2] INRA, UMR 1313 GABI, Plate-forme MIMA2, Jouy-en-Josas, France, [3] INRA, MICALIS Institute, AgroParisTech, Université Paris-Saclay, Jouy-en-Josas, France

OPEN ACCESS

Edited by:
Maria Alejandra Mussi, Consejo Nacional de Investigaciones Científicas y Técnicas (CONICET), Argentina

Reviewed by:
Maria Tomas, Complexo Hospitalario Universitario A Coruña, Spain
Filipa Grosso, Universidade do Porto, Portugal
Melissa Hackett Brown, Flinders University, Australia

***Correspondence:**
Jūratė Skerniškytė
jurate.skerniskyte@gf.vu.lt

Specialty section:
This article was submitted to Infectious Diseases, a section of the journal Frontiers in Microbiology

Received: *31 August 2018*
Accepted: *03 December 2018*
Published: *08 January 2019*

Citation:
Skerniškytė J, Krasauskas R, Péchoux C, Kulakauskas S, Armalytė J and Sužiedėlienė E (2019) Surface-Related Features and Virulence Among Acinetobacter baumannii Clinical Isolates Belonging to International Clones I and II. Front. Microbiol. 9:3116. doi: 10.3389/fmicb.2018.03116

Acinetobacter baumannii currently represents one of the most important nosocomial infection agent due to its multidrug-resistance and a propensity for the epidemic spread. The *A. baumannii* strains belonging to the international clonal lineages I (IC I) and II (IC II) are associated with the hospital outbreaks and a high virulence. However, the intra and inter lineage-specific features of strains belonging to these most worldwide spread *A. baumannii* clones are not thoroughly explored. In this study we have investigated a set of cell surface-related features of *A. baumannii* IC I (n = 20) and IC II (n = 16) lineage strains, representing 30 distinct pulsed-field gel electrophoresis types in the collection of clinical isolates obtained in Lithuanian tertiary care hospitals. We show that *A. baumannii* IC II strains are non-motile, do not form pellicle and display distinct capsular polysaccharide profile compared with the IC I strains. Moreover, in contrast to the overall highly hydrophobic IC I strains, IC II strains showed a greater variation in cell surface hydrophobicity. Within the IC II lineage, hydrophilic strains demonstrated reduced ability to form biofilm and adhere to the abiotic surfaces, also possessed twofold thicker cell wall and exhibited higher resistance to desiccation. Furthermore, these strains showed increased adherence to the lung epithelial cells and were more virulent in nematode and mouse infection model compared with the hydrophobic IC II strains. According to the polymerase chain reaction-based locus-typing, the reduction in hydrophobicity of IC II strains was not capsule or lipooligosaccharide locus type-dependent. Hence, this study shows that the most widespread *A. baumannii* clonal lineages I and II markedly differ in the series of cell surface-related phenotypes including the considerable phenotypic diversification of IC II strains at the intra-lineage level. These findings suggest that the genotypically related *A. baumannii* strains might evolve the features which could provide an advantage at the specific conditions outside or within the host.

Keywords: *Acinetobacter baumannii*, clonal lineages, surface-related features, virulence, hydrophobicity

INTRODUCTION

Gram-negative bacterium *Acinetobacter baumannii* is a difficult to treat infection agent, causing nosocomial infections worldwide (Eliopoulos et al., 2008; Holt et al., 2016). Characteristic features of this opportunistic pathogen include multidrug-resistance (MDR) phenotype, ability to withstand unfavorable environmental conditions for long periods of time and a high propensity for spread resulting in the hospital outbreaks, especially in the intensive care units (Manchanda et al., 2010; Eijkelkamp et al., 2014).

The worldwide spread of *A. baumannii* in clinical settings is characterized by the expansion of several predominant clones (Karah et al., 2012; Zarrilli et al., 2013). Of them, the international clonal lineages I (IC I) and II (IC II), otherwise known as European clones I and II, account for the most part of the *A. baumannii* infections (Zarrilli et al., 2013; Dahdouh et al., 2017). These clonal lineages have been identified around 1970s (Holt et al., 2016) and since then have been spread globally (Antunes et al., 2014). In particular, the IC II lineage strains are characterized through their high carbapenem-resistance and nosocomial spread in many countries during the recent years (Kim et al., 2017; Pournaras et al., 2017). The specific features contributing to the endemic nature of successful *A. baumannii* clones are of particular interest in exploring the virulome of *A. baumannii* (Di Nocera et al., 2011; Eijkelkamp et al., 2014; Ali et al., 2017) and identifying the novel candidates for the vaccine-based strategies to combat this infection agent (Ni et al., 2017). Most of the studies exploring virulent properties of *A. baumannii* are based on the experiments using several well-defined strains (Geisinger and Isberg, 2015; Tipton et al., 2015; Kentache et al., 2017). The data describing currently clinically relevant isolates are in scarce, despite findings that *A. baumannii* is characterized by its ability to change pathogenic features constantly (Antunes et al., 2014; Holt et al., 2016; Piepenbrink et al., 2016).

The cell surface structures are crucial for bacterial pathogens in sensing the environment and interacting with the host (Weber et al., 2016; Lee et al., 2017). In order to persist in clinical settings *A. baumannii* must be equipped with a set of cell surface features enabling it to adhere to the abiotic surfaces such metal and plastic found in medical devices and hospital equipment as well as to survive under desiccation stress (McConnell et al., 2013; Chiang et al., 2017). Multiple environmental and virulence-associated signals induce either biofilm formation or bacterial motility phenotypes through surface exposed sensors in *A. baumannii* (McConnell et al., 2013) assigning these features as possible survival-related factors. Moreover, specific cell surface determinants are required for *A. baumannii* to resist the host defense systems such as complement and macrophage-mediated killing as well as to mediate the attachment to the host cells at the sites of infection (Russo et al., 2010; Smani et al., 2012; Harding et al., 2018b).

In this study we present comprehensive comparative analysis of surface-related features and their relationship with *A. baumannii* IC I and IC II isolates and demonstrate that genotypically related strains display considerable cell-surface-related phenotypic differences that significantly impact their virulence properties displayed outside and within the host.

MATERIALS AND METHODS

Description of Bacterial Strains and Growth Conditions

The 36 *A. baumannii* strains representing different pulsed-field gel electrophoresis (PFGE) defined pulsotypes from the retrospective collection of 365 clinical isolates previously genotyped by Povilonis et al. (2013) were used in the study (**Supplementary Table S1**). The strains were previously assigned to the international clonal lineages I and II using trilocus sequence-based typing (3LST). On the basis of MLST-IP typing, the IC I and IC II strains were assigned to ST1 and ST2, respectively (Povilonis et al., 2013). Strains were named by their clonal dependence. Roman numerals I and II indicate IC I and IC II, respectively, and lowercase letters represent different pulsotypes. The MLST typing of selected isolates using the Oxford scheme was undertaken according to *A. baumannii* MLST website[1]. Strains were cultured on the Luria-Bertani (LB) agar plates at 37°C. Liquid cultures were inoculated in LB medium and grown overnight.

Determination of Cell Surface Hydrophobicity

Determination of cell surface hydrophobicity by salt aggregation test (SAT) was carried out as described by Nwanyanwu and Abu (2013). Briefly, *A. baumannii* were grown on LB plates at 37°C overnight. Cells were suspended in ddH_2O until slight turbidity and mixed with the equal volume of ammonium sulfate solution to yield concentrations ranging from 0.0625 to 2 M. Cell aggregation (clumping) was observed under the microscope at 50x magnification. The cell surface hydrophobicity was expressed as a lowest salt concentration, which caused bacterial cell aggregation.

Motility Assays

Twitching and swarming motilities were investigated as previously described (Eijkelkamp et al., 2011) with some modifications. Briefly, a single bacterial colony grown overnight, was collected using a sterile toothpick and stabbed through a semi-solid Tryptic Soy Broth medium (TSB) to the bottom of the Petri dish. For twitching and swarming motility assays, TSB medium with 0.75 and 0.25% agarose was used, respectively. Inoculated plates were kept in humid airtight containers and grown at 37°C for 24 or 48 h for surface motility and twitching motility, respectively. Motility was quantified by measuring the halo of growth around the inoculation site and expressed in millimeters.

[1]https://pubmlst.org/abaumannii/

Assessment of Pellicle Formation

The pellicle formation was measured as described by Giles et al. (2015) with some modifications. The 12-well plates [tissue culture plates (TPPs)] with 3 ml of TSB medium were inoculated with 1000-fold dilutions of overnight bacterial cultures and incubated without shaking at 30°C for 30 h. To remove the pellicle from the surface of the medium, 200 μL of isopropanol was added to each well. The floating pellicle was removed and dissolved in 0.5 ml of 10 mM of NaOH immediately followed by the neutralization with HCl. The OD_{600} of the suspension was measured.

Desiccation Assay

Acinetobacter baumannii were grown in LB medium at 37°C overnight and diluted into the same medium to the OD_{600} of 0.1. 10 μl of each of the sample were spotted on polystyrene, allowed to dry and incubated at 28°C for 24 h. Pre-desiccated samples were serially diluted by 10-fold dilutions and seeded on the LB plates. After desiccation, samples were resuspended in LB broth, serially diluted into 10-fold dilutions and seeded. LB plates were grown at 37°C overnight. Percentage of survived bacteria (D% – desiccation rate) was assessed by comparing obtained CFU counts of post-desiccated samples with those of the pre-desiccated samples.

Biofilm Formation Assay

Experiments were carried out in LB medium. Overnight bacterial cultures were diluted 1000-fold, 200 μl of suspension was inoculated into the wells of 96 U-form polystyrene plate (Nerbe Plus) and incubated in static conditions at 37°C for 18 h. OD_{600} of planktonic culture was measured. The wells were then washed three times with 0.9% NaCl to remove non-adherent bacteria. Biofilms were stained with 0.5% crystal violet dye for 5 min and washed three times with 0.9% NaCl. Dye was eluted with 96% ethanol by incubation for 5 min, and OD_{580} was determined. The $OD_{580/600}$ ratio was estimated to normalize the amount of formed biofilm to the total cell content.

Adhesion to Polystyrene Assay

The adhesion tests were performed by dispensing 200 μL of x5 diluted overnight bacterial culture grown in LB medium into the wells of 96 F-form polystyrene plate (Nerbe Plus) and incubated for 2 h at 28°C. Wells were rinsed three times with PBS and stained with crystal violet as described above. The $OD_{580/600}$ ratio was estimated to normalize the amount of adhered cells to the total cell content.

Cell Culture Assays

Mouse epithelial LL/2 (LLC1) and mouse macrophages J774 cell lines were grown in Dulbecco's modified Eagle's medium (DMEM) (Gibco, 31966021) supplemented with 10% fetal bovine serum (FBS) (Gibco, 12657029) at 37°C with 5% CO_2.

For adhesion experiment, lung epithelial cells were plated at a density of 1.5×10^4 cells/well into 96-well TPP. Cells were grown for 48 h to form fastened culture monolayer with ∼80% confluence.

A. baumannii strains were cultured for 12 h until the log phase in LB medium at 37°C with moderate shaking at 145 rpm. All bacterial suspensions were equalized to yield OD_{600} = 0.7, washed once with PBS. LL/2 cells were infected with bacteria at a multiplicity of infection (MOI, bacteria: eukaryotic cell ratio) ∼1000:1. The number of *A. baumannii* CFUs inoculated per well was determined by serial dilution of bacterial culture in PBS and plating on the LB medium.

Infected LL/2 cell monolayers were incubated for 90 min at 37°C. Wells were carefully washed with DPBS three times to remove unattached bacteria. Then LL/2 cells were lysed with ddH_2O by intense pipetting. Serially diluted lysates were plated onto LB medium to determine the number of adhered bacteria. Bacterial adherence (A%) to the LL/2 cells was expressed as a percentage of the CFU of adhered bacteria compared to the total number of CFUs of the initial inoculum.

Phagocytosis Assay

For the phagocytosis assay, macrophages J774 were plated at a density of 5.6×10^4 cells/well into 96-well TPPs and were grown for 14 h at 37°C with 5% CO_2. Macrophages were infected with bacteria at MOI ∼200:1. Infected macrophages were then incubated for 60 min, washed three times in PBS and incubated with DMEM supplemented with 400 μg/μl of gentamycin for 30 min. After three washes with PBS, macrophages were resuspended in ddH_2O and lysed by the intense pipetting. Serial dilutions were plated on the LB plates. Plates were incubated at 37°C overnight. Bacterial phagocytosis (P%) was expressed as a percentage of the CFU of intracellular bacteria compared to the total number of CFUs of the initial inoculum.

A. baumannii Growth Assays

Bacterial growth was evaluated in LB medium, heat inactivated FBS (htFBS) and active FBS. FBS was inactivated by incubation at 56°C for 30 min with the constant shaking. Overnight cultures were inoculated at x1000 dilution to LB medium and 80% FBS or htFBS (20% of LB medium). Growth curves were measured at 37°C with periodic shacking every 20 min by Tecan Infinite M200 Pro microplate reader.

Polymerase Chain Reaction

For the determination of capsule and lipooligosaccaharide (LOS) outer core (OC) locus types, a conventional polymerase chain reaction (PCR) was undertaken using primers listed in **Supplementary Table S2**. Conventional PCR volume was 20 μl and consisted of 2 μl of 10x Taq DNA polymerase reaction buffer with $(NH_4)_2SO_4$ (Thermo Fisher Scientific), 2 mM $MgCl_2$, 0.4 mM of each dNTPs, 400 nM of primers, 0.2 U Taq DNA polymerase (Thermo Fisher Scientific) and 1 μl of DNA template. Tm was calculated based on the primers sequences.

Generation of Capsule Negative (Δ*wza*) *A. baumannii* Mutant

Markerless gene deletion was performed as previously described (Oh et al., 2015). Briefly, upstream and downstream regions of *A. baumannii wza* gene were amplified using

primers listed in **Supplementary Table S2** and DNA of IC II strain III-a as a template. The amplicons were joined with gentamicin resistance cassette *aac3I* amplified from a clinical *A. baumannii* strain by overlap PCR. The resulting DNA was cloned into pUC19_sacB plasmid yielding pUC19_sacB_UDwzaGm plasmid (**Supplementary Table S2**). IC II III-a strain was transformed with the resulting plasmid by electroporation and colonies were selected on LB agar with gentamicin. Colonies were picked up with sterile toothpick and inoculated in LB medium for 4 h. Serial dilutions were plated on LB agar with 10% sucrose. Mutants were identified by PCR with specific primers and confirmed by sequencing.

Fractionation of Capsular Polysaccharides

For capsular polysaccharides (CPS) analysis, extracts of CPS from cell culture supernatants were prepared according to Geisinger and Isberg (2015). Briefly, cultures were grown on LB plates at 37°C overnight, suspended in PBS and normalized to an OD_{600} = 3. Polysaccharides were released into the supernatant by vortexing at maximum speed for 30 s. After centrifugation at 9000 × *g* for 10 min, polysaccharides were precipitated in 75% ice-cold ethanol overnight, followed by pelleting and air-drying. The pellet was resuspended in SDS sample buffer and boiled for 5 min. Samples were loaded on the 12% SDS-PAGE gels. After electrophoresis, gels were stained overnight with 0.1% (w/v) Alcian Blue as described in Mercaldi et al. (2008).

Transmission Electron Microscopy

Transmission electron microscopy (TEM) analysis was undertaken at Microscopy and Imaging Platform MIMA2 at Gabi UMR (Jouy-en-Josas, France). Bacteria were grown in LB medium at 37°C overnight and cells were fixed within 0.1 M sodium cacodylate buffer (pH 7.2) with 2% of glutaraldehyde for 3 h at room temperature. After treatment with 0.5% Oolong Tea Extract (OTE) in cacodylate buffer, post-fixation with 1% osmium tetroxide containing 1.5% potassium cyanoferrate, pellets were dehydrated in solutions of increasing ethanol concentrations and embedded in Epon. Ultrathin sections were collected on 200-mesh copper grids and counterstained with lead citrate. Grids were examined with a Hitachi HT7700 electron microscope operated at 80 kV (Elexience, France), and images were acquired with a charge-coupled device camera (AMT).

Caenorhabditis elegans Fertility Assay

Caenorhabditis elegans N2 eggs were grown to stage L1 and arrested overnight at 20°C to physiologically synchronize the worms. Nematodes were grown on nematode growth medium plates (NGM) with the culture of *Escherichia coli* OP50 strain until nematodes reached L2 stage. Overnight cultures of different *A. baumannii* strains were seeded on NGM medium. Ethanol was added to a final concentration of 1%, as it was demonstrated that ethanol induces *A. baumanni* virulence (Smith et al., 2007), and plates were grown at 21.5°C for 24 h. One L2 stage worm was placed over each *A. baumannii* strain and incubated at 21.5°C. On the third day after infection worm progeny was determined by counting *C. elegans* worms.

Sepsis Model in Mice

Eight- to twelve-week-old female BALB/c mice were purchased from Institute of Biochemistry, Life Science Center (Vilnius University, Vilnius). The animals were maintained and used in accordance with the recommendations of the directive 2010/63/EU of the European Parliament and of the Council of 22 September, 2010 on the protection of animals used for scientific purpose. Study was performed under permission of Lithuanian State Food and Veterinary Service No. G2-72.

A sepsis model was established as described previously (Huang et al., 2014). Briefly, *A. baumannii* cultures were grown in LB medium for 18 h at 37°C and adjusted to the designated concentrations with PBS according to the OD_{600} values based on previously determined concentrations by seeding serial dilutions and counting CFUs. Samples were prepared by mixing the bacterial suspension with 5% of porcine mucin (w/v; Sigma-Aldrich). Mice were injected intraperitoneally with 0.5 mL of the sample. CFUs corresponding the bacterial loads were determined by plating sequential dilutions on LB plates. Bacterial colonies obtained from animal sources were confirmed by PCR with *A. baumannii*-specific primers (**Supplementary Table S2**).

Statistical Analysis

All statistical comparisons were based on the one-way analysis of variance (ANOVA) with a Tukey HSD *post hoc* test. Statistical analysis was performed using the computing environment R version 3.5.1 (R Development Core Team, 2008). All quantitative data are representative of at least three independent experiments.

RESULTS

A. baumannii IC II Strains Are Non-motile and Pellicle-Non-Forming Compared With the IC I Strains

Thirty six *A. baumannii* clinical isolates, chosen for the present study, were representatives of 30 distinct PFGE types of IC I and IC II clonal lineages, and were obtained from Lithuanian hospitals during the period of June–November 2010 and characterized in a previous study (Povilonis et al., 2013). Twenty IC I isolates and 16 IC II isolates were selected (**Supplementary Table S1**). All isolates were multidrug-resistant (resistant to three or more antibiotic classes).

We were interested, whether representative strains of the two most common clonal lineages display specific pattern of surface-related features, which are thought to be important for *A. baumannii* growth and survival in clinical environment and within the host (Rumbo et al., 2014; Weber et al., 2016; Lee et al., 2017). Therefore, we first tested swarming and twitching motility of selected *A. baumannii* isolates. The

swarming distance, expressed by the majority of strains (92%, 33/36), was low and yielded approximately 6–14 mm. Only three strains, all representatives of IC I lineage, showed increased swarming motility yielding a value of >26 mm (**Figure 1A**). However, the majority of *A. baumannii* IC I lineage strains showed twitching motility in contrast to IC II strains, which lacked this property with the exception of a single strain (**Figure 1A**). The IV type pili have been proposed to be responsible for twitching motility in *A. baumannii* (Harding et al., 2013), therefore we looked for the presence of pili-like structures on the cell surface. The transmission electron microscopy of representative motile IC I strain 169 and non-motile IC II strain II-a showed marked differences in cell surface structures, the IC I strain displaying pili-like extended structures, which were absent in the IC II strain (**Supplementary Figure S1**).

According to the recent observations, the bacterial motility contributes to the formation of pellicle, a biofilm at the air–liquid interface (Giles et al., 2015; Hölscher et al., 2015). Hence, we tested the ability of our set of *A. baumannii* strains to form pellicle by growing them in TSB medium as described in Section "Materials and Methods". The vast majority of IC II lineage strains lacked the ability to form pellicle, whereas 85% (17/20) of IC I strains showed pellicle-forming phenotype (**Figure 1B**). The pellicle formation clearly was a trait of IC I lineage, though these strains were highly various in terms of the abundance of pellicle biomass. However, there was no obvious correlation among pellicle formation and swarming or twitching motility in IC I group, as for example I-d strain lacking twitching motility phenotype, was able to form a pellicle and I-gB strain with no pellicle forming feature was able to demonstrate twitching motility.

Therefore, results show evident differences in twitching motility and pellicle formation phenotypes between *A. baumannii* IC I and IC II lineage strains.

A. baumannii IC II Strains Express Different Type of Capsular Polysaccharide Profiles Compared With IC I Strains

Since exopolysaccharide represents one of the bacterial pellicle components (Armitano et al., 2014; Nait Chabane et al., 2014) and given the fact that IC I and IC II lineage strains exhibited marked differences in the pellicle formation, we next asked whether they differ in a production of cell surface glycoconjugates such as CPSs and lipooligosaccharide (LOS). **Figure 2** shows polysaccharide profiles of representative IC I (n = 5) and IC II (n = 11) isolates from our tested

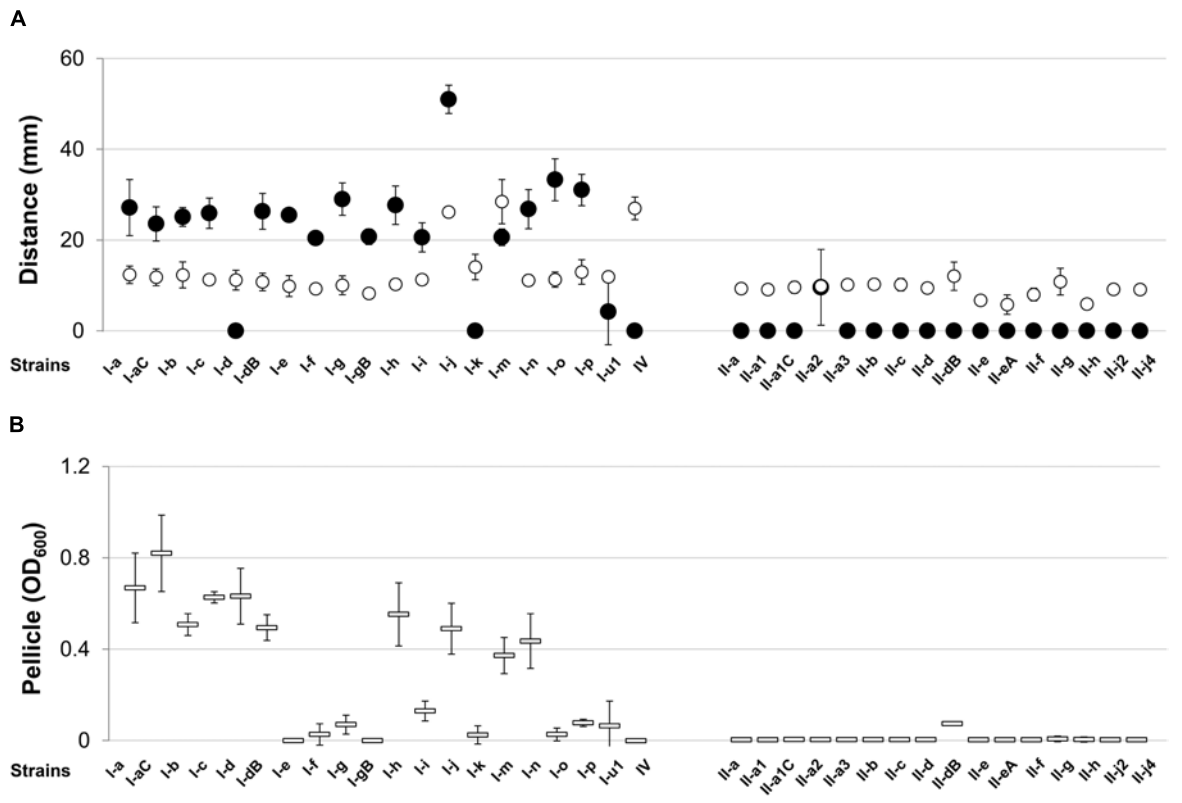

FIGURE 1 | Twitching and swarming motilities and pellicle formation of *Acinetobacter baumannii* IC I and IC II lineage strains. **(A)** Twitching (●) and swarming (o) motilities expressed as a distance in mm; **(B)** total pellicle biomass (=) was suspended in the aqueous solution and absorbance OD_{600} was measured. Data are given as mean ± standard deviations from three independent experiments. Roman numerals I and II in the strains names indicate IC I and IC II, respectively.

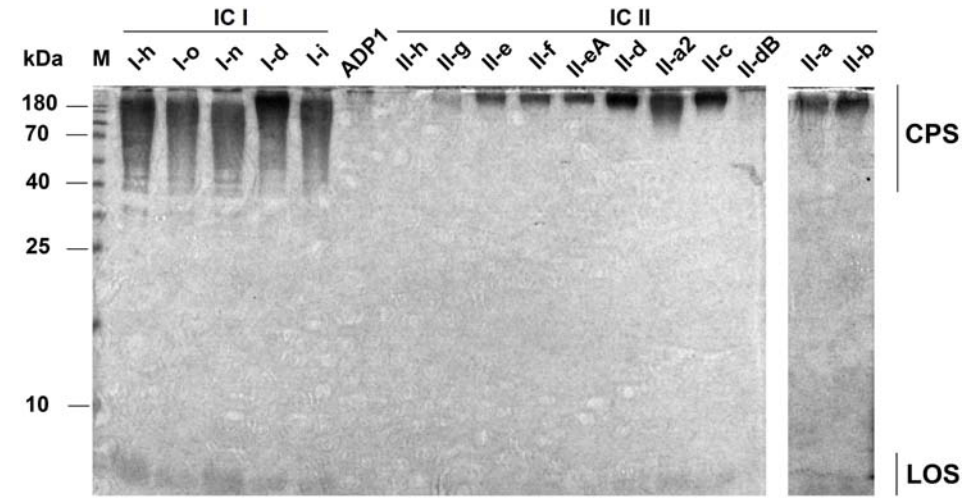

FIGURE 2 | Capsular polysaccharide (CPS) profiles of *A. baumannii* IC I and IC II lineage strains. 12% SDS-PAGE followed by Alcian Blue staining was undertaken to visualize CPS. *Acinetobacter baylyi* strain ADP1 was used as CPS-negative control. LOS denotes lipooligosaccharide (LOS). The positions of standard molecular mass markers [PageRuler^{TM} Prestained Protein Ladder (Thermo Fisher Scientific)] are shown on the left.

set of 36 isolates (profiles of the rest of isolates are given in the **Supplementary Figure S2**). Major differences can be observed in CPS profiles between representatives of two clonal lineages. The IC I strains express CPS of variable length, whereas the IC II strains with the few exceptions, produce only narrow distribution, high-molecular-weight CPS (**Supplementary Table S1**). Two IC II strains (II-h and II-dB) were found to be capsule-deficient at growth conditions used (**Figure 2**).

Therefore, these observations imply that *A. baumannii* belonging to the most widespread clonal lineages display lineage-specific CPS composition.

A. baumannii IC II Strains Exhibit Variation in the Surface Hydrophobicity Compared With IC I Strains

One of the most important characteristic of bacterial surface is cell surface hydrophobicity, whereas it plays a role in virulence-associated processes (Krasowska and Sigler, 2014). Since our tested strains differ in CPS production, we decided to access hydrophobicity of *A. baumannii* clinical isolates. We performed SAT, which is based on the clumping of bacteria in the presence of salt (Nwanyanwu and Abu, 2013).

All tested IC I strains were considered to have hydrophobic character based on the estimated SAT values, which ranged from 0.5 to 1 M (**Figure 3A**). In contrast, more than a half (56%, 9/16) of IC II strains displayed low surface hydrophobicity compared with the IC I group (SAT values $\geq$ 2 M) (**Figure 3A**). Of hydrophilic IC II strains, II-a2, II-c, II-d, and II-dB represented clonal isolates, with strains belonging to the pulsotypes retrieved repeatedly from the hospitals, whereas II-e, II-eA, II-f, II-g, II-h isolates were sporadic (**Supplementary Table S1**). We did not observe a correlation between hydrophobicity and sequence type (ST) by examining selected IC II isolates according the Oxford multilocus sequence typing (MLST) scheme[1]. Thus, strains II-a and II-f, differing significantly in hydrophobic features, were both assigned to a common sequence type ST208, whereas strains II-a2 and II-h displaying hydrophilic character were assigned to different STs, ST 440 and ST348, respectively.

Notably, the majority of the hydrophilic IC II strains showed significantly reduced growth rates in the LB medium compared with hydrophobic IC II strains, indicating altered bacterial fitness of hydrophilic strains (**Supplementary Figure S3**).

Hydrophilic *A. baumannii* IC II Strains Lack the Capacity to Form Biofilms and Adhere to the Plastic Surface

Since, it has been proposed that a degree of cell surface hydrophobicity could modulate adhesive properties of various commensal and pathogenic microorganisms (Krasowska and Sigler, 2014), we investigated how hydrophobic character of *A. baumannii* IC I and IC II strains impacts their ability to form biofilms and adhere to the abiotic and biotic surfaces. Interestingly, the trend of biofilm formation among IC I and IC II strains was different to that observed for pellicle phenotype (**Figure 3B**). All IC I strains and some IC II strains formed biofilm, albeit at the varying levels, whereas a group of IC II strains that were genetically close according to the PFGE analysis (Povilonis et al., 2013), namely, II-d, II-dB, II-e, II-eA, II-f, II-g, and II-h showed extremely weak biofilm-forming ability or entirely lacked this phenotype (**Figure 3B**). Biofilm non-forming phenotype of these isolates correlated with their low surface hydrophobicity according to the SAT assay.

Current model of biofilm formation involves attachment phase when bacteria comes into contact with the surface (Krasowska and Sigler, 2014). Due to the fact that different *A. baumannii* strains possess various surface hydrophobicity it

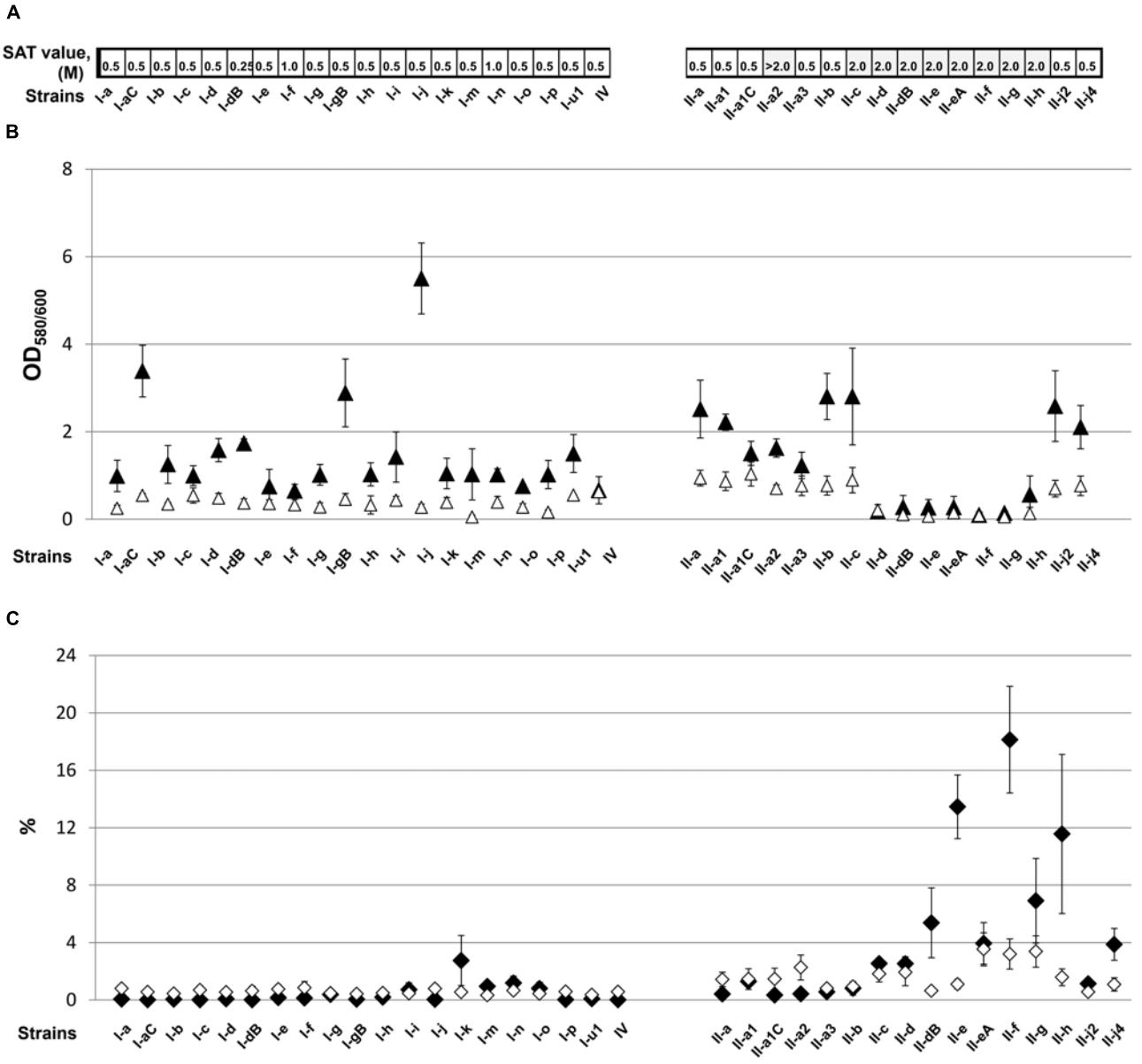

FIGURE 3 | The cell surface-associated features of *A. baumannii* IC I and IC II lineage strains. **(A)** Surface hydrophobicity, defined by the salt aggregation test (SAT) and expressed as a minimum ammonium sulfate concentration (M) required for bacterial aggregation; **(B)** biofilm formation (▲) and adherence to polystyrene (Δ) expressed as $OD_{580/600}$. Error bars represent standard deviations from three independent experiments; **(C)** desiccation resistance (♦) and adhesion to lung epithelium cells LL/2 (◇) expressed as percentages. Error bars represent standard errors from at least three independent experiments. Roman numerals I and II in the strains names indicate IC I and IC II, respectively.

could result in differences in the initial attachment. Therefore *A. baumannii* adherence to plastic was assessed. As can be seen in **Figure 3B**, all tested IC I lineage strains, except two (I-m and I-p), exhibited modest adherence to polystyrene. Again, IC II strains with the low cell surface hydrophobicity and impaired biofilm-forming phenotype, poorly adhered to the plastic, indicating that hydrophobicity in *A. baumannii* is essential in the initial attachment to the surface (**Figure 3B**).

Taken together, these results demonstrate that a high cell surface hydrophobicity of *A. baumannii* impacts important virulence traits such as biofilm formation and adherence to the abiotic surface.

Hydrophilic *A. baumannii* IC II Strains Survive Desiccation Stress Better Compared With Hydrophobic IC II Strains

Observation that some *A. baumannii* clinical strains exhibited low cell surface hydrophobicity, prompted as to evaluate how it impacts the ability to survive desiccation stress, feature which

contribute to bacterial survival and persistence in a hospital environment (Russotto et al., 2015).

Overall, the majority of IC I and a part of IC II strains poorly survived desiccation, yielding only 0.005 to 1.3% of survived cells (**Figure 3C**). However, a group of hydrophilic IC II strains was highly resistant to desiccation and displayed 2–14 times higher resistance compared with the rest of the IC II strains (**Figure 3C**). The decreased surface hydrophobicity possibly might increase water retention in the bacterial cell wall and thus contribute to the desiccation resistance. Moreover, we observed that the hydrophilic IC II strains II-e and II-f, displaying the highest desiccation resistance among tested strains, had approximately

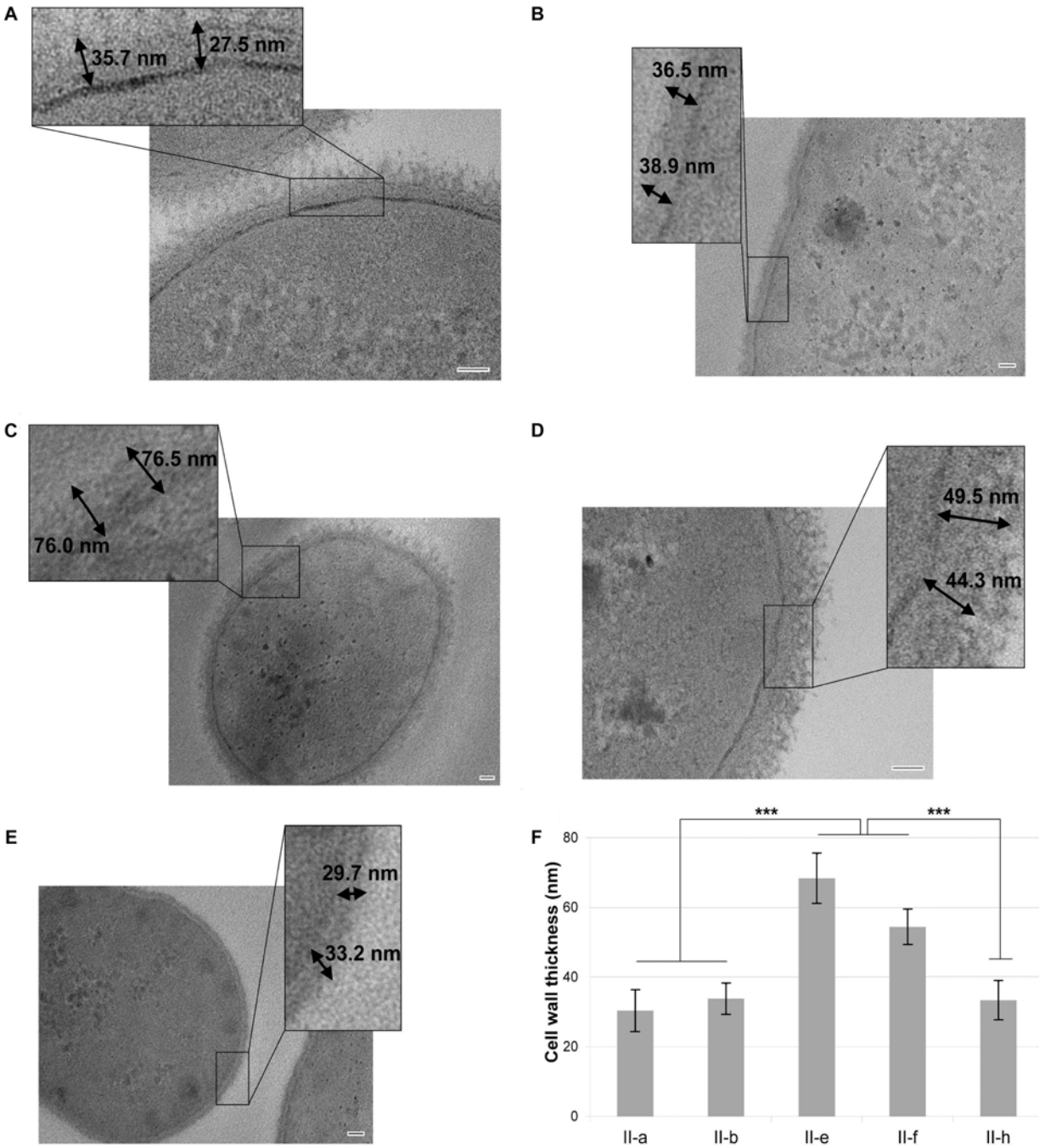

FIGURE 4 | Cell wall thickness of *A. baumannii* strains with different surface hydrophobicity, assessed by the transmission electron microscopy. *A. baumannii* II-b **(A),** II-a **(B)**, II-f **(C)**, II-e **(D)**, and II-h **(E)** strains were analyzed. Scale bar is 50 nm. Double arrows in the larger scale insets show the calculated thickness of the cell walls. **(F)** Average of cell wall thickness of the strains. Error bars represent standard deviations from three measurements of three different cells, significance was assessed by ANOVA. ***$p < 0.001$.

twofold thicker cell wall compared with the hydrophobic strains II-a and II-b and a capsule-deficient strain II-h according to the TEM analysis (**Figures 4A–F**).

Therefore, the hydrophilic nature of cell surface strongly impacts *A. baumannii* ability to resist desiccation.

Hydrophilic *A. baumannii* IC II Strains Adhere Better to the Lung Epithelial Cells Compared With the Hydrophobic IC II Strains

A. baumannii adherence to the epithelial cells is thought to be one of the essential features required for infection process (Smani et al., 2012). Therefore, we hypothesized that a degree of cell surface hydrophobicity might play a role in *A. baumannii* adherence to the host cells as well. Overall, the specific adherence of *A. baumannii* clinical strains to the mouse lung epithelial LL/2 cells was poor (**Figure 3C**). The IC I strains adhered at a rate of 0.3 to 0.8%, while the adhesion of IC II strains was more pronounced and yielded 0.5 to 3.5% rate. In the IC II group of hydrophilic strains, in particular II-a2, II-c, II-d, II-eA, II-f, II-g, and II-h strains showed a clear trend of increased ability to adhere to the epithelial cells (**Figure 3C**).

Therefore, the results presented above imply, that IC I and IC II strains might use different cell surface-related properties for an attachment to the host cells. Moreover, our observations with IC II strains also suggest that genetically related *A. baumannii* strains belonging to the same clonal lineage, display a marked variation in the surface-related properties. Therefore, we hypothesized that these phenotypic differences could have different impact on their virulence properties and decided to investigate them more thoroughly.

The Presence of *A. baumannii* Capsule Is Essential for the Resistance to Macrophage Phagocytosis and Serum-Mediated Killing

As the evasion of host defense systems such as phagocytic cells and complement are crucial in *A. baumannii* infection (Russo et al., 2010), we characterized our set of IC I and IC II isolates by the rate of macrophage-mediated phagocytosis and by the ability to survive serum-mediated killing. No correlation between strains clonal dependence or surface hydrophobicity and resistance to macrophage or serum killing was observed. All tested strains exhibited low rate of macrophage-mediated phagocytosis ranging from 0.01 to 0.18% with the exception of strains II-dB and II-h, which demonstrated approximately 5 and 10 times higher phagocytosis rate, respectively (**Figure 5** and **Supplementary Table S2**). Furthermore, these two strains showed reduced growth in serum-supplemented LB medium compared with the rest of the strains, which were considered resistant to complement system (R) (**Figure 5** and **Supplementary Table S2**). Notably, II-dB and II-h strains were the only ones CPS-deficient according the SDS-PAGE assay (**Figure 2**), indicating the crucial role of *A. baumannii* capsule in the evasion of host defense system. The role of capsule was further supported by the analysis of *A. baumannii* IC II strain III-a deletion mutant of *wza* gene, which is essential (Russo et al., 2010) for capsule synthesis. The Δ*wza* strain showed drastic increase in the FBS-sensitivity and displayed an impairment of CPS synthesis compared with the parent strain (**Supplementary Figure S4**).

Strikingly, the serum sensitive strain II-h was able to restore growth in the serum-containing LB medium after culturing for approximately 10 h (**Figure 6A**). Therefore, we asked, whether this restoration is due to the induction of CPS synthesis. Indeed,

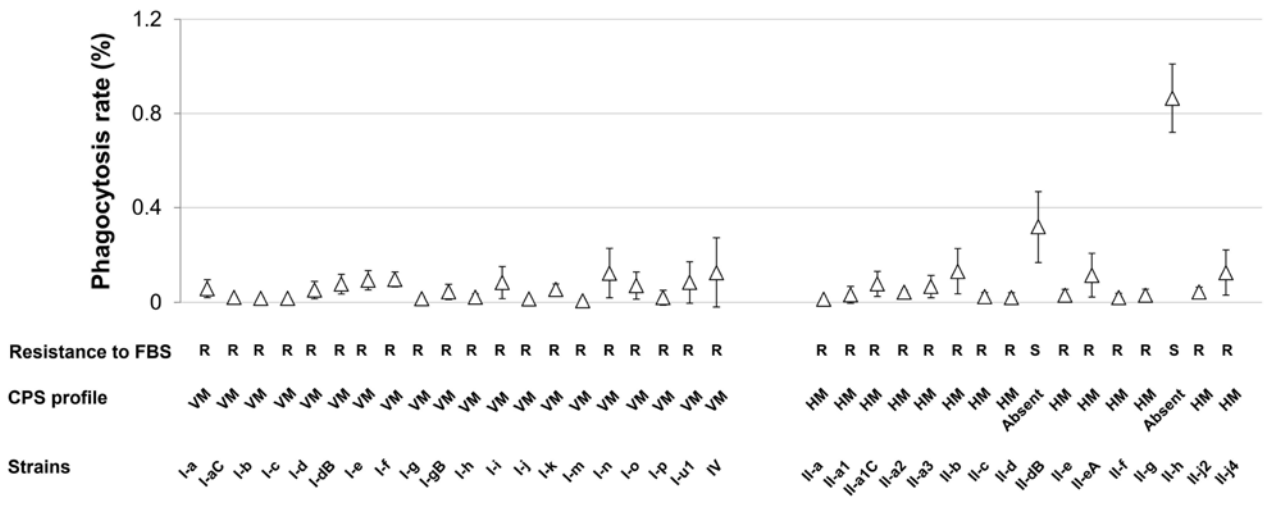

FIGURE 5 | Susceptibility of *A. baumannii* IC I and IC II lineage strains to macrophage and serum-mediated killing. Phagocytosis by J774 macrophages is expressed as percentages and shown in a graph (Δ). Error bars represent standard deviations from three independent experiments. R and S letters below the graph denote the strains that are FBS resistant and sensitive, respectively. HM and VM indicate profile of high and variable-molecular-mass CPS, respectively. Roman numerals I and II in the strains names indicate IC I and IC II, respectively.

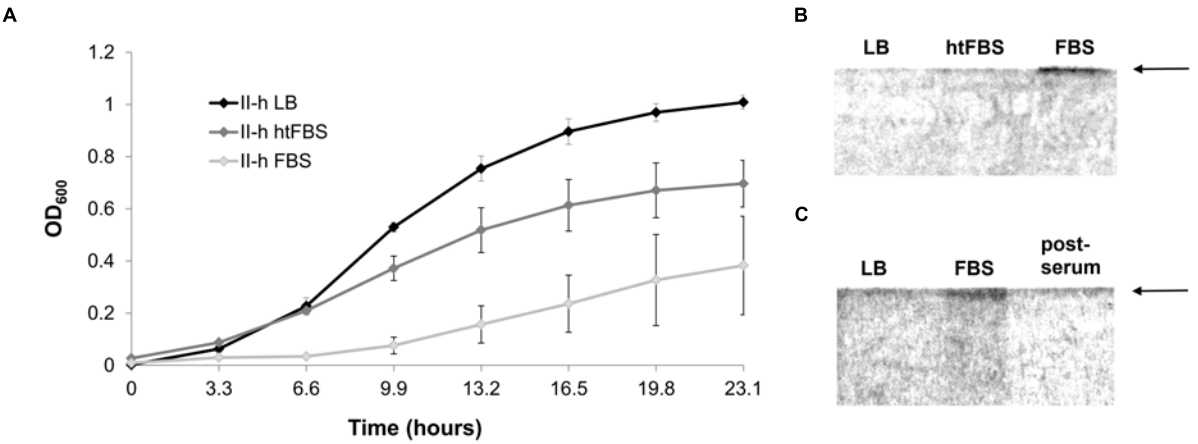

FIGURE 6 | Growth and CPS production by *A. baumannii* IC II strain II-h. **(A)** Growth curves in LB, LB supplemented with 80% of heat treated (htFBS) and untreated FBS. Error bars represent standard deviations from three independent experiments; **(B)** SDS-PAGE gel showing the polysaccharide profiles from cells cultured for ∼24 h in LB, LB supplemented with 80% of heat treated and untreated FBS; **(C)** SDS-PAGE gel showing the polysaccharide profiles from the cells cultured for 24 h in LB with FBS, then re-cultured for 24 h in fresh LB without FBS (post-serum). Gels were stained with Alcian Blue. Arrows on the right indicate the position of CPS.

the results of SDS-PAGE indicated the presence of a band corresponding CPS, which was absent in the same strain cultured in the LB medium or in the same medium supplemented with the heat inactivated serum (**Figure 6B**). Production of CPS was lost as soon as serum-induced bacteria were repeatedly re-grown in LB media (**Figure 6C**).

Thus, the results demonstrate that the capsule is essential for *A. baumannii* resistance to macrophages and serum-mediated killing and that capsule production might be induced by the presence of serum.

Hydrophilic *A. baumannii* IC II Strains Tend to Exhibit Enhanced Virulence in *C. elegans* and Murine Infection Model Compared With Hydrophobic IC II Strains

Next, we investigated virulence of *A. baumannii* using nematodes fertility assay and mouse sepsis infection model. First, to assess the virulence in *C. elegans*, we have selected a set of IC II strains, displaying different properties of surface hydrophobicity, resistance to desiccation and ability to adhere to the lung epithelial cells. The strains II-b and II-a are hydrophobic, show poor resistance to desiccation and have a weak capacity to adhere to the epithelial cells, whereas strains II-f, II-e, and II-h are hydrophilic, highly resistant to desiccation and show cell adherence ability (**Supplementary Table S1**). All selected strains except II-h express CPS under laboratory growth conditions (**Figure 2**).

Caenorhabditis elegans fertility assay demonstrated that a total number of progeny after 3 days upon infection was approximately two times lower in nematodes infected with the hydrophilic strains II-f, II-e, and II-h compared to those infected with the hydrophobic strains II-a and II-b and the difference was statistically significant ($p < 0.01$) (**Figure 7**). Moreover, other hydrophilic strains of IC II lineage also displayed a trend of increased virulence in nematodes compared with the hydrophobic strains of the same lineage (**Supplementary Figure S5**). Notably, strain II-h, being capsule-deficient under laboratory conditions, showed similar virulence features in *C. elegans* compared with capsule-producing strains II-e and II-f.

Next, we used an experimental murine model to assess the ability of selected IC II strains to establish a systemic infection. Representative IC II strain II-a with hydrophobic cell surface properties, II-f strain with hydrophilic character, and hydrophilic II-h strain, albeit displaying capsule-non-producing phenotype were used for infection. The mice survival rates were monitored for several days. The mice infected with II-f strain showed twofold higher mortality rate compare to those infected with II-a and II-h strains (80% vs. 40%) (**Figure 8A**). Spleens from the mice, infected with the II-f strain and examined *post-mortem* had 10 times higher bacterial load compared with those from the mice infected with II-a strain, and over 30 times higher load compared with those infected with capsule-deficient II-h strain (**Figure 8B**). Furthermore, the higher yield of bacteria was detected in spleen from the mouse, which survived after 48 h upon inoculation with II-f strain, while in the case of II-a strain the load of survived bacteria was mainly lower and only a few II-h colonies were observed after mice sacrifice and spleens examination (**Figure 8C**).

Therefore, the low cell surface hydrophobicity clearly impacts virulence of *A. baumannii*, although our study predicts that the capsule's presence is critically needed to establish an infection in vertebrate host, but not in *C. elegans* model.

Variations in Cell Surface Hydrophobicity Among *A. baumannii* IC II Strains Are Not Dependent on the Types of Capsule or Lipooligosaccharide Synthesis Loci

Observations that the low cell surface hydrophobicity of *A. baumannii* IC II strains correlates with their enhanced virulence *in vivo* prompted as to investigate the cell surface

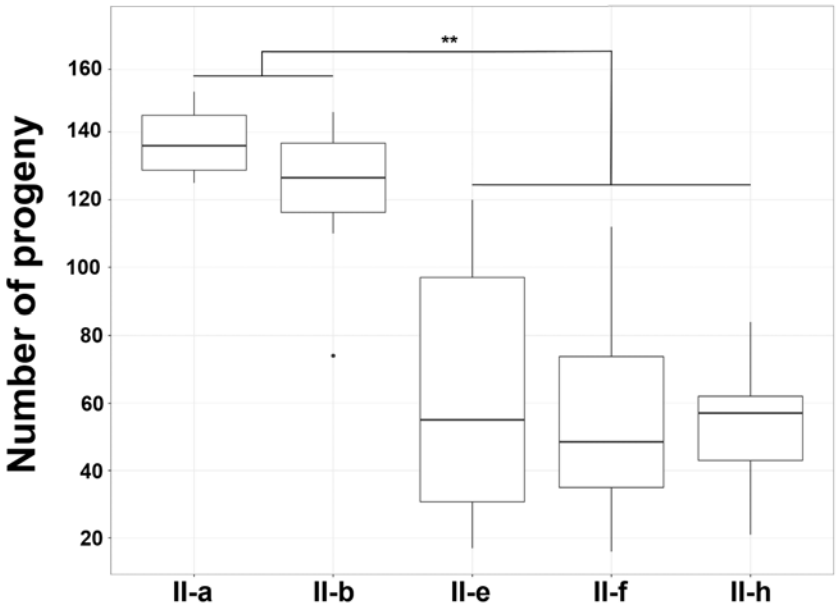

FIGURE 7 | *Caenorhabditis elegans* fertility assay. Box plot of the count of nematodes progeny after 3 days of incubation in the presence of *A. baumannii* IC II lineage strains exhibiting different cell surface hydrophobicity. Data are from three independent experiments, three to four plates were used in the each experiment. Black lines represent medians and whiskers – minimum to maximum values, significance was assessed by ANOVA. $^{**}p < 0.01$.

determinants that might be responsible for this phenotype. Earlier, it was demonstrated that changes in the structure of cell surface components, such as lipopolisaccharides, could alter bacterial surface hydrophobicity and biofilm formation in *E. coli* (Nakao et al., 2012).

First, we were interested whether IC II strains displaying different degree of cell surface hydrophobicity posses differences in CPS synthesis locus (K locus) organization, as *A. baumannii* is known to produce a high diversity of CPS, which impacts cell surface properties (Traub and Bauer, 2000). For this purpose, we intended to determine the variants of Wzy polymerase gene present in the K locus according to the *A. baumannii* K locus typing scheme developed by Hu et al. (2013). Wzy polymerase is responsible for polymerization of oligosaccharide units into CPS (Kenyon and Hall, 2013). Hu et al. (2013) have demonstrated a strong correlation between the *wzy* gene variant and organization of CPS synthesis gene cluster. We have chosen the IC II strain II-f for the amplification of approximately 8 kb in length K locus region with primer pair gnaaF/galuR (**Supplementary Table S2**). Sequencing of the resulting amplicon revealed the presence of PSgc12 gene cluster with the *wzy11* gene variant, what is in accordance with the typing scheme proposed. The *wzy11* gene variant so far was found to occur in *A. baumannii* possessing KL2 capsule type (Kenyon et al., 2014a). To identify whether *wzy11* gene variant was present in other IC II strains, we have designed *wzy11*-specific primers wzy11F/wzy11R and used them for PCR with the DNA of IC II strains. All tested IC II strains, except II-a2, II-g and II-h, yielded amplicons specific to *wzy11* gene variant suggesting the presence of the same type of CPS synthesis locus in the majority of IC II strains regardless their hydrophobic features. We have designed additional primer pairs targeting other possible *wzy* gene variants and probed them with the rest of the strains (**Supplementary Table S2**). All IC I strains, except I-e and I-f, coded for the *wzy* variant found in *A. baumannii* with the KL40 capsule type. The I-e and I-f strains carried *wzy* allele, present in strains assigned to KL1 type, whereas the IC II II-a2 strain had *wzy* gene variant found in *A. baumannii* strain with the KL27 capsule type. The designed primers were not able to target the *wzy* gene in IC I strain IV and IC II strains II-g and II-h.

Next, we identified the type of LOS by using typing scheme developed by Kenyon et al. (2014b). Typing scheme is based on the determination of a locus, responsible for the synthesis of the OC component of the LOS in *A. baumannii*. The strains of IC I and IC II lineages have been previously shown to display variations in the OC component (Kenyon et al., 2014b). The PCR with the RH1704/RH1705 primer pair (**Supplementary Table S2**) and the DNA obtained from *A. baumannii* IC II strains resulted in an amplicon corresponding to the *gtrOC4-gtrOC5* region in the OC gene cluster and thereby confirming the OCL1 variant for all tested strains.

Therefore, typing of *A. baumannii* genome regions responsible for the synthesis of polysaccharides suggest that neither capsule synthesis locus type, nor OC locus type of LOS are responsible for variations in the surface hydrophobicity displayed by the *A. baumannii* IC II strains.

DISCUSSION

In this study we have performed a comprehensive investigation of the cell surface-related phenotypic properties of *A. baumannii* clinical strains belonging to the international clonal lineages IC I

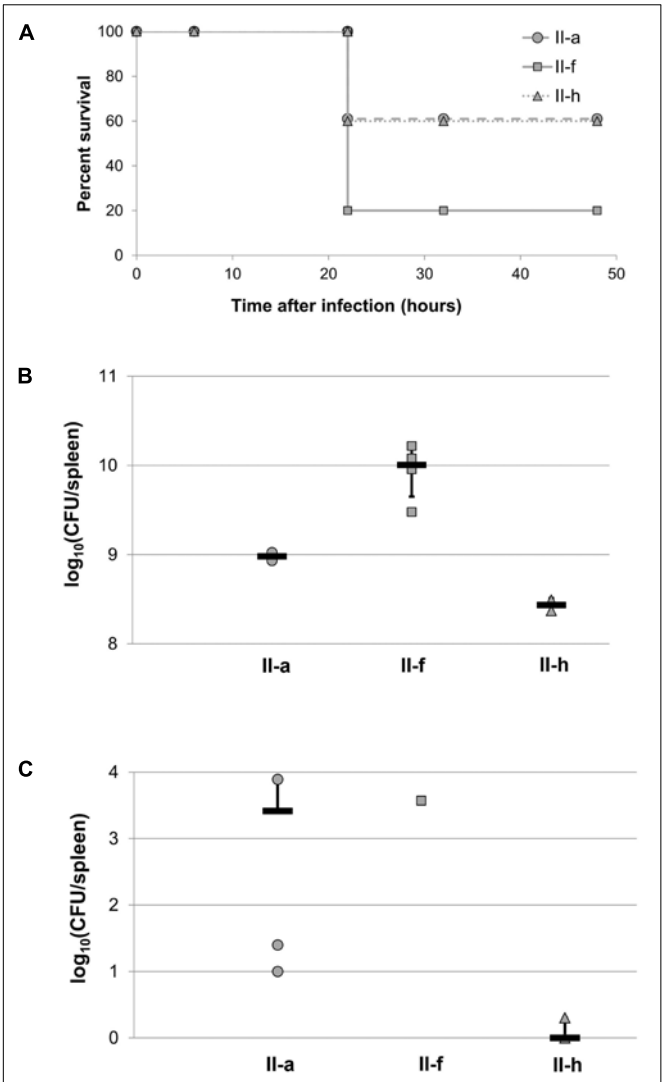

FIGURE 8 | *Acinetobacter baumannii* sepsis infection in BALB/c mice. Mice (n = 5 per group) were intraperitoneally infected with 1.25×10^6 CFU of II-a, 5.5×10^6 CFU of II-f and 2.25×10^6 CFU of II-h *A. baumannii* IC II lineage strains. **(A)** Survival of mice; **(B)** bacterial load, estimated in the spleen *post-mortem*; **(C)** bacterial load in the spleen after 48 h of infection. Survived mice were sacrificed and spleens were tested for bacterial loads. Black lines in **(B,C)** represent an average, error bars represent standard deviations.

and IC II. We aimed to identify their relations with the virulence, since specific clone-associated features are largely obscure.

In accordance with other studies (Eijkelkamp et al., 2011), our results show that swarming motility is rare phenotype, as we have identified only three strains with this type of motility. While swarming motility in the most of bacteria is flagella-depended, bioinformatic analysis did not indicate any flagellar genes in *A. baumanni* genomes (Clemmer et al., 2011). However it was observed that some *A. baumannii* strains indeed are able to express swarming motility on the solid surfaces (Clemmer et al., 2011; Eijkelkamp et al., 2011; McQueary et al., 2012). It was suggested that swarming motility in *A. baumannii* is rather flagella-independent, multifactorial and complex process (Harding et al., 2013).

Our results indicate that twitching motility and pellicle formation are features strongly associated with *A. baumannii* IC I lineage strains. These data are in the line with the previous observations of Eijkelkamp et al. (2011) from the analysis of Australian *A. baumannii* clinical isolates, where all IC I clone and only a few IC II clone members showed twitching motility. *A. baumannii* twitching motility is flagella-independent phenomenon and has been shown to require type IV pili (Harding et al., 2013). Comparative genomic studies demonstrated that IC I and IC II isolates carry the same sets of essential genes responsible for type IV pili biogenesis, although possess lineage-specific differences in a soluble domain of the major pili subunit PilA (Piepenbrink et al., 2016) hypothesizing that it might render differences in twitching motility observed between the lineages. Moreover, the IC II genomes, in contrast to the IC I, carry the *tfpO* gene, coding for a pilin glycosylating *O*-oligosaccharyltransferase (*O*-OTase) in addition to PglL-like *O*-OTase present in all *Acinetobacter* species (Harding et al., 2015). Strikingly, the possession of *tfpO* gene correlated with the presence of the C-terminal serine residue in the PilA protein (Harding et al., 2015), suggesting the C-terminal glycosylation event, which may affect pilin-associated phenotypes. However, our generated *A. baumannii tfpO* gene deletion in IC II strain II-d had no effect on the twitching motility (data not shown) indicating that other components are responsible for this phenotype. This observation is supported by the analysis of C-terminal glycosylation-deficient PilA S136A mutant of *A. nosocomialis*, which showed no pili-associated phenotypic changes compared with the parent strain (Piepenbrink et al., 2016).

Similarly to other Gram-negative pathogens, *A. baumannii* CPS and lipopolysaccharide (LPS), the latter thought to be deficient in extracellular polysaccharide portion in most *A. baumannii* strains (Harding et al., 2015) and called LOS, are essential virulence factors protecting from the host complement system (Russo et al., 2010) and mediating inflammatory responses (Moffatt et al., 2013). Our data show that nearly all clinical *A. baumannii* strains produce capsule, although IC I and IC II strains display lineage-specific CPS profile. According to the previous reports, *A. baumannii* genomic K locus, responsible for the CPS synthesis and export, is highly diverse (Hu et al., 2013; Kenyon and Hall, 2013). Strikingly, all our examined capsule-producing IC I strains synthesized polysaccharides of variable-molecular-mass, whereas IC II strains yielded exclusively high-molecular-mass CPS. The data on *A. baumannii* CPS profiling are in scarce. According to the recent reports, *A. baumannii* non-clonal strain ATCC 17978 produced high-molecular-mass CPS (Lees-Miller et al., 2013; Geisinger and Isberg, 2015), whereas IC I strain AB307-0294 yielded CPS of variable-molecular-mass (Russo et al., 2016). Interestingly, Dams-Kozlowska and Kaplan (2007) found that the length of the polysaccharide produced by *Acinetobacter venetianus* strain Rag-1 depends on the introduction of the point mutations into the proline-glycine rich region of the Wzc protein, a member of Wzy-dependent polysaccharide production

pathway (Hu et al., 2013). The Wzc tyrosine kinase belongs to the group of polysaccharide co-polymerases (PCPs), proposed to control the capsule polysaccharide length in Gram-negative bacteria (Kalynych et al., 2012). Wzc activity has been shown to be required for *A. baumannii* CPS assembly, since introduced mutations in the kinase Walker motifs and phosphorylation site resulted in the changes of CPS profile (Geisinger and Isberg, 2015). Recently, Harding et al. (2018a) found that introduction of a non-native ortholog of phosphoglycosyltransferase PglC resulted in a change of capsule serotype and CPS profile of *A. baumannii*, indicating that genetic alterations in other capsule-related genes might be involved in the capsule variations. We have performed phylogenetic analysis of Wzc and PglC proteins of *A. baumannii* IC I and IC II strains from the genomes available in the databases (**Supplementary Figure S6**). The sequences of Wzc and PglC proteins of non-clonal *A. baumannii* strain ATCC 17978 and *A. venetianus* strain Rag-1, for which CPS profiles have been determined, were also included. The IC II strains and non-clonal ATCC 17978 strain formed a separate cluster regarding both proteins, whereas *A. venetianus* strain Rag-1 tend to group with the IC I cluster. The observed clustering correlated with identified CSP profiles of IC II and IC I strains with the same capsule type as aligned *A. baumannii* strains from the databases as well as with reported CSP profiles for ATCC 17978 and *A. venetianus* strain Rag-1. This indicates that distinct CPS profiles could possibly be triggered by the genetic differences in capsule-related genes between two clones.

All our analyzed IC I and IC II strains showed low macrophage-mediated phagocytosis rate and high resistance to FBS, except for the capsule-deficient strains II-dB and II-h, thereby confirming the crucial role of capsule (Russo et al., 2010) in the evasion of host immunity components. Moreover, induction of capsule synthesis, demonstrated by strain II-h after prolonged incubation in the presence of FBS, indicates that capsule production might display a phase variation pattern, recently shown for capsule expression in *A. baumannii* strain AB5075 (Chin et al., 2018). Previously, *A. baumannii* CPS expression was also demonstrated to be depended on the presence of antibiotics, where hyperproduction of capsular exopolysaccharide was reversible and non-mutational (Geisinger and Isberg, 2015). Our results demonstrate that capsule-deficient strain II-h exhibited similar virulence in *C. elegans* infection model as did capsule-producing hydrophilic strains, while in a murine model its virulence was suppressed. The presence of the capsule might be crucial at the beginning of infection in vertebrates, when phagocytic cells and active complement proteins neutralize bacteria. The defense system in nematodes is based mostly on the antimicrobial peptides and lectins (Ermolaeva and Schumacher, 2014), there is no evidence for the presence of functional complement proteins or phagocytic cells. Russo et al. (2010) showed that capsule-negative *A. baumannii* mutant was unable to survive in the rat soft tissue infection model during the first hours after injection. However, in our study II-h strain was able to cause the death in murine model, possibly indicating ability to induce capsule production, reach infectious dose and expand the contagion.

Another feature that clearly distinguishes strains of IC I and IC II lineages is the inability of IC II strains to form pellicle in contrast to the most of IC I lineage members. Pellicle represents a biofilm formed by bacteria at the air–liquid interface (Armitano et al., 2014). It is composed of cells surrounded by complex extracellular matrix containing exopolysaccharides, LOSs, lipids, DNA and protein components (Nait Chabane et al., 2014). The plastic and metal surfaces might serve as a basis for the attachment of the formed pellicle (Nait Chabane et al., 2014; Giles et al., 2015), therefore medical devices containing the liquid represent niches for pellicle formation and *A. baumannii* colonization. The previous studies reported increased expression of virulence factors such as phospholipases, adhesion factors, type VI secretion system, siderophore iron uptake systems implies the role of *A. baumannii* pellicle in the virulence (Marti et al., 2011; Kentache et al., 2017). There is a controversy regarding observations on the impact of *A. baumannii* cell surface hydrophobicity on the capacity to form pellicle. While Nait Chabane et al. (2014) and Giles et al. (2015) observed a strong link between hydrophobicity and pellicle formation, McQueary and Actis (2011) found no correlation between these phenotypes. Our data show that while hydrophobicity might present a favorable property for pellicle formation, other cellular features should be involved, since none of the IC II strains with hydrophobic character demonstrated pellicle phenotype. However, hydrophobicity was clearly associated with the *A. baumannii* capacity to form conventional biofilm and adhere to the abiotic (plastic) surface, thereby suggesting that different surface properties underlie pellicle and conventional biofilm phenotypes. The recent structural analysis of principal adhesin of Csu pili, involved in *A. baumannii* biofilm formation, revealed three hydrophobic finger-like loops, found to mediate attachment to the hydrophobic surface (Pakharukova et al., 2018). Whether Csu adhesin plays a similar role in the formation of the pellicle, shown to contain the *A. bumannii* pili subunits in the matrix (Nait Chabane et al., 2014), remains to be elucidated.

Whereas our study confirms a link between *A. baumannii* hydrophobicity and biofilm formation as well as adherence to the abiotic surface, it demonstrates that hydrophobic phenotype renders *A. baumannii* to become more sensitive to desiccation and weakens its ability to adhere to the epithelial cells. Moreover, we observed that *A. baumannii* IC II strains, which displayed hydrophilic character, were more virulent compared to their hydrophobic counterparts using both *C. elegans* and murine infection models. This is in accordance with the observations made by Kempf et al. (2012) from the analysis of two *A. baumannii* strains recovered from the same patient, where a strain with hydrophobic features and biofilm forming ability did not show increased virulence compared to the strain with hydrophilic properties. Hu et al. (2016) provided data showing that biofilm forming phenotype of IC II strains did not correlated with their epidemicity suggesting that other virulence factors contribute to the success of this global clone. Nevertheless, most of our tested *A. baumannii*, including outbreak strains formed biofilm, whereas IC II strains with hydrophilic character, increased desiccation resistance and adherence to the epithelium cells, were mostly sporadic. However, the listed features of

hydrophilic *A. baumannii* strains might be superior at certain conditions such as long periods dryness or at the onset of host colonization and such strains might pose a high infection risk. The origin of significant diversification of cell surface hydrophobicity phenotype among closely related IC II strains, observed in this study, is of particular interest, since neither CPS synthesis locus type, nor OC locus type were found to be responsible for these phenotypic variations. It is possible that unknown point mutations or genetic rearrangements in so far identified types of K locus or OC locus could impair cell surface hydrophobicity, therefore comprehensive studies based on the deep-sequencing would be required. Moreover, changes in CPS or LOS resulting from the modifications could also play a role in cell surface hydrophobicity. It was observed, that phosphoethanolamine modification of lipid A reduces the fitness and decreases the biofilm formation in *A. baumannii* (Pelletier et al., 2013; Da Silva and Domingues, 2017). Strains with this type of lipid A modification, tend to demonstrate increased resistance to colistin. However, all our tested IC II isolates were found to be colistin-sensitive according to the analysis of minimal inhibitory concentration (MIC) (**Supplementary Figure S3**), suggesting that this modification is not responsible for the phenotypic differences. Possibly, unknown changes in CPS or LOS could play a role in cell surface hydrophobicity between hydrophilic IC II strains.

Tipton et al. (2015) have recently identified *A. baumannii* AB5075 strain generating two subpopulations with different virulence features. Virulent cells possessed a thicker capsule, showed increased resistance to hospital disinfectants and desiccation, reduced biofilm formation and were more virulent in animal models compared to the avirulent cells (Tipton et al., 2015; Chin et al., 2018). Chin et al. (2018) have shown the involvement of transcriptional regulator TetR in the phenotypic switch in *A. baumannii* AB5075 strain. Interestingly, the observed phenotypes for virulent subpopulation of *A. baumannii* AB5075 closely resemble the features of our investigated hydrophilic IC II strains, which were more virulent compared to the hydrophobic strains, therefore we have tested the *tetR* gene expression by qPCR in the representative strains II-a and II-f. However, no differences in gene expression were observed (data not shown), indicating additional adaptation pathways.

CONCLUSION

Our study revealed a set of lineage-specific cell-surface-associated features of clinical *A. baumannii* strains belonging to the most spread clonal lineages, suggesting distinct adaptation strategies. Moreover, a significant diversification of cell surface hydrophobicity-related phenotypes and their association with the virulence at the intra-lineage level was demonstrated for strains belonging to international clone lineage II thereby implying the high pathogenicity potential of this expanding clone. Indeed several countries reported the replacement of IC I *A. baumannii* isolates by IC II (Kim et al., 2017; Pournaras et al., 2017). The observed variations in an armory of virulence-associated features among IC II strains might favor a particular life-style within the clinical environment resulting in the different spreading routes and interaction with the host.

AUTHOR CONTRIBUTIONS

JS and RK designed the experiments. JS, RK, CP, SK, and JA performed the experiments. JS and ES analyzed the data and wrote the manuscript. All of the authors critically reviewed the manuscript and approved the final version.

ACKNOWLEDGMENTS

We thank I. Rinkūnaitė for excellent technical assistance and Dr. M. Rudgalvytė for sharing *C. elegans*.

SUPPLEMENTARY MATERIAL

The Supplementary Material for this article can be found online at: https://www.frontiersin.org/articles/10.3389/fmicb.2018.03116/full#supplementary-material

REFERENCES

Ali, H. M., Salem, M. Z. M., El-Shikh, M. S., Megeed, A. A., Alogaibi, Y. A., and Talea, I. A. (2017). Investigation of the virulence factors and molecular characterization of the clonal relations of multidrug-resistant *Acinetobacter baumannii* isolates. *J. AOAC Int.* 100, 152–158. doi: 10.5740/jaoacint.16-0139

Antunes, L. C., Visca, P., and Towner, K. J. (2014). *Acinetobacter baumannii*: evolution of a global pathogen. *Pathog. Dis.* 71, 292–301. doi: 10.1111/2049-632X.12125

Armitano, J., Méjean, V., and Jourlin-Castelli, C. (2014). Gram-negative bacteria can also form pellicles. *Environ. Microbiol. Rep.* 6, 534–544. doi: 10.1111/1758-2229.12171

Chiang, S. R., Jung, F., Tang, H. J., Chen, C. H., Chen, C. C., Chou, H. Y., et al. (2017). Desiccation and ethanol resistances of multidrug resistant *Acinetobacter baumannii* embedded in biofilm: the favorable antiseptic efficacy of combination chlorhexidine gluconate and ethanol. *J. Microbiol. Immunol. Infect.* doi: 10.1016/j.jmii.2017.02.003 [Epub ahead of print].

Chin, C. Y., Tipton, K. A., Farokhyfar, M., Burd, E. M., Weiss, D. S., and Rather, P. N. (2018). A high-frequency phenotypic switch links bacterial virulence and environmental survival in *Acinetobacter baumannii*. *Nat. Microbiol.* 3, 563–569. doi: 10.1038/s41564-018-0151-5

Clemmer, K. M., Bonomo, R. A., and Rather, P. N. (2011). Genetic analysis of surface motility in *Acinetobacter baumannii*. *Microbiology* 157, 2534–2544. doi: 10.1099/mic.0.049791-0

Da Silva, G. J., and Domingues, S. (2017). Interplay between colistin resistance, virulence and fitness in *Acinetobacter baumannii*. *Antibiotics* 6:E28. doi: 10.3390/antibiotics6040028

Dahdouh, E., Gómez-Gil, R., Pacho, S., Mingorance, J., Daoud, Z., and Suárez, M. (2017). Clonality, virulence determinants, and profiles of resistance of clinical *Acinetobacter baumannii* isolates obtained from a Spanish hospital. *PLoS One* 12:e0176824. doi: 10.1371/journal.pone.0176824

Dams-Kozlowska, H., and Kaplan, D. L. (2007). Protein engineering of wzc to generate new emulsan analogs. *Appl. Environ. Microbiol.* 73, 4020–4028. doi: 10.1128/AEM.00401-07

Di Nocera, P. P., Rocco, F., Giannouli, M., Triassi, M., and Zarrilli, R. (2011). Genome organization of epidemic *Acinetobacter baumannii* strains. *BMC Microbiol.* 11:224. doi: 10.1186/1471-2180-11-224

Eijkelkamp, B. A., Stroeher, U. H., Hassan, K. A., Papadimitrious, M. S., Paulsen, I. T., and Brown, M. H. (2011). Adherence and motility characteristics of clinical *Acinetobacter baumannii* isolates. *FEMS Microbiol. Lett.* 323, 44–51. doi: 10.1111/j.1574-6968.2011.02362.x

Eijkelkamp, B. A., Stroeher, U. H., Hassan, K. A., Paulsen, I. T., and Brown, M. H. (2014). Comparative analysis of surface-exposed virulence factors of *Acinetobacter baumannii*. *BMC Genomics* 15:1020. doi: 10.1186/1471-2164-15-1020

Eliopoulos, G. M., Maragakis, L. L., and Perl, T. M. (2008). *Acinetobacter baumannii*: epidemiology, antimicrobial resistance, and treatment options. *Clin. Infect. Dis.* 46, 1254–1263. doi: 10.1086/529198

Ermolaeva, M. A., and Schumacher, B. (2014). Insights from the worm: the *C. elegans* model for innate immunity. *Semin. Immunol.* 26, 303–309. doi: 10.1016/j.smim.2014.04.005

Geisinger, E., and Isberg, R. R. (2015). Antibiotic modulation of capsular exopolysaccharide and virulence in *Acinetobacter baumannii*. *PLoS Pathog.* 11:e1004691. doi: 10.1371/journal.ppat.1004691

Giles, S. K., Stroeher, U. H., Eijkelkamp, B. A., and Brown, M. H. (2015). Identification of genes essential for pellicle formation in *Acinetobacter baumannii*. *BMC Microbiol.* 15:116. doi: 10.1186/s12866-015-0440-6

Harding, C. M., Haurat, M. F., Vinogradov, E., and Feldman, M. F. (2018a). Distinct amino acid residues confer one of three UDP-sugar substrate specificities in *Acinetobacter baumannii* PglC phosphoglycosyltransferases. *Glycobiology* 28, 522–533. doi: 10.1093/glycob/cwy037

Harding, C. M., Hennon, S. W., and Feldman, M. F. (2018b). Uncovering the mechanisms of *Acinetobacter baumannii* virulence. *Nat. Rev. Microbiol.* 16, 91–102. doi: 10.1038/nrmicro.2017.148

Harding, C. M., Nasr, M. A., Kinsella, R. L., Scott, N. E., Foster, L. J., Weber, B. S., et al. (2015). Acinetobacter strains carry two functional oligosaccharyltransferases, one devoted exclusively to type IV pilin, and the other one dedicated to O-glycosylation of multiple proteins. *Mol. Microbiol.* 96, 1023–1041. doi: 10.1111/mmi.12986

Harding, C. M., Tracy, E. N., Carruthers, M. D., Rather, P. N., Actis, L. A., and Munson, R. S. Jr. (2013). *Acinetobacter baumannii* strain M2 produces type IV pili which play a role in natural transformation and twitching motility but not surface-associated motility. *mBio* 4:e00360-13. doi: 10.1128/mBio.00360-13

Hölscher, T., Bartels, B., Lin, Y. C., Gallegos-Monterrosa, R., Price-Whelan, A., Kolter, R., et al. (2015). Motility, chemotaxis and aerotaxis contribute to competitiveness during bacterial pellicle biofilm development. *J. Mol. Biol.* 427, 3695–3708. doi: 10.1016/j.jmb.2015.06.014

Holt, K., Kenyon, J. J., Hamidian, M., Scultz, M. B., Pickard, D. J., Dougan, G., et al. (2016). Five decades of genome evolution in the globally distributed, extensively antibiotic-resistant *Acinetobacter baumannii* global clone 1. *Open Microbiol.* 2:e000052. doi: 10.1099/mgen.0.000052

Hu, D., Liu, B., Dijkshoorn, L., Wang, L., and Reeves, P. R. (2013). Diversity in the major polysaccharide antigen of *Acinetobacter baumannii* assessed by DNA sequencing, and development of a molecular serotyping scheme. *PLoS One* 8:e70329. doi: 10.1371/journal.pone.0070329

Hu, Y., He, L., Tao, X., Meng, F., and Zhang, J. (2016). Biofilm may not be Necessary for the epidemic Spread of *Acinetobacter baumannii*. *Sci. Rep.* 6:32066. doi: 10.1038/srep320

Huang, W., Yao, Y., Long, Q., Yang, X., Sun, W., Liu, C., et al. (2014). Immunization against multidrug-resistant *Acinetobacter baumannii* effectively protects mice in both pneumonia and sepsis models. *PLoS One* 9:e100727. doi: 10.1371/journal.pone.0100727

Kalynych, S., Valvano, M. A., and Cygler, M. (2012). Polysaccharide co-polymerases: the enigmatic conductors of the O-antigen assembly orchestra. *Protein Eng. Des. Sel.* 25, 797–802. doi: 10.1093/protein/gzs075

Karah, N., Sundsfjord, A., Towner, K., and Samuelsen, Ö. (2012). Insights into the global molecular epidemiology of carbapenem non-susceptible clones of *Acinetobacter baumannii*. *Drug Resist. Updat.* 15, 237–247. doi: 10.1016/j.drup.2012.06.001

Kempf, M., Eveillard, M., Deshayes, C., Ghamrawi, S., Lefrancois, S., Bastiat, G., et al. (2012). Cell surface properties of two differently virulent strains of *Acinetobacter baumannii* isolated from a patient. *Can. J. Micorbiol.* 58, 311–317. doi: 10.1139/w11-131

Kentache, T., Ben Abdelkrim, A., Jouenne, T., Dé, E., and Hardouin, J. (2017). Global dynamic proteome study of a pellicle-forming *Acinetobacter baumannii* Strain. *Mol. Cell. Proteomics* 16, 100–112. doi: 10.1074/mcp.M116.061044

Kenyon, J. J., and Hall, R. M. (2013). Variation in the complex carbohydrate biosynthesis loci of *Acinetobacter baumannii* genomes. *PLoS One* 8:e62160. doi: 10.1371/journal.pone.0062160

Kenyon, J. J., Marzaioli, A. M., Hall, R. M., and De Castro, C. (2014a). Structure of the K2 capsule associated with the KL2 gene cluster of *Acinetobacter baumannii*. *Glycobiology* 24, 554–563. doi: 10.1093/glycob/cwu024

Kenyon, J. J., Nigro, S. J., and Hall, R. M. (2014b). Variation in the OC locus of *acinetobacter baumannii* genomes predicts extensive structural diversity in the lipooligosaccharide. *PLoS One* 9:e107833. doi: 10.1371/journal.pone.0107833

Kim, D. H., Jung, S. I., Kwon, K. T., and Ko, K. S. (2017). Occurrence of diverse AbGRI1-type genomic islands in *Acinetobacter baumannii* global clone 2 isolates from South Korea. *Antimicrob. Agents Chemother.* 72, 2944–2947. doi: 10.1128/AAC.01972-16

Krasowska, A., and Sigler, K. (2014). How microorganisms use hydrophobicity and what does this mean for human needs? *Front. Cell. Infect. Microbiol.* 4:112. doi: 10.3389/fcimb.2014.00112

Lee, C. R., Lee, J. H., Park, M., Park, K. S., Bae, I. K., Kim, Y. B., et al. (2017). Biology of *Acinetobacter baumannii*: pathogenesis, antibiotic resistance mechanisms, and prospective treatment options. *Front. Cell Infect. Microbiol.* 7:55. doi: 10.3389/fcimb.2017.00055

Lees-Miller, R. G., Iwashkiw, J. A., Scott, N. E., Seper, A., Vinogradov, E., Schild, S., et al. (2013). A common pathway for O-linked protein-glycosylation and synthesis of capsule in *Acinetobacter baumannii*. *Mol. Microbiol.* 89, 816–830. doi: 10.1111/mmi.12300

Manchanda, V., Sanchaita, S., and Singh, N. (2010). Multidrug resistant acinetobacter. *J. Glob. Infect. Dis.* 2, 291–304. doi: 10.4103/0974-777X.68538

Marti, S., Chabane, Y. N., Alexandre, S., Coquet, L., Vila, J., Jouenne, T., et al. (2011). Growth of *Acinetobacter baumannii* in pellicle enhanced the expression of potential virulence factors. *PLoS One* 6:e26030. doi: 10.1371/journal.pone.0026030

McConnell, M. J., Actis, L., and Pachón, J. (2013). *Acinetobacter baumannii*: human infections, factors contributing to pathogenesis and animal models. *FEMS Microbiol. Rev.* 37, 130–155. doi: 10.1111/j.1574-6976.2012.00344.x

McQueary, C. N., and Actis, L. A. (2011). *Acinetobacter baumannii* biofilms: variations among strains and correlations with other cell properties. *J. Microbiol.* 49, 243–250. doi: 10.1007/s12275-011-0343-7

McQueary, C. N., Kirkup, B. C., Si, Y., Barlow, M., Actis, L. A., Craft, D. W., et al. (2012). Extracellular stress and lipopolysaccharide modulate *Acinetobacter baumannii* surface-associated motility. *J. Microbiol.* 50, 434–443. doi: 10.1007/s12275-012-1555-1

Mercaldi, M. P., Dams-Kozlowska, H., Panilaitis, B., Joyce, A. P., and Kaplan, D. L. (2008). Discovery of the dual polysaccharide composition of emulsan and the isolation of the emulsion stabilizing component. *Biomacromolecules* 9, 1988–1996. doi: 10.1021/bm800239p

Moffatt, J. H., Harper, M., Mansell, A., Crane, B., Fitzsimons, T. C., Nation, R. L., et al. (2013). Lipopolysaccharide-Deficient *Acinetobacter baumannii* shows altered signaling through host toll-like receptors and increased susceptibility to the host antimicrobial peptide LL-37. *Infect. Immun.* 81, 684–689. doi: 10.1128/IAI.01362-12

Nait Chabane, Y., Marti, S., Rihouey, C., Alexandre, S., Hardouin, J., Lesouhaitier, O., et al. (2014). Characterisation of pellicles formed by *Acinetobacter baumannii* at the air-liquid interface. *PLoS One* 9:e111660. doi: 10.1371/journal.pone.0111660

Nakao, R., Ramstedt, M., Wai, S. N., and Uhlin, B. E. (2012). Enhanced biofilm formation by *Escherichia coli* LPS mutants defective in Hep biosynthesis. *PLoS One* 7:e51241. doi: 10.1371/journal.pone.0051241

Ni, Z., Chen, Y., Ong, E., and He, Y. (2017). Antibiotic resistance determinant-focused *Acinetobacter baumannii* vaccine designed using reverse vaccinology. *Int. J. Mol. Sci.* 18:458. doi: 10.3390/ijms18020458

Nwanyanwu, C. E., and Abu, G. O. (2013). Influence of growth media on hydrophobicity of phenol utilizing bacteria found in petroleum refinery effluent. *Int. Res. J. Biol. Sci.* 2, 6–11.

Oh, M. H., Lee, J. C., Kim, J., Choi, C. H., and Han, K. (2015). Simple method for markerless gene deletion in multidrug-resistant *Acinetobacter baumannii*. *Appl. Environ. Microbiol.* 81, 3357–3368. doi: 10.1128/AEM.03975-14

Pakharukova, N., Tuittila, M., Paavilainen, S., Malmi, H., Parilova, O., Teneberg, S., et al. (2018). Structural basis for *Acinetobacter baumannii* biofilm formation. *Proc. Natl. Acad. Sci. U.S.A.* 115, 5558–5563. doi: 10.1073/pnas.1800961115

Pelletier, M. R., Casella, L. G., Jones, J. W., Adams, M. D., Zurawski, D. V., Hazlett, K. R., et al. (2013). Unique structural modifications are present in the lipopolysaccharide from colistin-resistant strains of *Acinetobacter baumannii*. *Antimicrob. Agents Chemother.* 57, 4831–4840. doi: 10.1128/AAC.00865-13

Piepenbrink, K. H., Lillehoj, E., Harding, C. M., Labonte, J. W., Zuo, X., Rapp, C. A., et al. (2016). Structural Diversity in the Type IV Pili of Multidrug-resistant Acinetobacter. *J. Biol. Chem.* 291, 22924–22935. doi: 10.1074/jbc.M116.751099

Pournaras, S., Dafopoulou, K., Del Franco, M., Zarkotou, O., Dimitroulia, E., Protonotariou, E., et al. (2017). Predominance of international clone 2 OXA-23-producing-*Acinetobacter baumannii* clinical isolates in Greece, 2015: results of a nationwide study. *Int. J. Antimicrob. Agents* 49, 749–753. doi: 10.1016/j.ijantimicag.2017.01.028

Povilonis, J., Seputiene, V., Krasauskas, R., Juskaite, R., Miskinyte, M., Suziedelis, K., et al. (2013). Spread of carbapenem-resistant *Acinetobacter baumannii* carrying a plasmid with two genes encoding OXA-72 carbapenemase in Lithuanian hospitals. *J. Antimicrob. Chemother.* 68, 1000–1006. doi: 10.1093/jac/dks499

R Development Core Team (2008). *R: A Language and Environment for Statistical Computing*. Vienna: R Foundation for Statistical Computing. Available at: http://www.R-project.org

Rumbo, C., Tomás, M., Fernández Moreira, E., Soares, N. C., Carvajal, M., Santillana, E., et al. (2014). The *Acinetobacter baumannii* Omp33-36 porin is a virulence factor that induces apoptosis and modulates autophagy in human cells. *Infect. Immun.* 82, 4666–4680. doi: 10.1128/IAI.02034-14

Russo, T. A., Luke, N. R., Beanan, J. M., Olson, R., Sauberan, S. L., MacDonald, U., et al. (2010). The K1 capsular polysaccharide of *Acinetobacter baumannii* strain 307-0294 is a major virulence factor. *Infect. Immun.* 78, 3993–4000. doi: 10.1128/IAI.00366-10

Russo, T. A., Manohar, A., Beanan, J. M., Olson, R., MacDonald, U., Graham, J., et al. (2016). The response regulator BfmR is a potential drug target for *Acinetobacter baumannii*. *mSphere* 1:e00082-16. doi: 10.1128/mSphere.00082-16

Russotto, V., Cortegiani, A., Raineri, S. M., and Giarratano, A. (2015). Bacterial contamination of inanimate surfaces and equipment in the intensive care unit. *J. Intensive Care* 3:54. doi: 10.1186/s40560-015-0120-5

Smani, Y., McConnell, M. J., and Pachón, J. (2012). Role of fibronectin in the adhesion of *Acinetobacter baumannii* to host cells. *PLoS One* 7:e33073. doi: 10.1371/journal.pone.0033073

Smith, M. G., Gianoulis, T. A., Pukatzki, S., Mekalanos, J. J., Ornston, L. N., Gerstein, M., et al. (2007). New insights into *Acinetobacter baumannii* pathogenesis revealed by high-density pyrosequencing and transposon mutagenesis. *Genes Dev.* 21, 601–614. doi: 10.1101/gad.1510307

Tipton, K. A., Dimitrova, D., and Rather, P. N. (2015). Phase-variable control of multiple phenotypes in *Acinetobacter baumannii* strain AB5075. *J. Bacteriol.* 197, 2593–2599. doi: 10.1128/JB.00188-15

Traub, W. H., and Bauer, D. (2000). Surveillance of nosocomial cross-infections due to three Acinetobacter genospecies (*Acinetobacter baumannii*, genospecies 3 and genospecies 13) during a 10-Year Observation period: serotyping, macrorestriction analysis of Genomic DNA and antibiotic susceptibilities. *Chemotherapy* 46, 282–292. doi: 10.1159/000007300

Weber, B. S., Harding, C. M., and Feldman, M. F. (2016). Pathogenic Acinetobacter: from the Cell Surface to Infinity and Beyond. *J. Bacteriol.* 198, 880–887. doi: 10.1128/JB.00906-15

Zarrilli, R., Pournaras, S., Giannouli, M., and Tsakris, A. (2013). Global evolution of multidrug-resistant *Acinetobacter baumannii* clonal lineages. *Int. J. Antimicrob. Agents* 41, 11–19. doi: 10.1016/j.ijantimicag.2012.09.008

Conflict of Interest Statement: The authors declare that the research was conducted in the absence of any commercial or financial relationships that could be construed as a potential conflict of interest.

frontiers in Microbiology

MINI REVIEW
published: 09 January 2019
doi: 10.3389/fmicb.2018.03301

Diversity and Function of Capsular Polysaccharide in *Acinetobacter baumannii*

*Jennifer K. Singh, Felise G. Adams and Melissa H. Brown**

College of Science and Engineering, Flinders University, Bedford Park, SA, Australia

The Gram-negative opportunistic bacterium *Acinetobacter baumannii* is a significant cause of hospital-borne infections worldwide. Alarmingly, the rapid development of antimicrobial resistance coupled with the remarkable ability of isolates to persist on surfaces for extended periods of time has led to infiltration of *A. baumannii* into our healthcare environments. A major virulence determinant of *A. baumannii* is the presence of a capsule that surrounds the bacterial surface. This capsule is comprised of tightly packed repeating polysaccharide units which forms a barrier around the bacterial cell wall, providing protection from environmental pressures including desiccation and disinfection regimes as well as host immune responses such as serum complement. Additionally, capsule has been shown to confer resistance to a range of clinically relevant antimicrobial compounds. Distressingly, treatment options for *A. baumannii* infections are becoming increasingly limited, and the urgency to develop effective infection control strategies and therapies to combat infections is apparent. An increased understanding of the contribution of capsule to the pathobiology of *A. baumannii* is required to determine its feasibility as a target for new strategies to combat drug resistant infections. Significant variation in capsular polysaccharide structures between *A. baumannii* isolates has been identified, with over 100 distinct capsule types, incorporating a vast variety of sugars. This review examines the studies undertaken to elucidate capsule diversity and advance our understanding of the role of capsule in *A. baumannii* pathogenesis.

Keywords: *Acinetobacter*, capsule, polysaccharide, virulence factor, persistence

OPEN ACCESS

Edited by:
Maria Alejandra Mussi, Consejo Nacional de Investigaciones Científicas y Técnicas (CONICET), Argentina

Reviewed by:
Filipa Grosso, Universidade do Porto, Portugal
Ayush Kumar, University of Manitoba, Canada

****Correspondence:***
Melissa H. Brown
melissa.brown@flinders.edu.au

Specialty section:
This article was submitted to Infectious Diseases, a section of the journal Frontiers in Microbiology

Received: *08 October 2018*
Accepted: *18 December 2018*
Published: *09 January 2019*

Citation:
Singh JK, Adams FG and Brown MH (2019) Diversity and Function of Capsular Polysaccharide in Acinetobacter baumannii. Front. Microbiol. 9:3301. doi: 10.3389/fmicb.2018.03301

INTRODUCTION

Nosocomial infections caused by multidrug resistant *Acinetobacter baumannii* are becoming increasingly common worldwide, especially in the intensive care setting (Wieland et al., 2018). The success of this bacterium is facilitated by its ability to survive in a variety of environments compounded by its rapid ability to acquire multidrug resistance. Surface carbohydrates play key roles in the overall fitness and virulence of *A. baumannii* (Lees-Miller et al., 2013; Geisinger and Isberg, 2015; Weber et al., 2016). *A. baumannii* produces high molecular weight capsular polysaccharide (CPS) which surrounds the outer membrane (**Figure 1**) (Russo et al., 2010).

Comprised of tightly packed repeating oligosaccharide subunits (K units), CPS forms a discrete layer on the bacterial surface providing protection from diverse environmental conditions, assisting in evasion of host immune defenses, and increasing resistance to a number of antimicrobial compounds (Russo et al., 2010; Iwashkiw et al., 2012; Geisinger and Isberg, 2015).

In *A. baumannii*, capsule assembly and export occurs via a Wzy-dependent pathway (Hu et al., 2013; Kenyon and Hall, 2013; Willis and Whitfield, 2013; Woodward and Naismith, 2016) (**Figure 1**). Typically consisting of 4–6 sugars, the K unit is assembled on the lipid carrier molecule undecaprenyl pyrophosphate (Und-P) which provides a scaffold for the growing sugar chain (Whitfield, 2006). The first sugar in the K unit is recruited by an inner membrane (IM)-bound initial transferase (Itr), followed by the sequential addition of sugars to the growing K unit by specific glycosyl transferase (Gtr) enzymes (**Figure 1**) (Woodward and Naismith, 2016). Each K unit is then transferred to the periplasmic side of the IM by the Wzx translocase and polymerized by Wzy, which transfers the growing polysaccharide chain from one Und-P carrier to the next incoming subunit (**Figure 1**) (Collins et al., 2007). After the CPS polymer is synthesized, it is transported to the cell surface via a highly co-ordinated process involving the interaction of three proteins; Wza, Wzb, and Wzc, that comprise the export machinery (**Figure 1**). CPS synthesis represents one arm of a bifurcated pathway, as these K units are also used to decorate certain surface proteins via *O*-linked protein glycosylation (Lees-Miller et al., 2013). In this case, single K units are transferred to recipient proteins by the *O*-oligosaccharyltransferase PglL (**Figure 1**) (Iwashkiw et al., 2012). In *A. baumannii*, protein glycosylation contributes to biofilm formation by enhancing initial attachment and maturation of biofilms, and pathogenicity as demonstrated in a number of animal infection models (Iwashkiw et al., 2012; Scott et al., 2014; Harding et al., 2015). Biofilm is a growth state in which bacterial communities are enclosed within an exopolysaccharide matrix and has been shown to play a significant role in *A. baumannii* persistence and resistance.

Other surface carbohydrates known to influence pathogenicity of *A. baumannii* include lipooligosaccharide (LOS) and the exopolysaccharide poly-β-(1-6)-*N*-acetylglucosamine (PNAG) (Preston et al., 1996; Weber et al., 2016). PNAG forms the cohesive "glue" of biofilms and constitutes a substantial proportion of biofilms (Choi et al., 2009; Longo et al., 2014). Unlike most Gram-negative bacteria, *A. baumannii* does not produce traditional lipopolysaccharide, but instead a similar surface glyco-conjugate, LOS, comprised of a lipid A core that lacks O-antigen (Kenyon and Hall, 2013; Kenyon et al., 2014b). Loss of LOS production in *A. baumannii* decreases stability of the outer membrane leading to reduced fitness (Moffatt et al., 2010; Beceiro et al., 2014).

Although many carbohydrate moieties influence pathogenicity, it can be argued that CPS is a predominant virulence factor of *A. baumannii*. This review aims to consolidate what is known about *A. baumannii* capsule including selected structures, biosynthesis and gene organization, the role of CPS in virulence, and the potential for CPS as a target for future vaccine and drug development.

GENETIC ORGANIZATION OF K LOCI

As the complete genomes of more *A. baumannii* isolates become available, the true diversity of capsule structures present within this bacterium is becoming apparent. To date, over 100 unique capsule loci (KL) have been identified in *A. baumannii* (**Figure 2A**) (Shashkov et al., 2017). These regions typically range from 20 to 35 kb in size. Analysis of the genes directing CPS synthesis in ten complete *A. baumannii* genomes originally resulted in the designation of nine capsule types, KL1–KL9, which became the basis for a universal typing scheme for these loci (Kenyon and Hall, 2013). This scheme has subsequently expanded to accommodate the identification of new K loci. The chromosomal location of the K locus, between the *fkpA* and *lldP* genes, is highly conserved between *A. baumannii* strains and contains those genes required for the biosynthesis and export specific to each CPS type (**Figure 2**) (Hu et al., 2013; Kenyon and Hall, 2013). An exception to this rule are *A. baumannii* strains possessing KL19 and KL39 regions, where the gene encoding the Wzy polymerase, *wzy*, is found on a small genetic island elsewhere on the chromosome (Kenyon et al., 2016a). Additionally, the genes required for some of the common sugars seen in CPS are found elsewhere. All K loci show a similar genetic configuration, a highly variable cluster of synthesis and transferase genes required for the biosynthesis of unique KL-type complex sugars, flanked on one side by the highly conserved CPS export genes, and on the other side by a set of genes encoding conserved simple sugars and precursors (**Figure 2A**). The *wzx* and *wzy* genes required for repeat-unit processing are highly variable between K loci (**Figure 2A**, light blue), indicating specificity for particular K unit structures and, in general, the order of *gtr* determinants, encoding specific glycosyltransferases within the KL regions, inversely corresponds with the order of action.

The variable region of some KL gene clusters, such as KL37 and KL14, lack genes for complex sugar synthesis, as they only contain simple sugars in their K units (Arbatsky et al., 2015; Kenyon et al., 2015). Also adding to their diversity, several KL regions contain redundant genes which are not required for the synthesis of the final K unit. For example KL8 and KL9 contain two *itr* genes (Kenyon and Hall, 2013) and KL37 has the *pgt1* phosphoglyceroltransferase, but no corresponding phosphoglycerol residue in the determined structure (Arbatsky et al., 2015). Furthermore, in KL93, two insertion sequence elements (IS*Aba26* and IS*Aba22*) interrupt the *pgt1* determinant (**Figure 2**) (Kasimova et al., 2017). The genes required for specific sugar biosynthesis will not be discussed as these pathways have been covered previously and are beyond the scope of this review (Hu et al., 2013; Kenyon and Hall, 2013). Additionally, other genes located within the KL encode products predicted to be involved in acetylation or acylation modification of specific glycans (**Figure 2A**, pink). Although examination of the K loci can reveal a lot about K unit structures, chemical analysis and

biochemical testing is required to determine exact structures and identify specific linkages between repeat sugars.

CPS STRUCTURES

The earliest studies on CPS serotyping of *A. baumannii* were driven by the need to develop a method to discriminate *A. baumannii* isolates from other *Acinetobacter* species, as phenotypic analysis was burdened with ambiguity and misidentification (Traub, 1989). As described above, there is phenomenal diversity seen in *A. baumannii* CPS biosynthesis gene clusters, which translates into the diversity seen in K unit structure (Hu et al., 2013; Kenyon and Hall, 2013). Collectively, over 40 diverse *A. baumannii* K unit structures have been elucidated thus far using NMR spectroscopy and chemical analysis. K unit structures differ in sugar composition. They may include derivatives of common UDP-linked sugars such as glucose, galactose and glucuronic acid or rare and atypical sugars such as non-2-ulosonic acids. Structures vary in length and may consist of only two residues, as seen for K53 type CPS (Shashkov et al., 2018), or up to five or six monosaccharides, such as that seen in K37 (**Figure 2B**) (Arbatsky et al., 2015). Structures also differ in the linkages both within and between K units resulting in the production of K units that are linear or involve side branches, as seen in K1 and K93, respectively (**Figure 2B**) (Kenyon et al., 2016a; Kasimova et al., 2017). Differences in the location of specific glycosidic bonds and *O*-acetylation patterns of various oligosaccharides within a structure also contribute to K unit diversity.

Variation between K unit structures may be subtle, for example, K12 and K13 differ only by the linkage of two glycans, which requires the use of an alternate Wzy polymerase; accordingly, the K loci of both strains are identical except for the *wzy* gene (**Figure 2**). Alternatively the variation may be striking, such as the incorporation of rare sugars including pseudaminic, legionaminic, or acinetaminic acid derivatives as seen in K2/6, K49, and K12/13 structures, respectively (**Figure 2**) (Kenyon et al., 2014a, 2015; Vinogradov et al., 2014; Kasimova et al., 2018). Interestingly, acinetaminic acid derivatives have only been identified in *A. baumannii* and are found nowhere else in nature (Kenyon et al., 2017). Additionally, some K units incorporate unique derivatives of specific glycans, for instance the pseudaminic acid of K93 is acetylated with a (*R*)-3-hydroxybutanoyl group (Kasimova et al., 2017), whereas in K2 and K6 the pseudaminic acid is non-acetylated (**Figure 2**). Furthermore, the structure of K4 is unique as it contains only aminosugars, D-Qui*p*NAc, and one terminal *N*-acetyl-D-galactosamine (D-Gal*p*NAcA) branch which is capped with a pyruvyl group, a rare motif and the first to be described in *Acinetobacter* (**Figure 2A**, black) (Kenyon et al., 2016b). As the number of K unit structures elucidated increases, so does the confidence to infer the K unit structure from analysis of the biosynthesis clusters positioned in the *A. baumannii* KL. However, although informative, an understanding of the role CPS plays in pathogenesis is important to apply this knowledge to improving outcomes of *A. baumannii* infections.

ROLE IN VIRULENCE, ANTIMICROBIAL RESISTANCE, AND PERSISTENCE

It is beyond doubt that the presence of CPS is essential for *A. baumannii* pathogenicity. Not only is it necessary for evasion of host immune defenses (Russo et al., 2010; Geisinger and Isberg, 2015), but it is important for resistance to antimicrobial compounds and survival in adverse environments (Luke et al., 2010; Russo et al., 2010; Geisinger and Isberg, 2015). CPS mediates immune evasion in many *A. baumannii* strains by limiting interactions between immunogenic surface structures of the bacteria and host defenses (Preston et al., 1996; Wu et al., 2009; Russo et al., 2010; Umland et al., 2012; Lees-Miller et al., 2013; Geisinger and Isberg, 2015; Wang-Lin et al., 2017). The abolition of capsule in multiple different *A. baumannii* strains has shown reduced survival in human serum and ascites fluid, and attenuation in rat and murine infection models (Russo et al., 2010; Umland et al., 2012; Lees-Miller et al., 2013; Sanchez-Larrayoz et al., 2017). Furthermore, the up-regulation of capsule production in the commonly utilized *A. baumannii* strain ATCC 17978 (K3 CPS type) increased serum resistance and virulence in a mouse infection model (Geisinger and Isberg, 2015). Moreover, novel antimicrobial treatments could be developed for specific CPS types, for example those containing pseudaminic acid, as its presence has been correlated with enhanced virulence (Hitchen et al., 2010; Kao et al., 2016).

Besides protection from host defenses, in *A. baumannii* CPS production increases resistance to a range of antimicrobial compounds, including those used for disinfection in clinical

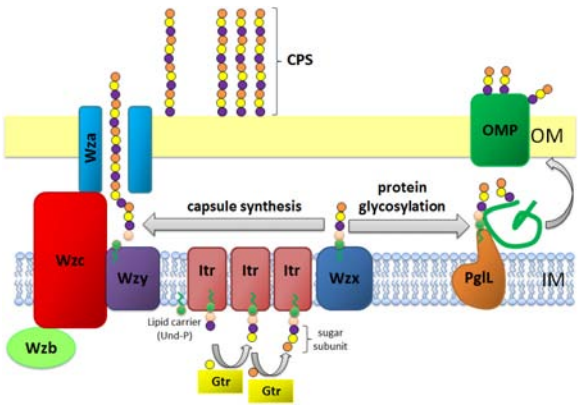

FIGURE 1 | Schematic representation of capsule polysaccharide assembly and export in *A. baumannii*. Synthesis begins with the initial transferase (Itr; maroon) located in the inner membrane (IM) transferring the first sugar of the repeating unit to a lipid carrier (Und-P; green circle). Subsequent sugars are then added to the growing unit by specific glycosyltransferases (Gtr; yellow) on the cytosolic side of the inner membrane. The capsule subunit (K unit) is then transferred to the periplasm via the integral membrane protein Wzx (dark blue). The sugar subunits are polymerized by the Wzy protein (purple) and the Wza/Wzb/Wzc complex (cyan, lime, red) coordinates high level polymerization and export of the growing chain, moving them to the outer membrane (OM). For glycosylation, PglL (orange) links the K units onto selected outer membrane proteins (OMP; dark green).

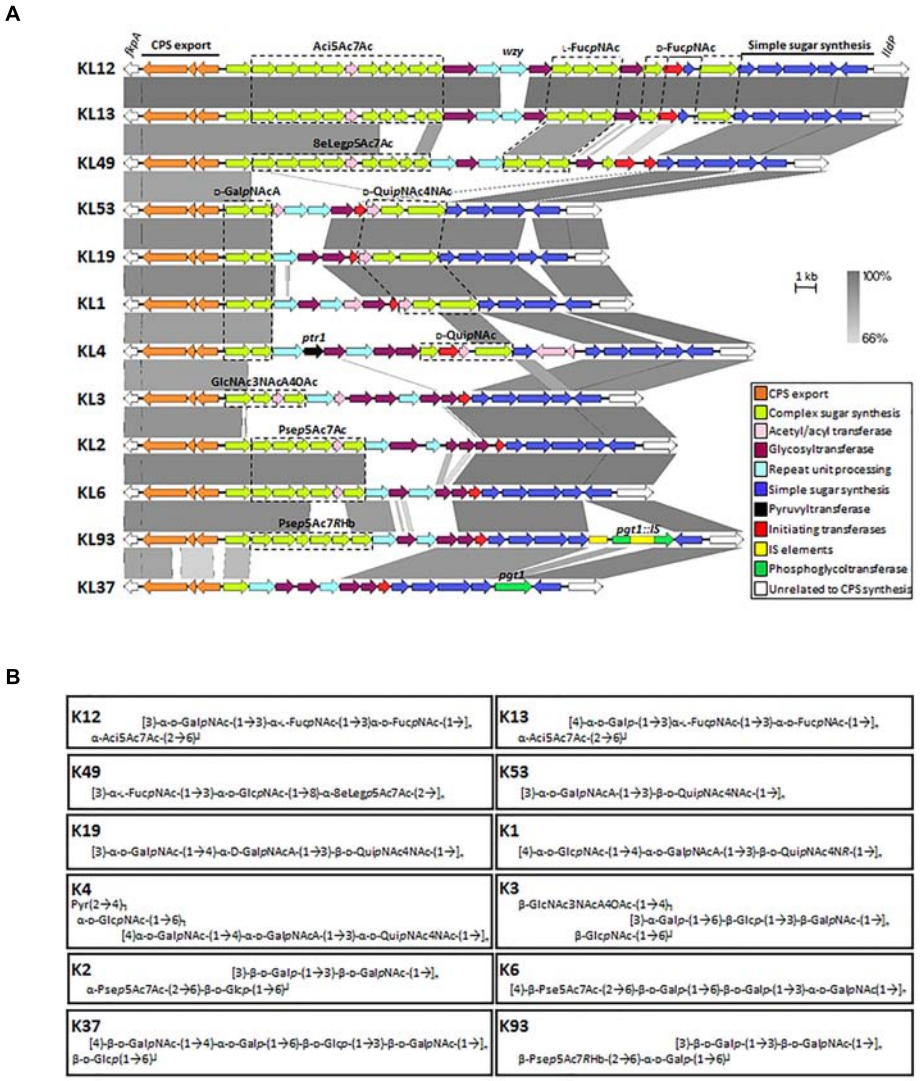

FIGURE 2 | Comparison of representative *A. baumannii* CPS biosynthesis gene clusters and corresponding structures. **(A)** Nucleotide sequences representing different KL regions focusing on genes between *fkpA* and *lldP* were obtained from the NCBI database and aligned using the Easyfig 2.2.2 tool (Sullivan et al., 2011). Genes are depicted by arrows and indicate direction of transcription whilst IS elements are represented by square boxes. Color scheme is based on homology to the putative function of gene products and are outlined in the key. Nucleotide sequence homology shared between regions is represented by color gradient. Figure is drawn to scale. Gene modules for sugar synthesis of interest are indicated, where Aci5Ac7Ac represents genes involved in the production of 5,7-di-*N*-acetylacinetaminic acid; L-Fuc*p*NAc, *N*-acetyl-L-fucosaminic acid; D-Fuc*p*NAc, *N*-acetyl-D-fucosaminic acid; 8eLeg*p*5Ac7Ac, 5,7-diacetamido-3,5,7,9- tetradeoxy-L-*glycero*-D-*galacto*-non-2-ulopyranosonic (di-*N*-acetyl-8-epilegionaminic) acid; D-Gal*p*NAcA, *N*-acetyl-D-galactosaminuronic acid; D-Qui*p*NAc4NAc, 2,4-diacetamido-2,4,6-trideoxy-D-glucopyranose (*N*,*N*'-diacetyl-bacillosamine); D-Qui*p*NAc, *N*-acetyl-D-quinovosaminic acid; GlcNAc3NAcA4OAc, 2,3-diacetamido-2,3-dideoxy -α-D-glucuronic acid with an additional *O*-acetyl group; Pse*p*5Ac7Ac, 5,7-diacetamido-3,5,7,9-tetradeoxy-L-*glycero*-L-*manno*-non-2-ulosonic (pseudaminic) acid and Pse*p*5Ac7*R*Hb, 5-acetamido-3,5,7,9-tetradeoxy-7-(3-hydroxybutanoylamino)-L-*glycero*-L-*manno*-non-2-ulosonic acid. Genes of interest are labeled above corresponding gene, see text for further details. Genbank accession numbers for sequences used in gene alignment are as follows; KL12, JN107991.2 (38.5 kb region; base position range 2332–40832); KL13, MF522810.1 (38.2 kb region); KL49, KT359616.1 (34.5 kb region); KL53, MH190222.1 (23.4 kb region); KL19, KU165787.1 (23.8 kb); KL1, CP001172.1 (24.9 kb; base position range 366401 to 3691388); KL4, JN409449.3 (30.9 kb; base position range 2375 to 33327); KL3, CP012004.1, (25.4 kb; base position range 3762660–3788118); KL2, CP000863.1 (27.1 kb; base position range 77125–104246); KL6, KF130871.1 (25.5 kb); KL93, CP021345.1 30.3 kb (base position range 3338210–3368604) and KL37 KX712115.1 (23.4 kb). **(B)** Capsule structures corresponding to KL gene regions in **(A)** are shown. Percentage of *O*-acetylation of specific glycans from K53, K19, K1 are not represented in structural configurations (Kenyon et al., 2016a; Shashkov et al., 2018).

settings (Geisinger and Isberg, 2015; Tipton et al., 2015; Chen et al., 2017). Furthermore, growth of *A. baumannii* in sub-inhibitory levels of antimicrobials influences CPS production. For example, exposure to the antibiotics chloramphenicol or erythromycin led to enhanced capsule synthesis in ATCC 17978 (Geisinger and Isberg, 2015) and meropenem exposure selected for mutations leading to a loss in CPS production in the isolate 37662 (Chen et al., 2017). Studies

conducted on a broader range of *A. baumannii* strains are required to identify if the protection against antimicrobials afforded by CPS is strain specific, capsule-type specific, or universal.

The ability of *A. baumannii* to persist in the clinical environment has undoubtedly enhanced colonization and infections in susceptible patients. *A. baumannii* is capable of surviving for months on hospital surfaces such as bed rails, furniture and medical devices, providing a reservoir that is often the source of transmission and infection (Wendt et al., 1997; Gayoso et al., 2013). The remarkable desiccation tolerance of *A. baumannii* is thought to be due to a "bust or boom" strategy, where a persistent subpopulation of cells survive at the expense of dying cells; CPS enhances desiccation tolerance by providing a physical barrier facilitating water retention (Roberts, 1996; Webster et al., 2000; Gayoso et al., 2013; Bravo et al., 2016). A direct role for CPS in desiccation resistance was recently demonstrated in the *A. baumannii* strain AB5075 (K25 CPS type). In this study, the acapsular variant of AB5075 displayed a 2.5-fold reduction in viability compared to the parental strain (Tipton et al., 2018). Furthermore, in two close relatives of *A. baumannii*, *Acinetobacter calcoaceticus* and *Acinetobacter baylyi*, production of exopolysaccharide and/or CPS has been shown to promote desiccation survival (Roberson and Firestone, 1992; Ophir and Gutnick, 1994). In addition to influencing resistance to desiccation, CPS has been associated with other virulence traits including motility (McQueary et al., 2012; Huang et al., 2014) and the production of biofilm (Umland et al., 2012; Lees-Miller et al., 2013), thus cementing its role as a pathogenic factor.

Recent studies have linked the phase-variable phenotype of *A. baumannii* AB5075 with alterations in CPS production, as highly virulent opaque variants produce a CPS layer with twice the thickness of their translucent counterparts (Chin et al., 2018). This transition from translucent to opaque also dramatically increased the pathogenic potential of *A. baumannii* AB5075. Resistance to common hospital disinfectants and a subset of aminoglycoside antibiotics were also increased (Tipton et al., 2015; Chin et al., 2018) and opaque variants were also more resistant to human lysozyme, the cathelicidin-related antimicrobial peptide LL37 and hydrogen peroxide compared to translucent colonies (Chin et al., 2018). Furthermore, opaque isolates had an increased tolerance to desiccated conditions and out-competed translucent counterparts in a mouse infection model (Chin et al., 2018). As multiple factors are involved in phase variation, further studies were performed to determine the contribution of CPS production to the more virulent opaque phenotype. In a following publication, the authors demonstrated that an acapsular variant was significantly more susceptible to lysozyme and disinfectants compared to its opaque AB5075 wild-type parent (Tipton et al., 2018). Interestingly, there was no difference in resistance to LL-37 and hydrogen peroxide between the opaque wild-type and acapsular strains, suggesting factors other than CPS production lead to this phenotype for opaque variants of *A. baumannii* (Tipton et al., 2018).

REGULATION OF CPS PRODUCTION

Environmental cues, such as temperature, osmotic pressure and changes in metabolite and ion availability can influence bacterial CPS production (Hagiwara et al., 2003; Lai et al., 2003; Mouslim et al., 2004; Willenborg et al., 2011). It is unsurprising that few regulatory mechanisms have been identified for CPS production as CPS levels are commonly regulated post-translationally through the phosphorylation of CPS export machinery (Whitfield and Paiment, 2003; Chiang et al., 2017). In *A. baumannii*, only two regulators of capsule production have thus far been identified; BfmRS and OmpR-EnvZ, both two component signal transduction systems which play multiple regulatory roles involved in envelope biogenesis (Geisinger and Isberg, 2015; Tipton and Rather, 2017; Geisinger et al., 2018). When subjected to antibiotic pressure, *A. baumannii* ATCC 17978 *cps* expression was increased in a BfmRS-dependent manner (Geisinger and Isberg, 2015). Phase variation, and thus potentially CPS production, is highly regulated by the OmpR-EnvZ system in *A. baumannii* AB5075, as mutations in either OmpR or EnvZ resulted in a significant increase in opaque to translucent switching frequency (Tipton and Rather, 2017). Although transition from translucent to opaque results in a two-fold increase in capsule thickness, transcriptomic analyses have not identified any differences in expression levels of KL genes between the two phases.

CPS AS A TARGET FOR THE DEVELOPMENT OF VACCINES AND TREATMENTS AGAINST *A. baumannii*

Antibiotic (specifically cabapenem) resistant *A. baumannii* are classified a World Health Organization Priority 1 Critical organism for the development of new antimicrobials (WHO, 2017). Although there are no non-antibiotic treatments or vaccines licensed for *A. baumannii* at present, there is an increased interest in their development and preliminary studies look promising. Surface exposure and prevalence in pathogenic strains of *A. baumannii* makes CPS an ideal target for both antimicrobial treatments and vaccines (Russo et al., 2013). These include the development of antibody-based therapies such as prophylactic vaccines, passive immunization, and phage therapy (García-Quintanilla et al., 2013).

Several studies have shown the efficacy of passive immunization in mice using a CPS-specific antibody, which is protective against bacterial challenge with 13–55% of clinical *A. baumannii* isolates (Russo et al., 2013; Yang et al., 2017; Lee et al., 2018). Additionally, inoculation with conjugate vaccines incorporating CPS glycans attached to a protein carrier elicit better immune protection than purified CPS against a diverse range of *A. baumannii* strains (Yang et al., 2017).

Interest in phage therapy to treat bacterial infections has increased in recent years in response to the current crisis of rising antimicrobial resistance. Phage therapy is attractive as a potential treatment avenue for multidrug resistant *A. baumannii* infections. For example, a phage encoding a CPS depolymerase

was found to degrade the CPS of approximately 10%, four out of 38, clinical multidrug resistant *A. baumannii* tested (Hernandez-Morales et al., 2018). Although the host range of this phage is limited, it could be incorporated as part of a phage cocktail to maximize effectiveness or target specific outbreaks (Hernandez-Morales et al., 2018). A phage which selectively cleaves the linkage of *A. baumannii* CPS at a pseudaminic acid branch may be valuable for phage therapy, or to efficiently manufacture purified CPS for vaccine and antibody development (Lee et al., 2018). Phage targeting *A. baumannii* were recently shown to be stable when impregnated in burn wound care products under a range of conditions including in the presence of antimicrobials (Merabishvili et al., 2017). However, as the majority of studies investigating *A. baumannii* CPS are usually confined to a particular *A. baumannii* strain, it is not known if these findings translate to all *A. baumannii* isolates or if they are strain or capsule type specific. Understanding what roles capsule plays in multiple strains is paramount in identifying CPS types which represent the best targets for new vaccines, or whether the development of antimicrobials targeting capsule biosynthesis pathway is indeed even feasible.

CONCLUDING REMARKS

Although capsule represents an important virulence trait of *A. baumannii* there are limited data available on the role different CPS types play in causing disease. To develop effective vaccines and therapies targeting CPS, we must first gain a comprehensive understanding towards the mechanisms behind its synthesis and expression, alongside the advantages that capsule conveys to the host bacteria. This research needs to be addressed in the context of the extreme variation of CPS serotypes found in *A. baumannii,* to ensure potential interventions work against strains producing diverse CPS structures. Further studies on CPS are required to provide a platform for the development of preventative measures and treatments against this increasingly persistent and deadly human pathogen.

AUTHOR CONTRIBUTIONS

JS wrote the first draft. MB provided academic input and critical revision of the article. FA produced genome alignments and provided critical revision of the manuscript. All authors approved the final version.

FUNDING

This work was supported by a Flinders Medical Research Foundation Grant to MB. FA was supported by AJ and IM Naylon and Playford Trust Ph.D. Scholarships. JS was supported by a AJ and IM Naylon Scholarship.

REFERENCES

Arbatsky, N. P., Shneider, M. M., Kenyon, J. J., Shashkov, A. S., Popova, A. V., Miroshnikov, K. A., et al. (2015). Structure of the neutral capsular polysaccharide of *Acinetobacter baumannii* NIPH146 that carries the KL37 capsule gene cluster. *Carbohydr. Res.* 413, 12–15. doi: 10.1016/j.carres.2015.05.003

Beceiro, A., Moreno, A., Fernández, N., Vallejo, J. A., Aranda, J., Adler, B., et al. (2014). Biological cost of different mechanisms of colistin resistance and their impact on virulence in *Acinetobacter baumannii*. *Antimicrob. Agents Chemother.* 58, 518–526. doi: 10.1128/AAC.01597-13

Bravo, Z., Orruño, M., Parada, C., Kaberdin, V., Barcina, I., and Arana, I. (2016). The long-term survival of *Acinetobacter baumannii* ATCC 19606T under nutrient-deprived conditions does not require the entry into the viable but non-culturable state. *Arch. Microbiol.* 198, 399–407. doi: 10.1007/s00203-016-1200-1

Chen, X., Meng, X., Gao, Q., Zhang, G., Gu, H., and Guo, X. (2017). Meropenem selection induced overproduction of the intrinsic carbapenemase as well as phenotype divergence in *Acinetobacter baumannii*. *Int. J. Antimicrob. Agents* 50, 419–426. doi: 10.1016/j.ijantimicag.2017.04.015

Chiang, S.-R., Jung, F., Tang, H.-J., Chen, C.-H., Chen, C.-C., Chou, H.-Y., et al. (2017). Desiccation and ethanol resistances of multidrug resistant *Acinetobacter baumannii* embedded in biofilm: the favorable antiseptic efficacy of combination chlorhexidine gluconate and ethanol. *J. Microbiol. Immunol. Infect.* 51, 770–777. doi: 10.1016/j.jmii.2017.02.003

Chin, C. Y., Tipton, K. A., Farokhyfar, M., Burd, E. M., Weiss, D. S., and Rather, P. N. (2018). A high-frequency phenotypic switch links bacterial virulence and environmental survival in *Acinetobacter baumannii*. *Nat. Microbiol.* 3, 563–569. doi: 10.1038/s41564-018-0151-5

Choi, A. H., Slamti, L., Avci, F. Y., Pier, G. B., and Maira-Litrán, T. (2009). The *pgaABCD* locus of *Acinetobacter baumannii* encodes the production of poly-β-1-6-*N*-acetylglucosamine, which is critical for biofilm formation. *J. Bacteriol.* 191, 5953–5963. doi: 10.1128/JB.00647-09

Collins, R. F., Beis, K., Dong, C., Botting, C. H., McDonnell, C., Ford, R. C., et al. (2007). The 3D structure of a periplasm-spanning platform required for assembly of group 1 capsular polysaccharides in *Escherichia coli*. *Proc. Natl. Acad. Sci. U.S.A.* 104, 2390–2395. doi: 10.1073/pnas.0607763104

García-Quintanilla, M., Pulido, M. R., López-Rojas, R., Pachón, J., and McConnell, M. J. (2013). Emerging therapies for multidrug resistant *Acinetobacter baumannii*. *Trends Microbiol.* 21, 157–163. doi: 10.1016/j.tim.2012.12.002

Gayoso, C. M., Mateos, J. S., Meìndez, J. A., Fernaìndez-Puente, P., Rumbo, C., Tomaìs, M., et al. (2013). Molecular mechanisms involved in the response to desiccation stress and persistence in *Acinetobacter baumannii*. *J. Proteome Res.* 13, 460–476. doi: 10.1021/pr400603f

Geisinger, E., and Isberg, R. R. (2015). Antibiotic modulation of capsular exopolysaccharide and virulence in *Acinetobacter baumannii*. *PLoS Pathog.* 11:e1004691. doi: 10.1371/journal.ppat.1004691

Geisinger, E., Mortman, N. J., Vargas-Cuebas, G., Tai, A. K., and Isberg, R. R. (2018). A global regulatory system links virulence and antibiotic resistance to envelope homeostasis in *Acinetobacter baumannii*. *PLoS Pathog.* 14:e1007030. doi: 10.1371/journal.ppat.1007030

Hagiwara, D., Sugiura, M., Oshima, T., Mori, H., Aiba, H., Yamashino, T., et al. (2003). Genome-wide analyses revealing a signaling network of the RcsC-YojN-RcsB phosphorelay system in *Escherichia coli*. *J. Bacteriol.* 185, 5735–5746. doi: 10.1128/JB.185.19.5735-5746.2003

Harding, C. M., Nasr, M. A., Kinsella, R. L., Scott, N. E., Foster, L. J., Weber, B. S., et al. (2015). Acinetobacter strains carry two functional oligosaccharyltransferases, one devoted exclusively to type IV pilin, and the other one dedicated to O-glycosylation of multiple proteins. *Mol. Microbiol.* 96, 1023–1041. doi: 10.1111/mmi.12986

Hernandez-Morales, A., Lessor, L., Wood, T., Migl, D., Mijalis, E., Cahill, J., et al. (2018). Genomic and biochemical characterization of Acinetobacter podophage petty reveals a novel lysis mechanism and tail-associated depolymerase activity. *J. Virol.* 92:e01064-17. doi: 10.1128/JVI.01064-17.

Hitchen, P., Brzostek, J., Panico, M., Butler, J. A., Morris, H. R., Dell, A., et al. (2010). Modification of the *Campylobacter jejuni* flagellin glycan by the product

of the Cj1295 homopolymeric-tract-containing gene. *Microbiology* 156, 1953–1962. doi: 10.1099/mic.0.038091-0

Hu, D., Liu, B., Dijkshoorn, L., Wang, L., and Reeves, P. R. (2013). Diversity in the major polysaccharide antigen of *Acinetobacter baumannii* assessed by DNA sequencing, and development of a molecular serotyping scheme. *PLoS One* 8:e70329. doi: 10.1371/journal.pone.0070329

Huang, T.-W., Lam, I., Chang, H.-Y., Tsai, S.-F., Palsson, B. O., and Charusanti, P. (2014). Capsule deletion via a lamda-Red knockout system perturbs biofilm formation and fimbriae expression in *Klebsiella pneumoniae* MGH 78578. *BMC Res. Notes* 7:13. doi: 10.1186/1756-0500-7-13

Iwashkiw, J. A., Seper, A., Weber, B. S., Scott, N. E., Vinogradov, E., Stratilo, C., et al. (2012). Identification of a general O-linked protein glycosylation system in *Acinetobacter baumannii* and its role in virulence and biofilm formation. *PLoS Pathog.* 8:e1002758. doi: 10.1371/journal.ppat.1002758

Kao, C.-Y., Sheu, B.-S., and Wu, J.-J. (2016). *Helicobacter pylori* infection: an overview of bacterial virulence factors and pathogenesis. *Biomed. J.* 39, 14–23. doi: 10.1016/j.bj.2015.06.002

Kasimova, A., Shneider, M., Arbatsky, N., Popova, A., Shashkov, A., Miroshnikov, K., et al. (2017). Structure and gene cluster of the K93 capsular polysaccharide of *Acinetobacter baumannii* B11911 containing 5-N-Acetyl-7-N-[(R)-3-hydroxybutanoyl] pseudaminic acid. *Biochemistry* 4, 483–489.

Kasimova, A. A., Kenyon, J. J., Arbatsky, N. P., Shashkov, A. S., Popova, A. V., Shneider, M. M., et al. (2018). *Acinetobacter baumannii* K20 and K21 capsular polysaccharide structures establish roles for UDP-glucose dehydrogenase Ugd2, pyruvyl transferase Ptr2 and two glycosyltransferases. *Glycobiology* 28, 876–884. doi: 10.1093/glycob/cwy074

Kenyon, J. J., and Hall, R. M. (2013). Variation in the complex carbohydrate biosynthesis loci of *Acinetobacter baumannii* genomes. *PLoS One* 8:e62160. doi: 10.1371/journal.pone.0062160

Kenyon, J. J., Hall, R. M., and De Castro, C. (2015). Structural determination of the K14 capsular polysaccharide from an ST25 *Acinetobacter baumannii* isolate, D46. *Carbohydr. Res.* 417, 52–56. doi: 10.1016/j.carres.2015.09.002

Kenyon, J. J., Marzaioli, A., Hall, R. M., and De Castro, C. (2014a). Structure of the K2 capsule associated with the KL2 gene cluster of *Acinetobacter baumannii*. *Glycobiology* 24, 554–563. doi: 10.1093/glycob/cwu024

Kenyon, J. J., Nigro, S. J., and Hall, R. M. (2014b). Variation in the OC Locus of *Acinetobacter baumannii* genomes predicts extensive structural diversity in the lipooligosaccharide. *PLoS One* 9:e107833. doi: 10.1371/journal.pone.0107833

Kenyon, J. J., Notaro, A., Hsu, L. Y., De Castro, C., and Hall, R. M. (2017). 5, 7-Di-N-acetyl-8-epiacinetaminic acid: a new non-2-ulosonic acid found in the K73 capsule produced by an *Acinetobacter baumannii* isolate from Singapore. *Sci. Rep.* 7:11357. doi: 10.1038/s41598-017-11166-4

Kenyon, J. J., Shneider, M. M., Senchenkova, S. N., Shashkov, A. S., Siniagina, M. N., Malanin, S. Y., et al. (2016a). K19 capsular polysaccharide of *Acinetobacter baumannii* is produced via a Wzy polymerase encoded in a small genomic island rather than the KL19 capsule gene cluster. *Microbiology* 162, 1479–1489. doi: 10.1099/mic.0.000313

Kenyon, J. J., Speciale, I., Hall, R. M., and De Castro, C. (2016b). Structure of repeating unit of the capsular polysaccharide from *Acinetobacter baumannii* D78 and assignment of the K4 gene cluster. *Carbohydr. Res.* 434, 12–17. doi: 10.1016/j.carres.2016.07.016

Lai, Y.-C., Peng, H.-L., and Chang, H.-Y. (2003). RmpA2, an activator of capsule biosynthesis in *Klebsiella pneumoniae* CG43, regulates K2 cps gene expression at the transcriptional level. *J. Bacteriol.* 185, 788–800. doi: 10.1128/JB.185.3.788-800.2003

Lee, I.-M., Yang, F.-L., Chen, T.-L., Liao, K.-S., Ren, C.-T., Lin, N.-T., et al. (2018). Pseudaminic acid on exopolysaccharide of *Acinetobacter baumannii* plays a critical role in phage-assisted preparation of glycoconjugate vaccine with high antigenicity. *J. Am. Chem. Soc.* 140, 8639–8643. doi: 10.1021/jacs.8b04078

Lees-Miller, R. G., Iwashkiw, J. A., Scott, N. E., Seper, A., Vinogradov, E., Schild, S., et al. (2013). A common pathway for O-linked protein-glycosylation and synthesis of capsule in *Acinetobacter baumannii*. *Mol. Microbiol.* 89, 816–830. doi: 10.1111/mmi.12300

Longo, F., Vuotto, C., and Donelli, G. (2014). Biofilm formation in *Acinetobacter baumannii*. *New Microbiol.* 37, 119–127.

Luke, N. R., Sauberan, S. L., Russo, T. A., Beanan, J. M., Olson, R., Loehfelm, T. W., et al. (2010). Identification and characterization of a glycosyltransferase involved in *Acinetobacter baumannii* lipopolysaccharide core biosynthesis. *Infect. Immun.* 78, 2017–2023. doi: 10.1128/IAI.00016-10

McQueary, C. N., Kirkup, B. C., Si, Y., Barlow, M., Actis, L. A., Craft, D. W., et al. (2012). Extracellular stress and lipopolysaccharide modulate *Acinetobacter baumannii* surface-associated motility. *J. Microbiol.* 50, 434–443. doi: 10.1007/s12275-012-1555-1

Merabishvili, M., Monserez, R., van Belleghem, J., Rose, T., Jennes, S., De Vos, D., et al. (2017). Stability of bacteriophages in burn wound care products. *PLoS One* 12:e0182121. doi: 10.1371/journal.pone.0182121

Moffatt, J. H., Harper, M., Harrison, P., Hale, J. D., Vinogradov, E., Seemann, T., et al. (2010). Colistin resistance in *Acinetobacter baumannii* is mediated by complete loss of lipopolysaccharide production. *Antimicrob. Agents Chemother.* 54, 4971–4977. doi: 10.1128/AAC.00834-10

Mouslim, C., Delgado, M., and Groisman, E. A. (2004). Activation of the RcsC/YojN/RcsB phosphorelay system attenuates *Salmonella* virulence. *Mol. Microbiol.* 54, 386–395. doi: 10.1111/j.1365-2958.2004.04293.x

Ophir, T., and Gutnick, D. L. (1994). A role for exopolysaccharides in the protection of microorganisms from desiccation. *Appl. Environ. Microbiol.* 60, 740–745.

Preston, A., Mandrell, R. E., Gibson, B. W., and Apicella, M. A. (1996). The lipooligosaccharides of pathogenic Gram-negative bacteria. *Crit. Rev. Microbiol.* 22, 139–180. doi: 10.3109/10408419609106458

Roberson, E. B., and Firestone, M. K. (1992). Relationship between desiccation and exopolysaccharide production in a soil *Pseudomonas* sp. *Appl. Environ. Microbiol.* 58, 1284–1291.

Roberts, I. S. (1996). The biochemistry and genetics of capsular polysaccharide production in bacteria. *Annu. Rev. Microbiol.* 50, 285–315. doi: 10.1146/annurev.micro.50.1.285

Russo, T. A., Beanan, J. M., Olson, R., MacDonald, U., Cox, A. D., Michael, F. S., et al. (2013). The K1 capsular polysaccharide from *Acinetobacter baumannii* is a potential therapeutic target via passive immunization. *Infect. Immun.* 81, 915–922. doi: 10.1128/IAI.01184-12

Russo, T. A., Luke, N. R., Beanan, J. M., Olson, R., Sauberan, S. L., MacDonald, U., et al. (2010). The K1 capsular polysaccharide of *Acinetobacter baumannii* strain 307-0294 is a major virulence factor. *Infect. Immun.* 78, 3993–4000. doi: 10.1128/IAI.00366-10

Sanchez-Larrayoz, A. F., Elhosseiny, N. M., Chevrette, M. G., Fu, Y., Giunta, P., Spallanzani, R. G., et al. (2017). Complexity of complement resistance factors expressed by *Acinetobacter baumannii* needed for survival in human serum. *J. Immunol.* 199, 2354–2368. doi: 10.4049/jimmunol.1700877

Scott, N. E., Kinsella, R. L., Edwards, A. V., Larsen, M. R., Dutta, S. M., Saba, J., et al. (2014). Diversity within the O-linked protein glycosylation systems of Acinetobacter species. *Mol. Cell. Proteomics* 13, 2354–2370. doi: 10.1074/mcp.M114.038315

Shashkov, A. S., Kenyon, J. J., Arbatsky, N. P., Shneider, M. M., Popova, A. V., Knirel, Y. A., et al. (2018). Genetics of biosynthesis and structure of the K53 capsular polysaccharide of *Acinetobacter baumannii* D23 made up of a disaccharide K unit. *Microbiology* 164, 1–4. doi: 10.1099/mic.0.000710

Shashkov, A. S., Liu, B., Kenyon, J. J., Popova, A. V., Shneider, M. M., Sof'ya, N. S., et al. (2017). Structures of the K35 and K15 capsular polysaccharides of *Acinetobacter baumannii* LUH5535 and LUH5554 containing amino and diamino uronic acids. *Carbohydr. Res.* 448, 28–34. doi: 10.1016/j.carres.2017.05.017

Sullivan, M. J., Petty, N. K., and Beatson, S. A. (2011). Easyfig: a genome comparison visualizer. *Bioinformatics* 27, 1009–1010. doi: 10.1093/bioinformatics/btr039

Tipton, K. A., Chin, C.-Y., Farokhyfar, M., Weiss, D. S., and Rather, P. N. (2018). Role of capsule in resistance to disinfectants, host antimicrobials and desiccation in *Acinetobacter baumannii*. *Antimicrob. Agents Chemother.* 62:e01188-18. doi: 10.1128/AAC.01188-18.

Tipton, K. A., Dimitrova, D., and Rather, P. N. (2015). Phase-variable control of multiple phenotypes in *Acinetobacter baumannii* strain AB5075. *J. Bacteriol.* 197, 2593–2599. doi: 10.1128/JB.00188-15

Tipton, K. A., and Rather, P. N. (2017). An ompR-envZ two-component system ortholog regulates phase variation, osmotic tolerance, motility, and virulence in *Acinetobacter baumannii* strain AB5075. *J. Bacteriol.* 199:e00705-16. doi: 10.1128/JB.00705-16

Traub, W. H. (1989). *Acinetobacter baumannii* serotyping for delineation of outbreaks of nosocomial cross-infection. *J. Clin. Microbiol.* 27, 2713–2716.

Umland, T. C., Schultz, L. W., MacDonald, U., Beanan, J. M., Olson, R., and Russo, T. A. (2012). In vivo-validated essential genes identified in *Acinetobacter baumannii* by using human ascites overlap poorly with essential genes detected on laboratory media. *mBio* 3:e00113-12. doi: 10.1128/mBio.00113-12

Vinogradov, E., MacLean, L., Xu, H. H., and Chen, W. (2014). The structure of the polysaccharide isolated from *Acinetobacter baumannii* strain LAC-4. *Carbohydr. Res.* 390, 42–45. doi: 10.1016/j.carres.2014.03.001

Wang-Lin, S. X., Olson, R., Beanan, J. M., MacDonald, U., Balthasar, J. P., and Russo, T. A. (2017). The capsular polysaccharide of *Acinetobacter baumannii* is an obstacle for therapeutic passive immunization strategies. *Infect. Immun.* 85:e00591-17. doi: 10.1128/IAI.00591-17

Weber, B. S., Harding, C. M., and Feldman, M. F. (2016). Pathogenic Acinetobacter: from the cell surface to infinity and beyond. *J. Bacteriol.* 198, 880–887. doi: 10.1128/JB.00906-15

Webster, C., Towner, K. J., and Humphreys, H. (2000). Survival of Acinetobacter on three clinically related inanimate surfaces. *Infect. Control Hosp. Epidemiol.* 21, 246–246. doi: 10.1086/503214

Wendt, C., Dietze, B., Dietz, E., and Rüden, H. (1997). Survival of *Acinetobacter baumannii* on dry surfaces. *J. Clin. Microbiol.* 35, 1394–1397.

Whitfield, C. (2006). Biosynthesis and assembly of capsular polysaccharides in *Escherichia coli*. *Annu. Rev. Biochem.* 75, 39–68. doi: 10.1146/annurev.biochem.75.103004.142545

Whitfield, C., and Paiment, A. (2003). Biosynthesis and assembly of Group 1 capsular polysaccharides in *Escherichia coli* and related extracellular polysaccharides in other bacteria. *Carbohydr. Res.* 338, 2491–2502. doi: 10.1016/j.carres.2003.08.010

WHO (2017). *Global Priority List of Antibiotic-Resistant Bacteria to Guide Research, Discovery, and Development of New Antibiotics*. Geneva: World Health Organisation.

Wieland, K., Chhatwal, P., and Vonberg, R.-P. (2018). Nosocomial outbreaks caused by *Acinetobacter baumannii* and *Pseudomonas aeruginosa*: results of a systematic review. *Am. J. Infect. Control* 46, 643–648. doi: 10.1016/j.ajic.2017.12.014

Willenborg, J., Fulde, M., de Greeff, A., Rohde, M., Smith, H. E., Valentin-Weigand, P., et al. (2011). Role of glucose and CcpA in capsule expression and virulence of *Streptococcus suis*. *Microbiology* 157, 1823–1833. doi: 10.1099/mic.0.046417-0

Willis, L. M., and Whitfield, C. (2013). "Chapter 17 - Capsule and lipopolysaccharide," in *Escherichia coli*, 2nd Edn, ed. M. S. Donnenberg (Boston, MA: Academic Press), 533–556. doi: 10.1016/B978-0-12-397048-0.00017-6

Woodward, L., and Naismith, J. H. (2016). Bacterial polysaccharide synthesis and export. *Curr. Opin. Struct. Biol.* 40, 81–88. doi: 10.1016/j.sbi.2016.07.016

Wu, M.-F., Yang, C.-Y., Lin, T.-L., Wang, J.-T., Yang, F.-L., Wu, S.-H., et al. (2009). Humoral immunity against capsule polysaccharide protects the host from magA++ *Klebsiella pneumoniae*-induced lethal disease by evading Toll-like receptor 4 signaling. *Infect. Immun.* 77, 615–621. doi: 10.1128/IAI.00931-08

Yang, F.-L., Lou, T.-C., Kuo, S.-C., Wu, W.-L., Chern, J., Lee, Y.-T., et al. (2017). A medically relevant capsular polysaccharide in *Acinetobacter baumannii* is a potential vaccine candidate. *Vaccine* 35, 1440–1447. doi: 10.1016/j.vaccine.2017.01.060

Conflict of Interest Statement: The authors declare that the research was conducted in the absence of any commercial or financial relationships that could be construed as a potential conflict of interest.

frontiers in Microbiology

ORIGINAL RESEARCH
published: 18 March 2019
doi: 10.3389/fmicb.2019.00545

The Capsule Depolymerase Dpo48 Rescues *Galleria mellonella* and Mice From *Acinetobacter baumannii* Systemic Infections

Yannan Liu[1], Sharon Shui Yee Leung[2], Yatao Guo[1], Lili Zhao[1], Ning Jiang[1], Liyuan Mi[3], Puyuan Li[4], Can Wang[4], Yanhong Qin[4], Zhiqiang Mi[3], Changqing Bai[4]* and Zhancheng Gao[1]**

[1] Department of Respiratory and Critical Care Medicine, Peking University People's Hospital, Beijing, China, [2] School of Pharmacy, The Chinese University of Hong Kong, Shatin, Hong Kong, [3] State Key Laboratory of Pathogen and Biosecurity, Beijing Institute of Microbiology and Epidemiology, Beijing, China, [4] Department of Respiratory and Critical Care Medicine, 307th Hospital of Chinese People's Liberation Army, Beijing, China

OPEN ACCESS

Edited by:
Raffaele Zarrilli,
University of Naples Federico II, Italy

Reviewed by:
Zuzanna Drulis-Kawa,
University of Wrocław, Poland
Younes Smani,
Institute of Biomedicine of Seville (IBIS), Spain

***Correspondence:**
Zhiqiang Mi
zhiqiangmi_jme@163.com
Changqing Bai
mlp1604@sina.com
Zhancheng Gao
zcgao@bjmu.edu.cn

Specialty section:
This article was submitted to Antimicrobials, Resistance and Chemotherapy, a section of the journal Frontiers in Microbiology

Received: 02 January 2019
Accepted: 01 March 2019
Published: 18 March 2019

Citation:
Liu Y, Leung SSY, Guo Y, Zhao L, Jiang N, Mi L, Li P, Wang C, Qin Y, Mi Z, Bai C and Gao Z (2019) The Capsule Depolymerase Dpo48 Rescues Galleria mellonella and Mice From Acinetobacter baumannii Systemic Infections. Front. Microbiol. 10:545. doi: 10.3389/fmicb.2019.00545

The emergence of multidrug- and extensively drug-resistant *Acinetobacter baumannii* has made it difficult to treat and control infections caused by this bacterium. Thus, alternatives to conventional antibiotics for management of severe *A. baumannii* infections is urgently needed. In our previous study, we found that a capsule depolymerase Dpo48 could strip bacterial capsules, and the non-capsuled *A. baumannii* were significantly decreased in the presence of serum complement *in vitro*. Here, we further explored its potential as a therapeutic agent for controlling systemic infections caused by extensively drug-resistant *A. baumannii.* Prior to mammalian studies, the anti-virulence efficacy of Dpo48 was first tested in a *Galleria mellonella* infection model. Survival rate of Dpo48-pretreated bacteria or Dpo48 treatment group was significantly increased compared to the infective *G. mellonella* without treatment. Furthermore, the safety and therapeutic efficacy of Dpo48 to mice were evaluated. The mice treated with Dpo48 displayed normal serum levels of TBIL, AST, ALT, ALP, Cr, BUN and LDH, while no significant histopathology changes were observed in tissues of liver, spleen, lung, and kidney. Treatment with Dpo48 could rescue normal and immunocompromised mice from lethal peritoneal sepsis, with the bacterial counts in blood, liver, spleen, lung, and kidney significantly reduced by 1.4–3.3 log colony-forming units at 4 h posttreatment. Besides, the hemolysis and cytotoxicity assays showed that Dpo48 was non-homolytic to human red blood cells and non-toxic to human lung, liver and kidney cell lines. Overall, the present study demonstrated the promising potential of capsule depolymerases as therapeutic agents to prevent antibiotic-resistant *A. baumannii* infections.

Keywords: *Acinetobacter baumannii*, capsule depolymerase, *Galleria mellonella* model, mouse model, systemic infection, antivirulence

INTRODUCTION

Acinetobacter baumannii is an opportunistic pathogen that often causes nosocomial infections, with the highest prevalence noted in immunocompromised and debilitated patients confined to intensive care units (ICUs) (Elhosseiny and Attia, 2018). Common *A. baumannii* infections include soft tissue infections (particularly in burn wards), urinary tract infections, post-surgical

endocarditis, pneumonia, meningitis, and sepsis (Garcia-Quintanilla et al., 2013; Wong et al., 2017). Comparatively, community-acquired infections caused by *A. baumannii* were rare but severe with a mortality rate reported as high as 64% (Dexter et al., 2015). Due to the extensive use of broad-spectrum antibiotics, especially carbapenems which are the most potent and reliable β-lactam antibiotics for the treatment of serious *A. baumannii* infections (Garnacho-Montero and Amaya-Villar, 2010), many *A. baumannii* strains isolated from patient specimens have become highly antibiotic resistant. Surveillance data in 2017 from China Antimicrobial Resistance Surveillance System (CARSS) indicated that about 66.7 and 69.3% of *A. baumannii* strains were resistant to imipenem and meropenem, respectively (Hu et al., 2018). Colistin has been increasingly used as the last-resort treatment against most carbapenem-resistant *A. baumannii*. However, parental administration of colistin can cause serious side effects including nephrotoxicity and neurotoxicity (Wong et al., 2017). Furthermore, the rapid emergence of colistin-resistant *A. baumannii* presents huge threats to public health that no effective antibiotics for infections caused by this problematic superbug. Hence, there is an urgent need for the development of novel strategies alternative to conventional antibiotics to combat severe *A. baumannii* infections.

In recent years, the safety and efficacy of lytic phages in combating infections caused by drug-resistant bacteria was demonstrated in numerous *in vitro* and *in vivo* studies (Wright et al., 2009; Fish et al., 2016; Leitner et al., 2017; Schooley et al., 2017). However, the use of intact phages to treat bacterial infections may not be ideal because a phage as a complete virion is hard to standardize for mass production and preservation. Moreover, whole phage genomes may contain some genes of unknown function, making it difficult to predict the long-term safety of phage therapy. Therefore, increasing attention has been drawn to investigate the potential of phage proteins in controlling bacterial infections. The effectiveness of endolysins against gram-positive bacteria have been demonstrated *in vitro* and *in vivo* (Chang et al., 2017a,b; Cheng et al., 2017; Zhou et al., 2017). However, reports of endolysins against gram-negative-bacterial infections are relatively limited due to the thick outer membrane surrounding the cell wall, protecting the gram-negative bacteria from the peptidoglycan-degrading enzymes. Outer-membrane permeabilizers were generally required to elevate antibacterial activity of some endolysins (Oliveira et al., 2014, 2016; Dong et al., 2015).

Recently, phage-encoded polysaccharide depolymerases have shown great potential as antivirulent agents in treating gram-negative-bacterial infections *in vitro* and *in vivo* (Lin et al., 2014, 2017; Lai et al., 2016; Majkowska-Skrobek et al., 2016; Guo et al., 2017; Hsieh et al., 2017). They can degrade the bacterial surface polysaccharides to expose the interior of bacteria for host immune attack (Lin et al., 2014, 2017; Hsieh et al., 2017). Although the structure, genomic and biochemical characterization of *A. baumannii* depolymerases have been reported (Lai et al., 2016; Lee et al., 2017; Oliveira et al., 2017, 2018; Hernandez-Morales et al., 2018), little is known regarding their efficacy as therapeutic agents *in vivo*. In our previous study, a capsule depolymerase Dpo48 was identified and characterized (Liu et al., 2019). *In vitro* experiments showed that the enzyme-treated *A. baumannii* were significantly decreased in the presence of serum complement. Here, we explored its potential as a therapeutic agent to control systemic infections induced by extensively drug-resistant *A. baumannii* using *Galleria mellonella* and mice infection models. Hemolysis assay on human red blood cells and cytotoxicity assays on human lung, liver and kidney cell lines were performed to confirm the safety of this enzyme for human application.

MATERIALS AND METHODS

A. baumannii Strain and the Capsule Depolymerase Dpo48

The extensively drug-resistant *A. baumannii* AB1610 was isolated from sputum samples from patients with severe pneumonia in the intensive care unit at 307th Hospital of Chinese People's Liberation Army, Beijing, China. This *A. baumannii* strain was identified by 16S ribosomal rRNA gene sequencing, and its antibiotic resistance profile was shown in our previous report (Liu et al., 2019).

Based on the annotation results of the phage IME200 sequence (GenBank accession number KT804908.2), the open reading frame 48 (GenBank accession number ALJ97635) was predicted to encode the capsule depolymerase Dpo48 with a predicted molecular weight of 75.141 kDa. The expression, purification and identification of this depolymerase, Dpo48, were described in detail previously (Liu et al., 2019). Briefly, the coding sequence of Dpo48 was cloned into the prokaryotic expression vector pET28a (Novagen, Madison, WI, United States), and the recombinant plasmid was transfected into the *Escherichia coli* BL21 cells. The protein was expressed under 0.1 mM isopropyl β-D-1-thiogalactopyranoside incubated at 16°C overnight. Then the sample was loaded into a Ni-nitrilotriacetic acid column (Sangon Biotech, Shanghai, China) and eluted with five volumes of imidazole-containing buffer (50 mM NaH_2PO_4, 300 mM NaCl, 250 mM imidazole, pH 8.0) via a step gradient to collect the purified Dpo48. The collected depolymerase was dialyzed with phosphate buffered saline (PBS) at 4°C overnight using a dialysis bag of 8–14 kDa molecular-mass-cutoff membrane (Viskase, Willowbrook, IL, United States). The concentration of Dpo48 was determined to be 0.5 mg/mL by the Bradford Protein Assay Kit (Thermo Fisher Scientific, MA, United States). The protein was stored at −80°C before use.

Galleria mellonella Infection Model

The treatment efficacy of Dpo48 *in vivo* was first tested in a *G. mellonella* infection model which is well established to assess novel therapeutics for bacterial pathogens (Peleg et al., 2009; Jacobs et al., 2014). The *G. mellonella* weighing about 250∼300 mg (Tianjin Huiyude Biotech Company, Tianjin, China) were used within 7 days of shipment from the vendor and kept in the dark at 21°C before infection. The 100% minimal lethal dose (MLD_{100}) of *G. mellonella* was conducted as described previously (Peleg et al., 2009;

Jacobs et al., 2014) with slight modifications. Briefly, a single clone of *A. baumannii* AB1610 was cultured in Luria-Bertani (LB; OXOID, Hampshire, United Kingdom) broth medium overnight at 37°C. Then, the overnight culture was washed three times with PBS. *G. mellonella* were infected by injecting the bacteria inoculum at a dose of 10^7, 10^6, 10^5, and 10^4 colony-forming units (CFU) in 10 μL PBS into the last left proleg using a 10 μL Hamilton syringe (Hamilton, Reno, NV, United States). The *G. mellonella* were then incubated at 37°C and observed at 12 h intervals over 3 days. The *G. mellonella* which did not respond to physical stimuli were considered dead. Each group included 10 *G. mellonella* with individual experiments repeated three times (n = 30). The MLD_{100} of *G. mellonella* determined to be 10^6 CFU by the Reed and Muench method (**Supplementary Table S1**) and used for the antivirulent experiment.

For the antivirulent experiment, *G. mellonella* were randomly divided into six groups. The positive control group was injected with 10^6 CFU bacteria (n = 30); one treatment group was injected with bacteria, which was pretreated with Dpo48 (final concentration, 50 μg/mL) for 1 h at 37°C and washed with PBS before final injection (n = 30); another treatment group was injected with 10^6 CFU bacteria and 5 μg Dpo48 in 10 μL PBS was administered within 5 min after bacterial infection (n = 30); the non-injected *G. mellonella* and *G. mellonella* injected with 10 μL PBS or Dpo48 as the negative control groups.

Assessment of Acute Toxicity of Dpo48 to Mice

Normal BALB/c female mice (19∼21 g, specificpathogen-free) were purchased from SPF Biotechnology Co., Ltd. (Beijing, China). All mice were housed in regulation boxes and given free access to food and water. All animal studies were performed according to the institutional guidelines for animal welfare, and approved by the Peking University People's Hospital Institutional Animal Care and Use Committee. Mice were sacrificed by CO_2 asphyxiation at the end of the experimental period in accordance with institutional guidelines.

To study the potential acute toxicity of Dpo48 *in vivo*, 50 μg (in 200 μL PBS) purified enzyme or 200 μL PBS was administered intraperitoneally (i.p.) to normal mice. Six mice from each group were sacrificed for blood biochemical analyses and histopathological observation after 24 h inoculation. The survival rate, body weight and abnormal behavior of other mice (n = 6) were recorded daily for 7 days.

Blood Biochemical Assays and Histopathological Observation

Blood samples of mice were centrifuged at 2000 rpm for 15 min to obtain serum, and some biochemical parameters of mice were determined by a Hitachi 7080 biochemical analyzer (Hitachi, Japan). Serum levels of total bilirubin (TBIL), aspartate aminotransferase (AST), alanine aminotransferase (ALT), and alkaline phosphatase (ALP) were measured to evaluate the liver function of mice. Blood creatinine (Cr) and urea nitrogen (BUN) levels were determined for the assessment of nephrotoxicity. Cell membrane injury and tissue damage were evaluated based on the measurements of lactate dehydrogenase (LDH).

For histopathological observation, liver, spleen, lung and kidney tissues were immediately fixed in 10% neutral buffered formalin, and subsequently embedded by paraffin. Tissues were cut into 4∼6 μm sections, stained with hematoxylin-eosin (HE; Solarbio, Beijing, China), and examined under light microscope (Ci-S, Nikon, Tokyo, Japan) for neutrophil infiltration and inflammatory changes.

Spreading of *A. baumannii* in Mice Organs

In order to determine the spreading of *A. baumannii* in mice organs, the MLD_{100} of mice was first assayed according to the method of assessing the MLD_{100} of *G. mellonella*. In brief, *A. baumannii* AB1610 was administered i.p. to each group of mice (n = 6) at a dose of 10^8, 5×10^7, 2×10^7, 10^7, 5×10^6, 2×10^6, or 10^6 CFU in 200 μL PBS, and observed for 7 days. A dose of 10^7 CFU of *A. baumannii* was determined as the MLD_{100} of mice by the Reed and Muench method (**Supplementary Table S2**). Next, three mice were injected i.p. with a dose of 10^7 CFU of *A. baumannii*, and euthanized 2 h postinoculation. Blood samples were obtained by the aorta abdominalis. Then, the liver, spleen, lung and kidney were aseptically removed from mice, weighed and homogenized in PBS. Serially diluted blood and homogenized tissues were plated onto brain heart infusion (BHI; BD, MD, United States) agar and incubated at 37°C for 24 h to determine bacterial counts. The amounts of bacteria in blood and organs were represented as CFU/mL and CFU per gram (g) of tissue, respectively.

Treatment of Dpo48 on Normal or Immunocompromised Mice With Peritoneal Sepsis

A total of 22 mice were inoculated i.p. with a dose of 10^7 CFU of *A. baumannii* and randomly divided into two groups: treated with 50 μg Dpo48 in 200 μL PBS or 200 μL PBS i.p. 2 h after bacterial challenged. Three mice of each group were euthanized 4 h posttreatment, and blood, liver, spleen, lung, and kidney samples were obtained for bacterial counting. The survival rate of other challenged mice (n = 8) were recorded for 7 days.

Immunocompromised mice model was developed by an i.p. injection of cyclophosphamide (CTX) with a single dose of 300 mg/kg (Thermo Fisher Scientific) in 200 μL PBS 3 days before bacterial challenge (Wang et al., 2016). The white blood cell numbers were counted at 0 and 3 days postinjection. The MLD_{100} of immunocompromised mice (**Supplementary Table S3**) and the efficacy of the Dpo48 therapy on the bacterial challenged immunocompromised mice were determined using the methods described above.

Hemolysis Assay

The effect of Dpo48 on the hemolysis of human red blood cells was performed using previously described methods (Wang et al., 2015; Oliveira et al., 2018) with minor modifications. The human blood sample from a healthy donor was centrifuged at 1000 rpm

for 10 min to remove the serum. The red blood cell pellets were washed with PBS (pH = 7.4) at least three times and then diluted to a concentration of 5% (v/v) with PBS. The Dpo48 (final concentration, 7.5 μg/mL) was added to the red blood cells and incubated at 37°C for 1 h with gentle shaking at 60 rpm, followed by centrifugation at 1000 rpm for 10 min. A volume of 100 μL supernatant was transferred to a 96-well microplate and topped up with another 100 μL of PBS to get a final volume of 200 μL. The erythrocytes in PBS and 0.1% Triton X-100 were recorded as negative and positive controls, respectively. The hemoglobin in supernatant was determined by measuring absorbance at 540 nm using a Synergy HT Multi-Detection Microplate Reader (BioTek, VT, United States). The experiments were performed in triplicate.

Cytotoxicity Assays of Dpo48 on Human Cell Lines

To evaluate the acute toxicity of Dpo48 toward human *in vitro*, HuH-7 (human liver cancer), A549 (human lung carcinoma) and 293T (human embryonic kidney) cell lines were obtained from ATCC (VA, United States) and used in this research. All cells were cultured in Dulbecco's Modified Eagle's Medium (DMEM; Gibco, NY, United States) supplemented with 10% fetal bovine serum (FBS; Gibco) under a humidified atmosphere of 5% CO_2 at 37°C, and sub-cultured every 2 days. The cytotoxicity of Dpo48 was determined by MTT assay according to previously methods with minor modifications (Oliveira et al., 2018). Briefly, cells were added into 96-well microtiter plates (5×10^3 cells/well) and incubated at 37°C for 24 h. The culture medium was removed, and cells were washed with PBS (pH = 7.4). Then, a final concentration of 7.5 μg/mL Dpo48 or PBS was added to cells and incubated at 37°C for 24 h. The toxicity of Dpo48 toward cells was conducted using the MTT Cell Proliferation and Cytotoxicity Assay Kit (Solarbio). Quantification of soluble formazan produced by cellular reduction of MTT was measured at 540 nm using a Synergy HT Multi-Detection Microplate Reader. The experiments were performed in triplicate.

Statistical Analysis

All experimental data are expressed as mean ± one standard deviation (SD). The independent Student's *t* test was utilized to compare two groups, and the one-way analysis of variance (ANOVA) was used to compare multiple groups. Survival rate of *G. mellonella* or mice was calculated by Kaplan-Meier survival analysis with a log-rank test. Result analysis were performed and plotted in Prism 7 (GraphPad software, CA, United States), with $P < 0.05$ considered statistically significant.

RESULTS

Antivirulent Efficacy of Dpo48 in the *G. mellonella* Infection Model

To assess the antivirulent efficacy of Dpo48, *G. mellonella* were injected with bacteria, Dpo48-pretreated bacteria, or Dpo48 within 5 min after bacterial challenge. As shown in **Figure 1**, approximately 65% of the *G. mellonella* died within 24 h after inoculated with 10^6 CFU of *A. baumannii* AB1610. On the contrary, the survival rate of Dpo48-pretreated bacteria group and Dpo48 treatment group was 100 and 76%, respectively. The mortality rate of untreated *G. mellonella* increased to 84% after 3 days. Administration of Dpo48 after bacterial challenged could only improve the survival rate of *G. mellonella* slightly to 26% ($P < 0.05$, log-rank test), whereas more than 93% of the *G. mellonella* challenged with enzyme-pretreated bacteria ($P < 0.0001$, log-rank test) survived after 3 days. *G. mellonella* received no injection, injected with PBS or Dpo48 showed a 100% survival rate.

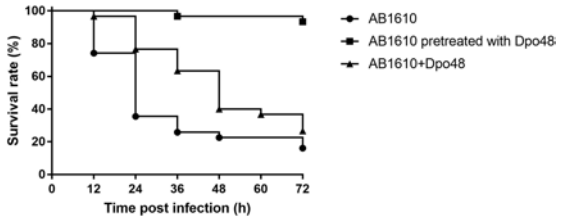

FIGURE 1 | Antivirulent efficacy of Dpo48 in the *Galleria mellonella* infection model. *G. mellonella* were inoculated with *Acinetobacter baumannii* AB1610 (10^6 CFU), or Dpo48-pretreated bacteria, or 5 μg enzyme within 5 min postinfection. Mortality of *G. mellonella* was recorded at 12 h intervals for 3 days. Kaplan-Meier survival analysis with a log-rank test was conducted. Survival rates of the enzyme-pretreated bacteria group ($n = 30$, $P < 0.0001$) and Dpo48 treatment group ($n = 30$, $P < 0.05$) were significantly higher than that of untreated group.

Acute Toxicity Study of Dpo48 to Mice

In order to evaluate the acute toxicity of Dpo48 to mice, the blood biochemical analyses of normal mice inoculated with PBS or enzyme were conducted, and the histopathological changes of mice tissues were examined. As depicted in **Figure 2**, there

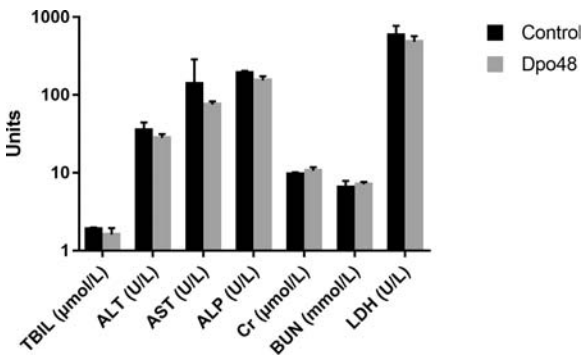

FIGURE 2 | Blood biochemical assays of mice. Normal mice were administered i.p. with Dpo48 (50 μg) or PBS, and sacrificed for blood biochemical analyses at 24 h postinjection. Serum levels of total bilirubin (TBIL), aspartate aminotransferase (AST), alanine aminotransferase (ALT), alkaline phosphatase (ALP), blood creatinine (Cr), urea nitrogen (BUN) and lactate dehydrogenase (LDH) were determined. Data are presented as means ± *SD* ($n = 6$), and the statistical analysis was assayed by the independent Student's *t* test ($P > 0.05$).

were no significant differences in serum levels of TBIL, AST, ALT, ALP, Cr, BUN, and LDH between the two groups after 24 h inoculation. Furthermore, no significantly histopathological changes were observed in tissues of liver, spleen, lung and kidney between the control and Dpo48-treated mice (**Figure 3**). All mice survived and appeared healthy without any abnormal behavior and obvious differences in body weight gain between the two groups during the 7-day observation period (data not shown). Therefore, the injected Dpo48 dose, 50 μg, caused no or little acute toxicity to mice.

Efficacies of Dpo48 Therapy on Mice Peritoneal Sepsis

After 2 h inoculation of *A. baumannii*, the average bacterial counts in liver, spleen, lung, kidney, and blood samples of mice reached 1.1×10^6, 1.2×10^6, 3.4×10^4, 7.2×10^4 CFU/g, and 1.5×10^6 CFU/mL (**Supplementary Figure S1**). Bacteria had been rapidly spread to blood and organs of mice by i.p. infection, suggesting that the *A. baumannii* infection was severe and systemic. A dose of 50 μg Dpo48 was injected into one group of mice 2 h postinoculation to evaluate the therapeutic efficacies of the enzyme. Survival rates of mice indicated that all mice injected with 10^7 CFU of *A. baumannii* died within 24 h postinoculation without treatment, whereas the infected mice treated with Dpo48 led to a 100% survival rate and appeared healthy through the 7-day observation period (**Figure 4A**). In other words, Dpo48 could effectively treat mice peritoneal sepsis caused by *A. baumannii* ($P < 0.0001$, log-rank test). Besides, the bacterial counts in blood and tissue samples of mice treated with Dpo48 were significantly decreased compared with that of the untreated mice 6 h postinoculation (**Figure 4B**).

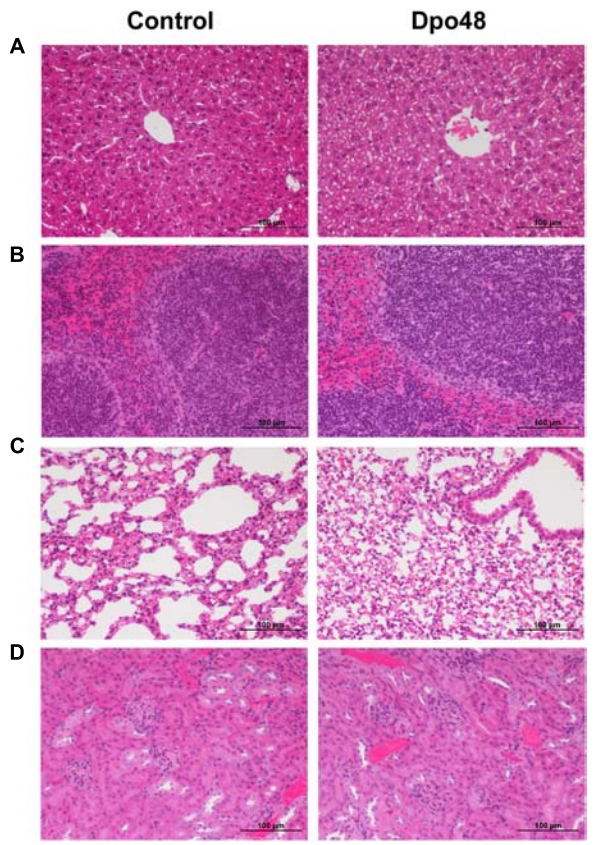

FIGURE 3 | Histopathology of mice tissues. Normal mice were injected i.p. with Dpo48 (50 μg) or PBS, and sacrificed for histopathological observation at 24 h postinjection. Tissues of liver **(A)**, spleen **(B)**, lung **(C)** and kidney **(D)** were stained with hematoxylin-eosin, and observed and recorded under light microscope (200×). There were no significantly histopathological changes in tissues between the control and Dpo48-treated mice.

Efficacies of Dpo48 Therapy on Immunocompromised Mice With Peritoneal Sepsis

Cyclophosphamide is an alkylating agent that interferes with DNA replication, which is often used as an immunosuppressive agent in rodent animal model development. It could inhibit mouse immune response or deteriorate its healthy status, which mimics the situation in clinical setting that *A. baumannii* often target immunocompromised patients. As depicted in **Figure 5A**, the white blood cell counts of the CTX-treated mice were significantly decreased 3 day postinjection ($P < 0.0001$). The immunocompromised mice also appeared with symptoms of slow movement, crowding together, eyes shut and ruffled fur. After injection with 10^7 CFU *A. baumannii*, all untreated immunocompromised mice died within 24 h infection. On the contrary, the survival rate of mice treated with Dpo48 at 2 h postinfection was 100% within the 7-day observation period (**Figure 5B**), with the mice gradually becoming more active. The results suggested that the immunocompromised mice were able to defense effectively against the enzyme-treated bacteria ($P < 0.0001$, log-rank test).

The Hemolysis and Toxicity of Dpo48 Toward Human Cells

The toxic effects of Dpo48 on human red blood cells and liver cancer, lung carcinoma and embryonic kidney cell lines were assessed *in vitro* to confirm the potential application and safety of the depolymerase to human. As shown in **Figure 6A**, Dpo48 displayed no hemolytic activity to erythrocytes based on the determination of hemoglobin in the supernatant. The enzyme also showed no toxic effects toward other human cells according to the quantification of soluble formazan produced by cellular reduction in the MTT assay (**Figure 6B**).

DISCUSSION

Antibiotics are important in curing minor or life threatening infections caused by bacteria. However, most clinical bacterial strains have shown to be resistant to at least three classes of antibiotics, presenting a significant global medical challenge for treatment of infections caused by superbugs. Alarmingly, there is no new antibiotics have reached the advanced development stages for infections caused by multidrug-resistant gram-negative

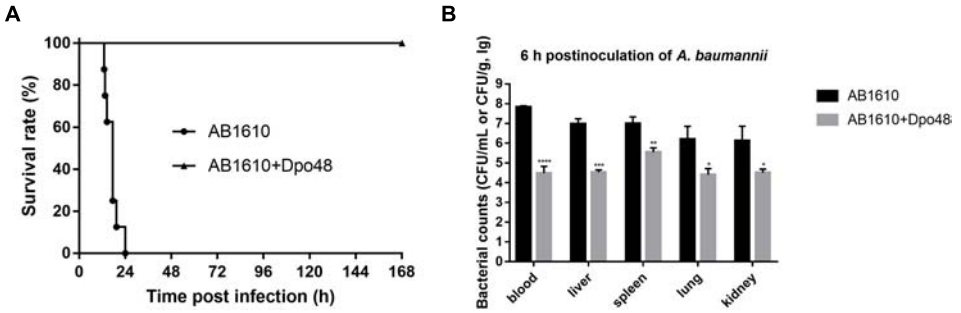

FIGURE 4 | Dpo48 rescues mice from peritoneal sepsis induced by *A. baumannii*. Normal mice were inoculated i.p. with *A. baumannii* AB1610 (10^7 CFU), and injected with Dpo48 (50 μg) or PBS at 2 h postinfection. **(A)** Mortality of mice was observed for 7 days, and comparison of the survival rates between the two groups was determined by Kaplan-Meier survival analysis with a log-rank test ($n = 8$, $P < 0.0001$). **(B)** Mice in each group were euthanized at 6 h postinoculation of *A. baumannii*, and the blood samples, liver, spleen, lung, and kidney were obtained and plated onto BHI agar for bacterial counting. The bacterial numbers are indicated as means ± *SD* ($n = 3$), and the data analysis was conducted by the independent Student's *t* test (*$P < 0.05$, **$P < 0.01$, ***$P < 0.001$, ****$P < 0.0001$).

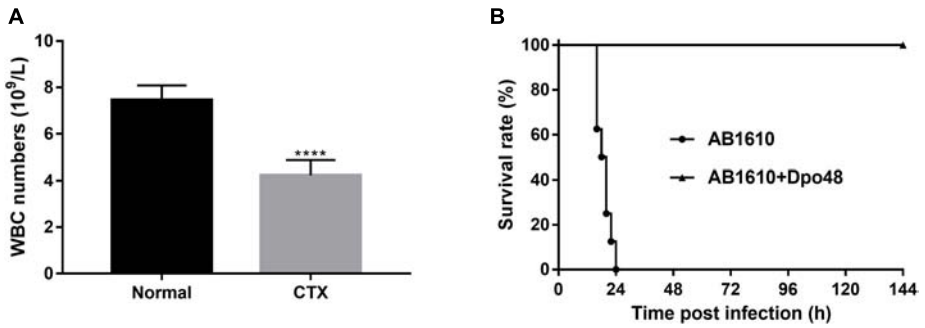

FIGURE 5 | Treatment application of Dpo48 on immunocompromised mice with peritoneal sepsis caused by *A. baumannii*. **(A)** Cyclophosphamide (300 mg/kg) was injected i.p. into normal mice. The white blood cell numbers of mice were determined at 0 and 3 days postinjection. The cell counts are shown as means ± *SD* ($n = 6$), and the comparison of two groups was adapted to the Student's *t* test (****$P < 0.0001$). **(B)** The immunocompromised mice were injected i.p. with *A. baumannii* AB1610 (10^7 cfu), and administered with Dpo48 (50 μg) or PBS at 2 h postinfection. Mice were observed for 7 days for mortality and the survival rate comparison was calculated by Kaplan-Meier survival analysis with a log-rank test ($n = 8$, $P < 0.0001$).

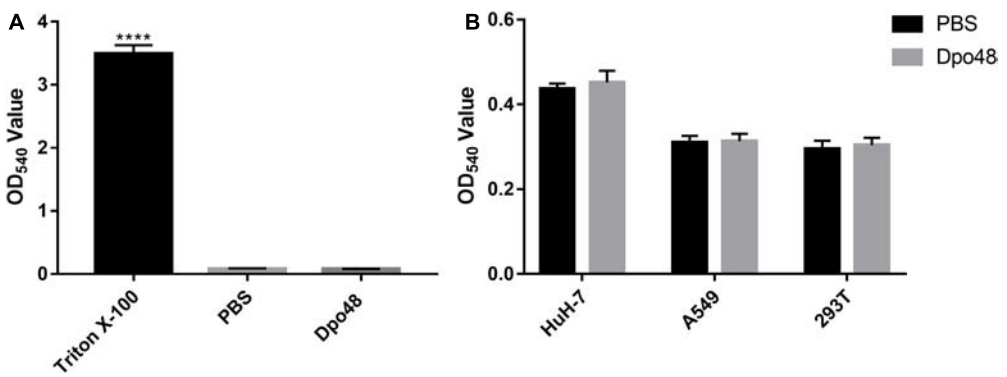

FIGURE 6 | Hemolysis and toxicity effect of Dpo48 on mammalian cells. **(A)** The Dpo48 (7.5 μg/mL) was added to a concentration of 5% (v/v) red blood cells and incubated at 37°C for 1 h with gentle shaking at 60 rpm, and the erythrocytes in PBS and 0.1% Triton X-100 were recorded as negative and positive controls, respectively. The hemoglobin of supernatant was determined at 540 nm. Data are represented as means ± *SD* ($n = 6$), and the one-way ANOVA was used to statistical analysis (****$P < 0.0001$). **(B)** HuH-7 (human liver cancer), A549 (human lung carcinoma), and 293T (human embryonic kidney) cell lines were seeded into 96-well microtiter plates (5×10^3 cells/well) and incubated at 37°C for 24 h. The Dpo48 (7.5 μg/mL) or PBS was added to cells and incubated at 37°C for 24 h. The quantification of soluble formazan produced by cellular reduction of MTT was measured at 540 nm. The values are expressed as means ± *SD* ($n = 6$), and the independent Student's *t* test was adopted in two groups comparison ($P > 0.05$).

bacteria (World Health Organization, 2017). Phage, as natural host of bacteria, have been refocused by many researchers on a global scale (Wright et al., 2009; Fish et al., 2016; Leitner et al., 2017; Schooley et al., 2017) and demonstrated as an effective alternative to antibiotics in combating drug-resistant bacteria. However, the current regulations bear significant challenges to allow full exploration of the benefits of this new therapeutic agent. Contrarily, phage-encoded endolysins and depolymerases, which have been identified as new class of antimicrobials, can follow the development of protein-based pharmaceutics, holding a greater potential to the market.

For most gram-negative bacteria, capsule polysaccharides are major determinants for promoting host virulence, and protection from phagocytosis and antimicrobials (Roach and Donovan, 2015). In our previous study, we have demonstrated the ability of Dpo48 to effectively degrade bacterial capsules and subsequently exposing the inner bacteria for immune attack *in vitro*. It is important to further evaluate the anti-virulence efficacy of this enzyme *in vivo*. Typically, murine or other rodent models were used to assess the toxicity and efficacy of new antimicrobial agents *in vivo*. However, this experimentation is not only costly and time consuming, but also requires full ethical consideration (Desbois and Coote, 2012). Hence, the antivirulent efficacy of Dpo48 in this research was first tested in a *G. mellonella* infection model because of its demonstrated suitability in assessing the efficacy of novel therapeutics for *A. baumannii* infections immediately prior to mammalian studies (Peleg et al., 2009; Jacobs et al., 2014). The better survival rate (10% higher, $P < 0.05$) of infected *G. mellonella* treated with Dpo48 compared with the untreated group confirmed that the enzyme could be an antivirulent agent to control *A. baumannii* infections *in vivo*. The results were in line with findings by Grazyna Majkowska-Skrobek (Majkowska-Skrobek et al., 2016). Although the treatment efficacy was not ideal, the much higher survival rate of the *G. mellonella* (93%) injected with enzyme-pretreated bacteria suggested that the loss of surficial capsules might cause the decrease the virulence of *A. baumannii*. Therefore, a part of the non-encapsulated *A. baumannii* might be cleared up by the innate immune system of *G. mellonella*, and the counts of remaining bacteria might not enough cause the death of *G. mellonella* despite the bacteria would restore the capsule during the propagation.

If depolymerases were considered to be used as therapeutic agents *in vivo*, the evaluation of their acute toxicity to mammalian tissues or cells was important. Mice injected with Dpo48 showed normal serum levels of TBIL, AST, ALT, ALP, Cr, BUN, and LDH after 24 h (**Figure 2**). Moreover, no significant histopathology changes were observed in mice tissues of liver, spleen, lung, and kidney (**Figure 3**), in agreement with other findings (Pan et al., 2015). The enzyme was also founded to be a non-hemolytic and non-toxic agent toward human cells (**Figures 6A,B**). However, the histidine tag and endotoxins in the Dpo48 preparation will need to be removed or reduced to lower levels before used in human trials.

Our previous study (Liu et al., 2019) indicated that a small amount of Dpo48 (10 μg/mL) could effectively strip the capsules of overnight *A. baumannii* with which subsequently killed by serum complement *in vitro*. Although previous research has proved that depolymerases could prevent rat or mice death from lethal bacteraemia, studies were focused on controlling systemic infections caused by *E. coli* and *Klebsiella pneumonia* infections (Mushtaq et al., 2004, 2005; Zelmer et al., 2010; Lin et al., 2014, 2017; Pan et al., 2015; Hsieh et al., 2017). This is the first study to evaluate the efficacy of a depolymerase, Dpo48, in treating *A. baumannii* infections *in vivo*. In addition, most previous studies demonstrated the efficacy of depolymerases against gram-negative bacteria were performed with co-administration of depolymerases and pathogenic bacteria at the same time (Mushtaq et al., 2005; Lin et al., 2014; Hsieh et al., 2017). In other words, the treatment could start before the pathogenic bacteria spread in all animal organs. This means these therapeutic methods might not reflect the clinical situation that treatments only take place after spreading of bacteria in systemic infections. To better representing the actual clinical practice, the present study was performed with the Dpo48 treatment initiated when the *A. baumannii* infection in mice was severe and systemic.

The 100% survival rates of the infected normal and immunocompromised mice revealed that Dpo48 could effectively treat peritoneal sepsis induced by *A. baumannii*. Comparing with the normal mice, the health status of immunocompromised mice was deteriorated. However, they were still capable of clearing the enzyme-degraded *A. baumannii*, because the level of serum complement was not reduced by cyclophosphamide (Li et al., 1987). This observation suggested that the complement-dependent mechanism is responsible for the clearance of enzyme-treated bacteria and protection for infection (Lin et al., 2014; Majkowska-Skrobek et al., 2018). As immunocompromised patients are at higher risk of developing *A. baumannii* infections, the exceptional survival rate of Dpo48 treated immunocompromised mice demonstrated clearly the potential of this enzyme against *A. baumannii* infections in clinical setting. The Dpo48 had better treatment efficacy in mice than that in *G. mellonella* could be due to the simpler innate immune system of insects. The insects only depend on germline-encoded factors for recognition and clearance pathogens (Wojda, 2017). Therefore, the insect models cannot replace the mammalian infection models completely. However, they can provide a rapid and economical approach to observe the effects of a new antimicrobial compound prior to further testing in a mammalian infection model (Desbois and Coote, 2012).

In conclusion, the safety and efficacy results suggested that the phage-encoded depolymerase, Dpo48, have a great potential as a therapeutic agent to prevent and control severe infections caused by *A. baumannii* in *G. mellonella* and mice models. However, the applicability of depolymerases against human infections still needs to be supported by further clinical trials.

AUTHOR CONTRIBUTIONS

YL conceived the project, designed the experiments, analyzed the data, and wrote the manuscript. SL helped to revise

and edit the manuscript. YL, YG, LZ, LM, and CW performed the biological experiments. YL, NJ, PL, and YQ prepared all figures and tables. ZM, CB, and ZG helped to conceive the project and design the experiments, and contributed to reagents or materials. All authors reviewed the manuscript.

FUNDING

This project was supported by the National Natural Science Foundation of China (Grant No. 81572045 and 81870010), the National Key R&D Program of China (Grant No. 2017YFF0108605) and the Capital Characteristic Clinic Project of Beijing (Grant No. Z161100000516181).

SUPPLEMENTARY MATERIAL

The Supplementary Material for this article can be found online at: https://www.frontiersin.org/articles/10.3389/fmicb.2019.00545/full#supplementary-material

FIGURE S1 | Spreading of *A. baumannii* in mice blood and organs. Normal mice were injected i.p. into a dose of 10^7 CFU of *A. baumannii* AB1610 and euthanized at 2 h postinoculation. The bacterial counts of mice blood, liver, spleen, lung, and kidney were assayed, and data are expressed as means ± *SD* (*n* = 3).

TABLE S1 | Determination the MLD_{100} of *Galleria mellonella* by using the Reed and Muench method.

TABLE S2 | Determination the MLD_{100} of Mice by using the Reed and Muench method.

TABLE S3 | Determination the MLD_{100} of Immunocompromised Mice by using the Reed and Muench method.

REFERENCES

Chang, Y., Kim, M., and Ryu, S. (2017a). Characterization of a novel endolysin LysSA11 and its utility as a potent biocontrol agent against *Staphylococcus aureus* on food and utensils. *Food Microbiol.* 68, 112–120. doi: 10.1016/j.fm.2017.07.004

Chang, Y., Yoon, H., Kang, D. H., Chang, P. S., and Ryu, S. (2017b). Endolysin LysSA97 is synergistic with carvacrol in controlling *Staphylococcus aureus* in foods. *Int. J. Food Microbiol.* 244, 19–26. doi: 10.1016/j.ijfoodmicro.2016.12.007

Cheng, M., Zhang, Y., Li, X., Liang, J., Hu, L., Gong, P., et al. (2017). Endolysin LysEF-P10 shows potential as an alternative treatment strategy for multidrug-resistant *Enterococcus faecalis* infections. *Sci. Rep.* 7:10164. doi: 10.1038/s41598-017-10755-7

Desbois, A. P., and Coote, P. J. (2012). Utility of greater wax moth larva (Galleria mellonella) for evaluating the toxicity and efficacy of new antimicrobial agents. *Adv. Appl. Microbiol.* 78, 25–53. doi: 10.1016/B978-0-12-394805-2.00002-6

Dexter, C., Murray, G. L., Paulsen, I. T., and Peleg, A. Y. (2015). Community-acquired *Acinetobacter baumannii*: clinical characteristics, epidemiology and pathogenesis. *Expert. Rev. Anti. Infect Ther.* 13, 567–573. doi: 10.1586/14787210.2015.1025055

Dong, H., Zhu, C., Chen, J., Ye, X., and Huang, Y. P. (2015). Antibacterial activity of *Stenotrophomonas maltophilia* Endolysin P28 against both gram-positive and gram-negative bacteria. *Front. Microbiol.* 6:1299. doi: 10.3389/fmicb.2015.01299

Elhosseiny, N. M., and Attia, A. S. (2018). Acinetobacter: an emerging pathogen with a versatile secretome. *Emerg. Microbes. Infect* 7:33. doi: 10.1038/s41426-018-0030-4

Fish, R., Kutter, E., Wheat, G., Blasdel, B., Kutateladze, M., and Kuhl, S. (2016). Bacteriophage treatment of intransigent diabetic toe ulcers: a case series. *J. Wound Care* 25(Suppl. 7), S27–S33. doi: 10.12968/jowc.2016.25.7.S27

Garcia-Quintanilla, M., Pulido, M. R., Lopez-Rojas, R., Pachon, J., and McConnell, M. J. (2013). Emerging therapies for multidrug resistant *Acinetobacter baumannii*. *Trends Microbiol.* 21, 157–163. doi: 10.1016/j.tim.2012.12.002

Garnacho-Montero, J., and Amaya-Villar, R. (2010). Multiresistant *Acinetobacter baumannii* infections: epidemiology and management. *Curr. Opin. Infect Dis.* 23, 332–339. doi: 10.1097/QCO.0b013e32833ae38b

Guo, Z., Huang, J., Yan, G., Lei, L., Wang, S., Yu, L., et al. (2017). Identification and characterization of Dpo42, a novel depolymerase derived from the *Escherichia coli* phage vB_EcoM_ECOO78. *Front. Microbiol.* 8:1460. doi: 10.3389/fmicb.2017.01460

Hernandez-Morales, A. C., Lessor, L. L., Wood, T. L., Migl, D., Mijalis, E. M., Russell, W. K., et al. (2018). Genomic and biochemical characterization of acinetobacter podophage petty reveals a novel lysis mechanism and tail-associated depolymerase activity. *J. Virol.* 92, e1064–e1017. doi: 10.1128/JVI.01064-17

Hsieh, P. F., Lin, H. H., Lin, T. L., Chen, Y. Y., and Wang, J. T. (2017). Two T7-like bacteriophages, K5-2 and K5-4, each encodes two capsule depolymerases: isolation and functional characterization. *Sci. Rep.* 7:4624. doi: 10.1038/s41598-017-04644-2

Hu, F., Guo, Y., Zhu, D., Wang, F., Jiang, X., Xu, Y., et al. (2018). Antimicrobial resistance profile of clinical isolates in hospitals across China: report from the CHINET surveillance program, 2017. *Chin. J. Infect. Chemother.* 18, 241–251.

Jacobs, A. C., Thompson, M. G., Black, C. C., Kessler, J. L., Clark, L. P., McQueary, C. N., et al. (2014). AB5075, a highly virulent isolate of *Acinetobacter baumannii*, as a model strain for the evaluation of pathogenesis and antimicrobial treatments. *MBio* 5, e1076–e1014. doi: 10.1128/mBio.01076-14

Lai, M. J., Chang, K. C., Huang, S. W., Luo, C. H., Chiou, P. Y., Wu, C. C., et al. (2016). The tail associated protein of *Acinetobacter baumannii* phage PhiAB6 Is the host specificity determinant possessing exopolysaccharide depolymerase activity. *PLoS One* 11:e0153361. doi: 10.1371/journal.pone.0153361

Lee, I. M., Tu, I. F., Yang, F. L., Ko, T. P., Liao, J. H., Lin, N. T., et al. (2017). Structural basis for fragmenting the exopolysaccharide of *Acinetobacter baumannii* by bacteriophage PhiAB6 tailspike protein. *Sci. Rep.* 7:42711. doi: 10.1038/srep42711

Leitner, L., Sybesma, W., Chanishvili, N., Goderdzishvili, M., Chkhotua, A., Ujmajuridze, A., et al. (2017). Bacteriophages for treating urinary tract infections in patients undergoing transurethral resection of the prostate: a randomized, placebo-controlled, double-blind clinical trial. *BMC Urol.* 17:90. doi: 10.1186/s12894-017-0283-6

Li, X. Y., Lin, Z. Y., Zhu, P. P., and Jin, Y. F. (1987). [Effect of cyclophosphamide on serum complement in mice]. *Zhongguo Yao Li Xue Bao* 8, 79–83.

Lin, H., Paff, M. L., Molineux, I. J., and Bull, J. J. (2017). Therapeutic application of phage capsule depolymerases against K1, K5, and K30 capsulated *E. coli* in mice. *Front. Microbiol.* 8:2257. doi: 10.3389/fmicb.2017.02257

Lin, T. L., Hsieh, P. F., Huang, Y. T., Lee, W. C., Tsai, Y. T., Su, P. A., et al. (2014). Isolation of a bacteriophage and its depolymerase specific for K1 capsule of *Klebsiella pneumoniae*: implication in typing and treatment. *J. Infect Dis.* 210, 1734–1744. doi: 10.1093/infdis/jiu332

Liu, Y., Mi, Z., Mi, L., Huang, Y., Li, P., Liu, H., et al. (2019). Identification and characterization of capsule depolymerase Dpo48 from *Acinetobacter baumannii* phage IME200. *PeerJ* 7:e6173. doi: 10.7717/peerj.6173

Majkowska-Skrobek, G., Latka, A., Berisio, R., Maciejewska, B., Squeglia, F., Romano, M., et al. (2016). Capsule-targeting depolymerase, derived from klebsiella KP36 phage, as a tool for the development of anti-virulent strategy. *Viruses* 8:324. doi: 10.3390/v8120324

Majkowska-Skrobek, G., Latka, A., Berisio, R., Squeglia, F., Maciejewska, B., Briers, Y., et al. (2018). Phage-borne depolymerases decrease *Klebsiella pneumoniae* resistance to innate defense mechanisms. *Front. Microbiol.* 9:2517. doi: 10.3389/fmicb.2018.02517

Mushtaq, N., Redpath, M. B., Luzio, J. P., and Taylor, P. W. (2004). Prevention and cure of systemic *Escherichia coli* K1 infection by modification of the bacterial phenotype. *Antimicrob. Agents Chemother.* 48, 1503–1508. doi: 10.1128/AAC.48.5.1503-1508.2004

Mushtaq, N., Redpath, M. B., Luzio, J. P., and Taylor, P. W. (2005). Treatment of experimental *Escherichia coli* infection with recombinant bacteriophage-derived capsule depolymerase. *J. Antimicrob. Chemother.* 56, 160–165. doi: 10.1093/jac/dki177

Oliveira, H., Costa, A. R., Ferreira, A., Konstantinides, N., Santos, S. B., Boon, M., et al. (2018). Functional analysis and anti-virulent properties of a new depolymerase from a myovirus that infects *Acinetobacter baumannii* capsule K45. *J. Virol.* 93, e1163–e1118. doi: 10.1128/JVI.01163-18

Oliveira, H., Costa, A. R., Konstantinides, N., Ferreira, A., Akturk, E., Sillankorva, S., et al. (2017). Ability of phages to infect Acinetobacter calcoaceticus-*Acinetobacter baumannii* complex species through acquisition of different pectate lyase depolymerase domains. *Environ. Microbiol.* 19, 5060–5077. doi: 10.1111/1462-2920.13970

Oliveira, H., Thiagarajan, V., Walmagh, M., Sillankorva, S., Lavigne, R., Neves-Petersen, M. T., et al. (2014). A thermostable *Salmonella* phage endolysin, Lys68, with broad bactericidal properties against gram-negative pathogens in presence of weak acids. *PLoS One* 9:e108376. doi: 10.1371/journal.pone.0108376

Oliveira, H., Vilas Boas, D., Mesnage, S., Kluskens, L. D., Lavigne, R., Sillankorva, S., et al. (2016). Structural and enzymatic characterization of ABgp46, a novel phage endolysin with broad anti-gram-negative bacterial activity. *Front. Microbiol.* 7:208. doi: 10.3389/fmicb.2016.00208

Pan, Y. J., Lin, T. L., Lin, Y. T., Su, P. A., Chen, C. T., Hsieh, P. F., et al. (2015). Identification of capsular types in carbapenem-resistant *Klebsiella pneumoniae* strains by wzc sequencing and implications for capsule depolymerase treatment. *Antimicrob. Agents Chemother.* 59, 1038–1047. doi: 10.1128/AAC.03560-14

Peleg, A. Y., Jara, S., Monga, D., Eliopoulos, G. M., Moellering, R. C., Jrand Mylonakis, E., et al. (2009). Galleria mellonella as a model system to study *Acinetobacter baumannii* pathogenesis and therapeutics. *Antimicrob. Agents Chemother.* 53, 2605–2609. doi: 10.1128/AAC.01533-08

Roach, D. R., and Donovan, D. M. (2015). Antimicrobial bacteriophage-derived proteins and therapeutic applications. *Bacteriophage* 5:e1062590. doi: 10.1080/21597081.2015.1062590

Schooley, R. T., Biswas, B., Gill, J. J., Hernandez-Morales, A., Lancaster, J., Lessor, L., et al. (2017). Development and use of personalized bacteriophage-based therapeutic cocktails to treat a patient with a disseminated resistant *Acinetobacter baumannii* infection. *Antimicrob. Agents Chemother.* 61, e954–e917. doi: 10.1128/AAC.00954-17

Wang, Y., El-Deen, A. G., Li, P., Oh, B. H., Guo, Z., Khin, M. M., et al. (2015). High-performance capacitive deionization disinfection of water with graphene oxide-graft-quaternized chitosan nanohybrid electrode coating. *ACS Nano* 9, 10142–10157. doi: 10.1021/acsnano.5b03763

Wang, Y., Mi, Z., Niu, W., An, X., Yuan, X., Liu, H., et al. (2016). Intranasal treatment with bacteriophage rescues mice from *Acinetobacter baumannii*-mediated pneumonia. *Future Microbiol.* 11, 631–641. doi: 10.2217/fmb.16.11

Wojda, I. (2017). Immunity of the greater wax moth *Galleria mellonella*. *Insect Sci.* 24, 342–357. doi: 10.1111/1744-7917.12325

Wong, D., Nielsen, T. B., Bonomo, R. A., Pantapalangkoor, P., Luna, B., and Spellberg, B. (2017). Clinical and pathophysiological overview of acinetobacter infections: a century of challenges. *Clin. Microbiol. Rev.* 30, 409–447. doi: 10.1128/CMR.00058-16

World Health Organization [WHO] (2017). *Antibacterial Agents in Clinical Development: An Analysis of the Antibacterial Clinical Development Pipeline, Including Tuberculosis*. Available at: http://www.who.int/iris/handle/10665/258965

Wright, A., Hawkins, C. H., Anggard, E. E., and Harper, D. R. (2009). A controlled clinical trial of a therapeutic bacteriophage preparation in chronic otitis due to antibiotic-resistant *Pseudomonas aeruginosa*; a preliminary report of efficacy. *Clin. Otolaryngol.* 34, 349–357. doi: 10.1111/j.1749-4486.2009.01973.x

Zelmer, A., Martin, M. J., Gundogdu, O., Birchenough, G., Lever, R., Wren, B. W., et al. (2010). Administration of capsule-selective endosialidase E minimizes upregulation of organ gene expression induced by experimental systemic infection with *Escherichia coli* K1. *Microbiology* 156(Pt 7), 2205–2215. doi: 10.1099/mic.0.036145-0

Zhou, Y., Zhang, H., Bao, H., Wang, X., and Wang, R. (2017). The lytic activity of recombinant phage lysin LysKDeltaamidase against staphylococcal strains associated with bovine and human infections in the Jiangsu province of China. *Res. Vet. Sci.* 111, 113–119. doi: 10.1016/j.rvsc.2017.02.011

Conflict of Interest Statement: The authors declare that the research was conducted in the absence of any commercial or financial relationships that could be construed as a potential conflict of interest.

frontiers in Microbiology

CORRECTION
published: 30 April 2019
doi: 10.3389/fmicb.2019.00942

Corrigendum: The Capsule Depolymerase Dpo48 Rescues *Galleria mellonella* and Mice From *Acinetobacter baumannii* Systemic Infections

OPEN ACCESS

Approved by:
Frontiers in Microbiology Editorial Office, Frontiers Media SA, Switzerland

***Correspondence:**
Zhiqiang Mi
zhiqiangmi_ime@163.com
Changqing Bai
mlp1604@sina.com
Zhancheng Gao
zcgao@bjmu.edu.cn

Specialty section:
This article was submitted to Antimicrobials, Resistance and Chemotherapy, a section of the journal Frontiers in Microbiology

Received: *03 April 2019*
Accepted: *12 April 2019*
Published: *30 April 2019*

Citation:
Liu Y, Leung SSY, Guo Y, Zhao L, Jiang N, Mi L, Li P, Wang C, Qin Y, Mi Z, Bai C and Gao Z (2019) Corrigendum: The Capsule Depolymerase Dpo48 Rescues Galleria mellonella and Mice From Acinetobacter baumannii Systemic Infections. Front. Microbiol. 10:942. doi: 10.3389/fmicb.2019.00942

Yannan Liu[1], Sharon Shui Yee Leung[2], Yatao Guo[1], Lili Zhao[1], Ning Jiang[1], Liyuan Mi[3], Puyuan Li[4], Can Wang[4], Yanhong Qin[4], Zhiqiang Mi[3], Changqing Bai[4]* and Zhancheng Gao[1]**

[1] Department of Respiratory and Critical Care Medicine, Peking University People's Hospital, Beijing, China, [2] School of Pharmacy, The Chinese University of Hong Kong, Shatin, Hong Kong, [3] State Key Laboratory of Pathogen and Biosecurity, Beijing Institute of Microbiology and Epidemiology, Beijing, China, [4] Department of Respiratory and Critical Care Medicine, 307th Hospital of Chinese People's Liberation Army, Beijing, China

Keywords: *Acinetobacter baumannii*, capsule depolymerase, *Galleria mellonella* model, mouse model, systemic infection, antivirulence

A Corrigendum on

The Capsule Depolymerase Dpo48 Rescues *Galleria mellonella* and Mice From *Acinetobacter baumannii* Systemic Infections

by Liu, Y., Leung, S. S. Y., Guo, Y., Zhao, L., Jiang, N., Mi, L., et al. (2019). Front. Microbiol. 10:545. doi: 10.3389/fmicb.2019.00545

In the published article, there was an error in the affiliation of Yannan Liu. The author is not connected to the second affiliation, 307th Hospital of Chinese People's Liberation Army. The authors apologize for this error and state that this does not change the scientific conclusions of the article in any way. The original article has been updated.

frontiers in Microbiology

ORIGINAL RESEARCH
published: 26 March 2019
doi: 10.3389/fmicb.2019.00559

Phenotypic and Genotypic Characterization of *Acinetobacter* spp. Panel Strains: A Cornerstone to Facilitate Antimicrobial Development

Roshan D'Souza[1,2], *Naina A. Pinto*[1,3], *Nguyen Le Phuong*[1,3], *Paul G. Higgins*[4,5], *Thao Nguyen Vu*[1,3], *Jung-Hyun Byun*[1,6], *Young Lag Cho*[5], *Jong Rak Choi*[1] and *Dongeun Yong*[1]*

[1] Department of Laboratory Medicine, Research Institute of Bacterial Resistance, Yonsei University College of Medicine, Seoul, South Korea, [2] J. Craig Venter Institute, Rockville, MD, United States, [3] Brain Korea 21 PLUS Project for Medical Science, Yonsei University, Seoul, South Korea, [4] Institute for Medical Microbiology, Immunology and Hygiene, University of Cologne, Cologne, Germany, [5] German Centre for Infection Research, Partner site Bonn-Cologne, Germany, [6] Department of Laboratory Medicine, Gyeongsang National University College of Medicine, Jinju, South Korea

OPEN ACCESS

Edited by:
Maria Soledad Ramirez, California State University, Fullerton, United States

Reviewed by:
Mariana Andrea Papalia, Universidad de Buenos Aires, Argentina
Timothy Meredith, Pennsylvania State University, United States

***Correspondence:**
Dongeun Yong
deyong@yuhs.ac

Specialty section:
This article was submitted to Infectious Diseases, a section of the journal Frontiers in Microbiology

Received: *10 December 2018*
Accepted: *05 March 2019*
Published: *26 March 2019*

Citation:
D'Souza R, Pinto NA, Phuong NL, Higgins PG, Vu TN, Byun J-H, Cho YL, Choi JR and Yong D (2019) Phenotypic and Genotypic Characterization of Acinetobacter spp. Panel Strains: A Cornerstone to Facilitate Antimicrobial Development. Front. Microbiol. 10:559. doi: 10.3389/fmicb.2019.00559

Acinetobacter spp. have emerged as significant pathogens causing nosocomial infections. Treatment of these pathogens has become a major challenge to clinicians worldwide, due to their increasing tendency to antibiotic resistance. To address this, much revenue and technology are currently being dedicated toward developing novel drugs and antibiotic combinations to combat antimicrobial resistance. To address this issue, we have constructed a panel of *Acinetobacter* spp. strains expressing different antimicrobial resistance determinants such as narrow spectrum β-lactamases, extended-spectrum β-lactamases, OXA-type-carbapenemase, metallo-beta-lactamase, and over-expressed AmpC β-lactamase. Bacterial strains exhibiting different resistance phenotypes were collected between 2008 and 2013 from Severance Hospital, Seoul. Antimicrobial susceptibility was determined according to the CLSI guidelines using agar dilution method. Selected strains were sequenced using Ion Torrent PGM system, annotated using RAST server and analyzed using Geneious pro 8.0. Genotypic determinants, such as acquired resistance genes, changes in the expression of efflux pumps, mutations, and porin alternations, contributing to the relevant expressed phenotype were characterized. Isolates expressing ESBL phenotype consisted of bla_{PER-1} gene, the overproduction of intrinsic AmpC beta-lactamase associated with IS*Aba1* insertion, and carbapenem resistance associated with production of carbapenem-hydrolyzing Ambler class D β-lactamases, such as OXA-23, OXA-66, OXA-120, OXA-500, and metallo-β-lactamase, SIM-1. We have analyzed the relative expression of Ade efflux systems, and determined the sequences of their regulators to correlate with phenotypic resistance. Quinolone resistance-determining regions were analyzed to understand fluoroquinolone-resistance. Virulence factors responsible for pathogenesis were also identified. Due to several mutations, acquisition of multiple resistance genes and transposon insertion, phenotypic resistance decision scheme for

for evaluating the resistance proved inaccurate, which highlights the urgent need for modification to this scheme. This complete illustration of mechanism contributing to specific resistance phenotypes can be used as a target for novel drug development. It can also be used as a reference strain in the clinical laboratory and for the evaluation of antibiotic efficacy for specific resistance mechanisms.

Keywords: *Acinetobacter*, panel strains, antimicrobial resistance, whole-genome sequencing, phenotypic characterization

INTRODUCTION

Acinetobacter spp. are non-motile, non-fermenting Gram-negative bacteria. Over the years, several species have been identified, and the most common and clinically significant are *Acinetobacter baumannii, Acinetobacter pittii,* and *Acinetobacter nosocomialis* (Chen et al., 2014). These bacteria have emerged as the most troublesome pathogens in hospital settings, due to their rapid colonization and infection. Incidence and mortality due to *A. nosocomialis* and *A. pittii* are lower than those due to *A. baumannii*; however, these are frequently isolated from nosocomial infections (Wisplinghoff et al., 2012). *Acinetobacter* spp. have been implicated in many pathological conditions such as ventilator-associated pneumonia, urinary tract infections, skin and wound infections, infective endocarditis, bacteremia, and secondary meningitis (Fishbain and Peleg, 2010; Garnacho-Montero and Amaya-Villar, 2010; Visca et al., 2011; Chusri et al., 2014). These infections have become challenging to treat due to their widespread multidrug resistance owing to mechanisms such as horizontal gene transfer, increased expression of β-lactamases, alterations of membrane permeability, and increased expression of efflux pumps (Singh et al., 2013); (Blair et al., 2015).

For several decades, numerous research have been conducted to understand the mechanisms of resistance and to control its dissemination in clinical settings. Considering the severity of infections, we have constructed a series of panel strains of *Acinetobacter* spp. expressing different resistance phenotypes such as narrow spectrum β-lactamase and oxacillinase, extended spectrum β-lactamase (ESBL), OXA-type carbapenemase, metallo-β-lactamase (MBL), and over-expressing AmpC β-lactamase. These strains were characterized genotypically using massive parallel sequencing (MPS) technology to understand the observed phenotypes. In this study, we have performed detailed analysis of the whole genome sequence (WGS) related to multidrug-resistance mechanisms, such as acquisition of β-lactamases, transposon insertions, mutations in porins, and changes in efflux pumps, and interpreted the discrepancy observed in phenotypic changes to relevant antibiotics. These panel strains can be used in hospital settings as reference strains, and also in the pharmaceutical industry to check the efficacy of new antibiotic drugs on pathogens expressing different resistance determinants. These strains can be distributed world-wide to institutions working on discovery of novel antibiotics, aiding in their characterization.

MATERIALS AND METHODS

Bacterial Strains

All bacterial strains were collected from Severance Hospital, Seoul from 2008 to 2013. Almost 4,000 strains were shortlisted depending on their *in-silico* resistance prediction from the hospital patient database, according to the resistance determination decision tree to interpret the type of resistance based on phenotypic observation by François et al. (2004) and Richard Bonnet (2010). Strains were categorized according to their resistance phenotype such as narrow spectrum β-lactamase and oxacillinase, ESBL, OXA-type-carbapenemase, MBL and over-expressed AmpC β-lactamase. Bacteria were identified using the direct colony method with MALDI-TOF MS (Bruker Daltonics, Bremen, Germany). In addition, RNA polymerase β-subunit gene (*rpoB*)-based identification was used to delineate species within the *Acinetobacter* genus (La Scola et al., 2006).

Susceptibility Tests

Initially, disc diffusion assays were performed on Muller Hinton agar plates with antibiotic discs containing piperacillin, ampicillin, piperacillin-tazobactam, ceftazidime, cefepime, imipenem, meropenem, ciprofloxacin, ceftazidime-clavulanate, ampicillin-sulbactam, and aztreonam to detect antibiotic susceptibility. In addition, the minimum-inhibitory concentrations (MIC) for bacterial strains were determined using agar dilution technique. E-test was used to measure the MIC of levofloxacin, trimethoprim/sulfamethoxazole, tigecycline, tetracycline, gentamicin, rifampicin, clindamycin, erythromycin and chloramphenicol. All of the procedures and results interpretation followed the Clinical and Laboratory Standards Institute (CLSI) guidelines. AmpC β-lactamase-, MBL, and ESBL-producing strains were selected using ertapenem-amino phenylboronic acid (APBA), imipenem-EDTA, and cefepime-clavulanate double disk synergy tests, respectively (Lee et al., 2001). Modified Hodge tests were also performed with cefoxitin disk for AmpC beta-lactamase detection, and imipenem disk for carbapenemase detection (Lee et al., 2010).

Whole Genome Sequencing and Bioinformatics Analysis

A few strains from each phenotypic resistance class were randomly selected and cultured overnight. Genomic DNA extractions were performed using Wizard genomic DNA purification kit (Promega, WI, USA) with a few modifications to the manufacturer's protocol, such as adding 5 μl of RNase

solution during cell lysis as well as incubating the supernatant carrying the DNA at −20°C for 1 h after addition of isopropanol. DNA concentration was measured using Qubit dsDNA BR assay kit (Molecular Probes, OR, USA) before sequencing.

Whole genome libraries were prepared using Ion plus fragment library kit, and Emulsion PCR was carried out using Ion one touch 200 Template kit v2 DL (Life technologies, CA, USA). Sequencing of the amplicon libraries was carried out on a 318 chip, using Ion Personal Genome Machine Ion Torrent sequencer through Ion Sequencing 200 kit (Life technologies, CA, USA). The resultant reads were assembled using MIRA plug-in (version 4.0) of Torrent suite software. Genome assemblies were annotated using RAST annotation pipeline, and further validated with Geneious pro 8.0 (Aziz et al., 2008; Kearse et al., 2012). Genes encoding the efflux systems, porins, and virulence factors of the panel strains were aligned using Clustal Omega, and verified for the polymorphisms (Sievers et al., 2011). Resistance genes were identified using Resfinder (Zankari et al., 2012), and manually curated using NCBI BLAST. Multi-locus sequence typing was performed using MLST 1.8 (Zankari et al., 2013) and *Acinetobacter baumannii* MLST website (Jolley and Maiden, 2010).

Outer Membrane Protein Detection

Bacterial cells were grown in Muller-Hinton broth until logarithmic phase, and centrifuged at 5,000 g for 15 min, washed twice in 10-mM phosphate buffer, and lysed by sonication at 18–20% amplitude for 2 × 30 s cycles, each comprised 6 × 5 s sonication steps separated by 1 s of no sonication, and 30 s of no sonication between the two cycles. Unbroken cells were eliminated using centrifugation at 3,000 g for 5 min, and outer membrane was solubilized with 2% sodium lauroyl sarcosinate. Insoluble outer membrane fraction was recovered by ultracentrifugation at 25,000 g for 1 h, as described previously (Hernandez-Alles et al., 1999). OMP profiles were determined using SDS-PAGE using Mini-Protean TGX gels (12%), followed by Coomassie blue staining (Bio-Rad, CA, USA). Additionally, OMPs were identified using Matrix-Assisted Laser Desorption-Time of Flight Mass Spectrometry on Tinkerbell LT (ASTA, Suwon, Korea), as described (Pinto et al., 2017). All experiments were repeated three times independently to check for reproducibility of the results.

Quantitative Real-Time RT-qPCR

Total RNA of the 12 *Acinetobacter* spp. isolates were extracted from exponentially grown bacterial cells with optical density at 600 nm of 0.7–0.8, using RNeasy Mini Kit (Qiagen, Hilden, Germany). Quantity and quality of RNA samples were checked using NanoDrop spectrophotometer (ND- 2000 Thermo scientific, USA). RNA samples with 260/280 ratio from 1.9 to 2.1, 260/230 ratio from 2.0 to 2.5 were used for further analysis. All of the RNA samples were adjusted to the same concentration. Then, 1 μg of total RNA was used to synthesize cDNA by reverse transcription using M-MLV cDNA Synthesis Kit (Enzynomics, Korea) in a 20 μl reaction using 50 μM random hexamers. cDNA was further diluted and stored at −20°C until PCR. Real-time PCR was performed with a 20-μl reaction volume containing 2 μl (100ng) of cDNA, 1X iQ SYBR Green Supermix (Bio-Rad, CA, USA), and gene-specific primers, 300 nM each (for *adeB*, *adeG*, *adeJ*, *baeSR*, *carO*, *33-36kDa omp,* and *oprD genes*), on StepOne Real-Time PCR System (Life technologies, CA, USA) with the following cycle: 1 cycle at 95°C for 3 min followed by 40 cycles of 95°C for 10 s and 56°C for 1 min. Dissociation curve was generated to check PCR amplification specificity. In each run, 2 μl RNase-free water was used as a no template control (NTC) for each gene. The primers used for RT-qPCR were designed using Primer3web (version 4.1.0) (Untergasser et al., 2012), validated using Geneious pro 8.0. (Kearse et al., 2012), synthesized commercially by Macrogen, Inc., Korea, and are shown in **Table S9**. Different primers were used for different species due to the polymorphism identified in efflux pumps. Each experiment was performed in triplicates at least twice independently. The changes in expression level for each gene was calculated according to a previous study (Livak and Schmittgen, 2001). In brief, for each sample, the threshold cycle (Ct) of target gene was determined and normalized to Ct value of *rpoB* gene, and then calculated relatively to the calibrator (strain YMC/2009/2/B2968) using formula $2^{-\Delta\Delta Ct}$ (data is represented as mean ± standard error). Detailed experimental conditions used in RT-qPCR based on MIQE requirements are described in **Table S10**.

RESULTS AND DISCUSSION

Among the 4,000 *Acinetobacter* spp. screened initially, we selected 26 isolates showing different phenotypic resistances, i.e., two ESBL-, six high-level AmpC β-lactamase-, ten OXA-type-carbapenemase-, five MBL-, two narrow-spectrum β-lactamase-, one narrow-spectrum oxacillinase-producing strains, in addition to a wild type strain, susceptible to all tested antibiotics (**Table S1**). Among these YMC2003/5/C86, YMC2003/1/R306 in ESBL's; YMC2009/2/B6756, YMC2012/7/R3167 among over-expressed AmpC beta-lactamase; YMC2011/2/C582, YMC2011/7/R812, YMC2012/1/R79, and YMC2012/9/R2209 in OXA-type-carbapenemase; YMC2013/3/R2081 in MBL; YMC2010/8/T346 in narrow spectrum beta-lactamase; and YMC2009/2/B2968 in narrow-spectrum oxacillinase were randomly picked and sequenced to further characterize the phenotypic and genotypic correlation (**Tables 1**, **2**). The draft genome sequences of strains YMC2003/5/C86, YMC2003/1/R306, YMC2009/2/B6756, YMC2012/7/R3167, YMC2011/2/C582, YMC2011/7/R812, YMC2012/1/R79, YMC2012/9/R2209, YMC2013/3/R2081, YMC2010/8/T346, and YMC2009/2/B2968 have been deposited at DDBJ/ENA/GenBank under the accession MKHG00000000, MKHH00000000, MKHI00000000, MKHJ00000000, MKHK00000000, MKHL00000000, MKHM00000000, MKHN00000000, MKHO00000000, and MKHP00000000, respectively.

Extended-Spectrum Beta-Lactamases

In Korea a high prevalence of bla_{PER-1} ESBL-producing *Acinetobacter* spp. was reported between 2001 and 2005 (Yong et al., 2003), and the level has been reducing over the years. The bla_{PER-1} belongs to class A extended-spectrum beta-lactamase,

which has been detected in *P. aeruginosa* (Ranellou et al., 2012), *P. mirabilis* (Pagani et al., 2004), *S. enterica* (Poirel et al., 2005), and *Acinetobacter* spp. (Naas et al., 2006), and disseminated worldwide since its first detection in France on 1993 (Nordmann et al., 1993). ESBLs are a class of group A β-lactamases, which hydrolyze third generation cephalosporin's but are inhibited by beta-lactamase inhibitors like clavulanic acid (Bradford, 2001; Jacoby and Munoz-Price, 2005). Antimicrobial susceptibility for beta-lactams is similar in ESBLs and high-level AmpC β-lactamase-producing *Acinetobacter* spp. We have categorized the strains depending according to the presence of ESBL or AmpC-producing genes, along with IS elements.

a) *Acinetobacter baumannii* YMC2003/5/C86: This strain was resistant to all antibiotics tested in this study, except ceftazidime-clavulanate. WGS analysis indicated the presence of $bla_{\mathrm{PER-1}}$, $bla_{\mathrm{TEM-1D}}$, $bla_{\mathrm{ADC-31}}$, and $bla_{\mathrm{OXA-82}}$. The $bla_{\mathrm{PER-1}}$ gene was flanked by the putative transposase gene *tpnA1* and *tpnA2* in upstream and downstream region. Insertion sequence IS*Aba1* was located immediate upstream region of AmpC beta-lactamase gene, $bla_{\mathrm{ADC-31}}$ and carbapenemase gene, $bla_{\mathrm{OXA-82}}$ (Zander et al., 2013) (**Figure S1**). Beta-lactam and cephalosporin resistance of this isolate can be clearly argued by the presence of these encoded β-lactamase genes along with the insertion elements, providing the additional promoters for their increased expression (Lin et al., 2010). Resistance to aminoglycosides and gentamicin are contributed by *aac(3′)-Ia*, *aac(6′)-Il, aph(3′)-Ic,* and *strAB* genes (**Tables 1**, **2**). Levofloxacin resistance was conferred due to the mutations observed in *gyrA* and *parC* genes (**Table 3**). Twenty to seventy-fold up-regulation of *adeB* and *adeJ* efflux pumps genes were confirmed, which are assumed to contribute to the resistance of levofloxacin, trimethoprim/sulfamethoxazole, tigecycline, clindamycin, chloramphenicol, and tetracyclines (**Table 1**, **Figure 1**).

b) *Acinetobacter nosocomialis* YMC2003/1/R306 was susceptible to imipenem, meropenem, and ciprofloxacin, intermediate to piperacillin-tazobactam, but resistant to piperacillin, ceftazidime, cefepime, and ampicillin-sulbactam. This isolate is an ideal candidate for ESBL strain, as it carries $bla_{\mathrm{PER-1}}$,which is identified as a part of composite transposon bracketed by two insertion elements *ISPa12* and *ISPa13*, belonging to IS4 family (**Figure S2**). Expression of this gene was driven by *ISPa12* promoter, and its genetic environment is similar to the $bla_{\mathrm{PER-1}}$ found in *Providencia stuartii* and *Pseudomonas aeruginosa* isolates, as reported previously (Yong et al., 2003; Poirel et al., 2005). Efflux pumps showed lower expression, which correlated to its increased susceptibility toward fluoroquinolones and tetracyclines (**Tables 1**, **3**, **Figure 1**).

Over-Expressed AmpC Beta-Lactamase

Overproduction of intrinsic cephalosporinase such as $bla_{\mathrm{ADC-25}}$, $bla_{\mathrm{ADC-30}}$, or $bla_{\mathrm{ADC-56}}$ coupled with insertion elements, such as IS*Aba1*, are responsible for cephalosporin resistance (Lopes and Amyes, 2012).

a) *Acinetobacter baumannii* YMC2009/2/B6756 was only susceptible to imipenem and meropenem, but resistant to all other antibiotics and beta-lactamase inhibitor combinations used in the study (**Table 1**). Genomic analysis indicated the presence of $bla_{\mathrm{TEM-1D}}$, $bla_{\mathrm{ADC-30}}$, and $bla_{\mathrm{OXA-66}}$ (a $bla_{\mathrm{OXA-51-like}}$ gene) (**Figure S3**). The $bla_{\mathrm{TEM-1D}}$ gene in this strain consisted of P3 promoter, which was initially found in Russia contributing to beta-lactam inhibitor-resistance (Edelstein et al., 2000; Leflon-Guibout et al., 2000; Constança and Manuela, 2003). Beta-lactam resistance in this isolate is attributed to the insertion of IS*Aba1* upstream of AmpC gene, $bla_{\mathrm{ADC-30}}$, mediating its over-expression (Li et al., 2015). OXA-66 is the intrinsic OXA-51 variant class D carbapenemase, which does not confer resistance to carbapenems, although it is associated with IS*Aba1*; however, a point mutation converts it into OXA-82, and this variant confers resistance to imipenem and meropenem (Zander et al., 2013) (**Figure S3**). OXA-82 and OXA-66 are associated with the International clone 2, which is the most prevalent clone found worldwide (Hu et al., 2007; Evans et al., 2008; Evans and Amyes, 2014). Decreased susceptibility toward levofloxacin, tetracycline, trimethoprim/sulfamethoxazole, rifampicin, chloramphenicol, and gentamicin (**Tables 1**, **3**) is contributed by *aacA4*, *aadA1*, *aac(3)-Ia*, *armA,* and *aac(6')Ib-cr* genes along with the more than 20-fold increased expression of *adeA*, *adeG*, *and adeJ* efflux pumps compared to the susceptible strain (Magnet et al., 2001; Coyne et al., 2010; Yoon et al., 2013) (**Figure 1**).

b) *Acinetobacter baumannii* YMC2012/7/R3167 was susceptible to piperacillin-tazobactam, imipenem, and meropenem, but resistant to ampicillin-sulbactam, piperacillin, ceftazidime, cefepime, ceftazidime-clavulanate (**Table 1**), and ciprofloxacin (**Table 3**). Whole genome analysis indicated the presence of β-lactamase genes, $bla_{\mathrm{ADC-30}}$, and $bla_{\mathrm{OXA-66}}$. (Hu et al., 2007; Zander et al., 2013) (**Figure S4**). Further analysis indicated the insertion of IS*Aba1* upstream of AmpC gene-$bla_{\mathrm{ADC-30}}$ which provided a stronger promoter leading to over-expression of AmpC beta-lactamase (Li et al., 2015) leading to multiple beta-lactam resistance. Genetic structure around $bla_{\mathrm{ADC-30}}$, and $bla_{\mathrm{OXA-66}}$ of this strain was identical to *A. baumannii* YMC2009/2/B6756. As opposed to the phenotypic resistance scheme for over-expressed AmpC beta-lactamase class, this strain was susceptible to piperacillin-tazobactam, and we were unable to explain the discrepancy for this phenotype. The expressions of *adeB* and *adeG* were similar to *A. baumannii* YMC2009/2/B6756. High-level resistance to tetracycline was observed due to *tet(B)* gene (Takahashi et al., 2002).

OXA-Type-Carbapenemases

Carbapenem resistance in *Acinetobacter* spp. is mediated by various mechanisms such as membrane impermeability due to loss of porins, but it is mostly mediated by enzymatic hydrolysis of antibiotics (Bou et al., 2000; Quale et al., 2003; Bonomo and Szabo, 2006; Poirel and Nordmann, 2006; Nordmann, 2010). Carbapenem-hydrolyzing class D beta-lactamases (CHDLs) or OXA-type-carbapenemases (OXA-51-like, 23-like, -58-like, -143-like, -40-like, and 235-like), often associated with upstream

TABLE 1 | Selected list of *Acinetobacter* spp. panel strains and its minimum inhibitory concentration with its sequence types.

Strains	ST	SAM	PIP	PIP-TZ	CAZ	FEP	IPM	MEM	CAZ-CLV	TET	TGC	TS	RI	CM	EM	CL	GM
ESBL			R	I/R	R	R	S	S									
A. baumannii YMC2003/5/C86	423	32, R	256, R	128, R	64, R	64, R	32, R	32, R	8, S	256, R	3	32	6	256	32	256	256, R
A. nosocomialis YMC2003/1/R306	948	32, R	256, R	32, I	64, R	64, R	2, S	4, S	4, S	24, R	0.19	4	4	128	12	16	64, R
Over-expressed AmpC β-lactamase			I/R	I/R	R	I/R	S	S									
A. baumannii YMC2009/2/B6756	191	32, R	256, R	256, R	256, R	32, R	2, S	4, S	64, R	64, R	1.5	32	4	256	256	256	256, R
A. baumannii YMC2012/7/R3167	208	32, R	256, R	8, S	64, R	32, R	1, S	4, S	64, R	256, R	1.5	1	6	256	12	256	4, S
OXA-type carbapenemase			R	R	S	S	I/R	I/R									
A. baumannii YMC2011/7/R812	1386	32, R	256, R	256, R	4, S	16, I	16, R	32, R	4, S	2, S	0.09	32	1.5	96	6	128	0.5, S
A. baumannii YMC2012/1/R79	191	32, R	256, R	256, R	256, R	128, R	32, R	64, R	64, R	256, R	1	32	3	256	256	256	256, R
A. baumannii YMC2011/2/C582	208	128, R	256, R	256, R	256, R	128, R	256, R	128, R	64, R	32, R	2	32	32	256	256	256	256, R
A. baumannii YMC2012/9/R2209	229	32, R	256, R	256, R	256, R	64, R	8, I	32, R	64, R	6, I	0.75	32	4	256	12	256	1.5, S
Metallo-β-lactamase			R	R	R	R	R	R									
A. pittii YMC2013/3/R2081	1030	16, R	256, R	4, S	256, R	64, R	4, S	64, R	32, R	32, R	0.38	32	32	192	256	128	256, R
Narrow-spectrum β-lactamase			I/R	I/R	S	S	S	S									
A. pittii YMC2010/8/T346	1385	4, S	32, I	0.5, S	4, S	4, S	2, S	16, R	4, S	4, S	0.19	0.38	3	96	32	64	1, S
Narrow-spectrum oxacillinase			R	R	S	S	S	S									
A. pittii YMC2009/2/B2968	1638	2, S	32, I	0.5, S	4, S	4, S	0.25, S	0.5, S	4, S	2, S	0.09	0.38	2	48	6	32	0.5, S
Wild type			S	S	S	S	S	S									
A. baumannii YMC2013/1/R3000		4, S	256, R	0.5, S	8, S	16, I	0.25, S	1, S	4, S	2, S	0.125	0.19	3	96	8	48	1.5, S

R, Resistant; I, Intermediate; S, susceptible; SAM, Ampicillin/sulbactam; PIP, piperacillin; PIP/TZ, piperacillin-tazobactam; CAZ, ceftazidime; FEP, cefepime; IPM, imipenem; MEM, meropenem; CAZ/CLV, ceftazidime-clavulanate, TET, Tetracycline; TGC, Tigecycline; TS, Trimethoprim sulfamethoxazole; RI, Rifampicin; CM, Clindamycin; EM, Erythromycin; CL, Chloramphenicol; GM, Gentamicin.

TABLE 2 | Resistome analysis of the *Acinetobacter* spp. strains representing β-Lactamases and Aminoglycoside-modifying enzymes.

	β-Lactamase																		Aminoglycoside-modifying enzyme								
				ADC's																							
	CARB-8	PER-1	TEM-1D	ADC-22	ADC-25	ADC-30	ADC-31	ADC-41	ADC-77	OXA-82	OXA-66	OXA-23	OXA-120	OXA-421	OXA-499	OXA-213	OXA-500	SIM-1	Aac(3')-Ia	Aac(6')-Il	Aph(3')-Ic	aadA1/24	aacA	aadB	armA	strA	strB
ESBL																											
YMC2003/5/C86		•	•				•			•									•	•	•					•	•
YMC2003/1/R306		•			•																			•		•	•
OVER-EXPRESSED AMPC β-LACTAMASE																											
YMC2009/2/B6756			•			•					•								•			•	•		•		
YMC2012/7/R3167						•					•															•	•
OXA-TYPE CARBAPENEMASES																											
YMC2011/7/R812									•			•	•														
YMC2012/1/R79			•			•					•	•							•			•			•		
YMC2011/2/C582		•				•					•	•									•	•			•	•	•
YMC2012/9/R2209						•				•																•	•
METALLO-β-LACTAMASE																											
YMC2013/3/R2081	•	•			•												•	•				•					
NARROW-SPECTRUM β-LACTAMASE																											
YMC2010/8/T346								•							•	•											
NARROW-SPECTRUM OXACILLINASE																											
YMC2009/2/B2968				•										•													

insertion elements, lead to their over-expression resulting in carbapenem resistance (Poirel et al., 2010). Studies have indicated that OXA-40- and OXA-143-type carbapenemases were not associated with insertion sequences nor integrons (Higgins et al., 2009; Evans and Amyes, 2014). Below we have illustrated the mechanism of few strains expressing OXA-type carbapenemases. According to the resistance determination decision tree, these strains were similar to the phenotype observed in metallo-beta lactamase producers, except its susceptibility toward ceftazidime and cefepime. However, due to the complex resistance mechanism involving multiple beta-lactamases and efflux pumps, most of the strains in this class were resistant to these two antibiotics.

a) *Acinetobacter baumannii* YMC2011/7/R812 was susceptible to ceftazidime, ceftazidime-clavulanate, ciprofloxacin, and levofloxacin, but resistant to ampicillin-sulbactam, piperacillin, piperacillin-tazobactam, imipenem, and meropenem (**Tables 1**, **3**). This strain carried CHDLs such as OXA-120, belonging to OXA-51 family, and OXA-23, along with cephalosporinase ADC-77 (**Table 2**). There were no insertion sequences located around $bla_{\mathrm{OXA-120}}$ and $bla_{\mathrm{ADC-77}}$, keeping their expressions at the basal level (**Figure S5-A**). However, there was an IS*Aba1* insertion upstream of $bla_{\mathrm{OXA-23}}$ leading to the overexpression of carbapenemase hydrolyzing activity, along with cefepime resistance (Turton et al., 2006; Lin et al., 2010). As illustrated by Naas and Nordmann (2010) and OXA-type carbapenemase detection scheme, these classes of bacteria are susceptible to ceftazidime and cefepime. This strain was susceptible to fluoroquinolones, tetracyclines, and aminoglycosides (**Tables 1**, **3**) due to absence of *adeRS* genes, which encode a two-component system regulating AdeABC expression system. In addition, none of the known aminoglycoside and fluoroquinolone resistant genes were present (**Tables 1**, **3**). In addition, *adeC* gene was also absent, along with truncation of *adeA* gene (**Figure S5-B**). The genetic structure around $bla_{\mathrm{OXA-120}}$ from *A. baumannii* YMC2011/7/R812 and $bla_{\mathrm{OXA-66}}$ from ESBL-producing *A. baumannii* YMC2009/2/B6756 and YMC2012/7/R3167 were identical, as both the beta-lactamases belongs to OXA-51-like group (Rafei et al., 2015).

b) *Acinetobacter baumannii* YMC2012/1/R79 was resistant to all of the antibiotics used in this study. This strain carried $bla_{\mathrm{TEM-1D}}$, $bla_{\mathrm{ADC-30}}$, $bla_{\mathrm{OXA-66}}$, and CHDL, $bla_{\mathrm{OXA-23}}$. The multi-drug resistant phenotype of this strain was contributed by IS*Aba1*-$bla_{\mathrm{OXA-23}}$ and IS*Aba1*-$bla_{\mathrm{ADC-30}}$ genes (Turton et al., 2006; Lin et al., 2010) (**Figure S6**). Resistance to aminoglycoside were seen due to the presence of *aadA1, aadA24, armA*, and *aac(6′)Ib-cr* genes, resistance to fluoroquinolones were due to the mutations in *gyrA* and *parC* genes, along with the moderately increased expressions of *adeB*, *adeG*, and *adeJ* efflux pumps (**Table 1**, **Figure 1**).

c) *Acinetobacter baumannii* YMC2011/2/C582 was resistant to all of the antibiotics and beta-lactam inhibitors used in this study for phenotypic screening (**Table 1**). WGS analysis indicated the presence of ESBL gene, $bla_{\mathrm{PER-1}}$, and wide variety of other β-lactamase genes, such as $bla_{\mathrm{OXA-66}}$, $bla_{\mathrm{OXA-23}}$, and $bla_{\mathrm{ADC-30}}$ (**Table 2**). The $bla_{\mathrm{PER-1}}$ gene and partial *glutathione-S-transferase* were bracketed by IS*Pa12* and IS*Pa13*, belonging to the IS4 family, regulating the expression of $bla_{\mathrm{PER-1}}$ gene driven by promoter sequences in IS*Pa12* (Poirel et al., 2005), similar to *A. nosocomialis* YMC2003/1/R306 strain (**Figures S2, S7**). In addition, there was insertion of IS*Aba1* upstream of $bla_{\mathrm{ADC-30}}$ and $bla_{\mathrm{OXA-23}}$, providing additional promoter leading to increased resistance due to overexpressions of AmpC beta-lactamase and carbapenemase, respectively. Increased expression of *adeb, adeG*, and *adeJ*, along with aminoglycoside and fluoroquinolones resistance genes such as *armA, aph(3′)-Ic, strAB, aph(3′)-VIb, aadA1*, and *aac(6′)Ib-cr* decreased the susceptibility toward gentamicin, tetracycline, trimethoprim/sulfamethoxazole, rifampicin, and chloramphenicol (**Table 1**, **Figure 1**). In addition, mutations were observed in *gyrA* and *parC* genes, which caused levofloxacin resistance (**Table 3**).

d) *Acinetobacter baumannii* YMC2012/9/R2209 was intermediate to imipenem but resistant to all other cephalosporin and carbapenems used in our study (**Table 1**). This isolate was AmpC beta-lactamase hyper-producer along with CHDL, which was revealed by the presence of IS*Aba1*-$bla_{\mathrm{OXA-82}}$ and IS*Aba1*-$bla_{\mathrm{ADC-30}}$ (**Figure S8**). Increased carbapenem resistance was caused by IS*Aba1*-$bla_{\mathrm{OXA-82}}$ (Zander et al., 2013). Susceptibility toward tigecycline, gentamicin and tetracycline were due to the absence of aminoglycoside resistance genes and lower expressions of *adeB* and *adeG* efflux pumps (**Table 1**, **Figure 1**). In contrast, increased relative expression of *adeJ* gene might have increased resistance to fluoroquinolones, such as ciprofloxacin and levofloxacin, along with *gyrA* and *parC* genes mutations.

MBL

MBL-producing *Acinetobacter* spp. have become an emerging therapeutic concern worldwide. Along with CHDLs, carbapenem resistance is attributed to MBLs such as IMP, VIM, GIM, SIM etc. (Kim et al., 2014). According to the resistance detection scheme, *Acinetobacter* spp. producing MBLs display similar phenotypic resistance as OXA-type carbapenemases, except the latter showing its susceptibility toward ceftazidime and cefepime. MBL producing *A. pittii* YMC2013/3/R2081 was susceptible to piperacillin-tazobactam and imipenem but resistant to ampicillin-sulbactam, piperacillin, ceftazidime, cefepime, meropenem, ceftazidime-clavulanate, and ciprofloxacin. This bacterium contains $bla_{\mathrm{CARB-8}}$, $bla_{\mathrm{PER-1}}$, $bla_{\mathrm{ADC-18}}$, $bla_{\mathrm{OXA-500}}$, and $bla_{\mathrm{SIM-1}}$ (**Tables 1**, **2**). Resistance to most of antibiotics can be explained due to ESBL gene along with IS element, *IS*CR1-$bla_{\mathrm{PER-1}}$, and MBL gene, $bla_{\mathrm{SIM-1}}$ (**Figure S9**). Despite SIM-1 production, this bacterium was susceptible to imipenem due to its strong activity against *Acinetobacter* spp (Lee et al., 2005). Genetic analysis indicated that $bla_{\mathrm{SIM-1}}$ along with *aar-3*, *carB3*, and *aadA1* genes were encoded by class 1 integron. The $bla_{\mathrm{CARB-8}}$ is carbencillin-hydrolyzing beta-lactamase, which

has the same hydrolytic profile as bla_{CARB-5} (Choury et al., 2000). This enzyme has been previously identified in various species such as *Oligella urethralis*, *Vibrio cholerae*, *Achromobacter xylosoxidans*, *A. baumannii*, and *Salmonella typhimurium*, which indicates inter-genus transferability of the gene (Decre et al., 1995; Ridley and Threlfall, 1998; Choury et al., 1999, 2000; Lin et al., 2010). Increased resistance to gentamicin was mediated by the *aac(3)-IId* gene (Ho et al., 2010), despite lower expression of *adeB*, *adeG*, and *adeJ* efflux pumps (**Table 1**, **Figure 1**).

Narrow Spectrum β-Lactamase

Acinetobacter pittii YMC2010/8/T346 belongs to a novel sequence type 1385 (ST 1385), and is susceptible to ampicillin-sulbactam, piperacillin-tazobactam, ceftazidime, cefepime, imipenem, ceftazidime-clavulanate, and ciprofloxacin but resistant to meropenem (**Tables 1**, **3**). Sequence analysis indicated the presence of $bla_{OXA-506}$, variant of *A. pittii* intrinsic $bla_{OXA-213-like}$, bla_{ADC-41}, and $bla_{OXA-499}$, which were not associated with insertion elements (**Table 2**, **Figure S10**). The $bla_{OXA-499}$ is a novel variant of carbapenem hydrolyzing oxacillinase, $bla_{OXA-143}$. This gene was first found in South Korea, and is the carbapenem hydrolyzing gene which explains its resistance to the meropenem, as reported previously (D'Souza et al., 2017). Wide susceptibility toward aminoglycosides, tetracyclines, and fluoroquinolones was observed due to the lower expression of efflux pumps and absence of any corresponding resistance genes (**Tables 1, 3, Figure 1**).

Narrow Spectrum Oxacillinase

Acinetobacter pittii YMC2009/2/B2968 belonging to novel ST1638, was not resistant to the antibiotics tested in this study (**Table 1**). Whole genome analysis revealed $bla_{OXA-421}$, a CHDL belonging to *A. pittii* intrinsic $bla_{OXA-213}$ family and bla_{ADC-22} (**Table 2**, **Figure S11**). However, no existing study has yet demonstrated that the carbapenemase activity of $bla_{OXA421.}$ bla_{ADC-22} is a naturally occurring cephalosporinase gene in *A. baumannii,* which is repressed under normal conditions (Beceiro et al., 2009; Li et al., 2015). This strain exhibited the highest susceptibility toward aminoglycosides, tetracyclines, and fluoroquinolones among all other panel strains, due to the absence of corresponding resistance genes and lowest expression of efflux pumps. Therefore, this was selected as the reference strain to calculate the relative expression of efflux pumps for other strains.

Analysis of QRDRs for *gyrA* and *parC* Genes and Fluoroquinolone Resistance

The MICs of ciprofloxacin and levofloxacin were determined (**Table 3**). Both antibiotics functioned by inhibiting DNA gyrase subunit A (GyrA), DNA gyrase subunit B (GyrB), and toposiomerase IV subunit C (ParC) (Drlica and Zhao, 1997), and hence exhibited similar resistance phenotypes for the panel strains. Resistance to fluoroquinolone in bacteria was mediated by spontaneous mutations in *gyrA*, *gyrB*, and *parC* genes (Park et al., 2011; Ardebili et al., 2015). We identified the substitutions in GyrA (Ser81Leu) and ParC (Ser84Leu) in all fluoroquinolone resistant strains (**Table 3**). Ser467Gly and Glu88Lys mutation in ParC did not correlate with the resistance phenotypes. As opposed to the previous studies, we found GyrA (Ser81Leu) and ParC (Ser467Gly) mutations in *A. nosocomialis* YMC2003/1/R306, which were susceptible to fluoroquinolone (Vila et al., 1995). We could not find Glu479Asp, Cys423Ser, Glu479Asp, Leu420Gln, Cys423Ser, Leu433His, Glu479Asp, and D644Y mutations in GyrB which were previously described as novel substitutions (Park et al., 2011), except A677V in *A. baumannii* YMC2003/5/C86.

Efflux-Mediated Antimicrobial Resistance

Overexpression of efflux pumps are one of the major mechanisms that contribute to the multidrug resistance in *Acinetobacter* species. Genes encoding these systems are carried by mobile genetic elements or chromosomes, and thus be responsible for acquired or intrinsic resistance (Coyne et al., 2011). Five categories of efflux pump systems have been described, which are responsible for pumping out diverse classes of antibiotics: resistance-nodulation-cell division (RND) family, ATP-binding cassette (ABC) transporters, major facilitator superfamily (MFS), small multidrug resistance (SMR) family, and the recently identified multidrug and toxic compound extrusion (MATE) family (Piddock, 2006; Vila et al., 2007). Considering the broad-range substrate specificity of the three RND-type efflux pump systems, AdeABC, AdeFGH, and AdeIJK, we investigated the expressions of *adeB*, *adeG*, and *adeJ* genes (**Figures 1A–C**). Reference gene *rpoB* was used as a control, and susceptible strain *A. pittii* YMC2009/2/B2968 was used as a reference. Tigecycline appeared to be the best substrate for *adeB* pump, which correlated with their increased resistance and seven to 50-fold increase in its expression. This was consistent with previous findings (Perez et al., 2007; Ruzin et al., 2007; Hornsey et al., 2010) (**Table 1**, **Figure 1**). In addition, decreased susceptibility toward tetracycline, trimethoprim/sulfamethoxazole, and gentamicin also correlated with the increased expression with few exceptions. We screened for mutations in AdeRS, a two-component regulator system that controls the expression of AdeRS. G186V substitution in AdeS and A136V in AdeR was detected in all of the isolates overexpressing *adeB* gene, which was previously linked to increased tigecycline resistance (Hornsey et al., 2010; Rumbo et al., 2013) (**Tables S3, S4**). The isolate *A. baumannii* YMC2011/7/R812 did not contain *adeRS*, *adeA*, and *adeC* genes (**Table S2**). The *adeC* gene was also absent from *A. baumannii* YMC2012/9/R2209 and all *A. pittii* strains (**Table S2**). The expressions of *adeG* and *adeJ* were variable and strain-specific. Therefore, we could not find the suitable phenotypic marker regulating the pump. Overall, *A. baumannii* isolates showed increased expression of three RND efflux systems compared to *A. pittii* and *A. nosocomialis*. AdeFGH and its LysR-type transcriptional regulator AdeL were present in all strains (**Table S5**). TetR transcriptional repressor AdeN, controlling AdeIJK were interrupted by IS*Aba1* insertion sequence in *A. baumannii* YMC2012/9/R2209, YMC2012/7/R3167, and YMC2011/2/C582, which increased AdeIJK expression (Rosenfeld et al., 2012) (**Table S5**). In addition, we were unable to correlate the expression of BaeSR two-component system, which was previously known to

TABLE 3 | MIC of the fluoroquinolone (ciprofloxacin and levofloxacin) and amino-acid substitutions in the QRDR of the *gyrA*, *gyrB,* and *parC* genes of panel strains.

	MIC(μg/ml)		Amino-acid substitutions in		
	CIP*	**LEV***	***gyrA***	***parC***	***gyrB***
ESBL					
YMC2003/5/C86	128, R	32, R	S81L	E88K	A677V
YMC2003/1/R306	0.5, S	0.75, R	S81L	–	–
OVER-EXPRESSED AMPCβ -LACTAMASE					
YMC2009/2/B6756	128, R	6, I	S81L	S81L	–
YMC2012/7/R3167	256, R	8, R	S81L	S81L	–
OXA-TYPE CARBAPENEMASES					
YMC2011/7/R812	0.5, S	0.19, S	–	–	–
YMC2012/1/R79	128, R	6, I	S81L	S81L	–
YMC2011/2/C582	128, R	24, R	S81L	S81L	–
YMC2012/9/R2209	256, R	16, R	S81L	S81L	–
METALLO-β-LACTAMASE					
YMC2013/3/R2081	128, R	6, I	S81L	S81L	–
NARROW-SPECTRUM β-LACTAMASE					
YMC2010/8/T346	0.25, S	0.19, S	–	–	–
NARROW-SPECTRUM OXACILLINASE					
YMC2009/2/B2968	0.12, S	0.125, S	–	–	–

*MIC assay was performed using Disk diffusion technique and E-test for ciprofloxacin and levofloxacin, respectively.

influence tigecycline susceptibility by regulating *adeABC* genes (Lin et al., 2014) (**Figure 1D**). The limitation of our qRT-PCR was using different primers for different species due to the polymorphism identified in efflux pumps. This might have led to different amplicon kinetics resulting in errors in differential expressions. Finally, we could also detect the genes related to non-RND efflux pumps such as *cra*, *amvA*, *abeM*, *abeS*, and *adeXYZ* in all of the *Acinetobacter* strains. The *adeDE* gene was identified in YMC2003/1/R306 and YMC2013/3/R2081, and *cmlA* was present only in isolate YMC2013/3/R2081 (**Table S6**).

Role of Porins in Resistance

Porins play a vital role in the mechanism of carbapenem resistance in *Enterobacteriaceae*. However, in *Acinetobacter* spp., their contributions toward resistance are debated, and their functions remain ambiguous (Marti et al., 2006). Previous studies indicated that loss of porins such as *CarO*, *OprD*, and *33-36Kda Omp* conferred carbapenem resistance (Bou et al., 2000; Fernandez-Cuenca et al., 2003; Mussi et al., 2005; Siroy et al., 2005; Peleg et al., 2008). To determine the potential role of these porins in resistance, we performed SDS-PAGE (data not shown) and MALDI-TOF (**Figure S12**). All of the panel strains showed identical OMP profiles, which were also confirmed by WGS analysis (**Table S7**). These results suggested that the porins did not have any role in carbapenem resistance among the panel strains. In addition, qRT-PCR for *CarO*, *oprD*, and *33-36Kda Omp* did not show any significant correlation to antimicrobial resistance (**Figure S13**).

Virulence Factors

Understanding the pathogenesis, along with its multi-drug resistance phenotype, is highly essential for infection control and investigation of alternate treatment options. The development of infection, and bacterial survival in the host depends on virulence factors such as biofilm formation, serum resistance, evasion of the host immune response, motility, host cell apoptosis, bacterial dissemination, transfer of genetic material between bacterial cells, and iron acquisition mechanisms (Choi et al., 2005; Jacobs et al., 2010; Luke et al., 2010; Jin et al., 2011; Gaddy et al., 2012; McConnell et al., 2013). Virulence factors capsular polysaccharide (*ptk* and *epsA*), phospholipase D, and penicillin-binding protein (*pbpG*) were present in all of the panel strains (**Table S8**). Virulent genes associated with biofilm formation, such as *OmpA* and BfmR, the response regulator component of two-component system BfmRS, were present in all of the strains (Gaddy et al., 2009; Liou et al., 2014). However, another key virulent gene, *bap* (Biofilm-associated protein), was absent in YMC2011/7/R812, YMC2012/9/R2209, YMC2013/3/R2081, and YMC2009/2/B2968 (Badmasti et al., 2015). Outer membrane proteins, CsuA/B, CsuC, and CsuD were absent from YMC2011/7/R812 and YMC2010/8/T346. *Acinetobacter nosocomialis* YMC2003/1/R306 did not carry the genes involved in acinetobactin-mediated iron acquisition system such as *bauA, bauB, bauC, bauD, bauE, basC,* and *basD*, and we did not find homologs of these systems either.

In summary, all of the panel strains in our study were shortlisted depending on the resistance scheme given by François et al. (2004) and Naas and Nordmann in Antibiogram (Naas and Nordmann, 2010). Similar to our previous study in *Klebsiella pneumoniae* (Dsouza et al., 2017), we found several discrepancies in the detection scheme. The ESBL strain YMC2003/5/C86 isolated in our study was resistant to carbapenems due to presence of OXA-82, albeit the scheme indicates that ESBL strains should be susceptible to carbapenems. Similarly, it also indicates that OXA-type carbapenemases are susceptible to ceftazidime and cefepime. However, the isolated strains in

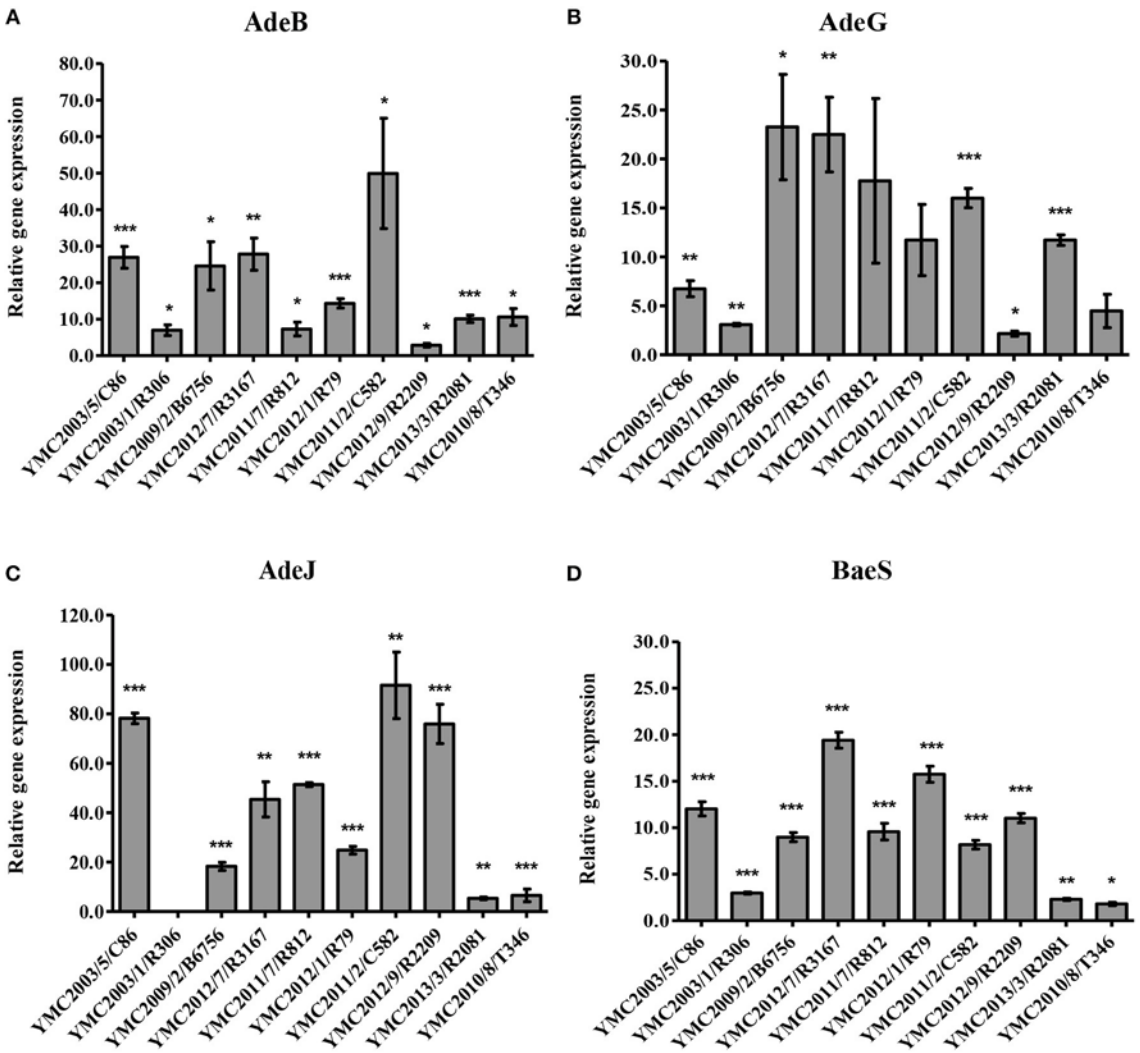

FIGURE 1 | Expression of **(A)** AdeB, **(B)** AdeG, **(C)** AdeJ, and **(D)** BaeS relative to rpoB. Susceptible strain *A. pittii* YMC2009/2/B2968 was used as a reference and each isolate was tested in triplicate in two independent experiments. The data represent the mean ± standard error for three independent replicates. The significant difference of expression levels between samples were indicated by bars and asterisks as follows: $*p < 0.05$, $**p < 0.01$, and $***p < 0.001$ using the Student's *t*-test.

this study were resistant to both antibiotics. Therefore, we suggest the scheme to be updated and modified considering the novel mutations, acquisition of multiple resistance genes, and transposon insertion, for better detection. The main drawback of this study was characterizing unequal number of strains in each resistance classes. Strains were obtained retrospectively and therefore, limiting the number of strains.

The basic rule in the pharmaceutical industry for developing new antibiotics, or for clinicians prescribing antibacterial therapy, depends on comprehensive understanding of the mechanism(s) of resistance. For some time now, *Acinetobacter* spp. have been implicated in several pathological conditions, and constant efforts are being undertaken to control the spread of these organisms in hospital and community settings (Maragakis and Perl, 2008; Vila and Pachon, 2008; Metan et al., 2009; Garnacho-Montero and Amaya-Villar, 2010; Evans et al., 2013; Wisplinghoff and Seifert, 2014; Dramowski et al., 2015). There are several mechanisms suggested for *Acinetobacter* spp. resistance for β-lactams and other antibiotics that we have outlined in this study. In hospital settings and research laboratories, it is quite common to encounter these pathogens with various resistance phenotypes. The genotypic and phenotypic correlations in our study would definitely help clinicians and researchers to better understand the mechanism associated, along with utilizing these pathogens as reference strains. In addition, these panel strains would be highly beneficial for evaluating the efficacy of novel antibiotics or antibiotic kit on *Acinetobacter* spp. displaying different resistance phenotypes. An in-depth study involving the genetic mechanism conferring resistance can open many opportunities for novel drug target study and ways to control the antimicrobial resistance. We have studied the role of various resistance genes attributing to the specific resistance in detail, by referring to previous publications. Therefore, we believe that we have constructed a single platform consisting of various

resistance genes illustrating its role, which can help antimicrobial researchers to understand the basics of antimicrobial resistance. Further, studies could be warranted to determine the lineage analysis on this strain and also understand the expression of virulence factors contributing toward the bacterial pathogenesis.

AUTHOR CONTRIBUTIONS

DY, JC, and YC designed the study and secured the funding. RD, NP, NLP, and TV performed the experiments. RD, PH, J-HB, and DY analyzed and interpreted the data and wrote the manuscript.

FUNDING

This work was supported by Korea Institute of Planning and Evaluation for Technology in Food, Agriculture, Forestry and Fisheries (IPET) through Agricultural Microbiome R&D Program, funded by Ministry of Agriculture, Food and Rural Affairs (MAFRA) (918003-4); by Nano Material Technology Development Program through the National Research Foundation of Korea (NRF) funded by the Ministry of Science and ICT (No.2017M3A7B4039936); by the Korea Health Technology R&D Project through the Korea Health Industry Development Institute (KHIDI), funded by the Ministry of Health & Welfare, Republic of Korea (grant number HI17C1807).

SUPPLEMENTARY MATERIAL

The Supplementary Material for this article can be found online at: https://www.frontiersin.org/articles/10.3389/fmicb.2019.00559/full#supplementary-material

REFERENCES

Ardebili, A., Lari, A. R., Beheshti, M., and Lari, E. R. (2015). Association between mutations in gyrA and parC genes of *Acinetobacter baumannii* clinical isolates and ciprofloxacin resistance. *Iran. J. Basic Med. Sci.* 18, 623–626.

Aziz, R. K., Bartels, D., Best, A. A., DeJongh, M., Disz, T., Edwards, R. A., et al. (2008). The RAST Server: rapid annotations using subsystems technology. *BMC Genomics* 9:75. doi: 10.1186/1471-2164-9-75

Badmasti, F., Siadat, S. D., Bouzari, S., Ajdary, S., and Shahcheraghi, F. (2015). Molecular detection of genes related to biofilm formation in multidrug-resistant *Acinetobacter baumannii* isolated from clinical settings. *J. Med. Microbiol.* 64(Pt 5), 559–564. doi: 10.1099/jmm.0.000058

Beceiro, A., Perez, A., Fernandez-Cuenca, F., Martinez-Martinez, L., Pascual, A., Vila, J., et al. (2009). Genetic variability among ampC genes from *Acinetobacter* genomic species 3. *Antimicrob. Agents Chemother.* 53, 1177–1184. doi: 10.1128/AAC.00485-08

Blair, J. M., Webber, M. A., Baylay, A. J., Ogbolu, D. O., and Piddock, L. J. (2015). Molecular mechanisms of antibiotic resistance. *Nat. Rev. Microbiol.* 13, 42–51. doi: 10.1038/nrmicro3380

Bonomo, R. A., and Szabo, D. (2006). Mechanisms of multidrug resistance in *Acinetobacter* species and *Pseudomonas aeruginosa*. *Clin. Infect. Dis.* 43 (Suppl. 2), S49–S56. doi: 10.1086/504477

Bou, G., Cervero, G., Dominguez, M. A., Quereda, C., and Martinez-Beltran, J. (2000). Characterization of a nosocomial outbreak caused by a multiresistant *Acinetobacter baumannii* strain with a carbapenem-hydrolyzing enzyme: high-level carbapenem resistance in *A. baumannii* is not due solely to the presence of beta-lactamases. *J. Clin. Microbiol.* 38, 3299–3305.

Bradford, P. A. (2001). Extended-spectrum β-lactamases in the 21st century: characterization, epidemiology, and detection of this important resistance threat. *Clin. Microbiol. Rev.* 14, 933–951. doi: 10.1128/CMR.14.4.933-951.2001

Chen, T. L., Lee, Y. T., Kuo, S. C., Yang, S. P., Fung, C. P., and Lee, S. D. (2014). Rapid identification of *Acinetobacter baumannii*, *Acinetobacter nosocomialis* and *Acinetobacter pittii* with a multiplex PCR assay. *J Med Microbiol* 63(Pt 9), 1154–1159. doi: 10.1099/jmm.0.071712-0

Choi, C. H., Lee, E. Y., Lee, Y. C., Park, T. I., Kim, H. J., Hyun, S. H., et al. (2005). Outer membrane protein 38 of *Acinetobacter baumannii* localizes to the mitochondria and induces apoptosis of epithelial cells. *Cell Microbiol.* 7, 1127–1138. doi: 10.1111/j.1462-5822.2005.00538.x

Choury, D., Aubert, G., Szajnert, M. F., Azibi, K., Delpech, M., and Paul, G. (1999). Characterization and nucleotide sequence of CARB-6, a new carbenicillin-hydrolyzing beta-lactamase from *Vibrio cholerae*. *Antimicrob. Agents Chemother.* 43, 297–301. doi: 10.1128/AAC.43.2.297

Choury, D., Szajnert, M. F., Joly-Guillou, M. L., Azibi, K., Delpech, M., and Paul, G. (2000). Nucleotide sequence of the bla(RTG-2) (CARB-5) gene and phylogeny of a new group of carbenicillinases. *Antimicrob. Agents Chemother.* 44, 1070–1074. doi: 10.1128/AAC.44.4.1070-1074.2000

Chusri, S., Chongsuvivatwong, V., Rivera, J. I., Silpapojakul, K., Singkhamanan, K., McNeil, E., et al. (2014). Clinical outcomes of hospital-acquired infection with *Acinetobacter nosocomialis* and *Acinetobacter pittii*. *Antimicrob. Agents Chemother.* 58, 4172–4179. doi: 10.1128/AAC.02992-14

Constança, P -F and Manuela, C. (2003). A novel sequence framework (bla(TEM-1G)) encoding the parental TEM-1 beta-lactamase. *FEMS Microbiol. Lett.* 220, 177–180. doi: 10.1016/S0378-1097(03)00123-X

Coyne, S., Courvalin, P., and Perichon, B. (2011). Efflux-mediated antibiotic resistance in *Acinetobacter* spp. *Antimicrob. Agents Chemother.* 55, 947–953. doi: 10.1128/AAC.01388-10

Coyne, S., Rosenfeld, N., Lambert, T., Courvalin, P., and Perichon, B. (2010). Overexpression of resistance-nodulation-cell division pump AdeFGH confers multidrug resistance in *Acinetobacter baumannii*. *Antimicrob. Agents Chemother.* 54, 4389–4393. doi: 10.1128/AAC.00155-10

Decre, D., Arlet, G., Bergogne-Berezin, E., and Philippon, A. (1995). Identification of a carbenicillin-hydrolyzing beta-lactamase in *Alcaligenes denitrificans* subsp. xylosoxydans. *Antimicrob. Agents Chemother.* 39, 771–774. doi: 10.1128/AAC.39.3.771

Dramowski, A., Cotton, M. F., Rabie, H., and Whitelaw, A. (2015). Trends in paediatric bloodstream infections at a South African referral hospital. *BMC Pediatr.* 15:33. doi: 10.1186/s12887-015-0354-3

Drlica, K., and Zhao, X. (1997). DNA gyrase, topoisomerase IV, and the 4-quinolones. *Microbiol. Mol. Biol. Rev.* 61, 377–392.

D'Souza, R., Pinto, N. A., Higgins, P. G., Hwang, I., Yong, D., Choi, J., et al. (2017). First report of the carbapenemase gene blaOXA-499 in *Acinetobacter pittii*. *Antimicrob. Agents Chemother.* 61, e02676–16. doi: 10.1128/AAC.02676-16

Dsouza, R., Pinto, N. A., Hwang, I., Cho, Y., Yong, D., Choi, J., et al. (2017). Panel strain of *Klebsiella pneumoniae* for beta-lactam antibiotic evaluation: their phenotypic and genotypic characterization. *PeerJ.* 5:e2896. doi: 10.7717/peerj.2896

Edelstein, M., Suvorov, M., Edelstein, I., and Kozlov, R. (2000). "Identification of the naturally occurring variant genes blaTEM-1d and blaTEM-70 encoding broad-spectrum TEM-Type b-lactamases," in *10th European Congress of Clinical Microbiology and Infectious Diseases* (Stockholm).

Evans, B. A., and Amyes, S. G. (2014). OXA beta-lactamases. *Clin. Microbiol. Rev.* 27, 241–263. doi: 10.1128/CMR.00117-13

Evans, B. A., Hamouda, A., and Amyes, S. G. (2013). The rise of carbapenem-resistant *Acinetobacter baumannii*. *Curr. Pharm. Des.* 19, 223–238. doi: 10.2174/138161213804070285

Evans, B. A., Hamouda, A., Towner, K. J., and Amyes, S. G. (2008). OXA-51-like beta-lactamases and their association with particular epidemic lineages of *Acinetobacter baumannii*. *Clin. Microbiol. Infect.* 14, 268–275. doi: 10.1111/j.1469-0691.2007.01919.x

Fernandez-Cuenca, F., Martinez-Martinez, L., Conejo, M. C., Ayala, J. A., Perea, E. J., and Pascual, A. (2003). Relationship between beta-lactamase production, outer membrane protein and penicillin-binding protein profiles on

the activity of carbapenems against clinical isolates of *Acinetobacter baumannii*. *J. Antimicrob. Chemother.* 51, 565–574. doi: 10.1093/jac/dkg097

Fishbain, J., and Peleg, A. Y. (2010). Treatment of *Acinetobacter* infections. *Clin. Infect. Dis.* 51, 79–84. doi: 10.1086/653120

François, J., Monique, C., and Michèle W., and Alain, G. (2004). *From Antibiogram to Prescription.* France: bioMérieux.

Gaddy, J. A., Arivett, B. A., McConnell, M. J., Lopez-Rojas, R., Pachon, J., and Actis, L. A. (2012). Role of acinetobactin-mediated iron acquisition functions in the interaction of *Acinetobacter baumannii* strain ATCC 19606T with human lung epithelial cells, *Galleria mellonella* caterpillars, and mice. *Infect. Immun.* 80, 1015–1024. doi: 10.1128/IAI.06279-11

Gaddy, J. A., Tomaras, A. P., and Actis, L. A. (2009). The *Acinetobacter baumannii* 19606 OmpA protein plays a role in biofilm formation on abiotic surfaces and in the interaction of this pathogen with eukaryotic cells. *Infect. Immun.* 77, 3150–3160. doi: 10.1128/IAI.00096-09

Garnacho-Montero, J., and Amaya-Villar, R. (2010). Multiresistant *Acinetobacter baumannii* infections: epidemiology and management. *Curr. Opin. Infect. Dis.* 23, 332–339. doi: 10.1097/QCO.0b013e32833ae38b

Hernandez-Alles, S., Alberti, S., Alvarez, D., Domenech-Sanchez, A., Martinez-Martinez, L., Gil, J., et al. (1999). Porin expression in clinical isolates of Klebsiella pneumoniae. *Microbiology* 145 (Pt 3), 673–679. doi: 10.1099/13500872-145-3-673

Higgins, P. G., Poirel, L., Lehmann, M., Nordmann, P., and Seifert, H. (2009). OXA-143, a novel carbapenem-hydrolyzing class D beta-lactamase in *Acinetobacter baumannii*. *Antimicrob. Agents Chemother.* 53, 5035–5038. doi: 10.1128/AAC.00856-09

Ho, P. L., Wong, R. C., Lo, S. W., Chow, K. H., Wong, S. S., and Que, T. L. (2010). Genetic identity of aminoglycoside-resistance genes in *Escherichia coli* isolates from human and animal sources. *J. Med. Microbiol.* 59(Pt 6), 702–707. doi: 10.1099/jmm.0.015032-0

Hornsey, M., Ellington, M. J., Doumith, M., Thomas, C. P., Gordon, N. C., Wareham, D. W., et al. (2010). AdeABC-mediated efflux and tigecycline MICs for epidemic clones of *Acinetobacter baumannii*. *J. Antimicrob. Chemother.* 65, 1589–1593. doi: 10.1093/jac/dkq218

Hu, W. S., Yao, S. M., Fung, C. P., Hsieh, Y. P., Liu, C. P., and Lin, J. F. (2007). An OXA-66/OXA-51-like carbapenemase and possibly an efflux pump are associated with resistance to imipenem in *Acinetobacter baumannii*. *Antimicrob. Agents Chemother.* 51, 3844–3852. doi: 10.1128/AAC.01512-06

Jacobs, A. C., Hood, I., Boyd, K. L., Olson, P. D., Morrison, J. M., Carson, S., et al. (2010). Inactivation of phospholipase D diminishes *Acinetobacter baumannii* pathogenesis. *Infect. Immun.* 78, 1952–1962. doi: 10.1128/IAI.00889-09

Jacoby, G. A., and Munoz-Price, L. S. (2005). The new beta-lactamases. *N. Engl. J. Med.* 352, 380–391. doi: 10.1056/NEJMra041359

Jin, J. S., Kwon, S. O., Moon, D. C., Gurung, M., Lee, J. H., Kim, S. I., et al. (2011). *Acinetobacter baumannii* secretes cytotoxic outer membrane protein A via outer membrane vesicles. *PLoS ONE* 6:e17027. doi: 10.1371/journal.pone.0017027

Jolley, K. A., and Maiden, M. C. (2010). BIGSdb: scalable analysis of bacterial genome variation at the population level. *BMC Bioinform.* 11:595. doi: 10.1186/1471-2105-11-595

Kearse, M., Moir, R., Wilson, A., Stones-Havas, S., Cheung, M., Sturrock, S., et al. (2012). Geneious basic: an integrated and extendable desktop software platform for the organization and analysis of sequence data. *Bioinformatics* 28, 1647–1649. doi: 10.1093/bioinformatics/bts199

Kim, U. J., Kim, H. K., An, J. H., Cho, S. K., Park, K. H., and Jang, H. C. (2014). Update on the epidemiology, treatment, and outcomes of carbapenem-resistant *Acinetobacter* infections. *Chonnam. Med. J.* 50, 37–44. doi: 10.4068/cmj.2014.50.2.37

La Scola, B., Gundi, V. A., Khamis, A., and Raoult, D. (2006). Sequencing of the rpoB gene and flanking spacers for molecular identification of *Acinetobacter* species. *J. Clin. Microbiol.* 44, 827–832. doi: 10.1128/JCM.44.3.827-832.2006

Lee, K., Chong, Y., Shin, H. B., Kim, Y. A., Yong, D., and Yum, J. H. (2001). Modified Hodge and EDTA-disk synergy tests to screen metallo-beta-lactamase-producing strains of *Pseudomonas* and *Acinetobacter* species. *Clin. Microbiol. Infect.* 7, 88–91. doi: 10.1046/j.1469-0691.2001.00204.x

Lee, K., Kim, C. K., Yong, D., Jeong, S. H., Yum, J. H., Seo, Y. H., et al. (2010). Improved performance of the modified hodge test with macconkey agar for screening carbapenemase-producing Gram-negative bacilli. *J. Microbiol. Methods* 83, 149–152. doi: 10.1016/j.mimet.2010.08.010

Lee, K., Yum, J. H., Yong, D., Lee, H. M., Kim, H. D., Docquier, J. D., et al. (2005). Novel acquired metallo-beta-lactamase gene, bla(SIM-1), in a class 1 integron from *Acinetobacter baumannii* clinical isolates from Korea. *Antimicrob. Agents Chemother.* 49, 4485–4491. doi: 10.1128/AAC.49.11.4485-4491.2005

Leflon-Guibout, V., Heym, B., and Nicolas-Chanoine, M. (2000). Updated sequence information and proposed nomenclature for bla(TEM) genes and their promoters. *Antimicrob. Agents Chemother.* 44, 3232–3234. doi: 10.1128/AAC.44.11.3232-3234.2000

Li, H., Liu, F., Zhang, Y., Wang, X., Zhao, C., Chen, H., et al. (2015). Evolution of carbapenem-resistant *Acinetobacter baumannii* revealed through whole-genome sequencing and comparative genomic analysis. *Antimicrob. Agents Chemother.* 59, 1168–1176. doi: 10.1128/AAC.04609-14

Lin, M. F., Lin, Y. Y., Yeh, H. W., and Lan, C. Y. (2014). Role of the BaeSR two-component system in the regulation of *Acinetobacter baumannii* adeAB genes and its correlation with tigecycline susceptibility. *BMC Microbiol.* 14:119. doi: 10.1186/1471-2180-14-119

Lin, Y. C., Hsia, K. C., Chen, Y. C., Sheng, W. H., Chang, S. C., Liao, M. H., et al. (2010). Genetic basis of multidrug resistance in *Acinetobacter* clinical isolates in Taiwan. *Antimicrob. Agents Chemother.* 54, 2078–2084. doi: 10.1128/AAC.01398-09

Liou, M. L., Soo, P. C., Ling, S. R., Kuo, H. Y., Tang, C. Y., and Chang, K. C. (2014). The sensor kinase BfmS mediates virulence in *Acinetobacter baumannii*. *J. Microbiol. Immunol. Infect.* 47, 275–281. doi: 10.1016/j.jmii.2012.12.004

Livak, K. J., and Schmittgen, T. D. (2001). Analysis of relative gene expression data using real-time quantitative PCR and the $2^{(-\Delta\Delta Ct)}$ Method. *Methods* 25, 402–408. doi: 10.1006/meth.2001.1262

Lopes, B. S., and Amyes, S. G. (2012). Role of ISAba1 and ISAba125 in governing the expression of blaADC in clinically relevant *Acinetobacter baumannii* strains resistant to cephalosporins. *J. Med. Microbiol.* 61(Pt 8), 1103–1108. doi: 10.1099/jmm.0.044156-0

Luke, N. R., Sauberan, S. L., Russo, T. A., Beanan, J. M., Olson, R., Loehfelm, T. W., et al. (2010). Identification and characterization of a glycosyltransferase involved in *Acinetobacter baumannii* lipopolysaccharide core biosynthesis. *Infect. Immun.* 78, 2017–2023. doi: 10.1128/IAI.00016-10

Magnet, S., Courvalin, P., and Lambert, T. (2001). Resistance-nodulation-cell division-type efflux pump involved in aminoglycoside resistance in *Acinetobacter baumannii* strain BM4454. *Antimicrob. Agents Chemother.* 45, 3375–3380. doi: 10.1128/AAC.45.12.3375-3380.2001

Maragakis, L. L., and Perl, T. M. (2008). Acinetobacter baumannii: epidemiology, antimicrobial resistance, and treatment options. *Clin. Infect. Dis.* 46, 1254–1263. doi: 10.1086/529198

Marti, S., Sanchez-Cespedes, J., Oliveira, E., Bellido, D., Giralt, E., and Vila, J. (2006). Proteomic analysis of a fraction enriched in cell envelope proteins of *Acinetobacter baumannii*. *Proteomics* 6(Suppl. 1), S82–87. doi: 10.1002/pmic.200500323

McConnell, M. J., Actis, L., and Pachon, J. (2013). *Acinetobacter baumannii*: human infections, factors contributing to pathogenesis and animal models. *FEMS Microbiol. Rev.* 37, 130–155. doi: 10.1111/j.1574-6976.2012.00344.x

Metan, G., Sariguzel, F., and Sumerkan, B. (2009). Factors influencing survival in patients with multi-drug-resistant *Acinetobacter bacteraemia*. *Eur. J. Intern. Med.* 20, 540–544. doi: 10.1016/j.ejim.2009.05.005

Mussi, M. A., Limansky, A. S., and Viale, A. M. (2005). Acquisition of resistance to carbapenems in multidrug-resistant clinical strains of *Acinetobacter baumannii*: natural insertional inactivation of a gene encoding a member of a novel family of beta-barrel outer membrane proteins. *Antimicrob. Agents Chemother.* 49, 1432–1440. doi: 10.1128/AAC.49.4.1432-1440.2005

Naas, T., Bogaerts, P., Bauraing, C., Degheldre, Y., Glupczynski, Y., and Nordmann, P. (2006). Emergence of PER and VEB extended-spectrum beta-lactamases in *Acinetobacter baumannii* in Belgium. *J. Antimicrob. Chemother.* 58, 178–182. doi: 10.1093/jac/dkl178

Naas, T., and Nordmann, P. (2010). *Antibiogram.* Paris: Eska Publishing.

Nordmann, P. (2010). Gram-negative bacteriae with resistance to carbapenems. *Med. Sci.* 26, 950–959. doi: 10.1051/medsci/20102611950

Nordmann, P., Ronco, E., Naas, T., Duport, C., Michel-Briand, Y., and Labia, R. (1993). Characterization of a novel extended-spectrum beta-lactamase

from *Pseudomonas aeruginosa*. *Antimicrob. Agents Chemother.* 37, 962–969. doi: 10.1128/AAC.37.5.962

Pagani, L., Mantengoli, E., Migliavacca, R., Nucleo, E., Pollini, S., Spalla, M., et al. (2004). Multifocal detection of multidrug-resistant *Pseudomonas aeruginosa* producing the PER-1 extended-spectrum beta-lactamase in Northern Italy. *J. Clin. Microbiol.* 42, 2523–2529. doi: 10.1128/JCM.42.6.2523-2529.2004

Park, S., Lee, K. M., Yoo, Y. S., Yoo, J. S., Yoo, J. I., Kim, H. S., et al. (2011). Alterations of gyrA, gyrB, and parC and activity of efflux pump in fluoroquinolone-resistant *Acinetobacter baumannii*. *Osong. Pub. Health Res. Perspect.* 2, 164–170. doi: 10.1016/j.phrp.2011.11.040

Peleg, A. Y., Seifert, H., and Paterson, D. L. (2008). Acinetobacter baumannii: emergence of a successful pathogen. *Clin. Microbiol. Rev.* 21, 538–582. doi: 10.1128/CMR.00058-07

Perez, F., Hujer, A. M., Hujer, K. M., Decker, B. K., Rather, P. N., and Bonomo, R. A. (2007). Global challenge of multidrug-resistant *Acinetobacter baumannii*. *Antimicrob. Agents Chemother.* 51, 3471–3484. doi: 10.1128/AAC.01464-06

Piddock, L. J. (2006). Clinically relevant chromosomally encoded multidrug resistance efflux pumps in bacteria. *Clin. Microbiol. Rev.* 19, 382–402. doi: 10.1128/CMR.19.2.382-402.2006

Pinto, N. A., D'Souza, R., Hwang, I. S., Choi, J., In, Y. H., Park, H. S., et al. (2017). Whole genome and transcriptome analysis reveal MALDI-TOF MS and SDS-PAGE have limited performance for the detection of the key outer membrane protein in carbapenem-resistant Klebsiella pneumoniae isolates. *Oncotarget* 8, 84818–84826. doi: 10.18632/oncotarget.19005

Poirel, L., Cabanne, L., Vahaboglu, H., and Nordmann, P. (2005). Genetic environment and expression of the extended-spectrum beta-lactamase blaPER-1 gene in gram-negative bacteria. *Antimicrob. Agents Chemother.* 49, 1708–1713. doi: 10.1128/AAC.49.5.1708-1713.2005

Poirel, L., Naas, T., and Nordmann, P. (2010). Diversity, epidemiology, and genetics of class D beta-lactamases. *Antimicrob. Agents Chemother.* 54, 24–38. doi: 10.1128/AAC.01512-08

Poirel, L., and Nordmann, P. (2006). Carbapenem resistance in *Acinetobacter baumannii*: mechanisms and epidemiology. *Clin. Microbiol. Infect.* 12, 826–836. doi: 10.1111/j.1469-0691.2006.01456.x

Quale, J., Bratu, S., Landman, D., and Heddurshetti, R. (2003). Molecular epidemiology and mechanisms of carbapenem resistance in *Acinetobacter baumannii* endemic in New York City. *Clin. Infect. Dis.* 37, 214–220. doi: 10.1086/375821

Rafei, R., Pailhories, H., Hamze, M., Eveillard, M., Mallat, H., Dabboussi, F., et al. (2015). Molecular epidemiology of *Acinetobacter baumannii* in different hospitals in Tripoli, Lebanon using bla(OXA-51-like) sequence based typing. *BMC Microbiol.* 15:103. doi: 10.1186/s12866-015-0441-5

Ranellou, K., Kadlec, K., Poulou, A., Voulgari, E., Vrioni, G., Schwarz, S., et al. (2012). Detection of *Pseudomonas aeruginosa* isolates of the international clonal complex 11 carrying the blaPER-1 extended-spectrum beta-lactamase gene in Greece. *J. Antimicrob. Chemother.* 67, 357–361. doi: 10.1093/jac/dkr471

Richard Bonnet, R. A. B. (2010). *Antibiogram.* Paris: Eska publishing.

Ridley, A., and Threlfall, E. J. (1998). Molecular epidemiology of antibiotic resistance genes in multiresistant epidemic *Salmonella typhimurium* DT 104. *Microb. Drug Resist.* 4, 113–118. doi: 10.1089/mdr.1998.4.113

Rosenfeld, N., Bouchier, C., Courvalin, P., and Perichon, B. (2012). Expression of the resistance-nodulation-cell division pump AdeIJK in *Acinetobacter baumannii* is regulated by AdeN, a TetR-type regulator. *Antimicrob. Agents Chemother.* 56, 2504–2510. doi: 10.1128/AAC.06422-11

Rumbo, C., Gato, E., Lopez, M., Ruiz de Alegria, C., Fernandez-Cuenca, F., Martinez-Martinez, L., et al. (2013). Contribution of efflux pumps, porins, and beta-lactamases to multidrug resistance in clinical isolates of *Acinetobacter baumannii*. *Antimicrob. Agents Chemother.* 57, 5247–5257. doi: 10.1128/AAC.00730-13

Ruzin, A., Keeney, D., and Bradford, P. A. (2007). AdeABC multidrug efflux pump is associated with decreased susceptibility to tigecycline in *Acinetobacter calcoaceticus-Acinetobacter baumannii* complex. *J. Antimicrob. Chemother.* 59, 1001–1004. doi: 10.1093/jac/dkm058

Sievers, F., Wilm, A., Dineen, D., Gibson, T. J., Karplus, K., Li, W., et al. (2011). Fast, scalable generation of high-quality protein multiple sequence alignments using clustal omega. *Mol. Syst. Biol.* 7:539. doi: 10.1038/msb.2011.75

Singh, H., Thangaraj, P., and Chakrabarti, A. (2013). *Acinetobacter baumannii*: a brief account of mechanisms of multidrug resistance and current and future therapeutic management. *J. Clin. Diagn. Res.* 7, 2602–2605. doi: 10.7860/JCDR/2013/6337.3626

Siroy, A., Molle, V., Lemaitre-Guillier, C., Vallenet, D., Pestel-Caron, M., Cozzone, A. J., et al. (2005). Channel formation by CarO, the carbapenem resistance-associated outer membrane protein of *Acinetobacter baumannii*. *Antimicrob. Agents Chemother.* 49, 4876–4883. doi: 10.1128/AAC.49.12.4876-4883.2005

Takahashi, H., Watanabe, H., Kuroki, T., Watanabe, Y., and Yamai, S. (2002). Identification of tet(B), encoding high-level tetracycline resistance, in *Neisseria meningitidis*. *Antimicrob. Agents Chemother.* 46, 4045–4046. doi: 10.1128/AAC.46.12.4045-4046.2002

Turton, J. F., Woodford, N., Glover, J., Yarde, S., Kaufmann, M. E., and Pitt, T. L. (2006). Identification of *Acinetobacter baumannii* by detection of the blaOXA-51-like carbapenemase gene intrinsic to this species. *J. Clin. Microbiol.* 44, 2974–2976. doi: 10.1128/JCM.01021-06

Untergasser, A., Cutcutache, I., Koressaar, T., Ye, J., Faircloth, B. C., Remm, M., et al. (2012). Primer3–new capabilities and interfaces. *Nucleic Acids Res.* 40:e115. doi: 10.1093/nar/gks596

Vila, J., Marti, S., and Sanchez-Cespedes, J. (2007). Porins, efflux pumps and multidrug resistance in *Acinetobacter baumannii*. *J. Antimicrob. Chemother.* 59, 1210–1215. doi: 10.1093/jac/dkl509

Vila, J., and Pachon, J. (2008). Therapeutic options for *Acinetobacter baumannii* infections. *Expert Opin. Pharmacother.* 9, 587–599. doi: 10.1517/14656566.9.4.587

Vila, J., Ruiz, J., Goni, P., Marcos, A., and Jimenez de Anta, T. (1995). Mutation in the gyrA gene of quinolone-resistant clinical isolates of *Acinetobacter baumannii*. *Antimicrob. Agents Chemother.* 39, 1201–1203. doi: 10.1128/AAC.39.5.1201

Visca, P., Seifert, H., and Towner, K. J. (2011). Acinetobacter infection–an emerging threat to human health. *IUBMB Life* 63, 1048–1054. doi: 10.1002/iub.534

Wisplinghoff, H., Paulus, T., Lugenheim, M., Stefanik, D., Higgins, P. G., Edmond, M. B., et al. (2012). Nosocomial bloodstream infections due to *Acinetobacter baumannii*, *Acinetobacter pittii* and *Acinetobacter nosocomialis* in the United States. *J. Infect.* 64, 282–290. doi: 10.1016/j.jinf.2011.12.008

Wisplinghoff, H., and Seifert, H. (2014). Epidemiology and clinical features of *Acinetobacter baumannii* infections in humans. *Berl. Munch. Tierarztl. Wochenschr.* 127, 447–457.

Yong, D., Shin, J. H., Kim, S., Lim, Y., Yum, J. H., Lee, K., et al. (2003). High prevalence of PER-1 extended-spectrum beta-lactamase-producing *Acinetobacter spp*. in Korea. *Antimicrob. Agents Chemother.* 47, 1749–1751. doi: 10.1128/AAC.47.5.1749-1751.2003

Yoon, E. J., Courvalin, P., and Grillot-Courvalin, C. (2013). RND-type efflux pumps in multidrug-resistant clinical isolates of *Acinetobacter baumannii*: major role for AdeABC overexpression and AdeRS mutations. *Antimicrob. Agents Chemother.* 57, 2989–2995. doi: 10.1128/AAC.02556-12

Zander, E., Chmielarczyk, A., Heczko, P., Seifert, H., and Higgins, P. G. (2013). Conversion of OXA-66 into OXA-82 in clinical *Acinetobacter baumannii* isolates and association with altered carbapenem susceptibility. *J. Antimicrob. Chemother.* 68, 308–311. doi: 10.1093/jac/dks382

Zankari, E., Hasman, H., Cosentino, S., Vestergaard, M., Rasmussen, S., Lund, O., et al. (2012). Identification of acquired antimicrobial resistance genes. *J. Antimicrob. Chemother.* 67, 2640–2644. doi: 10.1093/jac/dks261

Zankari, E., Hasman, H., Kaas, R. S., Seyfarth, A. M., Agersø, Y., Lund, O., et al. (2013). Genotyping using whole-genome sequencing is a realistic alternative to surveillance based on phenotypic antimicrobial susceptibility testing. *J. Antimicrob. Chemother.* 68, 771–777. doi: 10.1093/jac/dks496

Conflict of Interest Statement: The authors declare that the research was conducted in the absence of any commercial or financial relationships that could be construed as a potential conflict of interest.

frontiers in Microbiology

ORIGINAL RESEARCH
published: 29 March 2019
doi: 10.3389/fmicb.2019.00632

Adaptive *dif* Modules in Permafrost Strains of *Acinetobacter lwoffii* and Their Distribution and Abundance Among Present Day *Acinetobacter* Strains

*Sofia Mindlin[1], Alexey Beletsky[2], Andrey Mardanov[2] and Mayya Petrova[1]**

[1] *Laboratory of Molecular Genetics of Microorganisms, Institute of Molecular Genetics, Russian Academy of Sciences, Moscow, Russia,* [2] *Laboratory of Microorganism Genomics and Metagenomics, Institute of Bioengineering, Research Center of Biotechnology of the Russian Academy of Sciences, Moscow, Russia*

OPEN ACCESS

Edited by:
Maria Alejandra Mussi, Consejo Nacional de Investigaciones Científicas y Técnicas (CONICET), Argentina

Reviewed by:
Filipa Grosso, Universidade do Porto, Portugal
Alexandr Nemec, National Institute of Public Health (NIPH), Czechia

***Correspondence:**
Mayya Petrova
petrova@img.ras.ru

Specialty section:
This article was submitted to Infectious Diseases, a section of the journal Frontiers in Microbiology

Received: *15 November 2018*
Accepted: *13 March 2019*
Published: *29 March 2019*

Citation:
Mindlin S, Beletsky A, Mardanov A and Petrova M (2019) Adaptive dif Modules in Permafrost Strains of Acinetobacter lwoffii and Their Distribution and Abundance Among Present Day Acinetobacter Strains. Front. Microbiol. 10:632. doi: 10.3389/fmicb.2019.00632

The *dif*/Xer system of site-specific recombination allows resolution of chromosomal dimers during bacterial DNA replication. Recently, it was also shown to be involved in horizontal transfer of a few known Xer-dependent mobile elements. Here, we show that plasmids of various *Acinetobacter* species, including clinically important strains, often contain multiple p*dif* sites that are mainly located within their accessory regions. Chromosomes of *Acinetobacter* strains may also contain additional *dif* sites, and their similarity with plasmid p*dif* sites is higher than with the main chromosomal site *dif1*. We further identify putative mobile genetic elements containing p*dif* sites on both flanks of adaptive genes and analyze their distribution in *Acinetobacter* species. In total, we describe seven mobile elements containing genes with various adaptive functions from permafrost strains of *A. lwoffii* group. All of them are also spread in modern plasmids of different *Acinetobacter* species including *A. baumannii*. We could not detect p*dif* sites and corresponding mobile elements in closely related bacterial genera, including *Psychrobacter* and *Moraxella*. Thus, the widespread distribution of *dif* modules is a characteristic feature of *Acinetobacter* species and may contribute to their high adaptability both in the environment and in the clinic.

Keywords: plasmid p*dif* sites, additional chromosomal *dif* sites, *terC dif*, *ohr1 dif*, *sulP dif*, *kup dif*, *add dif*

INTRODUCTION

Acinetobacter strains are common everywhere due to their ability to adapt to various environments (Touchon et al., 2014). Many of them – first of all, *Acinetobacter baumannii*, but also *Acinetobacter nosocomialis*, *Acinetobacter pittii*, *Acinetobacter lwoffii*, *Acinetobacter ursingii*, *Acinetobacter haemolyticus*, *Acinetobacter parvus*, *Acinetobacter junii* – are among the most important pathogens in the clinic (Turton et al., 2010; Peleg et al., 2012; Evans and Amyes, 2014; Touchon et al., 2014). The rise of antimicrobial resistance in these strains is a burning medical problem, with a large number of mobile genetic elements involved in the spread of the resistance determinants (Martins et al., 2015; Da Silva and Domingues, 2016; Pagano et al., 2016).

Recently a novel class of mobile genetic elements whose transposition likely depends on the action of the *dif*/Xer recombination system was discovered in *Acinetobacter* species. Initially, a discrete DNA module that contained the gene encoding OXA-24 carbapenemase, flanked by conserved inverted repeats homologous to the XerC/XerD binding sites (*dif* sites), was revealed in an *A. baumannii* plasmid pABVA01a. It was shown that this element (later designated *dif* module) is also present in a different context in another *Acinetobacter* plasmid, suggesting its horizontal transfer (D'Andrea et al., 2009). Similar observations were soon made by other laboratories when studying plasmids containing the same gene OXA-24 (Merino et al., 2010; Grosso et al., 2012) and related carbapenemase genes OXA-72 (a variant of OXA-24) or OXA-58 (Povilonis et al., 2013; Blackwell and Hall, 2017). Subsequent studies demonstrated that other antibiotic resistance genes can also be included in *dif* modules. In particular, Blackwell and Hall (2017) described two novel *dif* modules containing genes encoding resistance to tetracycline and erythromycin.

The *dif* sites found in *Acinetobacter* plasmids (p*dif* sites) are similar to the chromosomal *dif1* site recognized by the dif/Xer system of site-specific recombination, which plays an essential role in the resolution of chromosomal and plasmid dimers (Carnoy and Roten, 2009; Castillo et al., 2017). Orphan p*dif* sites could also be revealed in a number of plasmids (Carnoy and Roten, 2009; Blackwell and Hall, 2017; Cameranesi et al., 2018), and the reaction of site-specific recombination could be observed between the two sites present in different plasmids, suggesting that this system is involved in the horizontal transfer of *dif* modules (Cameranesi et al., 2018).

Further studies have shown that the spread of *dif* sites and *dif* modules is not limited to plasmids of clinical *Acinetobacter* strains and that they can include a variety of genes, not only determinants of antibiotic resistance. In particular, we recently described a novel *dif* module containing chromium resistance genes (*chrAB dif*). Initially discovered in plasmids from ancient (permafrost) strains of *A. lwoffii* it was also found in plasmids of modern *Acinetobacter* strains (Mindlin et al., 2018). We also identified two other potential *dif* modules, *kup dif* and *sulP dif*, but did not characterize them in detail (Mindlin et al., 2018). Recently, putative new *dif* modules containing genes with potential adaptive functions were found in plasmids of the clinical isolate of *A. baumannii* D36 (Hamidian and Hall, 2018). This suggested that formation of mobile elements flanked by p*dif* sites and carrying various adaptive genes may be a characteristic feature of plasmids of the whole *Acinetobacter* genus.

In the present work, we investigated the distribution of *dif* sites in more than 180 *Acinetobacter* plasmids belonging to different species. The main emphasis was made on the identification and analysis of *dif* modules from ancient *A. lwoffii* plasmids and studies of their distribution in modern strains. As a result, we identified four novel adaptive *dif* modules, in addition to *chrAB dif*, *kup dif,* and *sulP dif*, and revealed their broad distribution in plasmids in environmental and clinical strains of the *Acinetobacter* genus. We also showed that most *Acinetobacter* chromosomes contain additional *dif* sites besides the main site *dif1*, which may contribute to the distribution of *dif* modules in this genus.

MATERIALS AND METHODS

Bacterial Strains and Growth Conditions

Acinetobacter strains ED23-35, ED45-23, ED9-5a, EK30A, and VS15 used in this study were previously isolated from 15 thousand to 3 million years old permafrost sediments collected from different regions of Kolyma Lowland. We here in referred to these strains as "ancient" strains, which never come into contact with clinical isolates. Initially they were identified as *A. lwoffii* based on metabolic testing and from 16S rRNA gene sequence analysis (Petrova et al., 2002; Kurakov et al., 2016; Mindlin et al., 2016). In this work, based on data from a recent article by Nemec et al. (2018), revising the taxonomy of the *Acinetobacter lwoffii* group we showed that strain ED9-5a actually belongs to the *Acinetobacter pseudolwoffii* species. The remaining permafrost strains do belong to *A. lwoffii*. In addition, we analyzed two sets of *Acinetobacter* strains obtained from publicly available databases ("modern" strains). These were (i) 38 strains of *A. baumannii* described by Shintani et al. (2015), and (ii) 30 strains belonging to other *Acinetobacter* species obtained from public databases before January 2018. Bacteria were grown in lysogeny broth (LB) medium or solidified LB medium (LA) at 30°C.

Confirmation of the Species Identification and Identification of Misidentified Isolates

Species identification was confirmed by comparison of partial *rpoB* gene sequences with the reference *Acinetobacter* genomes[1]. The *rpoB* gene nucleotide identity level of 98–100% was regarded as evidence that the compared genomes belong to the same species.

Whole-Genome Sequencing and Assembly of Plasmids

The genomes were sequenced with a Roche GS FLX genome sequencer (Roche, Switzerland) using the Titanium protocol to prepare shotgun genomic libraries. The GS FLX reads were assembled into contigs using the GS De Novo Assembler (Roche); protein coding genes were identified and annotated using the RAST web server. To identify potential plasmid contigs we used read coverage depth and annotation information, such as existence of genes for mobilization and/or replication of plasmids. Using 454 assembly graph file (output of the GS De Novo Assembler) we extended and merge our potential plasmid contigs with each other. Some additional merging of contigs was done using PCR. All manually assembled regions were checked using PCR. A plasmid was considered as finished if it was circular according to the 454 assembly graph and PCR check. The 454 reads were mapped back to the finished sequences using 454 GS Reference Mapper, and read mapping was visualized in IGV browser and manually inspected for potential missassemblies.

[1]https://apps.szu.cz/anemec/Genomes.pdf

Screening of *Acinetobacter* Plasmids and Chromosomes for the Presence of *dif* Sites

A collection of plasmids isolated from different *Acinetobacter* species (**Supplementary Table S1**) was screened for the presence of p*dif* sites by BLAST software. The XerC/XerD (3916–3943 bp) and XerD/XerC (6899–6926) p*dif* sites of plasmid pM131-6 [NC_025120] were used as a reference. Only sites that were at least 75–80% identical to the reference were taken into account. The same algorithm was used in the search for the main and additional *dif* sites in *Acinetobacter* chromosomes.

Bioinformatics Analysis

For the assembly and analysis of plasmid genomes from ancient strains, the program UGENE[2] was used. Similarity searches were performed using BLAST (Altschul et al., 1997) and REBASE (Roberts et al., 2009). Conserved domains and motifs were identified using the NCBI Conserved Domain Database (CDD) (Marchler-Bauer et al., 2011) and the Pfam database (Finn et al., 2009). Dif sites were clustered using blastclust from blast package with 95% identity threshold. Fasta files with dif sites were sorted according to blastclust results using custom perl script (dif sites from the same cluster follow each other, and clusters are sorted by size). The sorted fasta files were visualized in AliView as color blocks. The fasta files with dif sites were used to create sequence logos using WebLogo[3] (Crooks et al., 2004).

Identification of *dif* modules in permafrost plasmids and determination of their mobility was carried out manually in several stages. Initially, plasmids containing at least two different p*dif*-sites were selected. Then, the regions between the pairs of p*dif*-sites were analyzed, and, based on the presence of a potentially adaptive gene (s) in this region candidates for mobile modules were revealed. At the final stage, using the Blast software, the distribution of the identified modules among the ancient (isolated from permafrost) and modern strains of *Acinetobacter*'species was investigated. The presence of the same module with an identity level of 98–99% in different regions of different plasmids (contigs) isolated from *Acinetobacter* strains belonging to different species was regarded as evidence of its mobility.

Determination of the MIC for Tellurium and Organic Peroxide Resistance

The level of resistance was determined by the agar dilution method (Mindlin et al., 2016). Overnight cultures of bacterial strains were diluted 10-fold with fresh LB and grown at 30°C with shaking for 3–4 h; the cultures were then induced for 1 h by the addition of tert-butyl hydroperoxide (tBHP) at 0.1 mM. Five μl of the bacterial suspension (about 5×10^6 cells per ml) were plated onto LA supplemented with Na_2TeO_3 (Tel) or tBHP. The concentrations tested were as follows: Tel – 0.01; 0.02; 0.04 and 0.1 mg/ml and tBHP – 0.05; 0.1; 0.2; 0.3 and 0.4 mM. The plates were incubated at 30°C for 24 h and visually inspected. In each case, three independent experiments were performed.

Nucleotide Sequence Accession Numbers

The accession numbers for nucleotide sequences of the plasmids deposited in this work in the GenBank database are as follows: CP032112.1 (pALWED1.2); CP032113-CP032116.1 (pALWED1.4-1.7); CP032117.1-CP032124.1 (pALWED2.2-2.9); CP032287.1-CP032289.1 (pALWED3.2-3.4); CP032290.1 (pALWED3.6); CP032102.1 (pALWEK1.1); CP032105.1-CP032107.1 (pALWEK1.2-1.4); CP032108.1-CP032111.1 (pALWEK1.6-1.9); CP032103.1 (pALWEK1.10); CP032104.1 (pALWEK1.11).

RESULTS

Distribution of p*dif* Sites in Plasmids From Strains of Different *Acinetobacter* Species

For analysis of the occurrence of *pdif* sites in *Acinetobacter* plasmids, we studied plasmids found in strains of various *Acinetobacter* species, divided into three groups (see Materials and Methods): (1) plasmids of permafrost strains of *A. lwoffii* and *A. pseudolwoffii* isolated and studied in our group (35 plasmids, see below) together with plasmids from *A. lwoffii* ZS207 (10 plasmids, see **Supplementary Table S1**); (2) plasmids from *A. baumannii* strains, described in Shintani et al. (2015) (65 plasmids, **Supplementary Table S1**); (3) plasmids isolated from strains belonging to others *Acinetobacter* species available from public databases before January 2018 (73 plasmids, **Supplementary Table S1**).

The presence of p*dif* sites and the number of their copies in each plasmid were determined by the BLAST tool. The results obtained for each set of plasmids are presented in **Figure 1**, **Table 1**, and **Supplementary Table S1**. Plasmid p*dif* sites were found in more than 50% of the *Acinetobacter* plasmids in all three groups (**Table 1**). In most cases, the number of sites was 1–4, while some plasmids contained 5–8 copies of p*dif* or more (**Table 1**). Most p*dif* sites were found in small to middle size plasmids (6–30 kb), while very small plasmids (<6 kb) as a rule did not contain them.

Interestingly, multiple copies of *pdif* sites were found both in very large and in middle-size plasmids (22–400 kbp) (**Figure 1** and **Table 2**).

To determine the localization of p*dif* sites relative to the backbone and accessory plasmid regions, we analyzed their distribution in four plasmids, two middle size (pALWED2.3 and pOXA58-AP_882) and two large (pALWED2.1 and pXBB1-9), each containing more than 10 sites (**Table 2**). For all four plasmids, *pdif* sites were distributed unevenly across the plasmid sequence; notably, they were absent from the backbone regions and formed clusters in certain plasmid regions (**Figure 2**).

To our knowledge, there is currently no data on the distribution of typical p*dif* sites in the plasmids of bacteria from

[2]http://unipro.ru

[3]https://weblogo.berkeley.edu/logo.cgi

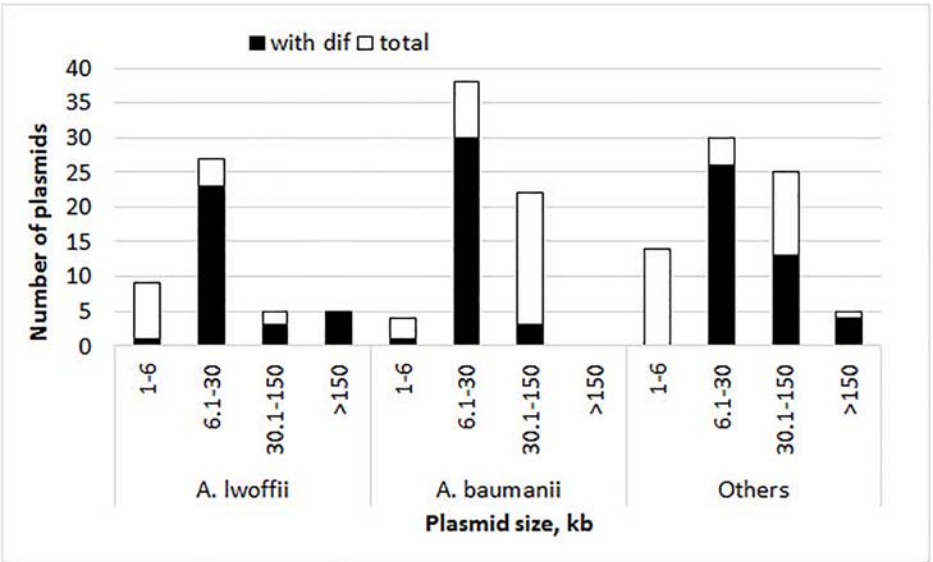

FIGURE 1 | Histograms of plasmid size and their numbers with and without p*dif* sites. The height of the column indicates the total number of plasmids, and its black part shows the number of plasmids containing p*dif* sites.

other systematic groups. To get insight into their abundance in closely related genera to *Acinetobacter*, we analyzed a total of 31 plasmids from 16 strains of *Psychrobacter* (2117–44793 bp) and 8 plasmids from 6 strains of *Moraxella* (1313–44215 bp) described by Shintani et al. (2015) and Moghadam et al. (2016). No p*dif* sites were detected in any of these plasmids. Therefore, the presence of a large number of p*dif* sites may be a unique feature of *Acinetobacter* plasmids.

Identification of *dif* Modules in Plasmids From Permafrost *A. lwoffii and A. pseudolwoffii* Strains

The primary search for *dif* modules was performed on the set of plasmids from five permafrost strains from our collection (ED23-35, ED45-23, ED9-5a, EK30A and VS15; **Supplementary Table S1**) (Petrova et al., 2002; Mindlin et al., 2016). In five fully sequenced genomes, a total of 35 plasmids of various sizes were found. In addition to previously described 8 plasmids (Mindlin et al., 2016, 2018), we have now assembled 27 new plasmids from the same strains (see details in Materials and Methods).

TABLE 1 | Distribution and abundance of p*dif* sites in *Acinetobacter* plasmids.

Species	Number (%) of plasmids with a given number of p*dif* sites in one plasmid				Total number of plasmids
	0 p*dif*	1–4 p*dif*	5–8 p*dif*	>8 p*dif*	
A. baumannii	31 (47,7)	28 (43,1)	4 (6,1)	2 (3,1)	65
A. lwoffii and *A. pseudolwoffii*	13 (28,9)	23 (51,1)	3 (6,7)	6 (13,3)	45
other species	30 (41,1)	28 (38,3)	12 (16,4)	3 (4,1)	73
Total	74 (40,4)	79 (43,2)	19 (10,4)	11 (6,0)	183

In 10 of the plasmids, sequences homologous to p*dif* sites were absent or only a single p*dif* site was detected (**Supplementary Table S1**). The remaining 25 plasmids with two or more p*dif* sites were analyzed for the presence of *dif* modules containing adaptive genes surrounded by two *pdif* sites (see Materials and Methods). In total, putative *dif* modules were detected in 12 plasmids; 6 of them contained one module; 4 contained two modules, and 2 contained three different modules (**Supplementary Table S2**).

In addition to the three modules identified previously (*chrAB dif, kup dif,* and *sulP dif*) (Mindlin et al., 2018), we revealed four new putative modules with adaptive genes: *terC dif*, *add dif*, *ohr dif,* and *sulP-uspA dif* (**Figure 3**).

In most cases, plasmids containing the same modules originated from different permafrost strains (**Supplementary Table S2**) suggesting their horizontal transfer. To test this hypothesis, we analyzed the distribution of all modules among

TABLE 2 | List of plasmids containing multiple p*dif* sites (>10).

Strain	Plasmid	Length, bp	Number of p*dif* sites		Accession No.
			C/D	D/C	
A. lwoffii ED45-23	pALWED2.1	191,611	8	8	KX426229
A. lwoffii ED45-23	pALWED2.3	22,771	6	5	CP032118.1
A. lwoffii EK30A	pALWEK1.1	209,982	7	5	KX528688
A. lwoffii ZS207	pmZS	198,391	9	14	CP019144.1
A. baumannii	pABIR	29,823	6	5	NC_010481
A. johnsonii XBB1	pXXB1-9	398,857	7	7	CP010351.1
A. pittii AP_882	pOXA58-AP_882	36,862	6	7	CP014479.1
A. sp NCu2D-2	Unnamed	309,964	6	7	CP015595.1

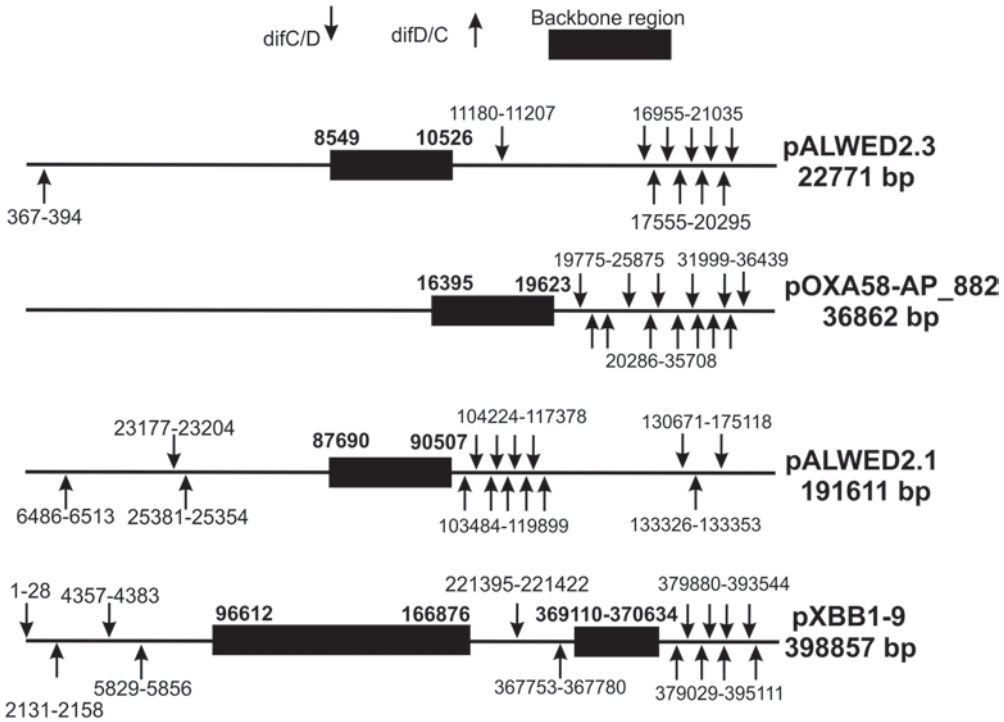

FIGURE 2 | Distribution of p*dif* sites over the plasmid genomes (not to scale).

plasmids (contigs) of modern *Acinetobacter* strains belonging to different *Acinetobacter* species (**Supplementary Table S2**). Below, we briefly describe characteristics and distribution of each of these modules (**Table 3**).

terC dif Module

We revealed the *terC dif* module (1221 bp) in four permafrost plasmids, pALWED1.4 from *A. lwoffii* ED23-35, pALWED2.1 from *A. lwoffii* ED45-23, pALWED3.6 from *A. pseudolwoffii* ED9-5a and pALWEK1.1 from *A. lwoffii* EK30A (**Supplementary Table S2**). It contained a single orf, identified as *terC* (978 bp), encoding resistance to tellurium. We also found the *terC dif* module in two modern plasmids and several contigs from modern strains belonging to different species of *Acinetobacter* (**Supplementary Table S2** and **Figure 3**).

Up to date, genetic determinants of resistance to tellurium were found in the genomes of different bacteria both in chromosomes and plasmids (Chasteen et al., 2009). We also detected the *terC* gene in the sequenced chromosomes of *Acinetobacter* strains, belonging to different species including *Acinetobacter baylyi* ADP1 [NC_005966.1] widely used in genetic studies.

However, the plasmidic and chromosomal *terC* genes were related only distantly (42–60% identity at the protein sequence level), and the chromosomal *terC* gene was not flanked by *dif* sites.

To determine the functional activity of the *terC dif* module, we compared the level of tellurium resistance of the permafrost strains of *A. lwoffii* and *A. pseudolwoffii* containing the *terC dif* module with the strain *A. lwoffii* VS15 that lacked this module in its plasmids. The results of three independent experiments showed that strains ED23-35, ED9-5a and EK30A have a significantly higher resistance level (MIC from 0.04 to 0.1 mg/ml) compared to strain VS15 (MIC $<$ 0.01 mg/ml); whereas strain ED45-23, characterized by very slow growth, does not differ from VS15. Thus, additional studies are needed to confirm the contribution of the *terC dif* module into the tellurium resistance of corresponding host strains.

add dif Module

Most prokaryotic chromosomes as well as many plasmids contain toxin-antitoxin (TA) systems consisting of a pair of genes that encode 2 components, a stable toxin and its cognate unstable antitoxin. TA systems are also known as addiction modules (Yamaguchi et al., 2011; Schuster and Bertram, 2013). In particular, many type II toxins are mRNA-specific endonucleases that arrest cell growth through RNA cleavage, thus preventing the process of translation (Bertram and Schuster, 2014). We revealed a number of type II TA modules in permafrost plasmids. Amongst them we found two related modules surrounded by p*dif* sites (both 768 bp long). Both modules contained two genes, one (297 bp) encoding a killer protein and another (291 bp) – an antidote protein. The first module was located in large plasmid pALWED2.1; the second was detected in medium-sized (22771 bp) plasmid pALWED2.3 and large plasmid pALWEK1.1. The difference in nucleotide sequences of the modules was 4%.

We also found variants of both *add dif* modules in plasmids and contigs of modern strains belonging to different

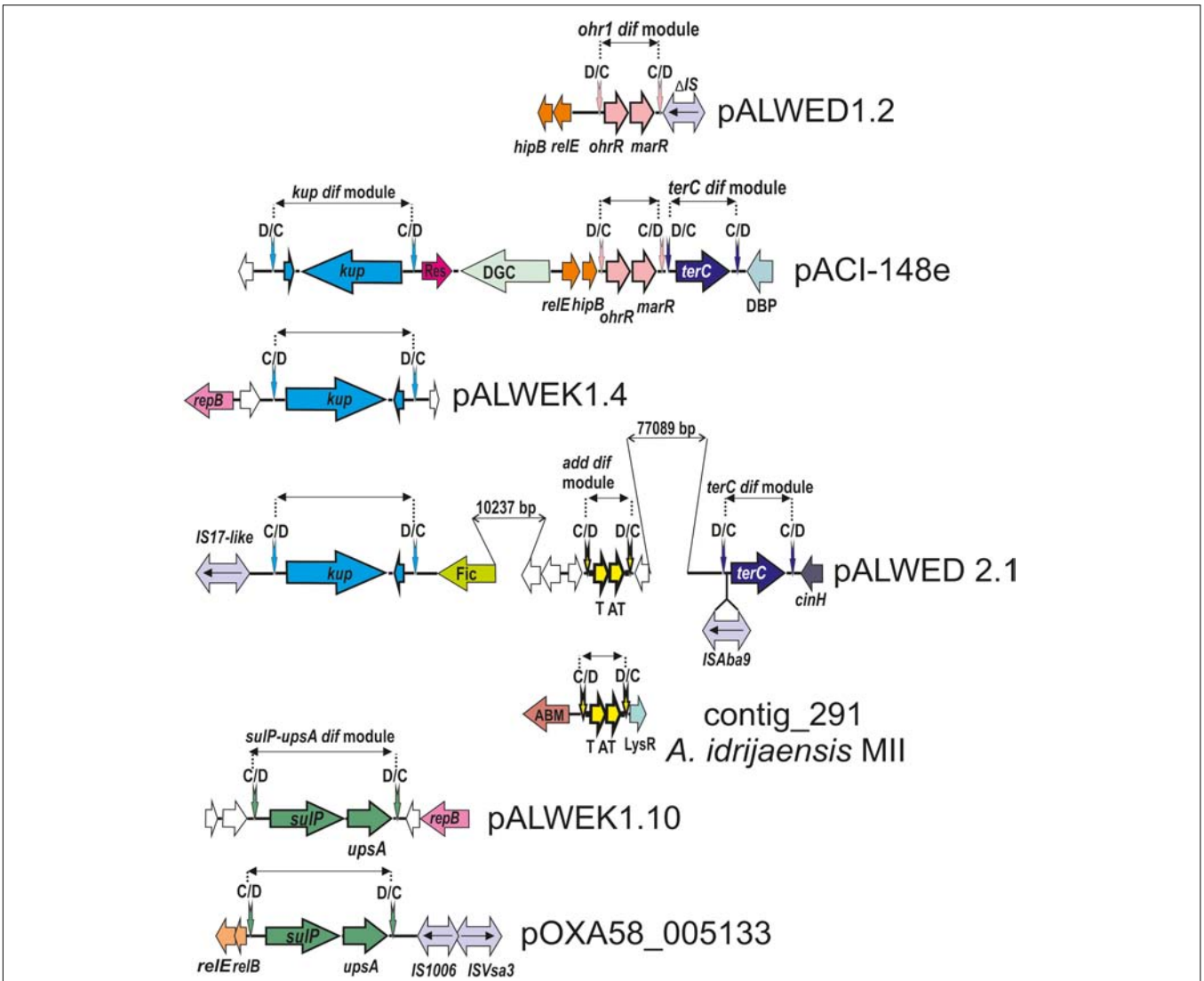

FIGURE 3 | Comparative genetic structures of plasmid regions containing *dif* modules. The locations and directions of genes and ORFs are shown by arrows. The components of the *dif* modules are represented by arrows with different colors. Vertical arrows indicate p*dif* sites with the orientation of the subsites shown above. Numbers (bp) show the size of the sequences located between different genes. Designations of gene products are as follows: DBP, DNA-binding protein; DGC, diguanylate cyclase; Res, resolvase; T, toxin; AT, antitoxin; Fic, Fic/DOC family protein; ABM, antibiotic biosynthesis monooxigenase; LysR, LysR family transcriptional regulator; unnamed ORFs, hypothetical proteins. Designations of IS-s: ISVsa3 -100% with ISVsa3; IS1006 – 1 mismatch with IS1006; ISAba9 – 2 mismatches with ISAba9; IS17-like -96% identity with IS17; ΔIS – truncated copy of an IS5 family element (IS427 group). The picture is drawn to scale.

Acinetobacter species (*A. lwoffii, A. baumannii, Acinetobacter towneri, Acinetobacter johnsonii)* (**Supplementary Table S2**). In most cases they were almost identical to the basic prototype modules (96–99% nucleotide identity level).

ohr dif Module

This genetic element contains two genes: a gene encoding organic hydroperoxide resistance, *ohr* (429 bp) and a second gene *ohrR* (432 bp) encoding transcription regulator from the MarR family of transcription factors (Sukchawalit et al., 2001; Atichartpongkul et al., 2010).

The *ohr dif* module was detected in plasmids from three permafrost strains *A. lwoffii*: pALWED1.2 from strain ED23-35; pALWVS1.1 from strain VS15 and pALWEK1.1 from strain EK30A (identity level 99%). However, the size and the boundaries of this module differed between the plasmids. We therefore analyzed its structure and distribution in more detail.

The *ohr/ohrR* genes with plasmid localization were first found by Dorsey et al. (2006) in the plasmid pMAC [AY541809.1] from a reference clinical strain *A. baumannii* ATCC 19606. The authors showed that *A. baumannii* ATCC 19606 is resistant to the organic peroxide-generating compounds cumene hydroperoxide (CHP) and tert-butyl hydroperoxide (t-BHP). We analyzed the genome of pMAC and detected typical p*dif* sites on both flanks of the *ohr* genes suggesting that pMAC contains an *ohr dif* module. The permafrost and clinical versions of the *ohr dif* module

TABLE 3 | The *dif* modules found in permafrost *A. lwoffii* strains and their distribution in modern strains.

Module	Length (b.p.)	Proposed function	Number of copies in plasmids/contigs	
			Environmental strains	Clinical strains
chrAB dif	3011	Resistance to chromium	9	2
terC dif	1221	Resistance to tellurium	8	1
kup dif	2549	Potassium uptake	7	0
ohr1 dif	1063	Resistance to organic peroxides	2	2
sulP dif	2159	Sulfate transporter	3	3
sulP-uspA dif	2739	Sulfate transporter	2	4
add dif	768	Toxin-antitoxin protein pair	5	3

are overall closely related (96% nucleotide identity) but reveal some specific differences: (*i*) the *ohr* module from the modern strain is 5 bp longer than the ancient one (1068 bp vs.1063 bp); (*ii*) both modules contain identical *ohrR* genes but their *ohrA* genes differ by 3%; (*iii*) region adjacent to the XerD/XerC site contains multiple substitutions. We therefore designated the ancient variant *ohr1 dif* and the modern variant *ohr2 dif* and studied the distribution of each of them separately.

Although we did not find the *ohr1 dif* module in the plasmids of modern strains, it was revealed among unassembled genomic sequences of various *Acinetobacter* species, in most cases in small-size contigs (**Supplementary Table S2**). The *ohr2 dif* module was detected both in plasmids and in contigs from various *Acinetobacter* species (**Supplementary Table S2**).

Interestingly, two plasmids (plasmid unnamed 2 [CP027180] and plasmid unnamed 4 [CP027186] from the modern strains of *A. baumannii* AR_0070 and *A. baumannii* AR_0052, respectively) contained numerous copies of the *ohr* 2 module, 14 in the first plasmid and 8 in the second.

The location of both *ohr dif* modules in various sequence contexts in different plasmids and contigs (**Figure 3**) strongly suggests their ability to move. Both modules likely originated from a common ancestor and then distributed independently among *Acinetobacter* species.

To test the functional activity of the *ohr1 dif* module, we compared resistance of permafrost strains, containing (group 1: ED23-35, VS15 and EK30A) or lacking (group 2: ED45-23 and ED9-5a) this module, to tert-butyl hydroperoxide (t-BHP) (see Materials and Methods). The results of three independent experiments demonstrated a higher level of resistance of group 1 strains (MIC = 0.2–0.4 mM) in comparison with group 2 strains (MIC = 0.1 mM).

dif Modules Containing Gene *sulP*

The gene *sulP* encodes sulfate permease (484 aa) that perform transport of inorganic anions into cells (Price et al., 2004). It is a member of the large and ubiquitous family of SulP proteins present in archaea, bacteria, fungi, plants and animals (Alper and Sharma, 2013).

We revealed two different mobile elements containing the *sulP* gene. The first module *sulP dif* (2159 bp), first found in our previous work (Mindlin et al., 2018), contained a small orf (198 bp) encoding hypothetical protein in addition to *sulP*; the second module *sulP-uspA dif* (2739 bp), detected in this work in the plasmid pALWEK1.10 from *A. lwoffii* EK30A, contained the *uspA* gene encoding a universal stress protein in addition to *sulP*. The *sulP* genes from the two modules are related (the identity level of 75%). The distribution of both *dif* modules in modern plasmids (contigs) is presented in **Supplementary Table S2** and **Figure 3** illustrates the location of the *sulP-uspA dif* module in different plasmids.

kup dif Module

A putative 2549 bp *dif* module containing the *kup* gene (1878 bp) encoding a potassium uptake transporter (Zakharyan and Trchounian, 2001) and an orf of unknown function (210 bp) was first revealed in our previous work (Mindlin et al., 2018). In this work we detected almost identical *kup dif* module in plasmids of three other permafrost strains (**Figure 3**) and studied its distribution in modern strains. The *kup dif* modules with identity level of 99% were found in plasmids and contigs from *Acinetobacter* strains belonging to different species (**Supplementary Table S2**). Importantly, seven out of 10 modern plasmids/contigs containing this module were isolated from environmental strains. The origin of the host strains for the remaining three plasmids [CP026424.1; APOG01000001.1; JWHB01000051.1] could not be established. Therefore, this module, which likely controls the uptake of potassium, may increase the fitness of *Acinetobacter* strains living in the environment but not in the clinic.

dif Sites and *dif* Modules in *Acinetobacter* Chromosomes

To reveal whether the presence of multiple *dif* sites is restricted to *Acinetobacter* plasmids, we next analyzed the number and location of *dif* sites in the *Acinetobacter* chromosomes. Usually a single *dif* locus involved in the resolution of chromosomal concatenates is located near the chromosome terminus (Carnoy and Roten, 2009). Surprisingly, we found that the *Acinetobacter* chromosomes are organized in a different way. Besides the main *dif* site (*dif1*), we revealed additional *dif* sites in most completely sequenced circular chromosomes of different species of the *Acinetobacter* genus. In total, we analyzed 20 sequenced chromosomes of 13 *Acinetobacter* species, and only one of them did not contain additional *dif* sites.

As a rule, the number of discovered *dif* sites varied from one to five and they were located far from *dif1* (e.g., *A. lwoffii* WJ10621 [CM001194.1]; *A. lwoffii* ZS207 [NZ_CP019143.1]; *A. johnsonii* XBB1 [CP010350.1]; *A. nosocomialis* SSA3 [CP020588.1]). Interestingly, we found two *Acinetobacter* strains that contained multiple additional *dif* sites in their chromosomes, *Acinetobacter indicus* SGAir0564 with 14 additional chromosomal *dif* sites

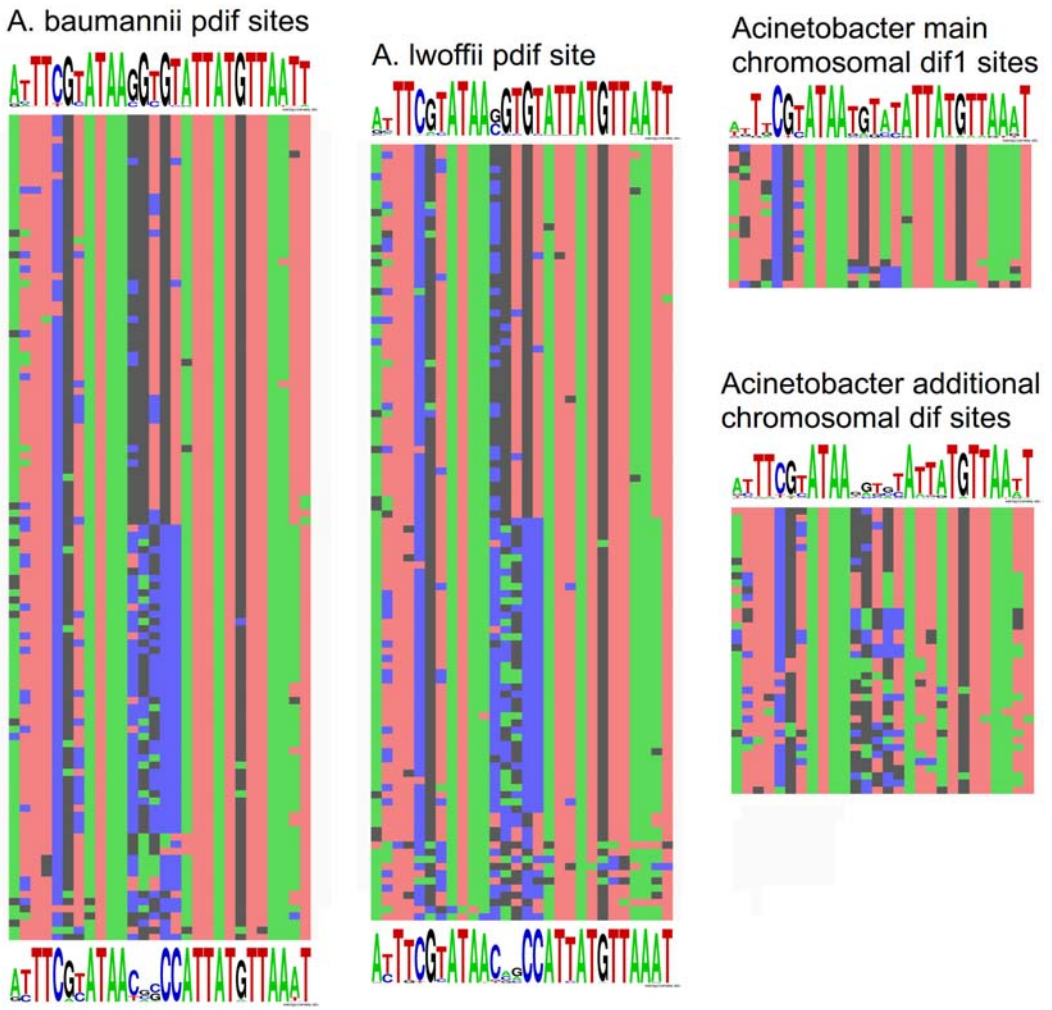

FIGURE 4 | Nucleotide variability within *dif* sites in *Acinetobacter* plasmids and chromosomes. All *dif* sequences analyzed in this study are presented in **Supplementary Table S1**.

[CP024620.1] and *Acinetobacter* sp. SWBY1 with 15 additional *dif* sites [CP026616.1].

It should be mentioned that strains containing multiple chromosomal *dif* sites were found occasionally when studying the distribution of different *dif* modules. In particular, the *terC dif* module, almost identical to that from plasmid pALWED1.4 (99% identity), was revealed in the chromosome *of A. indicus* SGAir0564 (CP024620.1). It was flanked by typical p*dif* sites (XerC/D and XerD/C) and was located at 2363397–2364617 bp, far from the main chromosomal *dif1* site at position 1526563. Similarly, we found a variant of the *add dif* module in the chromosome of the *Acinetobacter* sp strain SWBY1 [CP026616.1].

Comparative Analysis of Plasmid and Chromosomal *dif* Sites

To get insight into the origin and specific structure of the additional chromosomal *dif* sites, we compared their sequences with the main *dif1* sites from *Acinetobacter* chromosomes and with p*dif* sites from *A. baumannii* and *A. lwoffii* (see Materials and Methods). In total 109 p*dif* sites from 23 plasmids of *A. lwoffii*, 115 p*dif* sites from 33 plasmids of *A. baumannii*, 20 main *dif1* and 40 additional chromosomal *Acinetobacter dif* sites were analyzed.

All main features of classical *dif* sites were revealed in all studied groups (**Figure 4**). All of them have a length of 28 bp and are composed of two 11 bp regions comprising the binding sites for XerD (more conserved) and XerC (less conserved), separated by a more variable 6 bp central region. The inner parts of the XerC and XerD binding motifs contain inverted repeats forming a palindrome and are highly conserved while their outer regions are more variable (**Figure 4**).

Comparison of *dif* sites from different groups revealed that (**Figure 4**): (i) p*dif* sites from plasmids of distant species *A. baumannii* and *A. lwoffii* (*A. pseudolwoffii*) are very close to each other in their consensus structure and form two clusters

with different consensus sequences of five central nucleotides; (ii) additional chromosomal *dif* sites differ significantly in their structure from the main chromosomal *dif1* site, especially in their central part, while (iii) they are more similar to the plasmid p*dif* sites from both clusters. It should be mentioned that the structure of the main chromosomal *dif1* sites of *Acinetobacter* corresponds well to the consensus of *dif* sites from Proteobacteria chromosomes (Carnoy and Roten, 2009). Thus, it can be hypothesized that the plasmid p*dif* sites and additional chromosome *dif* sites have originated from a common genetic element, whose identity remains to be established.

DISCUSSION

The results of this and previous studies (D'Andrea et al., 2009; Merino et al., 2010; Grosso et al., 2012; Feng et al., 2016; Blackwell and Hall, 2017; Cameranesi et al., 2018; Hamidian and Hall, 2018) revealed the common presence of several (multiple) copies of *dif* sites and associated *dif* modules in plasmids and chromosomes of various *Acinetobacter* species including pathogens, commensals, and free-living bacteria belonging to different phylogenetic branches of the genus. Neither the additional copies of *dif* sites nor the mobile elements containing them are commonly found in other bacteria, even closely related to *Acinetobacter*, suggesting that their presence is a characteristic feature of the *Acinetobacter* genus. It should be noted that previous studies were mainly limited to the description of *dif* modules with antibiotic resistance genes (D'Andrea et al., 2009; Merino et al., 2010; Grosso et al., 2012; Povilonis et al., 2013; Blackwell and Hall, 2017). It was proposed that their distribution depends on the action of the site-specific recombination system *dif*/Xer. At the same time, the origin of the additional copies of *dif* sites, the mechanisms of their distribution and their role in the bacterial genome have not been studied in detail.

The results obtained in this study suggest that multiple *dif* sites present in *Acinetobacter* plasmids allow the formation of simple mobile elements containing various adaptive genes. In particular, analysis of the plasmid genomes from the ancient *A. lwoffii* (*A. pseudolwoffii*) strains revealed novel *dif* modules encoding different adaptive functions, including the resistance to chromium (*chrAB dif*, Mindlin et al., 2018), tellurium (*terC dif*) and organic peroxides (*ohr1 dif*), potassium (*kup dif*) and sulfate (*sulP dif*) transporters, toxin-antitoxin systems (*add dif*). All the detected genetic elements also have almost identical copies in the plasmids of modern *Acinetobacter* strains belonging to different species. It should be emphasized that the *dif* modules described in the present work were revealed in plasmids from only five studied permafrost strains of *A. lwoffii* group, and many more *dif* modules containing other adaptive genes are likely to be found in the future.

Based on their distribution, three groups of known *dif* modules can be distinguished: (i) mobile elements that encode metabolic and regulatory functions (e.g., resistance to chromium and tellurium, potassium uptake) and ensure survival under natural conditions, and mainly found in plasmids of environmental strains of *Acinetobacter* (described in this study); (ii) mobile elements found in both clinical and natural strains (including *dif* modules encoding sulfate permease, organic hydroperoxide resistance and toxin/antitoxin protein pairs, described in this study); (iii) mobile elements containing genes of antibiotic resistance and found almost without exception in plasmids of clinical strains of *Acinetobacter*, mainly *A. baumanni* (D'Andrea et al., 2009; Merino et al., 2010; Grosso et al., 2012; Blackwell and Hall, 2017). It is also appropriate to place in this group an *Acinetobacter* module encoding a putative virulence factor (Sel1-repeat protein) described by Lean and Yeo (2017). According to our preliminary data, it is flanked by XerC/D and XerD/C sites and is widely distributed in *A. baumannii* plasmids, similarly to classical *dif* modules.

Despite their different distribution, comparative molecular analysis of the *dif* modules described in this work and those containing antibiotic resistance genes described previously (D'Andrea et al., 2009; Merino et al., 2010; Grosso et al., 2012; Povilonis et al., 2013; Blackwell and Hall, 2017) suggests that they belong to the same group of unique genetic elements characteristic to the genus *Acinetobacter*. The wide distribution of such modules among plasmids of various *Acinetobacter* species indicates their ability to transfer horizontally and suggests that they form a special group of mobile genetic elements.

We demonstrated that multiple *dif* sites and *dif* modules can also be found in most *Acinetobacter* chromosomes. The main *dif1* site in the terminus region of the chromosome is required for the resolution of chromosome dimers by the XerC/XerD system and if it is transferred to other regions of the chromosome the process of dimer resolution is impaired, as shown for *Escherichia coli* (Cornet et al., 1996; Pérals et al., 2000). Thus, additional *dif* sites present in the *Acinetobacter* chromosomes are unlikely to function in the dimer resolution. Moreover, analysis of their sequences revealed that they are more closely related to p*dif* sites found in plasmids from various *Acinetobacter* species than to the chromosomal site *dif1*. Several examples of *dif* modules were also found in *Acinetobacter* chromosomes (this work). Thus, it can be proposed that the additional chromosomal *dif* sites may participate in the movement of *dif* modules encoding antibiotic resistance and various adaptive functions from plasmids to the chromosome and backward. Indeed, a *dif* module with the *Acinetobacter*-specific carbapenemase gene OXA-58 was recently found inserted into the XerC/XerD site of a prophage in the *Proteus mirabilis* chromosome (Girlich et al., 2017). As far as we know this is the first description of an XerC/XerD-dependent insertion of *Acinetobacter* antibiotic resistance genes within a bacterial chromosome.

It is natural to assume that the common role of all types of *dif* modules is to increase the fitness of their respective bacterial hosts in their habitats. Our results suggest that the *dif* modules possess the properties of mobile genetic elements capable to translocate between plasmids and chromosomes in *Acinetobacter* strains belonging to different species. Additional research is highly needed to assess the vast diversity of *dif* modules in

this clinically important genus and reveal their contribution to horizontal gene transfer and plasmid variability.

AUTHOR CONTRIBUTIONS

AM, AB, and MP conducted the sequencing and assembly of plasmids. All authors performed the bioinformatic analysis. MP performed the experiments. SM, MP, and AM wrote the manuscript. All authors contributed to the discussion and provided comments on the manuscript.

FUNDING

This research was supported by the Grant of the Ministry of Science and Higher Education of Russian Federation 14.W03.31.0007.

ACKNOWLEDGMENTS

We are grateful to A. Kulbachinskiy and two reviewers for helpful comments and suggestions and for critical reading of the manuscript and to A. Petrenko for help in assembly of plasmids.

SUPPLEMENTARY MATERIAL

The Supplementary Material for this article can be found online at: https://www.frontiersin.org/articles/10.3389/fmicb.2019.00632/full#supplementary-material

TABLE S1 | Distribution of *dif* sites in *Acinetobacter* plasmids and chromosomes.

TABLE S2 | Distribution of *dif* modules in ancient (permafrost) and modern *Acinetobacter* strains.

REFERENCES

Alper, S. L., and Sharma, A. K. (2013). The SLC26 gene family of anion transporters and channels. *Mol. Aspects Med.* 34, 494–515. doi: 10.1016/j.mam.2012.07.009

Altschul, S. F., Madden, T. L., Schaffer, A. A., Zhang, J., Zhang, Z., Miller, W., et al. (1997). Gapped BLAST and PSI-BLAST: a new generation of protein database search programs. *Nucleic Acids Res.* 25, 3389–3402. doi: 10.1093/nar/25.17.3389

Atichartpongkul, S., Fuangthong, M., Vattanaviboon, P., and Mongkolsuk, S. (2010). Analyses of the regulatory mechanism and physiological roles of *Pseudomonas aeruginosa* OhrR, a transcription regulator and a sensor of organic hydroperoxides. *J. Bacteriol.* 192, 2093–2101. doi: 10.1128/JB.01510-09

Bertram, R., and Schuster, C. F. (2014). Post-transcriptional regulation of gene expression in bacterial pathogens by toxin-antitoxin systems. *Front. Cell Infect. Microbiol.* 4:6. doi: 10.3389/fcimb.2014.00006

Blackwell, G. A., and Hall, R. M. (2017). The *tet39* determinant and the *msrE-mphE* genes in *Acinetobacter* plasmids are each part of discrete modules flanked by inversely oriented p*dif* (XerC-XerD) sites. *Antimicrob. Agents Chemother.* 61:e780-17. doi: 10.1128/AAC.00780-17

Cameranesi, M. M., Morán-Barrio, J., Limansky, A. S., Repizo, G. D., and Viale, A. M. (2018). Site-specific recombination at XerC/D sites mediates the formation and resolution of plasmid co-integrates carrying a *bla*OXA-58- and Tn*aphA6*-resistance module in *Acinetobacter baumannii*. *Front Microbiol.* 9:66. doi: 10.3389/fmicb.2018.00066

Carnoy, C., and Roten, C. A. (2009). The *dif*/Xer recombination systems in *Proteobacteria*. *PLoS One* 4:e6531. doi: 10.1371/journal.pone.0006531

Castillo, F., Benmohamed, A., and Szatmari, G. (2017). Xer site specific recombination: double and single recombinase systems. *Front Microbiol.* 8:453. doi: 10.3389/fmicb.2017.00453

Chasteen, T. G., Fuentes, D. E., Tantaleán, J. C., and Vásquez, C. C. (2009). Tellurite: history, oxidative stress, and molecular mechanisms of resistance. *FEMS Microbiol. Rev.* 33, 820–832. doi: 10.1111/j.1574-6976.2009.00177.x

Cornet, F., Louarn, J., Patte, J., and Louarn, J. M. (1996). Restriction of the activity of the recombination site dif to a small zone of the *Escherichia coli* chromosome. *Genes Dev.* 10, 1152–1161. doi: 10.1101/gad.10.9.1152

Crooks, G. E., Hon, G., Chandonia, J. M., and Brenner, S. E. (2004). WebLogo: a sequence logo generator. *Genome Res.* 14, 1188–1190. doi: 10.1101/gr.849004

Da Silva, G. J., and Domingues, S. (2016). Insights on the horizontal gene transfer of carbapenemase determinants in the opportunistic pathogen *Acinetobacter baumannii*. *Microorganisms* 4:E29. doi: 10.3390/microorganisms4030029

D'Andrea, M. M., Giani, T., D'Arezzo, S., Capone, A., Petrosillo, N., Visca, P., et al. (2009). Characterization of pABVA01, a plasmid encoding the OXA-24 carbapenemase from Italian isolates of *Acinetobacter baumannii*. *Antimicrob. Agents Chemother.* 53, 3528–3533. doi: 10.1128/AAC.00178-09

Dorsey, C. W., Tomaras, A. P., and Actis, L. A. (2006). Sequence and organization of pMAC, an *A. baumannii* plasmid harboring genes involved in organic peroxide resistance. *Plasmid* 56, 112–123. doi: 10.1016/j.plasmid.2006.01.004

Evans, B. A., and Amyes, S. G. (2014). OXA β-lactamases. *Clin. Microbiol. Rev.* 27, 241–263. doi: 10.1128/CMR.00117-13

Feng, Y., Yang, P., Wang, X., and Zong, Z. (2016). Characterization of *Acinetobacter johnsonii* isolate XBB1carrying nine plasmids and encoding NDM-1, OXA-58 and PER-1 by genome sequencing. *J. Antimicrob. Chemother.* 71, 71–75. doi: 10.1093/jac/dkv324

Finn, R. D., Mistry, J., Tate, J., Coggill, P., Heger, A., Pollington, J. E., et al. (2009). The Pfam protein families database. *Nucleic Acids Res.* 38, D211–D222. doi: 10.1093/nar/gkp985

Girlich, D., Bonnin, R. A., Bogaerts, P., De Laveleye, M., Huang, D. T., Dortet, L., et al. (2017). Chromosomal amplification of the blaOXA-58 carbapenemase gene in a *Proteus mirabilis* clinical isolate. *Antimicrob. Agents Chemother.* 61:e1697-16. doi: 10.1128/AAC.01697-16

Grosso, F., Quinteira, S., Poirel, L., Novais, Â, and Peixe, L. (2012). Role of common *bla*OXA-24/OXA-40-carrying platforms and plasmids in the spread of OXA-24/OXA-40 among *Acinetobacter* species clinical isolates. *Antimicrob. Agents Chemother.* 56, 3969–3972. doi: 10.1128/AAC.06255-11

Hamidian, M., and Hall, R. M. (2018). Genetic structure of four plasmids found in *Acinetobacter baumannii* isolate D36 belonging to lineage 2 of global clone 1. *PLoS One* 13:e0204357. doi: 10.1371/journal.pone.0204357

Kurakov, A., Mindlin, S., Beletsky, A., Shcherbatova, N., Rakitin, A., Ermakova, A., et al. (2016). The ancient small mobilizable plasmid pALWED1.8 harboring a new variant of the non-cassette streptomycin/spectinomycin resistance gene aadA27. *Plasmid* 8, 36–43. doi: 10.1016/j.plasmid.2016.02.005

Lean, S. S., and Yeo, C. C. (2017). Small, enigmatic plasmids of the nosocomial pathogen, *Acinetobacter baumannii*: good, bad, who knows? *Front. Microbiol.* 8:1547. doi: 10.3389/fmicb.2017.01547

Marchler-Bauer, A., Lu, S., Anderson, J. B., Chitsaz, F., Derbyshire, M. K., DeWeese-Scott, C., et al. (2011). CDD: a conserved domain database for the functional annotation of proteins. *Nucleic Acids Res.* 39(Suppl. 1), D225–D229. doi: 10.1093/nar/gkq1189

Martins, N., Picao, R. C., Adams-Sapper, S., Riley, L. W., and Moreira, B. M. (2015). Association of class 1 and 2 integrons with multidrug-resistant *Acinetobacter baumannii* international clones and *Acinetobacter nosocomialis* isolates. *Antimicrob. Agents Chemother.* 59, 698–701. doi: 10.1128/AAC.02415-14

Merino, M., Acosta, J., Poza, M., Sanz, F., Beceiro, A., Chaves, F., et al. (2010). OXA-24 carbapenemase gene flanked by XerC/XerD-Like recombination sites in different plasmids from different *Acinetobacter* species isolated during a nosocomial outbreak. *Antimicrob. Agents Chemother.* 54, 2724–2727. doi: 10.1128/AAC.01674-09

Mindlin, S., Petrenko, A., Kurakov, A., Beletsky, A., Mardanov, A., and Petrova, M. (2016). Resistance of ancient and modern *Acinetobacter lwoffii* strains to heavy metals and arsenic revealed by genome analysis. *BioMed. Res. Int.* 2016, 1–9. doi: 10.1155/2016/3970831

Mindlin, S., Petrenko, A., and Petrova, M. (2018). Chromium resistance genetic element flanked by XerC/XerD recombination sites and its distribution in environmental and clinical *Acinetobacter* strains. *FEMS Microbiol. Lett.* 365:fny047. doi: 10.1093/femsle/fny047

Moghadam, M. S., Albersmeier, A., Winkler, A., Cimmino, L., Rise, K., Hohmann-Marriott, M. F., et al. (2016). Isolation and genome sequencing of four Arctic marine *Psychrobacter* strains exhibiting multicopper oxidase activity. *BMC Genomics* 17:117. doi: 10.1186/s12864-016-2445-4

Nemec, A., Radolfová-Křížová, L., Maixnerová, M., Nemec, M., Clermont, D., Bzdil, J., et al. (2018). Revising the taxonomy of the *Acinetobacter lwoffii* group: the description of *Acinetobacter pseudolwoffii* sp. nov. and emended description of Acinetobacter lwoffii. *Syst. Appl. Microbiol.* 42, 159–167. doi: 10.1016/j.syapm.2018.10.004

Pagano, M., Martins, A. F., and Barth, A. L. (2016). Mobile genetic elements related to carbapenem resistance in *Acinetobacter baumannii*. *Braz. J. Microbiol.* 47, 785–792. doi: 10.1016/j.bjm.2016.06.005

Peleg, A. Y., de Breij, A., Adams, M. D., Cerqueira, G. M., Mocali, S., Galardini, M., et al. (2012). The success of acinetobacter species; genetic, metabolic and virulence attributes. *PLoS One* 7:e46984. doi: 10.1371/journal.pone.0046984

Pérals, K., Cornet, F., Merlet, Y., Delon, I., and Louarn, J. M. (2000). Functional polarization of the *Escherichia coli* chromosome terminus: the dif site acts in chromosome dimer resolution only when located between long stretches of opposite polarity. *Mol. Microbiol.* 36, 33–43. doi: 10.1046/j.1365-2958.2000.01847.x

Petrova, M. A., Mindlin, S. Z., Gorlenko, Zh. M, Kaliaeva, E. S., Soina, V. S., and Bogdanova, E. S. (2002). Mercury-resistant bacteria from permafrost sediments and prospects for their use in comparative studies of mercury resistance determinants. *Genetika* 38, 1569–1574.

Povilonis, J., Seputiene, V., Krasauskas, R., Juskaite, R., Miskinyte, M., Suziedelis, K., et al. (2013). Spread of carbapenem-resistant *Acinetobacter baumannii* carrying a plasmid with two genes encoding OXA-72 carbapenemase in Lithuanian hospitals. *J. Antimicrob. Chemother.* 68, 1000–1006. doi: 10.1093/jac/dks499

Price, G. D., Woodger, F. J., Badger, M. R., Howitt, S. M., and Tucker, L. (2004). Identification of a SulP-type bicarbonate transporter in marine cyanobacteria. *Proc. Natl. Acad. Sci. U.S.A.* 101, 18228–18233. doi: 10.1073/pnas.0405211101

Roberts, R. J., Vincze, T., Posfai, J., and Macelis, D. (2009). REBASE-a database for DNA restriction and modification: enzymes, genes and genomes. *Nucleic Acids Res.* 38, D234–D236. doi: 10.1093/nar/gkp874

Schuster, C. F., and Bertram, R. (2013). Toxin-antitoxin systems are ubiquitous and versatile modulators of prokaryotic cell fate. *FEMS Microbiol. Lett.* 340, 73–85. doi: 10.1111/1574-6968.12074

Shintani, M., Sanchez, Z. K., and Kimbara, K. (2015). Genomics of microbial plasmids: classification and identification based on replication and transfer systems and host taxonomy. *Front. Microbiol.* 6:242. doi: 10.3389/fmicb.2015.00242

Sukchawalit, R., Loprasert, S., Atichartpongkul, S., and Mongkolsuk, S. (2001). Complex regulation of the organic hydroperoxide resistance gene (ohr) from *Xanthomonas* involves OhrR, a novel organic peroxide-inducible negative regulator, and posttranscriptional modifications. *J. Bacteriol.* 183, 4405–4412. doi: 10.1128/JB.183.15.4405-4412.2001

Touchon, M., Cury, J., Yoon, E. J., Krizova, L., Cerqueira, G. C., Murphy, C., et al. (2014). The genomic diversification of the whole *Acinetobacter* genus: origins, mechanisms, and consequences. *Genome Biol. Evol.* 6, 2866–2882. doi: 10.1093/gbe/evu225

Turton, J. F., Shah, J., Ozongwu, C., and Pike, R. (2010). Incidence of Acinetobacter species other than A. baumannii among clinical isolates of *Acinetobacter*: evidence for emerging species. *J. Clin. Microbiol.* 48, 1445–1449. doi: 10.1128/JCM.02467-09

Yamaguchi, Y., Park, J., and Inouye, M. (2011). Toxin-antitoxin systems in bacteria and archaea. *Ann. Rev. Genet.* 45, 61–79. doi: 10.1146/annurev-genet-110410-132412

Zakharyan, E., and Trchounian, A. (2001). K+ influx by Kup in *Escherichia coli* is accompanied by a decrease in H+ efflux. *FEMS Microbiol. Lett.* 204, 61–64. doi: 10.1111/j.1574-6968.2001.tb10863.x

Conflict of Interest Statement: The authors declare that the research was conducted in the absence of any commercial or financial relationships that could be construed as a potential conflict of interest.

frontiers in Microbiology

ORIGINAL RESEARCH
published: 03 May 2019
doi: 10.3389/fmicb.2019.00930

Comparative Analysis of the Two *Acinetobacter baumannii* Multilocus Sequence Typing (MLST) Schemes

Stefano Gaiarsa[1,2], Gherard Batisti Biffignandi[2], Eliana Pia Esposito[3], Michele Castelli[4], Keith A. Jolley[5], Sylvain Brisse[6], Davide Sassera[2] and Raffaele Zarrilli[3]**

[1] Microbiology and Virology Unit, Fondazione IRCCS Policlinico San Matteo, Pavia, Italy, [2] Department of Biology and Biotechnology, University of Pavia, Pavia, Italy, [3] Department of Public Health, University of Naples "Federico II", Naples, Italy, [4] Romeo and Enrica Invernizzi Pediatric Research Center, Department of Biosciences, University of Milan, Milan, Italy, [5] Department of Zoology, University of Oxford, Oxford, United Kingdom, [6] Biodiversity and Epidemiology of Bacterial Pathogens, Institut Pasteur, Paris, France

OPEN ACCESS

Edited by:
Maria Soledad Ramirez, California State University, Fullerton, United States

Reviewed by:
Ruth M. Hall, University of Sydney, Australia
Spyros Pournaras, National and Kapodistrian University of Athens Medical School, Greece

***Correspondence:**
Davide Sassera
davide.sassera@uninpv.it
Raffaele Zarrilli
rafzarri@unina.it

Specialty section:
This article was submitted to Infectious Diseases, a section of the journal Frontiers in Microbiology

Received: *10 January 2019*
Accepted: *12 April 2019*
Published: *03 May 2019*

Citation:
Gaiarsa S, Batisti Biffignandi G, Esposito EP, Castelli M, Jolley KA, Brisse S, Sassera D and Zarrilli R (2019) Comparative Analysis of the Two Acinetobacter baumannii Multilocus Sequence Typing (MLST) Schemes. Front. Microbiol. 10:930. doi: 10.3389/fmicb.2019.00930

Acinetobacter species assigned to the *Acinetobacter calcoaceticus-baumannii* (Acb) complex, are Gram-negative bacteria responsible for a large number of human infections. The population structure of Acb has been studied using two 7-gene MLST schemes, introduced by Bartual and coworkers (Oxford scheme) and by Diancourt and coworkers (Pasteur scheme). The schemes have three genes in common but underlie two coexisting nomenclatures of sequence types and clonal complexes, which complicates communication on *A. baumannii* genotypes. The aim of this study was to compare the characteristics of the two schemes to make a recommendation about their usage. Using genome sequences of 730 strains of the Acb complex, we evaluated the phylogenetic congruence of MLST schemes, the correspondence between sequence types, their discriminative power and genotyping reliability from genomic sequences. *In silico* ST re-assignments highlighted the presence of a second copy of the Oxford *gdhB* locus, present in 553/730 genomes that has led to the creation of artefactual profiles and STs. The reliability of the two MLST schemes was tested statistically comparing MLST-based phylogenies to two reference phylogenies (core-genome genes and genome-wide SNPs) using topology-based and likelihood-based tests. Additionally, each MLST gene fragment was evaluated by correlating the pairwise nucleotide distances between each pair of genomes calculated on the core-genome and on each single gene fragment. The Pasteur scheme appears to be less discriminant among closely related isolates, but less affected by homologous recombination and more appropriate for precise strain classification in clonal groups, which within this scheme are more often correctly monophyletic. Statistical tests evaluate the tree deriving from the Oxford scheme as more similar to the reference genome trees. Our results, together with previous work, indicate that the Oxford scheme has important issues: *gdhB* paralogy, recombination, primers sequences, position of the genes on the genome. While there is no complete agreement in all analyses, when considered as a whole the above

results indicate that the Pasteur scheme is more appropriate for population biology and epidemiological studies of *A. baumannii* and related species and we propose that it should be the scheme of choice during the transition toward, and in parallel with, core genome MLST.

Keywords: multilocus sequence typing, *Acinetobacter baumannii*, comparative genomics, phylogeny, sequence types, clonal complexes

INTRODUCTION

Bacteria belonging to the genus *Acinetobacter* are glucose non-fermentative Gram-negative coccobacilli that are a frequent cause of health-care associated infections and hospital outbreaks, especially in intensive-care unit patients (Dijkshoorn et al., 2007; Zarrilli et al., 2013). *A. baumannii*, *A. nosocomialis*, *A. pittii*, *A. seifertii,* and *A. dijkshoorniae*, five of the most clinically relevant species, are genetically and phenotypically similar to the environmental species *A. calcoaceticus* and are therefore grouped into a species complex called the *A. calcoaceticus-A. baumannii* (Acb) complex (Dijkshoorn et al., 2007; Zarrilli et al., 2013; Marí-Almirall et al., 2017). *Acinetobacter spp*. isolates responsible for epidemics, in particular *A. baumannii* isolates, are frequently multidrug resistant (MDR) or extensively drug resistant (XDR). The majority of these strains are resistant to carbapenems and a fraction of them are resistant to last resource antimicrobial agent colistin (Zarrilli et al., 2013; Pournaras et al., 2017).

The rise of resistant Acb strains prompted the design and execution of epidemiological investigations of *A. baumannii* epidemics using a variety of molecular typing methods, among which multilocus sequence typing (MLST) has become the reference approach (Dijkshoorn et al., 1996; Dijkshoorn et al., 2007; Zarrilli et al., 2013). Among the advantages of MLST are its excellent reproducibility, its portability that allows global comparisons, and the ease of interpretation of data in evolutionary terms (Maiden et al., 1998; Maiden et al., 2013; Bialek-Davenet et al., 2014). Besides, a prominent benefit of MLST is a derived nomenclature of sequence types (STs), which have been rapidly and largely adopted by the community, allowing expansion of the global collective knowledge on the distribution, spread and biological features of the major clonal groups.

For *A. baumannii*, the advantages of an MLST nomenclature have been somewhat reduced by the co-existence of two MLST schemes, which are both widely used. Both schemes encompass *A. baumannii* and non-*baumannii Acinetobacter* species. The first scheme was introduced by Bartual and coworkers and is referred as the Oxford scheme, after the platform hosting it (Bartual et al., 2005; Wisplinghoff et al., 2008), whereas a second scheme was later published by Diancourt and coworkers (Pasteur scheme) (Diancourt et al., 2010). Although both schemes appeared to provide largely concordant classifications (Zarrilli et al., 2013, 2015), the co-existence of two nomenclatures (Zarrilli et al., 2015) calls for an assessment of their relative merits in terms of reliability, discrimination (which should be optimized for epidemiological purposes) and phylogenetic concordance of their derived classifications with "true" phylogenic relationships. Although the schemes were initially hosted at two different locations (both using first the mlstdbnet; Jolley et al., 2004) then the BIGSdb software (Jolley and Maiden, 2010), in 2013, the two schemes were united into a single database. This move facilitated curation requests (sometimes using both schemes for the same set of isolates) and harmonized the data analysis functionalities. The hosting of both schemes within a single BIGSdb database, which can incorporate genomic sequences, facilitated the joint MLST analysis of genomic sequences using both schemes.

Molecular epidemiology investigations revealed the occurrence of genetically distinct clonal lineages among populations of *A. baumannii* (Diancourt et al., 2010; Zarrilli et al., 2013). Three of these lineages, which were initially defined as European clones I to III and subsequently regarded as International Clones (IC) I to III, are distributed worldwide (IC I and IC II are also known as Global Clones, GC). The Pasteur scheme genotypes were numbered according to previous denominations, i.e., IC I, II, and III were named, respectively, as CC1, CC2, and CC3, with their dominant ST named ST1, ST2, and ST3, respectively (Dijkshoorn et al., 1996; van Dessel et al., 2004; Diancourt et al., 2010; Zarrilli et al., 2013). Other successful epidemic clonal lineages have been subsequently identified in the population structure of *A. baumannii* using the Pasteur MLST scheme, including sequence types ST10, ST15, ST25, ST32, ST78, ST79 (Diancourt et al., 2010; Zarrilli et al., 2013; Da Silva et al., 2014; Pournaras et al., 2014; Ou et al., 2015; Sahl et al., 2015). The Oxford MLST scheme was able to identify international clones I, II, and III and has been shown to possess higher discriminatory power than the Pasteur scheme (Feng et al., 2016; Tomaschek et al., 2016), but to suffer from problems due to recombination and technical artifacts (Hamouda et al., 2010; Hamidian et al., 2017). Recombination plays a crucial role in the evolution of the Acb genomes. Several specific loci are interested by this phenomenon. Among them is the *gpi* gene, which is part of the capsular operon (thus influencing the bacterium virulence) and one of the seven Oxford MLST scheme genes. Several works suggested to exploit this behavior for classification and adopt the Oxford scheme, as it allows to monitor the capsular type (Kenyon and Hall, 2013; Holt et al., 2016; Schultz et al., 2016; Hamidian et al., 2019).

The aims of the present study were to recapitulate the current status of both schemes, determine the characteristics of the Oxford and the Pasteur MLST schemes in terms of reliability of genotyping, denomination correspondence, phylogenetic congruence with genome-based phylogenies and discriminatory power.

MATERIALS AND METHODS

Python and Perl Scripts

All the scripts specifically developed and used for this work are available at https://github.com/MIDIfactory.

MLST Data

On 14 September 2018, we retrieved all sequence and profile definitions of both schemes from the PubMLST database[1] to evaluate them comparatively using different approaches.

Genome Datasets

Bacterial genomes included in the analysis were manually selected from the PubMLST database. In detail, we selected all complete genomes and all high-quality genomes, i.e., in which all loci of the MLST schemes and the ribosomal MLST scheme (Jolley et al., 2012) could be detected. The resulting dataset contains the genomes of 730 strains, belonging to the Acb complex, i.e., *A. baumannii* (n = 703), *A. nosocomialis* (n = 13), *A. seifertii* (n = 1), *A. dijkshoorniae* (n = 1), *A. pittii* (n = 7), *A. calcoaceticus* (n = 3) (see **Supplementary Figures S1A,B** for geographical and temporal distribution of the isolates, respectively). A complete list of the genomes is available here: https://pubmlst.org/bigsdb?db=pubmlst_abaumannii_isolates&page=projects.

The allelic variants of all gene fragments of both schemes were extracted from all the genomes, using an in-house Python script based on Blast (Altschul et al., 1990), keeping all results above 95% of identity with known alleles and subsequently selecting only perfect matches, procedure that allowed to assign the corresponding STs. The allelic sequences obtained were then aligned with Muscle (Edgar, 2004). The resulting alignments were concatenated using an in-house Perl script, to obtain two multigene alignments (one per MLST scheme) to be used as input for downstream analyses.

A core genome alignment was obtained to be used as a reference for determining the reliable phylogenetic trees. Gene calling was performed using Prodigal software v2.6.1 (Hyatt et al., 2010) on all 730 genomes in the dataset. A Perl script, which uses the double best Blast hit algorithm, was then used to identify genes orthologs to the previously published core genome by Higgins et al. (2017). Groups of ortholog genes were built and aligned using Muscle (v3.8.31, Edgar, 2004). The resulting core alignments were polished for poorly aligned positions and divergent regions using Gblocks software version 0.91b (Castresana, 2000), and merged in a concatenate of all ortholog genes, via another Perl script.

A Single-nucleotide polymorphism (SNP) alignment was built as a second reference. SNPs were detected using the procedure developed by Gaiarsa and coworkers (Gaiarsa et al., 2015) based on the software Mauve (Darling et al., 2004). Each genome was individually aligned to a reference (the complete genome AB307-0294), and alignments were then concatenated. Core SNPs were defined as single-nucleotide mutations flanked by conserved bases present in all the genomes in analysis.

[1]https://pubmlst.org/abaumannii/

Phylogenetic Analyses

Phylogenies of all four datasets (Oxford, Pasteur, core genes, core SNPs) were inferred using the same approach. The best model of evolution was determined using ModelTest-ng version 0.1.3 (Darriba et al., 2011). The selected model was GTRGAMMAIX for the three gene datasets, while the analysis for the SNP alignment was performed considering the ascertainment bias and using the Lewis correction (Lewis, 2001), thus with model ASC_GTRGAMMAX. Maximum Likelihood phylogeny was performed using RAxML (Stamatakis, 2014) with 100 bootstrap replicates.

Statistical Analysis

Three statistical tests were performed using the Core-genome and SNP phylogenetic trees as references and comparing them to the phylogenetic trees resulting from MLST gene concatenates. Two topology-based tests (Matching clusters, Robinson-Fould), were performed with TreeCmp (Bogdanowicz et al., 2012). The matching clusters test calculates the number of topology changes that should be performed in order to transform a tree into the reference one. The Robinson-Fould (R-F) test instead counts the different bipartitions between the two trees. In both cases, a value of zero indicates that the two analyzed trees are identical.

The other analysis, likelihood-based Shimodaira-Hasegawa test, was performed with RaxML (Stamatakis, 2014). In this test, a null hypothesis is stated, which assumes that two compared trees are both a correct interpretation of an alignment. The tested hypothesis is that one or more trees are a better representation of the data. *P*-values smaller than 0.05 indicate that two trees are significantly different.

In addition, the Gini-Simpson index was used to determine the discrimination power of both schemes. The index was calculated using the website service comparingpartitions.info on the entire dataset of 730 genomes and on the genomes of the three main International Clones.

Monophyly of Clonal Complexes

Clonal Complexes were defined using eBURST as described previously (Feil et al., 2004); CCs were defined as groups of Sequence Types that differ from one or more members of the group by just one allele. Monophyly of the CCs was checked on the core genome tree using the R environment and the library spider. Minimum spanning trees of sequence types (STs) were built using Phyloviz Online using the goeBURST algorithm (Ribeiro-Gonçalves et al., 2016). Minimum spanning trees were generated from the 7 alleles of each MLST scheme and species were assigned based on clustering with reference STs. The species field was updated in the PubMLST database for all STs with no ambiguous assignment.

Nucleotide Distance Analysis

To evaluate how well each gene fragment variation correlates with the genome variation, we compared the pairwise nucleotide distances between each pair of genomes in our dataset with the corresponding distances between each gene fragment pairs. The MLST gene fragment sequences, as well as all the concatenated

core genome gene sequences, were aligned with Muscle (Edgar, 2004) and then used to calculate pairwise genetic distances via the function "dist.dna" of the R package APE (Paradis et al., 2004).

In order to test the discrimination resolution of each MLST scheme, we plotted the pairwise sequence distance between each MLST locus for each pair of genomes, against the corresponding core genome-wide sequence distance. The correlation was determined adopting the regression linear model in the R environment. Due to an uneven large distribution of genomic distances, we decided to split each dataset in three blocks (as in Bleidorn and Gerth, 2018), based on the genomic distance (first block: 0.0–0.05, second block: 0.05–0.1, third: >0.1). Finally, a heatmap was generated to evaluate R^2 and slopes of all regression lines.

Recombination Rate

The recombination rate was calculated for each locus of both MLST schemes, using the RDP4 Software on the alignments of all alleles present the 730 genomes of the dataset (Martin et al., 2015), employing all available algorithms. This same analysis

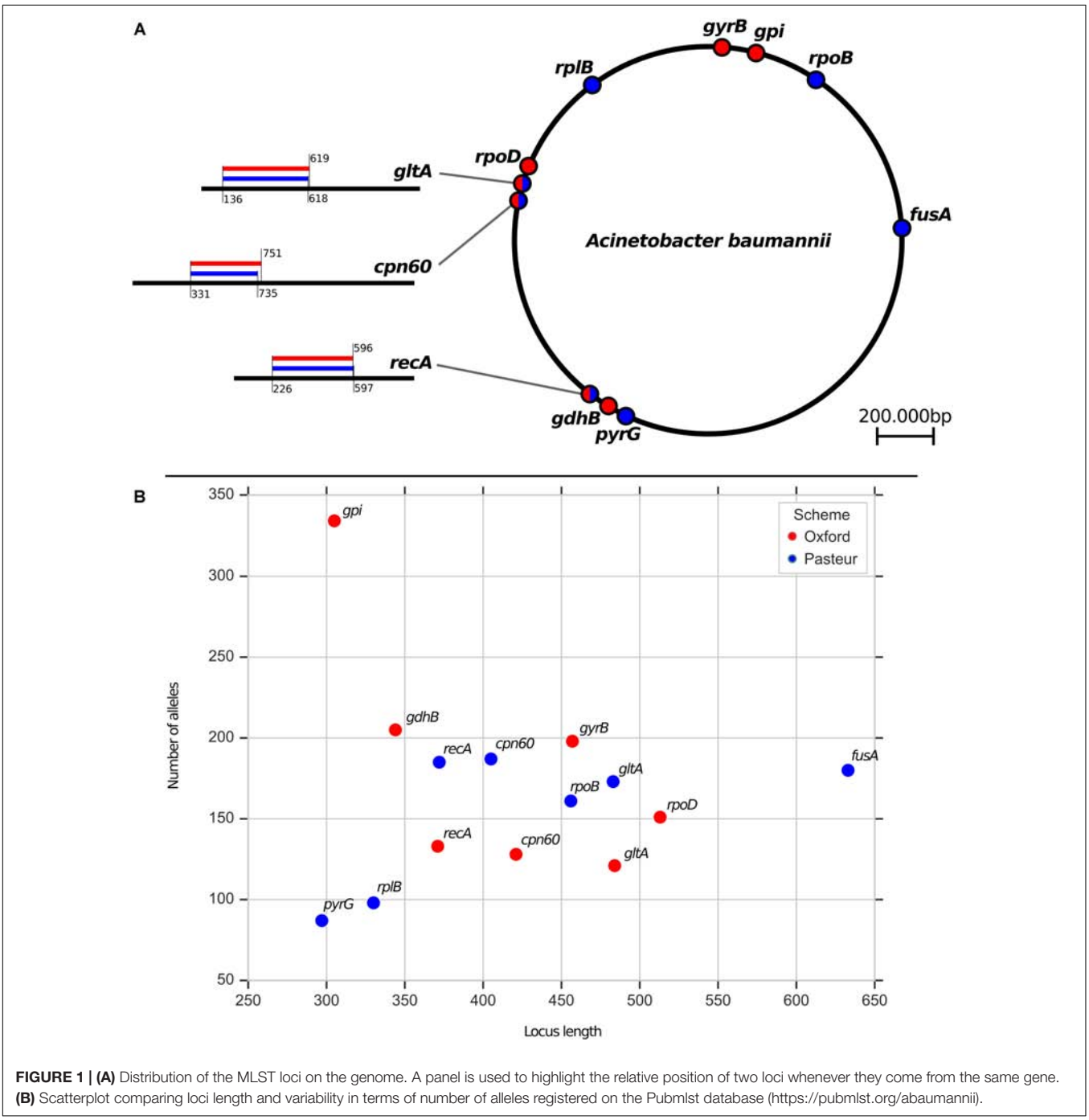

FIGURE 1 | (A) Distribution of the MLST loci on the genome. A panel is used to highlight the relative position of two loci whenever they come from the same gene. **(B)** Scatterplot comparing loci length and variability in terms of number of alleles registered on the Pubmlst database (https://pubmlst.org/abaumannii).

was also performed on a reduced dataset containing only the *A. baumannii* genome subset, to refine the recombination rate detection within this species.

GdhB Analysis

To investigate the Oxford scheme gene *gdhB* putative duplication, we extracted all variants of both gene copies from the 730 genomes in our dataset, including sequences not registered in the PubMLST database, through a custom approach based on Blast (identity > 95% with the *gdhB*-1 or the *gdhB*-182 allele).

To check primer alignment, the flanking region was extracted for all alleles found, and aligned with the PCR primers used to sequence the *gdhB* locus. Mismatches between the aligned sequences and the primers were calculated for the entire primer length and for the ten bases at the three-prime end.

Finally, all *gdhB* and *gdhB2* variants were analyzed with a phylogenetic approach. Variants were aligned with the software muscle (Edgar, 2004) and used as input for a Maximum Likelihood phylogeny, executed with fasttree (Price et al., 2010). The genes surrounding the *gdhB* and *gdhB2* sites were extracted using a python script and the software Prodigal (Hyatt et al., 2010). Functions were predicted using COGnitor (Galperin et al., 2015). Codon adaptation index was calculated for all coding sequences in all 730 genomes in the dataset using the CAIcalc script (Puigbo et al., 2008).

RESULTS

Status of the Database Contents of the Pasteur and Oxford MLST Schemes

In order to evaluate the two MLST schemes available for *A. baumannii*, we start by describing them in detail. Both schemes are built on 7 genes. The concatenation of allele 1 of the 7 Oxford and Pasteur genes yields 2895 and 2976 nucleotides, respectively. Three genes are shared between the two schemes: *cpn60*, *gltA*, and *recA*. The subsequences used for typing, though, differ between the two schemes, as depicted in **Figure 1A**.

We downloaded all sequence and profiles definitions on date 14 September 2018. Oxford contained 1866 profiles (STs), while the Pasteur scheme had 1234 STs defined. The number of alleles ranged from 121 to 334 for Oxford, 87–187 for Pasteur. Regarding the three common genes, the allele numbers were 128(Oxford)/187(Pasteur) for *cpn60*, 121(Oxford)/173(Pasteur) for *gltA*, 133(Oxford)/185(Pasteur) for *recA*. Thus, the Pasteur scheme seemed to encompass more diversity in the common genes, although more STs were defined by Oxford overall (**Figure 1B**).

A gdhB Paralog Complicates *in silico* Determination of the Oxford ST

730 genomes of the Acb complex were selected and downloaded to be used as dataset. The database included mostly genomes of *A. baumannii* isolates (703, 96.3%), but also genomes of *A. nosocomialis, A. seifertii, A. dijkshoorniae, A. pittii,* and *A. calcoaceticus* isolates. MLST alleles of both schemes were first defined from genomic sequences. While extracting alleles, a consistent proportion of the genomes appeared to have two variants of the *gdhB* gene. This issue was investigated further, revealing that an alternative *gdhB* locus (corresponding to alleles 182, 189 and variants of them) was present in 553 (76%) of 730 strains, all belonging to the *A. baumannii* species. This locus is often annotated in these genomes as *gdhB2* and has a sequence similarity with allele 1 of *gdhB* ranging from 73.98 to 77.94%. Primers used for molecular MLST were aligned to

TABLE 1 | Minimum and maximum number of mutations obtained when sequencing primers are aligned to all *gdhB* loci in the dataset.

	Entire sequence		Last 10 nt	
	Forward primer	**Reverse primer**	**Forward primer**	**Reverse primer**
gdhB site	0–1	3–4	0–1	1–3
alternative *gdhB* site	4–18	6–6	3–10	4–4

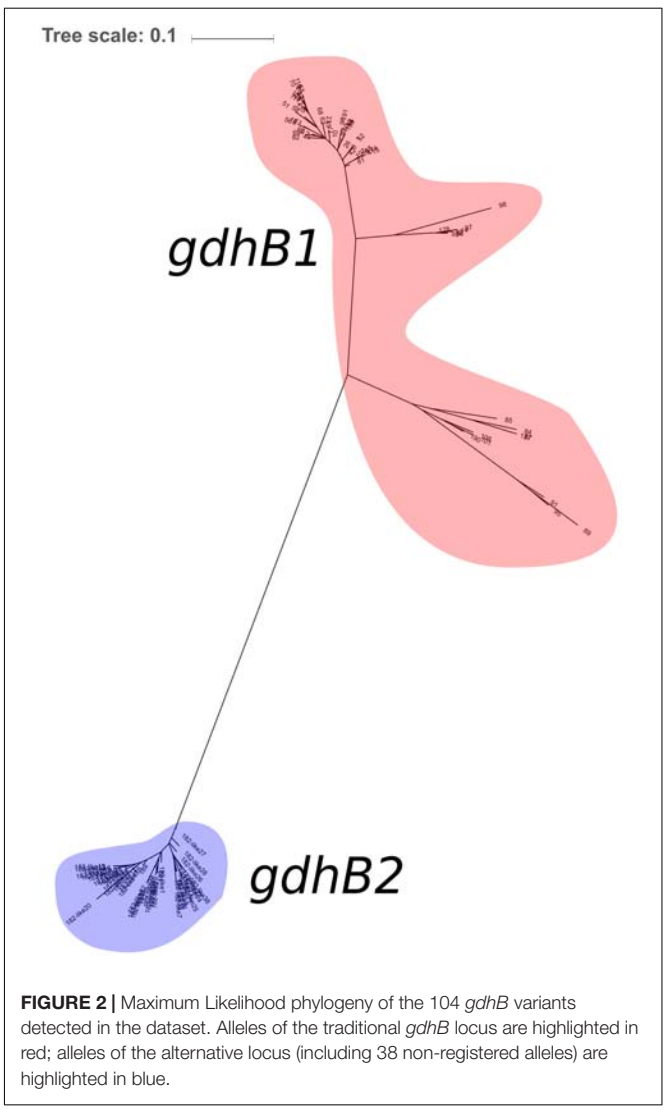

FIGURE 2 | Maximum Likelihood phylogeny of the 104 *gdhB* variants detected in the dataset. Alleles of the traditional *gdhB* locus are highlighted in red; alleles of the alternative locus (including 38 non-registered alleles) are highlighted in blue.

both genomic regions, showing a low affinity for the alternative *gdhB2* locus (**Table 1**). For this reason, we can hypothesize that the *gdhB2* locus cannot be amplified with these PCR primers, and indeed all alleles of the paralogous locus were defined only using *in-silico* methods for ST determination from genomic sequences. In order to evaluate the relationships between *gdhB* and *gdhB2*, a phylogeny of all 64 *gdhB* and the 40 *gdhB2* alleles was determined. The resulting tree clearly showed two main clusters, one containing only the putative *gdhB2* sequences, i.e., allele 182 and related variants, only found in *A. baumannii* (**Figure 2**). The other main cluster, containing the original *gdhB* variants, on the other hand presents genomes from all the analyzed Acb species, and each species appears grouped in a monophyletic cluster. The genomic surroundings of the two variants (i.e., the three genes upstream and downstream the *gdhB* and *gdhB2* sites) are clearly different. Nucleotide composition analysis was performed on *gdhB* and *gdhB2*, showing that both genes have a codon composition that is significantly different from the average of the respective genomes. A subset of isolates that are characterized in the Oxford scheme with STs that include alleles of *gdhB2* instead of the original locus where manually analyzed. When replacing the artefactual *gdhB2* allele with the correct *gdhB* locus, the obtained profiles correspond to existing STs, including ST231, a strain of epidemiological importance due to the report of the presence of the carbapenemase gene $bla_{\mathrm{OXA-23}}$. Therefore, the wrong calling of alleles at *gdhB2* locus has artifactually inflated the diversity recorded using the Oxford scheme.

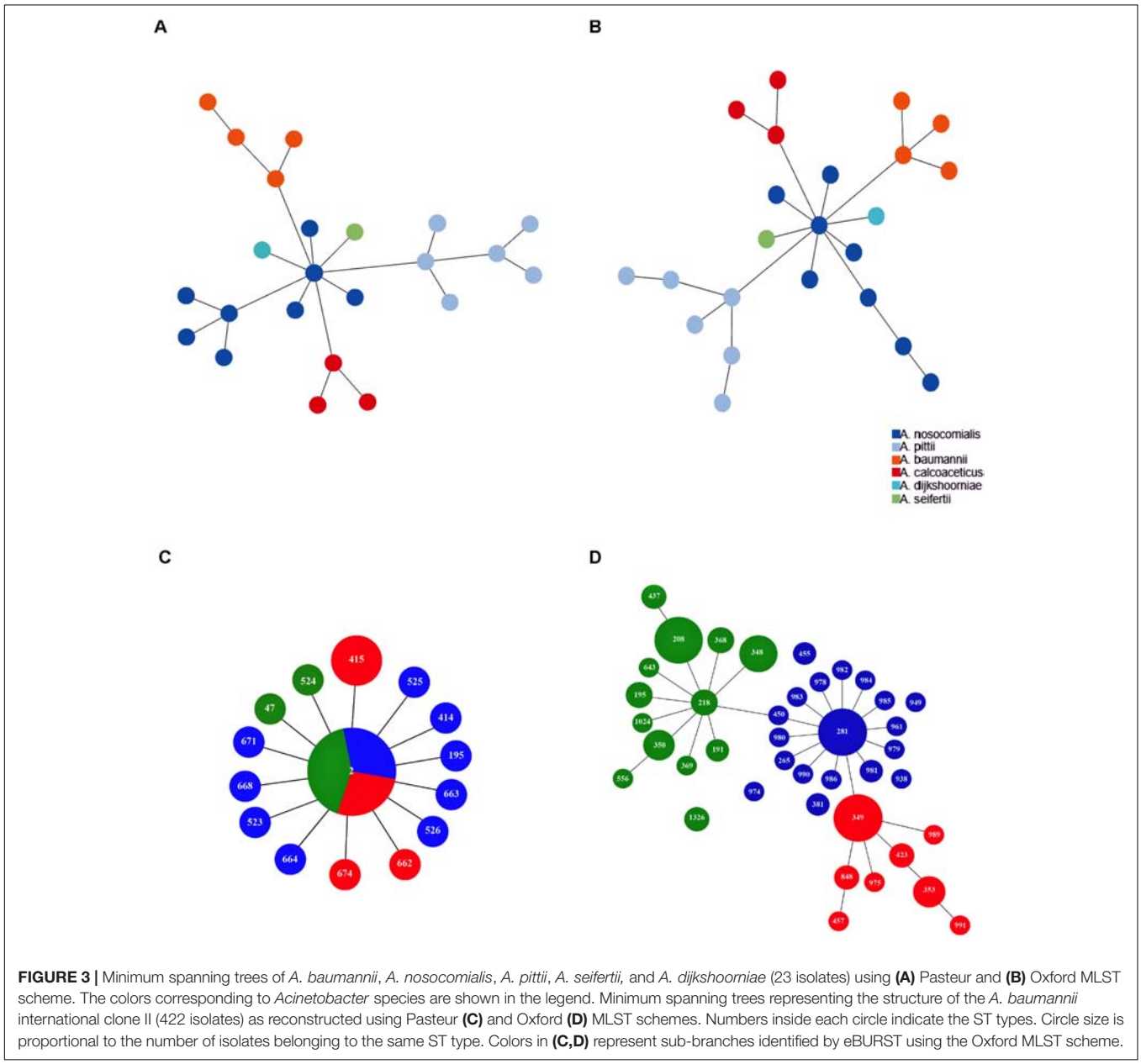

FIGURE 3 | Minimum spanning trees of *A. baumannii*, *A. nosocomialis*, *A. pittii*, *A. seifertii,* and *A. dijkshoorniae* (23 isolates) using **(A)** Pasteur and **(B)** Oxford MLST scheme. The colors corresponding to *Acinetobacter* species are shown in the legend. Minimum spanning trees representing the structure of the *A. baumannii* international clone II (422 isolates) as reconstructed using Pasteur **(C)** and Oxford **(D)** MLST schemes. Numbers inside each circle indicate the ST types. Circle size is proportional to the number of isolates belonging to the same ST type. Colors in **(C,D)** represent sub-branches identified by eBURST using the Oxford MLST scheme.

Oxford and Pasteur Comparison

Minimum spanning tree analysis demonstrated that both MLST schemes gene sets discriminate the existing species within the Acb complex (**Figures 3A,B**, MLST-based species identification). ST assignments and eBURST analyses using our 730 genomes dataset generated a convenient and expandable table of correspondence between the two MLST schemes, represented in **Table 2** and in **Figure 4** and **Supplementary Figure S2** as Sankey diagrams.

Then, we extracted CCs from both schemes and checked their monophyly on the core genome phylogeny. The Pasteur scheme had 12 CCs comprising a total of 47 STs, i.e., 35.34% of all STs. Additionally, there were 86 singleton Pasteur STs, while nine CCs are monophyletic. The Oxford scheme had 16 CCs comprising in total 82 STs, i.e., 44.56% of all STs. Additionally, there were 102 singleton Oxford STs and 11 monophyletic CCs. The Pasteur scheme appeared to be less discriminant, but more appropriate for precise strain classification into clonal groups. On the other hand, the Oxford scheme was able to identify additional genotypes and to differentiate isolates belonging to international clone II into three distinct clonal groups (**Table 2** and **Figures 3C,D**).

The Gini-Simpson index of the 730 genomes was almost one order of magnitude higher when classifying the dataset using the Pasteur STs (0.70–0.93 for Oxford). When repeating the calculation on the genomes of the three International Clones, the score difference was lower but still important. The Pasteur scheme obtained values close to 0, being of low discrimination within the three ICs (**Table 3**).

TABLE 2 | Correspondence of *A. baumannii* clonal lineages as assessed by Oxford and Pasteur MLST schemes.

International clonal lineages[a]	Pasteur's MLST[b]	Oxford's MLST[b]	References[c]
I	CC1	CC231	Diancourt et al., 2010; Hamidian et al., 2017
II	CC2	CC208 CC281 CC349	Diancourt et al., 2010; Feng et al., 2016; Hamidian et al., 2017
III	ST3	CC928	van Dessel et al., 2004; Diancourt et al., 2010
	CC10	CC447	Zarrilli et al., 2013
	ST15	ST950	Di Popolo et al., 2011; Zarrilli et al., 2013
	ST25	CC229	Zarrilli et al., 2013; Sahl et al., 2015;
	ST32	ST172	Zarrilli et al., 2013; Da Silva et al., 2014
	CC52	ST931	Diancourt et al., 2010; Zarrilli et al., 2013
	ST78	ST944	Giannouli et al., 2010; Carretto et al., 2011; Zarrilli et al., 2013
	CC422	CC124	Grosso et al., 2011; Villalon et al., 2011; Zarrilli et al., 2013

[a] The International clonal lineages are identified by amplified fragment length polymorphism (AFLP) analysis. [b] Clonal complexes (CCs) are numbered according to the most prevalent clone. STs are indicated when singletons. [c] Key publications on each clone are reported.

Topologies Comparison and Statistical Analysis

To evaluate the two MLST schemes with respect to phylogenetic inference, we constructed four phylogenies (**Figure 5**): two using the concatenated alleles of the Pasteur and Oxford scheme as input, and two references using genome-wide data (a core-genome of 1409 high quality genes, and an alignment of 68,340 SNPs). We then statistically compared the trees to evaluate the reliability of MLST concatenates in relationship with the two references. All tests applied suggested a better congruence between the Oxford scheme and the references. Full results are reported in **Table 4**, which includes the results of cross check tests between the two reference phylogenies. In **Figure 5**, International Clones I, II, and III (calculated according to the Pasteur CC 1, 2, and 3) are highlighted in all four trees. In the tree obtained using the Oxford genes, the genomes of IC I are split in two separate, non-monophyletic, clades.

Recombination Analysis

A recombination analysis was run on the alignments of all MLST gene fragments. All gene sequences presented signs of recombination in the *non-baumannii* genomes. This suggested that the analysis was biased by an uneven evolutionary distance and was repeated only on the 703 *A. baumannii* genomes. This step allowed detecting a recombination in the *gpi* locus of the Oxford scheme, while all other loci appeared to be recombination free. These data are in partial agreement with a previous study, which detected recombination in the topologies of the phylogenetic trees generated for the *gyrB* and *gpi* genes using the Oxford MLST scheme (Hamouda et al., 2010). High recombinogenicity of the *gpi* locus was also detected in other studies, which focused on the genomic plasticity of the capsular loci (Kenyon and Hall, 2013; Holt et al., 2016; Schultz et al., 2016; Hamidian et al., 2019). Accordingly, the recombining locus *gpi* happens to have the highest variability in alleles (**Figure 1B**). These results suggest that the Pasteur scheme allele diversification is less affected by homologous recombination. Accordingly, the recombining locus *gpi* happens to have the highest variability in alleles (**Figure 1B**).

MLST Correlation With Genomic Distance

The pairwise sequence distance between each MLST locus of each pair of genomes was plotted against the corresponding genome-wide distance in order to test its correlation. The test was repeated focusing on three different ranges of genome-wide distances (as in Bleidorn and Gerth, 2018). A total of 56 plots was obtained and reported in **Supplementary Figure S3**. We expected high quality genes to have a regression line with a positive slope (direct correlation between genomic and locus distance), as close as possible to a value of 1 (this means that the evolution of the MLST sequence follows the same pace as the genome). We thus summarized the slope data in two heatmaps: one with the slope values (**Figure 6**) and one with the R^2-values (**Supplementary Figure S4**) to assess reliability of the regression. In general, both schemes perform better at lower genomic distances. This trend

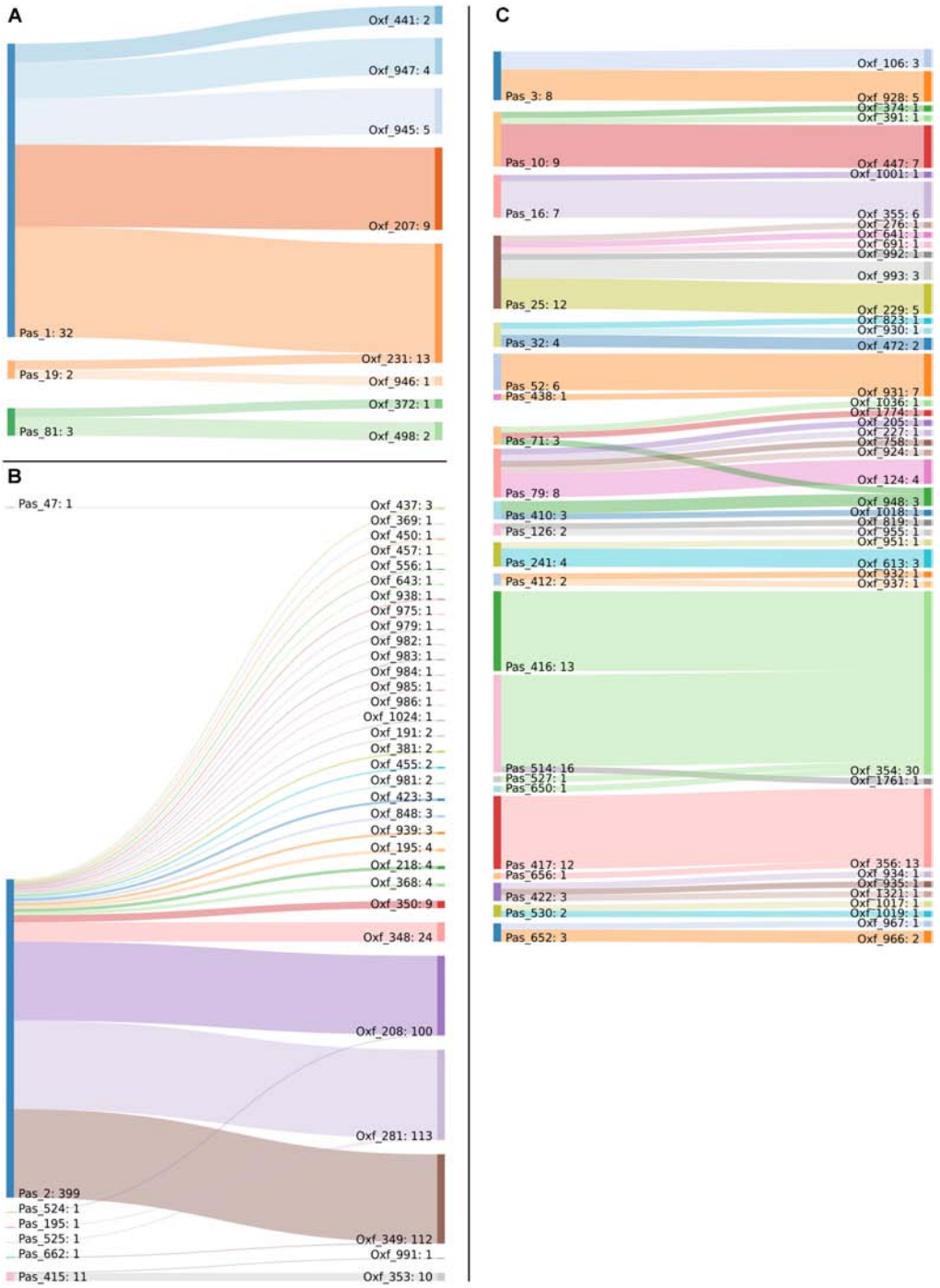

FIGURE 4 | Sankey diagram of the MLST classification of the 730 genomes in use, as performed with the Pasteur and Oxford schemes. Two-way corresponding STs were removed to improve image clarity. Captions show the corresponding STs belonging to **(A)** International Clone 1, **(B)** International Clone 2, and **(C)** all the other genomes.

is highlighted especially in the *recA* gene, shared between the two schemes. Generally speaking, Pasteur alleles perform well when analyzing high genomic distances, while Oxford alleles have better scores at lower genomic distances. Finally, the *gpi* gene deserves a particular mention: at low genomic distances, the locus shows a quicker evolution than the genomic reference, while at high genomic distances, it shows an inverted evolution (i.e., at higher genomic distances correspond lower *gpi* distances). This could be probably due to the recombination detected in the gene sequence: at lower evolutionary distances, recombinations can

TABLE 3 | Gini-Simpson index values obtained using the STs of both schemes on the entire dataset of 730 genomes and separately on the three International Clones.

Scheme	Total	IC_I	IC_II	IC_III
Oxford	0.927543629	0.768518519	0.7799125	0.46875
Pasteur	0.695552637	0.203703704	0.0049875	0

increase variation, while they can act as equalizers at larger scales, having a cohesive effect (Doroghazi and Buckley, 2011).

DISCUSSION

The aim of this investigation was to compare the two MLST schemes that are widely used to genotype isolates of the Acb species complex. We decided to tackle the problem evaluating the two schemes, their reproducibility, discrimination, strain classification into CCs and compatibility among MLST-based phylogenies and genome-based phylogenies.

Starting from a curated dataset of 730 genomes, two phylogenomic trees were obtained from information collected throughout the whole genomes (core genes and core SNPs). The two resulting trees showed highly similar topologies and can be considered close approximations of the real evolutionary history of the Acb species complex. For this reason, they were used as reliable and unbiased references for the analyses. A phylogeny was obtained from the concatenate alignment of the alleles of each of the two MLST schemes and compared with the two references using three different statistical methods. In all three cases, the tree obtained from the Oxford scheme resulted in a closer approximation of the references.

On the other hand, previous publications described a series of limitations and issues of the Oxford scheme (Hamouda et al., 2010; Hamidian et al., 2017), such as the inclusion of the primers in the registered allele sequences of two of the seven MLST genes. This unusual procedure leads to replacing the true sequence with the primer sequence at these locations, creating mosaic sequences (primerF + internal sequence from isolate + primerR), and removing variation at priming sites when sequenced using primer-based methods. This issue was recognized and corrected previously, so it should not affect future identification, but it remains for all the previously investigated strains that were analyzed by PCR and not *in silico* (Hamidian et al., 2017).

Here, we detected an entirely novel problem with *in silico* determination of Oxford profiles, namely the presence of a

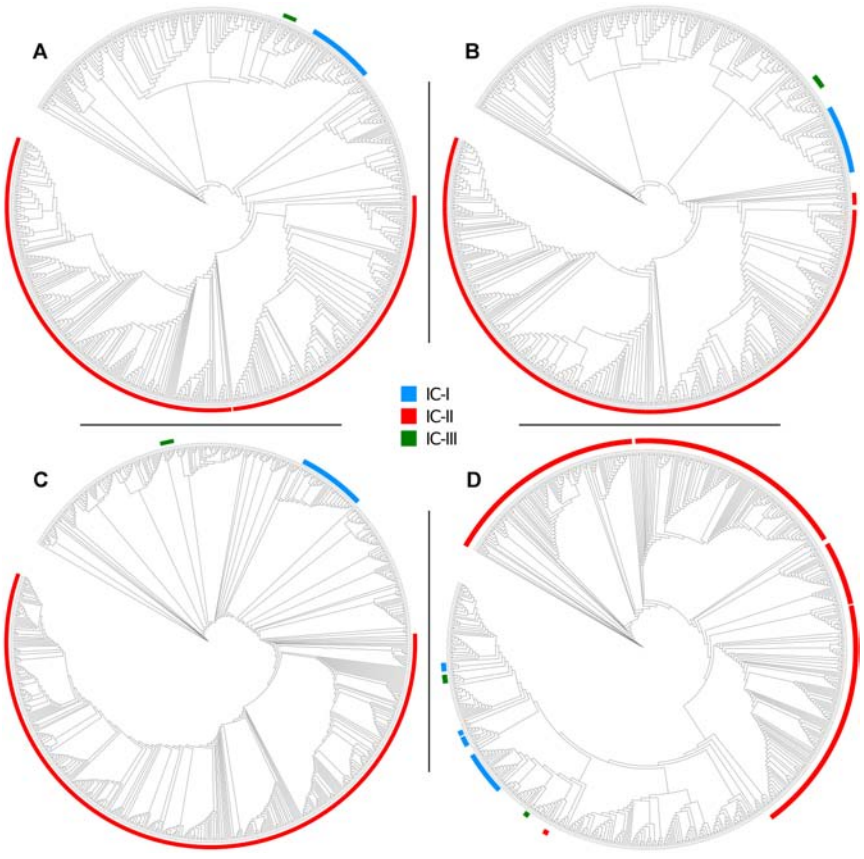

FIGURE 5 | Maximum Likelihood phylogenies of 730 genomes of the *Acb* complex, inferred from **(A)** a concatenate of 1409 orthologous core genes, **(B)** a concatenate of 68,340 SNP positions, **(C)** a concatenate of the seven alleles used in the Pasteur MLST scheme, and **(D)** a concatenate of the seven alleles used in the Oxford MLST scheme. Major clonal complexes are highlighted: International clone I in blue, International clone II in red, International clone III in green.

TABLE 4 | Statistical comparison of the phylogenies obtained using the MLST loci of both schemes to the two reference trees obtained with genome-wide SNPS and core genes.

Reference tree	Tree	Matching clusters	R-F clusters	SH test		
				D (LH)	SD	*P*-value
Core genome	Oxford	17149	653	−560419,8575	4728,447118	<1%
Core genome	Pasteur	22348	669	−1114308,906	14114,36962	<1%
SNP	Oxford	15958	654	−226406,4429	2748,796098	<1%
SNP	Pasteur	22679	669	−576957,8653	10208,8312	<1%
SNP	Core genome	6197	497	−12777,39132	988,204341	<1%
Core genome	SNP	6197	497	−34788,30168	1285,842838	<1%

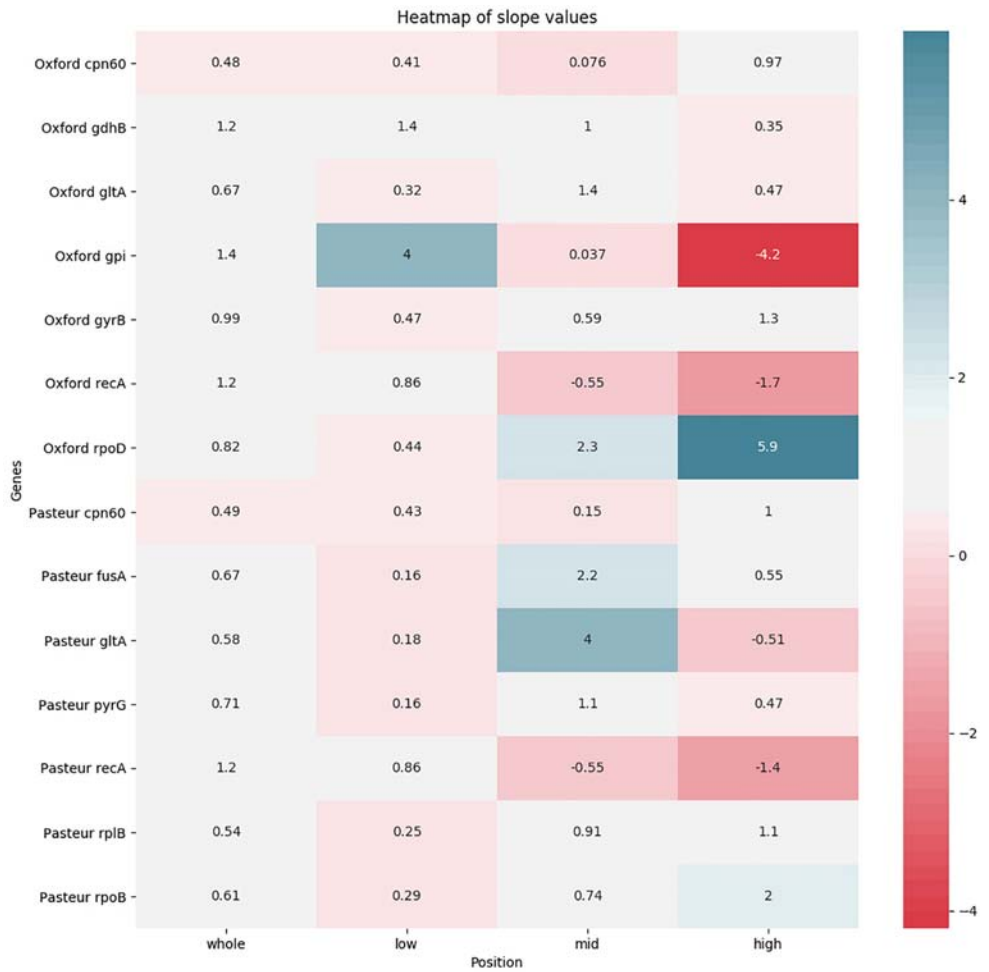

FIGURE 6 | Heatmap showing the levels of agreement of each MLST locus to a reference alignment based on the core genome. Agreement levels are shown in terms of regression line slopes obtained from distance values between genome pairs. For each locus four regression were obtained, based, respectively, on the entirety of genome-wide distances and three subranges. White color indicates that a MLST locus represents the genome-wide distances well, showing a similar evolutionary pace. Red shades (indicating a negative correlation) and blue shades (indicating that the MLST locus shows an evolutionary pace much higher than the genome wide distances) indicate that the locus variation does not well represent genome variation.

paralog of the Oxford gene *gdhB* in a high proportion (553 out of the 730) of Acb genomes, a locus that we found to be often annotated as *gdhB2*, and that is located in a different genomic region. On multiple occasions, allele sequences resulting from this duplication were incorrectly used to establish new Oxford STs that do not actually exist, as they are based on alleles of the paralog *gdhB2*. This issue can be explained with an event of gene duplication, or of horizontal gene transfer, the second being more probable considering the low identity between the two paralogs (around 73%). Such event would have occurred early

in the evolution of the Acb complex, possibly at the root of the *A. baumannii* species, followed by a quick sequence divergence of *gdhB2* and by the loss of this gene in a number of representatives of the Acb complex (177 out of 730 in our dataset). Nucleotide composition analysis shows that both *gdhB* and *gdhB2* have higher than average codon adaptation index, thus not allowing to understand which of the two events could be more likely.

The incorrect alleles are, to date (14 September 2018) 182 and 189 and have led to the determination of 30 STs: 1567, 1604, 1677, 1678, 1793, 1794, 1796, 1800, 1804, 1805, 1806, 1807, 1808, 1809, 1813, 1815, 1816, 1833, 1834, 1835, 1836, 1837, 1838, 1839, 1840, 1841, 1843, 1851, 1852, 1857. Other 38 unregistered 182-like alleles were found in the dataset used in this project and should not be registered if submitted to the MLST database. We suggest that these *gdhB2*-based alleles should be removed from the database, and each of the genomes belonging to these STs should be re-analyzed excluding the paralog *gdhB2* (a stringent allele calling filter on genetic similarity could be useful for this purpose) to find the correct *gdhB* allele and subsequently the current ST. The inclusion of the paralog allele in the database is due to the bioinformatics methods used, which did not take into account the possible presence of such paralog. This does not appear to have ever happened in PCR-based classification, as the *gdhB* primers are sufficiently specific to amplify only the correct locus. While this issue can be solved using bioinformatics, in silico MLST can be performed with different software tools including in-house scripts, so we cannot rule out the possibility of novel *gdhB2*-based alleles to appear in the future.

Another issue of the Oxford scheme, albeit one that mostly impact phylogenetic analyses, is the presence of possible recombinations, previously reported for two of the loci used, *gpi* and *gyrB* (Hamouda et al., 2010). Our analysis does not show a clear signal of recombination in the *gyrB* gene, but we detected a strong recombination signal in the *gpi* gene. The fact that recombination in the *gyrB* locus was detected previously but not within this study could be explained by the use of different methods, as Hamouda and colleagues used a general phylogenetic approach (Hamouda et al., 2010), while we chose an *ad hoc* recombination detection software.

Clearly, the most reliable classification method for *Acinetobacte*r isolates would be one based on genome-wide information, such as a core genome MLST (cgMLST) (Maiden et al., 2013). Whole genome sequencing, which is required to extract cgMLST data, is now a routine task in many research laboratories, with costs comparable to performing the seven PCR amplifications and Sanger sequencing required for the traditional MLST. Whole genome sequencing has been used to study *A. baumannii* phylogeny (Snitkin et al., 2011; Sahl et al., 2013; Chan et al., 2015; Wallace et al., 2016), but only two studies so far used cgMLST schemes for *A. baumannii* (Fitzpatrick et al., 2016; Higgins et al., 2017). The cgMLST scheme by Fitzpatrick and colleagues analyzed genetic similarity based on SNPs in the core genome of a limited number of Acb complex bloodstream isolates, 116 *A. baumannii*, 28 *A. pittii,* and 3 *A. nosocomialis*, and showed higher discriminatory power than PFGE and MLST (Fitzpatrick et al., 2016). Higgins et al. (2017) developed a cgMLST scheme based on 1,339 *A. baumannii* genomes and validated on 53 *A. baumannii* genomes. The cgMLST clustering showed a good correlation between PFGE types and also matched the classification of *A. baumannii* international clones as previously determined by DiversiLab typing or MLST (Higgins et al., 2017). The set of genes by Higgins works well when analyzing strains of *A. baumannii sensu stricto* but is not fit for the other species of the Acb complex (Higgins et al., 2017) and should thus be restricted to shared genes in order to allow broader use.

As NGS is not yet accessible in all diagnostic laboratories in the world, cgMLST is probably still unfit to be a globally shared typing technique. Additionally, cgMLST classification could in some cases be incompatible with previous works that used MLST classifications, especially if specific STs are found to be polyphyletic and considering that determining STs *in silico* must be done with caution, as highlighted by our discovery of incorrect *gdhB* alleles identified based on a paralog sequence. Therefore, 7-gene MLST is likely to continue being used widely in the near future.

CONCLUSION

In conclusion, the two MLST schemes have complementary characteristics, each with their own advantages: the Pasteur scheme shows lower discrimination, is able to better identify clonal lineages, and in general performs better when comparing evolutionary distant clones. The Oxford scheme in turn shows higher concordance with phylogenies and works better for discrimination among strains at short evolutionary distances. However, a novel and important issue of the Oxford scheme in the genomic era is the presence of an alternative *gdhB* locus in the majority (533/730) of the *A. baumannii* genomes. Besides, the presence of primers in sequence templates of two of the genes may have resulted in a few artefactual allele calls.

Previous works recommended the Oxford scheme due to the presence of the *gpi* gene, which is part of the capsular locus, and thus can provide a link between typing and phenotypic information (Kenyon and Hall, 2013; Holt et al., 2016). Other authors criticize both schemes due to the low level of resolution or polyphyly of Sts (Castillo-Ramírez and Graña-Miraglia, 2019). An opposite view could recommend the use of both schemes to provide a finer characterization. On the other hand, our opinion is to recommend the Pasteur scheme because of the following reasoning: both the link to phenotypic information and the finer characterization will be soon accomplished by the blooming cgMLST method, and will thus not be required for classical MLST schemes in the future. An MLST scheme in the genome era, however, retains great importance as a fundamental nomenclature tool. As such, absence of recombination, absence of wrongly called variants, and better adherence to the main epidemiological clones should be considered the main reasons to choose one of the two available schemes.

To summarize, we recommend the utilization of the Pasteur scheme for 7-gene MLST classification of *Acinetobacter* isolates of the Acb complex, and that future cgMLST nomenclature of genotypic groups should inherit, as much as possible, the Pasteur MLST denominations that were themselves inherited from pre-MLST international clone nomenclatures.

AUTHOR CONTRIBUTIONS

SG, SB, DS, and RZ designed the project. EE, KJ, and RZ curated the database and performed eburst analyses. SG and GB performed the bulk of the bioinformatic analyses. MC performed the phylogenetic analyses. SG, KJ, SB, DS, and RZ wrote the manuscript. All authors read and approved the final manuscript.

FUNDING

This work was supported in part by grants from Wellcome Trust Biomedical Resource (Grant 104992 to KJ), University of Naples "Federico II" (Fondo d'Ateneo per la Ricerca to RZ) and the Italian Ministry of Education, University and Research (MIUR): PRIN2017 (Grant 2017SFBFER to RZ), Dipartimenti di Eccellenza Program (2018–2022) – Department of Biology and Biotechnology "L. Spallanzani," University of Pavia (to DS).

ACKNOWLEDGMENTS

We thank the team of curators of the Pasteur and Oxford Acinetobacter MLST schemes for curating the data and making them publicly available at http://pubmlst.org/abaumannii/. RZ dedicates this study to the memory of Carmelo Bruno Bruni, his mentor of microbial genetics.

SUPPLEMENTARY MATERIAL

The Supplementary Material for this article can be found online at: https://www.frontiersin.org/articles/10.3389/fmicb.2019.00930/full#supplementary-material

FIGURE S1 | (A) Geographic and **(B)** temporal characterization of the database of 730 genomes used in the present work.

FIGURE S2 | Complete Sankey diagram of the MLST classification of the 730 genomes in use, as performed with the Pasteur and Oxford schemes.

FIGURE S3 | Plots showing the correlation of genetic distances of *Acinetobacter* genomes between MLST loci and genome-wide distances. Each data-point corresponds to a single pair of *Acinetobacter* genomes, and shows the divergence of each locus related to core-genome-based distance. For each locus, we show the full range of genome-wide distances and three different subregions representing different genomic distances (first block: 0.0–0.05, second block: 0.05–0.1, third: > 0.1).

FIGURE S4 | Heatmap representing the correlation of each MLST locus in comparison to a reference alignment based on the core genome. Four plots were produced for each locus, based on genome-wide distances (see **Supplementary Figure 3**). In this figure, we report the R^2-values of the interpolation lines.

REFERENCES

Altschul, S. F., Gish, W., Miller, W., Myers, E. W., and Lipman, D. J. (1990). Basic local alignment search tool. *J. Mol. Biol.* 215, 403–410. doi: 10.1016/S0022-2836(05)80360-2

Bartual, S. G., Seifert, H., Hippler, C., Luzon, M. A., Wisplinghoff, H., and Rodriguez-Valera, F. (2005). Development of a multi-locus sequence typing scheme for characterization of clinical isolates of *Acinetobacter baumannii*. *J. Clin. Microbiol.* 43, 4382–4390. doi: 10.1128/jcm.43.9.4382-4390.2005

Bialek-Davenet, S., Criscuolo, A., Ailloud, F., Passet, V., Jones, L., Delannoy-Vieillard, A. S., et al. (2014). Genomic definition of hypervirulent and multidrug-resistant *Klebsiella pneumoniae* clonal groups. *Emerg. Infect. Dis.* 20, 1812–1820. doi: 10.3201/eid2011.140206

Bleidorn, C., and Gerth, M. (2018). A critical re-evaluation of multilocus sequence typing (MLST) efforts in Wolbachia. *FEMS Microbiol. Ecol.* 94:fix163. doi: 10.1093/femsec/fix163

Bogdanowicz, D., Giaro, K., and Wróbel, B. (2012). TreeCmp: comparison of trees in polynomial time. *Evol. Bioinform. Online* 8, 475–487. doi: 10.4137/EBO.S9657

Carretto, E., Barbarini, D., Dijkshoorn, L., van der Reijden, T. J., Brisse, S., Passet, V., et al. (2011). Widespread carbapenem resistant *Acinetobacter baumannii* clones in Italian hospitals revealed by a multicenter study. *Infect. Genet. Evol.* 11, 1319–1326. doi: 10.1016/j.meegid.2011.04.024

Castillo-Ramírez, S., and Graña-Miraglia, L. (2019). Inaccurate multilocus sequence typing of *Acinetobacter baumannii*. *Emerg. Infect. Dis.* 25, 186–187. doi: 10.3201/eid2501.180374

Castresana, J. (2000). Selection of conserved blocks from multiple alignments for their use in phylogenetic analysis. *Mol. Biol. Evol.* 17, 540–552. doi: 10.1093/oxfordjournals.molbev.a026334

Chan, A. P., Sutton, G., DePew, J., Krishnakumar, R., Choi, Y., Huang, X. Z., et al. (2015). A novel method of consensus pan-chromosome assembly and large-scale comparative analysis reveal the highly flexible pan-genome of *Acinetobacter baumannii*. *Genome Biol.* 21:143. doi: 10.1186/s13059-015-0701-6

Da Silva, G. J., Van Der Reijden, T., Domingues, S., Mendonça, N., Petersen, K., and Dijkshoorn, L. (2014). Characterization of a novel international clonal complex (CC32) of *Acinetobacter baumannii* with epidemic potential. *Epidemiol. Infect.* 142, 1554–1558. doi: 10.1017/S0950268813002288

Darling, A. C. E., Mau, B., Blattner, F. R., and Perna, N. T. (2004). Mauve: multiple alignment of conserved genomic sequence with rearrangements. *Genome Res.* 14, 1394–1403. doi: 10.1101/gr.2289704

Darriba, D., Taboada, G. L., Doallo, R., and Posada, D. (2011). Prottest 3: fast selection of best-fit models of protein evolution. *Bioinformatics* 27, 1164–1165. doi: 10.1093/bioinformatics/btr088

Di Popolo, A., Giannouli, M., Triassi, M., Brisse, S., and Zarrilli, R. (2011). Molecular epidemiology of multidrug-resistant *Acinetobacter baumannii* strains in four Mediterranean countries with a multilocus sequence typing scheme. *Clin. Microbiol. Infect.* 17, 197–201. doi: 10.1111/j.1469-0691.2010.03254.x

Diancourt, L., Passet, V., Nemec, A., Dijkshoorn, L., and Brisse, S. (2010). The population structure of *Acinetobacter baumannii*: expanding multiresistant clones from an ancestral susceptible genetic pool. *PLoS One* 5:e10034. doi: 10.1371/journal.pone.0010034

Dijkshoorn, L., Aucken, H., Gerner Smidt, P., Janssen, P., Kaufmann, M. E., Garaizar, J., et al. (1996). Comparison of outbreak and nonoutbreak *Acinetobacter baumannii* strains by genotypic and phenotypic methods. *J. Clin. Microbiol.* 34, 1519–1525.

Dijkshoorn, L., Nemec, A., and Seifert, H. (2007). An increasing threat in hospitals: multidrug resistant *Acinetobacter baumannii*. *Nat. Rev. Microbiol.* 5, 939–951. doi: 10.1038/nrmicro1789

Doroghazi, J. R., and Buckley, D. H. (2011). A model for the effect of homologous recombination on microbial diversification. *Genome Biol. Evol.* 3, 1349–1356. doi: 10.1093/gbe/evr110

Edgar, R. C. (2004). MUSCLE: multiple sequence alignment with high accuracy and high throughput. *Nucleic Acids Res.* 32, 1792–1797. doi: 10.1093/nar/gkh340

Feil, E. J., Li, B. C., Aanensen, D. M., Hanage, W. P., and Spratt, B. G. (2004). eBURST: inferring patterns of evolutionary descent among clusters of related bacterial genotypes from multilocus sequence typing data. *J. Bacteriol.* 186, 1518–1530. doi: 10.1128/JB.186.5.1518-1530.2004

Feng, Y., Ruan, Z., Shu, J., Chen, C. L., and Chiu, C. H. (2016). A glimpse into evolution and dissemination of multidrug-resistant *Acinetobacter baumannii* isolates in East Asia: a comparative genomics study. *Sci. Rep.* 6:24342. doi: 10.1038/srep24342

Fitzpatrick, M. A., Ozer, E. A., and Hauser, A. R. (2016). Utility of whole-genome sequencing in characterizing *Acinetobacter* epidemiology and analyzing hospital outbreaks. *J. Clin. Microbiol.* 54, 593–612. doi: 10.1128/JCM.01818-15

Gaiarsa, S., Comandatore, F., Gaibani, P., Corbella, M., Dalla Valle, C., Epis, S., et al. (2015). Genomic epidemiology of *Klebsiella pneumoniae* in Italy and novel insights into the origin and global evolution of its resistance to carbapenem antibiotics. *Antimicrob. Agents Chemother.* 59, 389–396. doi: 10.1128/AAC.04224-14

Galperin, M. Y., Makarova, K. S., Wolf, Y. I., and Koonin, E. V. (2015). Expanded microbial genome coverage and improved protein family annotation in the COG database. *Nucleic Acids Res.* 43, D261–D269. doi: 10.1093/nar/gku1223

Giannouli, M., Cuccurullo, S., Crivaro, V., Di Popolo, A., Bernardo, M., Tomasone, F., et al. (2010). Molecular epidemiology of multidrug-resistant *Acinetobacter baumannii* in a tertiary care hospital in Naples, Italy, shows the emergence of a novel epidemic clone. *J. Clin. Microbiol.* 48, 1223–1230. doi: 10.1128/JCM.02263-09

Grosso, F., Carvalho, K. R., Quinteira, S., Ramos, A., Carvalho-Assef, A. P., Asensi, M. D., et al. (2011). OXA-23-producing *Acinetobacter baumannii*: a new hotspot of diversity in Rio de Janeiro? *J. Antimicrob. Chemother.* 66, 62–65. doi: 10.1093/jac/dkq406

Hamidian, M., Hawkey, J., Wick, R., Holt, K. E., and Hall, R. M. (2019). Evolution of a clade of *Acinetobacter baumannii* global clone 1, lineage 1 via acquisition of carbapenem- and aminoglycoside-resistance genes and dispersion of ISAba1. *Microb. Genom.* 5:e000242. doi: 10.1099/mgen.0.000242

Hamidian, M., Nigro, S. J., and Hall, R. M. (2017). Problems with the Oxford multilocus sequence typing scheme for *Acinetobacter baumannii*: do sequence type 92 (ST92) and ST109 exist? *J. Clin. Microbiol.* 55, 2287–2289. doi: 10.1128/JCM.00533-17

Hamouda, A., Evans, B. A., Towner, K. J., and Amyes, S. G. (2010). Characterization of epidemiologically unrelated *Acinetobacter baumannii* isolates from four continents by use of multilocus sequence typing, pulsed-field gel electrophoresis, and sequence-based typing of *bla* (OXA-51-like) genes. *J. Clin. Microbiol.* 48, 2476–2483. doi: 10.1128/JCM.02431-09

Higgins, P. G., Prior, K., Harmsen, D., and Seifert, H. (2017). Development and evaluation of a core genome multilocus typing scheme for whole-genome sequence-based typing of *Acinetobacter baumannii*. *PLoS One* 12:e0179228. doi: 10.1371/journal.pone.0179228

Holt, K., Kenyon, J. J., Hamidian, M., Schultz, M. B., Pickard, D. J., Dougan, G., et al. (2016). Five decades of genome evolution in the globally distributed, extensively antibiotic-resistant *Acinetobacter baumannii* global clone 1. *Microb. Genom.* 2:e000052. doi: 10.1099/mgen.0.000052

Hyatt, D., Chen, G. L., Locascio, P. F., Land, M. L., Larimer, F. W., and Hauser, L. J. (2010). Prodigal: prokaryotic gene recognition and translation initiation site identification. *BMC Bioinformatics* 11:119. doi: 10.1186/1471-2105-11-119

Jolley, K. A., Bliss, C. M., Bennett, J. S., Bratcher, H. B., Brehony, C., Colles, F. M., et al. (2012). Ribosomal multilocus sequence typing: universal characterization of bacteria from domain to strain. *Microbiology* 158(Pt 4), 1005–1015. doi: 10.1099/mic.0.055459-0

Jolley, K. A., Chan, M. S., and Maiden, M. C. (2004). mlstdbNet - distributed multi-locus sequence typing (MLST) databases. *BMC Bioinformatics* 5:86. doi: 10.1186/1471-2105-5-86

Jolley, K. A., and Maiden, M. C. J. (2010). BIGSdb: scalable analysis of bacterial genome variation at the population level. *BMC Bioinformatics* 11:595. doi: 10.1186/1471-2105-11-595

Kenyon, J. J., and Hall, R. M. (2013). Variation in the complex carbohydrate biosynthesis loci of *Acinetobacter baumannii* genomes. *PLoS One* 8:e62160. doi: 10.1371/journal.pone.0062160

Lewis, P. O. (2001). A likelihood approach to estimating phylogeny from discrete morphological character data. *Syst. Biol.* 50, 913–925. doi: 10.1080/106351501753462876

Maiden, M. C., Bygraves, J. A., Feil, E., Morelli, G., Russell, J. E., Urwin, R., et al. (1998). Multilocus sequence typing: a portable approach to the identification of clones within populations of pathogenic microorganisms. *Proc. Natl. Acad. Sci. U.S.A.* 95, 3140–3145. doi: 10.1073/pnas.95.6.3140

Maiden, M. C., Jansen van Rensburg, M. J., Bray, J. E., Earle, S. G., Ford, S. A., Jolley, K. A., et al. (2013). MLST revisited: the gene-by-gene approach to bacterial genomics. *Nat. Rev. Microbiol.* 11, 728–736. doi: 10.1038/nrmicro3093

Marí-Almirall, M., Cosgaya, C., Higgins, P. G., Van Assche, A., Telli, M., Huys, G., et al. (2017). MALDI-TOF/MS identification of species from the Acinetobacter baumannii (Ab) group revisited: inclusion of the novel *A. seifertii* and *A. dijkshoorniae* species. *Clin. Microbiol. Infect.* 23:210.e1-210.e9. doi: 10.1016/j.cmi.2016.11.020

Martin, D. P., Murrell, B., Golden, M., Khoosal, A., and Muhire, B. (2015). RDP4: detection and analysis of recombination patterns in virus genomes. *Virus Evol.* 1:vev003. doi: 10.1093/ve/vev003

Ou, H. Y., Kuang, S. N., He, X., Molgora, B. M., Ewing, P. J., Deng, Z., et al. (2015). Complete genome sequence of hypervirulent and outbreak-associated *Acinetobacter baumannii* strain LAC-4: epidemiology, resistance genetic determinants and potential virulence factors. *Sci. Rep.* 5:8643. doi: 10.1038/srep08643

Paradis, E., Claude, J., and Strimmer, K. (2004). APE: analyses of phylogenetics and evolution in R language. *Bioinformatics* 20, 289–290. doi: 10.1093/bioinformatics/btg412

Pournaras, S., Dafopoulou, K., Del Franco, M., Zarkotou, O., Dimitroulia, E., Protonotariou, E., et al. (2017). Predominance of international clone 2 OXA-23-1 producing-*Acinetobacter baumannii* clinical isolates in Greece, 2015: results of a nationwide study. *Int. J. Antimicrob. Agents* 49, 749–753. doi: 10.1016/j.ijantimicag.2017.01.028

Pournaras, S., Gogou, V., Giannouli, M., Dimitroulia, E., Dafopoulou, K., Tsakris, A., et al. (2014). Single-locus-sequence-based typing of *bla*OXA-51-like genes for rapid assignment of *Acinetobacter baumannii* clinical isolates to international clonal lineages. *J. Clin. Microbiol.* 52, 1653–1657. doi: 10.1128/JCM.03565-13

Price, M. N., Dehal, P. S., and Arkin, A. P. (2010). FastTree 2–approximately maximum-likelihood trees for large alignments. *PLoS One* 5:e9490. doi: 10.1371/journal.pone.0009490

Puigbo, P., Bravo, I. G., and Garcia-Vallve, S. (2008). CAIcal: a combined set of tools to assess codon usage adaptation. *Biol. Direct.* 3:38. doi: 10.1186/1745-6150-3-38

Ribeiro-Gonçalves, B., Francisco, A. P., Vaz, C., Ramirez, M., and Carriço, J. A. (2016). PHYLOViZ online: web-based tool for visualization, phylogenetic inference, analysis and sharing of minimum spanning trees. *Nucleic Acids Res.* 44, W246–W251. doi: 10.1093/nar/gkw359

Sahl, J. W., Del Franco, M., Pournaras, S., Colman, R. E., Karah, N., Dijkshoorn, L., et al. (2015). Phylogenetic and genomic diversity in isolates from the globally distributed *Acinetobacter baumannii* ST25 lineage. *Sci. Rep.* 5:15188. doi: 10.1038/srep15188

Sahl, J. W., Gillece, J. D., Schupp, J. M., Waddell, V. G., Driebe, E. M., Engelthaler, D. M., et al. (2013). Evolution of a pathogen: a comparative genomics analysis identifies a genetic pathway to pathogenesis in Acinetobacter. *PLoS One* 8:e54287. doi: 10.1371/journal.pone.0054287

Schultz, M. B., Pham Thanh, D., Tran Do Hoan, N., Wick, R. R., Ingle, D. J., Hawkey, J., et al. (2016). Repeated local emergence of carbapenem-resistant *Acinetobacter baumannii* in a single hospital ward. *Microb. Genom.* 2:e000050. doi: 10.1099/mgen.0.000050

Snitkin, E. S., Zelazny, A. M., Montero, C. I., Stock, F., Mijares, L., Nisc Comparative Sequence Program, et al. (2011). Genome-wide recombination drives diversification of epidemic strains of *Acinetobacter baumannii*. *Proc. Natl. Acad. Sci. U.S.A.* 108, 13758–13763. doi: 10.1073/pnas.1104404108

Stamatakis, A. (2014). RAxML version 8: a tool for phylogenetic analysis and post-analysis of large phylogenies. *Bioinformatics* 30, 1312–1313. doi: 10.1093/bioinformatics/btu033

Tomaschek, F., Higgins, P. G., Stefanik, D., Wisplinghoff, H., and Seifert, H. (2016). Head-to-head comparison of two multi-locus sequence typing (MLST) schemes for characterization of *Acinetobacter baumannii* outbreak and sporadic isolates. *PLoS One* 11:e0153014. doi: 10.1371/journal.pone.0153014

van Dessel, H., Dijkshoorn, L., van der Reijden, T., Bakker, N., Paauw, A., van den Broek, P., et al. (2004). Identification of a new geographically widespread multiresistant *Acinetobacter baumannii* clone from European hospitals. *Res. Microbiol.* 155, 105–112. doi: 10.1016/j.resmic.2003.10.003

Villalon, P., Valdezate, S., Medina-Pascual, M. J., Rubio, V., Vindel, A., and Saez-Nieto, J. A. (2011). Clonal diversity of nosocomial epidemic *Acinetobacter baumannii* strains isolated in Spain. *J. Clin. Microbiol.* 49, 875–882. doi: 10.1128/JCM.01026-10

Wallace, L., Daugherty, S. C., Nagaraj, S., Johnson, J. K., Harris, A. D., and Rasko, D. A. (2016). Use of comparative genomics to characterize the diversity of *Acinetobacter baumannii* surveillance isolates in a health care

institution. *Antimicrob. Agents Chemother.* 60, 5933–5941. doi: 10.1128/AAC.00477-16

Wisplinghoff, H., Hippler, C., Bartual, S. G., Haefs, C., Stefanik, D., Higgins, P. G., et al. (2008). Molecular epidemiology of clinical *Acinetobacter baumannii* and *Acinetobacter* genomic species 13TU isolates using a multilocus sequencing typing scheme. *Clin. Microbiol. Infect.* 14, 708–715. doi: 10.1111/j.1469-0691.2008.02010.x

Zarrilli, R., Pournaras, S., Giannouli, M., and Tsakris, A. (2013). Global evolution of multidrug-resistant *Acinetobacter baumannii* clonal lineages. *Int. J. Antimicrob. Agents* 41, 11–19. doi: 10.1016/j.ijantimicag.2012.09.008

Zarrilli, R., Wisplinghoff, H., Passet, V., Seifert, H., Jolley, K. A., and Brisse, S. (2015). "Reconciliation of *Acinetobacter baumannii* MLST nomenclatures using a genome database," in *Proceedings of the 10th International Symposium on the Biology of Acinetobacter*, (Athens), 41.

Conflict of Interest Statement: SB was one of the developers of the Pasteur MLST scheme for *Acinetobacter* strains of the Acb complex.

The remaining authors declare that the research was conducted in the absence of any commercial or financial relationships that could be construed as a potential conflict of interest.

frontiers in Microbiology

ORIGINAL RESEARCH
published: 18 June 2019
doi: 10.3389/fmicb.2019.01375

Genetic and Phenotypic Features of a Novel Acinetobacter Species, Strain A47, Isolated From the Clinical Setting

*Sareda T. J. Schramm[1], Kori Place[1], Sabrina Montaña[2], Marisa Almuzara[3], Sammie Fung[1], Jennifer S. Fernandez[1], Marisel R. Tuttobene[4], Adrián Golic[4], Matías Altilio[4], German M. Traglia[3], Carlos Vay[3], Maria Alejandra Mussi[4], Andres Iriarte[5] and Maria Soledad Ramirez[1]**

[1] Department of Biological Science, California State University Fullerton, Fullerton, CA, United States, [2] Facultad de Medicina, Instituto de Microbiología y Parasitología Médica (IMPaM, UBA-CONICET), Universidad de Buenos Aires, Buenos Aires, Argentina, [3] Laboratorio de Bacteriología Clínica, Departamento de Bioquímica Clínica, Hosp. de Clínicas José de San Martín, Facultad de Farmacia y Bioquímica, Universidad de Buenos Aires, Buenos Aires, Argentina, [4] Centro de Estudios Fotosintéticos y Bioquímicos (CEFOBI – CONICET), Rosario, Argentina, [5] Laboratorio de Biología Computacional, Departamento de Desarrollo Biotecnológico, Instituto de Higiene, Facultad de Medicina, Universidad de la República, Montevideo, Uruguay

In 2014, a novel species of *Acinetobacter*, strain A47, determined to be hospital-acquired was recovered from a single patient soft tissue sample following a traumatic accident. The complexity of the *Acinetobacter* genus has been established, and every year novel species are identified. However, specific features and virulence factors that allow members of this genus to be successful pathogens are not well understood. Utilizing both genomic and phenotypic approaches, we identified distinct features and potential virulence factors of the A47 strain to understand its pathobiology. *In silico* analyses confirmed the uniqueness of this strain and other comparative and sequence analyses were used to study the evolution of relevant features identified in this isolate. The A47 genome was further analyzed for genes associated with virulence and genes involved in type IV pili (T4P) biogenesis, hemolysis, type VI secretion system (T6SS), and novel antibiotic resistance determinants were identified. A47 exhibited natural transformation with both genomic and plasmid DNA. It was able to form biofilms on different surfaces, to cause hemolysis of sheep and rabbit erythrocytes, and to kill competitor bacteria. Additionally, surface structures with non-uniform length were visualized with scanning electron microscopy and proposed as pili-like structures. Furthermore, the A47 genome revealed the presence of two putative BLUF type photoreceptors, and phenotypic assays confirmed the modulation by light of different virulence traits. Taken together, these results provide insight into the pathobiology of A47, which exhibits multiple virulence factors, natural transformation, and the ability to sense and respond to light, which may contribute to the success of an A47 as a hospital dwelling pathogen.

Keywords: *Acinetobacter* spp., biofilm, antibiotic resistance, virulence traits, biofilm, natural transformation

OPEN ACCESS

Edited by:
Lisa Sedger,
University of Technology Sydney, Australia

Reviewed by:
Ariadnna Cruz-Córdova,
Children's Hospital, Mexico Federico Gómez, Mexico
Mario Feldman,
University of Alberta, Canada

****Correspondence:***
Maria Soledad Ramirez
msramirez@fullerton.edu

Specialty section:
This article was submitted to Infectious Diseases, a section of the journal Frontiers in Microbiology

Received: *26 March 2019*
Accepted: *03 June 2019*
Published: *18 June 2019*

Citation:
Schramm STJ, Place K, Montaña S, Almuzara M, Fung S, Fernandez JS, Tuttobene MR, Golic A, Altilio M, Traglia GM, Vay C, Mussi MA, Iriarte A and Ramirez MS (2019) Genetic and Phenotypic Features of a Novel Acinetobacter Species, Strain A47, Isolated From the Clinical Setting. Front. Microbiol. 10:1375. doi: 10.3389/fmicb.2019.01375

INTRODUCTION

The genus *Acinetobacter* represents an important group of pathogens. Currently, there are 52 species of *Acinetobacter* with assigned names[1]. However, the majority of research focuses on *Acinetobacter baumannii*, the most frequent cause of hospital-acquired infections (Turton et al., 2010; Lee et al., 2011; Weber et al., 2016). Recently with the development of other diagnostic tools and technological advancements, other members of the *Acinetobacter* genus have also been identified as causative agents of hospital-acquired infections (Turton et al., 2010; Karah et al., 2011). Although *A. baumannii* is still the most significant and common nosocomial pathogen, additional *Acinetobacter* species are gaining in clinical relevance.

The extreme genome plasticity and the ability to acquire foreign DNA has played an essential role in making some species of *Acinetobacter* successful pathogens. Horizontal gene transfer (HGT) allows bacteria to acquire and share DNA through different processes (conjugation, transduction, and transformation). Natural transformation is not fully understood, but its relevance in the spread of antibiotic resistance is unprecedented. Several species of *Acinetobacter* have been documented to naturally acquire foreign DNA (Palmen et al., 1993; Traglia et al., 2014). Transmembrane type IV pili (T4P) represent an important mechanism for acquiring exogenous DNA from the environment (Fronzes et al., 2008). T4P, which are complex structures composed of many proteins, is implicated in both the acquisition of exogenous DNA and the ability to overcome repulsive electrostatic forces during bacterial attachment to surfaces (Giltner et al., 2012; Berne et al., 2015). Initial attachment is imperative for the formation of complex biofilms, allowing the bacteria to survive antimicrobial treatment and maintain virulence. Biofilms protect the associated bacteria by decreasing the diffusion of some antibiotics or rendering them inactive before they can reach a subcellular target (Anderl et al., 2000). Additionally, some susceptible bacteria can tolerate antibiotics within the biofilm due to recalcitrance of biofilm bacteria toward antibiotics (Lebeaux et al., 2014). Biofilms are a unique virulence factor which provides bacteria with the ability to survive or tolerate antimicrobial treatment. It was previously recognized that *A. baumannii* perceives and responds to light modulating global features of its physiology through the BlsA photoreceptor encoded in its genome (Mussi et al., 2010). Light can modulate motility, biofilm formation, and virulence against *Candida albicans* in *A. baumannii* (Mussi et al., 2010). Furthermore, light regulates metabolic pathways, susceptibility and tolerance to some antibiotics, antioxidant enzyme levels such as catalase, likely contributing to bacterial persistence in adverse environments (Ramirez et al., 2015; Muller et al., 2017).

Extensive genome variation has generated interesting phenotypic variations throughout the *Acinetobacter* genus. One example of his is hemolytic activity, which not only varies by species but also between isolates (Tayabali et al., 2012; Dahdouh et al., 2016). Studies have identified all three types of hemolytic activity (α, β, and γ) in *Acinetobacter*, being the most uncommon the β-hemolysis (Tayabali et al., 2012; Dahdouh et al., 2016).

A taxonomically unique strain, *Acinetobacter* strain A47 (referred to as A47) recovered from a single patient soft tissue samples following a traumatic accident in 2014 was previously described (Almuzara et al., 2015; Traglia et al., 2015).

In this study, using both genomic and phenotypic approach, we aimed to characterize important mechanisms which may influence the pathobiology of A47 infections. *In silico* analyses revealed the phylogenetic position of this isolate among closely related strains and showed the uniqueness of it. The analysis of the A47 genome identified all T4P genes, and associated phenotypes with a functional T4P, such as natural competence and biofilm formation, were confirmed. Additionally, A47 was shown to modulate different virulence traits under blue light. Further genetic analyses led to the identification of multiple virulence factors, including genes associated with hemolysis and antibiotic resistance determinants. Although A47 was found to be susceptible to ampicillin-sulbactam, piperacillin-tazobactam, ceftazidime, cefepime, imipenem, meropenem, amikacin, gentamicin, ciprofloxacin, colistin, and trimethoprim-sulfamethoxazole (Almuzara et al., 2015; Traglia et al., 2015), the potential for this species to become a more significant threat should not be ignored, as previous studies have demonstrated antibiotic resistance and virulence are not consistently correlated (Tayabali et al., 2012; Giannouli et al., 2013). A47 harbors virulence factors which may cause additional problems concerning treatment options and pathobiology. As this is the initial isolation of A47, identifying mechanisms of virulence at a genetic and phenotypic level adds not only to the understanding of this novel *Acinetobacter* species but also to the growing knowledge of the *Acinetobacter* genus.

MATERIALS AND METHODS

Bacterial Strains and Plasmids

Acinetobacter strain A47, a taxonomically unique species recovered from a single patient soft tissue sample following a traumatic accident, was used in the present work (Almuzara et al., 2015). Moreover, *A. baumannii* strains ATCC 17978, A144, Ab33405, and *A. haemolyticus* strain A23 were also used (Vilacoba et al., 2013). Plasmids pDSRed (4.5 kbp) and pJHCMW1 (11.3 kbp) which harbor a Kan^R gene were extracted from *Escherichia coli* TOP10 cells using QIAprep Spin Miniprep Kit following manufacturer protocol (Qiagen Germantown, MD, United States) and used for transformation assays.

Whole Genome Sequence

The genome of A47 was previously sequenced using Illumina MiSeq at the Argentinian Consortium of Genomic Technology and reported in Traglia et al. (2015). Open reading frame (ORF) prediction was previously performed using the RAST server (Aziz et al., 2008). SEED source genome annotations identified known genes in the A47 genome under default parameters

[1]http://www.bacterio.net/acinetobacter.html

(Overbeek et al., 2014). Gene annotation was confirmed by BLAST (version 2.0) software at NCBI[2].

Homologous Gene Clustering, Phylogenetic Analysis, and Average Nucleotide Identity

The phylogenetic position of A47 within *Acinetobacter* genus was previously defined (Traglia et al., 2015). In order to get a more detailed phylogenetic position of A47 a group of closely related genomes to A47 strain was defined based on this previous published result. Then, a phylogenetic analysis of this group was done. The closely related genome group used for comparative analyses comprises 55 strains plus A47 (**Supplementary Table S1**). Homologous gene families among the 56 analyzed genomes were identified using the OrthoMCL method (Li et al., 2003) implemented in the get_homologous software package, version 07082017 (Contreras-Moreira and Vinuesa, 2013). Blastp search minimums for e-value, identity and query coverage were 1×10^{-5}, 30 and 75%, respectively. Thousand three hundred and eighty-three clusters of putative orthologous sequences were identified among the analyzed genomes. Clustal Omega v1.2.0 was used to align protein sequences (Sievers et al., 2011). Gblock with default parameters was used to trim low quality aligned regions (Castresana, 2000).

Two different strategies were used for phylogenetic reconstruction: (1) PHYML version 3.1 was used to generate a maximum-likelihood phylogenetic tree for each alignment of orthologous protein sequences, using five random starting trees. Sumtrees.py script was then used to generate a consensus tree from the 1383 generated phylograms (Sukumaran and Holder, 2010). (2) The alignments of the 1383 orthologous proteins were concatenated. Then, FastTree version 2.1 was used for building an approximately maximum-likelihood phylogenetic tree. In both cases, consensus and concatenated approaches, the amino acid LG + G model were used with eight categories (Guindon and Gascuel, 2003). Branch supports were evaluated using the SH-like test (Guindon et al., 2010; **Supplementary Figure S2**).

The average nucleotide identity (ANI) score between A47 and other closely related genomes were estimated. The ANI is used to delineate species using genome sequence data. Two genomes displaying an ANI value of 95% or higher are considered to be the same species (Goris et al., 2007). Two-way ANI (reciprocal best hits based comparison) was estimated by the ani.rb script, developed by Luis M. Rodriguez-R and available at enveomics.blogspot.com.

Comparative Genomic Analysis, Gene Content, and Sequence Analysis

Comparative genome analysis was performed with the open-source MAUVE aligner version 2.3.1 (Darling et al., 2004). ARG-ANNOT and ISfinder softwares were used to identify antibiotic resistance genes and insertion sequences, respectively (Siguier et al., 2006; Gupta et al., 2014). Phage and prophage sequences were identified using PHAST (Zhou et al., 2011). PlasmidFinder was used to detect the presence of *Enterobacteriaceae* plasmids (Carattoli et al., 2014). In addition, CRISPRCASFinder and RASTA-Bacteria software were used to searched for the CRISPR-Cas and toxin-antitoxin systems, respectively (Sevin and Barloy-Hubler, 2007; Couvin et al., 2018).

The group of unique genes of strain A47 was defined based on the get_homologous result, see above.

Molecular Evolutionary Studies of *bla*$_{\text{OXA-like}}$ Genes and Phylogenetic Distribution of Hemolytic Activity-Related Genes

Homologous sequences of the *bla*$_{\text{OXA-like}}$ gene and putative hemolytic related genes found in A47 were identified in closely related genomes using the BLASTP tool. A minimum identity value of 40% and a minimum coverage of 75% were set as thresholds for positive hits. *bla*$_{\text{OXA-like}}$ homologous proteins were aligned using Clustal Omega v1.2.0. Then, a phylogeny was build using PHYML v3.1 as mention above (Sukumaran and Holder, 2010). Amino acid pairwise *p*-distance was estimated in MEGA version 7.0 (Kumar et al., 2016). Aligned proteins were back-translated to the known DNA sequences by means of the tranalign program from the EMBOSS package (Rice et al., 2000) and visualized using Bioedit v7.5 (Hall, 2011). Site and branch models dN/dS selection tests were done in the Datamonkey web server (Weaver et al., 2018), Fixed Effects Likelihood test and adaptive Branch Site REL tests (Kosakovsky Pond and Frost, 2005; Smith et al., 2015), respectively. The ratio of non-synonymous changes per non-synonymous sites (dN) over synonymous changes per synonymous sites (dS) is used to identify sites or lineages that evolve under negative, neutral or positive selection regimes. Hemolytic related genes were mapped in the phylogeny of the group according to the BLAST results, using the iTOL web server (Letunic and Bork, 2016).

Transformation Assays

To perform the transformation assays, two KAN^R plasmids, pJHCMW1 (11.3 kbp) or pDSRed (4.5 kbp) (Sarno et al., 2002; Traglia et al., 2016), were used. *A. baumannii* A144 and Ab33405 (GenBank accession numbers JQSF01000000 and JPXZ00000000, respectively) strains, known to harbor many genes conferring resistance to aminoglycosides (Vilacoba et al., 2013), were used as the source of total genomic DNA (gDNA).

Transformation assays were carried out as previously described (Ramirez et al., 2010). Briefly, late-stationary-phase cells (OD_{600}:1) of A47 were mixed with either donor gDNA or plasmid DNA, incubated for 1h at 37°C, and then plated on LB agar supplemented with 10 μg/ml KAN overnight at 37°C. Following incubation, KAN^R colonies representing individual transformation events were counted. An average of 15 colonies (transformants) were checked and confirmed in every independent transformation experiment by PCR reactions targeting the genes *aac(6′)-Ib*, *aac(3)-IIa*, and *aph(3′)-Ia*. Total colony forming units (CFUs) were quantified by plating dilutions of non-transformed A47 cells on LB agar and incubated at 37°C overnight. The calculated transformation frequency represented

[2]www.ncbi.nlm.nih.gov/BLAST

the number of KAN^R colonies per CFU. Experiments were repeated three times (n = 3) and statistical significance was determined using ANOVA.

Antimicrobial susceptibility testing was performed to assess susceptibility levels of selected transformants cells. Disk diffusion was used to assess susceptibility levels to amikacin (AK), ceftazidime (CAZ), ciprofloxacin (CIP), gentamicin (GN), cefepime (FEP), imipenem (IMP), meropenem (MEM), minocycline (MH), trimethoprim/sulfamethoxazole (SXT), tetracycline (TE), and tigecycline (TGC) disks (Oxoid™, Basingstoke, United Kingdom) according to the Clinical and Laboratory Standards Institute (Clinical and Laboratory Standards Institute, 2017). Minimum Inhibitory Concentration (MIC) to AK, CAZ, GN, and cefotaxime (CT) were measured using commercial strips (bioMérieux, Marcy-l'Etoile, FR) following the gradient diffusion method (E-test method) as recommended by the supplier (Jorgensen and Ferraro, 2009).

Biofilm Formation

Quantification of biofilm production, in glass and polystyrene tube, was carried out using a protocol adapted from previously described methods (O'toole and Kolter, 1998; Tomaras et al., 2003; Mussi et al., 2010). Quantification of biofilm was reported as a ratio of biofilm to total biomass (OD_{580}/OD_{600}) for three independent experiments (n = 3). By reporting biofilm as a ratio of total biomass, each value is normalized to the total biomass to account for any variation in growth due to the different abiotic tubes. *A. baumannii* strain ATCC 17978 was used as a control (Eijkelkamp et al., 2011; Nait Chabane et al., 2014). Additionally, by normalizing to total cell mass, differences due to the growth rates of A47 and ATCC 17978 do not obscure reported biofilm formation. Statistical significance was determined using a two-tailed Student's t-test and one-way ANOVA using GraphPad Prism (GraphPad Software, San Diego, CA, United States).

Scanning Electron Microscopy

The surface of A47 was visualized using scanning electron microscopy (SEM). A working protein fixing solution (2% formaldehyde, 2% glutaraldehyde, and 0.1 M phosphate buffer) was used to fix A47 cells. A section of A47 was extracted and transferred into a sterile glass vial. Lipids and fatty acids were fixed with 2% osmium tetroxide. The sample was dehydrated with ethanol and mounted to a degreased stub using double stick tape. The stub was coated in gold/platinum and imaged with the Hitachi S-2400 scanning electron microscope.

Hemolysis Assays

Hemolytic activity was determined using a previously described protocol with minor changes (Tayabali et al., 2012). Tryptic soy agar (TSA) plates supplemented with 5% sheep's blood (blood agar plates; Hardy Diagnostics, Santa Maria, CA, United States) were inoculated by transferring colonies of A47 to a blood agar plate. Blood agar plates were incubated for up to 72 h at 37°C. At 24, 48, and 72 h post-inoculation the diameter of the colony (D_1) and the diameter of the clearing (D_2) was measured and recorded in mm. Hemolysis was quantified by calculating the ratio of the diameter of the clearing to the diameter of the colony (D_2/D_1). Independent biological samples were used for every trial (n = 16). *A. haemolyticus* strain A23 strain was used for comparison.

An additional assay was conducted to measure hemolytic activity using defibrinated rabbit erythrocytes, following a previously described protocol with modifications (Ramsey et al., 2016). Individual colonies of A47 were cultured in 5 mL LB broth overnight with agitation, then diluted 1/100 with LB broth. Defibrinated rabbit erythrocytes (Hemostat Laboratories, Dixon, CA, United States) were diluted to 10% (v/v) in 1X phosphate buffered saline (PBS). 60 μL of 1/100 A47 cultures and 140 μL of 10% rabbit blood were combined in wells of a flat-bottom 96-well plate and incubated for 12 h at 37°C. The plate was then centrifuged for 10 min at 3000 rpm, 100 μL of the supernatant was transferred to a new well; absorbance of the supernatant was measured at 540 and 630 nm. Independent biological samples were used for every trial (n = 4) and performed in quadruplicates. LB without bacteria served as a negative control, as well as a normalization for hemolysis.

Blue Light Treatments

Blue light treatments were performed as described in previous studies (Mussi et al., 2010; Golic et al., 2013; Ramirez et al., 2015). Cells were incubated for 26 h (or else specified) at 24°C in the dark or under blue light emitted by nine-LED (light-emitting diode) arrays with an intensity of 6–10 μmol photons/m^2/s. Each array was built using three-LED module strips emitting blue light with emission peaks centered at 462 nm determined using a LI-COR LI-1800 spectroradiometer (Mussi et al., 2010).

Growth of A47 on Phenylacetic Acid

To test the ability of A47 to grow on phenylacetic acid (PAA), 1/100 dilutions of overnight cultures grown in LB Difco were washed with PBS 1X and inoculated in either M9 solid medium supplemented with 5 or 10 mM PAA or in LB Difco medium (Fisher Scientific) and incubated at 24°C under blue light or in the dark. The experiments were performed in triplicates.

Quantification of Trehalose

The strain was grown in LB Difco medium until it reached an OD660 of 0.4 under blue light or in the dark, and sugars were extracted from bacterial cells as described in Zeidler et al. (2017). Trehalose content was quantified as previously described by measuring glucose increments after trehalase (Sigma) treatment (Muller et al., 2017). Glucose calibration curves were generated using glucose (Sigma) as standards and glucose was measured using a glucose oxidase kit (Glicemia enzimaìtica AA liìquida) under the recommendations of the manufacturer (Wiener, Argentina) before and after trehalase treatment. The experiments were performed in triplicates.

Cell Motility

Cell motility was tested on "swimming agarose" (Tryptone 1%, NaCl 0.5%, agarose 0.3%; 5) or LB agarose (Peptone 1%, NaCl 1%, yeast extract 0.5%, agarose 0.3%) plates incubated in the presence or absence of light, as described previously (Mussi et al., 2010; Golic et al., 2013). All assays were performed in triplicates for both light and dark conditions.

RESULTS

A47 Genome Features and Comparative Genomic Analysis

The genome of A47 is 3,915,593 bp with a corresponding G+C content of 44.5% (Traglia et al., 2015). RAST annotation software predicted a total of 3627 ORFs, of which 281 are unique genes, which are defined as genes with no homologs in any closely related genome. These unique genes are distributed in at least 28 clusters (**Supplementary Table S2**). Almost 70% of the identified singletons are hypothetical proteins; and other unique genes coding for transporters, phage-related proteins, transcriptional regulators, among other functional categories. ANI values support the previous report that A47 does not belong to any hitherto known taxa and represents a unique species of *Acinetobacter* (**Supplementary Table S3**). Phylogenetic analysis using 56 publicly available genomes identified the genetic relationship between A47 and closely related strains. Two robust phylogenetic trees were built based on the sequences of 1383 aligned orthologs. Implemented strategies showed highly similar branching pattern; however, the phylogenetic tree generated with FastTree was built based on concatenated sequences and displayed higher node support values (**Figure 1**). A47 grouped with strong statistical support as a monophyletic cluster with two lineages that also represent new species (node support = 100) (see ANI results in **Supplementary Table S3**). Then, as a sister group of this monophyletic cluster, three equally distant and defined species were found: *A. gyllenbergii*, *A. colistiniresistens*, and *A. proteolyticus*.

Genetic Analysis of Virulence Genes Associated With Distinct Phenotypes

Initial phenotypic testing of A47 indicated it was β-hemolytic (Almuzara et al., 2015), leading to the search for putative genes related with hemolytic activity. Thus, four protein-coding genes were identified in the A47 genome including a putative hemolysin (WP_038344358.1) with 85% identity to a previously described protein in *A. haemolyticus* TJS01 (Accession number: APR70514.1), a putative hemolysin translocator protein, HylD (WP_038343297.1) with 97% identity to a protein in *Acinetobacter* sp. WC-323, a predicted membrane protein (WP_038343513.1) with 78% identity to hemolysin III, Hly III, present in *A. junni* 65 (Accession number: CP019041.1), and ahemolysin activation/secretion family protein, HecB, (WP_052209140.1) with 77% identity to a protein identified in *A. baumannii* strain 1437282. We studied the phylogenetic distribution of these proteins among closely related genomes (**Supplementary Figure S1**). Hly III was found in all studied genomes, and all but three genomes have at least one hemolysin homologous proteins coded. HylD is almost completely conserved, only missing in a specific basal lineage. Interestingly, this lineage is characterized not only by the absence of HylD but also for the absence of Hec-B. Hec-B homologous genes seem to be restricted to non-related specific lineages, displaying a non-uniform phylogenetic distribution (**Supplementary Figure S1**). In addition, other putative hemolytic related proteins were identified in the genome of A47; but annotation data is inconclusive about its role in the hemolytic activity. This is the case of WP_038342744.1, an RND transporter subunit, and WP_038342201.1, a 21 kDa hemolysin precursor with 81% identity to a BON domain-containing protein.

Due to the contribution of T4P to virulence, genes associated with its biogenesis were searched and all T4P associated genes were identified in A47 and are described in **Table 1**.

A47 is resistant to ampicillin, cefalotin, cefoxitin, and cefotaxime, and exhibits susceptibility to a variety of other antibiotics. Considering that ubiquitous β-lactamases have been reported in all *Acinetobacter* genomes, we searched for β-lactamases in A47 genome. A novel chromosomally located $bla_{\mathrm{OXA-like}}$ gene (897 bp) was identified (Nucleotide accession number: KT835650). This gene exhibits the highest percent nucleotide identity (79%) to $bla_{\mathrm{OXA-298}}$ from *Acinetobacter* sp. NIPH 3623 (Accession number: NG_049593). The predicted protein sequence corresponding to this novel β-lactamase is 288 residues and has the highest percent (73%) identity to a class D β-lactamase from *Acinetobacter* sp. YK3 (Accession number: WP_069578983). Additionally, this novel β-lactamase exhibits 72% amino acid identity to a class D β-lactamase from *Acinetobacter* sp. Neg1 (Accession number: WP_047430089.1), OXA-295 from *Acinetobacter* sp. NIPH 2168 (Accession number: WP_005260134.1) and OXA-294 from *Acinetobacter* sp. NIPH 758 (Accession number: WP_004776204.1). The genetic context of the novel β-lactamase is shown in **Figure 2**. A BLAST search revealed only one isolate of *A. haemolyticus* TJS01 sharing 75% identity to the genetic context (5 kbp upstream and downstream) of the $bla_{\mathrm{OXA-like}}$ gene.

The molecular evolution of $bla_{\mathrm{OXA-like}}$ and homologous sequences in closely related genomes was studied. The phylogenetic reconstruction and the estimated amino acid *p*-distance suggest that the $bla_{\mathrm{OXA-like}}$ protein found in A47 (WP_052209191.1) has significantly diverged from other homologs found in closely related genomes (**Supplementary Figure S3**). On average the more similar group of $bla_{\mathrm{OXA-like}}$ proteins has a *p*-distance of 0.245 (G2 in **Supplementary Figure S3A**). This group is formed for OXA-298 and OXA-297 proteins found in *Acinetobacter* sp. NIPH 3623 and *Acinetobacter* sp. NIPH 1847, respectively. On the other hand, the most distantly related $bla_{\mathrm{OXA-like}}$ proteins found were OXA-58 proteins. The effect of selection at the molecular level was studied by means of the dN/dS test. Results suggest there is evidence of episodic diversifying selection in the lineage of the $bla_{\mathrm{OXA-like}}$ gene found in A47. This is also true in three other independent lineages. Significance was assessed using the Likelihood Ratio Test at a threshold of $P \leq 0.05$, after correcting for multiple testing. The site model dN/dS test found evidence of positive/diversifying selection in two amino acid sites, when considering the whole alignment (**Supplementary Figure S3C**). Taken together, these results suggest that the $bla_{\mathrm{OXA-like}}$ protein found in A47 and other homologous proteins found in closely related genomes may be evolving under positive selection. An incomplete aminoglycoside resistance gene (*aac(6′)-Ir*) was also identified. We searched for the presence of efflux pump systems in the A47 genome. AdeIJK system, with 81% identity with

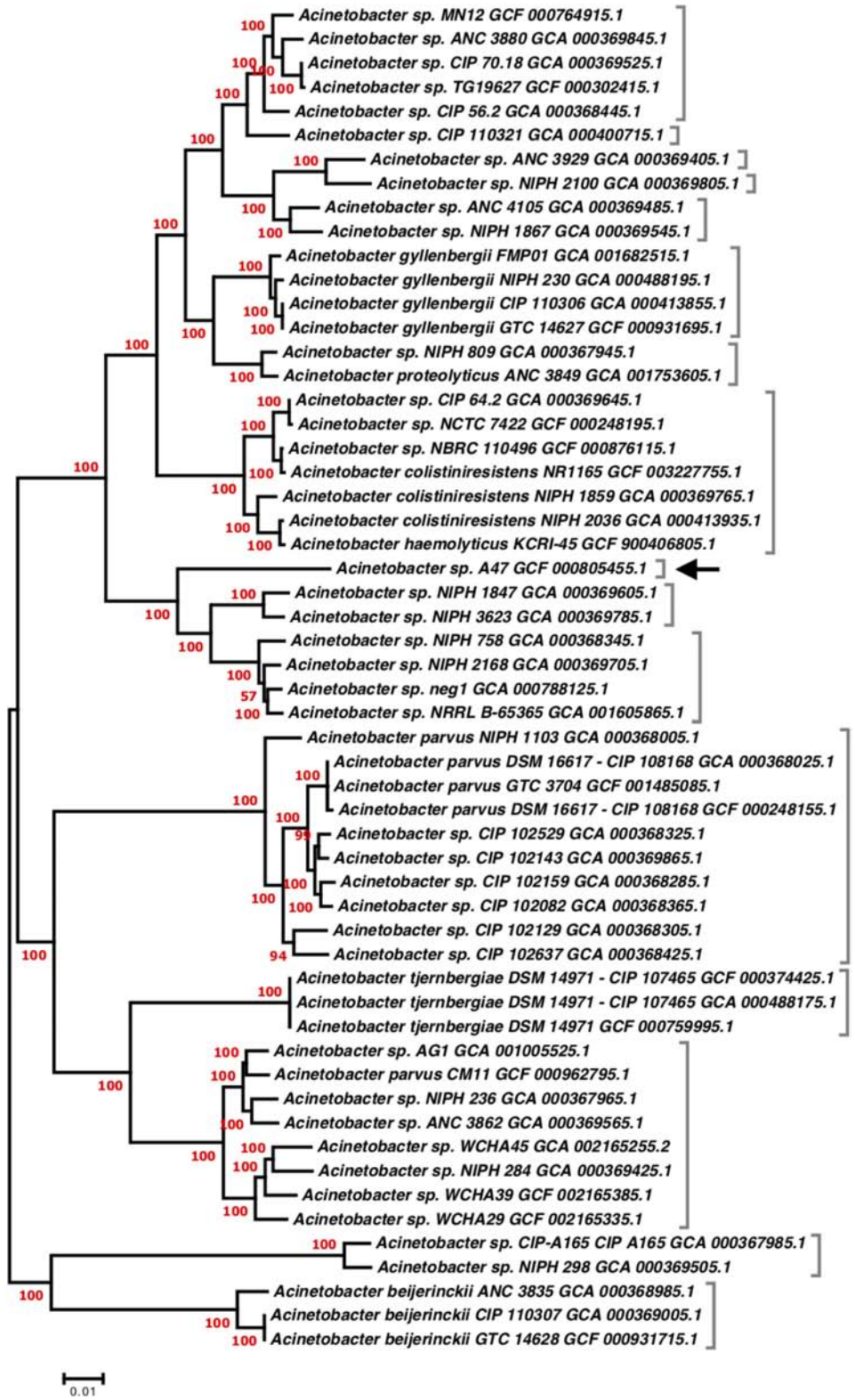

FIGURE 1 | Approximate maximum likelihood phylogenetic tree of A47 and closely related assemblies. The phylogenetic tree was build based on 1383 concatenated orthologous proteins. The tree was inferred using FastTree version 2.1, with LG + G model. The SH-like test was used to evaluate branch supports and indicated as red values next to nodes. Genomes from the same species based on two-way ANI score (>95%) were indicated with brackets. The position of A47 is indicated with a black arrow.

TABLE 1 | Type IV pili genes identified in the A47 genome and predicted function with relation to T4P biogenesis and function.

Gene	Predicted function
pilA	Major pilin
pilB	Type 4 fimbrial biogenesis protein
pilC	Type 4 fimbrial assembly protein
pilD	Type 4 prepilin-like proteins leader peptide processing enzyme
pilE	Type 4 pilus assembly protein and pilin like competence factor
pilF	Type 4 fimbrial biogenesis protein
pilG	Twitching motility two-component system response regulator
pilH	Twitching motility two-component system response regulator
pilI	Twitching motility protein
pilJ	Type 4 pilus biogenesis protein
pilM	Type 4 pilus assembly protein
pilN	Type 4 pilus assembly protein
pilO	Type 4 pilus assembly protein
pilP	Type 4 pilus assembly protein
pilQ	Type 4 pilus assembly protein
pilR	Type 4 fimbriae expression regulatory protein
pilS	Sensor protein
pilT	Putative type 4 fimbrial biogenesis protein and twitching motility protein
pilU	Twitching motility protein
pilV	Type 4 fimbrial biogenesis protein
pilW	Type 4 pilus assembly protein
pilX	Putative type 4 fimbrial biogenesis protein
pilY1	Type 4 pilus assembly protein
pilZ	Type 4 fimbrial biogenesis protein
fimB	Type 4 fimbrial assembly protein
fimT	Type 4 pilus assembly protein

Adapted from a supplemental table originally presented by Antunes et al. (2011).

A. junii strain 65 (AN CP019041) and the AdeABC proteins with 78, 79, and 72% identity, respectively with *A. baumannii* BM4454 (AN AF370885) were found. Two regulatory (*adeS* and *adeR*) genes of the AdeABC system were also found, with 72 and 78% identity with *A. calcoaceticus* NCTC7364 (AN LT605059) and *A. lactucae* OTEC-02 (AN CP020015), respectively. Further genomic analysis revealed the absence of insertion sequences in A47 genome. Using the PHAST tool to predict phage sequences, two intact prophages, one incomplete prophage, and two questionable prophages were identified in A47 genome.

In addition, CRISPR-cas systems were searched and a CRISPR-cas system, which belongs to subtype IF, was identified in A47 genome. The system contains the cluster *cas* genes including the *cas1*, *cas3-cas2*, *csy1*, *csy2*, *csy3*, and *cas* and a 91 spacer (GTTCATGGCGGCATACGCCATTTAGAAA). This variant of Cas-IF type was previously described in other bacterial species such as *Shewanella putrefaciens* and *Yersinia pseudotuberculosis* (Makarova et al., 2018). No toxin-antitoxin systems were identified in A47 genome.

The distribution of the T6SS components in *Acinetobacter* was studied, showing a large variability in the presence or absence of the 13 T6SS core genes in *Acinetobacter* species (Traglia et al., 2018). To address the presence of this system in A47 genome, the thirteen genes coding for the core proteins of this system were searched for within the A47 genome, and their presence was confirmed showing 94–100% amino acid sequence identity against the available genes deposited in the GenBank.

A47 Can Naturally Acquire Genomic and Plasmid DNA

Considering that the genes required for T4P biogenesis in A47 were found, the implications of T4P in A47 DNA-acquisition were investigated. Transformations, using plasmid and gDNA, were carried out as previously described (Ramirez et al., 2010). A47 was successfully transformed with all DNA sources tested, suggesting that A47 is naturally competent under the tested condition.

Transformation frequencies using two DNA sources (plasmid and gDNA) were calculated in A47. We observed that A47 can be transformed with DNA both sources. Transforming with gDNA resulted in A47::A33405 and A47::A144 with transformation frequencies of 1.19×10^{-6} TF/CFU (SD $\pm$ 7.83×10^{-7}) and 3.07×10^{-6} TF/CFU (SD $\pm$ 3.14×10^{-6}), respectively. Plasmid transformation frequencies were 7.20×10^{-7} TF/CFU (SD $\pm$ 1.96×10^{-7}) and 3.56×10^{-6} TF/CFU (SD $\pm$ 3.61×10^{-6}) for A47::pDSRed and A47::pJHCMW1, respectively.

Randomly selected transformant colonies were picked and assessed for changes in resistance profile using a disk diffusion screening method. We observed a variety of changes in the susceptibility profile of the transformant colonies (data not shown). To further determine the level of susceptibility of A47 and transformants, MIC was performed. The most

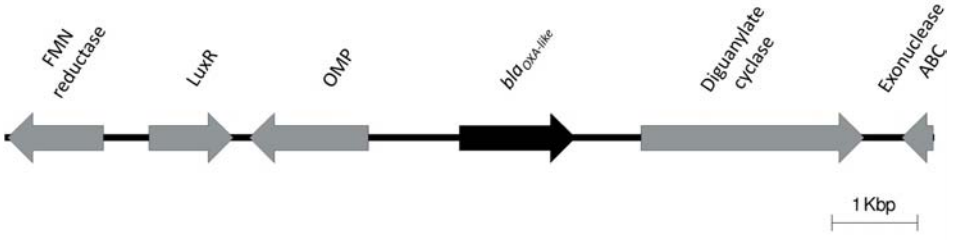

FIGURE 2 | Genetic context of the novel $bla_{OXA-like}$ identified in the A47 genome. Direction of the arrows indicate directionality of the coding genes.

substantial increase in MIC was observed with AK and GN for A47::Ab33405 (**Table 2**).

A47 Can Form Biofilms on Two Different Abiotic Surfaces and Exhibits Type IV Pili (T4P) Like Structures on Its Cell Surface

A47 ability to form biofilms on both polystyrene plastic and borosilicate glass abiotic surfaces was observed (**Figure 3A**). As *A. baumannii* ATCC 17978 is a known biofilm producer, this strain was used as an experimental control as well as a means of comparison for A47 biofilm production (Nait Chabane et al., 2014). A47 forms biofilms on both polystyrene plastic and borosilicate glass abiotic surfaces (**Figure 3A**). On average, A47 produces a larger amount of biofilm on polystyrene plastic than borosilicate glass (**Figure 3A**). Comparison of A47 OD_{580}/OD_{600} on the two abiotic surfaces is not statistically significant ($P > 0.05$) by a two-tailed Mann–Whitney U test. Comparison between A47 and ATCC 17978 OD_{580}/OD_{600} did not yield statistically significant results ($P > 0.05$) as determined by an ANOVA test under the tested conditions (**Figure 3B**).

Upon identification of all T4P genes in A47, SEM was used to visualize the surface of A47 cells. SEM images of A47 exhibit multiple surface appendages and a coccobacilli shape. The appendages vary in size and distribution; however, the most common and distinct appendages are long cellular extensions and shorter potential pili-like structures unevenly distributed (**Figure 3B**). Longer appendages are variable in length and appear to connect individual bacteria or anchor bacteria (**Figure 3B**). Short pili-like appendages are The coccobacilli shape is in line with what has previously been observed for *Acinetobacter*.

TABLE 2 | Comparison of A47 and transformed A47 MIC's.

Strain	AK	CAZ	GN	CT
A47	1.5	1.0–1.5	0.19–0.25	1.5
A47::A33405	**16–24**	1.5–2.0	3.0–4.0	6.0
A47::A144	n/a	1.5	1.0–1.5	n/a
A47::pDSRed	6.0	1.0–1.5	**6.0**	n/a

Following the 2017 CLSI breakpoints for Acinetobacter spp. MIC's are expressed as μg/mL. Bold numbers represent intermediate susceptibility levels.

A47 Exhibits a High Hemolytic Activity

With the aim to characterize A47 hemolytic activity, two different approaches were performed. As *A. haemolyticus* is a well-studied hemolytic species of *Acinetobacter*, the *A. haemolyticus* strain A23 was used as a positive control for β-hemolysis. Only A47 showed lysis of red blood cells after 24 h, as indicated by a zone of clearing surrounding the colony. A23 did not exhibit β-hemolysis until 48 h post-inoculation (**Figure 4A**). When using defibrinated rabbit blood in a 96-well microplate, A47 was shown to exhibit hemolytic activity. After 12 h, there was significant hemolytic activity in A47 conditions, in contrast to the control negative LB conditions ($P < 0.005$) (**Figure 4B**). Hemolytic activity of A47 bacteria was also visible based on the color change of the wells (**Figure 4C**).

A47 Exhibits Photoregulation of Different Virulence Traits

Analysis of the A47 genome reveals the presence of two BLUF-type photoreceptors (**Figure 5A**), one of which – peg 1386 – is 82% identical with respect to the BlsA homolog present in *A. baumannii* ATCC 17978 strain. This putative photoreceptor is globally synthenic to the genes located upstream with respect to *blsA*, showing differences mostly in the length of the intergenic region. On the contrary, no conservation is observed in the genes located downstream to *blsA*, except peg 1389 which codes for a putative sodium/glutamate symport protein. The second BLUF-coding protein, peg 1430, shows 52% identity respect to *A. baumannii* ATCC 17978 BlsA. It is flanked by a putative isochorismatase (peg 1429), enzymes involved in the synthesis of 2,3-dihydroxy-2,3-dihydrobenzoate and pyruvate from isochorismate, which are frequently involved in siderophore synthesis. Located next to this gene is a

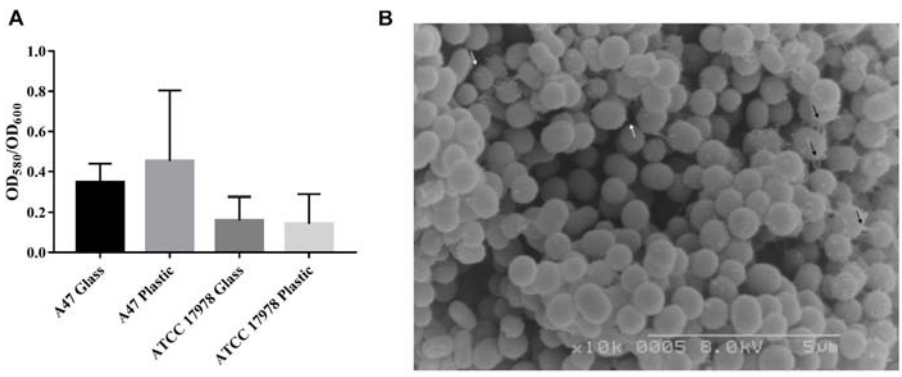

FIGURE 3 | (A) Amount of biofilm formed by A47 and ATCC 17978 on polystyrene plastic or borosilicate glass reported as a ratio of biofilm (OD580) to total biomass (OD600). Difference in amount of biofilm formed relative to biomass are not statistically significant ($P > 0.05$) between the two abiotic surfaces as evaluated using a paired Student's t-test. Means for each condition are represented by black bars ($n = 3$). **(B)** SEM magnified (10×) image of A47 exhibits a coccobacilli shape and surface structures which vary in length. Longer cellular appendages are indicated by black arrows and white arrows indicate short pili-like appendages.

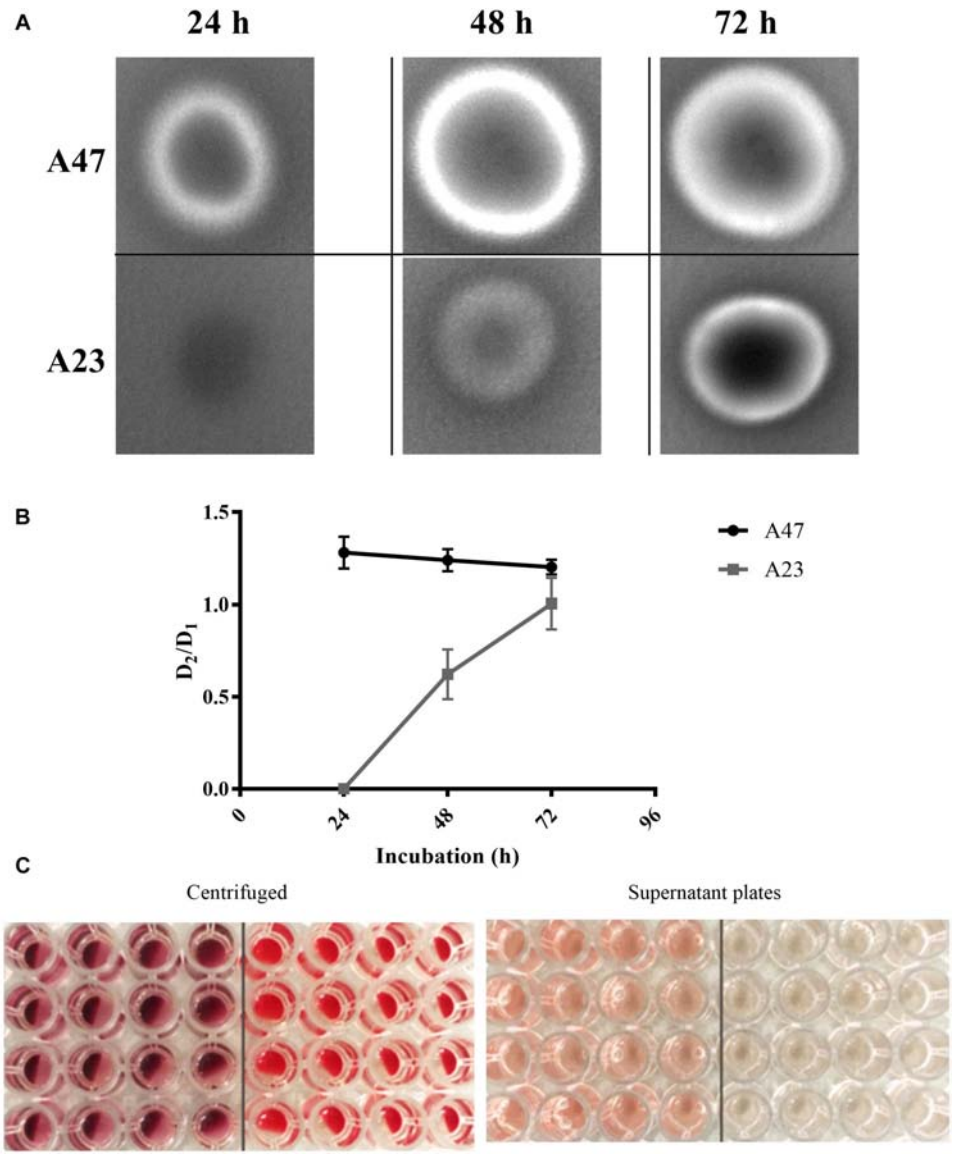

FIGURE 4 | (A) Observed hemolytic activity in A47 and A23. TSA supplemented with 5% rabbits's blood was inoculated with A47 and *A. haemolyticus* A23, incubated at 37°C and imaged at 24, 48, and 72 h post-inoculation. A47 and A23 exhibit β-hemolysis generating a zone of clearing around colonies, representative of complete lysis of red blood cells. **(B)** Quantification A47 and A23 hemolysis. Blood agar plates were aseptically inoculated with colonies of A47 and A23, and incubated at 37°C. The diameters of lytic zones (D2) and colonies (D1) was measured at 24, 48, and 72 h. Hemolysis is reported as the average ratio (D2/D1), data points represent individual ratios for each biological samples (n = 16). The curve intersects at the average D2/D1 for each time point. **(C)** A47 exhibits visible signs of hemolytic activity. Compared to LB conditions on right half, A47 wells exhibit visible signs of hemolytic activity, evidenced in both centrifuged (C1) and supernatant plates (C2). The deep red color change indicates hemolytic activity in (C1), and the effect of lysed blood cells bleeding out into the supernatant is shown in (C2).

putative 3-hydroxyisobutyrate dehydrogenase (peg 1428), which participates in leucine, valine and isoleucine degradation, and there is a gene coding for a putative polihydroxyalcanoic acid synthase (peg 1427). 3′ downstream from the *blsA* homolog, there is a gene coding for a quaternary ammonium compound resistance protein (peg 1431), followed by a phage lysin coding gene (peg 1432).

We have studied whether A47 can sense and respond to light by studying different cellular processes. As shown in **Figure 5B**, A47 exhibits photoregulation of motility at 24°C. Motility was inhibited under blue light, while the bacteria grew and spread over the surface of the plate in the dark. At 37°C, A47 still shows photoregulation of motility, although to a lesser extent than at 24°C. In addition, we studied other traits previously shown to be photoregulated in *A. baumannii*, such as metabolism (Muller et al., 2017). **Figure 5C** shows that light modulates the PAA utilization pathway at 24°C, just as it does in *A. baumannii* (Muller et al., 2017). On the contrary, we were not able to detect photoregulation of trehalose biosynthesis (data not shown).

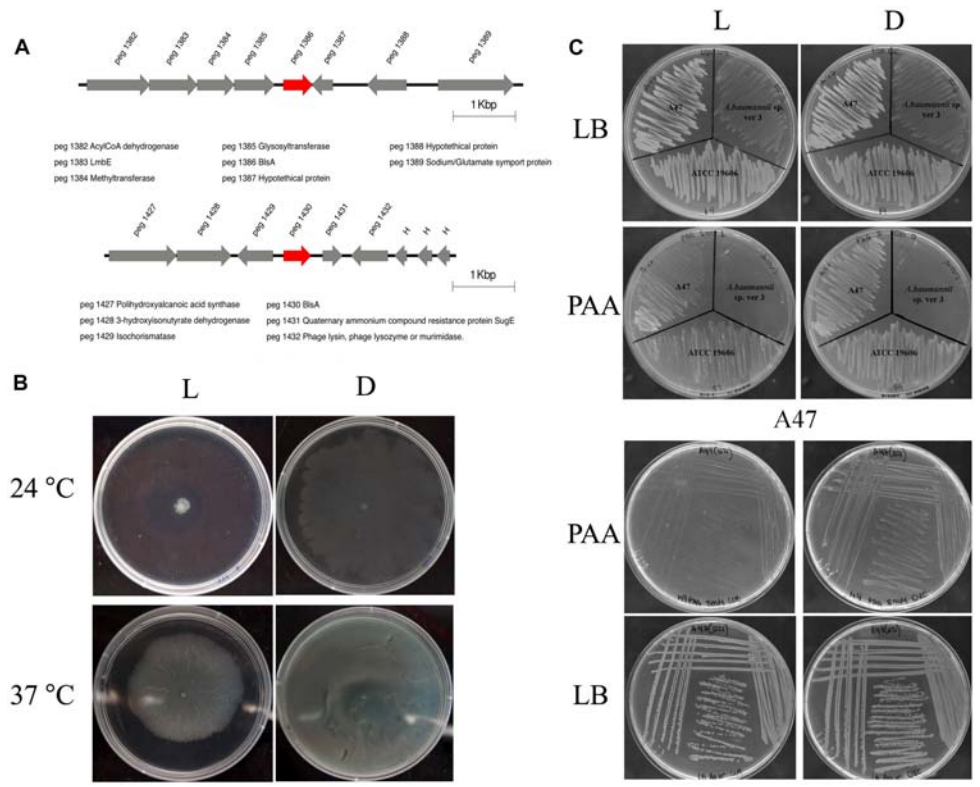

FIGURE 5 | (A) Genomic context of BLUF-domain containing genes in *Acinetobacter* sp. A47. Gene annotations are indicated below the scheme. In red are indicated BLUF photoreceptors. The figure was constructed using information retrieved from RAST and the seed viewer. **(B)** Effects of light and temperature on motility. Cells of *Acinetobacter* sp. A47 were inoculated on the surface of motility plates. Plates were inspected and photographed after overnight incubation in darkness (D) or in the presence of blue light (L) at 24°C or 37°C. **(C)** Light inhibits growth of *Acinetobacter* sp. A47 in PAA. Growth of *Acinetobacter* sp. A47 in M9 minimal agar medium supplemented with 5 mM PAA as a sole carbon source and incubated stagnantly at 24°C under blue light or in the dark. Also shown is growth of *A. baumannii* ATCC 19606 and *Acinetobacter* sp. ver 3 as controls, as well as growth in LB to show no effect of light on viability of the strains. Shown are representative results obtained from three independent experiments.

DISCUSSION

The genus *Acinetobacter* represents an important group of pathogens mainly due to the extreme genome plasticity and the ability to acquire foreign DNA.

Our results, including phylogenetic and comparative genomic analysis, indicate that *Acinetobacter* A47 represents a new species. More importantly, according to the phylogenetic and the ANI analyses, we found that many strains with closely related genomes are likely misidentified: *A. gyllenbergii*, *A. colistiniresistens*, *A. proteolyticus*, *A. parvus*, *A. tjernbergiae*, and *A. beijerinckii*.

When analyzing genes associated with pathogenesis, four genes putatively involved in hemolytic activity were identified in the genome of A47. There is significant documented variation in hemolysis in the *Acinetobacter* genus, with the most uncommon type of hemolytic activity being the β-hemolysis (Tayabali et al., 2012; Dahdouh et al., 2016). Our results show that the novel species A47 exhibits β-hemolysis, falling within a small subset of β-hemolytic *Acinetobacter* species. Analyses of hemolysis-related genes and their distribution showed that three of the putative genes are highly conserved in the studied genomes (**Supplementary Figure S1**). However, Hec-B-like gene was identified in different and independent lineages, displaying a patchy phylogenetic distribution. Thus, many of the analyzed genomes, which share the four analyzed hemolysis-related homologs, may also exhibit β-hemolysis activity, though none have currently been reported in the literature.

In addition, genomic analysis revealed the presence of a novel OXA-like β-lactamase gene. This OXA-like gene is unique and may be ubiquitous in this novel species, but more isolates will need to be recovered before this can be determined. No signs of pseudogenization has been found in this gene, and at least one fourth of the amino acids residues in this protein are different to its closest related homologs found in the studied genomes. Note, however, that many putative functional residues are also conserved in this protein (**Supplementary Figure S3C**). The observed highly divergence may in part be explained in the observed susceptibility to the tested β-lactams. Interestingly, molecular evolution tests found evidence of positive selection driving the evolution of the coding sequence of this new $bla_{\mathrm{OXA-like}}$ gene. This suggests that amino acid changes may be related to a functional change of the coded protein. Another possible scenario is that this gene is not derived from OXA-like homologs found in closely related genomes. In other words, the

observed divergence could be explained by a horizontal transfer event. This scenario, although not entirely improbable, is not compatible with the observation that highly similar sequences in public databases belong to closely related genomes (data not shown). Future research into this novel β-lactamase could investigate the affinity of this enzyme to different β-lactams and/or possible novel functions. In addition, we performed molecular docking studies to assess the mechanism of A47 OXA-like and we observed that this enzyme has similar binding affinity against imipenem and doripenem comparing with OXA-51, and stronger affinity for oxacillin (**Supplementary Figure S4** and **Supplementary Table S4**). Further phenotypic studies are needed to confirm this observation.

Genes coding for T4P were found in A47' genome and its ability to naturally acquire different types of DNA was also confirmed. Acquisition of exogenous DNA is not specific to the nature of DNA, as evidenced by the bacteria's ability to acquire plasmid and gDNA fragments. This was previously observed in *A. calcoaceticus* BD413 (also referred to as *A. baylyi* ADP1), and the same system of DNA uptake was found to be utilized in both instances (Palmen et al., 1993). The mechanism A47 uses to uptake foreign DNA was not examined in depth, although T4P have previously been implicated in the acquisition of exogenous DNA (Harding et al., 2013). It is interesting to note that there is no significant difference between transformation frequencies when A47 was transformed with plasmid or gDNA. Furthermore, biofilm formation was also observed in A47 on plastic and glass. Comparisons of A47 biofilm formation on polystyrene plastic or borosilicate glass was not statistically significant ($P > 0.05$). Additionally, no statistically significant differences between A47 biofilm formation and ATCC 17978 biofilm formation were observed between the tested surfaces ($P > 0.05$). ATCC 17978 has been characterized as a weak biofilm producer, and the findings here suggest that A47 is a poor biofilm producer as well. Images obtained using SEM showed the presence of multiple cellular surface appendages of variable length. De Breij and colleagues similarly examined surface structures of *A. baumannii* and identified long cellular-like projections as well as potential pili-like surface structures (De Breij et al., 2010). Although these results do not confirm that these surface structures are T4P, they provide substantial evidence that A47 does express non-uniform surface appendages. These images combined with the genetic identification of all the T4P genes within the A47 genome support the hypothesis that A47 expresses T4P.

The T6SS was recently recognized as a key system for bacterial competition and involved in HGT (Cooper et al., 2017; Ringel et al., 2017). Genomic results showed the presence of the T6SS genomic locus in A47, which could contribute to its repertoire of potential virulent traits.

Additionally, *A. baumannii* and other members of the *Acinetobacter* genus have been shown to sense and respond to light (Mussi et al., 2010; Muller et al., 2017). While various BLUF type photoreceptors are present in non-*baumannii* species, BlsA is the only BLUF protein that has been detected in *A. baumannii*. Our data indicates the presence of two BLUF-type photoreceptors in the genome of *Acinetobacter* sp. A47, and we have verified the ability of this strain to photoregulate both motility as well as the utilization of PAA.

CONCLUSION

The work presented here provides an initial characterization of some of A47's virulence factors and demonstrates why A47 represents an important new species of *Acinetobacter*. The general phylogenetic background and specific aspects of this isolate's evolution were studied. The genome of A47 harbors a novel β-lactamase is susceptible to all tested antibiotics, forms biofilms, can naturally acquire foreign DNA, is a member of a small group of *Acinetobacter* that carry out β-hemolysis and possesses the genes coding for the T6SS, and has the ability to sense and response to light, regulating motility and PAA catabolism. This novel species of *Acinetobacter* can greatly improve the current understanding of this genus due to its unique characteristics.

DATA AVAILABILITY

All datasets generated for this study are included in the manuscript and/or the **Supplementary Files**.

AUTHOR CONTRIBUTIONS

STJS, AI, and MSR conceived the study and designed the experiments. STJS, KP, SM, SF, JSF, MRT, GMT, MAM, AI, MA2, and MSR performed the experiments and genomics and bioinformatics analyses. STJS, SM, SF, JSF, GMT, MAM, MA1, MA2, MRT, AI, and MSR analyzed the data and interpreted the results. MAM, AI, and MSR contributed reagents, materials, and analysis tools. MA1 and CV contributed with the strains. STJS, SF, SM, MRT, MA, AI, and MSR wrote the manuscript. All authors read and approved the final manuscript.

FUNDING

This work was supported by the NIH SC3GM125556 to MSR. JSF was supported by the grant MHIRT 2T37MD001368 from the National Institute on Minority Health and Health Disparities, National Institutes of Health.

ACKNOWLEDGMENTS

The content is solely the responsibility of the authors and does not necessarily represent the official views of the National Institutes of Health. GMT has a postdoctoral fellowship from the CONICET. SM has a doctoral fellowship from the CONICET. JSF has a SOAR-ELEVAR scholar fellowship from Latina/o Graduate Students from the U.S. Department of Education. We thank Steve Karl for his technical assistance.

SUPPLEMENTARY MATERIAL

The Supplementary Material for this article can be found online at: https://www.frontiersin.org/articles/10.3389/fmicb.2019.01375/full#supplementary-material

FIGURE S1 | Phylogenetic distribution of putative hemolysis-related genes found in closely related genomes studied. A47 genome is indicated with a black arrow. The visualization was generated in the iTOL web server available at itol.embl.de.

FIGURE S2 | Approximate maximum likelihood phylogenetic tree of A47 and closely related assemblies. The phylogenetic tree was build based on 1383 concatenated orthologous proteins. The tree was inferred using FastTree version 2.1, with LG + G model. The SH-like test was used to evaluate branch supports and indicated as red values next to nodes. Genomes from the same species based on two-way ANI score (>95%) were indicated with brackets. The position of A47 is indicated with a black arrow.

FIGURE S3 | Molecular evolution and sequence analyses of $bla_{OXA-like}$ homologs. **(A)** Maximum likelihood phylogenetic reconstruction of homologs found in closely related genomes. The phylogenetic tree was build based on proteins sequences using the PHYML version 3.1 software, with the LG + G model. The SH-like test was used to evaluate branch supports. Groups are indicated next to basal nodes with "G." The position of $bla_{OXA-like}$ gene found in A47 is indicated with a black arrow. Evidence of positive selection was found in four lineages, indicated in magenta. **(B)** Average amino acid *p*-distance estimated between monophyletic groups in the lower triangular matrix, standard deviation of the average estimation in the upper triangular matrix. Groups are defined in phylogeny shown in panel **(A)**. **(C)** Clustal-omega alignment of OXA-like proteins ordered according to monophyletic groups, as stated in A. Two sites evolving under positive selection are indicated with black arrows.

FIGURE S4 | Computed two-dimensional structure of the OXA-like (UCSF Chimera 1.12) and the interaction between OXA-like and oxacillin. **(A)** Ribbon structure of OXA-like colored in rainbow style. **(B)** Surface topology of OXA-like colored by Coulombic surface coloring (UCSF Chimera 1.12). Surface was calculated using AMBER ff 14SB charge model on three color scale of red, −10 kcal/(mol e), white, 0 kcal/(mol e), and blue, 10 kcal/(mol e), where e is unit electron charge. **(E)** Ramachandran plot analysis of the OXA-like structure. Binding of various antibiotic molecules with **(C)** the OXA-like and **(D)** OXA-51. Different antibiotics was colored in violet and residues was colored in orange. H-bond lines between different residues and the ligands was colored in green.

TABLE S1 | List of 56 genomes used in the present study.

TABLE S2 | List of putative unique genes in *Acinetobacter* sp. 47.

TABLE S3 | Two-way average nucleotide identity estimated among closely related genomes that belongs to the A47 strain monophylogenetic cluster.

TABLE S4 | Predicted binding affinity between OXA-like from *Acinetobacter* sp. A47 and OXA-51 from *A. baumannii* against to doripenem, imipenem, and oxacillin.

REFERENCES

Almuzara, M., Traglia, G. M., Krizova, L., Barberis, C., Montana, S., Bakai, R., et al. (2015). A taxonomically unique *Acinetobacter* strain with proteolytic and hemolytic activities recovered from a patient with a soft tissue injury. *J. Clin. Microbiol.* 53, 349–351. doi: 10.1128/JCM.02625-14

Anderl, J. N., Franklin, M. J., and Stewart, P. S. (2000). Role of antibiotic penetration limitation in *Klebsiella pneumoniae* biofilm resistance to ampicillin and ciprofloxacin. *Antimicrob. Agents Chemother.* 44, 1818–1824. doi: 10.1128/aac.44.7.1818-1824.2000

Antunes, L. C. S., Imperi, F., Towner, K. J., and Visca, P. (2011). Genome-assisted identification of putative iron-utilization genes in *Acinetobacter baumannii* and their distribution among a genotypically diverse collection of clinical isolates. *Res. Microbiol.* 162, 279–284. doi: 10.1016/j.resmic.2010.10.010

Aziz, R. K., Bartels, D., Best, A. A., Dejongh, M., Disz, T., Edwards, R. A., et al. (2008). The RAST server: rapid annotations using subsystems technology. *BMC Genomics* 9:75. doi: 10.1186/1471-2164-9-75

Berne, C., Ducret, A., Hardy, G. G., and Brun, Y. V. (2015). Adhesins involved in attachment to abiotic surfaces by gram-negative bacteria. *Microbiol. Spectr.* 3. doi: 10.1128/microbiolspec.MB-0018-2015

Carattoli, A., Zankari, E., Garcia-Fernandez, A., Voldby Larsen, M., Lund, O., Villa, L., et al. (2014). In silico detection and typing of plasmids using plasmid finder and plasmid multilocus sequence typing. *Antimicrob. Agents Chemother.* 58, 3895–3903. doi: 10.1128/AAC.02412-14

Castresana, J. (2000). Selection of conserved blocks from multiple alignments for their use in phylogenetic analysis. *Mol. Biol. Evol.* 17, 540–552. doi: 10.1093/oxfordjournals.molbev.a026334

Clinical and Laboratory Standards Institute (2017). *Performance standards for antimicrobial susceptibility testing. Twenty-seven Informational Supplement. CLSI document M100–S27*. Wayne, PA: Clinical and Laboratory Standards Institute.

Contreras-Moreira, B., and Vinuesa, P. (2013). GET_HOMOLOGUES, a versatile software package for scalable and robust microbial pangenome analysis. *Appl. Environ. Microbiol.* 79, 7696–7701. doi: 10.1128/AEM.02411-13

Cooper, R. M., Tsimring, L., and Hasty, J. (2017). Inter-species population dynamics enhance microbial horizontal gene transfer and spread of antibiotic resistance. *Elife* 6:e25950. doi: 10.7554/eLife.25950

Couvin, D., Bernheim, A., Toffano-Nioche, C., Touchon, M., Michalik, J., Neron, B., et al. (2018). CRISPRCasFinder, an update of CRISRFinder, includes a portable version, enhanced performance and integrates search for Cas proteins. *Nucleic Acids Res.* 46, W246–W251. doi: 10.1093/nar/gky425

Dahdouh, E., Hajjar, M., Suarez, M., and Daoud, Z. (2016). *Acinetobacter baumannii* isolated from lebanese patients: phenotypes and genotypes of resistance, clonality, and determinants of pathogenicity. *Front. Cell. Infect. Microbiol.* 6:163. doi: 10.3389/fcimb.2016.00163

Darling, A. C., Mau, B., Blattner, F. R., and Perna, N. T. (2004). Mauve: multiple alignment of conserved genomic sequence with rearrangements. *Genome Res.* 14, 1394–1403. doi: 10.1101/gr.2289704

De Breij, A., Dijkshoorn, L., Lagendijk, E., Van Der Meer, J., Koster, A., Bloemberg, G., et al. (2010). Do biofilm formation and interactions with human cells explain the clinical success of *Acinetobacter baumannii*? *PLoS One* 5:e10732. doi: 10.1371/journal.pone.0010732

Eijkelkamp, B. A., Stroeher, U. H., Hassan, K. A., Papadimitrious, M. S., Paulsen, I. T., Brown, M. H., et al. (2011). Adherence and motility characteristics of clinical *Acinetobacter baumannii* isolates. *FEMS Microbiol. Lett.* 323, 44–51. doi: 10.1111/j.1574-6968.2011.02362.x

Fronzes, R., Remaut, H., and Waksman, G. (2008). Architectures and biogenesis of non-flagellar protein appendages in Gram-negative bacteria. *EMBO J.* 27, 2271–2280. doi: 10.1038/emboj.2008.155

Giannouli, M., Antunes, L. C., Marchetti, V., Triassi, M., Visca, P., and Zarrilli, R. (2013). Virulence-related traits of epidemic *Acinetobacter baumannii* strains belonging to the international clonal lineages I-III and to the emerging genotypes ST25 and ST78. *BMC Infect. Dis.* 13:282. doi: 10.1186/1471-2334-13-282

Giltner, C. L., Nguyen, Y., and Burrows, L. L. (2012). Type IV pilin proteins: versatile molecular modules. *Microbiol. Mol. Biol. Rev.* 76, 740–772. doi: 10.1128/MMBR.00035-12

Golic, A., Vaneechoutte, M., Nemec, A., Viale, A. M., Actis, L. A., and Mussi, M. A. (2013). Staring at the cold sun: blue light regulation is distributed within the genus *Acinetobacter*. *PLoS One* 8:e55059. doi: 10.1371/journal.pone.0055059

Goris, J., Konstantinidis, K. T., Klappenbach, J. A., Coenye, T., Vandamme, P., and Tiedje, J. M. (2007). DNA-DNA hybridization values and their relationship to whole-genome sequence similarities. *Int. J. Syst. Evol. Microbiol.* 57, 81–91. doi: 10.1099/ijs.0.64483-0

Guindon, S., Dufayard, J. F., Lefort, V., Anisimova, M., Hordijk, W., and Gascuel, O. (2010). New algorithms and methods to estimate maximum-likelihood phylogenies: assessing the performance of PhyML 3.0. *Syst. Biol.* 59, 307–321. doi: 10.1093/sysbio/syq010

Guindon, S., and Gascuel, O. (2003). A simple, fast, and accurate algorithm to estimate large phylogenies by maximum likelihood. *Syst. Biol.* 52, 696–704. doi: 10.1080/10635150390235520

Gupta, S. K., Padmanabhan, B. R., Diene, S. M., Lopez-Rojas, R., Kempf, M., Landraud, L., et al. (2014). ARG-ANNOT, a new bioinformatic tool to discover antibiotic resistance genes in bacterial genomes. *Antimicrob. Agents Chemother.* 58, 212–220. doi: 10.1128/AAC.01310-13

Hall, T. (2011). BioEdit: an important software for molecular biology. *GERF Bull. Biosci.* 2, 60–61. doi: 10.1016/j.compbiolchem.2019.02.002

Harding, C. M., Tracy, E. N., Carruthers, M. D., Rather, P. N., Actis, L. A., and Munson, R. S. Jr. (2013). Acinetobacter baumannii strain M2 produces type IV pili which play a role in natural transformation and twitching motility but not surface-associated motility. *MBio* 4:e00360-13. doi: 10.1128/mBio.00360-13

Jorgensen, J. H., and Ferraro, M. J. (2009). Antimicrobial susceptibility testing: a review of general principles and contemporary practices. *Clin. Infect. Dis.* 49, 1749–1755. doi: 10.1086/647952

Karah, N., Haldorsen, B., Hegstad, K., Simonsen, G. S., Sundsfjord, A., and Samuelsen, O. (2011). Species identification and molecular characterization of *Acinetobacter* spp. blood culture isolates from Norway. *J. Antimicrob. Chemother.* 66, 738–744. doi: 10.1093/jac/dkq521

Kosakovsky Pond, S. L., and Frost, S. D. (2005). Not so different after all: a comparison of methods for detecting amino acid sites under selection. *Mol. Biol. Evol.* 22, 1208–1222. doi: 10.1093/molbev/msi105

Kumar, S., Stecher, G., and Tamura, K. (2016). MEGA7: molecular evolutionary genetics analysis version 7.0 for Bigger Datasets. *Mol. Biol. Evol.* 33, 1870–1874. doi: 10.1093/molbev/msw054

Lebeaux, D., Ghigo, J. M., and Beloin, C. (2014). Biofilm-related infections: bridging the gap between clinical management and fundamental aspects of recalcitrance toward antibiotics. *Microbiol. Mol. Biol. Rev.* 78, 510–543. doi: 10.1128/MMBR.00013-14

Lee, K., Yong, D., Jeong, S. H., and Chong, Y. (2011). Multidrug-resistant *Acinetobacter* spp.: increasingly problematic nosocomial pathogens. *Yonsei Med. J.* 52, 879–891. doi: 10.3349/ymj.2011.52.6.879

Letunic, I., and Bork, P. (2016). Interactive tree of life (iTOL) v3: an online tool for the display and annotation of phylogenetic and other trees. *Nucleic Acids Res.* 44, W242–W245. doi: 10.1093/nar/gkw290

Li, L., Stoeckert, C. J. Jr., and Roos, D. S. (2003). OrthoMCL: identification of ortholog groups for eukaryotic genomes. *Genome Res.* 13, 2178–2189. doi: 10.1101/gr.1224503

Makarova, K. S., Wolf, Y. I., and Koonin, E. V. (2018). Classification and Nomenclature of CRISPR-Cas systems: where from here? *CRISPR J.* 1, 325–336. doi: 10.1089/crispr.2018.0033

Muller, G. L., Tuttobene, M., Altilio, M., Martinez Amezaga, M., Nguyen, M., Cribb, P., et al. (2017). Light modulates metabolic pathways and other novel physiological traits in the human pathogen *Acinetobacter baumannii*. *J. Bacteriol.* 199:e00011-17. doi: 10.1128/JB.00011-17

Mussi, M. A., Gaddy, J. A., Cabruja, M., Arivett, B. A., Viale, A. M., Rasia, R., et al. (2010). The opportunistic human pathogen *Acinetobacter baumannii* senses and responds to light. *J. Bacteriol.* 192, 6336–6345. doi: 10.1128/JB.00917-10

Nait Chabane, Y., Mlouka, M. B., Alexandre, S., Nicol, M., Marti, S., Pestel-Caron, M., et al. (2014). Virstatin inhibits biofilm formation and motility of *Acinetobacter baumannii*. *BMC Microbiol.* 14:62. doi: 10.1186/1471-2180-14-62

O'toole, G. A., and Kolter, R. (1998). Initiation of biofilm formation in *Pseudomonas* fluorescens WCS365 proceeds via multiple, convergent signalling pathways: a genetic analysis. *Mol. Microbiol.* 28, 449–461. doi: 10.1046/j.1365-2958.1998.00797.x

Overbeek, R., Olson, R., Pusch, G. D., Olsen, G. J., Davis, J. J., Disz, T., et al. (2014). The SEED and the rapid annotation of microbial genomes using subsystems technology (RAST). *Nucleic Acids Res.* 42, D206–D214.

Palmen, R., Vosman, B., Buijsman, P., Breek, C. K., and Hellingwerf, K. J. (1993). Physiological characterization of natural transformation in *Acinetobacter calcoaceticus*. *J. Gen. Microbiol.* 139, 295–305. doi: 10.1099/00221287-139-2-295

Ramirez, M. S., Don, M., Merkier, A. K., Bistue, A. J., Zorreguieta, A., Centron, D., et al. (2010). Naturally competent *Acinetobacter baumannii* clinical isolate as a convenient model for genetic studies. *J. Clin. Microbiol.* 48, 1488–1490. doi: 10.1128/JCM.01264-09

Ramirez, M. S., Muller, G. L., Perez, J. F., Golic, A. E., and Mussi, M. A. (2015). More Than just light: clinical relevance of light perception in the nosocomial pathogen *Acinetobacter baumannii* and other members of the genus *Acinetobacter*. *Photochem. Photobiol.* 91, 1291–1301. doi: 10.1111/php.12523

Ramsey, M. M., Freire, M. O., Gabrilska, R. A., Rumbaugh, K. P., and Lemon, K. P. (2016). *Staphylococcus aureus* Shifts toward Commensalism in response to *Corynebacterium* Species. *Front. Microbiol.* 7:1230. doi: 10.3389/fmicb.2016.01230

Rice, P., Longden, I., and Bleasby, A. (2000). EMBOSS: the european molecular biology open software suite. *Trends Genet.* 16, 276–277. doi: 10.1016/s0168-9525(00)02024-2

Ringel, P. D., Hu, D., and Basler, M. (2017). The role of type VI secretion system effectors in target cell lysis and subsequent horizontal gene transfer. *Cell Rep.* 21, 3927–3940. doi: 10.1016/j.celrep.2017.12.020

Sarno, R., Mcgillivary, G., Sherratt, D. J., Actis, L. A., and Tolmasky, M. E. (2002). Complete nucleotide sequence of *Klebsiella pneumoniae* multiresistance plasmid pJHCMW1. *Antimicrob. Agents Chemother.* 46, 3422–3427. doi: 10.1128/aac.46.11.3422-3427.2002

Sevin, E. W., and Barloy-Hubler, F. (2007). RASTA-Bacteria: a web-based tool for identifying toxin-antitoxin loci in prokaryotes. *Genome Biol.* 8:R155.

Sievers, F., Wilm, A., Dineen, D., Gibson, T. J., Karplus, K., Li, W., et al. (2011). Fast, scalable generation of high-quality protein multiple sequence alignments using Clustal Omega. *Mol. Syst. Biol.* 7, 539–539. doi: 10.1038/msb.2011.75

Siguier, P., Perochon, J., Lestrade, L., Mahillon, J., and Chandler, M. (2006). ISfinder: the reference centre for bacterial insertion sequences. *Nucleic Acids Res.* 34, D32–D36.

Smith, M. D., Wertheim, J. O., Weaver, S., Murrell, B., Scheffler, K., and Kosakovsky Pond, S. L. (2015). Less is more: an adaptive branch-site random effects model for efficient detection of episodic diversifying selection. *Mol. Biol. Evol.* 32, 1342–1353. doi: 10.1093/molbev/msv022

Sukumaran, J., and Holder, M. T. (2010). DendroPy: a Python library for phylogenetic computing. *Bioinformatics* 26, 1569–1571. doi: 10.1093/bioinformatics/btq228

Tayabali, A. F., Nguyen, K. C., Shwed, P. S., Crosthwait, J., Coleman, G., and Seligy, V. L. (2012). Comparison of the virulence potential of Acinetobacter strains from clinical and environmental sources. *PLoS One* 7:e37024. doi: 10.1371/journal.pone.0037024

Tomaras, A. P., Dorsey, C. W., Edelmann, R. E., and Actis, L. A. (2003). Attachment to and biofilm formation on abiotic surfaces by *Acinetobacter baumannii*: involvement of a novel chaperone-usher pili assembly system. *Microbiology* 149, 3473–3484. doi: 10.1099/mic.0.26541-0

Traglia, G., Chiem, K., Quinn, B., Fernandez, J. S., Montana, S., Almuzara, M., et al. (2018). Genome sequence analysis of an extensively drug-resistant *Acinetobacter baumannii* indigo-pigmented strain depicts evidence of increase genome plasticity. *Sci. Rep.* 8:16961. doi: 10.1038/s41598-018-35377-5

Traglia, G. M., Almuzara, M., Barberis, C., Montana, S., Schramm, S. T., Enriquez, B., et al. (2015). Draft genome sequence of a taxonomically unique acinetobacter clinical strain with proteolytic and hemolytic activities. *Genome Announc.* 3:e00030-15. doi: 10.1128/genomeA.00030-15

Traglia, G. M., Chua, K., Centron, D., Tolmasky, M. E., and Ramirez, M. S. (2014). Whole-genome sequence analysis of the naturally competent *Acinetobacter baumannii* clinical isolate A118. *Genome Biol. Evol.* 6, 2235–2239. doi: 10.1093/gbe/evu176

Traglia, G. M., Quinn, B., Schramm, S. T. J., Soler-Bistue, A., and Ramirez, M. S. (2016). Serum Albumin and Ca(2+) are natural competence inducers in the human pathogen *Acinetobacter baumannii*. *Antimicrob. Agents Chemother.* 60, 4920–4929. doi: 10.1128/AAC.00529-16

Turton, J. F., Shah, J., Ozongwu, C., and Pike, R. (2010). Incidence of Acinetobacter species other than *A. baumannii* among clinical isolates of Acinetobacter: evidence for emerging species. *J. Clin. Microbiol.* 48, 1445–1449. doi: 10.1128/JCM.02467-09

Vilacoba, E., Almuzara, M., Gulone, L., Rodriguez, R., Pallone, E., Bakai, R., et al. (2013). Outbreak of extensively drug-resistant *Acinetobacter baumannii* indigo-pigmented strains. *J. Clin. Microbiol.* 51, 3726–3730. doi: 10.1128/JCM.01388-13

Weaver, S., Shank, S. D., Spielman, S. J., Li, M., Muse, S. V., and Kosakovsky Pond, S. L. (2018). Datamonkey 2.0: a modern web application for characterizing selective and other evolutionary processes. *Mol. Biol. Evol.* [Epub ahead of print],

Weber, B. S., Harding, C. M., and Feldman, M. F. (2016). Pathogenic *Acinetobacter*: from the cell surface to infinity and beyond. *J. Bacteriol.* 198, 880–887. doi: 10.1128/JB.00906-15

Zeidler, S., Hubloher, J., Schabacker, K., Lamosa, P., Santos, H., and Muller, V. (2017). Trehalose, a temperature- and salt-induced solute with implications in pathobiology of *Acinetobacter baumannii*. *Environ. Microbiol.* 19, 5088–5099. doi: 10.1111/1462-2920.13987

Zhou, Y., Liang, Y., Lynch, K. H., Dennis, J. J., and Wishart, D. S. (2011). PHAST: a fast phage search tool. *Nucleic Acids Res.* 39, W347–W352. doi: 10.1093/nar/gkr485

Conflict of Interest Statement: The authors declare that the research was conducted in the absence of any commercial or financial relationships that could be construed as a potential conflict of interest.

frontiers in Microbiology

ORIGINAL RESEARCH
published: 20 June 2019
doi: 10.3389/fmicb.2019.01376

Quorum and Light Signals Modulate Acetoin/Butanediol Catabolism in *Acinetobacter* spp.

Marisel Romina Tuttobene[1†], Laura Fernández-García[2†], Lucía Blasco[2], Pamela Cribb[3], Anton Ambroa[2], Gabriela Leticia Müller[1], Felipe Fernández-Cuenca[4,5,6], Inés Bleriot[1], Ramiro Esteban Rodríguez[3], Beatriz G. V. Barbosa[7], Rafael Lopez-Rojas[4,5,6], Rocío Trastoy[2], María López[2], Germán Bou[1], María Tomás[2‡] and María A. Mussi[1*‡]*

[1] Centro de Estudios Fotosintéticos y Bioquímicos de Rosario (CEFOBI-CONICET), Facultad de Ciencias Bioquímicas y Farmacéuticas, Universidad Nacional de Rosario, Rosario, Argentina, [2] Microbiology Department-Biomedical Research Institute A Coruña (INIBIC), Hospital A Coruña (CHUAC), University of A Coruña (UDC), A Coruña, Spain, [3] Instituto de Biología Molecular y Celular de Rosario (IBR-CONICET), Rosario, Argentina, [4] Clinical Unit for Infectious Diseases, Microbiology and Preventive Medicine, Hospital Universitario Virgen Macarena, Seville, Spain, [5] Department of Microbiology and Medicine, University of Seville, Seville, Spain, [6] Biomedicine Institute of Seville (IBIS), Seville, Spain, [7] Microbial Resistance Laboratory, Biological Sciences Institute, University of Pernambuco (UPE), Recife, Brazil

OPEN ACCESS

Edited by:
Miklos Fuzi,
Semmelweis University, Hungary

Reviewed by:
Liming Liu,
Jiangnan University, China
Xian Zhang,
Jiangnan University, China

***Correspondence:**
Maria Tomás
ma.del.mar.tomas.carmona@sergas.es
María A. Mussi
mussi@cefobi-conicet.gov.ar

[†]These authors have contributed equally to this work as co-first authors

[‡]These authors have contributed equally to this work as co-corresponding authors

Specialty section:
This article was submitted to Infectious Diseases, a section of the journal Frontiers in Microbiology

Received: *28 March 2019*
Accepted: *03 June 2019*
Published: *20 June 2019*

Citation:
Tuttobene MR, Fernández-García L, Blasco L, Cribb P, Ambroa A, Müller GL, Fernández-Cuenca F, Bleriot I, Rodríguez RE, Barbosa BGV, Lopez-Rojas R, Trastoy R, López M, Bou G, Tomás M and Mussi MA (2019) Quorum and Light Signals Modulate Acetoin/Butanediol Catabolism in Acinetobacter spp. Front. Microbiol. 10:1376. doi: 10.3389/fmicb.2019.01376

Acinetobacter spp. are found in all environments on Earth due to their extraordinary capacity to survive in the presence of physical and chemical stressors. In this study, we analyzed global gene expression in airborne *Acinetobacter* sp. strain 5-2Ac02 isolated from hospital environment in response to quorum network modulators and found that they induced the expression of genes of the acetoin/butanediol catabolism, volatile compounds shown to mediate interkingdom interactions. Interestingly, the *acoN* gene, annotated as a putative transcriptional regulator, was truncated in the downstream regulatory region of the induced acetoin/butanediol cluster in *Acinetobacter* sp. strain 5-2Ac02, and its functioning as a negative regulator of this cluster integrating quorum signals was confirmed in *Acinetobacter baumannii* ATCC 17978. Moreover, we show that the acetoin catabolism is also induced by light and provide insights into the light transduction mechanism by showing that the photoreceptor BlsA interacts with and antagonizes the functioning of AcoN in *A. baumannii*, integrating also a temperature signal. The data support a model in which BlsA interacts with and likely sequesters AcoN at this condition, relieving acetoin catabolic genes from repression, and leading to better growth under blue light. This photoregulation depends on temperature, occurring at 23°C but not at 30°C. BlsA is thus a dual regulator, modulating different transcriptional regulators in the dark but also under blue light, representing thus a novel concept. The overall data show that quorum modulators as well as light regulate the acetoin catabolic cluster, providing a better understanding of environmental as well as clinical bacteria.

Keywords: acetoin, BLSA, AcoN, light, *Acinetobacter*

INTRODUCTION

Acinetobacter baumannii has recently been recognized by the World Health Organization (WHO) as one of the most threatening pathogens deserving urgent action (Tacconelli et al., 2018). With the aid of new taxonomic tools and technological advancements, other members of the *Acinetobacter* genus have also been identified as causative agents of hospital acquired infections and are gaining

clinical relevance (Turton et al., 2010; Karah et al., 2011). Key factors determining their success as pathogens include their extraordinary ability to develop resistance to antimicrobials as well as to persist in the hospital environment despite adverse conditions such as desiccation, lack of nutrients, etc. (McConnell et al., 2013; Spellberg and Bonomo, 2014; Yakupogullari et al., 2016). It is known that some members of the genus can be transmitted by air. In fact, some genotypes of *A. baumannii* have been shown to survive for up to 4 weeks in the air in intensive care units (ICUs) (Yakupogullari et al., 2016). It is becoming increasingly clear, despite not very much studied, the importance of this kind of transmission since it leads to recontamination of already decontaminated surfaces, transmission between patients, airborne contamination of healthcare providers as well as of medical instruments (Spellberg and Bonomo, 2013). We have recently reported the genome sequence of *Acinetobacter* sp. strain 5-2Ac02 (closely related to *Acinetobacter towneri*), which has been recovered from the air in an ICU of a hospital in Rio de Janeiro, Brazil (Barbosa et al., 2016). This strain was shown to harbor a much reduced genome and higher content of insertion sequences than other *Acinetobacter* sp. Moreover, four different toxin–antitoxin (TA) systems as well as heavy metal resistance operons were found encoded in its genome (Barbosa et al., 2016). Interestingly, some bacteria have been shown to produce and release a large diversity of small molecules, including organic and inorganic volatile compounds such as acetoin and 2,3-butanediol (BD), referred as bacterial volatile compounds (BVCs), which can mediate airborne bacterial interactions (Audrain et al., 2015). BVCs can mediate cross-kingdom interactions with fungi, plants, and animals, and can even modulate antibiotic resistance, biofilm formation, and virulence (Audrain et al., 2015).

Several molecular mechanisms have been associated with the development of bacterial tolerance or persistence under stress conditions (environmental or drug-related) (Trastoy et al., 2018). Among these are included the general stress response (RpoS-mediated), tolerance to reactive oxygen species (ROS), energy metabolism, drug efflux pumps, the SOS response, and TA systems, with the quorum network (quorum sensing/quorum quenching) regulating many of them (Trastoy et al., 2018). The finding that many bacterial pathogens are able to sense and respond to light modulating diverse aspects related to bacterial virulence and persistence in the environment is particularly pertinent in this context. Indeed, light has been shown to modulate biofilm formation, motility, and virulence against *C. albicans*, a microorganism sharing habitat with *A. baumannii*, at environmental temperatures in this pathogen. Moreover, light modulates metabolic pathways including trehalose biosynthesis and the phenylacetic acid degradation pathway, antioxidant enzyme levels such as catalase, and susceptibility or tolerance to some antibiotics (Ramirez et al., 2015; Muller et al., 2017). In addition, light induced the expression of whole gene clusters and pathways, including those involved in modification of lipids, the complete type VI secretion system (T6SS), acetoin catabolism, and efflux pumps (Muller et al., 2017). Many of these processes are controlled by BlsA, the only canonical photoreceptor codified in the genome of *A. baumannii*, which is a short blue light using flavin (BLUF) protein. BlsA has been shown to function at moderate temperatures such as 23°C but not at 37°C by a mechanism that includes control of transcription as well as photoactivity by temperature (Mussi et al., 2010; Abatedaga et al., 2017; Tuttobene et al., 2018). Knowledge of these mechanisms will potentially enable the implementation of several clinical or industrial applications.

In this study, we characterized the airborne *Acinetobacter* sp. strain 5-2Ac02, analyzing gene expression adjustments in response to environmental stressors such as mitomycin C and acyl-homoserine-lactones, which modulate the quorum network. The results showed that genes involved in the SOS response, TA systems, and heavy metal resistance were induced in response to mitomycin, while genes involved in acetoin and aromatic amino acid catabolism were modulated as a response to quorum sensing signals. The fact that acetoin catabolic genes were also found to be induced by light in *A. baumannii* (Muller et al., 2017) prompted us to deepen the study on this metabolism. In bacteria, the butanediol fermentation is characterized by the production of BD and acetoin from pyruvate. The production of butanediol is favored under slightly acidic conditions and is a way for the bacteria to limit the decrease in external pH caused by the synthesis of organic acids from pyruvate. The catabolic α-acetolactate-forming enzyme (ALS) condenses two molecules of pyruvate to form one α-acetolactate, which is unstable and can be converted to acetoin by α-acetolactate decarboxylase (ALDC) or diacetyl as a minor by-product by non-enzymatic oxidative decarboxylation. Diacetyl can be irreversibly transformed into its reductive state acetoin, and acetoin can be reversibly transformed into its reductive state BD, both catalyzed by 2,3-butanediol dehydrogenase (BDH). The acetoin breakdown in many bacteria is catalyzed by the acetoin dehydrogenase enzyme system (AoDH ES), which consists of acetoin:2,6-dichlorophenolindophenol oxidoreductase, encoded by *acoA* and *acoB*; dihydrolipoamide acetyltransferase, encoded by *acoC*; and dihydrolipoamide dehydrogenase, encoded by *acoL* (Xiao and Xu, 2007). Our results show that the *acoN* gene codes for a negative regulator of the acetoin/butanediol catabolic cluster and is involved in photoregulation of acetoin catabolism in *A. baumannii* through the BlsA photoreceptor. Most importantly, we provide strong evidence on the mechanism of light signal transduction, which is far from being understood for BlsA or other short BLUF photoreceptors, taking into account in addition that BlsA is a global regulator in *A. baumannii*. In this sense, we have recently shown that this photoreceptor binds to and antagonizes the functioning of the Fur repressor only in the dark at 23°C, presumably by reducing its ability to bind to acinetobactin promoters, thus relieving repression at the transcriptional level as well as growth under iron limitation at this condition (Tuttobene et al., 2018). Here, we further show that BlsA directly interacts with the acetoin catabolism negative regulator AcoN at 23°C but, in this case, in the presence of blue light rather than in the dark. In fact, growth on acetoin was much better supported under blue light than in the dark through BlsA and AcoN. Moreover, acetoin catabolic genes were induced at this condition in a BlsA- and AcoN-dependent manner. Opposite behavior was observed for Δ*blsA* and Δ*acoN* mutants, being BlsA necessary

for the observed induction while AcoN for repression, thus indicating that BlsA antagonizes AcoN. Finally, yeast two-hybrid (Y2H) assays indicate that BlsA interacts with AcoN only under blue light but not in the dark. The results strongly suggest that BlsA interacts with and likely sequesters the acetoin repressor under blue light but not in the dark. Thus, in the presence of light, acetoin catabolic genes are relieved from repression resulting in much better bacterial growth in this condition. Here again, the phenomena depends on temperature, occurring at low–moderate temperatures such as 23°C but not at 30°C, consistent with previous findings of our group for BlsA functioning (Mussi et al., 2010; Abatedaga et al., 2017; Tuttobene et al., 2018).

MATERIALS AND METHODS

Bacterial Strains, Plasmids, and Media

Bacterial strains and plasmids used in this work are listed in **Table 1**. Luria-Bertani (LB) broth (Difco) and agar (Difco) were used to grow and maintain bacterial strains. Broth cultures were incubated at the indicated temperatures either statically or with shaking at 200 rpm.

TABLE 1 | Minimal inhibitory concentrations (MICs) of several antibiotics and heavy metals for *Acinetobacter* sp. strain 5-2Ac02.

Antimicrobial	MIC (μg/mL)	Category[a]
Sulbactam	0.5	Susceptible
Piperacillin	0.06	Susceptible
Ceftazidime	4	Susceptible
Imipenem	0.06	Susceptible
Meropenem	0.03	Susceptible
Doripenem	0.015	Susceptible
Ciprofloxacin	1	Susceptible
Amikacin	1	Susceptible
Gentamicin	0.25	Susceptible
Tobramycin	0.5	Susceptible
Netilmicin	0.25	Susceptible
Tetracycline	0.5	Susceptible
Minocycline	<0.002	Susceptible
Doxycycline	0.03	Susceptible
Tigecycline	0.25	Susceptible
Colistin	0.125	Susceptible
Clavulanic acid	4	Susceptible
Azithromycin	16	Susceptible
Heavy metal	**MIC (μg/mL)**	**Category[b]**
Arsenic	>2048	**Resistant**
Cadmium	64	Susceptible
Cobalt	16	Susceptible
Cooper	266	**Resistant**
Chromium	128	Susceptible
Tellurite	2	Susceptible
Zinc	256	Susceptible

[a]*MICs were determined by the microdilution method, in accordance with general procedures recommended by CLSI. For specific details, please refer to the section "Materials and Methods."* [b]*Determined according to Taylor et al. (2002) and Akinbowale et al. (2007). In bold are shown the resistance category.*

Plasmid Construction

Y2H Plasmid Construction

PCR amplification of *blsA* and *acoN* coding sequences was performed from *A. baumannii* ATCC 17978 genomic DNA using primers blsAdh and acoNdh (**Supplementary Table S2**). The amplification products were subsequently cloned into the BamHI and XhoI sites of Gateway entry vector pENTR3C (Invitrogen) (**Supplementary Table S1**). The cloned fragments were then transferred to pGBKT7-Gw and pGADT7-Gw Y2H vectors (Clontech) by using LR Clonase (Cribb and Serra, 2009; Tuttobene et al., 2018). In the yeast host, these plasmids express the cloned coding sequences as fusion proteins to the GAL4 DNA-binding domain (DB) or activation domain (AD), respectively, under the control of the constitutive ADH1 promoter. Automated DNA sequencing confirmed correct construction of each plasmid.

pWHAcoN Plasmid Construction

acoN coding sequence and its promoter were amplified by PCR using *A. baumannii* ATCC 17978 genomic DNA as template and primers PAcoNF and PAcoNR (**Supplementary Table S2**), which contained BamHI restriction site tails. The amplification product was cloned into pWH1266 through the BamHI sites. Automated DNA sequencing confirmed the proper construction of pWHAcoN plasmid.

Susceptibility to Antimicrobials and Heavy Metals (MICs)

The antibiotic and heavy metal susceptibility profile by microdilution was determined according to CLSI recommendations (**Table 1**). Heavy metal susceptibility was determined by broth microdilution following CLSI instructions for cobalt, chromium, copper, arsenic, and zinc (Akinbowale et al., 2007). The susceptibility to tellurite was determined by serial plate dilution, with concentrations ranging from 1 to 1024 μg/mL *Escherichia coli* K12 were used as reference strain (Akinbowale et al., 2007). The breakpoints adopted for resistance phenotype were as follows: ≥100 μg/mL for cadmium; ≥200 μg/mL for copper, arsenic, and zinc; ≥400 μg/mL for cobalt; ≥800 μg/mL for chromium; and >128 μg/mL for tellurite.

Growth curves in the presence of heavy metals were performed as follow: one colony of *Acinetobacter* sp. strain 5-2Ac02 was grown overnight, diluted 1:100 in 20 mL of low nutrient LB broth, and incubated at 37°C with shaking (180 rpm) (Lopez et al., 2018). The cultures were grown for 4 h to the exponential phase; and then, the heavy metals were added. For each isolate, the proportion of survivors was determined: (i) in the control without heavy metals, (ii) in the presence of arsenic (0.50× MIC), (iii) in the presence of cupper (0.5× MIC). Bacterial concentrations ($\log_{10}$ CFU/mL) were determined at 0, 2, 4, 24, and 48 h by serial dilution and plating on LB agar. All experiments were performed in duplicate.

Gene Expression by Microarrays Under Stress Conditions: Mitomycin and AHLs

Acinetobacter sp. strain 5-2Ac02 cells were grown in LB medium to an exponential phase about OD_{600} = 0.5 before addition of 10 μg/mL of mitomycin C (SOS response) or a mixture of 1 μM each acyl-homoserine lactones composed by *N*-(butyl, heptanoyl, hexanoyl, β-ketocaproyl, octanoyl, and tetradecanoyl)-DL-homoserine lactones or 10 μM 3-oxo-dodecanoyl-HSL (3-oxo-C12-HSL) (Quorum Network). After incubation of the mixtures for 2 h, 1 mL of each culture was used for RNA extraction. RNA was purified using the High Pure RNA Isolation Kit (Roche, Germany). The microarrays were specifically designed for this strain using eArray (Agilent). The microarray assays were performed with 12,664 probes to study 2,795 genes. Labeling was carried out by two-color microarray-based prokaryote analysis and Fair Play III labeling, version 1.3 (Agilent). Three independent RNAs per condition (biological replicates) were used in each experiment. Statistical analysis was carried out using Bioconductor, implemented in the RankProd software package for the R computing environment. A gene was considered induced when the ratio of the treated to the untreated preparation was 1.5 and the *p*-value was <0.05 (Lopez et al., 2017b).

Bacterial Killing Curves

The MICs of ampicillin, ciprofloxacin, and mitomycin C were determined for *Acinetobacter* sp. strain 5-2Ac02 (0.5, 1, and 0.5 μg/mL) versus *A. baumannii* strain ATCC 17978 (8, ≤0.12, and 2 μg/mL). Briefly, an initial inoculum of 5×10^5 CFU/mL was incubated at 37°C with shaking (250 rpm) in 20 mL of low nutrient LB broth (LN-LB; 2 g/L tryptone, 1 g/L yeast extract, and 5 g/L NaCl) (Lopez et al., 2017a,b). The cultures were grown for 4 h to the exponential phase; and then, the antibiotics were added. For each isolate, the proportion of survivors was determined: (i) in the control without antibiotic, (ii) in the presence of mitomycin C (0.25× MIC), (iii) in the presence of ampicillin (10× MIC), (iv) in the presence of ciprofloxacin (10× MIC), (v) in the presence of mitomycin C and ampicillin (0.25× MIC and 10× MIC), and (vi) in the presence of mitomycin C and ciprofloxacin (0.25× MIC and 10× MIC). Bacterial concentrations ($\log_{10}$ CFU/mL) were determined at 0, 1, 2, 3, 4, 20, 24, 28, and 48 h by serial dilution and plating on Mueller-Hinton agar. All experiments were performed in triplicate. This protocol was performed following previously described indications (Hofsteenge et al., 2013). Finally, the persister sub-population was determined from the percentage of survivors.

Gene Deletion in *A. baumannii* ATCC 17978

The negative regulator of the acetoin operon was deleted following the double recombination method, using the pMO-TelR plasmid and *E. coli* DH5α strain to multiply the plasmid with the construct (Hamad et al., 2009; Aranda et al., 2010). All primer sequences used were designed in this study and are listed in **Supplementary Table S2**.

Isolation of RNA and Analyses of Genes Expression by qRT-PCR

Acinetobacter baumannii cells were grown stagnantly in LN-LB at 37°C with the addition of 10 μM of 3-oxo-C12-HSL or 10 μM of 3-hydroxy-dodecanoyl-HSL (3-OH-C12-HSL) when appropriate, or in M9 liquid medium supplemented with 15 mM acetoin as carbon source at 23 or 30°C until an OD_{600} of 0.4–0.6 was reached, as indicated. RNA extraction and qRT-PCR were performed following procedures described in Lopez et al. (2018) and Tuttobene et al. (2018). Results are informed as normalized relative quantities (NRQs) calculated using qBASE (Hellemans et al., 2007), with *recA* and *rpoB* genes as normalizers (Muller et al., 2017). The UPL Taqman Probes (Universal Probe Library-Roche, Germany) and primers used are listed in **Supplementary Table S3**.

Growth in the Presence of Acetoin

Wild-type and derivative strains *A. baumannii* ATCC 17978 were grown on acetoin as the sole carbon source. To test the ability of the *A. baumannii* strains used in this work to grow on acetoin as the sole carbon source, 1/100 dilutions of overnight cultures grown in LB Difco were washed and inoculated in M9 liquid medium supplemented with 5, 10, or 15 mM acetoin or in LB Difco medium and grown without shaking, under blue light or in the dark at 23 or 30°C. Aliquots were removed at the times indicated in the figures in order to measure the A660 of the culture.

Blue Light Treatments

Blue light treatments were conducted as reported before (Mussi et al., 2010; Golic et al., 2013; Abatedaga et al., 2017; Muller et al., 2017; Tuttobene et al., 2018). Briefly, cells were grown in the dark or under blue light emitted by an array composed of 3 × 3-LED module strips emitting an intensity of 6–10 μol photons/m^2/s, with emission peaks centered at 462 nm (Mussi et al., 2010).

Yeast Two-Hybrid (Y2H) Assays

Yeast two-hybrid experiments were conducted following procedures described before (Cribb and Serra, 2009; Tuttobene et al., 2018). *Saccharomyces cerevisiae* Mav 203 strain (MATa, *leu*2-3,112, *trp*1-901, *his*3-D200, *ade*2-101, *gal*4D, *gal*80D, SPAL10::URA3, GAL1::*lacZ*, HIS3UAS GAL1::HIS3, LYS2, *can*1R, and *cyh*2R) was transformed with the different expression vectors. First, BlsA and AcoN were analyzed for self-activation. For this purpose, MaV203 yeast strain containing the pGAD-T7 empty vector was transformed with the DNA DB-fusion protein expressing vectors (pGBK-X) (X = BlsA or AcoN). Conversely, MaV203 yeast strain containing the pGBK-T7 empty vector was then transformed with the AD-fusion protein expressing vectors (pGAD-Y) (Y = BlsA or AcoN). In addition, these strains were used for determination of the optimal 3-amino-1,2,4-triazole (3AT) concentration required to titrate basal *HIS3* expression. MaV203/pGBK-X strains were afterward transformed with each pGAD-Y plasmids. Transformations using one or both Y2H plasmids were performed by the lithium acetate/single-stranded carrier DNA/polyethylene glycol method described in Gietz and Woods (2002), and plated in convenient minimal selective

medium [synthetic complete (SC) medium without leucine (-leu) for pGAD-Y transformants, SC without tryptophan (-trp) for pGBK-X transformants, and SC-leu-trp transformants carrying both plasmids]. The plates were then incubated at 23°C for 72 h to allow growth of transformants. A "Master Plate" was then prepared using SC-leu-trp media, in which we patched: four to six clones of each pGBK-X/pGAD-Y containing yeasts, four to six self-activation control clones pGBK-X/pGAD and pGBK/pGAD-Y (Y DNA-binding negative control), and two isolated colonies of each of the five yeast control strains (A–E). The plates were incubated for 48–72 h at 23°C. This Master Plate was then replica plated to SC–leu–trp–his+3AT and to SC–leu–trp–ura to test for growth in the absence of histidine (*his*) and uracil (*ura*), respectively (*his*3 and *ura*3 reporter activation), under the different conditions analyzed, i.e., dark/light; 23/30°C, for at least 72 h. For development of blue color as a result of β-galactosidase (β-Gal) expression, transformed yeasts were replica plated on a nitrocellulose filter on top of a YPAD medium plate and grown at the different conditions (dark/light; 23/30°C). Then, the cells on the nitrocellulose filter were permeabilized with liquid nitrogen and soaked in X-Gal solution (5-bromo-4-chloro-3-indolyl-b-D-galactopyranoside in Z buffer (60 mM Na_2HPO_4, 40 mM NaH_2PO_4, 10 mM KCl, 1 mM $MgSO_4$, pH 7.0) maintaining the different incubation conditions to be tested.

Accession Numbers

The genome of the *Acinetobacter* sp. 5-2Ac02 is deposited in GenBank database (GenBank accession number MKQS00000000; Bioproject PRJNA345289). The genome of *A. baumannii* ATCC17978 is deposited in GenBank (accession number CP018664.1). Finally, the gene expression microarray results are deposits in GEO database (GEO accession number GSE120392).

RESULTS

Transcriptome Adjustments in Response to Mitomycin C Show Induction of Defense and Stress Response Systems in *Acinetobacter* sp. Strain 5-2Ac02

The airborne *Acinetobacter* sp. 5-2Ac02 isolate was first characterized to learn about its antibiotic as well as heavy metal susceptibility profiles, since its genome harbored genes of the *ter* (tellurite resistance) operon (*terZABCDEF*); *klaA* and *klaB* genes from the *kil* operon, which is associated with the previous one (O'Gara et al., 1997); as well as the arsenic-resistance operon *arsC1-arsRarsC2-ACR3*-arsH (**Table 1**). The data presented in **Table 1** show that *Acinetobacter* sp. 5-2Ac02 is susceptible to all antibiotic tested but resistant to copper as well as to arsenic, as previously reported (Barbosa et al., 2016). This information was confirmed by growth curves in the presence of these heavy metals (**Supplementary Figure S1**).

Arrays performed in the presence of the stressor mitomycin C revealed induction of SOS genes such as those coding for recombinases, polymerases, as well as DNA repair proteins, all with a fold change (FC) > 3 in *Acinetobacter* sp. strain 5-2Ac02. Also, genes coding for components of six TA systems were found to be induced with a FC > 4.9 in all cases: the RelBE systems (x2), the HigBA system, the ParDE system, and two new putative systems (x2). The data also showed induction of genes involved in heavy metal resistance genes, among which can be highlighted cobalt–zinc–cadmium, copper, and arsenic resistance genes. In addition, the gene coding for colicin V protein was induced with a FC of 3.716 (**Table 2**). Finally, many mobile element genes, which are extraordinarily abundant in the genome of *Acinetobacter* sp. 5-2Ac02 strain, were also induced (not shown).

The TA systems have been shown to be involved both in tolerance and persistence (Fernandez-Garcia et al., 2018). We next analyzed the fraction of tolerant or persister cells in populations of *Acinetobacter* sp. strain 5-2Ac02 by determining the time-kill responses in the presence of ampicillin, ciprofloxacin, mitomycin C, and combinations of these (**Figure 1**), following protocols described in Hofsteenge et al. (2013). The data show a large decrease in colonies of *Acinetobacter* sp. strain 5-2Ac02 during the first 24 h in the presence of ampicillin, ciprofloxacin, as well as in the presence of the combination of ampicillin and mitomycin C. Interestingly, the presence of a combination of mitomycin C with ciprofloxacin showed a tolerant population displaying slow growth at 4, 24, and 48 h (**Figure 1**) under this stress condition, which may result from activation of defense mechanisms such as the toxins and antitoxins systems as well as SOS response.

Quorum Sensing Signals Modulate Expression of the Acetoin/Butanediol Catabolic Cluster in *Acinetobacter* spp., Being AcoN a Negative Regulator in *A. baumannii*

Array expression studies of *Acinetobacter* sp. 5-2Ac02 in the presence of a mixture of *N*-acyl-homoserine lactones (AHLs) or 3-oxo-C12-HSL, which are modulators of the quorum network in *A. baumannii* (Lopez et al., 2018), indicated induction of the acetoin/butanediol catabolic pathway genes, each with a FC > 1.5 (**Tables 3**, **4**, respectively). We show the genomic arrangement of this cluster in the genomes of *Acinetobacter* sp. 5-2Ac02 and *A. baumannii* ATCC 17978 strain (**Figures 2A,B**). The same genomic configuration in *A. baumannii* strain ATCC 17978 was observed in 18 clinical *A. baumannii* strains isolated in the "II Spanish Study of *A. baumannii* GEIH-REIPI 2000–2010" which included 45 Spanish hospitals with 246 patients (GenBank Umbrella Bioproject PRJNA422585) (**Supplementary Table S4**).

Ten genes were identified in the ATCC 17978 cluster, likely coding for a putative transcriptional regulator (gene 1) followed by a putative lipoyl synthase (gene 2), two oxidoreductases homologous to *acoA* and *acoB* (genes 3 and 4), a deaminase homologous to *acoC* (gene 5), a dehydrogenase homologous to *acoD* (gene 6), a BDH reductase (gene 7), and a BDH (gene 8), all of which are followed by a hypothetical protein (gene 9) and a putative transcriptional regulator (gene 10) (**Figure 2A**). Gene 2 is homologous to *acoK* (**Figure 2A**) and gene 1 is

TABLE 2 | Gene expression adjustments in response to mitomycin C in *Acinetobacter* sp. strain 5-2Ac02.

Protein ID (RAST server)[a]	Description	Fold change	System	Mechanism
202956.5.peg.1643	*recA*	5.7671	Recombinases	SOS response
202956.5.peg.129	*recT*	25.3753		
202956.5.peg.1972	*recF*	13.1351		
202956.5.peg.2285	*umuD*	5.0572	Polymerases V	
202956.5.peg.1220	*umuD*	21.6016		
202956.5.peg.2284	*umuC*	3.7093		
202956.5.peg.1221	*umuC*	4.1229		
202956.5.peg.1236	*rmlC-like cupin*	29.8694	DNA repair protein	
202956.5.peg.2036	*rmlC-like cupin*	10.1388		
202956.5.peg.274	*relB*	5.3331	RelEB system	Toxin–antitoxin modules
202956.5.peg.2563	*relB*	7.4618		
202956.5.peg.275	*relE*	5.8337		
202956.5.peg.2564	*relE*	7.8490		
202956.5.peg.411	*higA*	7.3751	HigBA system	
202956.5.peg.412	*higB*	14.9347		
202956.5.peg.2515	Antitoxin	6.7492	New putative TA system	
202956.5.peg.2516	Toxin	9.5133		
202956.5.peg.2550	Antitoxin	8.6098		
202956.5.peg.2551	Toxin	10.5546		
202956.5.peg.797	*parD*	5.8254	ParDE system	
202956.5.peg.796	*parE*	4.9563		
202956.5.peg.984	*aphC*	2.3370	Reductase	Oxidant tolerance (ROS response)
202956.5.peg.319	*rpoS* regulon	28.4676	Regulatory system	
202956.5.peg.1019	*arsC* (arsenate reductase)	3.7665	Reductase	Heavy metals resistance
202956.5.peg.1000	*copA* (*copD*)	2.1898	Copper resistance operon	
202956.5.peg.1009	*copB*	2.3034		
202956.5.peg.1001	*copC*	3.2015		
202956.5.peg.2458	*czcA*	4.6191	Cobalt–zinc–cadmium resistance operon	
202956.5.peg.1476	*czcD*	3.1468		
202956.5.peg.2744	*cvpA* (colicin V)	3.7163	Bacteriocin protein	Antibiotic peptides

Genes showing FC >2 are indicated. [a]RAST server was used to identify the protein-coding genes, rRNA and tRNA genes, and to assign predictive functions to these genes.

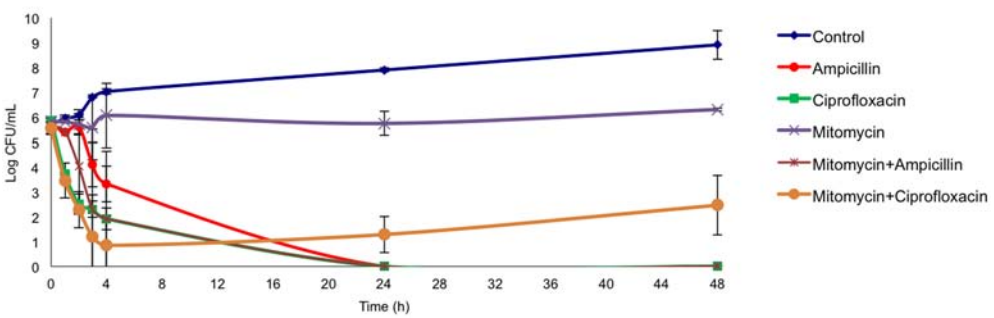

FIGURE 1 | Killing curves of *Acinetobacter* sp. 5-2Ac02 in the presence of antimicrobials and/or mitomycin C.

TABLE 3 | Expression of genes in *Acinetobacter* sp. strain 5-2Ac02 by quorum network molecules (AHLs mix).

Protein ID (RAST server)[a]	Gene/predicted protein description	Fold change	System	Mechanism
202956.5.peg.1419	*acoA*/acetoin dehydrogenase E1 alpha-subunit	3.9966	Acetoin/butanediol cluster (degradation)	QS system
202956.5.peg.1420	*acoB*/acetoin dehydrogenase E1 beta-subunit	3.7291		
202956.5.peg.1421	*acoC*/dihydrolipoamide acetyltransferase (E2) acetoin	3.6752		
202956.5.peg.1422	*acoD*/dihydrolipoamide dehydrogenase of acetoin dehydrogenase	3.3919		
202956.5.peg.1423	2,3-BDH/2,3-butanediol dehydrogenase, S-alcohol forming, (S)-acetoin-specific	2.9770		
202956.5.peg.1424	2,3-BDH/2,3-butanediol dehydrogenase, R-alcohol forming, (R)- and (S)-acetoin-specific	1.9456		
202956.5.peg.2091	1,2-Dihydroxycyclohexa-3,5-diene-1-carboxylate dehydrogenase	2.4396	Aromatic compounds biodegradation cluster	QS system
202956.5.peg.2092	Benzoate dioxygenase, ferredoxin reductase	2.8198		
202956.5.peg.2093	Benzoate 1,2-dioxygenase beta-subunit	3.2909		
202956.5.peg.2094	Benzoate 1,2-dioxygenase alpha-subunit	3.3731		
202956.5.peg.2095	Catechol 1,2-dioxygenase	3.5774		
202956.5.peg.2096	Muconolactone isomerase	3.1273		

[a] *RAST server was used to identify the protein-coding genes, rRNA and tRNA genes, and to assign functions to these genes.*

homologous to a positive transcriptional regulator (activator) homologous to *acoR* in different organisms (**Figure 2A**). The genomic configuration in *Acinetobacter* sp. strain 5-2Ac02 is similar to that of ATCC 17978 except that genes coding for the hypothetical protein and the putative transcriptional regulator (9 and 10 in ATCC 17978, respectively) are absent, while three genes coding for putative transposases were identified following gene 8 (**Figure 2B**).

Finally, in presence of the AHL mixture, the arrays also revealed increased expression (FC > 2) of genes involved in biodegradation of aromatic compounds (**Table 4**).

We suspected that the absence of the putative transcriptional regulator in *Acinetobacter* sp. strain 5-2Ac02, designated as gene 10 in the genome locus of *A. baumannii* ATCC17978 (**Figure 2A**) and renamed here from now on as *acoN*, might be responsible for the induced expression of the acetoin catabolic genes in response to quorum network signals.

We reasoned that whether this was the case, then a knockout mutant in *acoN* in *A. baumannii* ATCC 17978, which would resemble the situation in the so far genetically intractable *Acinetobacter* sp. strain 5-2Ac02, would result in induction of the acetoin catabolic genes in the presence of quorum sensing signals. As can be observed in **Figure 3**, the presence of quorum sensing signals resulted in induction of the transcript levels of BDH (*bdh*, acetoin/butanediol cluster) (RE > twofold) in the *A. baumannii* ATCC 17978 Δ*acoN* mutant with respect to the wild-type strain. This provides the first clue that AcoN functions as a negative regulator of acetoin catabolic genes.

Further studies showed that the Δ*acoN* mutant grew much better in media supplemented with acetoin (5 mM) as sole carbon source than the wild-type strain in the dark at 23°C (**Figure 4A**), which barely grew at this condition. The Δ*acoN* mutant containing the pWHAcoN plasmid, which expresses *acoN* directed from its own promoter, behaved as the wild type showing a reduced ability to grow on acetoin as sole carbon source at 23°C in the dark, restoring therefore the wild-type phenotype (**Figure 4B**). Similar results were obtained at 30°C and are discussed later in the manuscript. These results provide further evidence of the role of AcoN gene as a negative regulator of the acetoin catabolic cluster.

Finally, expression of acetoin catabolic genes such as *acoA*, *acoB*, and *acoC* was induced approximately 150-folds in the Δ*acoN* mutant with respect to the wild type at 23°C in the dark (**Figure 5**). These results confirm the functioning of AcoN as a negative regulator of the acetoin catabolic pathway in *A. baumannii*.

Light Modulates Acetoin Catabolism Through BlsA and AcoN at Moderate Temperatures in *A. baumannii*

Acetoin catabolic genes such as *acoA*, *acoB*, *acoC*, and *acoD* have been previously shown to be induced by light at moderate temperatures in *A. baumannii* ATCC 19606 by RNA-seq studies (Muller et al., 2017). We thus studied whether light modulated acetoin catabolism in ATCC 17978 at 23°C and found a differential ability of this strain to grow in the presence of acetoin as sole carbon source between light and dark conditions (**Figure 4** and **Supplementary Figure S2**).

Figure 4A shows that *A. baumannii* ATCC 17978 grows much poorer in 5 mM acetoin in the dark rather than under blue light at 23°C. The Δ*blsA* mutant, which lacks the only traditional photoreceptor encoded in the *A. baumannii* genome, behaved as the wild type in the dark both under blue light or in the dark (**Figure 4A**), as also did the mutant containing the empty vector pWH1266 (**Figure 4B**). In contrast, the Δ*blsA* mutant containing pWHBlsA, which expresses *blsA* directed from its own promoter, grew better on acetoin under blue light than in the dark, restoring thus the wild-type phenotype (**Figure 4B**). The Δ*acoN* mutant,

TABLE 4 | Expression of genes in *Acinetobacter* sp. strain 5-2Ac02 by quorum network molecules (3-oxo-C12-HSL).

Protein ID (RAST server)[a]	Gene/predicted protein description	Fold change	System	Mechanism
202956.5.peg.1419	*acoA*/acetoin dehydrogenase E1 alpha-subunit	2.3803	Acetoin/butanediol cluster	QS system
202956.5.peg.1420	*acoB*/acetoin dehydrogenase E1 beta-subunit	2.5212		
202956.5.peg.1421	*acoC*/dihydrolipoamide acetyltransferase (E2) of acetoin dehydrogenase complex	2.7127	Acetoin/butanediol cluster	QS system
202956.5.peg.1422	*acoD*/dihydrolipoamide dehydrogenase of acetoin dehydrogenase	2.2546		
202956.5.peg.1423	2,3-BDH/2,3-butanediol dehydrogenase, S-alcohol forming, (S)-acetoin-specific	2.0217		
202956.5.peg.2196	Aminoacid transporter	3.6649		Others
202956.5.peg.2630	Short-chain dehydrogenase	2.8179		
202956.5.peg.2505	Amide	2.6736		
202956.5.peg.2388	Transporter (DMT) superfamily	2.6240		
202956.5.peg.2137	Alcohol dehydrogenase	2.5237		
202956.5.peg.517	Ribonucleotide reductase	2.3017		
202956.5.peg.2100	dcaP	2.2854		
202956.5.peg.1418	Lipoate synthase	2.2626		
202956.5.peg.691	Monooxygenase	2.1241		
202956.5.peg.2775	Cyclic AMP receptor	2.0731		
202956.5.peg.2753	*cspA*	2.0635		
202956.5.peg.451	NAD(P)	2.0352		
202956.5.peg.434	Protein-export membrane protein SecD	2.0152		
202956.5.peg.1121	Putrescine importer	2.0026		

[a] *RAST server was used to identify the protein-coding genes, rRNA and tRNA genes, and to assign functions to these genes.*

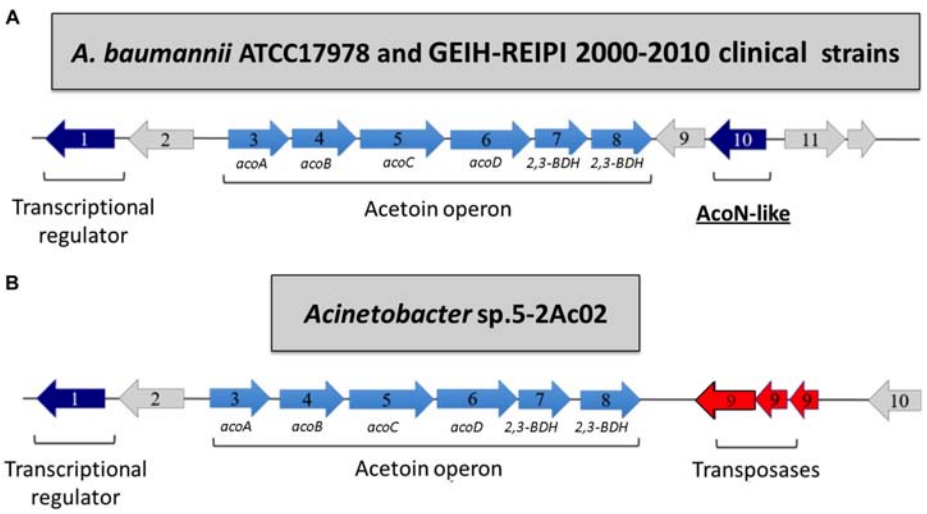

FIGURE 2 | Acetoin/butanediol cluster from *A. baumannii* ATCC 17978 (GenBank accession number CP018664.1; *acoN*-like AU097_16290) as well as clinical *A. baumannii* strains isolated in the "II Spanish Study of *A. baumannii* GEIH-REIPI 2000–2010" involving 45 Spanish hospitals with 246 patients (GenBank Umbrella Bioproject PRJNA422585) **(A)** and Acinetobacter sp. strain 5-2Ac02 (GenBank accession number MKQS00000000; Bioproject PRJNA345289) **(B)**. The following proteins from the acetoin/butanediol cluster are indicated by arrows: (1) putative transcriptional regulator; (2) hypothetical protein; (3) *acoA*, acetoin dehydrogenase E1 alpha-subunit; (4) *acoB*, acetoin dehydrogenase E1 beta-subunit; (5) *acoC*, dihydrolipoamide acetyltransferase (E2) acetoin; (6) *acoD*, dihydrolipoamide dehydrogenase subunit of acetoin dehydrogenase; (7) 2,3-BDH/2,3-butanediol dehydrogenase, S-alcohol forming, (S)-acetoin-specific; (8) 2,3-BDH/2,3-butanediol dehydrogenase, R-alcohol forming, (R)- and (S)-acetoin-specific; (9) hypothetical protein (*A. baumannii* ATCC17978) and transposases (*Acinetobacter* sp. 5-2Ac02 strain); (10) putative transcriptional regulator (AcoN, *A. baumannii* ATCC17978) and hypothetical protein (*Acinetobacter* sp. 5-2Ac02 strain).

both under blue light and in the dark, behaved as the wild type under blue light, i.e., showed enhanced growth with respect to the wild type in the dark, congruent with the absence of the negative regulator (**Figure 4A**); as also did the Δ*acoN* mutant containing pWH1266 (**Figure 4B**). The Δ*acoN* mutant containing pWHAcoN, which expresses *acoN* directed from its

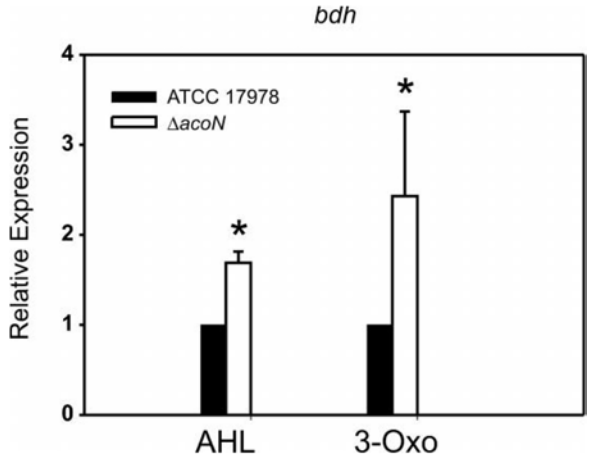

FIGURE 3 | The BDH (*bdh*) gene is induced by quorum network signals in the Δ*acoN* mutant. Estimation of the relative levels of the BDH mRNA by qRT-PCR in the presence of AHLs or 3-oxo-C12-HSL in the wild-type *A. baumannii* ATCC 17978 and Δ*acoN* genetic backgrounds. The data shown are mean ± SD of the expression levels relative to the wild type from at least three biological replicates. Asterisks indicate significant differences in Δ*acoN* compared to wild type as indicated by *t*-test ($p < 0.01$).

own promoter, grew better on acetoin under blue light than in the dark, therefore restoring the wild-type phenotype (**Figure 4B**). Similar results were obtained when acetoin 10 and 15 mM was used as sole carbon source (**Supplementary Figure S2**).

These results show that light modulation of acetoin catabolism depends on the BlsA photoreceptor and the AcoN negative regulator in *A. baumannii* ATCC 17978. Opposite behavior is observed for Δ*blsA* and Δ*acoN* mutants regarding modulation of growth on acetoin by light, indicating that BlsA is necessary for the observed induction, while AcoN for repression. The overall evidence prompts us to postulate a model in which BlsA interacts with AcoN under blue light at 23°C antagonizing this repressor, with the concomitant induction of acetoin catabolic genes' expression as well as growth on acetoin in this condition. It is important to mention that the viability of cells was not affected by light, as similar growth curves were obtained for the different strains in the complex media LB under blue light and in the dark (**Figures 4C,D**).

Light Regulates Expression of the Acetoin Catabolic Pathway Through BlsA and AcoN at Moderate Temperatures in *A. baumannii*

We then monitored AcoN functioning in response to light by measuring the expression of AcoN-regulated genes under different illumination conditions and genetic backgrounds. To this end, the expression of the acetoin catabolic genes *acoA*, *acoB*, and *acoC* (**Figures 5A–C** respectively) was analyzed by qRT-PCR at different light conditions at moderate temperatures in *A. baumannii* strain ATCC 17978. Our results show that the expression levels of these genes were basal in the dark at 23°C in M9 minimal medium with acetoin as sole carbon source. However, their expression was significantly induced in the presence of blue light (**Figure 5**). In Δ*blsA* mutants, expression of *acoA–C* genes was basal and comparable between blue light and dark, and similar to that observed for the wild type in the dark at 23°C (**Figure 5**). Thus, light modulates the expression of the acetoin catabolic genes, *acoA–C* through BlsA. On its side, the Δ*acoN* mutant also lost photoregulation, i.e., expression levels of *acoA–C* genes were similar between the illuminated or dark conditions. However, for this mutant, expression levels were much higher even than those registered in the wild-type under blue light, i.e., in the induced condition (**Figure 5**). Indeed, *acoA* expression levels in the Δ*acoN* mutant were approximately twofold higher than in the wild type under blue light, while *acoB* and *acoC* expression levels were about threefold higher, and >100-folds higher than the wild type in the dark. Opposite behavior is observed for Δ*blsA* and Δ*acoN* mutants regarding modulation of *acoA–C* genes' expression, suggesting that BlsA is necessary for the observed induction while AcoN for repression. Altogether, BlsA antagonizes the functioning of AcoN under blue light at 23°C, with the concomitant induction of the expression of AcoN-regulated genes at this condition. By analogy with a mechanism described previously for BlsA and Fur (Tuttobene et al., 2018), we hypothesized that BlsA might interact with the AcoN negative regulator, antagonizing its functioning.

BlsA Interacts With the Acetoin Catabolic Negative Regulator AcoN Under Illumination at Moderate Temperatures in *A. baumannii*

Yeast two-hybrid assay experiments were conducted to study if BlsA interacts with AcoN, using an adapted system from ProQuest™ Two-Hybrid System, as previously described (Tuttobene et al., 2018). The system includes strain Mav 203, which harbors three reporter genes with different promoters to avoid false positives: *lacZ* and two auxotrophic markers HIS3 and URA3. If the two proteins studied do interact, the appearance of blue color as well as growth in the absence of histidine or uracil would be observed. Gateway-system vectors pGAD-T7Gw and pGBK-T7Gw adapted to Y2H express each of the studied genes, *blsA* and *acoN*, as fusions to GAL4 DNA DB or AD. In each plate were also included self-activation controls (pGAD-T7Gw and pGBK-T7Gw empty vectors) as well as different strength interaction controls (A–E), to give an indication of the reporter genes' expression levels. In our previous report (Tuttobene et al., 2018), we observed that BlsA protein interactions depend on illumination and temperature conditions, so we decided to test its interaction with AcoN, the acetoin catabolism negative regulator, under different conditions. **Figure 6** shows results of Y2H assay experiments at the different conditions analyzed. At 23°C under blue light (**Figure 6**), the interaction between BlsA and AcoN was demonstrated by the appearance of blue color and growth in SC defined media without the supplementation of histidine or uracil, i.e., results were consistent for the three reporters analyzed. The interactions occurred independently of the vector used, as both pGAD*blsA*/pGBK*acoN* and pGAD*acoN*/pGBK*blsA* combinations produced signals (**Table 5**). Growth on SC–Ura

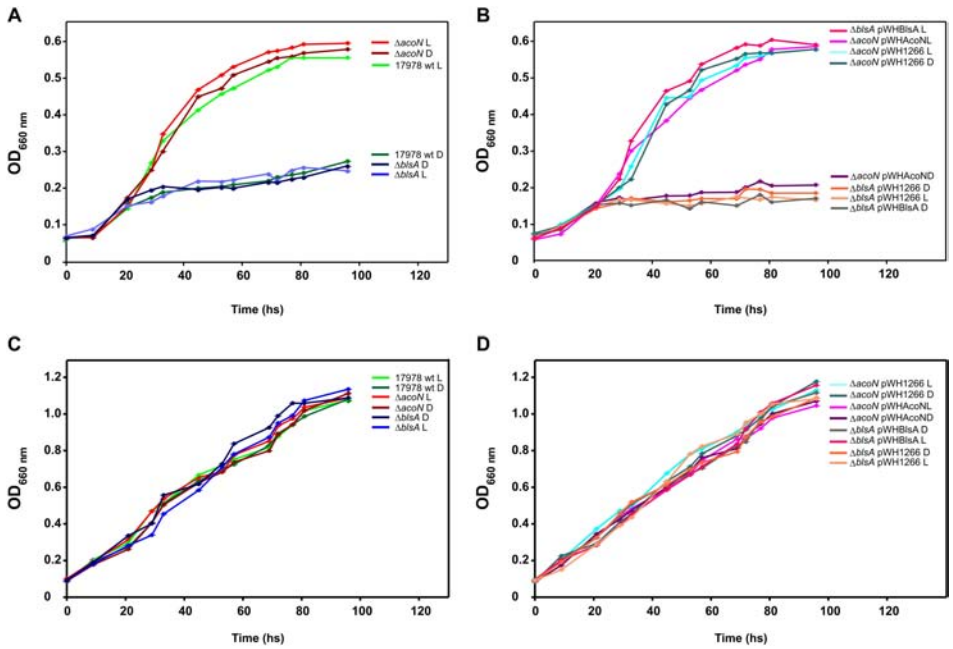

FIGURE 4 | Light modulates acetoin catabolism at moderate temperatures in *A. baumannii* ATCC 17978. **(A,B)** Growth curves in M9 minimal medium supplemented with acetoin 5 mM as sole carbon source of *A. baumannii* ATCC 17978 wild-type and derivative strains, incubated stagnantly at 23°C under blue light (L) or in the dark (D). **(C,D)** Growth curves in LB medium of *A. baumannii* ATCC 17978 wild-type and derivative strains incubated stagnantly at 23°C under blue light (L) or in the dark (D). Growth was measured by determining the optical density at 660 nm. The experiments were performed at least in triplicate, including three replicates for each strain at each condition. Representative results are shown.

plates indicates a strong interaction between BlsA and AcoN in the conditions analyzed, since the *URA3* reporter is the least sensitive[1]. Moreover, controls indicated absence of self-activation of each protein fused to DB or AD: (pGAD-T7/pGBK*blsA* or pGBK*acoN*) or (pGBK-T7/pGAD*blsA* or pGAD*acoN*) (**Table 5**). The overall data provide convincing evidence indicating that BlsA interacts with AcoN at 23°C under blue light. However, no positive signal was detected for AcoN–BlsA interaction by Y2H assays for any of the reporters tested at 23°C in the dark, while interaction controls behaved as expected (**Figure 6** and **Table 5**). Altogether, the data account for BlsA interacting with AcoN in a light-dependent manner at moderate temperatures. **Table 5** summarizes the results obtained for Y2H.

AcoN Does Not Modulate A1S_1697 Expression in Response to Light

We next analyzed the possibility that AcoN would be directly controlling the expression of the other putative transcriptional regulator identified in this cluster (gene 1, A1S_1697) in *A. baumannii* (**Figure 2**), which by analogy with *acoR* from *B. subtilis* might be an activator of the acetoin cluster. Whether this hypothesis is correct, AcoN would modulate *acoA–C* in response to light indirectly by modulation of the functioning of the putative activator. For this purpose, we studied A1S_1697 expression at different illumination conditions and genetic backgrounds. If AcoN functions as a negative regulator of A1S_1697 expression in a light-dependent manner, then A1S_1697 transcripts levels would vary between light and dark conditions. This variation would level in the Δ*acoN* mutant between light and dark, and reach higher expression levels than the wild type, had it been the negative regulator. However, and as seen in **Figure 7**, A1S_1697 transcripts levels were similar between light and dark for all the genetic backgrounds analyzed, namely, the wild-type strain, and the Δ*blsA* and Δ*acoN* mutants. These results indicate that AcoN does not regulate A1S_1697 expression in response to light.

BlsA–AcoN Interaction Is Significantly Reduced at Higher Temperatures

Since BlsA and AcoN interact at 23°C under blue light, we wondered whether this interaction is conserved at higher temperatures. Thus, BlsA–AcoN interactions were studied by Y2H at a temperature that supports yeast growth such as 30°C. A control at 23°C under blue light was always included for each repetition. **Figure 6** shows representative Y2H results indicating null or negligible BlsA–AcoN interactions at 30°C, neither in the dark nor under blue light.

Light Does Not Modulate Acetoin Catabolism at Higher Temperatures

We next studied whether acetoin catabolic gene expression and growth was modulated by light at 30°C, since no interaction between BlsA and AcoN was detected at this temperature. As

[1]http://www.invitrogen.com/content/sfs/manuals/10835031.pdf

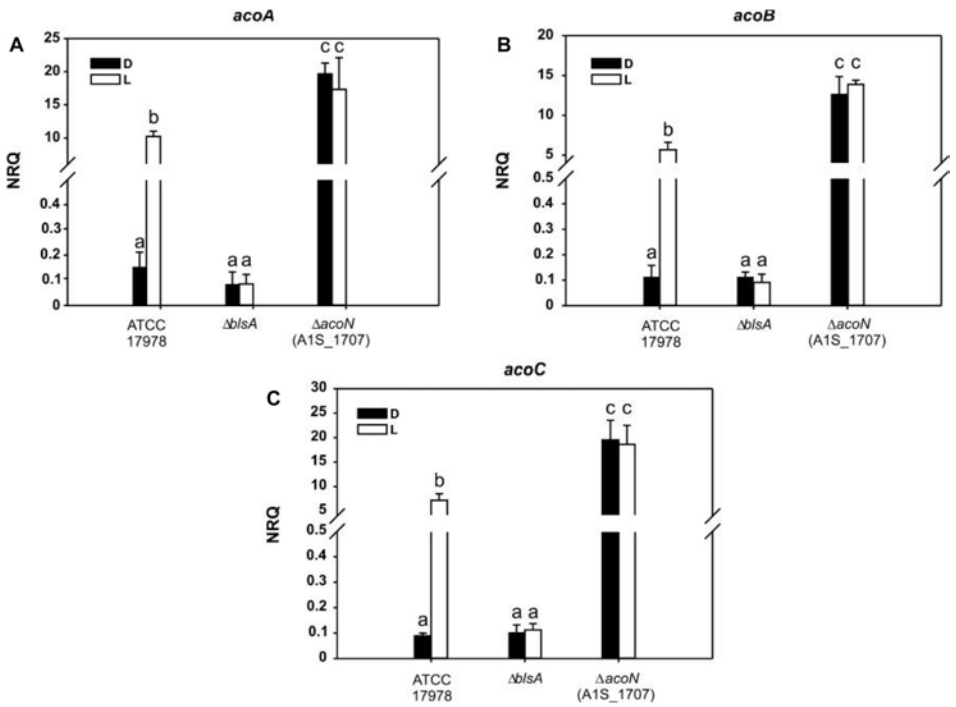

FIGURE 5 | Acetoin catabolism genes are induced under blue light at moderate temperatures. **(A–C)** Estimation of the expression levels of representative genes of the acetoin catabolic cluster, acoA–C, by RT-qPCR in *A. baumannii* ATCC 17978 wild-type as well as Δ*blsA* and Δ*acoN* genetic backgrounds at 23°C under blue light (L) or in the dark (D). The data shown are mean ± SD of normalized relative quantities (NRQs) calculated from transcript levels measured in samples grown in M9 minimal media supplemented with acetoin as sole carbon source under blue light or in the dark at 23°C, in at least three biological replicates. Different letters indicate significant differences as determined by ANOVA followed by Tukey's multiple comparison test ($p < 0.01$).

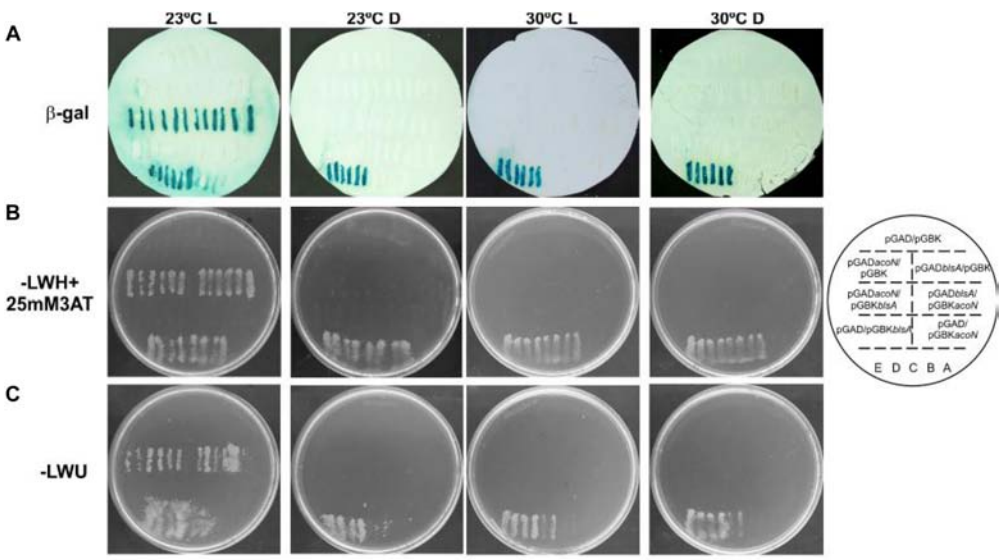

FIGURE 6 | BlsA interacts with AcoN only under blue light at moderate temperatures in *A. baumannii*. BlsA–AcoN interaction was analyzed by Y2H assays at different conditions including 23°C under blue light (L) or in the dark (D), and 30°C under blue light (L) or in the dark, following procedures described in Cribb and Serra (2009) and Tuttobene et al. (2018). In each plate were patched six clones of MaV203/pGAD-*blsA* or MaV203/pGAD-*acoN* transformed with plasmids pGBK-*acoN* or pGBK-*blsA*, respectively, as well as plasmid pGBK-T7 as negative control. Reciprocal combinations were also included, as well as self-activation and different strength interaction controls (strains A–E). The scheme on the right side represents the order of yeast streaks on each plate. Panel **A** shows results for the *lacZ* reporter, panel **B** for the histidine auxothropic reporter and panel **C** for the uracil reporter. Experiments were performed in triplicates and representative results are shown.

TABLE 5 | The interaction between AcoN and BlsA was determined by the yeast two hybrid assay, using GAL4 activation domain (AD) and DNA-binding domain (BD) fusion proteins.

β-Gal	Empty vector pGAD-T7	BlsA_AD	AcoN_AD
Empty vector pGBK-T7	–	–	–
AcoN BD	–	+	ND
BlsA_BD	–	ND	+
HIS 3			
Empty vector pGBK-T7	–	–	–
AcoN BD	–	+	ND
BlsA_BD	–	ND	+
URA3			
Empty vector pGBK-T7	–	–	–
AcoN BD	–	+	ND
BlsA_BD	–	ND	+

Both combinations of fusion proteins (AcoN_BD vs. BlsA_AD and BlsA _BD vs. AcoN_AD) were assayed giving the same results with all three reporter genes (β-Gal, HIS 3, and URA 3). +, means reporter gene expression induced by a positive interaction; –, means no interaction, confirming that no "self-activation" of the fusion proteins may result in the reporters expression (interactions using pGAD-T7 and pGBK-T7 empty vectors in combination with the fusion proteins); ND, means that self-interactions of AcoN and BlsA were not determined.

expected, *acoA*, *acoB*, and *acoC* gene expression showed no differential modulation by light neither in *A. baumannii* ATCC 17978 wild type, nor in the Δ*blsA* or Δ*acoN* mutants at this condition (**Figure 8A**). At 30°C, *acoA–C* expression levels in the Δ*blsA* mutant were similar to the wild-type strain both under blue light and in the dark, i.e., were repressed; while they were induced in the Δ*acoN* mutant both under blue light and in the dark. This behavior was congruent with growth curves performed in M9 minimal media supplemented with acetoin as sole carbon source, which showed no significant difference between light and dark for any of the studied strains (**Figures 8B,C**). Here again, the Δ*acoN* mutant showed enhanced growth consistent with the absence of the negative regulator, as also did the Δ*acoN* mutant containing pWH1266 (**Figures 8B,C**). The overall data indicate that light does not influence acetoin catabolism at 30°C or above, and are in agreement with available knowledge regarding BlsA functioning (Mussi et al., 2010; Golic et al., 2013; Abatedaga et al., 2017).

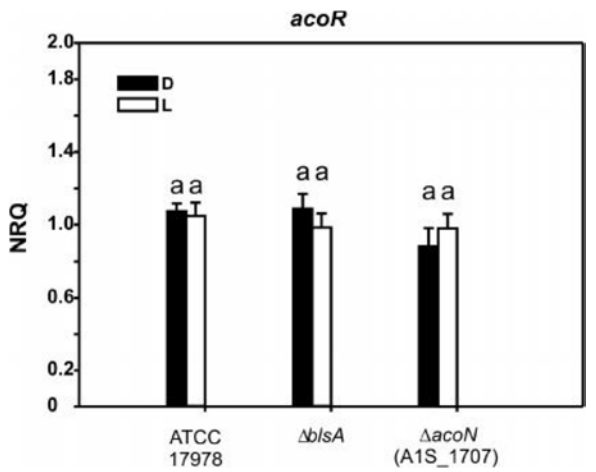

FIGURE 7 | A1S_1697 expression does not depend on light nor on AcoN. Estimation of the expression levels of A1S_1697 by RT-qPCR in *A. baumannii* ATCC 17978 wild-type as well as Δ*blsA* and Δ*acoN* genetic backgrounds at 23°C under blue light (L) or in the dark (D). The data shown are mean ± SD of NRQs calculated from transcript levels measured in samples grown in M9 minimal media supplemented with acetoin as sole carbon source under blue light or in the dark at 23°C, in at least three biological replicates. Different letters indicate significant differences as determined by ANOVA followed by Tukey's multiple comparison test ($p < 0.01$).

DISCUSSION

Acinetobacter sp. are extremely well adapted to different hostile environments thanks to several molecular mechanisms that enable survival under stress conditions. Here, we characterized the *Acinetobacter* sp. 5-2Ac02 strain isolated from the air in a hospital from Brazil. *Acinetobacter* sp. 5-2Ac02 showed an antibiotic susceptible profile. It includes a bla_{oxa-58} gene as well as *tet* genes, which have been related to resistance to tetracycline, coded in its genome. This susceptible strain carrying these cryptic genes hence represents a clinical threat as it may act as a reservoir of resistance genes. The high arsenic MIC for *Acinetobacter* sp. strain 5-2Ac02 may be attributed to the arsenic operon, arsC1–arsR–arsC2–ACR–arsH, which has only been described in the *Pseudomonas stutzeri* TS44 (Barbosa et al., 2016).

We further analyzed the global gene expression adjustments in this strain in response to environmental stressors such as mitomycin C and found induction of genes coding for components of the SOS response, genes involved in numerous TA systems (RelBE, HigBA, parDE, and other two new TA systems) (Barbosa et al., 2016), and resistance to heavy metals and antioxidant enzymes. The TA systems have been shown to be involved both in tolerance and persistence, which presuppose the ability of the bacteria to grow slowly or enter into a dormant state, respectively, to cope with the presence of a stressor (Fernandez-Garcia et al., 2018). It is thus not surprising that in the presence of mitomycin C and ciprofloxacin a tolerance phenotype was observed in killing curves (**Figure 1**). Furthermore, the ability of *A. baumannii* to survive for long periods of desiccation has been related to the achievement of dormant states, via mechanisms affecting control of cell cycling, DNA coiling, transcriptional and translational regulation, protein stabilization, antimicrobial resistance, and toxin synthesis (Gayoso et al., 2014). The fact that this airborne strain, in which desiccation is a common feature in its lifestyle, harbors and modulates numerous determinants leading to persistence in adverse environmental conditions is thus aligned with this notion.

Under pressure from the quorum network, both AHLs and 3-oxo-C12-HSL compounds induced the expression of a cluster involved in acetoin/butanediol metabolism in *Acinetobacter* sp. 5-2Ac02, which was also shown to be induced by light

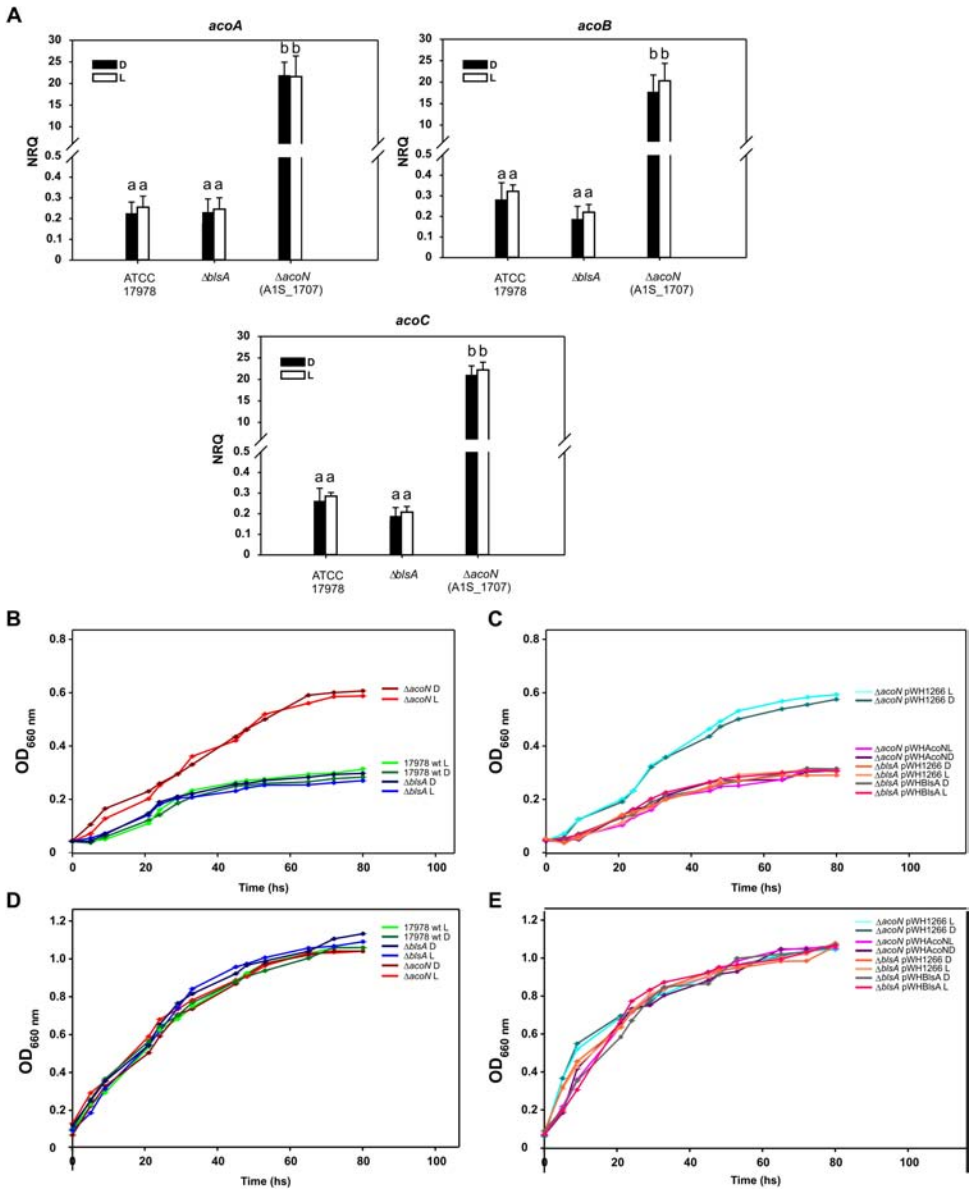

FIGURE 8 | Light does not modulate acetoin catabolism at higher temperatures. **(A)** Estimation of the expression levels of representative genes components of the acetoin catabolic cluster, *acoA–C*, by RT-qPCR in *A. baumannii* ATCC 17978 wild-type as well as Δ*blsA* and Δ*acoN* genetic backgrounds under blue light (L) or in the dark (D) at 30°C. The data shown are mean ± SD of NRQs calculated from transcript levels measured in samples grown in M9 minimal media supplemented with acetoin as sole carbon source under blue light or in the dark at 30°C, in at least three biological replicates. Different letters indicate significant differences as determined by ANOVA followed by Tukey's multiple comparison test ($p < 0.01$). **(B,C)** Growth curves in M9 minimal media supplemented with acetoin as sole carbon source of *A. baumannii* ATCC 17978 wild-type and derivative strains incubated stagnantly under blue light or in the dark at 30°C. **(D,E)** Growth curves of *A. baumannii* ATCC 17978 wild-type and derivative strains in LB media incubated stagnantly under blue light (L) or in the dark (D) at 30°C. Growth was measured by determining the optical density at 660 nm. The experiments were performed at least in triplicates, including three repetitions for each strain at each condition. Representative results are shown.

in *A. baumannii* (Muller et al., 2017). Acetoin (3-hydroxy-2-butanone) is a four carbon neutral molecule used as substrate by various microorganisms, with multiple usages in flavor, cosmetic, and chemical synthesis (Xiao et al., 2007). In *B. subtilis*, acetoin is a significant product generated from glucose metabolism in aerobiosis. Given its neutral nature, acetoin allows the consumption of important quantities of glucose without acidification of the medium. It can also serve as a carbon reserve which can be expelled to the exterior and later re-internalized (Ali et al., 2001). Acetoin and BD are also BVCs, which can influence bacterial pathogenesis (Audrain et al., 2015) by altering the production of virulence factors (Venkataraman et al., 2014) or by affecting host cell functions (Kurita-Ochiai et al., 1995). In addition to the

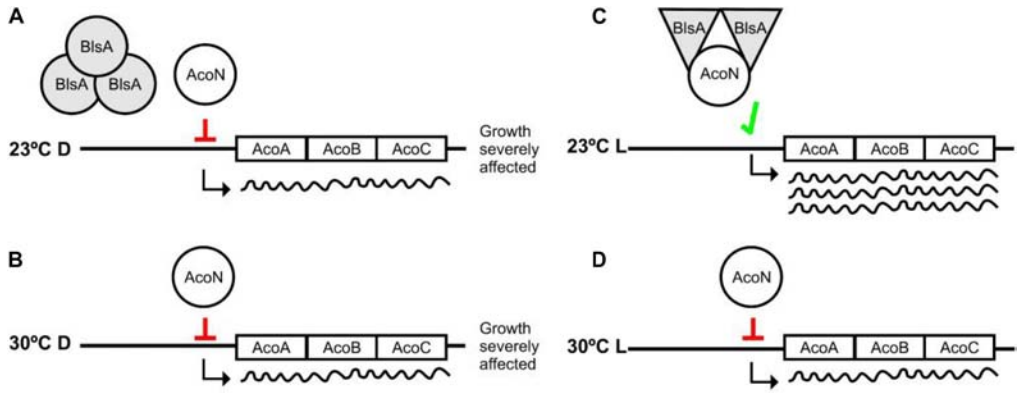

FIGURE 9 | Working model representing photoregulation of acetoin catabolism through AcoN and BlsA. At 23°C in the dark, BlsA and AcoN do not interact, and AcoN represses expression of the acetoin catabolic genes acoA, acoB, and acoC **(A)**. As a result, growth on acetoin as sole carbon source is severely affected. Under blue light, BlsA acquires an excited state now capable of interacting with AcoN, antagonizing its functioning, allowing expression from the acetoin catabolic operon, and supporting growth **(B)**. Overall, BlsA finely tunes AcoN levels in response to light, modulating therefore acetoin catabolism. At 30°C, both under blue light or in the dark, BlsA does not interact with AcoN maintaining therefore its functioning as a repressor **(C,D)**, resulting growth severely affected at this condition.

fundamental ecological interest, a better understanding of environmental bacteria and of the roles of BVCs (including BD), metabolic pathways, and mechanisms involved could provide new information about the bacterial response to the environment, thus potentially leading to clinical or industrial applications.

Comparisons of the genetic organization of this cluster from *Acinetobacter* sp. 5-2Ac02 with that of *A. baumannii* ATCC 17978 guided us to further study a gene annotated as a putative transcriptional regulator, then designated AcoN by us. We show here that it behaves as a negative regulator of the acetoin/butanediol cluster in an *A. baumannii* and is involved in photoregulation of acetoin catabolism in *A. baumannii* through the photoreceptor BlsA. In this context, we have recently shown that BlsA binds to and antagonizes the functioning of the transcriptional repressor Fur only in the dark at 23°C, likely by reducing its ability to bind to acinetobactin promoters with the concomitant enhanced gene expression and growth under iron deprivation at this condition (Tuttobene et al., 2018). In this work, we have broadened our understanding of BlsA functioning by showing that this photoreceptor can antagonize the functioning of other transcriptional regulators also under blue light such as AcoN. Our results support a model in which the system is at a basal level or repressed state in most conditions, for example in the dark at 23°C as well as at 30°C both in the dark or under blue light, i.e., AcoN is repressing acetoin catabolic genes' transcription resulting in basal gene expression levels as well as severely affected growth on acetoin (**Figure 9**). However, under blue light at 23°C the system gets derepressed: BlsA binds to the acetoin repressor AcoN antagonizing its functioning, likely by reducing its ability to bind to acetoin catabolic genes' promoters, allowing thus their expression at this condition (**Figure 9**). Overall, the global regulator BlsA functions both under blue light and in the dark at low–moderate temperatures modulating different transcriptional regulators, such as Fur and AcoN, as well as the corresponding sets of regulated genes and the corresponding cellular processes. In this sense, BlsA probes to be unique among described photoreceptors regarding its dual activity under illumination and in the dark. Indeed, many photoreceptors have been shown to antagonize transcriptional repressors (Tuttobene et al., 2018), such as AppA from *Rhodobacter sphaeroides* (Pandey et al., 2017), PixD from *Synechocystis* sp. PCC6803 (Fujisawa and Masuda, 2017), and YcgF from *E. coli* (Tschowri et al., 2012). However, their functioning has been reported to occur in the dark for the first two or under blue light for the last one. This constitutes therefore the first report showing that a single photoreceptor can act both under blue light and in the dark for differential modulation by light of diverse cellular processes.

The fact that BlsA-Fur modulates photoregulation of iron uptake, while BlsA–AcoN modulates photoregulation of acetoin catabolism in *A. baumannii* at low–moderate temperatures such as 23°C but not 30°C, is consistent with previous findings of our group. In fact, we have previously showed that BlsA integrates a temperature signal in addition to light by mechanisms affecting different points of regulation. On the one side, *blsA* expression levels are very much reduced at 30 or 37°C with respect to 23°C, which correlates with negligible photoreceptor levels in the cells at 37°C (Abatedaga et al., 2017; Tuttobene et al., 2018), while the other point of control by temperature affects BlsA photoactivity (Abatedaga et al., 2017).

The mechanism by which BlsA perceives light and differentially binds to transcriptional regulators is not clear and could result from differential properties displayed by the photoreceptor at each condition, for example regarding the oligomerization state. In this sense, our results show that BlsA forms oligomers both under blue light or in the dark at 23°C (Tuttobene et al., 2018). Yet, variations in the composition or order level of these oligomers at each condition could account

for differential functioning, as is the case of *Synechocystis* sp. PCC6803 PixD (Fujisawa and Masuda, 2017).

Many questions arise from our findings such as why photoregulation of acetoin catabolism at moderate temperatures has evolved in this pathogen. Likely, the answer lies in the lifestyle carried out by the microorganism at this condition. In this context, and as mentioned before, it has been shown that utilization of BD, a common fermentation product of *P. aeruginosa* co-habitant bacteria, significantly increases virulence and infection of the microorganism (Venkataraman et al., 2014; Nguyen et al., 2016; Liu et al., 2018). The activation of the pathway of BD utilization through acetoin by light observed could plausibly go in this same sense too in *A. baumannii*. Indeed, we have already seen that light induces factors related to virulence and/or persistence in the environment such as the type VI secretion system T6SS, the phenylacetic acid catabolic pathway, trehalose biosynthesis, tolerance to antibiotics, production of antioxidant enzymes, etc. (Muller et al., 2017), which could ultimately contribute to persistence and competition with other microorganisms in the habitat.

Future experiments will be devoted to provide a detailed characterization of the mechanism of photoregulation directed by BlsA, AcoN, and their targets. First, we will conduct gel mobility assays (EMSA) to prove that AcoN is a DNA-binding transcriptional regulator, as is strongly suggested by BLAST sequence homology analyses, which show 97–100% identity with proteins annotated as sigma-54-dependent Fis family DNA-binding transcriptional regulators in *A. baumannii*. If BlsA interacts with AcoN under blue light avoiding or reducing its ability to bind to target promoter regions, as proposed by the evidence accumulated in this work, then the addition of BlsA to these EMSA assays should reduce the delay observed for the AcoN-DNA probe. DNase protection assays will further characterize the AcoN-DNA binding region. Furthermore, by solving the 3D structures and conducting ultrafast structural dynamic studies of BlsA alone as well as bound to AcoN under blue light, we expect to gain detailed knowledge on structural as well as photochemical aspects of the light signal transduction mechanism.

Finally, we show in this work that quorum network modulators as well as light both regulate the acetoin catabolic cluster. Whether these are independent signals or share totally or partially the signal transduction cascade components is actually under study in our laboratories.

DATA AVAILABILITY

The datasets generated for this study can be found in GEO, GSE120392.

AUTHOR CONTRIBUTIONS

MRT and GLM performed the experiments. PC performed the experiments and collaborated in writing the manuscript. LF-G, LB, and AA performed the experiments and mutant strain. RER and RL-R analyzed the experiments. FF-C and IB analyzed the array studies. BB, RT, ML, and GB developed the RT-PCR experiments. MT designed the experiments. MAM and MT designed the experiments, wrote the manuscript, and provided funding.

FUNDING

This study was funded by grant PI16/01163 awarded to MT within the State Plan for R+D+I 2013–2016 (National Plan for Scientific Research, Technological Development and Innovation 2008–2011) and co-financed by the ISCIII-Deputy General Directorate for Evaluation and Promotion of Research – European Regional Development Fund "A way of Making Europe" and Instituto de Salud Carlos III FEDER, Spanish Network for the Research in Infectious Diseases (REIPI, RD16/0016/0001, RD16/0016/0006, and RD16/0016/0008) and by the Study Group on Mechanisms of Action and Resistance to Antimicrobials, GEMARA (SEIMC, http://www.seimc.org/). MT was financially supported by the Miguel Servet Research Program (SERGAS and ISCIII). RT and LF-G were financially supported by, respectively, a SEIMC grant and predoctoral fellowship from the Xunta de Galicia (GAIN, Axencia de Innovación). BB was financially supported by CAPES, Process: PDSE 99999.001069/2014-04. This work was also supported by grants from the Agencia Nacional de Promoción Científica y Tecnológica (PICT 2014-1161) and ASaCTeI (Ministerio de Ciencia, Tecnología e Innovación Productiva de la Provincia de Santa Fe) 2010-147-16 to MAM. PC, GLM, and MAM are career investigators of CONICET. MRT is a fellow from the same institution.

ACKNOWLEDGMENTS

We are very grateful to Prof. Elizabeth A. Marques and Prof. Robson Souza Leão (Department of Chemistry and Microbiology, Roberto Alcántara Gomes Institute, Universidade do Estado do Río de Janeiro, Rio de Janeiro, Brazil) for assistance with this research. We also thank Dr. Luis Martinez-Martinez (Department of Microbiology, Reina Sofia University Hospital, Spain) and Dr. Alvaro Pascual (Department of Microbiology, University Hospital Virgen, Macarena, Spain) for critical review of the manuscript.

SUPPLEMENTARY MATERIAL

The Supplementary Material for this article can be found online at: https://www.frontiersin.org/articles/10.3389/fmicb.2019.01376/full#supplementary-material

REFERENCES

Abatedaga, I., Valle, L., Golic, A. E., Muller, G. L., Cabruja, M., Moran Vieyra, F. E., et al. (2017). Integration of temperature and blue-light sensing in *Acinetobacter baumannii* through the BlsA sensor. *Photochem. Photobiol.* 93, 805–814. doi: 10.1111/php.12760

Akinbowale, O. L., Peng, H., Grant, P., and Barton, M. D. (2007). Antibiotic and heavy metal resistance in motile aeromonads and pseudomonads from rainbow trout (*Oncorhynchus mykiss*) farms in Australia. *Int. J. Antimicrob. Agents* 30, 177–182. doi: 10.1016/j.ijantimicag.2007.03.012

Ali, N. O., Bignon, J., Rapoport, G., and Debarbouille, M. (2001). Regulation of the acetoin catabolic pathway is controlled by sigma L in *Bacillus subtilis*. *J. Bacteriol.* 183, 2497–2504. doi: 10.1128/JB.183.8.2497-2504.2001

Aranda, J., Poza, M., Pardo, B. G., Rumbo, S., Rumbo, C., Parreira, J. R., et al. (2010). A rapid and simple method for constructing stable mutants of *Acinetobacter baumannii*. *BMC Microbiol.* 10:279. doi: 10.1186/1471-2180-10-279

Audrain, B., Letoffe, S., and Ghigo, J. M. (2015). Airborne bacterial interactions: functions out of thin air? *Front. Microbiol.* 6:1476. doi: 10.3389/fmicb.2015.01476

Barbosa, B. G., Fernandez-Garcia, L., Gato, E., Lopez, M., Blasco, L., Leao, R. S., et al. (2016). Genome sequence of airborne *Acinetobacter* sp. strain 5-2ac02 in the hospital environment, close to the species of *Acinetobacter towneri*. *Genome Announc.* 4:e01343-16. doi: 10.1128/genomeA.01343-16

Castañeda-Tamez, P., Ramírez-Peris, J., Pérez-Velázquez, J., Kuttler, C., Jalalimanesh, A., Saucedo-Mora, M. Á., et al. (2018). Pyocyanin Restricts Social Cheating in *Pseudomonas aeruginosa*. *Front. Microbiol.* 9:1348. doi: 10.3389/fmicb.2018.01348

Cribb, P., and Serra, E. (2009). One- and two-hybrid analysis of the interactions between components of the *Trypanosoma cruzi* spliced leader RNA gene promoter binding complex. *Int. J. Parasitol.* 39, 525–532. doi: 10.1016/j.ijpara.2008.09.008

Fernández-Cuenca, F., Tomás, M., Caballero-Moyano, F. J., Bou, G., Martínez-Martínez, L., Vila, J., et al. (2015). Reduced susceptibility to biocides in *Acinetobacter baumannii*: association with resistance to antimicrobials, epidemiological behaviour, biological cost and effect on the expression of genes encoding porins and efflux pumps. *J. Antimicrob. Chemother.* 70, 3222-3229. doi: 10.1093/jac/dkv262

Fernandez-Garcia, L., Fernandez-Cuenca, F., Blasco, L., Lopez-Rojas, R., Ambroa, A., Lopez, M., et al. (2018). Relationship between tolerance and persistence mechanisms in *Acinetobacter baumannii* strains with AbkAB toxin-antitoxin system. *Antimicrob. Agents Chemother.* 62:e00250-18. doi: 10.1128/AAC.00250-18

Fujisawa, T., and Masuda, S. (2017). Light-induced chromophore and protein responses and mechanical signal transduction of BLUF proteins. *Biophys. Rev.* 10, 327–337. doi: 10.1007/s12551-017-0355-6

Gayoso, C. M., Mateos, J., Mendez, J. A., Fernandez-Puente, P., Rumbo, C., Tomas, M., et al. (2014). Molecular mechanisms involved in the response to desiccation stress and persistence in *Acinetobacter baumannii*. *J. Proteome Res.* 13, 460–476. doi: 10.1021/pr400603f

Gietz, R. D., and Woods, R. A. (2002). Transformation of yeast by lithium acetate/single-stranded carrier DNA/polyethylene glycol method. *Methods Enzymol.* 350, 87–96.

Golic, A., Vaneechoutte, M., Nemec, A., Viale, A. M., Actis, L. A., and Mussi, M. A. (2013). Staring at the cold sun: blue light regulation is distributed within the genus *Acinetobacter*. *PLoS One* 8:e55059. doi: 10.1371/journal.pone.0055059

Hamad, M. A., Zajdowicz, S. L., Holmes, R. K., and Voskuil, M. I. (2009). An allelic exchange system for compliant genetic manipulation of the select agents *Burkholderia pseudomallei* and *Burkholderia mallei*. *Gene* 430, 123–131. doi: 10.1016/j.gene.2008.10.011

Hellemans, J., Mortier, G., De Paepe, A., Speleman, F., and Vandesompele, J. (2007). qBase relative quantification framework and software for management and automated analysis of real-time quantitative PCR data. *Genome Biol.* 8:R19. doi: 10.1186/gb-2007-8-2-r19

Hofsteenge, N., van Nimwegen, E., and Silander, O. K. (2013). Quantitative analysis of persister fractions suggests different mechanisms of formation among environmental isolates of *E. coli*. *BMC Microbiol.* 13:25. doi: 10.1186/1471-2180-13-25

Hunger, M., Schmucker, R., Kishan, V., and Hillen, W. (1990). Analysis and nucleotide sequence of an origin of DNA replication in *Acinetobacter calcoaceticus* and its use for *Escherichia coli* shuttle plasmids. *Gene* 87, 45–51. doi: 10.1016/0378-1119(90)90494-C

Karah, N., Haldorsen, B., Hegstad, K., Simonsen, G. S., Sundsfjord, A., Samuelsen, O., et al. (2011). Species identification and molecular characterization of *Acinetobacter* spp. blood culture isolates from Norway. *J. Antimicrob. Chemother.* 66, 738–744. doi: 10.1093/jac/dkq521

Kurita-Ochiai, T., Fukushima, K., and Ochiai, K. (1995). Volatile fatty acids, metabolic by-products of periodontopathic bacteria, inhibit lymphocyte proliferation and cytokine production. *J. Dent. Res.* 74, 1367–1373. doi: 10.1177/00220345950740070801

Liu, Q., Liu, Y., Kang, Z., Xiao, D., Gao, C., Xu, P., et al. (2018). 2,3-Butanediol catabolism in *Pseudomonas aeruginosa* PAO1. *Environ. Microbiol.* 20, 3927–3940. doi: 10.1111/1462-2920.14332

Lopez, M., Blasco, L., Gato, E., Perez, A., Fernandez-Garcia, L., Martinez-Martinez, L., et al. (2017a). Response to bile salts in clinical strains of *Acinetobacter baumannii* lacking the AdeABC efflux pump: virulence associated with quorum sensing. *Front. Cell Infect. Microbiol.* 7:143. doi: 10.3389/fcimb.2017.00143

Lopez, M., Mayer, C., Fernandez-Garcia, L., Blasco, L., Muras, A., Ruiz, F. M., et al. (2017b). Quorum sensing network in clinical strains of *A. baumannii*: AidA is a new quorum quenching enzyme. *PLoS One* 12:e0174454. doi: 10.1371/journal.pone.0174454

Lopez, M., Rueda, A., Florido, J. P., Blasco, L., Fernandez-Garcia, L., Trastoy, R., et al. (2018). Evolution of the quorum network and the mobilome (plasmids and bacteriophages) in clinical strains of *Acinetobacter baumannii* during a decade. *Sci. Rep.* 8:2523. doi: 10.1038/s41598-018-20847-7

McConnell, M. J., Actis, L., and Pachon, J. (2013). *Acinetobacter baumannii*: human infections, factors contributing to pathogenesis and animal models. *FEMS Microbiol. Rev.* 37, 130–155. doi: 10.1111/j.1574-6976.2012.00344.x

Muller, G. L., Tuttobene, M., Altilio, M., Martinez Amezaga, M., Nguyen, M., Cribb, P., et al. (2017). Light modulates metabolic pathways and other novel physiological traits in the human pathogen *Acinetobacter baumannii*. *J. Bacteriol.* 199:e00011-17. doi: 10.1128/JB.00011-17

Mussi, M. A., Gaddy, J. A., Cabruja, M., Arivett, B. A., Viale, A. M., Rasia, R., et al. (2010). The opportunistic human pathogen *Acinetobacter baumannii* senses and responds to light. *J. Bacteriol.* 192, 6336–6345. doi: 10.1128/JB.00917-10

Nguyen, M., Sharma, A., Wu, W., Gomi, R., Sung, B., Hospodsky, D., et al. (2016). The fermentation product 2,3-butanediol alters *P. aeruginosa* clearance, cytokine response and the lung microbiome. *ISME J.* 10, 2978–2983. doi: 10.1038/ismej.2016.76

O'Gara, J. P., Gomelsky, M., and Kaplan, S. (1997). Identification and molecular genetic analysis of multiple loci contributing to high-level tellurite resistance in *Rhodobacter sphaeroides* 2.4.1. *Appl. Environ. Microbiol.* 63, 4713–4720.

Pandey, R., Armitage, J. P., and Wadhams, G. H. (2017). Use of transcriptomic data for extending a model of the AppA/PpsR system in *Rhodobacter sphaeroides*. *BMC Syst. Biol.* 11:146. doi: 10.1186/s12918-017-0489-y

Ramirez, M. S., Muller, G. L., Perez, J. F., Golic, A. E., and Mussi, M. A. (2015). More than just light: clinical relevance of light perception in the nosocomial pathogen *Acinetobacter baumannii* and other members of the genus *Acinetobacter*. *Photochem. Photobiol.* 91, 1291–1301. doi: 10.1111/php.12523

Spellberg, B., and Bonomo, R. A. (2013). "Airborne assault": a new dimension in *Acinetobacter baumannii* transmission. *Crit. Care Med.* 41, 2042–2044. doi: 10.1097/CCM.0b013e31829136c3

Spellberg, B., and Bonomo, R. A. (2014). The deadly impact of extreme drug resistance in *Acinetobacter baumannii*. *Crit. Care Med.* 42, 1289–1291. doi: 10.1097/CCM.0000000000000181

Tacconelli, E., Carrara, E., Savoldi, A., Harbarth, S., Mendelson, M., Monnet, D. L., et al. (2018). Discovery, research, and development of new antibiotics: the WHO priority list of antibiotic-resistant bacteria and tuberculosis. *Lancet Infect. Dis.* 18, 318–327. doi: 10.1016/S1473-3099(17)30753-3

Taylor, D. E., Rooker, M., Keelan, M., Ng, L. K., Martin, I., Perna, N. T., et al. (2002). Genomic variability of O islands encoding tellurite resistance in enterohemorrhagic *Escherichia coli* O157:H7 isolates. *J. Bacteriol.* 184, 4690–4698.

Trastoy, R., Manso, T., Fernandez-Garcia, L., Blasco, L., Ambroa, A., Perez Del Molino, M. L., et al. (2018). Mechanisms of bacterial tolerance and persistence in the gastrointestinal and respiratory environments. *Clin. Microbiol. Rev.* 31:e00023-18. doi: 10.1128/CMR.00023-18

Tschowri, N., Lindenberg, S., and Hengge, R. (2012). Molecular function and potential evolution of the biofilm-modulating blue light-signalling pathway of *Escherichia coli*. *Mol. Microbiol.* 85, 893–906. doi: 10.1111/j.1365-2958.2012.08147.x

Turton, J. F., Shah, J., Ozongwu, C., and Pike, R. (2010). Incidence of Acinetobacter species other than *A. baumannii* among clinical isolates of Acinetobacter: evidence for emerging species. *J. Clin. Microbiol.* 48, 1445–1449. doi: 10.1128/JCM.02467-09

Tuttobene, M. R., Cribb, P., and Mussi, M. A. (2018). BlsA integrates light and temperature signals into iron metabolism through Fur in the human pathogen *Acinetobacter baumannii*. *Sci. Rep.* 8:7728. doi: 10.1038/s41598-018-26127-8

Venkataraman, A., Rosenbaum, M. A., Werner, J. J., Winans, S. C., and Angenent, L. T. (2014). Metabolite transfer with the fermentation product 2,3-butanediol enhances virulence by *Pseudomonas aeruginosa*. *ISME J.* 8, 1210–1220. doi: 10.1038/ismej.2013.232

Xiao, Z., and Xu, P. (2007). Acetoin metabolism in bacteria. *Crit. Rev. Microbiol.* 33, 127–140. doi: 10.1080/10408410701364604

Xiao, Z. J., Liu, P. H., Qin, J. Y., and Xu, P. (2007). Statistical optimization of medium components for enhanced acetoin production from molasses and soybean meal hydrolysate. *Appl. Microbiol. Biotechnol.* 74, 61–68. doi: 10.1007/s00253-006-0646-5

Yakupogullari, Y., Otlu, B., Ersoy, Y., Kuzucu, C., Bayindir, Y., Kayabas, U., et al. (2016). Is airborne transmission of *Acinetobacter baumannii* possible: a prospective molecular epidemiologic study in a tertiary care hospital. *Am. J. Infect. Control* 44, 1595–1599. doi: 10.1016/j.ajic.2016.05.022

Conflict of Interest Statement: The authors declare that the research was conducted in the absence of any commercial or financial relationships that could be construed as a potential conflict of interest.

frontiers in Microbiology

REVIEW
published: 17 July 2019
doi: 10.3389/fmicb.2019.01601

The Mechanisms of Disease Caused by *Acinetobacter baumannii*

*Faye C. Morris[1], Carina Dexter[1], Xenia Kostoulias[1], Muhammad Ikhtear Uddin[1] and Anton Y. Peleg[1,2]**

[1]Infection and Immunity Program, Department of Microbiology, Monash Biomedicine Discovery Institute, Monash University, Clayton, VIC, Australia, [2]Department of Infectious Diseases, The Alfred Hospital and Central Clinical School, Monash University, Melbourne, VIC, Australia

Acinetobacter baumannii is a Gram negative opportunistic pathogen that has demonstrated a significant insurgence in the prevalence of infections over recent decades. With only a limited number of "traditional" virulence factors, the mechanisms underlying the success of this pathogen remain of great interest. Major advances have been made in the tools, reagents, and models to study *A. baumannii* pathogenesis, and this has resulted in a substantial increase in knowledge. This article provides a comprehensive review of the bacterial virulence factors, the host immune responses, and animal models applicable for the study of this important human pathogen. Collating the most recent evidence characterizing bacterial virulence factors, their cellular targets and genetic regulation, we have encompassed numerous aspects important to the success of this pathogen, including membrane proteins and cell surface adaptations promoting immune evasion, mechanisms for nutrient acquisition and community interactions. The role of innate and adaptive immune responses is reviewed and areas of paucity in our understanding are highlighted. Finally, with the vast expansion of available animal models over recent years, we have evaluated those suitable for use in the study of *Acinetobacter* disease, discussing their advantages and limitations.

Keywords: *A. baumannii*, host-pathogen interactions, animal models, immune response, bacterial virulence factors

OPEN ACCESS

Edited by:
Maria Alejandra Mussi, National Council for Scientific and Technical Research (CONICET), Argentina

Reviewed by:
Jason Sahl, Northern Arizona University, United States
Jose Ramos-Vivas, Instituto de Investigación Marques de Valdecilla (IDIVAL), Spain

***Correspondence:**
Anton Y. Peleg
anton.peleg@monash.edu

Specialty section:
This article was submitted to Infectious Diseases, a section of the journal Frontiers in Microbiology

Received: *15 January 2019*
Accepted: *26 June 2019*
Published: *17 July 2019*

Citation:
Morris FC, Dexter C, Kostoulias X, Uddin MI and Peleg AY (2019) The Mechanisms of Disease Caused by Acinetobacter baumannii. Front. Microbiol. 10:1601. doi: 10.3389/fmicb.2019.01601

INTRODUCTION

Acinetobacter baumannii is a Gram negative, obligate aerobe, coccobacillus, and one of the most prevalent causes of nosocomial infections (Martín-Aspas et al., 2018). The burgeoning resistance of *A. baumannii* to primary antimicrobial therapies has created a deadly combination of pathogenicity and antimicrobial resistance that plagues hospitals (Roca et al., 2012). Classified as an ESKAPE pathogen (*Enterococcus faecium, Staphylococcus aureus, Klebsiella pneumoniae, Acinetobacter baumannii, Pseudomonas aeruginosa*, and *Enterobacter* species), carbapenem-resistant *A. baumannii* is considered the World Health Organization's number one critical priority pathogen for which new therapeutics are urgently required (Shlaes and Bradford, 2018). Concerns continue to grow that without a significant intervention, hospital-acquired *A. baumannii* infections will soon be untreatable.

Acinetobacter phylogenetics has undergone significant changes, originally described as *Micrococcus*, with the designation of *Acinetobacter* only being proposed in the 1950's (Peleg et al., 2008a). Since then, *Acinetobacter* taxonomy has been reclassified and over 50 different species have been identified to date (Harding et al., 2017a). While *A. baumannii*, *A. nosocomialis*

and *A. pittii* are the most commonly isolated hospital species, *A. baumannii* international clonal types 1 and 2 are the most prominent, with lineage 3 largely restricted to Europe (Wallace et al., 2016; Weber et al., 2016). For more information on genomic diversity, the reader is directed to the following articles (Diancourt et al., 2010; Antunes et al., 2014; Touchon et al., 2014; Meumann et al., 2019).

With only a limited number of "traditional" virulence factors, which are not always present or conserved across all strains, the mechanisms contributing to the success of *A. baumannii* are of increasing interest to researchers and clinicians alike. This article summarizes the knowledge of characterized virulence factors (depicted in **Figure 1**) and the host immune responses (depicted in **Figure 2**) that contribute to both its success and clearance *in vivo*, with a final overview of the available animal models, evaluating their advantages and limitations.

CLINICAL SIGNIFICANCE

A. baumannii causes a range of infections in both the hospital and community, including skin and soft tissue, urinary tract infections, meningitis, bacteremia, and pneumonia, with the latter being the most frequently reported infection in both settings (Dexter et al., 2015). Hospital-acquired infections are most commonly seen in critically ill patients; specific risk factors for developing an *A. baumannii* infection include prolonged hospital stays, immune suppression, advanced age, presence of comorbid diseases, major trauma or burns, previous antibiotic use, invasive procedures, and presence of indwelling catheters or mechanical ventilation (García-Garmendia et al., 2001; Robenshtok et al., 2006; Karageorgopoulos and Falagas, 2008; Wong et al., 2017). Due to the already poor prognosis of critically ill patients who acquire *A. baumannii* infections, it is difficult to attribute a definitive mortality rate (Freire et al., 2016); however crude morality rates have ranged from 23 to 68% (Eliopoulos et al., 2008).

Community-acquired infections present as a distinct and severe clinical syndrome in countries with hot and humid climates. These infections typically occur in individuals with underlying health conditions, including diabetes mellitus and chronic obstructive pulmonary disease, or in those that are heavy smokers or drink alcohol in excess (Falagas et al., 2007; Dexter et al., 2015). Mortality rates for community-acquired *A. baumannii* infections have been reported as high as 64% (Anstey et al., 1992; Patamatamkul et al., 2017); however, it is currently unknown as to whether host or bacterial factors are responsible for the difference in disease presentation between community and hospital infections.

BACTERIAL PATHOGENESIS

Virulence Factors

Outer Membrane Components

Outer Membrane Proteins

Outer membrane protein A (OmpA, previously Omp38) is the most abundant *A. baumannii* outer membrane protein (OMP)

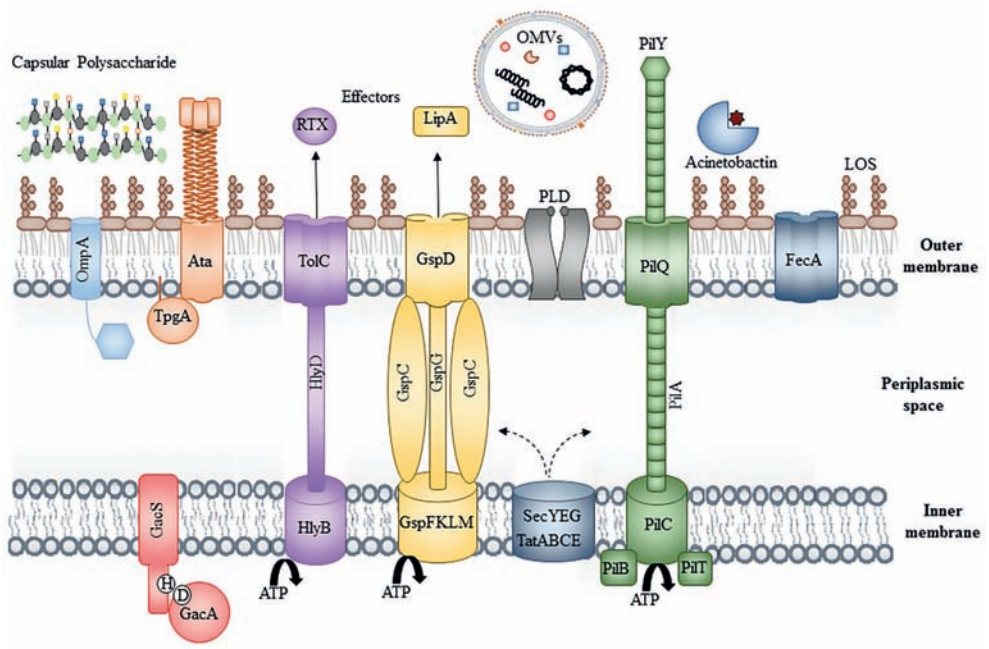

FIGURE 1 | Bacterial virulence factors. Schematic of the bacterial cell envelope depicting some of the known virulence factors, including OmpA, the Type II, IV, and V secretion systems, phospholipase D (PLD), iron acquisition systems (Acinetobactin and FecA), the inner membrane two-component system, GacAS and extracellular factors, including lipid oligosaccharide, capsular polysaccharide, and outer membrane vesicles. For simplicity, peptidoglycan has been excluded and individual components are not to scale.

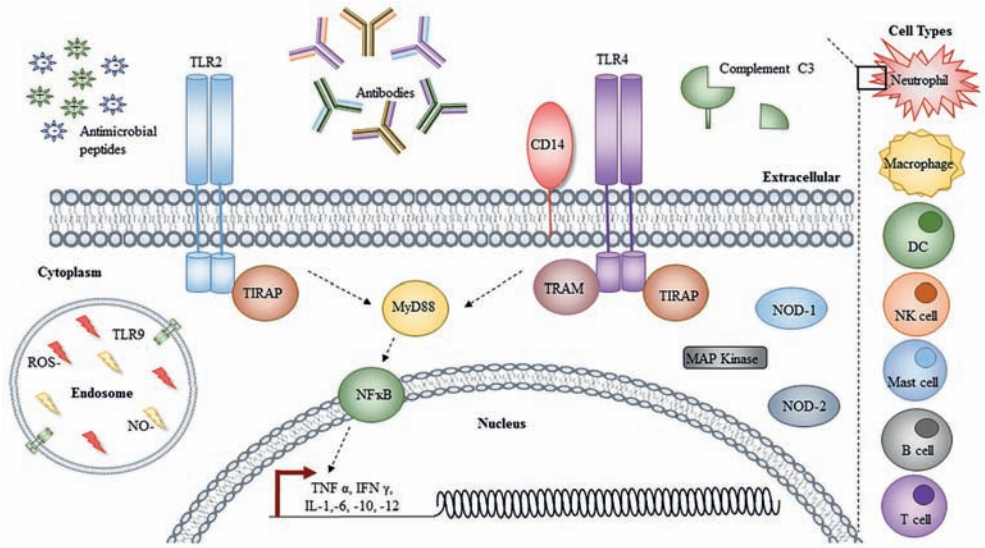

FIGURE 2 | Immune responses to *Acinetobacter.* Immune cells involved in the clearance of *Acinetobacter* infections are denoted on the right-hand side, with an insert depicting the cellular components responsible. The toll-like receptor (TLR) 2 and 4 signaling leads to activation of NFκB *via* MyD88, resulting in transcriptional activation and the synthesis of a range of cytokines and chemokines. Other cytoplasmic proteins shown to be involved in response to *Acinetobacter* infection are highlighted, with TLR9 localized to the endosome, in conjugation with reactive oxygen species (ROS) and nitric oxide (NO). Extracellular components, including cationic and anionic antimicrobial peptides, antibodies, and C3 complement are depicted left to right. For simplicity, not all proteins involved in the TLR signaling pathways are depicted and individual components are not to scale.

(Hee et al., 2008) and one of the most well-characterized virulence factors. OmpA is highly conserved, with 83 of 103 clinical isolates showing greater than 99% sequence identity, with the most diverse having 85% sequence identity (Ahmad et al., 2016; Ansari et al., 2018; Iyer et al., 2018). As such, OmpA has often been promoted as an attractive target for vaccine development. OmpA forms an eight-stranded β barrel in the OM, with a 2-nm pore diameter and C-terminal periplasmic globular extension, accommodating molecules up to 500 Da (Sugawara and Nikaido, 2012; Iyer et al., 2018). In contrast to other major porins, such as OmpF/C from *E. coli*, *A. baumannii* OmpA has significantly reduced permeability, thought to contribute to the overall reduction in *A. baumannii* OM permeability (Sugawara and Nikaido, 2012). To date, only the C-terminal periplasmic domain has been crystalized (1.6 Å) and shown to directly interact with peptidoglycan through Asp271 and Arg286 binding to diaminopimelate (Park et al., 2012). This interaction is thought to influence the packing of OMPs into outer membrane vesicles (OMVs), though this has yet to be confirmed, and may be merely a consequence of altered membrane homeostasis in an *ompA* mutant (Moon et al., 2012).

During normal growth and *in vivo* infection, OmpA is preferentially concentrated into OMVs (Moon et al., 2012). The interaction of OmpA (on the bacterial cell surface or OMVs) with eukaryotic cells induces cytotoxicity, through binding and adhesion to eukaryotic cell surface death receptors (Ahmad et al., 2016). Upon internalization, OmpA translocates to either the mitochondria or the nucleus (Hee et al., 2005, 2008; Rumbo et al., 2014). In the mitochondria, OmpA induces proapoptotic signals, through the activation of Bcl-2 family proteins, the release of cytochrome C and apoptosis-inducing factor (Hee et al., 2005). OmpA can also be translocated to the nucleus courtesy of its self-encoded nuclear localization signal (KTKEGRAMNRR), which is absent from other *A. baumannii* OMPs, and causes host DNA degradation in a DNase I-like manner (Hee et al., 2008; Choi et al., 2008a; Rumbo et al., 2014). In addition to its cytotoxic properties, OmpA modulates a range of other virulence attributes, including resistance to alternate complement-mediated killing through factor H binding and promoting adhesion to extracellular matrix proteins, including fibronectin, which is important for lung epithelial colonization (Kim et al., 2009; Smani et al., 2012).

Recent years have seen an expansion in our knowledge of other OMPs contributing to *A. baumannii* pathogenesis. Omp34 (otherwise termed Omp33–36) is highly conserved in *A. baumannii*, present in >1,600 strains with ≥98% identity (Rumbo et al., 2014). Similar to OmpA, Omp34 induces apoptosis in eukaryotic cells through caspase-dependent mechanisms and inhibition of autophagy, promoting bacterial persistence in the autophagosome (Rumbo et al., 2014; Jahangiri et al., 2018). Omp34 has also been shown to bind fibronectin and is selectively concentrated into OMVs (Smani et al., 2012). Shown to be important for systemic virulence in murine models, Omp34 is highly immunogenic, driving potent IgA/G/M antibody responses in sera from infected patients (Islam et al., 2011; Jahangiri et al., 2018). Additionally, OmpW also forms an eight-stranded OM β barrel protein, which is both highly immunogenic and concentrated in OMVs, though the functional role of this protein is thought to be related to iron acquisition and antibiotic resistance (Huang et al., 2015; Manuella et al., 2016).

Surface Antigen 1 (SurA) is another OMP that was identified from the chicken isolate CCGGD201101 (Liu et al., 2016). The relevance of this OMP to human clinical isolates is yet to be determined. While numerous other OMPs have been identified and characterized, these are discussed later in the context of bacterial nutrient acquisition, as they do not encode conventional virulence factors.

Lipopolysaccharide, Lipoolgiosaccharide, and Capsule

Similar to all other OM components, the Lipopolysaccharide (LPS), Lipoolgiosaccharide (LOS), and capsule are all synthesized in the cytoplasm and translocated to the outer leaflet of the cell envelop by dedicated proteinaceous machinery.

LPS is comprised of three distinct components: the lipid A anchor, glycosylated with core oligosaccharides, to which the O-antigen repeat is attached. In contrast, LOS does not contain O-antigen and instead has extended core oligosaccharides (Whitfield and Trent, 2014; Weber et al., 2016; Joseph and Stephen, 2018). Synthesized in the cytoplasm by the multistep Raetz pathway, both types are transported from the inner membrane to the cell surface by the Lpt pathway. Despite encoding two potential *waaL* O-antigen ligase homologs, *A. baumannii* does not produce O-antigen or LPS, and instead decorates the OM with LOS. Furthermore, subsequent analysis of these *waaL* genes has shown they are responsible for protein glycosylation (Iwashkiw et al., 2012).

Lipid A is the immunostimulatory component of LPS and LOS and previously thought to be essential in all Gram negative bacteria. Within the last decade, *Acinetobacter* has become only the third Gram negative pathogen capable of survival in the absence of lipid A, where previously only *Neisseria meningitidis* and *Moraxella catarrhalis* were thought to have this capacity (Moffatt et al., 2010). Lipid A minus *A. baumannii* was first identified in response to *in vitro* colistin exposure, resulting in inactivation of *lpxA*, *lpxC*, or *lpxD* in ATCC 19606 (Moffatt et al., 2010). Interestingly, with the exception of *lpxA*, *lpxC*, *lpxD*, and *lptD*, all other LOS biosynthetic genes are essential due to the resultant accumulation of toxic intermediates (Joseph and Stephen, 2018). For several years, the loss of lipid A was thought to be restricted to specific *A. baumannii* strains; however, recent efforts have shown that the levels of penicillin-binding protein PBP1a and, specifically, its glycosyltransferase activity are critical to the ability to lose lipid A (Boll et al., 2016). As lipid A is the major stimulus for toll like receptor (TLR) 4, it is unsurprising that lipid A minus strains reduce TLR4 signaling, but elevate TLR2 stimulation (Moffatt et al., 2013), thought to be as a result of the increased OM lipoprotein exposure. In contrast to LOS deficiency, *A. baumannii* more frequently modifies the lipid A moiety to promote antimicrobial resistance. Unlike other Gram negative pathogens, *A. baumannii* does not encode a PagP homolog; therefore, modification of the hexa-acylated lipid A occurs through the addition of one and two lauryl acyl chains during synthesis by the activity of LpxL and LpxM, respectively (Boll et al., 2015; Lopalco et al., 2017). This modification results in hepta-acylated lipid A that is more resistant to cationic antimicrobial peptides, less stimulatory of TLR4 and implicated in desiccation survival (Boll et al., 2015). By contrast to that of LOS minus strains, lipid A modification does not induce the same biological burden, and thus is readily detected in clinical isolates.

Capsule forms a protective layer on the extracellular surface, mediating resistance to cationic antimicrobial peptides and serum, subsequently enhancing *in vivo* survival (Geisinger and Isberg, 2015). Capsule loci in *A. baumannii* are highly variable, with conserved 5′ and 3′ genes capping the variable central cluster (Hu et al., 2013; Geisinger and Isberg, 2015). The 5′ *wza*, *wzb*, and *wzc* encode the assembly and export machinery complex spanning the inner and outer membranes, promoting transport of capsular polysaccaride from the periplasm to the cell surface (Kenyon and Hall, 2013; Senchenkova et al., 2015). The 3′ genes encode UDP-linked sugar synthases and epimerases, responsible for the conversion of UDP-D-glucose, UDP-D-galactose, and UDP-D-glucuronic acid to UDP-N acetyl-D-glucosaminuronic acid or UDP-N acetyl-D-galactosaminuronic acid, respectively (Hu et al., 2013; Kenyon and Hall, 2013). Other epimerases are encoded by central genes and/or at distinct sites around the chromosome, while glycosyltransferases and UndP lipid carriers responsible for the construction of the repeating unit, work in concert with wzx and wzy to translocate these components to the periplasm for polymerization and presentation to the Wzabc complex (Kenyon and Hall, 2013).

Capsule production is negatively regulated by the BfmRS two-component regulatory system (TCS) in response to environmental stimuli, including particular antibiotics (chloramphenicol and erythromycin), resulting in increased expression and antimicrobial resistance (Geisinger and Isberg, 2015). Furthermore, the presence or absence of capsule has also been linked to *Acinetobacter* phenotypic switching, whereby the opaque virulent form is characterized by enhanced capsule production, in contrast with the translucent avirulent form, which displays two-fold less capsule production (Chin et al., 2018).

Phospholipase

Phospholipases are well-established virulence factors and *Acinetobacter* encodes both phospholipase C and D enzymes, differentiated by their cleavage position preference resulting in a phospho head group (phospholipase C) or phosphatidic acid and a separate head group (phospholipase D) (Schmiel and Miller, 1999). *A. baumannii* encodes two phospholipase C and three phospholipase D enzymes, all with substrate specificity toward the eukaryotic membrane component, phosphatidylcholine (Stahl et al., 2015; Fiester et al., 2016). Interestingly, both enzymes are transcriptionally regulated by the ferric uptake regulator (Fur) and display hemolytic activity against human erythrocytes, aiding in iron acquisition (Fiester et al., 2016). Consistent with this important role, phospholipase C is conserved across numerous strains, including ATCC 19606, ATCC 17978, ACICU, AYE, and AB0057 (Fiester et al., 2016).

Similarly, the three phospholipase D genes are associated with serum resistance, epithelial cell invasion, and *in vivo* pathogenesis (Jacobs et al., 2010; Stahl et al., 2015). Two phospholipase D enzymes appear to be as a result of a gene duplication, identifiable by two catalytic domains containing the HxKx4Dx6GS/GGxN (HKD) motif, while phospholipase

D3 contains only one (Stahl et al., 2015). Despite the similarity, phospholipase D2 has been shown to be more important for invasion than the other two, though the deletion of all three induces only marginal defects in virulence in a *Galleria mellonella* model (Stahl et al., 2015).

Secretion Systems

Acinetobacter encodes a diverse range of secretion systems. The Type I secretion system (T1SS) is a tripartite system, delivering proteins from the cytosol to the extracellular environment. In *Acinetobacter*, the T1SS is homologous to that of the prototypical HlyBD-TolC system from *E. coli*, consisting of an IM ATP-binding protein, periplasmic adaptor, and OM pore (Harding et al., 2017b). *A. nosocomialis* strain M2 was the first *Acinetobacter* strain shown to encode an active T1SS, with two putative effector proteins, RTX (containing an RTX toxin domain) and Bap (homologous to the biofilm associated protein) (Harding et al., 2017b). Interestingly, the activity of the T1SS in this strain was shown to have a direct impact on the Type VI secretion system (T6SS), suggestive of cross talk between these systems (Harding et al., 2017b).

The Type IV secretion system (T4SS) is responsible for conjugative transfer of DNA, plasmids, and other mobile genetic elements. To date, only three reports address the T4SS in *Acinetobacter* (Smith et al., 2007; Iacono et al., 2008; Liu et al., 2014). *A. baumannii* strain ATCC 17978 encodes eight genes homologous to those of the *Legionella/Coxiella* T4SS, while strains ACICU and TYTH-1 harbor plasmids encoding complete *tra* loci on pACICU2 and pAB-CC, respectively (Smith et al., 2007; Iacono et al., 2008; Liu et al., 2014). While these features are of critical importance in the transfer of genetic material, particularly that of antibiotic resistance determinants, their role in host-pathogen interactions has yet to be elucidated.

T6SSs are capable of targeting both eukaryotic and prokaryotic cells, though in *Acinetobacter* the T6SS exclusively targets other bacteria, secreting a range of toxins, including peptidoglycan hydrolases, nucleases, or those targeting cell membranes (Elhosseiny and Attia, 2018; Fitzsimons et al., 2018). Interestingly, despite its role in bacterial competition, clinical isolates with active T6SS are isolated from immunocompromised patients at higher frequencies (Repizo, 2017), suggestive of a competitive advantage, although this may be due to their bactericidal activity against competing pathogens.

Type II Secretion System

The Type II secretion system (T2SS) is a two step secretion mechanism, dependent on Sec or Tat for substrate translocation to the periplasm prior to secretion. The T2SS was first described in ATCC 17978, with the apparatus encoded by genes designated, general secretory pathway (GspA-O), distributed across discrete clusters and not a single operon (Eijkelkamp et al., 2014). Effector proteins include enzymes such as lipase, elastase, alkaline phosphatase, and phospholipases, critical for *A. baumannii* virulence (Elhosseiny and Attia, 2018).

In *A. baumannii*, specific T2SS effectors include the lipases, LipA and LipH, hydrolyzing long-chain fatty acids as carbon sources for growth, the metallo-endopeptidase, CpaA, responsible for fibrinogen and factor V degradation, while the PilD peptidase is shared between the T2SS and T4SS (Harding et al., 2016; Johnson et al., 2016; Weber et al., 2017). The importance of this system is delineated by the observed attenuation of various mutants (*gspD* and *lipA*) in both *G. mellonella* and murine models (Harding et al., 2016; Johnson et al., 2016).

Type V Secretion System

The Type V secretion system (T5SS) (autotransporters) is the simplest and most widespread secretion system in Gram negative bacteria (Henderson et al., 2000). They are identifiable by their distinct domain architecture, including a N-terminal Sec-dependent signal peptide, a central passenger domain and C-terminal β barrel (Henderson et al., 2004). To date, five subdivisions of this family have been identified termed Type Va-Ve (Leo et al., 2012); however, *Acinetobacter* encodes only two, Type Vb (AbFhaB/C and CdiA/B) and one Type Vc (Ata) (Bentancor et al., 2012a,b; Pérez et al., 2017; Elhosseiny and Attia, 2018).

In the Type Vb subclass, the passenger and β domains are encoded as two distinct proteins from an operon termed TspA (AbFhaB) and TspB (AbFhaC), respectively (Jacob-Dubuisson et al., 2001; Pérez et al., 2017). AbFhaC encodes the 16-stranded β barrel, with two periplasmic polypeptide transport-associated domains for the recognition and translocation of AbFhaB to the cell surface, where the arginine-glycine-aspartate (RGD) motif binds eukaryotic integrin and fibronectin molecules (Jacob-Dubuisson et al., 2009; Pérez et al., 2017). Interestingly, while disruption of AbFhaC and subsequent loss of AbFhaB result in increased fertility of *Caenorhabditis elegans* and increased murine survival, it does not completely attenuate virulence (Pérez et al., 2017).

Contact-dependent inhibition (CDI) was first identified in 2005 as a T6SS-independent mechanism of bacterial cell killing. CdiA/B are considered to be Type Vb autotransporters, whereby CdiB forms the OM pore for the secretion of the CdiA toxin (containing numerous filamentous hemagglutinin domains) (Harding et al., 2017b). In contrast to traditional Type Vb autotransporters, a third component termed CdiI encodes an immunity protein (Harding et al., 2017b). Initially identified in *A. nosocomialis*, this operon has since been identified in the *A. baumannii* strains ATCC 19606 and 1225 (Harding et al., 2017b), although the mechanism of killing has yet to be determined.

Type Vc, Ata forms a trimeric autotransporter, with an extended signal peptide, and a smaller C-terminal β domain. Each monomer encodes 101 amino acids, contributing four β strands to the final homotrimer (Bentancor et al., 2012a). The passenger domain of each monomer consists of three subdomains, head, neck, and stalk, which trimerise to form the functional moiety (Koiwai et al., 2016). Ata contains four pentameric collagen-binding consensus sequences (SVAIG) and an RGD motif important for binding to extracellular matrix and basal proteins, including collagen I, III, IV, and V and laminin (Bentancor et al., 2012a). Deletion of this protein significantly reduces the ability of ATCC 17978 to form biofilms and completely attenuates *in vivo* virulence (Bentancor et al., 2012a).

Interestingly, Ata is produced in concert with TpgA, an OM lipoprotein anchor for Ata and although similar chaperones have been observed for other trimeric autotransporters, TpgA is unique in its OM localization (Ishikawa et al., 2016).

Efflux Systems

Bacterial efflux systems are membrane spanning, tripartite systems exhibiting broad substrate specificity, extruding potentially toxic compounds from the periplasm to the extracellular environment. To date, six bacterial efflux pump families have been identified, including the major facilitator superfamily (MFS), the multidrug and toxin extrusion family (MATE), the small multidrug resistance family (SMR), the resistance-nodulation-cell division superfamily (RND), and the proteobacterial antimicrobial compound efflux family (Du et al., 2018). In other Gram negative pathogens, efflux pumps play critical roles in the extrusion of bile salts and antimicrobial fatty acids and peptides or actively secrete virulence factors such as siderophores (Du et al., 2018). In *Acinetobacter*, AceI and the AdeABC efflux pumps promote resistance to biocides and aminoglycosides, respectively (Marchand et al., 2004; Hassan et al., 2013; Liu et al., 2018). While the majority of characterized efflux pumps have only been linked to the exclusion of toxic molecules, the AdeABC pump has been shown to impact bacterial fitness *in vivo* (Yoon et al., 2016). Overexpression of this particular pump in the drug susceptible strain BM4587 was shown to reduce bacterial burdens in the lungs and spleen at 8 h post infection when administered *via* the intraperitoneal route (Yoon et al., 2016). Conversely, transposon insertion mutants in AdeIJK and the toluene tolerance efflux transporter in AB5075 and ATCC17978, respectively, result in reduced bacterial persistence in *Galleria* larvae and a murine pneumonia model (Wang et al., 2014; Gebhardt et al., 2015). Although the mechanisms by which these efflux pumps contribute to virulence have yet to be elucidated, their complex genetic regulation implies a more significant role in bacterial homeostasis that has yet to be determined.

Outer Membrane Vesicles

OMVs are small, spherical vesicles, ranging in size between 10 and 300 nm, produced by all Gram negative species examined to date under varying growth conditions, indicative of an evolutionary conserved mechanism (Roier et al., 2016). In contrast to the name, these vesicles are an encapsulation of cytoplasmic components, IM, periplasmic proteins, and OM (Kulkarni and Jagannadham, 2014; Roier et al., 2016). Despite previously being considered a consequence of cell envelope stress, vesicle formation has recently been shown to be a natural process, though the exact mechanism of their biogenesis and differential packaging regarding the enrichment or depletion of particular OMPs or lipid species has yet to be determined (McBroom and Kuehn, 2005, 2007; Roier et al., 2016). It is unclear whether a dedicated mechanism exists or whether this is just a general secretory pathway responsive to different environmental conditions (Kato et al., 2002; Kuehn and Kesty, 2005; McMahon et al., 2012; Cahill et al., 2015). Currently, three hypotheses exist for their biogenesis: firstly, the loss of OM lipoprotein-peptidoglycan interactions leads to membrane protrusion and vesicle formation; second, the accumulation of misfolded proteins and peptidoglycan fragments in the periplasm lead to membrane bulging; third, the enrichment of molecules driving membrane curvature induces vesicle formation (Roier et al., 2016). Roiser et al. have shown that the OM lipoprotein VacJ in *Haemophilus influenzae* and *Vibrio cholerae* influences OMV phospholipid content, while in *A. baumannii* OmpA influences the OMP composition and abundance in OMVs, though further investigation is required to elucidate the mechanism (Moon et al., 2012; Roier et al., 2016).

OMVs have long been hypothesized to function as a bacterial defense mechanism against the host innate immune system (Beceiro et al., 2013) due to their association with bacterial signaling, modulation of host-pathogen interactions and immune evasion. *A. baumannii* OMVs provide an important mechanism for the secretion of OmpA and other putative virulence factors to host cells, through interactions with eukaryotic cholesterol micro-domains (Kwon et al., 2009; Jin et al., 2011). *In vivo* OMVs can stimulate immune responses through the activation of TLR signaling or modulate immune evasion through sequestration of innate immune factors (Kaparakis-Liaskos and Ferrero, 2015). For example in *E. coli*, OMVs have been shown to be produced in response to treatment with antimicrobial peptides, while in *H. influenzae* and *Moraxella catarrhalis*, OMVs promote serum resistance through the depletion of complement factors (Thuan Tong et al., 2007; Manning and Kuehn, 2011; Roier et al., 2016). Furthermore, OMVs provide a unique opportunity for bacterial dissemination of encapsulated genetic material within communities or across species. *Pseudomonas aeruginosa* OMVs have been shown to contain DNA and RNA capable of modulating host immune responses (Koeppen et al., 2016; Bitto et al., 2017). Similarly, multiple groups have shown *A. baumannii* clinical isolates utilize OMVs as a mechanism for dissemination of plasmids containing carbapenem resistance genes, including $bla_{\text{OXA-24}}$ and $bla_{\text{NDM-1}}$ (Rumbo et al., 2011; Chatterjee et al., 2017), highlighting the versatility of this system and the requirement for more in-depth analysis.

Nutrient Acquisition

Metal Acquisition

Iron

Iron is the most restricted nutrient in the human body. Bacteria have developed two scavenging mechanisms: direct uptake through receptors and transporters and high-affinity secreted iron chelator proteins (siderophores) (Eijkelkamp et al., 2011; De Léséleuc et al., 2014). *A. baumannii* strains encode up to five different siderophores. Cluster 1 comprises eight genes and a MFS family efflux pump, cluster 2 (only present in ATCC 17978) includes 15 genes with a separate MFS and MATE efflux pumps, cluster 3 is the well-characterized acinetobactin and ABC efflux pump, while cluster 4 is only found in strain 8399, and cluster 5 is present in most strains with the exception of ATCC 17978 (Eijkelkamp et al., 2011). Despite cluster variability, those described to date are all transcriptionally regulated by Fur, identifiable by the presence

of a Fur box sequence (a palindromic 25-nucleotide sequence) in their respective promoters (Eijkelkamp et al., 2011). In isolates, such as LAC-4 and SDF, the iron transporters and receptors FecI, FecR, and FecA are reported to enhance pathogenesis and growth capabilities of these strains through the utilization of heme (De Léséleuc et al., 2014).

Given the importance of iron-scavenging systems, it is unsurprising that disruption of these mechanisms causes dysregulation of other systems and virulence attenuation. In ATCC 17978, iron limitation results in a downregulation of Type 1 and Type IV pili (Eijkelkamp et al., 2011), while in ATCC 19606, disruption of the acinetobactin OM receptor, BauA, or the biosynthetic component, BasD, impairs intracellular persistence and killing of lung epithelial cells *in vitro*, though only varying degrees of attenuation are observed in *G. mellonella* and murine models (Gaddy et al., 2012). Similarly, disruption of Fur, iron-sulfur cluster assembly system (Isc), and/or other putative iron transporters (FeoA), leads to reduced bacterial biofilm formation, oxidative stress resistance, and *in vivo* pathogenesis (Ajiboye et al, 2018; Álvarez-Fraga et al., 2018). The phenotypes reported for *fur* mutants should be judged with caution due to the cross regulation with OxyR and SoxRS systems, which are associated with reactive oxygen detoxification and superoxide dismutase activation, and result in increased intracellular iron interacting with free radicals (Ajiboye et al., 2018). In contrast to that observed in the *G. mellonella* model, Fleming et al. reported that *A. baumannii* pathogenesis can be alleviated by the supply of excess iron to the surrounding environment when using a murine wound infection model, preventing the activation of iron-scavenging systems and virulence (Fleming et al., 2017).

Zinc and Manganese

Similar to iron, zinc is biologically important, acting as both a natural catalyst and cofactor for numerous proteins, with as many as 8% of *E. coli*-encoded proteins containing zinc-binding domains (Hood and Skaar, 2012). During the course of infection, the host can sequester metals by the action of the chelator protein calprotectin in a tactic termed "nutritional immunity" (Hood and Skaar, 2012; Nairn et al., 2016). *A. baumannii* regulates intracellular zinc concentrations by the activity of the ZnuABC transporter and ZigA GTPase, transcriptionally controlled by Zur (Mortensen et al., 2014; Nairn et al., 2016). While ZnuABC imports zinc into the cell, ZigA promotes its release through HutH activation and histidine catabolism (Mortensen et al., 2014; Nairn et al., 2016). This delicate balance between availability and toxicity results in a mild attenuation of *zigA* mutants in a murine pneumonia model, with less systemic dissemination from the lungs after infection (Nairn et al., 2016).

Although not characterized to the same degree, manganese starvation is of equal importance, whereby the NRAMP family transporter MumT and urea carboxylase, MumC, facilitate manganese accumulation in response to calprotectin (Juttukonda et al., 2016). Disruption of *mumT* significantly impacts bacterial colonization and dissemination from the lungs during pneumonia, a phenotype that is abolished in calprotectin-deficient mice (Juttukonda et al., 2016), further emphasizing the interplay of host and bacterial proteins in pathogenesis.

Community Interactions

Quorum Sensing

The ability of bacteria to sense, respond to, and communicate with neighboring cells is critical to the success of the population. Quorum sensing is the process by which bacteria detect and respond to hormone like molecules, such as acyl homoserine lactone, regulating numerous phenotypes, including motility and biofilm formation (Bhargava et al., 2010; Rutherford and Bassler, 2012). In the LuxRI family of proteins, LuxI synthesizes the acyl homoserine lactone, which interacts with the LuxR protein mediating the transcriptional response (Bhargava et al., 2010). In *A. baumannii*, *abaI* is responsible for the synthesis of N-(3-hydroxydodecanoyl)-L-HSL (3-hydroxy-C12-HSL), functioning in conjugation with the *abaR* LuxR homolog, to regulate biofilm maturation (Niu et al., 2008). Furthermore, the importance of this system in virulence has been demonstrated by the significant increase in murine survival rates during infection with *abaI* mutants (Bhuiyan et al., 2016).

Biofilm Formation

Biofilms are a bacterial lifestyle, constituting dynamic community environments, comprised of a heterogeneous protein matrix, nucleic acids, polysaccharides, and bacterial microcolonies, dispersed with water channels (Hall-Stoodley et al., 2004). *A. baumannii* forms biofilms on both biotic and abiotic surfaces, promoting survival on indwelling medical devices, hospital surfaces, or in otherwise unfavorable conditions. Biofilm formation is a multistage process, commencing with the initial attachment, proceeding to strong adhesion and aggregation of cells into microcolonies, followed by biofilm growth and maturation, prior to cell dispersal into the environment (Hall-Stoodley et al., 2004).

Biofilm formation on abiotic surfaces has contributed to the success of this pathogen in hospital environments, with their ability to adhere to medically relevant surfaces, such as titanium and polystyrene (Loehfelm et al., 2008; Brossard and Campagnari, 2011). Numerous strains encode for the Csu Type 1 chaperone-usher pili, associated with cell-to-cell attachment and biofilm initiation (Tomaras et al., 2008; Brossard and Campagnari, 2011). The operon contains six genes *csuA/B*, *A*, *B*, *C*, *D*, and *E*, encoding for pili and minor subunits, the chaperone, the usher and adhesive tip, respectively (Moon et al., 2017). Despite being predominantly regulated by BfmRS TCS, the GacAS TCS also modulates its expression, in addition to a putative folate-responsive riboswitch identified in the *csu* and *bfmR* promoters (Cerqueira et al., 2014; Moon et al., 2017), emphasizing the interplay between environmental signals and population dynamics. Despite BfmRS being predominantly associated with abiotic biofilms, this system is also linked to eukaryotic cell adhesion and antimicrobial resistance (Liou et al., 2014).

A. baumannii also produce the T1SS effector biofilm-associated protein, Bap, associated with abiotic and biotic biofilms. Homologous to that previously identified in *Staphylococcus*, it is defined by its immense size (over 800 kDa) and

immunoglobulin-like fold (Loehfelm et al., 2008; Brossard and Campagnari, 2011). In contrast to *Staphylococcus*, *A. baumannii* Bap contains four modules, A–D, with numerous internal repeats, promoting cell-to-cell adhesion and eukaryotic cell adhesion, through modulation of cell surface hydrophobicity (Loehfelm et al., 2008; Brossard and Campagnari, 2011). Interestingly, despite their clearly defined roles in biofilm formation, numerous strains contain mutations which disrupt the *csu* operon or *bap* gene abolishing their production, though the significance of these findings has yet to be determined (Goh et al., 2013; Wright et al., 2016).

In addition to the Csu pilus, *A. baumannii* encodes a second shorter (29 nm in length) chaperone usher Pap pilus, homologous to that of *E. coli* P pilin that is associated with eukaryotic cell adhesion (De Breij et al., 2009; Marti et al., 2011; Cerqueira et al., 2014). In addition to pilus complexes, proteins such as the autotransporter Ata and the extracellular poly-β-1,6-*N*-acetylglucosamine (PNAG) encoded for by *pgaABCD* locus have also been shown to mediate attachment and adhesion of cells in the biofilm (Choi et al., 2009; Brossard and Campagnari, 2011).

Genetic Regulation of Virulence Phenotypes

Transcriptional Regulation

In addition to TCS, a recent study identified a Tet-R family transcription factor (encoded by *ABUW_1645* in strain AB5075) involved in the regulation of phenotypic switching between two colony types, termed opaque and translucent (Tipton et al., 2015; Chin et al., 2018). These morphological differences were not due to genetic mutations, and instead were driven by changes in the expression of *ABUW_1645*, which regulates ~70% of the differentially expressed genes including capsule biosynthesis (Chin et al., 2018). Interestingly, it is this phase variation and morphological difference that causes striking differences in *in vivo* pathogenesis, with the translucent form being avirulent, and frequent reversion to the opaque form is observed in cultures recovered from murine lungs post infection (Tipton et al., 2015; Chin et al., 2018). Consistent with this virulence phenotype, the opaque form shows resistance to cathelicidin-related antimicrobial peptides, reactive oxygen species (ROS), lysozyme, disinfectant, and desiccation. Thus, unsurprisingly, the opaque form is routinely isolated from clinical samples (Chin et al., 2018). The translucent form is thought to be associated with environmental settings and bacteriophage resistance, with its increased biofilm formation at lower temperatures, reduced capsule and upregulated nutrient acquisition and catabolism-related genes (Chin et al., 2018).

H-NS

The H-NS transcription factor is associated with silencing horizontally acquired and/or AT-rich genes, limiting their potentially detrimental effects (Eijkelkamp et al., 2013). Previous studies have shown disruption of *hns* in either ATCC 17978 or clinical isolates results in a myriad of phenotypes including hypermotility, increased colistin resistance, adhesion to epithelial cells, and *in vivo* virulence in *Caenorhabditis elegans* (Eijkelkamp et al., 2013; Deveson Lucas et al., 2018). Transcriptomic analysis of *hns* disruption mutants reveals a vast number of dysregulated genes, including the significant overexpression of those associated with quorum sensing, OMPs, T5SS, T6SS, and fatty acid biosynthesis (Eijkelkamp et al., 2013).

Two-Component Regulatory Systems

Two-component regulatory systems (TCSs) impact a diverse range of phenotypes by modulating transcriptional regulation. They are usually found as a pair of regulatory proteins, including a membrane-bound sensor kinase and a separate DNA-binding transcriptional regulator, which respond to environmental conditions and/or cell stress (Stock et al., 2000; Zschiedrich et al., 2016). To our knowledge, six TCSs have been described in *A. baumannii*, including BfmSR associated with morphology, biofilm formation and adhesion to eukaryotic cells (Tomaras et al., 2008; Liou et al., 2014), PmrAB, modulating lipid A modifications in response to antimicrobial peptides and polymyxin (Adams et al., 2009; Arroyo et al., 2011), BaeSR and AdeRS, which modulate the expression of the AdeABC efflux pump (Marchand et al., 2004; Lin et al., 2014), CheAY regulating the chaperone/usher pili and AbaI quorum sensing (Chen et al., 2017) and GacAS, associated with pathogenesis and host immune evasion (Cerqueira et al., 2014; Bhuiyan et al., 2016).

While all the TCSs play important roles in bacterial homeostasis and physiology, the GacAS system plays a critical role in bacterial pathogenesis and host-pathogen interactions. GacAS is a global regulator, whereby disruption of either *gacA* or *gacS* abolishes the ability of ATCC 17978 to cause lethality in either *Candida albicans* or murine models (Cerqueira et al., 2014). GacS forms the inner membrane sensor kinase, with conserved histidine and aspartic acid residues at H299 and D719/771, respectively, responsible for the phosphorylation of the transcriptional response regulator GacA (Cerqueira et al., 2014). Although GacAS regulates a variety of genes, including *ompA*, *csu* operon, and *motB* to name but a few, its role in the regulation of the phenylacetate catabolite pathway (*paa* operon) is a significant factor contributing to pathogenesis (Cerqueira et al., 2014). Inhibition of this pathway resulted in increased neutrophil migration to the site of infection and bacterial clearance (Cerqueira et al., 2014; Bhuiyan et al., 2016). It should be noted though, consistent with other previously described TCSs, GacAS does display some degree of cross regulation with others; however, *paa* transcriptional regulation is specific to GacAS.

Post-transcriptional Regulation by Hfq

The global RNA chaperone Hfq is an important regulator of bacterial virulence in a range of pathogens. In *Salmonella* and *E. coli*, *hfq* mutations result in pleotropic effects, including reduced growth rates, changes in motility, biofilm formation, OMP levels, and attenuated *in vivo* virulence (Tsui et al., 1994; Bossi et al., 2008; Kulesus et al., 2008). Hfq can positively or negatively regulate messenger and/or small RNAs (sRNA) (Jousselin et al., 2009). Interestingly, *Acinetobacter* Hfq is almost double the size of that found in other gamma Proteobacteria, with an elongated C terminal, though the functional significance of this remains unknown (Kuo et al., 2017). Similar to other

species, *A. baylyi* and *A. baumannii hfq* mutants display pleotropic phenotypes, including reduced growth rates, elevated sensitivity to environmental stress, reductions in OMV production, fimbriae, biofilm formation and adhesion, invasion and survival in eukaryotic cells (Schilling and Gerischer, 2009; Kuo et al., 2017). Furthermore, changes in cytokine stimulation have been reported with these mutants, though these effects are cell line specific (Kuo et al., 2017). Despite *hfq* not being essential in ATCC 17978, this does not appear to be the case for all strains, as no *hfq* transposon insertion mutant is available in the AB5075 library generated by Gallagher et al. (2015). These datasets highlight the critical need for further investigations into the role of these important and dynamic proteins in different strains in order to elucidate their roles and association with other accessory factors.

IMMUNE RESPONSES

Innate Immune Response

Cellular Immunity

Neutrophils

The importance of neutrophils in response to *A. baumannii* was first noted regarding the increased prevalence of this pathogen in neutropenic patients. However, it was a further 10 years until Faassen and colleagues confirmed their importance in resistance to *Acinetobacter* respiratory infections (Van Faassen et al., 2007). Numerous *in vivo* studies show neutrophil recruitment to the site of infection occurs as early as 4 h, peaking at 24 h, and while their depletion results in enhanced lethality, this effect can be strain specific (Bruhn et al., 2015; Bhuiyan et al., 2016; García-Patiño et al., 2017). The recruitment and activation of neutrophils can be stimulated by a range of host factors, including cytokines and chemokines, though only the bacterial metabolic by-product phenylacetate has been shown to act as a bacterial-derived chemoattractant in the case of *A. baumannii* (Bhuiyan et al., 2016).

Neutrophils elicit antibacterial effects through phagocytosis, degranulation, and neutrophil extracellular trap (NETs) formation (Konstantinidis et al., 2016). Phagocytosis is mediated by TLR activation, IgG opsonization or complement-mediated receptor binding (Nordenfelt and Tapper, 2011). The process is extremely rapid, occurring in as little as 20 s, through pseudopod and filopodia generation, with phagocytic arms capable of retaining and engulfing the bacteria (Nordenfelt and Tapper, 2011; Lázaro-Díez et al., 2017). Once phagocytosed, rapid killing is dependent on ROS and granular fusion, releasing a plethora of antimicrobial molecules, including human defensins and lysosome into the phagosome (Greenwald and Ganz, 1987; Borregaard and Cowland, 1997; Qiu et al., 2009; Nordenfelt and Tapper, 2011; Harding et al., 2017a). However, it is the capacity of neutrophils to kill *A. baumannii* that is contentious, with some *in vitro* studies reporting their co-culture does not affect the viability of either (Kamoshida et al., 2015, 2016). Instead, *A. baumannii* preferentially adhere to the neutrophil surface, in an IL-8-dependent manner, promoting their dissemination (Kamoshida et al., 2016). While others have shown *in vitro* neutrophil phagocytosis kills *A. baumannii*, a finding consistent with *in vivo* studies (Lázaro-Díez et al., 2017). The reasoning behind such conflicting reports is most likely due to the experimental details, in that Kamoshida et al. tested only a single *A. baumannii* strain, ATCC 19606, at 1 h post infection, while Lázaro-Díez et al. performed an extensive assessment, testing 11 strains, including 5 *A. baumannii* and 6 *A. pittii* over a time course, emphasizing the importance of testing multiple strains.

NETs are an important mechanism by which neutrophils control pathogens, though their induction in response to *A. baumannii* is equally controversial (Brinkmann et al., 2004; Brinkmann and Zychlinsky, 2012; Kamoshida et al., 2015, 2018; Konstantinidis et al., 2016). NETs constitute a mesh of chromatin, impregnated with antimicrobial proteins and peptides, including myeloperoxidase, neutrophil elastase, and LL-37, respectively (Konstantinidis et al., 2016). NETs have been linked to the control of bacterial infections, while *A. baumannii* has been reported to inhibit their formation (Kamoshida et al., 2018). This mechanism of inhibition has yet to be fully elucidated and confirmed *in vivo*, though the neutrophil cell surface receptors CD11a and CD11b have been implicated in the observed reduced adhesion of *A. baumannii* to neutrophils (Kamoshida et al., 2018).

While cytokines such as IL-8 and tumor necrosis factor (TNF)-α have stimulatory and chemoattractive effects on neutrophils, it should be noted that TNF-α induces concentration-dependent effects, including cytokine release and MAP kinase activation or cell apoptosis (March et al., 2010; Kikuchi-Ueda et al., 2017). Other host factors such as neutrophil phosphatase, Wip1, and serum amyloid A and P can also regulate neutrophil migration and pro-inflammatory cytokine secretion (Renckens et al., 2006; Sun et al., 2014).

Macrophages

Similar to neutrophils, the role of macrophages in *A. baumannii* infection is equally controversial. While their depletion in zebrafish has no effect, in murine models, macrophage depletion reduces pro-inflammatory cytokines and elevates bacterial burdens when depleted in conjunction with complement (Qiu et al., 2012; Bruhn et al., 2015; Bhuiyan et al., 2016). However, macrophages are important early defenders, promoting neutrophil recruitment and phagocytosis (Qiu et al., 2009, 2012). Alveolar macrophages provide the first line of defense against *A. baumannii* in the lungs, capable of microfilament and microtubule-dependent phagocytosis of the bacteria, stimulating high levels of IL-6, TNF-α, and macrophage inflammatory protein-2, potent chemoattractants for neutrophils, with additional IL-1β and IL-10 produced at latter time points (Qiu et al., 2012). Though macrophages kill phagocytosed *A. baumannii,* they do so at a significantly slower rate than that of neutrophils; however, they can phagocytose bacteria in as little as 10 min (Qiu et al., 2012; Lázaro-Díez et al., 2017).

Natural Killer Cells, Dendritic Cells, and Mast Cells

Natural killer (NK) cells are an important defense against viral infections, intra- and extracellular bacteria; however, their role in *A. baumannii* infection remains largely unexplored (Small et al., 2008; Waggoner et al., 2016; Paidipally et al., 2018).

In a murine pneumonia model, depletion of NK cells led to reduced survival and impaired bacterial clearance, though the impact of the NK cells was indirect, and mediated *via* the production of the neutrophil chemoattractant, keratinocyte chemoattractant (Tsuchiya et al., 2012). *A. baumannii* attachment to the natural cytotoxicity receptors on the surface of NK cells, has very low or no affinity, indicative that the interaction is indirect (Esin et al., 2008). Furthermore, NK cell cytotoxicity is significantly reduced in mice with *A. baumannii* septicaemia compared to uninfected controls; however, the mechanism defining this impact has not been explored (Cirioni et al., 2016).

Dendritic cells (DCs) are unique antigen-presenting cells linking the innate and adaptive immune systems. *A. baumannii* OmpA activates DCs in a dose-dependent manner, resulting in maturation, MAP kinase and NF-κB signaling, leading to the induction of a CD4+ Th_1 T cell responses or early onset apoptosis and delayed necrosis (Lee et al., 2007). DC death is *via* mitochondrial targeting and production of ROS, consistent with OmpAs mechanism of action, suggestive that *A. baumannii* may modulate T cell response *via* this cell type (Lee et al., 2010). Furthermore, despite the identification of neutrophil-DC hybrids several years ago (Geng et al., 2013; Matsushima et al., 2013), it remains to be determined whether they contribute to the control of *Acinetobacter* infections.

Mast cells are considered sentinels of mucosal layers, sensing and responding to pathogen invasion. Lung mast cells have been shown to secrete IL-8 and TNF-α in response to *A. baumannii*, enhancing neutrophil recruitment to the site (Kikuchi-Ueda et al., 2017).

Cell Signaling in Response to *Acinetobacter*

Toll-Like Receptor Signaling

Toll-like receptor (TLR) signaling is an important mechanism by which hosts recognize and respond to pathogens. Of the 11 reported TLRs, TLR2, 4, and 9 are critical for the recognition and response to *A. baumannii*, through the detection of lipoproteins, peptidoglycan, porins, lipoteichoic acid (TLR2), LOS (TLR4), and unmethylated CpG DNA motifs (TLR9) (Knapp et al., 2006; Lin et al., 2012; Moffatt et al., 2013; Noto et al., 2015).

Host signaling *via* TLR2 and 4 has been extensively documented, whereby activation of either receptor, in the presence or absence of the soluble GPI-linked glycoprotein, CD14, leads to NF-κB activation in a MyD88-dependent fashion, resulting in the secretion of pro-inflammatory cytokines including TNF-α; IFN-γ; IL-1, 6, 8, 10, and 12 (Lin et al., 2012; Moffatt et al., 2013; García-Patiño et al., 2017). TLR2 is important for DC recognition of *A. baumannii* OmpA; however, there are conflicting reports regarding the impact of TLR2 knockout, whereby Kim et al. reported increased bacterial burdens in the first 24 h of infection in TLR2 −/− mice, while Knapp et al. observed significantly lower bacterial burdens at the same time point (Knapp et al., 2006; Kim et al., 2014; García-Patiño et al., 2017). These differences may be attributed to the use of different *A. baumannii* isolates, though further investigation is clearly warranted. By contrast, TLR4 −/− and/or CD14 −/− both result in increased bacterial burdens in pneumonia models, as a result of reduced pro-inflammatory cytokine responses and neutrophil recruitment. Interestingly though, TLR4 knockout has also been shown to reduce the lethality of *A. baumannii* septicaemia, by limiting septic shock caused by LOS (Lin et al., 2012). Consistent with this finding, *A. baumannii* virulence has also been linked to the levels of LOS shedding and TLR4 signaling (Lin et al., 2012). Similarly, the treatment of *A. baumannii*-infected animals with LpxC inhibitors protects against lethality, by enhancing TLR2 stimulation and reducing NF-κB signaling and TNF-α secretion by four- and two-fold respectively, promoting opsonophagocytic killing in response to increased surface PNAG (Lin et al., 2012; Moffatt et al., 2013). By contrast, *A. baumannii* isolates with phosphoethalomine-modified lipid A induce significantly higher levels of TLR4 signaling compared to unmodified LOS (Lin et al., 2012).

In contrast to TLR2 and TLR4, TLR9 signaling in response to *A. baumannii* is the least well characterized. TLR9 is an internal receptor of the endolysosome, responsible for the detection of bacterial and viral DNA (Noto et al., 2015; Harding et al., 2017a). Similarly, its stimulation promotes NF-κB activation and pro-inflammatory cytokine responses, whereby TLR9 −/− mice have reduced TNF-α and IFN-ϒ in response to *A. baumannii* lung infections, causing elevated bacterial burdens, systemic dissemination, and increased tissue damage (Noto et al., 2015).

Soluble Secreted Factors

The production of pro-inflammatory cytokines in response to *A. baumannii* is primarily *via* NF-κB activation, with each cytokine driving a different response. For example, NLRP3-caspase 1- caspase 11 activation leads to the release of IL-1β and IL-18 from infected lung epithelia resulting in tissue damage (Dikshit et al., 2017). IL-17, however, promotes granulocytopoiesis and drives secretion of GM-CSF and IL-8, stimulating the antimicrobial peptide LL-37 (García-Patiño et al., 2017). With the release of IL-8 and TNF-α, neutrophils are recruited and activated (March et al., 2010; Bist et al., 2014). However, while IL-33 represses IL-8 secretion, it is known to also promote neutrophil migration and stimulation (Peng et al., 2018).

Epithelial cells and neutrophils also secrete an array of antimicrobial peptides, including human β-defensin 2 and 3, the cathelicidin LL-37 and CD14 enhancing TLR4 ligand interactions through myeloid differentiation factor 2 binding (March et al., 2010; García-Patiño et al., 2017; Harding et al., 2017a). *A. baumannii* is highly susceptible to human β-defensin 2, which causes membrane disruption and increased permeability, although the potential for cell death *via* non-membrane lytic methods (i.e., inhibition of nucleic acid synthesis) or synergy with other antimicrobial peptides cannot be excluded (Cobo and Chadee, 2013). Interestingly, only LOS-deficient *A. baumannii* demonstrates elevated sensitivity to the antimicrobial peptide LL-37, despite the target considered to be LOS (Moffatt et al., 2013).

Intracellular Responses

Despite *A. baumannii* being considered an extracellular pathogen, *in vitro* evidence exists for their ability to invade lung epithelial cells and macrophages (Choi et al., 2008b; Qiu et al., 2012),

though this observation is controversial, and the evidence should be viewed with caution, given the limitations of the studies. In both instances, only a single *A. baumannii* strain was tested, with extracellular bacteria eliminated using gentamicin; however, the authors neglect to provide either the minimum inhibitory concentration for their respective strains or suitable microscopy to support their observations. In contrast to these reports, other studies testing a range of *A. baumannii* strains have been unable to visualize a direct interaction or invasion of the lung epithelial cell line A549, irrespective of MOI or incubation duration (Lázaro-Díez et al., 2016). Furthermore, Qiu et al. observed a reduction in bacterial viability during co-culture with macrophages (Qiu et al., 2012), suggesting that these observations are purely phagocytosis as opposed to active invasion and their significance in the context of *in vivo* infection has yet to be confirmed.

In addition to TLR9, the cytosolic family of NOD-like receptors, including Nod1 and Nod2 associated with pathogen-associated molecular pattern recognition, induce NF-κB, but not MAP kinase through interactions with Rip2 (Bist et al., 2014). This NF-κB activation induces IL-8, TNF-α and β-defensin, although it should be noted these responses are cell type specific (Bist et al., 2014). ROS and nitric oxide play critical and moderate roles in the control of intracellular *A. baumannii,* respectively (Qiu et al., 2009, 2012). Evident by the fact that $gp91^{phox-/-}$ mice, deficient in the NADPH phagosomal oxidase (and thus ROS), are more susceptible to *A. baumannii* infection than neutropenic mice, while those defective for nitric oxide production demonstrate only moderate increases in bacterial burdens (Qiu et al., 2009).

Complement-Mediated Killing

Complement-mediated killing is an important non-cellular innate immune component, consisting of multiple soluble factors, acting in a cascade promoting either bacterial cell lysis or opsonophagocytosis. Three pathways exist for the deposition of complement factors on to bacterial surfaces, although in human serum, the alternative complement pathway is required for *A. baumannii* killing (Garcia et al., 2000; Kim et al., 2009; King et al., 2009; Bruhn et al., 2015). Resistance is frequently reported in clinical *A. baumannii* isolates and *in vitro* serum resistance may correlate with more severe disease (Bruhn et al., 2015).

The alternative complement pathway is regulated by factor H, a soluble component important for the recognition of host cell markers (Ferreira et al., 2010). Activation of the alternative complement pathway leads to the deposition of C3 on the surface of serum-sensitive isolates, though discrepancies exist surrounding the binding of factor H to bacterial cells and subsequent inhibition of C3 deposition, promoting serum resistance in *A. baumannii* (Dave et al., 2001; King et al., 2009; Laarman et al., 2011). Previously, Kim et al. reported that factor H bound to *A. baumannii* OMPs, promoting serum resistance (Kim et al., 2009). While King et al. were unable to identify bound factor H on their serum-resistant isolates (King et al., 2009), suggesting that factor H acquisition is not solely responsible.

Furthermore, the *A. baumannii* plasminogen-binding protein, CipA, was also shown to inhibit the alternative complement pathway *via* C3b cleavage and degradation of fibrin networks, by mechanisms that have yet to be fully elucidated (Koenigs et al., 2016). Consistent with the role of CipA in complement resistance, *cipA* deletion mutants are also more susceptible to killing by human serum (King et al., 2013).

Genes involved in *A. baumannii* cell envelope homeostasis also contribute to serum resistance. For example, disruption of the TCS *bfmS*, which regulates pilus and capsule biosynthesis, leads to serum resistance (Geisinger et al., 2018). *A. baumannii* genes associated with capsule biosynthesis and glycosylation, including *ptk, epsA, mltB,* and *pglC,* encoding a putative tyrosine kinase, OM polysaccharide exporter, lytic transglycosylase and glycosyltransferase, respectively, are required for resistance to killing in human ascites fluid and serum, highlighting the importance of capsule in resisting complement (Russo et al., 2010; Lees-Miller et al., 2013; Crépin et al., 2018).

Adaptive Immune Response

While numerous studies have examined the ability of different bacterial components to induce a range of adaptive immune responses (McConnell and Pachón, 2010; McConnell et al., 2011a,b; García-Quintanilla et al., 2014; Badmasti et al., 2015; Kuolee et al., 2015; Garg et al., 2016; Ainsworth et al., 2017; Bazmara et al., 2017; Pulido et al., 2018; Song et al., 2018), very little work has been done to examine these during the course of infection, due to several confounding factors, including the available animal models, rate of disease progression and severity.

To our knowledge, the importance of Th_1 vs. Th_2 or Th_{17} responses has yet to be fully elucidated with regard to *A. baumannii* infection. Despite IL-17 being important for neutrophil recruitment and secretion of β-defensin, deletion of IL-17A in mice has no impact on bacterial burdens (Breslow et al., 2011; Yan et al., 2016). Furthermore, Qui et al. demonstrated that mice which recover from sub-lethal infections do not have increased survival compared to naïve mice when infected with a lethal dose of *A. baumannii* 6 weeks later, despite having significantly higher levels of CD4+ and CD8α+ T cells and CD19+ B lymphocytes (Qiu et al., 2016). This suggests that adaptive immune responses play only a minor role in the resolution of *A. baumannii* infections. By contrast, some studies have shown the induction of antibody subtypes, IgM and IgG (isotypes IgG1 and 2c), and cytokines, IFN-ϒ, IL-4, and IL-17, can promote bacterial killing and improve host survival (McConnell et al., 2011b; Luo et al., 2012; García-Quintanilla et al., 2014). Further work is needed to clarify the significance of different adaptive immune components in the clearance of and resistance to *A. baumannii* infections.

IN VIVO MODELS FOR THE STUDY OF *A. BAUMANNII* HOST-PATHOGEN INTERACTIONS

Mammalian Models

Murine models have been the predominant mammalian model used to study *Acinetobacter* infections over the last 30 years,

with a small number of studies also utilizing rabbits (Rodríguez-Hernández et al., 2004; Pachón-Ibáñez et al., 2010) and guinea pigs (Bernabeu-Wittel et al., 2005). While initial studies focused on assessing antibiotic efficacy, more recent studies have investigated bacterial pathogenesis, host interactions, immunity and alternative therapeutic treatments (Obana et al., 1985; Joly-Guillou et al., 1997; Ko et al., 2004; Knapp et al., 2006; Jacobs et al., 2010; Cerqueira et al., 2014; Lood et al., 2015; Noto et al., 2015; Sebe et al., 2016; Dikshit et al., 2017; Murray et al., 2017; Peng et al., 2017). A number of models have been developed for skin and soft tissue infection, endocarditis, osteomyelitis, bloodstream infection, and pneumonia, with the latter two being the most commonly used given the frequency and severity of these infections in hospital and community settings (Peleg et al., 2008a; McConnell et al., 2013).

Bloodstream Infection

Several bacterial virulence factors have been confirmed using bloodstream infection models, including the acinetobactin iron acquisition system, the universal stress protein A (UspA), and the TCS GacAS (Gaddy et al., 2012; Cerqueira et al., 2014; Elhosseiny et al., 2015). A recent investigation utilized a bacteremia model to determine the global gene expression profile of *A. baumannii* ATCC 17978 during a life-threatening infection, and compared expression profiles between *in vitro* and *in vivo* growth, revealing 886 differentially expressed genes (Murray et al., 2017).

Recently, bloodstream infection models have been expanded to test the efficacy of bacteriophage therapy to treat lethal infections. Lood et al. used purified, recombinant autolysin from a bacteriophage to treat mice infected with a lethal dose of *A. baumannii,* resulting in increased survival in lysin-treated mice (up to 50%) and reduced *A. baumannii* burdens (Lood et al., 2015). Similar results were observed with a more recent study using another bacteriophage lysin (Peng et al., 2017).

Pneumonia

Lung infection models were first used in 1997 to evaluate the efficacy of imipenem *in vivo* against acute *A. baumannii* pneumonia (Joly-Guillou et al., 1997). Two lung infection methods are most commonly used to induce pneumonia in mice: intra-tracheal, where the trachea of an anesthetized mouse is cannulated with a blunt-ended needle and the inoculum instilled; or intranasal, where the inoculum is pipetted over the nares of anesthetized mice (Joly-Guillou et al., 1997; Eveillard et al., 2010). Both methods induce inflammatory and histological responses consistent with acute pneumonia and a number of virulence factors have been assessed using these models, including phospholipase D, OmpA, and a heme oxygenase (Choi et al., 2008b; Jacobs et al., 2010; De Léséleuc et al., 2014). Assessment of essential *A. baumannii* genes in the context of pneumonia has also been performed using a transposon mutant library of *A. baumannii* ATCC 17978 and comparing input and output mutant pools after lung infection (Wang et al., 2014). This approach identified 157 genes, including OmpA and several novel virulence factors that are required for a pneumonia infection.

Over the last 15 years, mouse pneumonia models have been increasingly used to understand the host immune response to *A. baumannii* as described above. Furthermore, vaccine efficacy studies have now also been performed using mouse infection models. (McConnell and Pachón, 2010; McConnell et al., 2011a; Luo et al., 2012; Russo et al., 2013; Qiu et al., 2016).

With the rise in studies, it is also now recognized that different strains of *A. baumannii* elicit different immune responses in mice (De Breij et al., 2012; Dikshit et al., 2017). This is an important finding considering that for many years, strains such as ATCC 17978 and 19606 have been used to study *A. baumannii* pathogenesis; however, they are not representative of the dominant clinical strains found in hospitals today. When compared to international clonal Type I and II strains, they have reduced virulence and elicit different immune responses (Eveillard et al., 2010; De Breij et al., 2012; Dikshit et al., 2017).

Other Infection Models

As previously described, a number of other infection models exist for studying *A. baumannii* infections. Skin and soft tissue models have been developed in both mice and rats for treatment studies and as a screening tool for determining gene essentiality (Shankar et al., 2007; Russo et al., 2008; Dai et al., 2009). Several groups have tried to develop an osteomyelitis model in mice and rats with varying levels of success (Crane et al., 2009; Collinet-Adler et al., 2011). Crane et al. were able to establish a non-lethal infection in mice by implanting stainless steel pins into their tibias, while Collinet-Adler et al. were unable to establish chronic bone infections in rats (Crane et al., 2009; Collinet-Adler et al., 2011). Rabbits have been used for studying meningitis and endocarditis, and guinea pigs used to study pneumonia (Rodríguez-Hernández et al., 2004; Bernabeu-Wittel et al., 2005; Pachón-Ibáñez et al., 2010). While larger animals allow researchers to sample the same animal at multiple time points, the increased costs and ethical concerns associated with larger animals have limited their use thus far.

The increasing costs and growing ethical concerns regarding mammalian models have spurred the development of non-mammalian models such as *C. elegans*, *G. mellonella*, and zebrafish for studying *A. baumannii* host-pathogen interactions. Despite their clear differences from mice and humans, non-mammalian models have proved useful for the assessment of mutants, screening compounds, and enabling visualization of host-pathogen interactions.

Caenorhabditis elegans

C. elegans, a small soil-dwelling nematode was the first non-mammalian model to be used to study *A. baumannii* pathogenesis (Smith et al., 2004). The small size (1 mm), transparency, short replication cycle (2–3 days), and well-characterized genome make it an ideal model to study bacterial-host interactions. It was first used by Smith et al. to study *A. baumannii* pathogenesis in the presence of ethanol, with a later method developed using proliferation and brood size as the outcome measure rather than worm death (Smith et al., 2004, 2007).

Polymicrobial interactions between *A. baumannii* and *Candida albicans* have also been assessed in *C. elegans,* where *A. baumannii* reduced *C. albicans* filament production and virulence within the worm (Peleg et al., 2008b). *C. elegans* has most recently been used to screen potential antimicrobial agents (Jayamani et al., 2015; Mohamed et al., 2017). Jayamani et al. used a liquid infection assay in a 384-well format to concurrently assess the antimicrobial activity of peptides in parallel to evaluating host toxicity, revealing 15 molecules that prolonged worm survival (Jayamani et al., 2015). A disadvantage of *C. elegans* though is their requirement to be maintained at 25°C, with 37°C causing worm death. This may impact the virulence of pathogens including *A. baumannii* (Peleg et al., 2009; De Silva et al., 2017).

Galleria mellonella

G. mellonella (caterpillars of the greater wax moth) have a considerable advantage over *C. elegans* in that they can be maintained at 37°C and a precise inoculum or therapeutic dose can be administered into the body of the caterpillar (Peleg et al., 2009; Hornsey et al., 2013). *G. mellonella* also have a more advanced immune system with both humoral and phagocytic cells (Peleg et al., 2009). *A. baumannii* kills *G. mellonella* in a dose-dependent manner and survival can be prolonged by the administration of antibiotics (Peleg et al., 2009). *G. mellonella* has since been used to test the efficacy of antibiotic combinations, assess the virulence of mutants, or compare pathogenicity between strains (Peleg et al., 2009; Antunes et al., 2011; Hornsey and Wareham, 2011; Gaddy et al., 2012; Iwashkiw et al., 2012; Wand et al., 2012; Hornsey et al., 2013; O'Hara et al., 2013; Yang et al., 2015; Betts et al., 2017). A disadvantage of note is that *G. mellonella* sourced from different suppliers can show significant variance in results (Betts et al., 2017). However, with their increasing use, more standardized models have been developed that control for age, size, and food supply.

Dictyostelium discoideum

D. discoideum is a unicellular amoeba that feeds on bacteria, with previous work having highlighted similarities between amoeba phagocytosis and mammalian immune cell phagocytosis (Hasselbring et al., 2011). It has therefore been proposed that when used in conjunction with other non-mammalian models, such as *C. elegans,* which kill *via* extracellular methods, the two can represent multiple areas of a mammalian infection (Smith et al., 2007). In order to determine whether bacteria are killed by *D. discoideum,* liquid cultures of the two are mixed and plated, allowing the faster growing bacteria to form a lawn, with formation of plaques if amoeba are able to phagocytose bacteria (Smith et al., 2007; Iwashkiw et al., 2012; Weber et al., 2013). *D. discoideum* and *C. elegans* have been jointly used to screen transposon mutant libraries for attenuated mutants (Smith et al., 2007). Two other studies were performed using *D. discoideum* and *C. elegans* and showed that the T6SS is not required for virulence, while a glycosylation pathway was (Iwashkiw et al., 2012; Weber et al., 2013).

Zebrafish

Zebrafish (*Danio rerio*) are the most recent non-mammalian model to be utilized for host-pathogen interaction studies. Zebrafish are a small (3–4 cm) freshwater fish native to India, Pakistan, and Bhutan and are susceptible to a range of bacteria, including *Vibrio cholera, S. aureus*, and *Shigella flexneri* (Prajsnar et al., 2008; Mostowy et al., 2013; Runft et al., 2014). A considerable advantage of zebrafish to other non-mammalian models is their advanced immune system development with innate immune cells present at 25 h post fertilization and a fully functional adaptive immune system developed by adulthood (Van Der Sar et al., 2004). Transparency can be maintained to allow for real-time visualization, numerous transgenic fish lines are available, including fluorescently tagged neutrophils and macrophages and immune cell-depleted fish (Hall et al., 2007; White et al., 2008; Ellett et al., 2010; Li et al., 2010). The establishment of zebrafish to study *A. baumannii* pathogenesis has recently been published, and showed that *A. baumannii* is lethal toward zebrafish in a dose-dependent manner, with interactions between *A. baumannii* and neutrophils easily imaged (Bhuiyan et al., 2016). The unique advantages of real-time imaging during infection allowed the authors to elucidate novel findings related to neutrophil migration in the context of an *A. baumannii* infection.

CONCLUSIONS

Taken together, this review highlights the real advances that have been made in our understanding of *A. baumannii* pathogenesis, but further highlights areas in need of more in-depth analysis. Consistency and transparency in the field and subsequent publications will optimize the success of future studies. The selection of multiple and appropriate *A. baumannii* strains, encompassing those that are representative of modern-day clinical isolates and human infections, combined with the standardization of cell lines, animal models, and procedures will provide a level of uniformity across all studies. Such consistency will not only enable direct comparison between studies, but also advance our overall understanding of this important pathogen.

However, the future does hold promise with more innovative techniques and the rapid advancement of technology, new approaches are providing greater insight into the intricacies of regulatory networks not only in the bacterial cell but also in the host. As cross-disciplinary research continues to grow, so too does our understanding of this important pathogen and its hosts.

AUTHOR CONTRIBUTIONS

CD wrote the "*In vivo models*" section and the "Introduction". XK wrote the "Natural Killer Cells, Dendritic Cells, and Mast Cells" section. MU wrote the section "Neutrophils". FM wrote all remaining sections and prepared the figures. AP edited the manuscript.

REFERENCES

Adams, M. D., Nickel, G. C., Bajaksouzian, S., Lavender, H., Murthy, A. R., Jacobs, M. R., et al. (2009). Resistance to colistin in *Acinetobacter baumannii* associated with mutations in the PmrAB two-component system. *Antimicrob. Agents Chemother.* 53, 3628–3634. doi: 10.1128/AAC.00284-09

Ahmad, T. A., Tawfik, D. M., Sheweita, S. A., Haroun, M., and El-Sayed, L. H. (2016). Development of immunization trials against *Acinetobacter baumannii*. *Trials Vaccinol.* 5, 53–60. doi: 10.1016/j.trivac.2016.03.001

Ainsworth, S., Ketter, P. M., Yu, J.-J., Grimm, R. C., May, H. C., Cap, A. P., et al. (2017). Vaccination with a live attenuated *Acinetobacter baumannii* deficient in thioredoxin provides protection against systemic *Acinetobacter* infection. *Vaccine* 35, 3387–3394. doi: 10.1016/j.vaccine.2017.05.017

Ajiboye, T. O., Skiebe, E., and Wilharm, G. (2018). Contributions of ferric uptake regulator fur to the sensitivity and oxidative response of *Acinetobacter baumannii* to antibiotics. *Microb. Pathog.* 119, 35–41. doi: 10.1016/j.micpath.2018.03.060

Álvarez-Fraga, L., Vázquez-Ucha, J. C., Martínez-Guitián, M., Vallejo, J. A., Bou, G., Beceiro, A., et al. (2018). Pneumonia infection in mice reveals the involvement of the *feoA* gene in the pathogenesis of *Acinetobacter baumannii*. *Virulence* 9, 496–509. doi: 10.1080/21505594.2017.1420451

Ansari, H., Doosti, A., Kargar, M., Bijanzadeh, M., and Jaafarinia, M. (2018). Cloning of *ompA* gene from *Acinetobacter baumannii* into the eukaryotic expression vector pBudCE4.1 as DNA vaccine. *Indian J. Microbiol.* 58, 174–181. doi: 10.1007/s12088-017-0705-x

Anstey, N. M., Currie, B. J., and Withnall, K. M. (1992). Community-acquired *Acinetobacter* pneumonia in the northern territory of Australia. *Clin. Infect. Dis.* 14, 83–91. doi: 10.1093/clinids/14.1.83

Antunes, L. C. S., Imperi, F., Carattoli, A., and Visca, P. (2011). Deciphering the multifactorial nature of *Acinetobacter baumannii* pathogenicity. *PLoS One* 6:e22674. doi: 10.1371/journal.pone.0022674

Antunes, L. C. S., Visca, P., and Towner, K. J. (2014). *Acinetobacter baumannii*: evolution of a global pathogen. *Pathog. Dis.* 71, 292–301. doi: 10.1111/2049-632X.12125

Arroyo, L. A., Herrera, C. M., Fernandez, L., Hankins, J. V., Trent, M. S., and Hancock, R. E. W. (2011). The *pmrCAB* operon mediates polymyxin resistance in *Acinetobacter baumannii* ATCC 17978 and clinical isolates through phosphoethanolamine modification of lipid A. *Antimicrob. Agents Chemother.* 55, 3743–3751. doi: 10.1128/AAC.00256-11

Badmasti, F., Ajdary, S., Bouzari, S., Fooladi, A. A. I., Shahcheraghi, F., and Siadat, S. D. (2015). Immunological evaluation of OMV(PagL)+Bap(1-487aa) and AbOmpA(8-346aa)+Bap(1-487aa) as vaccine candidates against *Acinetobacter baumannii* sepsis infection. *Mol. Immunol.* 67, 552–558. doi: 10.1016/j.molimm.2015.07.031

Bazmara, H., Rasooli, I., Jahangiri, A., Sefid, F., Astaneh, S. D. A., and Payandeh, Z. (2017). Antigenic properties of iron regulated proteins in *Acinetobacter baumannii:* an in silico approach. *Int. J. Pept. Res. Ther.* 25, 205–213. doi: 10.1007/s10989-017-9665-6

Beceiro, A., Tomás, M., and Bou, G. (2013). Antimicrobial resistance and virulence: a successful or deleterious association in the bacterial world? *Clin. Microbiol. Rev.* 26, 185–230. doi: 10.1128/CMR.00059-12

Bentancor, L. V., Camacho-Peiro, A., Bozkurt-Guzel, C., Pier, G. B., and Maira-Litrán, T. (2012a). Identification of Ata, a multifunctional trimeric autotransporter of *Acinetobacter baumannii*. *J. Bacteriol.* 194, 3950–3960. doi: 10.1128/JB.06769-11

Bentancor, L. V., Routray, A., Bozkurt-Guzel, C., Camacho-Peiro, A., Pier, G. B., and Maira-Litrán, T. (2012b). Evaluation of the trimeric autotransporter Ata, as a vaccine candidate against *Acinetobacter baumannii* infections. *Infect. Immun.* 80, 3387–3388. doi: 10.1128/IAI.06096-11

Bernabeu-Wittel, M., Pichardo, C., García-Curiel, A., Pachón-Ibáñez, M. E., Ibáñez-Martínez, J., Jiménez-Mejías, M. E., et al. (2005). Pharmacokinetic/pharmacodynamic assessment of the *in-vivo* efficacy of imipenem alone or in combination with amikacin for the treatment of experimental multiresistant *Acinetobacter baumannii* pneumonia. *Clin. Microbiol. Infect.* 11, 319–325. doi: 10.1111/j.1469-0691.2005.01095.x

Betts, J. W., Hornsey, M., Wareham, D. W., and La Ragione, R. M. (2017). *In vitro* and *In vivo* activity of theaflavin-epicatechin combinations versus multidrug-resistant *Acinetobacter baumannii*. *Infect. Dis. Ther.* 6, 435–442. doi: 10.1007/s40121-017-0161-2

Bhargava, N., Sharma, P., and Capalash, N. (2010). Quorum sensing in *Acinetobacter*: an emerging pathogen. *Crit. Rev. Microbiol.* 36, 349–360. doi: 10.3109/1040841X.2010.512269

Bhuiyan, M. S., Ellett, F., Murray, G. L., Kostoulias, X., Cerqueira, G. M., Schulze, K. E., et al. (2016). *Acinetobacter baumannii* phenylacetic acid metabolism influences infection outcome through a direct effect on neutrophil chemotaxis. *Proc. Natl. Acad. Sci.* 113, 9599–9604. doi: 10.1073/pnas.1523116113

Bist, P., Dikshit, N., Koh, T. H., Mortellaro, A., Tan, T. T., and Sukumaran, B. (2014). The Nod1, Nod2, and Rip2 axis contributes to host immune defense against intracellular *Acinetobacter baumannii* infection. *Infect. Immun.* 82, 1112–1122. doi: 10.1128/IAI.01459-13

Bitto, N. J., Chapman, R., Pidot, S., Costin, A., Lo, C., Choi, J., et al. (2017). Bacterial membrane vesicles transport their DNA cargo into host cells. *Sci. Rep.* 7:7072. doi: 10.1038/s41598-017-07288-4

Boll, J. M., Crofts, A. A., Peters, K., Cattoir, V., Vollmer, W., Davies, B. W., et al. (2016). A penicillin-binding protein inhibits selection of colistin-resistant, lipooligosaccharide-deficient *Acinetobacter baumannii*. *Proc. Natl. Acad. Sci.* 113, E6228–E6237. doi: 10.1073/pnas.1611594113

Boll, J. M., Tucker, A. T., Klein, D. R., Beltran, A. M., Brodbelt, J. S., Davies, B. W., et al. (2015). Reinforcing lipid A acylation on the cell surface of *Acinetobacter baumannii* promotes cationic antimicrobial peptide resistance and desiccation survival. *MBio* 6, e00478–e00415. doi: 10.1128/mBio.00478-15

Borregaard, N., and Cowland, J. B. (1997). Granules of the human neutrophilic polymorphonuclear leukocyte. *Blood* 89, 3503–3521.

Bossi, L., Maloriol, D., and Figueroa-Bossi, N. (2008). Porin biogenesis activates the sigma E response in *Salmonella hfq* mutants. *Biochimie* 90, 1539–1544. doi: 10.1016/j.biochi.2008.06.001

Breslow, J. M., Meissler, J. J., Hartzell, R. R., Spence, P. B., Truant, A., Gaughan, J., et al. (2011). Innate immune responses to systemic *Acinetobacter baumannii* infection in mice: neutrophils, but not Interleukin-17, mediate host resistance. *Infect. Immun.* 79, 3317–3327. doi: 10.1128/IAI.00069-11

Brinkmann, V., Reichard, U., Goosmann, C., Fauler, B., Uhlemann, Y., Weiss, D. S., et al. (2004). Neutrophil extracellular traps kill bacteria. *Science* 303, 1532–1535. doi: 10.1126/science.1092385

Brinkmann, V., and Zychlinsky, A. (2012). Neutrophil extracellular traps: is immunity the second function of chromatin? *J. Cell Biol.* 198, 773–783. doi: 10.1083/jcb.201203170

Brossard, K. A., and Campagnari, A. A. (2011). The *Acinetobacter baumannii* biofilm associated protein (Bap) plays a role in adherence to human epithelial cells. *Infect. Immun.* 80, 228–233. doi: 10.1128/IAI.05913-11

Bruhn, K. W., Pantapalangkoor, P., Nielsen, T., Tan, B., Junus, J., Hujer, K. M., et al. (2015). Host fate is rapidly determined by innate effector-microbial interactions during *Acinetobacter baumannii* bacteremia. *J. Infect. Dis.* 211, 1296–1305. doi: 10.1093/infdis/jiu593

Cahill, B. K., Seeley, K. W., Gutel, D., and Ellis, T. N. (2015). *Klebsiella pneumoniae* O antigen loss alters the outer membrane protein composition and the selective packaging of proteins into secreted outer membrane vesicles. *Microbiol. Res.* 180, 1–10. doi: 10.1016/j.micres.2015.06.012

Cerqueira, G. M., Kostoulias, X., Khoo, C., Aibinu, I., Qu, Y., Traven, A., et al. (2014). A global virulence regulator in *Acinetobacter baumannii* and its control of the phenylacetic acid catabolic pathway. *J. Infect. Dis.* 210, 46–55. doi: 10.1093/infdis/jiu024

Chatterjee, S., Mondal, A., Mitra, S., and Basu, S. (2017). *Acinetobacter baumannii* transfers the *bla*NDM-1 gene via outer membrane vesicles. *J. Antimicrob. Chemother.* 72, 2201–2207. doi: 10.1093/jac/dkx131

Chen, R., Lv, R., Xiao, L., Wang, M., Du, Z., Tan, Y., et al. (2017). A1S_2811, a CheA/Y-like hybrid two-component regulator from *Acinetobacter baumannii* ATCC17978, is involved in surface motility and biofilm formation in this bacterium. *MicrobiologyOpen* 6:e00510. doi: 10.1002/mbo3.510

Chin, C. Y., Tipton, K. A., Farokhyfar, M., Burd, E. M., Weiss, D. S., and Rather, P. N. (2018). A high-frequency phenotypic switch links bacterial virulence and environmental survival in *Acinetobacter baumannii*. *Nat. Microbiol.* 3, 563–569. doi: 10.1038/s41564-018-0151-5

Choi, C. H., Hyun, S. H., Kim, J., Lee, Y. C., Seol, S. Y., Cho, D. T., et al. (2008a). Nuclear translocation and DNAse I-like enzymatic activity of *Acinetobacter baumannii* outer membrane protein A. *FEMS Microbiol. Lett.* 288, 62–67. doi: 10.1111/j.1574-6968.2008.01323.x

Choi, C. H., Lee, J. S., Lee, Y. C., Park, T. I., and Lee, J. C. (2008b). *Acinetobacter baumannii* invades epithelial cells and outer membrane protein A mediates interactions with epithelial cells. *BMC Microbiol.* 8:216. doi: 10.1186/1471-2180-8-216

Choi, A. H. K., Slamti, L., Avci, F. Y., Pier, G. B., and Maira-Litrán, T. (2009). The *pgaABCD* locus of *Acinetobacter baumannii* encodes the production of poly-β-1-6-N-acetylglucosamine, which is critical for biofilm formation. *J. Bacteriol.* 191, 5953–5963. doi: 10.1128/JB.00647-09

Cirioni, O., Simonetti, O., Pierpaoli, E., Barucca, A., Ghiselli, R., Orlando, F., et al. (2016). Colistin enhances therapeutic efficacy of daptomycin or teicoplanin in a murine model of multiresistant *Acinetobacter baumannii* sepsis. *Diagn. Microbiol. Infect. Dis.* 86, 392–398. doi: 10.1016/j.diagmicrobio.2016.09.010

Cobo, E. R., and Chadee, K. (2013). Antimicrobial human β-defensins in the colon and their role in infectious and non-infectious diseases. *Pathogens* 2, 177–192. doi: 10.3390/pathogens2010177

Collinet-Adler, S., Castro, C. A., Ledonio, C. G. T., Bechtold, J. E., and Tsukayama, D. T. (2011). *Acinetobacter baumannii* is not associated with osteomyelitis in a rat model: a pilot study. *Clin. Orthop. Relat. Res.* 469, 274–282. doi: 10.1007/s11999-010-1488-0

Crane, D. P., Gromov, K., Li, D., Søballe, K., Wahnes, C., Büchner, H., et al. (2009). Efficacy of colistin-impregnated beads to prevent multidrug-resistant *A. baumannii* implant-associated osteomyelitis. *J. Orthop. Res.* 27, 1008–1015. doi: 10.1002/jor.20847

Crépin, S., Ottosen, E. N., Peters, K., Smith, S. N., Himpsl, S. D., Vollmer, W., et al. (2018). The lytic transglycosylase MltB connects membrane homeostasis and *in vivo* fitness of *Acinetobacter baumannii*. *Mol. Microbiol.* 109, 745–762. doi: 10.1111/mmi.14000

Dai, T., Tegos, G. P., Lu, Z., Huang, L., Zhiyentayev, T., Franklin, M. J., et al. (2009). Photodynamic therapy for *Acinetobacter baumannii* burn infections in mice. *Antimicrob. Agents Chemother.* 53, 3929–3934. doi: 10.1128/AAC.00027-09

Dave, S., Brooks-Walter, A., Pangburn, M. K., and McDaniel, L. S. (2001). PspC, a pneumococcal surface protein, binds human factor H. *Infect. Immun.* 69, 3435–3437. doi: 10.1128/IAI.69.5.3435-3437.2001

De Breij, A., Eveillard, M., Dijkshoorn, L., Van Den Broek, P. J., Nibbering, P. H., and Joly-Guillou, M.-L. (2012). Differences in *Acinetobacter baumannii* strains and host innate immune response determine morbidity and mortality in experimental pneumonia. *PLoS One* 7:e30673. doi: 10.1371/journal.pone.0030673

De Breij, A., Gaddy, J., Van Der Meer, J., Koning, R., Koster, A., Van Den Broek, P., et al. (2009). CsuA/BABCDE-dependent pili are not involved in the adherence of *Acinetobacter baumannii* ATCC19606T to human airway epithelial cells and their inflammatory response. *Res. Microbiol.* 160, 213–218. doi: 10.1016/j.resmic.2009.01.002

De Léséleuc, L., Harris, G., Kuolee, R., Xu, H. H., and Chen, W. (2014). Serum resistance, gallium nitrate tolerance and extrapulmonary dissemination are linked to heme consumption in a bacteremic strain of *Acinetobacter baumannii*. *Int. J. Med. Microbiol.* 304, 360–369. doi: 10.1016/j.ijmm.2013.12.002

De Silva, P. M., Chong, P., Fernando, D. M., Westmacott, G., and Kumar, A. (2017). Effect of incubation temperature on antibiotic resistance and virulence factors of *Acinetobacter baumannii* ATCC 17978. *Antimicrob. Agents Chemother.* 62, e01514–e01517. doi: 10.1128/AAC.01514-17

Deveson Lucas, D., Crane, B., Wright, A., Han, M.-L., Moffatt, J., Bulach, D., et al. (2018). Emergence of high-level colistin resistance in an *Acinetobacter baumannii* clinical isolate mediated by inactivation of the global regulator H-NS. *Antimicrob. Agents Chemother.* 62, e02442-17. doi: 10.1128/AAC.02442-17

Dexter, C., Murray, G. L., Paulsen, I. T., and Peleg, A. Y. (2015). Community-acquired *Acinetobacter baumannii:* clinical characteristics, epidemiology and pathogenesis. *Expert Rev. Anti-Infect. Ther.* 13, 567–573. doi: 10.1586/14787210.2015.1025055

Diancourt, L., Passet, V., Nemec, A., Dijkshoorn, L., and Brisse, S. (2010). The population structure of *Acinetobacter baumannii*: expanding multiresistant clones from an ancestral susceptible genetic Pool. *PLoS One* 5:e10034. doi: 10.1371/journal.pone.0010034

Dikshit, N., Kale, S. D., Khameneh, H. J., Balamuralidhar, V., Tang, C. Y., Kumar, P., et al. (2017). NLRP3 inflammasome pathway has a critical role in the host immunity against clinically relevant *Acinetobacter baumannii* pulmonary infection. *Mucosal Immunol.* 11, 257–272. doi: 10.1038/mi.2017.50

Du, D., Wang-Kan, X., Neuberger, A., Van Veen, H. W., Pos, K. M., Piddock, L. J. V., et al. (2018). Multidrug efflux pumps: structure, function and regulation. *Nat. Rev. Microbiol.* 16, 523–539. doi: 10.1038/s41579-018-0048-6

Eijkelkamp, B. A., Hassan, K. A., Paulsen, I. T., and Brown, M. H. (2011). Investigation of the human pathogen *Acinetobacter baumannii* under iron limiting conditions. *BMC Genomics* 12:126. doi: 10.1186/1471-2164-12-126

Eijkelkamp, B. A., Stroeher, U. H., Hassan, K. A., Elbourne, L. D. H., Paulsen, I. T., and Brown, M. H. (2013). H-NS plays a role in expression of *Acinetobacter baumannii* virulence features. *Infect. Immun.* 81, 2574–2583. doi: 10.1128/IAI.00065-13

Eijkelkamp, B. A., Stroeher, U. H., Hassan, K. A., Paulsen, I. T., and Brown, M. H. (2014). Comparative analysis of surface-exposed virulence factors of *Acinetobacter baumannii*. *BMC Genomics* 15:1020. doi: 10.1186/1471-2164-15-1020

Elhosseiny, N. M., Amin, M. A., Yassin, A. S., and Attia, A. S. (2015). *Acinetobacter baumannii* universal stress protein A plays a pivotal role in stress response and is essential for pneumonia and sepsis pathogenesis. *Int. J. Med. Microbiol.* 305, 114–123. doi: 10.1016/j.ijmm.2014.11.008

Elhosseiny, N. M., and Attia, A. S. (2018). *Acinetobacter*: an emerging pathogen with a versatile secretome. *Emerg. Microb. Infect.* 7, 1–15. doi: 10.1038/s41426-018-0030-4

Eliopoulos, G. M., Maragakis, L. L., and Perl, T. M. (2008). *Acinetobacter baumannii:* epidemiology, antimicrobial resistance, and treatment options. *Clin. Infect. Dis.* 46, 1254–1263. doi: 10.1086/529198

Ellett, F., Pase, L., Hayman, J. W., Andrianopoulos, A., and Lieschke, G. J. (2010). *mpeg1* promoter transgenes direct macrophage-lineage expression in zebrafish. *Blood* 117, e49–e56. doi: 10.1182/blood-2010-10-314120

Esin, S., Batoni, G., Counoupas, C., Stringaro, A., Brancatisano, F. L., Colone, M., et al. (2008). Direct binding of human NK cell natural cytotoxicity receptor NKp44 to the surfaces of *Mycobacteria* and other bacteria. *Infect. Immun.* 76, 1719–1727. doi: 10.1128/IAI.00870-07

Eveillard, M., Soltner, C., Kempf, M., Saint-André, J.-P., Lemarié, C., Randrianarivelo, C., et al. (2010). The virulence variability of different *Acinetobacter baumannii* strains in experimental pneumonia. *J. Inf. Secur.* 60, 154–161. doi: 10.1016/j.jinf.2009.09.004

Falagas, M., Karveli, E., Kelesidis, I., and Kelesidis, T. (2007). Community-acquired *Acinetobacter* infections. *Eur. J. Clin. Microbiol. Infect. Dis.* 26, 857–868. doi: 10.1007/s10096-007-0365-6

Ferreira, V. P., Pangburn, M. K., and Cortés, C. (2010). Complement control protein factor H: the good, the bad, and the inadequate. *Mol. Immunol.* 47, 2187–2197. doi: 10.1016/j.molimm.2010.05.007

Fiester, S. E., Arivett, B. A., Schmidt, R. E., Beckett, A. C., Ticak, T., Carrier, M. V., et al. (2016). Iron-regulated phospholipase C activity contributes to the cytolytic activity and virulence of *Acinetobacter baumannii*. *PLoS One* 11:e0167068. doi: 10.1371/journal.pone.0167068

Fitzsimons, T. C., Lewis, J. M., Wright, A., Kleifeld, O., Schittenhelm, R. B., Powell, D., et al. (2018). Identification of novel *Acinetobacter baumannii* type VI secretion system anti-bacterial effector and immunity pairs. *Infect. Immun.* 86, e00297-18. doi: 10.1128/IAI.00297-18

Fleming, I. D., Krezalek, M. A., Belogortseva, N., Zaborin, A., Defazio, J., Chandrasekar, L., et al. (2017). Modeling *Acinetobacter baumannii* wound infections: the critical role of iron. *J. Trauma Acute Care Surg.* 82, 557–565. doi: 10.1097/TA.0000000000001338

Freire, M. P., De Oliveira Garcia, D., Garcia, C. P., Campagnari Bueno, M. F., Camargo, C. H., Kono Magri, A. S. G., et al. (2016). Bloodstream infection caused by extensively drug-resistant *Acinetobacter baumannii* in cancer patients: high mortality associated with delayed treatment rather than with the degree of neutropenia. *Clin. Microbiol. Infect.* 22, 352–358. doi: 10.1016/j.cmi.2015.12.010

Gaddy, J. A., Arivett, B. A., McConnell, M. J., López-Rojas, R., Pachón, J., and Actis, L. A. (2012). Role of Acinetobactin-mediated iron acquisition functions in the interaction of *Acinetobacter baumannii* strain ATCC 19606T with human lung epithelial cells, *Galleria mellonella* caterpillars, and mice. *Infect. Immun.* 80, 1015–1024. doi: 10.1128/IAI.06279-11

Gallagher, L. A., Ramage, E., Weiss, E. J., Radey, M., Hayden, H. S., Held, K. G., et al. (2015). Resources for genetic and genomic analysis of emerging pathogen *Acinetobacter baumannii*. *J. Bacteriol.* 197, 2027–2035. doi: 10.1128/JB.00131-15

Garcia, A., Solar, H., Gonzalez, C., and Zemelman, R. (2000). Effect of EDTA on the resistance of clinical isolates of *Acinetobacter baumannii* to the

bactericidal activity of normal human serum. *J. Med. Microbiol.* 49, 1047–1050. doi: 10.1099/0022-1317-49-11-1047

García-Garmendia, J.-L., Ortiz-Leyba, C., Garnacho-Montero, J., Jiménez-Jiménez, F.-J., Pérez-Paredes, C., Barrero-Almodóvar, A. E., et al. (2001). Risk factors for *Acinetobacter baumannii* nosocomial bacteremia in critically ill patients: a cohort study. *Clin. Infect. Dis.* 33, 939–946. doi: 10.1086/322584

García-Patiño, M. G., García-Contreras, R., and Licona-Limón, P. (2017). The immune response against *Acinetobacter baumannii*, an emerging pathogen in nosocomial infections. *Front. Immunol.* 8:441. doi: 10.3389/fimmu.2017.00441

García-Quintanilla, M., Pulido, M. R., Pachón, J., and McConnell, M. J. (2014). Immunization with lipopolysaccharide-deficient whole cells provides protective immunity in an experimental mouse model of *Acinetobacter baumannii* infection. *PLoS One* 9:e114410. doi: 10.1371/journal.pone.0114410

Garg, N., Singh, R., Shukla, G., Capalash, N., and Sharma, P. (2016). Immunoprotective potential of in silico predicted *Acinetobacter baumannii* outer membrane nuclease, NucAb. *Int. J. Med. Microbiol.* 306, 1–9. doi: 10.1016/j.ijmm.2015.10.005

Gebhardt, M. J., Gallagher, L. A., Jacobson, R. K., Usacheva, E. A., Peterson, L. R., Zurawski, D. V., et al. (2015). Joint transcriptional control of virulence and resistance to antibiotic and environmental stress in *Acinetobacter baumannii*. *MBio* 6, e01660-15. doi: 10.1128/mBio.01660-15

Geisinger, E., and Isberg, R. R. (2015). Antibiotic modulation of capsular exopolysaccharide and virulence in *Acinetobacter baumannii*. *PLoS Pathog.* 11:e1004691. doi: 10.1371/journal.ppat.1004691

Geisinger, E., Mortman, N. J., Vargas-Cuebas, G., Tai, A. K., and Isberg, R. R. (2018). A global regulatory system links virulence and antibiotic resistance to envelope homeostasis in *Acinetobacter baumannii*. *PLoS Pathog.* 14:e1007030. doi: 10.1371/journal.ppat.1007030

Geng, S., Matsushima, H., Okamoto, T., Yao, Y., Lu, R., Page, K., et al. (2013). Emergence, origin, and function of neutrophil–dendritic cell hybrids in experimentally induced inflammatory lesions in mice. *Blood* 121, 1690–1700. doi: 10.1182/blood-2012-07-445197

Goh, H. M. S., Beatson, S. A., Totsika, M., Moriel, D. G., Phan, M.-D., Szubert, J., et al. (2013). Molecular analysis of the *Acinetobacter baumannii* biofilm-associated protein. *Appl. Environ. Microbiol.* 79, 6535–6543. doi: 10.1128/AEM.01402-13

Greenwald, G. I., and Ganz, T. (1987). Defensins mediate the microbicidal activity of human neutrophil granule extract against *Acinetobacter calcoaceticus*. *Infect. Immun.* 55, 1365–1368.

Hall, C., Flores, M. V., Storm, T., Crosier, K., and Crosier, P. (2007). The zebrafish lysozyme C promoter drives myeloid-specific expression in transgenic fish. *BMC Dev. Biol.* 7:42. doi: 10.1186/1471-213X-7-42

Hall-Stoodley, L., Costerton, J. W., and Stoodley, P. (2004). Bacterial biofilms: from the natural environment to infectious diseases. *Nat. Rev. Microbiol.* 2, 95–108. doi: 10.1038/nrmicro821

Harding, C. M., Hennon, S. W., and Feldman, M. F. (2017a). Uncovering the mechanisms of *Acinetobacter baumannii* virulence. *Nat. Rev. Microbiol.* 16, 91–102. doi: 10.1038/nrmicro.2017.148

Harding, C. M., Kinsella, R. L., Palmer, L. D., Skaar, E. P., and Feldman, M. F. (2016). Medically relevant *Acinetobacter* species require a type II secretion system and specific membrane-associated chaperones for the export of multiple substrates and full virulence. *PLoS Pathog.* 12:e1005391. doi: 10.1371/journal.ppat.1005391

Harding, C. M., Pulido, M. R., Di Venanzio, G., Kinsella, R. L., Webb, A. I., Scott, N. E., et al. (2017b). Pathogenic *Acinetobacter* species have a functional type I secretion system and contact-dependent inhibition systems. *J. Biol. Chem.* 292, 9075–9087. doi: 10.1074/jbc.M117.781575

Hassan, K. A., Jackson, S. M., Penesyan, A., Patching, S. G., Tetu, S. G., Eijkelkamp, B. A., et al. (2013). Transcriptomic and biochemical analyses identify a family of chlorhexidine efflux proteins. *Proc. Natl. Acad. Sci.* 110, 20254–20259. doi: 10.1073/pnas.1317052110

Hasselbring, B. M., Patel, M. K., and Schell, M. A. (2011). *Dictyostelium discoideum* as a model system for identification of *Burkholderia pseudomallei* virulence factors. *Infect. Immun.* 79, 2079–2088. doi: 10.1128/IAI.01233-10

Hee, C. C., Hee, H. S., Young, L. J., Sik, L. J., Seok, L. Y., Ae, K. S., et al. (2008). *Acinetobacter baumannii* outer membrane protein A targets the nucleus and induces cytotoxicity. *Cell. Microbiol.* 10, 309–319. doi: 10.1111/j.1462-5822.2007.01041.x

Hee, C. C., Young, L. E., Chul, L. Y., In, P. T., Jung, K. H., Hee, H. S., et al. (2005). Outer membrane protein 38 of *Acinetobacter baumannii* localizes to the mitochondria and induces apoptosis of epithelial cells. *Cell. Microbiol.* 7, 1127–1138. doi: 10.1111/j.1462-5822.2005.00538.x

Henderson, I. R., Cappello, R., and Nataro, J. P. (2000). Autotransporter proteins, evolution and redefining protein secretion. *Trends Microbiol.* 8, 529–532. doi: 10.1016/S0966-842X(00)01853-9

Henderson, I. R., Navarro-Garcia, F., Desvaux, M., Fernandez, R. C., and Ala'aldeen, D. (2004). Type V protein secretion pathway: the autotransporter story. *Microbiol. Mol. Biol. Rev.* 68, 692–744. doi: 10.1128/MMBR.68.4.692-744.2004

Hood, M. I., and Skaar, E. P. (2012). Nutritional immunity: transition metals at the pathogen–host interface. *Nat. Rev. Microbiol.* 10, 525–537. doi: 10.1038/nrmicro2836

Hornsey, M., Phee, L., Longshaw, C., and Wareham, D. W. (2013). *In vivo* efficacy of telavancin/colistin combination therapy in a *Galleria mellonella* model of *Acinetobacter baumannii* infection. *Int. J. Antimicrob. Agents* 41, 285–287. doi: 10.1016/j.ijantimicag.2012.11.013

Hornsey, M., and Wareham, D. W. (2011). *In vivo* efficacy of glycopeptide/colistin combination therapies in a *Galleria mellonella* model of *Acinetobacter baumannii* infection. *Antimicrob. Agents Chemother.* 55, 3534–3537. doi: 10.1128/AAC.00230-11

Hu, D., Liu, B., Dijkshoorn, L., Wang, L., and Reeves, P. R. (2013). Diversity in the major polysaccharide antigen of *Acinetobacter baumannii* assessed by DNA sequencing, and development of a molecular serotyping scheme. *PLoS One* 8:e70329. doi: 10.1371/journal.pone.0083821

Huang, W., Wang, S., Yao, Y., Xia, Y., Yang, X., Long, Q., et al. (2015). OmpW is a potential target for eliciting protective immunity against *Acinetobacter baumannii* infections. *Vaccine* 33, 4479–4485. doi: 10.1016/j.vaccine.2015.07.031

Iacono, M., Villa, L., Fortini, D., Bordoni, R., Imperi, F., Bonnal, R. J. P., et al. (2008). Whole-genome pyrosequencing of an epidemic multidrug-resistant *Acinetobacter baumannii* strain belonging to the European clone II group. *Antimicrob. Agents Chemother.* 52, 2616–2625. doi: 10.1128/AAC.01643-07

Ishikawa, M., Yoshimoto, S., Hayashi, A., Kanie, J., and Hori, K. (2016). Discovery of a novel periplasmic protein that forms a complex with a trimeric autotransporter adhesin and peptidoglycan. *Mol. Microbiol.* 101, 394–410. doi: 10.1111/mmi.13398

Islam, A. H. M. S., Singh, K.-K. B., and Ismail, A. (2011). Demonstration of an outer membrane protein that is antigenically specific for *Acinetobacter baumannii*. *Diagn. Microbiol. Infect. Dis.* 69, 38–44. doi: 10.1016/j.diagmicrobio.2010.09.008

Iwashkiw, J. A., Seper, A., Weber, B. S., Scott, N. E., Vinogradov, E., Stratilo, C., et al. (2012). Identification of a general O-linked protein glycosylation system in *Acinetobacter baumannii* and its role in virulence and biofilm formation. *PLoS Pathog.* 8:e1002758. doi: 10.1371/journal.ppat.1002758

Iyer, R., Moussa, S. H., Durand-Réville, T. F., Tommasi, R., and Miller, A. (2018). *Acinetobacter baumannii* OmpA is a selective antibiotic permeant porin. *ACS Infect. Dis.* 4, 373–381. doi: 10.1021/acsinfecdis.7b00168

Jacob-Dubuisson, F., Locht, C., and Antoine, R. (2001). Two-partner secretion in gram-negative bacteria: a thrifty, specific pathway for large virulence proteins. *Mol. Microbiol.* 40, 306–313. doi: 10.1046/j.1365-2958.2001.02278.x

Jacob-Dubuisson, F., Villeret, V., Clantin, B., Delattre, A. S., and Saint, N. (2009). First structural insights into the TpsB/Omp85 superfamily. *Biol. Chem.* 390, 675–684. doi: 10.1515/BC.2009.099

Jacobs, A. C., Hood, I., Boyd, K. L., Olson, P. D., Morrison, J. M., Carson, S., et al. (2010). Inactivation of phospholipase D diminishes *Acinetobacter baumannii* pathogenesis. *Infect. Immun.* 78, 1952–1962. doi: 10.1128/IAI.00889-09

Jahangiri, A., Rasooli, I., Owlia, P., Imani Fooladi, A. A., and Salimian, J. (2018). Highly conserved exposed immunogenic peptides of Omp34 against *Acinetobacter baumannii*: an innovative approach. *J. Microbiol. Methods* 144, 79–85. doi: 10.1016/j.mimet.2017.11.008

Jayamani, E., Rajamuthiah, R., Larkins-Ford, J., Fuchs, B. B., Conery, A. L., Vilcinskas, A., et al. (2015). Insect-derived cecropins display activity against *Acinetobacter baumannii* in a whole-animal high-throughput *Caenorhabditis elegans* model. *Antimicrob. Agents Chemother.* 59, 1728–1737. doi: 10.1128/AAC.04198-14

Jin, J. S., Kwon, S.-O., Moon, D. C., Gurung, M., Lee, J. H., Kim, S. I., et al. (2011). *Acinetobacter baumannii* secretes cytotoxic outer membrane protein

A via outer membrane vesicles. *PLoS One* 6:e17027. doi: 10.1371/journal.pone.0017027

Johnson, T. L., Waack, U., Smith, S., Mobley, H., and Sandkvist, M. (2016). *Acinetobacter baumannii* is dependent on the type II secretion system and its substrate LipA for lipid utilization and *in vivo* fitness. *J. Bacteriol.* 198, 711–719. doi: 10.1128/JB.00622-15

Joly-Guillou, M. L., Wolff, M., Pocidalo, J. J., Walker, F., and Carbon, C. (1997). Use of a new mouse model of *Acinetobacter baumannii* pneumonia to evaluate the postantibiotic effect of imipenem. *Antimicrob. Agents Chemother.* 41, 345–351. doi: 10.1128/AAC.41.2.345

Joseph, P. M., and Stephen, T. M. (2018). Expanding the paradigm for the outer membrane: *Acinetobacter baumannii* in the absence of endotoxin. *Mol. Microbiol.* 107, 47–56. doi: 10.1111/mmi.13872

Jousselin, A., Metzinger, L., and Felden, B. (2009). On the facultative requirement of the bacterial RNA chaperone, Hfq. *Trends Microbiol.* 17, 399–405. doi: 10.1016/j.tim.2009.06.003

Juttukonda, L. J., Chazin, W. J., and Skaar, E. P. (2016). *Acinetobacter baumannii* coordinates urea metabolism with metal import to resist host-mediated metal limitation. *MBio* 7, e01475-16. doi: 10.1128/mBio.01475-16

Kamoshida, G., Kikuchi-Ueda, T., Nishida, S., Tansho-Nagakawa, S., Ubagai, T., and Ono, Y. (2018). Pathogenic bacterium *Acinetobacter baumannii* inhibits the formation of neutrophil extracellular traps by suppressing neutrophil adhesion. *Front. Immunol.* 9:178. doi: 10.3389/fimmu.2018.00178

Kamoshida, G., Kikuchi-Ueda, T., Tansho-Nagakawa, S., Nakano, R., Nakano, A., Kikuchi, H., et al. (2015). *Acinetobacter baumannii* escape from neutrophil extracellular traps (NETs). *J. Infect. Chemother.* 21, 43–49. doi: 10.1016/j.jiac.2014.08.032

Kamoshida, G., Tansho-Nagakawa, S., Kikuchi-Ueda, T., Nakano, R., Hikosaka, K., Nishida, S., et al. (2016). A novel bacterial transport mechanism of *Acinetobacter baumannii* via activated human neutrophils through interleukin-8. *J. Leukoc. Biol.* 100, 1405–1412. doi: 10.1189/jlb.4AB0116-023RR

Kaparakis-Liaskos, M., and Ferrero, R. L. (2015). Immune modulation by bacterial outer membrane vesicles. *Nat. Rev. Immunol.* 15, 375–387. doi: 10.1038/nri3837

Karageorgopoulos, D. E., and Falagas, M. E. (2008). Current control and treatment of multidrug-resistant *Acinetobacter baumannii* infections. *Lancet Infect. Dis.* 8, 751–762. doi: 10.1016/S1473-3099(08)70279-2

Kato, S., Kowashi, Y., and Demuth, D. R. (2002). Outer membrane-like vesicles secreted by *Actinobacillus actinomycetemcomitans* are enriched in leukotoxin. *Microb. Pathog.* 32, 1–13. doi: 10.1006/mpat.2001.0474

Kenyon, J. J., and Hall, R. M. (2013). Variation in the complex carbohydrate biosynthesis loci of *Acinetobacter baumannii* genomes. *PLoS One* 8:e62160. doi: 10.1371/journal.pone.0062160

Kikuchi-Ueda, T., Kamoshida, G., Ubagai, T., Nakano, R., Nakano, A., Akuta, T., et al. (2017). The TNF-α of mast cells induces pro-inflammatory responses during infection with *Acinetobacter baumannii*. *Immunobiology* 222, 1025–1034. doi: 10.1016/j.imbio.2017.05.015

Kim, S. W., Choi, C. H., Moon, D. C., Jin, J. S., Lee, J. H., Shin, J.-H., et al. (2009). Serum resistance of *Acinetobacter baumannii* through the binding of factor H to outer membrane proteins. *FEMS Microbiol. Lett.* 301, 224–231. doi: 10.1111/j.1574-6968.2009.01820.x

Kim, C., Kim, D., Lee, S., Jeong, Y., Kang, M., Lee, J., et al. (2014). Toll-like receptor 2 promotes bacterial clearance during the initial stage of pulmonary infection with *Acinetobacter baumannii*. *Mol. Med. Rep.* 9, 1410–1414. doi: 10.3892/mmr.2014.1966

King, L. B., Pangburn, M. K., and McDaniel, L. S. (2013). Serine protease PKF of *Acinetobacter baumannii* results in serum resistance and suppression of biofilm formation. *J. Infect. Dis.* 207, 1128–1134. doi: 10.1093/infdis/jis939

King, L. B., Swiatlo, E., Swiatlo, A., and McDaniel, L. S. (2009). Serum resistance and biofilm formation in clinical isolates of *Acinetobacter baumannii*. *FEMS Immunol. Med. Microbiol.* 55, 414–421. doi: 10.1111/j.1574-695X.2009.00538.x

Knapp, S., Wieland, C. W., Florquin, S., Pantophlet, R., Dijkshoorn, L., Tshimbalanga, N., et al. (2006). Differential roles of CD14 and toll-like receptors 4 and 2 in murine *Acinetobacter* pneumonia. *Am. J. Respir. Crit. Care Med.* 173, 122–129. doi: 10.1164/rccm.200505-730OC

Ko, W.-C., Lee, H.-C., Chiang, S.-R., Yan, J.-J., Wu, J.-J., Lu, C.-L., et al. (2004). *In vitro* and *in vivo* activity of meropenem and sulbactam against a multidrug-resistant *Acinetobacter baumannii* strain. *J. Antimicrob. Chemother.* 53, 393–395. doi: 10.1093/jac/dkh080

Koenigs, A., Stahl, J., Averhoff, B., Göttig, S., Wichelhaus, T. A., Wallich, R., et al. (2016). CipA of *Acinetobacter baumannii* is a novel plasminogen binding and complement inhibitory protein. *J. Infect. Dis.* 213, 1388–1399. doi: 10.1093/infdis/jiv601

Koeppen, K., Hampton, T. H., Jarek, M., Scharfe, M., Gerber, S. A., Mielcarz, D. W., et al. (2016). A novel mechanism of host-pathogen interaction through sRNA in bacterial outer membrane vesicles. *PLoS Pathog.* 12:e1005672. doi: 10.1371/journal.ppat.1005672

Koiwai, K., Hartmann, M. D., Linke, D., Lupas, A. N., and Hori, K. (2016). Structural basis for toughness and flexibility in the C-terminal passenger domain of an *Acinetobacter* trimeric autotransporter adhesin. *J. Biol. Chem.* 291, 3705–3724. doi: 10.1074/jbc.M115.701698

Konstantinidis, T., Kambas, K., Mitsios, A., Panopoulou, M., Tsironidou, V., Dellaporta, E., et al. (2016). Immunomodulatory role of clarithromycin in *Acinetobacter baumannii* infection via formation of neutrophil extracellular traps. *Antimicrob. Agents Chemother.* 60, 1040–1048. doi: 10.1128/AAC.02063-15

Kuehn, M. J., and Kesty, N. C. (2005). Bacterial outer membrane vesicles and the host–pathogen interaction. *Genes Dev.* 19, 2645–2655. doi: 10.1101/gad.1299905

Kulesus, R. R., Diaz-Perez, K., Slechta, E. S., Eto, D. S., and Mulvey, M. A. (2008). Impact of the RNA chaperone Hfq on the fitness and virulence potential of uropathogenic *Escherichia coli*. *Infect. Immun.* 76, 3019–3026. doi: 10.1128/IAI.00022-08

Kulkarni, H. M., and Jagannadham, M. V. (2014). Biogenesis and multifaceted roles of outer membrane vesicles from gram-negative bacteria. *Microbiology* 160, 2109–2121. doi: 10.1099/mic.0.079400-0

Kuo, H.-Y., Chao, H.-H., Liao, P.-C., Hsu, L., Chang, K.-C., Tung, C.-H., et al. (2017). Functional characterization of *Acinetobacter baumannii* lacking the RNA chaperone Hfq. *Front. Microbiol.* 8:2068. doi: 10.3389/fmicb.2017.02068

Kuolee, R., Harris, G., Yan, H., Xu, H. H., Conlan, W. J., Patel, G. B., et al. (2015). Intranasal immunization protects against *Acinetobacter baumannii*-associated pneumonia in mice. *Vaccine* 33, 260–267. doi: 10.1016/j.vaccine.2014.02.083

Kwon, S.-O., Gho, Y. S., Lee, J. C., and Kim, S. I. (2009). Proteome analysis of outer membrane vesicles from a clinical *Acinetobacter baumannii* isolate. *FEMS Microbiol. Lett.* 297, 150–156. doi: 10.1111/j.1574-6968.2009.01669.x

Laarman, A. J., Ruyken, M., Malone, C. L., Van Strijp, J. A. G., Horswill, A. R., and Rooijakkers, S. H. M. (2011). *Staphylococcus aureus* metalloprotease aureolysin cleaves complement C3 to mediate immune evasion. *J. Immunol.* 186, 6445–6453. doi: 10.4049/jimmunol.1002948

Lázaro-Díez, M., Chapartegui-González, I., Redondo-Salvo, S., Leigh, C., Merino, D., Segundo, D. S., et al. (2017). Human neutrophils phagocytose and kill *Acinetobacter baumannii* and *A. pittii*. *Sci. Rep.* 7:4571. doi: 10.1038/s41598-017-04870-8

Lázaro-Díez, M., Navascués-Lejarza, T., Remuzgo-Martínez, S., Navas, J., Icardo, J. M., Acosta, F., et al. (2016). *Acinetobacter baumannii* and *A. pittii* clinical isolates lack adherence and cytotoxicity to lung epithelial cells in vitro. *Microbes Infect.* 18, 559–564. doi: 10.1016/j.micinf.2016.05.002

Lee, J. S., Choi, C. H., Kim, J. W., and Lee, J. C. (2010). *Acinetobacter baumannii* outer membrane protein a induces dendritic cell death through mitochondrial targeting. *J. Microbiol.* 48, 387–392. doi: 10.1007/s12275-010-0155-1

Lee, J. S., Lee, J. C., Lee, C.-M., Jung, I. D., Jeong, Y.-I., Seong, E.-Y., et al. (2007). Outer membrane protein A of *Acinetobacter baumannii* induces differentiation of CD4+ T cells toward a Th1 polarizing phenotype through the activation of dendritic cells. *Biochem. Pharmacol.* 74, 86–97. doi: 10.1016/j.bcp.2007.02.012

Lees-Miller, R. G., Iwashkiw, J. A., Scott, N. E., Seper, A., Vinogradov, E., Schild, S., et al. (2013). A common pathway for O-linked protein-glycosylation and synthesis of capsule in *Acinetobacter baumannii*. *Mol. Microbiol.* 89, 816–830. doi: 10.1111/mmi.12300

Leo, J. C., Grin, I., and Linke, D. (2012). Type V secretion: mechanism(s) of autotransport through the bacterial outer membrane. *Philos. Trans. R. Soc. Bio. Sci.* 367, 1088–1101. doi: 10.1098/rstb.2011.0208

Li, L., Jin, H., Xu, J., Shi, Y., and Wen, Z. (2010). Irf8 regulates macrophage versus neutrophil fate during zebrafish primitive myelopoiesis. *Blood* 117, 1359–1369. doi: 10.1182/blood-2010-06-290700

Lin, M.-F., Lin, Y.-Y., Yeh, H.-W., and Lan, C.-Y. (2014). Role of the BaeSR two-component system in the regulation of *Acinetobacter baumannii adeAB* genes and its correlation with tigecycline susceptibility. *BMC Microbiol.* 14:119. doi: 10.1186/1471-2180-14-119

Lin, L., Tan, B., Pantapalangkoor, P., Ho, T., Baquir, B., Tomaras, A., et al. (2012). Inhibition of LpxC protects mice from resistant *Acinetobacter baumannii* by modulating inflammation and enhancing phagocytosis. *MBio* 3, e00312-12. doi: 10.1128/mBio.00312-12

Liou, M.-L., Soo, P.-C., Ling, S.-R., Kuo, H.-Y., Tang, C. Y., and Chang, K.-C. (2014). The sensor kinase BfmS mediates virulence in *Acinetobacter baumannii*. *J. Microbiol. Immunol. Infect.* 47, 275–281. doi: 10.1016/j.jmii.2012.12.004

Liu, Q., Hassan, K. A., Ashwood, H. E., Gamage, H. K. A. H., Li, L., Mabbutt, B. C., et al. (2018). Regulation of the *aceI* multidrug efflux pump gene in *Acinetobacter baumannii*. *J. Antimicrob. Chemother.* 73, 1492–1500. doi: 10.1093/jac/dky034

Liu, C.-C., Kuo, H.-Y., Tang, C. Y., Chang, K.-C., and Liou, M.-L. (2014). Prevalence and mapping of a plasmid encoding a type IV secretion system in *Acinetobacter baumannii*. *Genomics* 104, 215–223. doi: 10.1016/j.ygeno.2014.07.011

Liu, D., Liu, Z.-S., Hu, P., Cai, L., Fu, B.-Q., Li, Y.-S., et al. (2016). Characterization of surface antigen protein 1 (SurA1) from *Acinetobacter baumannii* and its role in virulence and fitness. *Vet. Microbiol.* 186, 126–138. doi: 10.1016/j.vetmic.2016.02.018

Loehfelm, T. W., Luke, N. R., and Campagnari, A. A. (2008). Identification and characterization of an *Acinetobacter baumannii* biofilm-associated protein. *J. Bacteriol.* 190, 1036–1044. doi: 10.1128/JB.01416-07

Lood, R., Winer, B. Y., Pelzek, A. J., Diez-Martinez, R., Thandar, M., Euler, C. W., et al. (2015). Novel phage lysins capable of killing the multidrug resistant gram-negative bacterium *Acinetobacter baumannii* in a mouse sepsis model. *Antimicrob. Agents Chemother.* 59, 1983–1991. doi: 10.1128/AAC.04641-14

Lopalco, P., Stahl, J., Annese, C., Averhoff, B., and Corcelli, A. (2017). Identification of unique cardiolipin and monolysocardiolipin species in *Acinetobacter baumannii*. *Sci. Rep.* 7:2972. doi: 10.1038/s41598-017-03214-w

Luo, G., Lin, L., Ibrahim, A. S., Baquir, B., Pantapalangkoor, P., Bonomo, R. A., et al. (2012). Active and passive immunization protects against lethal, extreme drug resistant-*Acinetobacter baumannii* infection. *PLoS One* 7:e29446. doi: 10.1371/journal.pone.0051008

Manning, A. J., and Kuehn, M. J. (2011). Contribution of bacterial outer membrane vesicles to innate bacterial defense. *BMC Microbiol.* 11, 258–258. doi: 10.1186/1471-2180-11-258

Manuella, C.-F., Sara, M., Laurent, G., Luis, J., Gaël, C., Virginie, M., et al. (2016). The outer membrane porin OmpW of *Acinetobacter baumannii* is involved in iron uptake and colistin binding. *FEBS Lett.* 590, 224–231. doi: 10.1002/1873-3468.12050

March, C., Regueiro, V., Llobet, E., Moranta, D., Morey, P., Garmendia, J., et al. (2010). Dissection of host cell signal transduction during *Acinetobacter baumannii* – triggered inflammatory response. *PLoS One* 5:e10033. doi: 10.1371/journal.pone.0010033

Marchand, I., Damier-Piolle, L., Courvalin, P., and Lambert, T. (2004). Expression of the RND-type efflux pump AdeABC in *Acinetobacter baumannii* is regulated by the AdeRS two-component system. *Antimicrob. Agents Chemother.* 48, 3298–3304. doi: 10.1128/AAC.48.9.3298-3304.2004

Marti, S., Nait Chabane, Y., Alexandre, S., Coquet, L., Vila, J., Jouenne, T., et al. (2011). Growth of *Acinetobacter baumannii* in pellicle enhanced the expression of potential virulence factors. *PLoS One* 6:e26030. doi: 10.1371/journal.pone.0026030

Martín-Aspas, A., Guerrero-Sánchez, F. M., García-Colchero, F., Rodríguez-Roca, S., and Girón-González, J.-A. (2018). Differential characteristics of *Acinetobacter baumannii* colonization and infection: risk factors, clinical picture, and mortality. *Inf. Drug Resist.* 11, 861–872. doi: 10.2147/IDR.S163944

Matsushima, H., Geng, S., Lu, R., Okamoto, T., Yao, Y., Mayuzumi, N., et al. (2013). Neutrophil differentiation into a unique hybrid population exhibiting dual phenotype and functionality of neutrophils and dendritic cells. *Blood* 121, 1677–1689. doi: 10.1182/blood-2012-07-445189

McBroom, A. J., and Kuehn, M. J. (2005). Outer membrane vesicles. *EcoSal Plus* 1. doi: 10.1128/ecosal.2.2.4

McBroom, A. J., and Kuehn, M. J. (2007). Release of outer membrane vesicles by gram-negative bacteria is a novel envelope stress response. *Mol. Microbiol.* 63, 545–558. doi: 10.1111/j.1365-2958.2006.05522.x

McConnell, M. J., Actis, L., and Pachón, J. (2013). *Acinetobacter baumannii*: human infections, factors contributing to pathogenesis and animal models. *FEMS Microbiol. Rev.* 37, 130–155. doi: 10.1111/j.1574-6976.2012.00344.x

McConnell, M. J., Domínguez-Herrera, J., Smani, Y., López-Rojas, R., Docobo-Pérez, F., and Pachón, J. (2011a). Vaccination with outer membrane complexes elicits rapid protective immunity to multidrug-resistant *Acinetobacter baumannii*. *Infect. Immun.* 79, 518–526. doi: 10.1128/IAI.00741-10

McConnell, M. J., and Pachón, J. (2010). Active and passive immunization against *Acinetobacter baumannii* using an inactivated whole cell vaccine. *Vaccine* 29, 1–5. doi: 10.1016/j.vaccine.2010.10.052

McConnell, M. J., Rumbo, C., Bou, G., and Pachón, J. (2011b). Outer membrane vesicles as an acellular vaccine against *Acinetobacter baumannii*. *Vaccine* 29, 5705–5710. doi: 10.1016/j.vaccine.2011.06.001

McMahon, K. J., Castelli, M. E., Vescovi, E. G., and Feldman, M. F. (2012). Biogenesis of outer membrane vesicles in *Serratia marcescens* is thermoregulated and can be induced by activation of the Rcs phosphorelay system. *J. Bacteriol.* 194, 3241–3249. doi: 10.1128/JB.00016-12

Meumann, E. M., Anstey, N. M., Currie, B. J., Piera, K. A., Kenyon, J. J., Hall, R. M., et al. (2019). Genomic epidemiology of severe community-onset *Acinetobacter baumannii* infection. *Microb. Genom.* 5:e000258. doi: 10.1099/mgen.0.000258.

Moffatt, J. H., Harper, M., Harrison, P., Hale, J. D. F., Vinogradov, E., Seemann, T., et al. (2010). Colistin resistance in *Acinetobacter baumannii* is mediated by complete loss of lipopolysaccharide production. *Antimicrob. Agents Chemother.* 54, 4971–4977. doi: 10.1128/AAC.00834-10

Moffatt, J. H., Harper, M., Mansell, A., Crane, B., Fitzsimons, T. C., Nation, R. L., et al. (2013). Lipopolysaccharide-deficient *Acinetobacter baumannii* shows altered signaling through host toll-like receptors and increased susceptibility to the host antimicrobial peptide LL-37. *Infect. Immun.* 81, 684–689. doi: 10.1128/IAI.01362-12

Mohamed, M. F., Brezden, A., Mohammad, H., Chmielewski, J., and Seleem, M. N. (2017). A short D-enantiomeric antimicrobial peptide with potent immunomodulatory and antibiofilm activity against multidrug-resistant *Pseudomonas aeruginosa* and *Acinetobacter baumannii*. *Sci. Rep.* 7:6953. doi: 10.1038/s41598-017-07440-0

Moon, D. C., Choi, C. H., Lee, J. H., Choi, C.-W., Kim, H.-Y., Park, J. S., et al. (2012). *Acinetobacter baumannii* outer membrane protein a modulates the biogenesis of outer membrane vesicles. *J. Microbiol.* 50, 155–160. doi: 10.1007/s12275-012-1589-4

Moon, K. H., Weber, B. S., and Feldman, M. F. (2017). Subinhibitory concentrations of trimethoprim and sulfamethoxazole prevent biofilm formation by *Acinetobacter baumannii* through inhibition of Csu Pilus expression. *Antimicrob. Agents Chemother.* 61, e00778-17. doi: 10.1128/AAC.00778-17

Mortensen, B. L., Rathi, S., Chazin, W. J., and Skaar, E. P. (2014). *Acinetobacter baumannii* response to host-mediated zinc limitation requires the transcriptional regulator Zur. *J. Bacteriol.* 196, 2616–2626. doi: 10.1128/JB.01650-14

Mostowy, S., Boucontet, L., Mazon Moya, M. J., Sirianni, A., Boudinot, P., Hollinshead, M., et al. (2013). The Zebrafish as a new model for the *in vivo* study of *Shigella flexneri* interaction with phagocytes and bacterial autophagy. *PLoS Pathog.* 9:e1003588. doi: 10.1371/journal.ppat.1003588

Murray, G. L., Tsyganov, K., Kostoulias, X. P., Bulach, D. M., Powell, D., Creek, D. J., et al. (2017). Global gene expression profile of *Acinetobacter baumannii* during bacteremia. *J. Infect. Dis.* 215, S52–S57. doi: 10.1093/infdis/jiw529

Nairn, B. L., Lonergan, Z. R., Wang, J., Braymer, J. J., Zhang, Y., Calcutt, M. W., et al. (2016). The response of *Acinetobacter baumannii* to zinc starvation. *Cell Host Microbe* 19, 826–836. doi: 10.1016/j.chom.2016.05.007

Niu, C., Clemmer, K. M., Bonomo, R. A., and Rather, P. N. (2008). Isolation and characterization of an autoinducer synthase from *Acinetobacter baumannii*. *J. Bacteriol.* 190, 3386–3392. doi: 10.1128/JB.01929-07

Nordenfelt, P., and Tapper, H. (2011). Phagosome dynamics during phagocytosis by neutrophils. *J. Leukoc. Biol.* 90, 271–284. doi: 10.1189/jlb.0810457

Noto, M. J., Boyd, K. L., Burns, W. J., Varga, M. G., Peek, R. M., and Skaar, E. P. (2015). Toll-like receptor 9 contributes to defense against *Acinetobacter baumannii* infection. *Infect. Immun.* 83, 4134–4141. doi: 10.1128/IAI.00410-15

O'Hara, J. A., Ambe, L. A., Casella, L. G., Townsend, B. M., Pelletier, M. R., Ernst, R. K., et al. (2013). Activity of Vancomycin-containing regimens against colistin-resistant *Acinetobacter baumannii* clinical strains. *Antimicrob. Agents Chemother.* 57, 2103–2108. doi: 10.1128/AAC.02501-12

Obana, Y., Nishino, T., and Tanino, T. (1985). *In-vitro* and *in-vivo* activities of antimicrobial agents against *Acinetobacter calcoaceticus*. *J. Antimicrob. Chemother.* 15, 441–448. doi: 10.1093/jac/15.4.441

Pachón-Ibáñez, M. E., Docobo-Pérez, F., López-Rojas, R., Domínguez-Herrera, J., Jiménez-Mejias, M. E., García-Curiel, A., et al. (2010). Efficacy of Rifampin and its combinations with imipenem,

sulbactam, and colistin in experimental models of infection caused by imipenem-resistant *Acinetobacter baumannii*. *Antimicrob. Agents Chemother.* 54, 1165–1172. doi: 10.1128/AAC.00367-09

Paidipally, P., Tripathi, D., Van, A., Radhakrishnan, R. K., Dhiman, R., Venkatasubramanian, S., et al. (2018). Interleukin-21 regulates natural killer cell responses during *Mycobacterium tuberculosis* infection. *J. Infect. Dis.* 217, 1323–1333. doi: 10.1093/infdis/jiy034

Park, J. S., Lee, W. C., Yeo, K. J., Ryu, K.-S., Kumarasiri, M., Hesek, D., et al. (2012). Mechanism of anchoring of OmpA protein to the cell wall peptidoglycan of the gram-negative bacterial outer membrane. *FASEB J.* 26, 219–228. doi: 10.1096/fj.11-188425

Patamatamkul, S., Klungboonkrong, V., Praisarnti, P., and Jirakiat, K. (2017). A case-control study of community-acquired *Acinetobacter baumannii* pneumonia and melioidosis pneumonia in Northeast Thailand: an emerging fatal disease with unique clinical features. *Diagn. Microbiol. Infect. Dis.* 87, 79–86. doi: 10.1016/j.diagmicrobio.2016.10.014

Peleg, A. Y., Jara, S., Monga, D., Eliopoulos, G. M., Moellering, R. C., and Mylonakis, E. (2009). *Galleria mellonella* as a model system to study *Acinetobacter baumannii* pathogenesis and therapeutics. *Antimicrob. Agents Chemother.* 53, 2605–2609. doi: 10.1128/AAC.01533-08

Peleg, A. Y., Seifert, H., and Paterson, D. L. (2008a). *Acinetobacter baumannii*: emergence of a successful pathogen. *Clin. Microbiol. Rev.* 21, 538–582. doi: 10.1128/CMR.00058-07

Peleg, A. Y., Tampakakis, E., Fuchs, B. B., Eliopoulos, G. M., Moellering, R. C., and Mylonakis, E. (2008b). Prokaryote–eukaryote interactions identified by using *Caenorhabditis elegans*. *Proc. Natl. Acad. Sci.* 105, 14585–14590. doi: 10.1073/pnas.0805048105

Peng, C., Han, J., Ye, X., and Zhang, X. (2018). IL-33 treatment attenuates the systemic inflammation reaction in *Acinetobacter baumannii* pneumonia by suppressing TLR4/NF-κB signaling. *Inflammation* 41, 870–877. doi: 10.1007/s10753-018-0741-7

Peng, S.-Y., You, R.-I., Lai, M.-J., Lin, N.-T., Chen, L.-K., and Chang, K.-C. (2017). Highly potent antimicrobial modified peptides derived from the *Acinetobacter baumannii* phage endolysin LysAB2. *Sci. Rep.* 7:11477. doi: 10.1038/s41598-017-11832-7

Pérez, A., Merino, M., Rumbo-Feal, S., Álvarez-Fraga, L., Vallejo, J. A., Beceiro, A., et al. (2017). The FhaB/FhaC two-partner secretion system is involved in adhesion of *Acinetobacter baumannii* AbH12O-A2 strain. *Virulence* 8, 959–974. doi: 10.1080/21505594.2016.1262313

Prajsnar, T. K., Cunliffe, V. T., Foster, S. J., and Renshaw, S. A. (2008). A novel vertebrate model of *Staphylococcus aureus* infection reveals phagocyte-dependent resistance of zebrafish to non-host specialized pathogens. *Cell. Microbiol.* 10, 2312–2325. doi: 10.1111/j.1462-5822.2008.01213.x

Pulido, M. R., García-Quintanilla, M., Pachón, J., and McConnell, M. J. (2018). Immunization with lipopolysaccharide-free outer membrane complexes protects against *Acinetobacter baumannii* infection. *Vaccine* 36, 4153–4156. doi: 10.1016/j.vaccine.2018.05.113

Qiu, H., Kuolee, R., Harris, G., and Chen, W. (2009). Role of NADPH phagocyte oxidase in host defense against acute respiratory *Acinetobacter baumannii* infection in mice. *Infect. Immun.* 77, 1015–1021. doi: 10.1128/IAI.01029-08

Qiu, H., Kuolee, R., Harris, G., Van Rooijen, N., Patel, G. B., and Chen, W. (2012). Role of macrophages in early host resistance to respiratory *Acinetobacter baumannii* infection. *PLoS One* 7:e40019. doi: 10.1371/journal.pone.0040019

Qiu, H., Li, Z., Kuolee, R., Harris, G., Gao, X., Yan, H., et al. (2016). Host resistance to intranasal *Acinetobacter baumannii* reinfection in mice. *Pathog. Dis.* 74, ftw048–ftw048. doi: 10.1093/femspd/ftw048

Renckens, R., Roelofs, J. J. T. H., Knapp, S., De Vos, A. F., Florquin, S., and Van Der Poll, T. (2006). The acute-phase response and serum amyloid A inhibit the inflammatory response to *Acinetobacter baumannii* pneumonia. *J. Infect. Dis.* 193, 187–195. doi: 10.1086/498876

Repizo, G. D. (2017). Prevalence of *Acinetobacter baumannii* strains expressing the type 6 secretion system in patients with bacteremia. *Virulence* 8, 1099–1101. doi: 10.1080/21505594.2017.1346768

Robenshtok, E., Paul, M., Leibovici, L., Fraser, A., Pitlik, S., Ostfeld, I., et al. (2006). The significance of *Acinetobacter baumannii* bacteraemia compared with *Klebsiella pneumoniae* bacteraemia: risk factors and outcomes. *J. Hosp. Infect.* 64, 282–287. doi: 10.1016/j.jhin.2006.06.025

Roca, I., Espinal, P., Vila-Farrés, X., and Vila, J. (2012). The *Acinetobacter baumannii* oxymoron: commensal hospital dweller turned pan-drug-resistant menace. *Front. Microbiol.* 3:148. doi: 10.3389/fmicb.2012.00148

Rodríguez-Hernández, M. J., Jiménez-Mejias, M. E., Pichardo, C., Cuberos, L., García-Curiel, A., and Pachón, J. (2004). Colistin efficacy in an experimental model of *Acinetobacter baumannii* endocarditis. *Clin. Microbiol. Infect.* 10, 581–584. doi: 10.1111/j.1469-0691.2004.00910.x

Roier, S., Zingl, F. G., Cakar, F., Durakovic, S., Kohl, P., Eichmann, T. O., et al. (2016). A novel mechanism for the biogenesis of outer membrane vesicles in gram-negative bacteria. *Nat. Commun.* 7:a10515. doi: 10.1038/ncomms10515

Rumbo, C., Fernández-Moreira, E., Merino, M., Poza, M., Mendez, J. A., Soares, N. C., et al. (2011). Horizontal transfer of the OXA-24 carbapenemase gene via outer membrane vesicles: a new mechanism of dissemination of carbapenem resistance genes in *Acinetobacter baumannii*. *Antimicrob. Agents Chemother.* 55, 3084–3090. doi: 10.1128/AAC.00929-10

Rumbo, C., Tomás, M., Fernández Moreira, E., Soares, N. C., Carvajal, M., Santillana, E., et al. (2014). The *Acinetobacter baumannii* Omp33-36 porin is a virulence factor that induces apoptosis and modulates autophagy in human cells. *Infect. Immun.* 82, 4666–4680. doi: 10.1128/IAI.02034-14

Runft, D. L., Mitchell, K. C., Abuaita, B. H., Allen, J. P., Bajer, S., Ginsburg, K., et al. (2014). Zebrafish as a natural host model for *Vibrio cholerae* colonization and transmission. *Appl. Environ. Microbiol.* 80, 1710–1717. doi: 10.1128/AEM.03580-13

Russo, T. A., Beanan, J. M., Olson, R., MacDonald, U., Cox, A. D., St. Michael, F., et al. (2013). The K1 capsular polysaccharide from *Acinetobacter baumannii* is a potential therapeutic target via passive immunization. *Infect. Immun.* 81, 915–922. doi: 10.1128/IAI.01184-12

Russo, T. A., Beanan, J. M., Olson, R., Macdonald, U., Luke, N. R., Gill, S. R., et al. (2008). Rat pneumonia and soft-tissue infection models for the study of *Acinetobacter baumannii* biology. *Infect. Immun.* 76, 3577–3586. doi: 10.1128/IAI.00269-08

Russo, T. A., Luke, N. R., Beanan, J. M., Olson, R., Sauberan, S. L., Macdonald, U., et al. (2010). The K1 capsular polysaccharide of *Acinetobacter baumannii* strain 307-0294 is a major virulence factor. *Infect. Immun.* 78, 3993–4000. doi: 10.1128/IAI.00366-10

Rutherford, S. T., and Bassler, B. L. (2012). Bacterial quorum sensing: its role in virulence and possibilities for its control. *Cold Spring Harb. Perspect. Med.* 2:a012427. doi: 10.1101/cshperspect.a012427

Schilling, D., and Gerischer, U. (2009). The *Acinetobacter baylyi hfq* gene encodes a large protein with an unusual C terminus. *J. Bacteriol.* 191, 5553–5562. doi: 10.1128/JB.00490-09

Schmiel, D. H., and Miller, V. L. (1999). Bacterial phospholipases and pathogenesis. *Microbes Infect.* 1, 1103–1112. doi: 10.1016/S1286-4579(99)00205-1

Sebe, I., Ostorhazi, E., Fekete, A., Kovacs, K. N., Zelko, R., Kovalszky, I., et al. (2016). Polyvinyl alcohol nanofiber formulation of the designer antimicrobial peptide APO sterilizes *Acinetobacter baumannii*-infected skin wounds in mice. *Amino Acids* 48, 203–211. doi: 10.1007/s00726-015-2080-4

Senchenkova, S. Y. N., Shashkov, A. S., Popova, A. V., Shneider, M. M., Arbatsky, N. P., Miroshnikov, K. A., et al. (2015). Structure elucidation of the capsular polysaccharide of *Acinetobacter baumannii* AB5075 having the KL25 capsule biosynthesis locus. *Carbohydr. Res.* 408, 8–11. doi: 10.1016/j.carres.2015.02.011

Shankar, R., He, L.-K., Szilagyi, A., Muthu, K., Gamelli, R. L., Filutowicz, M., et al. (2007). A novel antibacterial gene transfer treatment for multidrug-resistant *Acinetobacter baumannii*-induced burn sepsis. *J. Burn Care Res.* 28, 6–12. doi: 10.1097/BCR.0b013e31802c8861

Shlaes, D. M., and Bradford, P. A. (2018). Antibiotics—from there to where? *Pathog. Immun.* 3, 19–43. doi: 10.20411/pai.v3i1.231

Small, C.-L., McCormick, S., Gill, N., Kugathasan, K., Santosuosso, M., Donaldson, N., et al. (2008). NK cells play a critical protective role in host defense against acute extracellular *Staphylococcus aureus* bacterial infection in the lung. *J. Immunol.* 180, 5558–5568. doi: 10.4049/jimmunol.180.8.5558

Smani, Y., McConnell, M. J., and Pachón, J. (2012). Role of fibronectin in the adhesion of *Acinetobacter baumannii* to host cells. *PLoS One* 7:e33073. doi: 10.1371/journal.pone.0033073

Smith, M. G., Des Etages, S. G., and Snyder, M. (2004). Microbial synergy via an ethanol-triggered pathway. *Mol. Cell. Biol.* 24, 3874–3884. doi: 10.1128/MCB.24.9.3874-3884.2004

Smith, M. G., Gianoulis, T. A., Pukatzki, S., Mekalanos, J. J., Ornston, L. N., Gerstein, M., et al. (2007). New insights into *Acinetobacter baumannii* pathogenesis revealed by high-density pyrosequencing and transposon mutagenesis. *Genes Dev.* 21, 601–614. doi: 10.1101/gad.1510307

Song, X., Zhang, H., Zhang, D., Xie, W., and Zhao, G. (2018). Bioinformatics analysis and epitope screening of a potential vaccine antigen TolB from *Acinetobacter baumannii* outer membrane protein. *Infect. Genet. Evol.* 62, 73–79. doi: 10.1016/j.meegid.2018.04.019

Stahl, J., Bergmann, H., Göttig, S., Ebersberger, I., and Averhoff, B. (2015). *Acinetobacter baumannii* virulence is mediated by the concerted action of three phospholipases D. *PLoS One* 10:e0138360. doi: 10.1371/journal.pone.0138360

Stock, A. M., Victoria L. Robinson, A., and Goudreau, P. N. (2000). Two-component signal transduction. *Annu. Rev. Biochem.* 69, 183–215. doi: 10.1146/annurev.biochem.69.1.183

Sugawara, E., and Nikaido, H. (2012). OmpA is the principal nonspecific slow porin of *Acinetobacter baumannii*. *J. Bacteriol.* 194, 4089–4096. doi: 10.1128/JB.00435-12

Sun, B., Hu, X., Liu, G., Ma, B., Xu, Y., Yang, T., et al. (2014). Phosphatase Wip1 negatively regulates neutrophil migration and inflammation. *J. Immunol.* 192, 1184–1195. doi: 10.4049/jimmunol.1300656

Thuan Tong, T., Mörgelin, M., Forsgren, A., and Riesbeck, K. (2007). Haemophilus influenzae survival during complement-mediated attacks is promoted by *Moraxella catarrhalis* outer membrane vesicles. *J. Infect. Dis.* 195, 1661–1670. doi: 10.1086/517611

Tipton, K. A., Dimitrova, D., and Rather, P. N. (2015). Phase-variable control of multiple phenotypes in *Acinetobacter baumannii* strain AB5075. *J. Bacteriol.* 197, 2593–2599. doi: 10.1128/JB.00188-15

Tomaras, A. P., Flagler, M. J., Dorsey, C. W., Gaddy, J. A., and Actis, L. A. (2008). Characterization of a two-component regulatory system from *Acinetobacter baumannii* that controls biofilm formation and cellular morphology. *Microbiology* 154, 3398–3409. doi: 10.1099/mic.0.2008/019471-0

Touchon, M., Cury, J., Yoon, E.-J., Krizova, L., Cerqueira, G. C., Murphy, C., et al. (2014). The genomic diversification of the whole *Acinetobacter genus*: origins, mechanisms, and consequences. *Genome Biol. Evol.* 6, 2866–2882. doi: 10.1093/gbe/evu225

Tsuchiya, T., Nakao, N., Yamamoto, S., Hirai, Y., Miyamoto, K., and Tsujibo, H. (2012). NK1.1+ cells regulate neutrophil migration in mice with *Acinetobacter baumannii* pneumonia. *Microbiol. Immunol.* 56, 107–116. doi: 10.1111/j.1348-0421.2011.00402.x

Tsui, H. C., Leung, H. C., and Winkler, M. E. (1994). Characterization of broadly pleiotropic phenotypes caused by an *hfq* insertion mutation in *Escherichia coli* K-12. *Mol. Microbiol.* 13, 35–49. doi: 10.1111/j.1365-2958.1994.tb00400.x

Van Der Sar, A. M., Appelmelk, B. J., Vandenbroucke-Grauls, C. M. J. E., and Bitter, W. (2004). A star with stripes: zebrafish as an infection model. *Trends Microbiol.* 12, 451–457. doi: 10.1016/j.tim.2004.08.001

Van Faassen, H., Kuolee, R., Harris, G., Zhao, X., Conlan, J. W., and Chen, W. (2007). Neutrophils play an important role in host resistance to respiratory infection with *Acinetobacter baumannii* in mice. *Infect. Immun.* 75, 5597–5608. doi: 10.1128/IAI.00762-07

Waggoner, S. N., Reighard, S. D., Gyurova, I. E., Cranert, S. A., Mahl, S. E., Karmele, E. P., et al. (2016). Roles of natural killer cells in antiviral immunity. *Curr. Opin. Virol.* 16, 15–23. doi: 10.1016/j.coviro.2015.10.008

Wallace, L., Daugherty, S. C., Nagaraj, S., Johnson, J. K., Harris, A. D., and Rasko, D. A. (2016). Use of comparative genomics to characterize the diversity of *Acinetobacter baumannii* surveillance isolates in a health care institution. *Antimicrob. Agents Chemother.* 60, 5933–5941. doi: 10.1128/AAC.00477-16

Wand, M. E., Bock, L. J., Turton, J. F., Nugent, P. G., and Sutton, J. M. (2012). *Acinetobacter baumannii* virulence is enhanced in *Galleria mellonella* following biofilm adaptation. *J. Med. Microbiol.* 61, 470–477. doi: 10.1099/jmm.0.037523-0

Wang, N., Ozer, E. A., Mandel, M. J., and Hauser, A. R. (2014). Genome-wide identification of *Acinetobacter baumannii* genes necessary for persistence in the lung. *MBio* 5, e01163-14. doi: 10.1128/mBio.01163-14

Weber, B. S., Harding, C. M., and Feldman, M. F. (2016). Pathogenic *Acinetobacter*: from the cell surface to infinity and beyond. *J. Bacteriol.* 198, 880–887. doi: 10.1128/JB.00906-15

Weber, B. S., Kinsella, R. L., Harding, C. M., and Feldman, M. F. (2017). The secrets of *Acinetobacter* secretion. *Trends Microbiol.* 25, 532–545. doi: 10.1016/j.tim.2017.01.005

Weber, B. S., Miyata, S. T., Iwashkiw, J. A., Mortensen, B. L., Skaar, E. P., Pukatzki, S., et al. (2013). Genomic and functional analysis of the type VI secretion system in *Acinetobacter*. *PLoS One* 8:e55142. doi: 10.1371/journal.pone.0055142

White, R. M., Sessa, A., Burke, C., Bowman, T., Leblanc, J., Ceol, C., et al. (2008). Transparent adult Zebrafish as a tool for *in vivo* transplantation analysis. *Cell Stem Cell* 2, 183–189. doi: 10.1016/j.stem.2007.11.002

Whitfield, C., and Trent, M. S. (2014). Biosynthesis and export of bacterial lipopolysaccharides. *Annu. Rev. Biochem.* 83, 99–128. doi: 10.1146/annurev-biochem-060713-035600

Wong, D., Nielsen, T. B., Bonomo, R. A., Pantapalangkoor, P., Luna, B., and Spellberg, B. (2017). Clinical and pathophysiological overview of *Acinetobacter* infections: a century of challenges. *Clin. Microbiol. Rev.* 30, 409–447. doi: 10.1128/CMR.00058-16

Wright, M. S., Iovleva, A., Jacobs, M. R., Bonomo, R. A., and Adams, M. D. (2016). Genome dynamics of multidrug-resistant *Acinetobacter baumannii* during infection and treatment. *Genome Med.* 8, 1–26. doi: 10.1186/s13073-016-0279-y

Yan, Z., Yang, J., Hu, R., Hu, X., and Chen, K. (2016). *Acinetobacter baumannii* infection and IL-17 mediated immunity. *Mediat. Inflamm.* 2016, 1–5. doi: 10.1155/2016/9834020

Yang, H., Chen, G., Hu, L., Liu, Y., Cheng, J., Li, H., et al. (2015). *In vivo* activity of daptomycin/colistin combination therapy in a *Galleria mellonella* model of *Acinetobacter baumannii* infection. *Int. J. Antimicrob. Agents* 45, 188–191. doi: 10.1016/j.ijantimicag.2014.10.012

Yoon, E.-J., Balloy, V., Fiette, L., Chignard, M., Courvalin, P., and Grillot-Courvalin, C. (2016). Contribution of the Ade resistance-nodulation-cell division-type efflux pumps to fitness and pathogenesis of *Acinetobacter baumannii*. *MBio* 7, e00697–e00716. doi: 10.1128/mBio.00697-16

Zschiedrich, C. P., Keidel, V., and Szurmant, H. (2016). Molecular mechanisms of two-component signal transduction. *J. Mol. Biol.* 428, 3752–3775. doi: 10.1016/j.jmb.2016.08.003

Conflict of Interest Statement: The authors declare that the research was conducted in the absence of any commercial or financial relationships that could be construed as a potential conflict of interest.

frontiers in Microbiology

ORIGINAL RESEARCH
published: 23 July 2019
doi: 10.3389/fmicb.2019.01599

Identification of Potential Virulence Factors in the Model Strain *Acinetobacter baumannii* A118

*Maria S. Ramirez[1], William F. Penwell[2], German M. Traglia[3], Daniel L. Zimbler[2], Jennifer A. Gaddy[2,4], Nikolas Nikolaidis[1], Brock A. Arivett[2], Mark D. Adams[5], Robert A. Bonomo[6], Luis A. Actis[2] and Marcelo E. Tolmasky[1]**

[1] Department of Biological Science, Center for Applied Biotechnology Studies, California State University, Fullerton, Fullerton, CA, United States, [2] Department of Microbiology, Miami University, Oxford, OH, United States, [3] Laboratorio de Bacteriología Clínica, Departamento de Bioquímica Clínica, Facultad de Farmacia y Bioquímica, Hospital de Clínicas "José de San Martín", Buenos Aires, Argentina, [4] Department of Medicine, Vanderbilt University Medical Center, Nashville, TN, United States, [5] Department of Genetics, School of Medicine, Case Western Reserve University, Cleveland, OH, United States, [6] Departments of Pharmacology and Molecular Biology and Microbiology, Louis Stokes Cleveland Veterans Affairs Medical Center, School of Medicine, Case Western Reserve University, Cleveland, OH, United States

OPEN ACCESS

Edited by:
Miklos Fuzi, Semmelweis University, Hungary

Reviewed by:
Andres Felipe Opazo-Capurro, Universidad de Concepción, Chile
Paolo Visca, Roma Tre University, Italy
Lenie Dijkshoorn, Leiden University Medical Center, Netherlands

***Correspondence:**
Marcelo E. Tolmasky
mtolmasky@fullerton.edu

Specialty section:
This article was submitted to Infectious Diseases, a section of the journal Frontiers in Microbiology

Received: *01 March 2019*
Accepted: *26 June 2019*
Published: *23 July 2019*

Citation:
Ramirez MS, Penwell WF, Traglia GM, Zimbler DL, Gaddy JA, Nikolaidis N, Arivett BA, Adams MD, Bonomo RA, Actis LA and Tolmasky ME (2019) Identification of Potential Virulence Factors in the Model Strain Acinetobacter baumannii A118. Front. Microbiol. 10:1599. doi: 10.3389/fmicb.2019.01599

Acinetobacter baumannii A118, a strain isolated from the blood of an infected patient, is naturally competent and unlike most clinical strains, is susceptible to a variety of different antibiotics including those usually used for selection in genetic manipulations. These characteristics make strain A118 a convenient model for genetic studies of *A. baumannii*. To identify potential virulence factors, its complete genome was analyzed and compared to other *A. baumannii* genomes. *A. baumannii* A118 includes gene clusters coding for the acinetobactin and baumannoferrin iron acquisition systems. Iron-regulated expression of the BauA outer membrane receptor for ferric-acinetobactin complexes was confirmed as well as the utilization of acinetobactin. *A. baumannii* A118 also possesses the *feoABC* genes, which code for the main bacterial ferrous uptake system. The functionality of baumannoferrin was suggested by the ability of *A. baumannii* A118 culture supernatants to cross feed an indicator BauA-deficient strain plated on iron-limiting media. *A. baumannii* A118 behaved as non-motile but included the *csuA/BABCDE* chaperone-usher pilus assembly operon and produced biofilms on polystyrene and glass surfaces. While a known capsular polysaccharide (K) locus was identified, the outer core polysaccharide (OC) locus, which belongs to group B, showed differences with available sequences. Our results show that despite being susceptible to most antibiotics, strain A118 conserves known virulence-related traits enhancing its value as model to study *A. baumannii* pathogenicity.

Keywords: *Acinetobacter*, virulence factors, pathogenicity, hospital infection, community infection, ESKAPE

INTRODUCTION

Acinetobacter baumannii infections used to be rare a few decades ago (Hartstein et al., 1988). However, its importance as an opportunistic human pathogen kept increasing and it is now responsible for a growing number of community and nosocomial infections including bacteremia, urinary tract infections, wound infections, meningitis, and pneumonia (Maragakis and Perl, 2008; Zurawski et al., 2012; McConnell et al., 2013; Harding et al., 2018). It mainly affects compromised

patients but it has also been identified as an important causative agent of infections in wounded military personnel (Peleg et al., 2008; Petersen et al., 2011; Arivett et al., 2016). The success as an opportunistic pathogen, especially in hospital environments is due to its ability to resist desiccation and persist in the most diverse hospital locations combined with a growing resistance to disinfectants and major antibacterials (Jawad et al., 1998; Dijkshoorn et al., 2007; Perez et al., 2007; Peleg et al., 2008; Rodriguez-Bano and Bonomo, 2008; Farrow et al., 2018). Furthermore, the problematic nature of *A. baumannii* infections is enhanced by its acquisition of resistance to carbapenems, which now exceed 90% in some geographical regions with a mortality rate of about 60% (Isler et al., 2018). Recent studies identified pathogenic and resistance islands (Fournier et al., 2006; Smith et al., 2007; Post et al., 2010; Krizova et al., 2011) as well as several potential virulence factors (Harding et al., 2018) such as iron and other micronutrients uptake (Zimbler et al., 2009; Gaddy et al., 2012; Moore et al., 2014; Penwell et al., 2015), motility (Mussi et al., 2010; Eijkelkamp et al., 2013; Wood et al., 2018), production of cytotoxic and protection factors (Russo et al., 2010; Jin et al., 2011), and adhesion and biofilm formation on abiotic and biotic surfaces (Gaddy et al., 2009; Longo et al., 2014).

We have described *A. baumannii* A118, a naturally competent isolate obtained from blood of an infected patient, that is susceptible to numerous antibiotics including those commonly used in molecular genetics (Ramirez et al., 2010, 2011; Traglia et al., 2014). We proposed that these characteristics make this strain a convenient experimental model studying the pathobiology of this relevant human pathogen. Accordingly, *A. baumannii* A118 has been used in numerous studies to assess the efficiency of metal/ionophore complexes to override aminoglycoside resistance (Lin et al., 2014), to understand the effect of serum albumin in competency stability (Traglia et al., 2016; Quinn et al., 2018) and acquisition of mobile genetic elements (Ramirez et al., 2012; Domingues et al., 2018), the role of osmolarity in uptake of exogenous DNA (Domingues et al., 2019), and in the discovery of a novel bacteriophage (Turner et al., 2016). The growing number of research groups utilizing *A. baumannii* A118 as model makes characterizing this strain in greater detail desirable. In this work we focus our analysis in characteristics associated to *Acinetobacter* pathogenicity and virulence.

MATERIALS AND METHODS

Bacterial Strains, Genomes, and Culture Conditions

Acinetobacter baumannii A118 was isolated from the bloodstream of an infected patient in an intensive care unit (Merkier and Centron, 2006; Ramirez et al., 2010). *Escherichia coli* TOP10 (Invitrogen, San Diego, CA, United States) was used as host in DNA recombinant cloning. *A. baumannii* ATCC 17978, ATCC 19606^T (Bouvet and Grimont, 1986) and the isogenic ATCC 19606^T s1 (BasD$^-$) and t6 (BauA$^-$) derivatives (Dorsey et al., 2004) were used in bioassays to test acinetobactin production and utilization, respectively. Iron-rich and iron-limiting conditions were attained by supplementing the growth media with 100 μM $FeCl_3$ or 100 μM 2,2′-dipyridyl (DIP), respectively.

The presence or absence of specific coding regions in the genome sequence of *A. baumannii* A118 (GenBank Accession Number AEOW00000000) (Ramirez et al., 2011) was determined using BLAST (Altschul et al., 1990). BLASTp searches were performed with A minimum value of 30% amino acid identity, 70% coverage and a minimum *e*-value of 1×10^{-5}. The reference genomes for sequence comparison were ATCC 17978 (Accession Number CP000521), ATCC 19606 (Accession Number ACQB00000000.1), and ACICU (Accession Number NC 010611) (**Supplementary Table 1**). For K Locus and OC Locus sequence analysis, we used the most related genetic structures in GenBank Database (**Supplementary Table 1**).

Production and Utilization of Acinetobactin

Bioassays to test production or utilization of siderophore were carried out as previously (Dorsey et al., 2004). Briefly, supernatants from cultures using succinate medium were sterilized by filtration and spotted on filter disks placed on L agar plates containing 225 μM DIP seeded with the ATCC 19606^T t6 strain, which does not produce the acinetobactin receptor protein BauA. The plates were incubated for 24 h at 37°C, growth halos around the filters were an indication of production of a siderophore different from acinetobactin. The presence of the outer membrane protein BauA in *A. baumannii* strains was determined by western blotting with anti-BauA polyclonal antiserum using total lysates of bacterial cells cultured under iron-limiting or iron-rich conditions as described before (Dorsey et al., 2004). Briefly, total proteins from cells cultured under iron-rich or iron-limiting conditions were separated by SDS–PAGE using 12.5% polyacrylamide gels, transferred to a nitrocellulose membrane, and incubated in the presence of anti-BauA serum. The immunocomplexes were detected by chemiluminescence using HRP-labeled protein A (Dorsey et al., 2004).

Cell Motility and Biofilm Assays

Cell motility was assessed using semi-solid plates containing 0.3% agarose as described before (Mussi et al., 2010). The plates were inoculated on the surface with bacteria using flat-ended sterile wooden sticks or depositing 0.003 ml of LB cultures grown to an OD_{600} of 0.3. Plates were incubated for 24 h at 24°C or 37°C in the dark or under blue light (emission peak centered at 462 nm) emitted by nine-LED (light-emitting diode) arrays with an intensity of 10 to 20 μmol photons/m^2/s. Biofilms formed on the walls of polystyrene or glass tubes were stained with crystal violet, visually inspected and quantified after elution of the stain as previously described (Tomaras et al., 2003). The amount of biofilm formed by each sample was normalized to its total biomass, which was determined by measuring the OD_{600} of duplicate cultures as described before (Tomaras et al., 2003). Triplicate assays were done at least three times using fresh samples each time.

Infection Assays

Randomly chosen *Galleria mellonella* larvae were injected with 1×10^5 *A. baumannii* cells resuspended in sterile phosphate-buffered saline (PBS), or with PBS as negative control. After injection, the larvae were incubated at 37°C in the dark, and killing was assessed at 24-h intervals over 6 days. Caterpillars were considered dead and removed from the study if they displayed no response to probing. The results of the trial were omitted if more than two deaths occurred in the control groups. The experiments were repeated six times using 10 larvae per experimental group, and the resulting survival curves were plotted using the Kaplan-Meier method. *P*-values < 0.05 are considered statistically significant.

RESULTS AND DISCUSSION

Acinetobacter baumannii A118 is characterized for its susceptibility to a variety of antimicrobial agents such as ceftazidime, cefepime, piperacillin, minocycline, amikacin, gentamicin, sulfamethoxazole-trimethoprim, imipenem, meropenem, and ciprofloxacin (Ramirez et al., 2010). This characteristic makes it more suitable as a model for genetic analysis than most other isolates that exhibit multiresistance to antibiotics usually used for selection in a variety of techniques. To facilitate its use as model of infection we identify the presence of genes and functions previously associated with *A. baumannii* pathogenicity. The results discussed in this article are summarized in **Table 1**.

Iron Uptake Systems (IUSs)

A non-specific defense system of vertebrate animals against bacterial infection is the chelation of iron by high-affinity iron-binding proteins such as transferrin and lactoferrin (Crosa and Walsh, 2002). Consequently, bacteria have evolved very efficient iron-acquisition systems to scavenge iron from the iron-binding proteins of their hosts. These systems are varied and include synthesis of a siderophore (a high-affinity ferric iron chelator) that uptakes iron and mediates its internalization through a specific energy-dependent transport system (Crosa and Walsh, 2002; Di Lorenzo and Stork, 2014; Li and Ma, 2017), production of outer membrane receptors that recognize lactoferrin, transferrin, heme or non-indigenous siderophores (Koster, 2005; Antunes et al., 2011; Di Lorenzo and Stork, 2014; Huang and Wilks, 2017), or direct binding and transport of ferrous iron (Lau et al., 2016). The siderophore-mediated iron uptake systems identified in *A. baumannii* strains are those that utilize acinetobactin (Echenique et al., 1992; Actis et al., 1993, 1999), baumannoferrin (Penwell et al., 2015), or fimsbactins, which are represented by a family of six related chatechol/hydroxamate compounds (Proschak et al., 2013). Since the acinetobactin system, originally described in the ATCC 19606^T strain (Dorsey et al., 2004; Mihara et al., 2004), is the most widespread among *A. baumannii* isolates we identified the presence of the gene cluster as well as *entA* and *entB* orthologs, which code for functions required for the biosynthesis of the acinetobactin precursor 2,3-dihydroxybenzoic acid (Penwell et al., 2012). We also carried out assays to identify the regulated expression of BauA, the outer membrane receptor of ferric-acinetobactin complexes (**Figure 1A**), as well as the growth of *A. baumannii* A118 at increasing concentrations of DIP (**Figure 1B**). The levels and iron regulation of BauA in *A. baumannii* A118 were similar to those in the control strains ATCC 19606^T. Both strains showed higher production of this protein as compared to the levels detected in strain ATCC 17978 (**Figure 1A**). However, comparison of growth of all three strains showed that while the OD_{600} levels reached by strains A118 and ATCC 17978 at increasing concentrations of DIP were nearly identical, strain ATCC 19606^T proved to be more sensitive to iron chelation, the growth of which was completely inhibited at a lower DIP concentration when compared with the two other tested strains (**Figure 1B**). The *A. baumannii* ATCC 19606^T s1 mutant, deficient in production of acinetobactin due to lack of the biosynthetic enzyme BasD was inhibited at the lowest DIP concentration of all four strains tested (**Figure 1B**). The ability of the strains A118 and ATCC 17978 to grow at higher DIP concentrations when compared to strain ATCC 19606^T could be due to the presence/expression of one or more additional iron acquisition systems or to a higher production of acinetobactin. It is known that *A. baumannii* ATCC 19606^T does not possess the genes coding for a fimsbactin siderophore and cannot express a functional baumanoferrin iron uptake system in spite of including the cognate gene cluster. This is supported by the observation that an ATCC 19606^T acinetobactin biosynthetic mutant cannot grow in the presence of DIP (Dorsey et al., 2004; Penwell et al., 2012, 2015). In addition to the acinetobactin gene cluster, *A. baumannii* ATCC 17978 includes the cluster coding for fimsbactin and baumannoferrin iron-uptake systems (Antunes et al., 2011; Eijkelkamp et al., 2011). Thus, the higher iron proficiency can be explained by the expression of one or both of these systems. Analysis of the *A. baumannii* A118 genome showed that it possesses the baumannoferrin gene cluster but not that one coding for a fimsbactin siderophore iron uptake system. To determine if besides the acinetobactin system, *A. baumannii* A118 expresses an additional iron uptake system we conducted a siderophore-utilization bioassays using the ATCC 19606^T

TABLE 1 | Characteristics of *A. baumannii* strains.

	A. baumannii		
	A118	**ATCC 19606^T**	**ATCC 17978**
IUS – Acinetobactin	+	+	+
IUS – Baumannoferrin	+	−	+
IUS – Fimsbactin	−	−	+
Heme cluster 1	+	+	+
Heme cluster 2	−	−	−
IUS – FeoABC	+	+	+
Biofilm	+	−	+
Motility	+	−	+
Capsular polysaccharide – locus K[1]	PSgc8	PSgc9	PSgc9
Capsular polysaccharide – locus OC[2]	New	OCL1	OCL2

Plus signs denote functional systems. [1]According to the classification described in Hu et al. (2013). [2]According to the classification described in Kenyon et al. (2014).

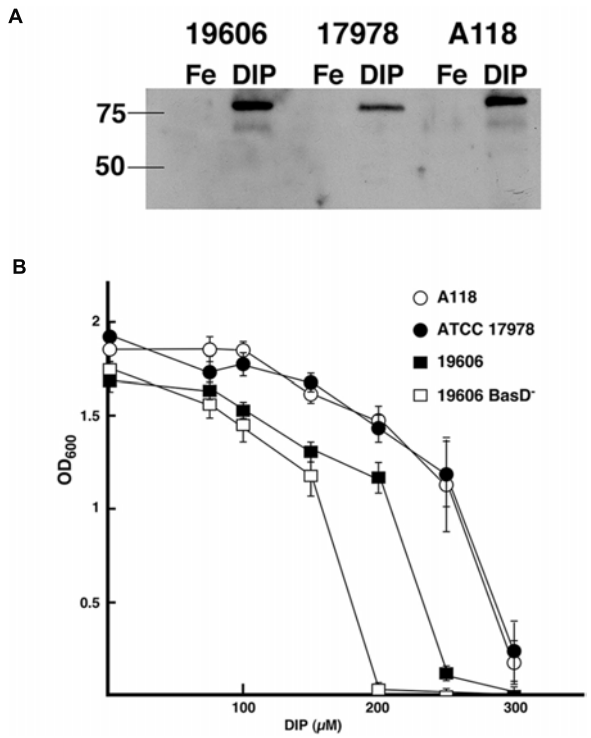

FIGURE 1 | Acinetobactin iron uptake system. **(A)** Synthesis and regulation of BauA. Total proteins from *A. baumannii* ATCC 19606^T, ATCC 17978, and A118 cultured under iron-rich (100 μM $FeCl_3$) and iron-limiting (100 μM DIP) conditions were separated on a 12.5% SDS–PAGE, transferred onto nitrocellulose, and probed with anti-BauA serum. The "Precision" molecular-mass protein markers (Bio-Rad) were detected with StrepTactin-HRP conjugate. The positions of the 50- and 75-kDa protein markers are shown on the left side to the gel. 19606, ATCC 19606^T; 17978, ATCC 17978; Fe, iron-rich conditions; DIP, iron-limiting conditions. **(B)** Bacterial growth under iron limiting conditions. The strains were cultured overnight at 37°C in L broth containing increasing concentrations of the iron chelator DIP.

t6 BauA-deficient strain, which cannot use acinetobactin to grow under iron-chelated conditions. **Table 2** shows that the *A. baumannii* ATCC 19606^T t6 BauA-deficient indicator strain was able to grow around the disks spotted with supernatants obtained from cultures of strains ATCC 17978 and A118 under iron-limiting conditions. These results strongly suggest that *A. baumannii* A118 secretes an additional siderophore that, given the presence the appropriate gene cluster, it most probably is baumannoferrin. However, further chemical assays are needed to prove that A118 produces baumanoferrin.

A search for genetic determinants of a heme-acquisition system showed that *A. baumannii* A118 posseses the heme uptake cluster 2 (Antunes et al., 2011). There is at least one report proposing that heme contributes to overcoming the iron limitation caused by the host's high affinity iron binding proteins (de Leseleuc et al., 2014). *A. baumannii* A118 also includes the *feoABC* genes, which code for the main bacterial Feo ferrous uptake system (Cartron et al., 2006). The cluster specifies three proteins, FeoA of unknown function, the repressor FeoC, and FeoB that participates in translocation of iron across the inner membrane. A recent study showed that although the Feo system enhances growth in heat-inactivated human serum and contributes to resistance to human serum, it is not essential for virulence (Runci et al., 2019).

TABLE 2 | Siderophore utilization bioassays.

Crossfeeding sample	Halo around the filter disks (mm)
H_2O	0
$FeCl_3$	13.25 ± 0.96
ATCC 19606^T Sp	0
ATCC 19606^T s1 (BasD$^-$) Sp	0
ATCC 17978 Sp	15.75 ± 1.71
A118 Sp	13.75 ± 2.22

Strains to be tested were cultured in succinate medium for 24 h at 37°C. Culture supernatants (Sp), obtained by filter sterilization, were spotted onto filter disks that were placed on L agar plates containing 225 μM DIP and seeded with the reporter A. baumannii ATCC 19606^T t6 strain deficient in the production of the BauA outer membrane acinetobactin receptor. Halos were measured after incubation for 24 h at 37°C. H_2O or $FeCl_3$ were spotted as negative and positive controls, respectively.

Biofilm Formation

The ability of *A. baumannii* strains to form biofilms on abiotic surfaces (Tomaras et al., 2003) is partially or totally responsible for their persistence in different environments such as the surface of medical devices and other common artifacts like furniture, linens, soap dispensers, phones and computer keyboards (Hartstein et al., 1988, 1990; Neely, 2000; Villegas and Hartstein, 2003; Borer et al., 2005; Espinal et al., 2012). Comparative analysis of the *A. baumannii* A118 nucleotide sequence with *A. baumannii* genomes showed that the *csuA/BABCDE* chaperon-usher pilus assembly system is present in the A118 strain and the identities of the deduced amino acid sequence of the products of the cognate open reading frames is 96% or higher when compared to those from strain ATCC 17978. Standard crystal violet biofilm assays using polystyrene tubes showed that *A. baumannii* A118 formed a distinctive biofilm ring on the surface of the tubes as it was described for ATCC 19606^T cells (Tomaras et al., 2003). Control assays showed a stronger ring in the case of the strain ATCC 19606^T while significantly reduced biofilm was formed by strain ATCC 17978. Quantification of total biofilms formed on polystyrene and glass showed that strain A118 produced a significant amount of biofilm on glass and polystyrene surfaces (**Figure 2**). It was of interest that while the biofilm mass was higher for strain A118 than for strain ATCC 19606^T on glass, the opposite was true for biofilm formed on plastic (**Figure 2**). Although the molecular and cellular bases of these differences are unknown, variations in the amount of biofilms formed by different strains on the same or different types of surfaces seem to be a common property among *A. baumannii* clinical isolates (McQueary and Actis, 2011; Runci et al., 2017; Quinn et al., 2018; Wood et al., 2018).

Motility

Acinetobacter baumannii lacks flagellum and therefore cannot show flagellum-mediated swimming motility (Towner et al., 1991). However, it has been shown that *Acinetobacter* strains

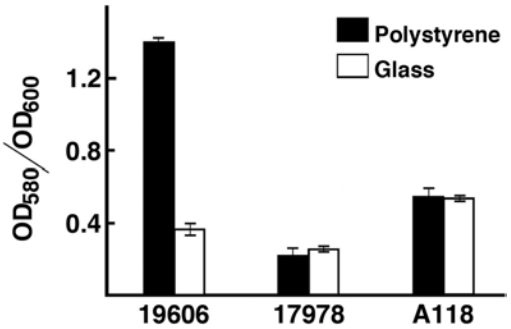

FIGURE 2 | Production of biofilm. Quantification of biofilm formation on polystyrene and glass tubes by *A. baumannii* strains ATCC 19606^T, ATCC 17978, and A118 after static incubation at 37°C. Quantification was carried out as described in "Materials and Methods."

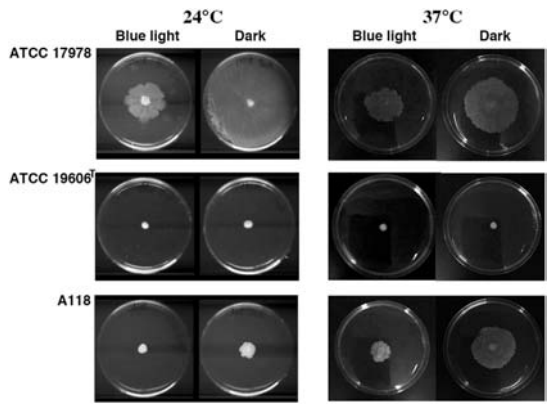

FIGURE 3 | Surface motility on a semi-solid surface. Cells were inoculated on the surface of motility plates and incubated overnight at 24°C or 37°C in the dark or under blue light.

are capable of motility on semi-solid agar (Barker and Maxted, 1975; Mussi et al., 2010; Eijkelkamp et al., 2011; Quinn et al., 2018; Wood et al., 2018), and the movement is dependent on the concentration of iron in the environment and possibly on other stress related factors (Eijkelkamp et al., 2011; Quinn et al., 2018; Wood et al., 2018). Furthermore, it has been shown that at 24°C strain ATCC 17978 shows low or no signs of motility when growing exposed to light but this situation is reversed when growing in the dark (Mussi et al., 2010; **Figure 3**). This regulation depends on the expression of BlsA, a photoreceptor and transcriptional regulator (Mussi et al., 2010), and the newly identified PrpABCD type I pilus assembly system (Wood et al., 2018). In contrast, as it was shown before, ATCC 17978 cells displayed comparable surface motility independently of illumination when cultured at 37°C (Mussi et al., 2010). Analysis of *A. baumannii* A118 showed that this strain was unable to exhibit motility under blue light at 24°C but it showed slight motility in the dark (**Figure 3**). This motility was more evident at 37°C in the dark although cells displayed a reduced motility when cultured at this temperature under illumination (**Figure 3**). *A. baumannii* ATCC 19606^T did not show motility in any of the assayed conditions (**Figure 3**). Analysis of the *A. baumannii* A118 genome showed the presence of all the genes associated with a type IV pilus system (T4P), known to play a role in *A. baumannii* twitching motility and surface-associated. Taken together, these results indicate that *A. baumannii* A118 is motile under the right conditions and that light and temperature affect the motility responses of different *A. baumannii* strains by mechanisms that remain to characterized.

Locus K and Locus OC

Acinetobacter baumannii strains produce a capsular polysaccharide coded for by a gene cluster known as K locus, which exhibits sequence variations among isolates (Kenyon and Hall, 2013). Another surface polysaccharide produced by this bacterium is part of the lipooligosaccharide formed by the lipid A and the inner and outer core oligosaccharides (Kenyon et al., 2014). While the inner core oligosaccharide is well conserved, the outer core is highly variable (Erridge et al., 2007). The group of genes

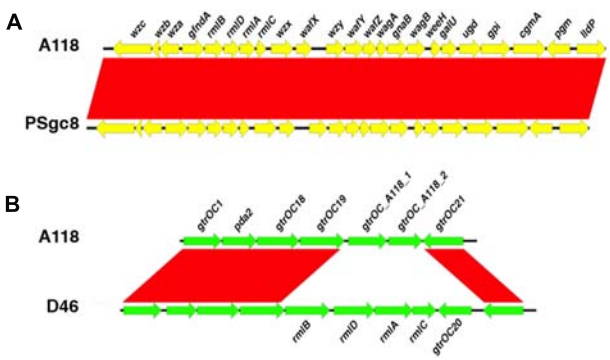

FIGURE 4 | K and OC loci comparisons. **(A)** Comparison of the K loci from *A. baumannii* strains A118 and PSgc8 (Accession Number LUH5538). Comparison was performed using BLAST (version 2.2.31) and the graphic representation was generated using the software EasyFig (version 2.1). Proteins coded for by the genes are: *wzc*, Tyrosine-protein kinase; *wzb*, protein-tyrosine-phosphatase; *wza*, periplasmic protein; *gnaA*, UDP-glucose/GDP-mannose dehydrogenase; *rmlB*, dTDP-D-glucose-4,6-dehydratase; *rmlD*, dTDP-4-dehydrorhamnose reductase; *rmlA*, dTDP-glucose pyrophosphorylase; *rmlC*, dTDP-4-keto-6-deoxy-D-glucose-3,5-epimerase; *wzx*, flippase; *wafX*, glycosyltransferase; *wzy*, O antigen polymerase; *wafY*, glycosyltransferase; *wafZ*, glycosyltransferase; *wagA*, acetyltransferase; *gnaB*, NAD-dependent epimerase/dehydratase; *wagB*, glycosyl transferase; *weeH*, glycosyltransferase; *galU*, UDP-glucose pyrophosphorylase; *ugd*, UDP-glucose 6-dehydrogenase; *gpi*, glucose-6-phosphate isomerase; *cgmA*, cyclic beta-1,2-glucan modification transmembrane protein; *pgm*, phosphoglucomutase; *lldP*, L-lactate permease. **(B)** Comparison of the OC loci from *A. baumannii* strains A118 and D46 (Accession Number KF030679). All three strains, D46, ZW85-1 (Accession Number CP006768), and 6200 (Accession Number CP010397), have identical OC loci. Proteins coded for by the genes are: *gtrOC1*, glycosyltransferase; *pda2*, polysaccharide deacetylase; *gtrOC18*, glycosyltransferase; *gtrOC19*, glycosyltransferase; *gtrOC20*, glycosyltransferase; *gtrOC21*, glycosyltransferase; *gtrOC_A118_1*, capsular protein, polysaccharide synthesis; *gtrOC_A118_2*, glycosyltransferase.

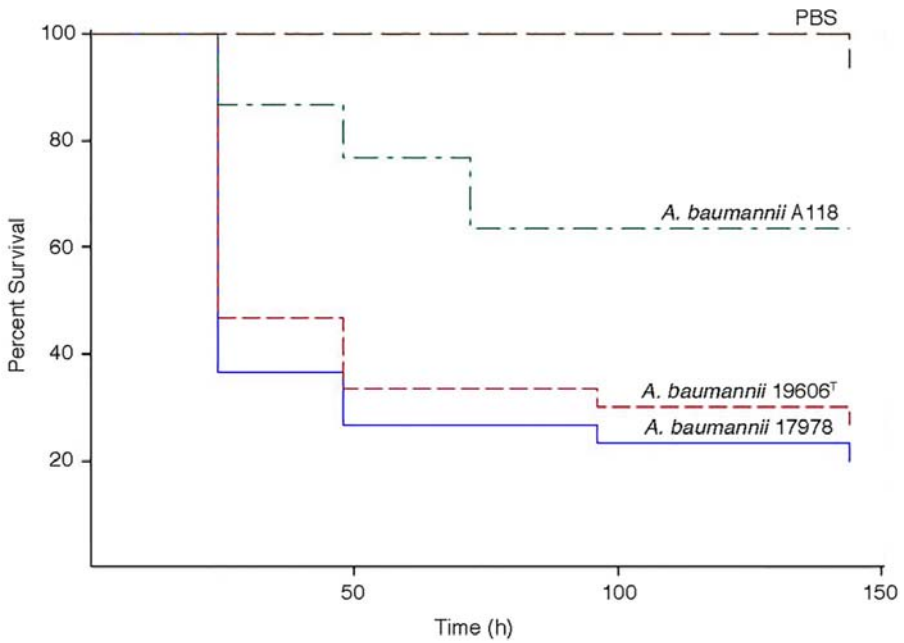

FIGURE 5 | *Galleria mellonella* infection assays. Infections were carried out as described in Materials and Methods. Larvae were injected with 1×10^5 cells of *A. baumannii* A118, 19606^T, or 17978 resuspended in sterile PBS. Negative controls were injected with PBS.

coding for the outer core oligosaccharide are known as the OC locus. The surface carbohydrates have been linked to the virulence of *A. baumannii* in numerous studies (Russo et al., 2010; Iwashkiw et al., 2012; Geisinger and Isberg, 2015). We found the *A. baumannii* A118 K locus structure located between the *fkpA* and *lldP* genes as it has been reported for other strains (Kenyon and Hall, 2013). Nucleotide sequence comparison of this locus showed 99% identity (100% cover) with that of the strain Sv8/PSgc8 described by Hu et al. (2013); (**Figure 4A**). A search to identify the OC locus showed that an *A. baumannii* A118 gene cluster exhibited 98% identity (79% cover) with those present in strains D46, ZW85-1, and 6200 (**Figure 4B**). None of the reported versions of the OC locus was identical to that of the *A. baumannii* A118 strain. The two genes not represented in strain D46 show 100% amino acid sequence identity with those found in strain Naval-72. On the other hand, the *rmlB*, *rmlD*, *rmlA* y *rmlC* genes present in this locus in strain D46 are located in the K locus in *A. baumannii* A118 (see **Figures 4A,B**). According to the OC loci classification proposed by Kenyon et al. (2014), the *A. baumannii* A118 OC locus belongs to group B.

Experimental Infections

The virulence of *A. baumannii* A118 was assessed using the *G. mellonella* model of infection. **Figure 5** shows that larvae infections with this strain results in a significant increase in mortality as compared to the negative control. However, strain A118 showed lower virulence when compared to the *A. baumannii* ATCC 17978 and ATCC 19606T strains, both of which produced comparable larvae survival rates (**Figure 5**).

CONCLUDING REMARKS

There is an urgent need to find answers to the problem of infections with bacteria belonging to the ESKAPE group (Boucher et al., 2013), which includes *A. baumannii*. Research on this bacterium presents numerous challenges due to its tremendous genetic plasticity and diversity, as well as its multiresistance to most antibiotics used for selection in the molecular biology laboratory (Ramirez et al., 2010; Wright et al., 2016; Traglia et al., 2019). We have analyzed functions related to the antibiotic resistance/susceptibility profile of the model strain *A. baumannii* A118 (Ramirez et al., 2010, 2011). Building on the characterization of this strain we show here the presence of genetic and cellular traits that could be associated to its pathogenicity. It most probably includes at least two iron uptake systems, those mediated by the siderophores acinetobactin and baumannoferrin (Dorsey et al., 2003, 2004; Mihara et al., 2004; Eijkelkamp et al., 2011). The presence of the *csu* operon is compatible with the ability of *A. baumannii* A118 to form biofilms on polystyrene and glass to levels comparable to strain ATCC 19606^T. The K and OC loci were identified and characterized, while the K locus has been found in another isolated, the OC locus was still undescribed. Although *A. baumannii* A118 displayed more surface motility than ATCC 19606^T under all tested conditions, its motility seems reduced when compared to ATCC17978, particularly under illumination at 37°C. This response could be due to the absence of the gene coding for a fimbrial protein that might be involved in this response. In conclusion, *A. baumannii* A118 possesses the main potential virulence factors found in other clinical isolates

reinforcing the usefulness of this strain as a model of genetic manipulation and pathogenic studies.

DATA AVAILABILITY

All datasets generated for this study are included in the manuscript and/or the **Supplementary Files**.

AUTHOR CONTRIBUTIONS

MT, MR, LA, and RB conceived and designed the experiments. MR, WP, JG, GT, DZ, NN, BA, MA, LA, and MT performed the experiments. MR, WP, JG, NN, GT, DZ, BA, MA, LA, and MT analyzed the data. MA, MR, MT, and NN contributed reagents, mutant strains, materials, and analysis tools. MR and MT wrote the manuscript. MR, MT, LA, RB, and NN revised the manuscript.

FUNDING

This study was supported by Public Health Service grants 2R15AI047115 (to MT), AI070174 (to LA), R01AI00560, R01AI0AI063517, R21AI11458, and R01AI072219 (to RB), and SC3G-M125556 (to MR) from the National Institutes of Health, award 1I01BX001974 (to RB) from the BLRDS (Veterans Administration Office of Research and Development), and award VISN10 (to RB) from the Geriatric Research and Educational and Clinical Center. The funders had no role in study design, data collection and analysis, decision to publish, or preparation of the manuscript.

SUPPLEMENTARY MATERIAL

The Supplementary Material for this article can be found online at: https://www.frontiersin.org/articles/10.3389/fmicb.2019.01599/full#supplementary-material

REFERENCES

Actis, L. A., Smoot, J. C., Barancin, C. E., and Findlay, R. H. (1999). Comparison of differential plating media and two chromatography techniques for the detection of histamine production in bacteria. *J. Microbiol. Methods* 39, 79–90. doi: 10.1016/s0167-7012(99)00099-8

Actis, L. A., Tolmasky, M. E., Crosa, L. M., and Crosa, J. H. (1993). Effect of iron-limiting conditions on growth of clinical isolates of *Acinetobacter baumannii*. *J. Clin. Microbiol.* 31, 2812–2815.

Altschul, S. F., Gish, W., Miller, W., Myers, E. W., and Lipman, D. J. (1990). Basic local alignment search tool. *J. Mol. Biol.* 215, 403–410. doi: 10.1006/jmbi.1990.9999

Antunes, L. C., Imperi, F., Towner, K. J., and Visca, P. (2011). Genome-assisted identification of putative iron-utilization genes in *Acinetobacter baumannii* and their distribution among a genotypically diverse collection of clinical isolates. *Res. Microbiol.* 162, 279–284. doi: 10.1016/j.resmic.2010.10.010

Arivett, B. A., Ream, D. C., Fiester, S. E., Kidane, D., and Actis, L. A. (2016). Draft genome sequences of *Acinetobacter baumannii* isolates from wounded military personnel. *Genome Announc.* 4:e773-16. doi: 10.1128/genomeA.00773-16

Barker, J., and Maxted, H. (1975). Observations on the growth and movement of *Acinetobacter* on semi-solid media. *J. Med. Microbiol.* 8, 443–446. doi: 10.1099/00222615-8-3-443

Borer, A., Gilad, J., Smolyakov, R., Eskira, S., Peled, N., Porat, N., et al. (2005). Cell phones and *Acinetobacter* transmission. *Emerg. Infect. Dis.* 11, 1160–1161.

Boucher, H. W., Talbot, G. H., Benjamin, D. K. Jr., Bradley, J., Guidos, R. J., Jones, R. N., et al. (2013). 10 x ′20 Progress–development of new drugs active against gram-negative bacilli: an update from the infectious diseases society of America. *Clin. Infect. Dis.* 56, 1685–1694. doi: 10.1093/cid/cit152

Bouvet, P. J. M., and Grimont, P. A. D. (1986). Taxonomy of the genus *Acinetobacter* with the recognition of *Acinetobacter baumannii* sp. *nov., Acinetobacter haemolyticus* sp. nov., *Acinetobacter johnsonii* sp. nov., and *Acinetobacter junii* sp. nov. and emended descriptions of *Acinetobacter calcoaceticus* and *Acinetobacter lwoffii*. *Int. J. Syst. Bacteriol.* 36, 228–240. doi: 10.1099/00207713-36-2-228

Cartron, M. L., Maddocks, S., Gillingham, P., Craven, C. J., and Andrews, S. C. (2006). Feo–transport of ferrous iron into bacteria. *Biometals* 19, 143–157. doi: 10.1007/s10534-006-0003-2

Crosa, J. H., and Walsh, C. T. (2002). Genetics and assembly line enzymology of siderophore biosynthesis in bacteria. *Microbiol. Mol. Biol. Rev.* 66, 223–249. doi: 10.1128/mmbr.66.2.223-249.2002

de Leseleuc, L., Harris, G., Kuolee, R., Xu, H. H., and Chen, W. (2014). Serum resistance, gallium nitrate tolerance and extrapulmonary dissemination are linked to heme consumption in a bacteremic strain of *Acinetobacter baumannii*. *Int. J. Med. Microbiol.* 304, 360–369. doi: 10.1016/j.ijmm.2013.12.002

Di Lorenzo, M., and Stork, M. (2014). Plasmid-encoded iron uptake systems. *Microbiol. Spectr.* 2:6.

Dijkshoorn, L., Nemec, A., and Seifert, H. (2007). An increasing threat in hospitals: multidrug-resistant *Acinetobacter baumannii*. *Nat. Rev. Microbiol.* 5, 939–951. doi: 10.1038/nrmicro1789

Domingues, S., Rosario, N., Ben Cheikh, H., and Da Silva, G. J. (2018). IS*Aba1* and Tn*6168* acquisition by natural transformation leads to third-generation cephalosporins resistance in *Acinetobacter baumannii*. *Infect. Genet. Evol.* 63, 13–16. doi: 10.1016/j.meegid.2018.05.007

Domingues, S., Rosario, N., Candido, A., Neto, D., Nielsen, K. M., and Da Silva, G. J. (2019). Competence for natural transformation is common among clinical strains of resistant *Acinetobacter* spp. *Microorganisms* 7:30. doi: 10.3390/microorganisms7020030

Dorsey, C. W., Tolmasky, M. E., Crosa, J. H., and Actis, L. A. (2003). Genetic organization of an *Acinetobacter baumannii* chromosomal region harbouring genes related to siderophore biosynthesis and transport. *Microbiol. SGM* 149, 1227–1238. doi: 10.1099/mic.0.26204-0

Dorsey, C. W., Tomaras, A. P., Connerly, P. L., Tolmasky, M. E., Crosa, J. H., and Actis, L. A. (2004). The siderophore-mediated iron acquisition systems of *Acinetobacter baumannii* ATCC 19606 and *Vibrio anguillarum* 775 are structurally and functionally related. *Microbiology* 150, 3657–3667. doi: 10.1099/mic.0.27371-0

Echenique, J. R., Arienti, H., Tolmasky, M. E., Read, R. R., Staneloni, R. J., Crosa, J. H., et al. (1992). Characterization of a high-affinity iron transport system in *Acinetobacter baumannii*. *J. Bacteriol.* 174, 7670–7679. doi: 10.1128/jb.174.23.7670-7679.1992

Eijkelkamp, B. A., Hassan, K. A., Paulsen, I. T., and Brown, M. H. (2011). Investigation of the human pathogen *Acinetobacter baumannii* under iron limiting conditions. *BMC Genomics* 12:126. doi: 10.1186/1471-2164-12-126

Eijkelkamp, B. A., Stroeher, U. H., Hassan, K. A., Elbourne, L. D., Paulsen, I. T., and Brown, M. H. (2013). H-NS plays a role in expression of *Acinetobacter baumannii* virulence features. *Infect. Immun.* 81, 2574–2583. doi: 10.1128/IAI.00065-13

Erridge, C., Moncayo-Nieto, O. L., Morgan, R., Young, M., and Poxton, I. R. (2007). *Acinetobacter baumannii* lipopolysaccharides are potent stimulators of human monocyte activation via toll-like receptor 4 signalling. *J. Med. Microbiol.* 56, 165–171. doi: 10.1099/jmm.0.46823-0

Espinal, P., Marti, S., and Vila, J. (2012). Effect of biofilm formation on the survival of *Acinetobacter baumannii* on dry surfaces. *J. Hosp. Infect.* 80, 56–60. doi: 10.1016/j.jhin.2011.08.013

Farrow, J. M. III, Wells, G., and Pesci, E. C. (2018). Desiccation tolerance in *Acinetobacter baumannii* is mediated by the two-component response regulator BfmR. *PLoS One* 13:e0205638. doi: 10.1371/journal.pone.0205638

Fournier, P. E., Vallenet, D., Barbe, V., Audic, S., Ogata, H., Poirel, L., et al. (2006). Comparative genomics of multidrug resistance in *Acinetobacter baumannii*. *PLoS Genet.* 2:e7. doi: 10.1371/journal.pgen.0020007

Gaddy, J. A., Arivett, B. A., Mcconnell, M. J., Lopez-Rojas, R., Pachon, J., and Actis, L. A. (2012). Role of acinetobactin-mediated iron acquisition functions in the interaction of *Acinetobacter baumannii* strain ATCC 19606T with human lung epithelial cells, *Galleria mellonella* caterpillars, and mice. *Infect. Immun.* 80, 1015–1024. doi: 10.1128/IAI.06279-11

Gaddy, J. A., Tomaras, A. P., and Actis, L. A. (2009). The *Acinetobacter baumannii* 19606 OmpA protein plays a role in biofilm formation on abiotic surfaces and in the interaction of this pathogen with eukaryotic cells. *Infect. Immun.* 77, 3150–3160. doi: 10.1128/IAI.00096-09

Geisinger, E., and Isberg, R. R. (2015). Antibiotic modulation of capsular exopolysaccharide and virulence in *Acinetobacter baumannii*. *PLoS Pathog.* 11:e1004691. doi: 10.1371/journal.ppat.1004691

Harding, C. M., Hennon, S. W., and Feldman, M. F. (2018). Uncovering the mechanisms of *Acinetobacter baumannii* virulence. *Nat. Rev. Microbiol.* 16, 91–102. doi: 10.1038/nrmicro.2017.148

Hartstein, A. I., Morthland, V. H., Rourke, J. W. Jr., Freeman, J., Garber, S., Sykes, R., et al. (1990). Plasmid DNA fingerprinting of *Acinetobacter calcoaceticus* subspecies anitratus from intubated and mechanically ventilated patients. *Infect. Control Hosp. Epidemiol.* 11, 531–538. doi: 10.2307/30151321

Hartstein, A. I., Rashad, A. L., Liebler, J. M., Actis, L. A., Freeman, J., Rourke, J. W., et al. (1988). Multiple intensive care unit outbreak of *Acinetobacter calcoaceticus* subspecies anitratus respiratory infection and colonization associated with contaminated, reusable ventilator circuits and resuscitation bags. *Am. J. Med.* 85, 624–631. doi: 10.1016/0002-9343(88)90683-3

Hu, D., Liu, B., Dijkshoorn, L., Wang, L., and Reeves, P. R. (2013). Diversity in the major polysaccharide antigen of *Acinetobacter baumannii* assessed by DNA sequencing, and development of a molecular serotyping scheme. *PLoS One* 8:e70329. doi: 10.1371/journal.pone.0070329

Huang, W., and Wilks, A. (2017). Extracellular heme uptake and the challenge of bacterial cell membranes. *Annu. Rev. Biochem.* 86, 799–823. doi: 10.1146/annurev-biochem-060815-014214

Isler, B., Doi, Y., Bonomo, R. A., and Paterson, D. L. (2018). New treatment options against carbapenem-resistant *Acinetobacter baumannii* infections. *Antimicrob. Agents Chemother.* 63, e01110–e01118. doi: 10.1128/AAC.01110-18

Iwashkiw, J. A., Seper, A., Weber, B. S., Scott, N. E., Vinogradov, E., Stratilo, C., et al. (2012). Identification of a general O-linked protein glycosylation system in *Acinetobacter baumannii* and its role in virulence and biofilm formation. *PLoS Pathog.* 8:e1002758. doi: 10.1371/journal.ppat.1002758

Jawad, A., Seifert, H., Snelling, A. M., Heritage, J., and Hawkey, P. M. (1998). Survival of *Acinetobacter baumannii* on dry surfaces: comparison of outbreak and sporadic isolates. *J. Clin. Microbiol.* 36, 1938–1941.

Jin, J. S., Kwon, S. O., Moon, D. C., Gurung, M., Lee, J. H., Kim, S. I., et al. (2011). *Acinetobacter baumannii* secretes cytotoxic outer membrane protein a via outer membrane vesicles. *PLoS One* 6:e17027. doi: 10.1371/journal.pone.0017027

Kenyon, J. J., and Hall, R. M. (2013). Variation in the complex carbohydrate biosynthesis loci of *Acinetobacter baumannii* genomes. *PLoS One* 8:e62160. doi: 10.1371/journal.pone.0062160

Kenyon, J. J., Nigro, S. J., and Hall, R. M. (2014). Variation in the OC locus of *Acinetobacter baumannii* genomes predicts extensive structural diversity in the lipooligosaccharide. *PLoS One* 9:e107833. doi: 10.1371/journal.pone.0107833

Koster, W. (2005). Cytoplasmic membrane iron permease systems in the bacterial cell envelope. *Front. Biosci.* 10:462–477.

Krizova, L., Dijkshoorn, L., and Nemec, A. (2011). Diversity and evolution of AbaR genomic resistance islands in *Acinetobacter baumannii* strains of European clone I. *Antimicrob. Agents Chemother.* 55, 3201–3206. doi: 10.1128/AAC.00221-11

Lau, C. K., Krewulak, K. D., and Vogel, H. J. (2016). Bacterial ferrous iron transport: the Feo system. *FEMS Microbiol. Rev.* 40, 273–298. doi: 10.1093/femsre/fuv049

Li, Y., and Ma, Q. (2017). Iron acquisition strategies of *Vibrio anguillarum*. *Front. Cell Infect. Microbiol.* 7:342. doi: 10.3389/fcimb.2017.00342

Lin, D. L., Tran, T., Alam, J. Y., Herron, S. R., Ramirez, M. S., and Tolmasky, M. E. (2014). Inhibition of aminoglycoside 6'-*N*-acetyltransferase type Ib by zinc: reversal of amikacin resistance in *Acinetobacter baumannii* and *Escherichia coli* by a zinc ionophore. *Antimicrob. Agents Chemother.* 58, 4238–4241. doi: 10.1128/AAC.00129-14

Longo, F., Vuotto, C., and Donelli, G. (2014). Biofilm formation in *Acinetobacter baumannii*. *New Microbiol.* 37, 119–127.

Maragakis, L. L., and Perl, T. M. (2008). *Acinetobacter baumannii*: epidemiology, antimicrobial resistance, and treatment options. *Clin. Infect. Dis.* 46, 1254–1263. doi: 10.1086/529198

McConnell, M. J., Actis, L., and Pachon, J. (2013). *Acinetobacter baumannii*: human infections, factors contributing to pathogenesis and animal models. *FEMS Microbiol. Rev.* 37, 130–155. doi: 10.1111/j.1574-6976.2012.00344.x

McQueary, C. N., and Actis, L. A. (2011). *Acinetobacter baumannii* biofilms: variations among strains and correlations with other cell properties. *J. Microbiol.* 49, 243–250. doi: 10.1007/s12275-011-0343-7

Merkier, A. K., and Centron, D. (2006). bla(OXA-51)-type beta-lactamase genes are ubiquitous and vary within a strain in *Acinetobacter baumannii*. *Int. J. Antimicrob. Agents* 28, 110–113. doi: 10.1016/j.ijantimicag.2006.03.023

Mihara, K., Tanabe, T., Yamakawa, Y., Funahashi, T., Nakao, H., Narimatsu, S., et al. (2004). Identification and transcriptional organization of a gene cluster involved in biosynthesis and transport of acinetobactin, a siderophore produced by *Acinetobacter baumannii* ATCC 19606T. *Microbiology* 150, 2587–2597. doi: 10.1099/mic.0.27141-0

Moore, J. L., Becker, K. W., Nicklay, J. J., Boyd, K. L., Skaar, E. P., and Caprioli, R. M. (2014). Imaging mass spectrometry for assessing temporal proteomics: analysis of calprotectin in *Acinetobacter baumannii* pulmonary infection. *Proteomics* 14, 820–828. doi: 10.1002/pmic.201300046

Mussi, M. A., Gaddy, J. A., Cabruja, M., Arivett, B. A., Viale, A. M., Rasia, R., et al. (2010). The opportunistic human pathogen *Acinetobacter baumannii* senses and responds to light. *J. Bacteriol.* 192, 6336–6345. doi: 10.1128/JB.00917-10

Neely, A. N. (2000). A survey of gram-negative bacteria survival on hospital fabrics and plastics. *J. Burn. Care Rehabil.* 21, 523–527. doi: 10.1097/00004630-200021060-00009

Peleg, A. Y., Seifert, H., and Paterson, D. L. (2008). *Acinetobacter baumannii*: emergence of a successful pathogen. *Clin. Microbiol. Rev.* 21, 538–582. doi: 10.1128/CMR.00058-07

Penwell, W. F., Arivett, B. A., and Actis, L. A. (2012). The *Acinetobacter baumannii* ent A gene located outside the acinetobactin cluster is critical for siderophore production, iron acquisition, and virulence. *PLoS One* 7:e36493. doi: 10.1371/journal.pone.0036493

Penwell, W. F., Degrace, N., Tentarelli, S., Gauthier, L., Gilbert, C. M., Arivett, B. A., et al. (2015). Discovery and characterization of new hydroxamate siderophores, Baumannoferrin A and B, produced by *Acinetobacter baumannii*. *Chembiochem* 16, 1896–1904. doi: 10.1002/cbic.201500147

Perez, F., Hujer, A. M., Hujer, K. M., Decker, B. K., Rather, P. N., and Bonomo, R. A. (2007). Global challenge of multidrug-resistant *Acinetobacter baumannii*. *Antimicrob. Agents Chemother.* 51, 3471–3484.

Petersen, K., Cannegieter, S. C., Van Der Reijden, T. J., Van Strijen, B., You, D. M., Babel, B. S., et al. (2011). Diversity and clinical impact of *Acinetobacter baumannii* colonization and infection at a military medical center. *J. Clin. Microbiol.* 49, 159–166. doi: 10.1128/JCM.00766-10

Post, V., White, P. A., and Hall, R. M. (2010). Evolution of AbaR-type genomic resistance islands in multiply antibiotic-resistant *Acinetobacter baumannii*. *J. Antimicrob. Chemother.* 65, 1162–1170. doi: 10.1093/jac/dkq095

Proschak, A., Lubuta, P., Grun, P., Lohr, F., Wilharm, G., De Berardinis, V., et al. (2013). Structure and biosynthesis of fimsbactins A-F, siderophores from *Acinetobacter baumannii* and *Acinetobacter baylyi*. *Chembiochem* 14, 633–638. doi: 10.1002/cbic.201200764

Quinn, B., Rodman, N., Jara, E., Fernandez, J. S., Martinez, J., Traglia, G. M., et al. (2018). Human serum albumin alters specific genes that can play a role in survival and persistence in *Acinetobacter baumannii*. *Sci. Rep.* 8:14741. doi: 10.1038/s41598-018-33072-z

Ramirez, M. S., Adams, M. D., Bonomo, R. A., Centron, D., and Tolmasky, M. E. (2011). Genomic analysis of *Acinetobacter baumannii* A118 by comparison of optical maps: identification of structures related to its susceptibility phenotype. *Antimicrob. Agents Chemother.* 55, 1520–1526. doi: 10.1128/AAC.01595-10

Ramirez, M. S., Don, M., Merkier, A. K., Bistue, A. J., Zorreguieta, A., Centron, D., et al. (2010). Naturally competent *Acinetobacter baumannii* clinical isolate as a convenient model for genetic studies. *J. Clin. Microbiol.* 48, 1488–1490. doi: 10.1128/JCM.01264-09

Ramirez, M. S., Merkier, A. K., Quiroga, M. P., and Centron, D. (2012). *Acinetobacter baumannii* is able to gain and maintain a plasmid harbouring In35 found in *Enterobacteriaceae* isolates from Argentina. *Curr. Microbiol.* 64, 211–213. doi: 10.1007/s00284-011-0052-9

Rodriguez-Bano, J., and Bonomo, R. A. (2008). Multidrug-resistant *Acinetobacter baumannii*: eyes wide shut? *Enferm. Infecc. Microbiol. Clin.* 26, 185–186. doi: 10.1016/s0213-005x(08)72688-0

Runci, F., Bonchi, C., Frangipani, E., Visaggio, D., and Visca, P. (2017). *Acinetobacter baumannii* biofilm formation in human serum and disruption by gallium. *Antimicrob. Agents Chemother.* 61:e1563-16. doi: 10.1128/AAC.01563-16

Runci, F., Gentile, V., Frangipani, E., Rampioni, G., Leoni, L., Lucidi, M., et al. (2019). Contribution of active iron-uptake to *Acinetobacter baumannii* pathogenicity. *Infect. Immun.* 87:e755-18. doi: 10.1128/IAI.00755-18

Russo, T. A., Luke, N. R., Beanan, J. M., Olson, R., Sauberan, S. L., Macdonald, U., et al. (2010). The K1 capsular polysaccharide of *Acinetobacter baumannii* strain 307-0294 is a major virulence factor. *Infect. Immun.* 78, 3993–4000. doi: 10.1128/IAI.00366-10

Smith, M. G., Gianoulis, T. A., Pukatzki, S., Mekalanos, J. J., Ornston, L. N., Gerstein, M., et al. (2007). New insights into *Acinetobacter baumannii* pathogenesis revealed by high-density pyrosequencing and transposon mutagenesis. *Genes Dev.* 21, 601–614. doi: 10.1101/gad.1510307

Tomaras, A. P., Dorsey, C. W., Edelmann, R. E., and Actis, L. A. (2003). Attachment to and biofilm formation on abiotic surfaces by *Acinetobacter baumannii*: involvement of a novel chaperone-usher pili assembly system. *Microbiology* 149, 3473–3484. doi: 10.1099/mic.0.26541-0

Towner, K. J., Bergogne-Berezin, E., and Fewson, C. A. (1991). "Acinetobacter: portrait of a genus," in *The Biology of Acinetobacter*, ed. C. A. Fewson (New York, NY: Plenum Press), 1–24. doi: 10.1007/978-1-4899-3553-3_1

Traglia, G. M., Chua, K., Centron, D., Tolmasky, M. E., and Ramirez, M. S. (2014). Whole-genome sequence analysis of the naturally competent *Acinetobacter baumannii* clinical isolate A118. *Genome Biol. Evol.* 6, 2235–2239. doi: 10.1093/gbe/evu176

Traglia, G. M., Place, K., Dotto, C., Fernandez, J. S., Montana, S., Bahiense, C. D. S., et al. (2019). Interspecies DNA acquisition by a naturally competent *Acinetobacter baumannii* strain. *Int. J. Antimicrob. Agents* 53, 483–490. doi: 10.1016/j.ijantimicag.2018.12.013

Traglia, G. M., Quinn, B., Schramm, S. T., Soler-Bistue, A., and Ramirez, M. S. (2016). Serum albumin and Ca2+ are natural competence inducers in the human pathogen *Acinetobacter baumannii*. *Antimicrob. Agents Chemother.* 60, 4920–4929. doi: 10.1128/AAC.00529-16

Turner, D., Wand, M. E., Sutton, J. M., Centron, D., Kropinski, A. M., and Reynolds, D. M. (2016). Genome sequence of vB_AbaS_TRS1, a viable prophage isolated from *Acinetobacter baumannii* strain A118. *Genome Announc.* 4:e1051-16. doi: 10.1128/genomeA.01051-16

Villegas, M. V., and Hartstein, A. I. (2003). Acinetobacter outbreaks, 1977–2000. *Infect. Control. Hosp. Epidemiol.* 24, 284–295. doi: 10.1086/502205

Wood, C. R., Ohneck, E. J., Edelmann, R. E., and Actis, L. A. (2018). A light-regulated type I pilus contributes to *Acinetobacter baumannii* biofilm, motility, and virulence functions. *Infect. Immun.* 86:e442-18. doi: 10.1128/IAI.00442-18

Wright, M. S., Iovleva, A., Jacobs, M. R., Bonomo, R. A., and Adams, M. D. (2016). Genome dynamics of multidrug-resistant *Acinetobacter baumannii* during infection and treatment. *Genome Med.* 8:26. doi: 10.1186/s13073-016-0279-y

Zimbler, D. L., Penwell, W. F., Gaddy, J. A., Menke, S. M., Tomaras, A. P., Connerly, P. L., et al. (2009). Iron acquisition functions expressed by the human pathogen *Acinetobacter baumannii*. *Biometals* 22, 23–32. doi: 10.1007/s10534-008-9202-3

Zurawski, D. V., Thompson, M. G., Mcqueary, C. N., Matalka, M. N., Sahl, J. W., Craft, D. W., et al. (2012). Genome sequences of four divergent multidrug-resistant *Acinetobacter baumannii* strains isolated from patients with sepsis or osteomyelitis. *J. Bacteriol.* 194, 1619–1620. doi: 10.1128/JB.06749-11

Conflict of Interest Statement: The authors declare that the research was conducted in the absence of any commercial or financial relationships that could be construed as a potential conflict of interest.

frontiers in Microbiology

ORIGINAL RESEARCH
published: 21 August 2019
doi: 10.3389/fmicb.2019.01925

BlsA Is a Low to Moderate Temperature Blue Light Photoreceptor in the Human Pathogen *Acinetobacter baumannii*

Adrián E. Golic[1†], Lorena Valle[2†], Paula C. Jaime[2], Clarisa E. Álvarez[1], Clarisa Parodi[1], Claudio D. Borsarelli[2], Inés Abatedaga[2] and María Alejandra Mussi[1]**

[1] Centro de Estudios Fotosintéticos y Bioquímicos (CEFOBI-CONICET), Universidad Nacional de Rosario (UNR), Rosario, Argentina, [2] Instituto de Bionanotecnología del NOA (INBIONATEC) CONICET-Universidad Nacional de Santiago del Estero (UNSE), Santiago del Estero, Argentina

OPEN ACCESS

Edited by:
Yuji Morita,
Meiji Pharmaceutical University, Japan

Reviewed by:
Karl Hassan,
University of Newcastle, Australia
Emily Jean Ohneck,
Advanced Testing Laboratory, United States
Steven Fiester,
University of South Carolina, United States

***Correspondence:**
Inés Abatedaga
inesabatedaga@conicet.gov.ar
María Alejandra Mussi
mussi@cefobi-conicet.gov.ar

[†]These authors have contributed equally to this work

Specialty section:
This article was submitted to Infectious Diseases, a section of the journal Frontiers in Microbiology

Received: *24 February 2019*
Accepted: *05 August 2019*
Published: *21 August 2019*

Citation:
Golic AE, Valle L, Jaime PC, Álvarez CE, Parodi C, Borsarelli CD, Abatedaga I and Mussi MA (2019) BlsA Is a Low to Moderate Temperature Blue Light Photoreceptor in the Human Pathogen Acinetobacter baumannii. Front. Microbiol. 10:1925. doi: 10.3389/fmicb.2019.01925

Light is an environmental signal that produces extensive effects on the physiology of the human pathogen *Acinetobacter baumannii*. Many of the bacterial responses to light depend on BlsA, a bluelight using FAD (BLUF)-type photoreceptor, which also integrates temperature signals. In this work, we disclose novel mechanistic aspects of the function of BlsA. First, we show that light modulation of motility occurs only at temperatures lower than 24°C, a phenotype depending on BlsA. Second, *blsA* transcript levels were significantly reduced at temperatures higher than 25°C, in agreement with BlsA protein levels in the cell which were undetectable at 26°C and higher temperatures. Also, quantum yield of photo-activation of BlsA (lBlsA) between 14 and 37°C, showed that BlsA photoactivity is greatly compromised at 25°C and absent above 28°C. Fluorescence emission and anisotropy of the cofactor together with the intrinsic protein fluorescence studies suggest that the FAD binding site is more susceptible to structural changes caused by increments in temperature than other regions of the protein. Moreover, BlsA itself gains structural instability and strongly aggregates at temperatures above 30°C. Overall, BlsA is a low to moderate temperature photoreceptor, whose functioning is highly regulated in the cell, with control points at expression of the cognate gene as well as photoactivity.

Keywords: *Acinetobacter baumannii*, BLUF, motility, photoactivity, temperature modulation

INTRODUCTION

Blue light modulates multiple cellular processes in the important human pathogen *Acinetobacter baumannii* including metabolic pathways such as the phenylacetic acid (PAA) degradation pathway and trehalose biosynthesis, tolerance to some antibiotics as well as antioxidant enzyme levels such as catalase. These traits likely contribute to the bacterial persistence in adverse environments (Müller et al., 2017). Moreover, the expression of whole pathways and gene clusters, such as genes involved in lipid metabolism, the complete type VI secretion system, as well as efflux pumps related to antibiotic resistance, are differentially induced by blue light (Müller et al., 2017). In

previous work, we further showed that in *A. baumannii*, blue light also modulates motility, biofilm formation, and virulence against *Candida albicans* (Mussi et al., 2010).

Most of these blue light-depending processes are governed by BlsA, a Blue Light Using FAD (BLUF) photoreceptor. BlsA is therefore a global regulator, capable of modulating different cellular processes simultaneously in a light-dependent way (Mussi et al., 2010; Müller et al., 2017; Tuttobene et al., 2018). Recently, we have demonstrated that BlsA directly interacts and antagonizes the functioning of diverse transcriptional regulators as the ferric uptake regulator (Fur) in the dark, enabling expression of the acinetobactin siderophore gene cluster, as well as growth under iron deprived conditions (Tuttobene et al., 2018). Also, BlsA interacts with and antagonizes the functioning of the acetoin catabolism repressor, AcoN, but only under blue light (Tuttobene et al., 2019b). In the last years only a few combinations of BLUF domains and protein partners have been characterized; e.g., photosynthesis-related gene expression in the purple bacterium *Rhodobacter sphaeroides* is controlled by AppA-PpsR (Pandey et al., 2011), biofilm formation in *Escherichia coli* by YcgF-YcgE (Tschowri et al., 2009) and the phototaxis response in the cyanobacterium *Synechocystis* sp. PCC6803 by PixD–PixE (Fujisawa and Masuda, 2018). However, BlsA is the only so far shown to function as a global regulator.

Therefore, getting insight into the mechanism of BlsA function would provide clues regarding photoregulation in *A. baumannii*, which governs important traits related to bacterial persistence in the environment and virulence. In addition, this knowledge would enlarge our understanding of short BLUFs, which represent most of the BLUF-domain containing proteins present in bacterial genomes. Short BLUFs harbor only a short amino acidic extension of approximately 50 amino acids after the BLUF domain with no significant homology (van der Horst and Hellingwerf, 2007). Indeed, the absence of an output domain within the same molecule is overcome by interacting with other protein partner/s leading to signal transduction to multiple effectors in the case of BlsA, thus explaining its nature as a global regulator (Gomelsky and Hoff, 2011). We have previously demonstrated that BlsA also integrates temperature signals in addition to the blue-light input (Mussi et al., 2010; Abatedaga et al., 2017). Indeed, photoregulation of motility occurs at 24°C but not at 37°C in wild type cells (Mussi et al., 2010; Wood et al., 2018). Concomitantly, *blsA* expression and photoreceptor levels were significantly reduced at 37°C when compared to 24°C, likely accounting for the absence of photoregulation at this temperature (Abatedaga et al., 2017). In this sense, the *E. coli* photoreceptor YcgF, a fosfodiesterase which harbors a BLUF domain as a sensor in its architecture (Hasegawa et al., 2006; Nakasone et al., 2007; Tschowri et al., 2009), has also been proposed to be a blue light photoreceptor temperature sensitive (Nakasone et al., 2010). Another point of control that governs the functionality of BlsA is at the photocycle level, since spectroscopic analysis indicated that the protein looses all functionality above 30°C (Abatedaga et al., 2017). Most likely the displacement of the FAD cofactor from the adequate orientation within its pocket alters the prompt photoinduced electron-transfer (ET) coupled with a fast proton transfer with the conserved Tyr7 (Dragnea et al., 2005; Gauden et al., 2006; Mathes et al., 2012). Moreover, even under dark conditions, a fraction of the protein precipitated above 30°C, probably by massive BlsA aggregation due to drastic conformational modification. We hypothesized that external and internal conformational changes driven by temperature must occur in BlsA, since the activation energies for the formation of the light-activated state and its relaxation back to the dark form (lBlsA and dBlsA, respectively) follows an enthalpy-entropy compensation effect (Abatedaga et al., 2017), probably due to the breakdown of hydrogen-bonding interactions between the cofactor and surrounding residues in the FAD pocket. In fact, structural modifications in BlsA were also demonstrated by vibrational studies proving that the C2=O of FAD loses hydrogen-bonding interactions with the concomitant weakening of BlsA β-sheet upon illumination, with significant differences in the β5 strand (Brust et al., 2014).

In this work, we have investigated the influence of temperature on photoregulation mediated by BlsA in *A. baumannii*, by determining the critical temperature of BlsA functioning through monitoring a phenotype that depends on BlsA such as motility (Mussi et al., 2010; Abatedaga et al., 2017; Wood et al., 2018). A critical temperature for photoregulation of motility of 25 ± 1°C was determined, consistent with a significantly reduced *blsA* expression as well as photoreceptor levels in the cells at higher temperatures. In particular, we were able to detect photoregulation of motility at 18, 21, 23, and 24°C while at 25, 26, 27, 28, 30, and 35°C the photoregulation was lost, indicating 24°C being a critical temperature. Second, *blsA* expression levels were significantly reduced at temperatures higher than 25°C such as 26 or 30°C, while at 21 and 23°C expression of *blsA* was significant, with higher levels observed in the dark rather than under blue light. These results are in agreement with BlsA levels in the cell, which were undetectable from 26°C on. Furthermore, the critical temperature in which BlsA has the ability to form the light-activated state was determined to be 25°C, confirming that this photoreceptor experiences sufficient structural compromises in the FAD nanocavity so that its ability to respond to blue light is affected. Finally, the quaternary structure of BlsA and the dynamic changes of its aggregation with temperature confirmed that a small fraction of soluble protein is still present in solution, despite precipitation and loss of activity observed for the rest. The overall data indicate that BlsA is a low to moderate temperature light-sensor, which governs the response to light at low to moderate temperatures in the human pathogen *A. baumannii*.

MATERIALS AND METHODS

Blue Light Treatments

Blue light treatments were performed as described previously (Mussi et al., 2010; Golic et al., 2013; Müller et al., 2017). Briefly, cells were incubated as specified in the dark or under blue light emitted by 9-light-emitting diode (LED) arrays, with an intensity of 6 to 10 μEinsteins m^{-2} s^{-1}. Each array was built using 3-LED module strips emitting blue light.

Motility Assays

These experiments were performed as described previously (Mussi et al., 2010). Briefly, the plates were inoculated on the surface with bacteria lifted from overnight LB (Sambrook and Russell, 2001) agar cultures using flat-ended sterile wooden sticks. In these assays, pairs of plates (one in the dark and the other under blue light) were analyzed, at any given temperature. Plates were incubated until the cells of at least one of the plates of the analyzed pair just reached the edge of the dish at each given temperature. The area of plates covered with bacteria was measured with ImageJ (NIH), and then the percentage of plate coverage was calculated. Three independent experiments were performed for each condition.

Analyses of Gene Expression by qRT-PCR

Reverse transcription and qRT-PCR analysis were performed as described in references (Müller et al., 2017; Tuttobene et al., 2018), using *blsA* primers described in Müller et al. (2017). Data are presented as NRQ (Normalized relative quantities) calculated by the qBASE method (Hellemans et al., 2007), using *recA* and *rpoB* genes as normalizers (Müller et al., 2017). For motility assays, pairs of plates (one in the dark and the other under blue light) were analyzed, at any given temperature. Cells were harvested from complete plates, at time points in which the cells of at least one of the plates of the analyzed pair just reached the edge of the dish at each given temperature. Three biological replicates were used for each condition.

To analyze the variation of *blsA* transcripts in the short term as a result of light or temperature changes, ATCC®17978 cells were grown until OD = 0.5 in LB at 24°C in the dark (D) ($t = 0$), and then switched to light conditions, or rather, the cells were grown until OD = 0.5 in LB in the dark (D) at 24°C ($t = 0$), and then switched to 37°C (Mussi et al., 2010). Three biological replicates were used for each condition.

Protein Analyses

Protein extraction, quantification, SDS-PAGE separation and western blots were performed as indicated in Abatedaga et al. (2017). Recombinant BlsA was produced and purified also as performed in Abatedaga et al. (2017). Western blots were repeated at least twice using biological replicates.

Quantum Yield of Photoactivation (dBlsA + $h\nu$ → lBlsA)

Light adapted state for BlsA (lBlsA) was obtained by blue light irradiation of the dark-adapted form (dBlsA) using a 1 W Royal Blue LED (Luxeon Star Leds) at 443 ± 20 nm. The apparent quantum yield of formation of lBlsA state (Φ_{lBlsA}) was estimated following a methodology previously described (Abatedaga et al., 2017). Briefly, for each analyzed temperature, Φ_{lBlsA} was calculated using Eq. (1), where C_{lBlsA} the concentration of lBlsA determinated from the absorbance plateau at 510 nm of the growth kinetic profiles, using $\Delta\varepsilon_{510}$ = 3800 M^{-1} cm^{-1} profiles, and $q_{n,p}$ is the photon flux, determined by chemical actinometry using potassium ferrioxalate (Fukushima et al., 2005; Abatedaga et al., 2017).

$$\Phi_{\mathrm{lBlsA}} = C_{lBlsA} / q_{n,p} \quad (1)$$

Spectroscopic Measurements

UV-vis absorption spectra were registered using a modular miniature spectrophotometer USB2000+ (Ocean Optics, United States) connected via optic fiber to UV-vis light source (Analytical Instruments System, United States), by placing 300 μL of BlsA in buffer *TRIS* (2-Amino-2-(hydroxymethyl)propane-1,3-diol) 20 mM, NaCl 500 mM, pH 8 in a 5 × 5 mm quartz cuvettes, mounted on a Peltier-driven temperature-controlled cuvette holder (Flash 300 of Quantum Northwest) (Abatedaga et al., 2017).

Emission spectra of the cofactor or the protein were obtained with Hitachi F-2500 spectrofluorometer by selective excitation at 460 nm or 295 nm, respectively. Steady state fluorescence anisotropy r was determined using the classical L-format and calculated as previously described (Villegas et al., 2014).

Time-resolved fluorescence anisotropy $r(t)$ of the cofactor emission of BlsA as a function of the temperature was calculated by measuring the fluorescence emission decays using a Tempro-01 time-correlated single photon counting (TCSPC) system (Horiba, Glasgow), by ultrafast excitation with a 1 MHz Nanoled®emitting at 460 (±20) nm. Fluorescence decays were registered at 510 and 540 nm with an emission bandwidth of ±12 nm (Valle et al., 2015). The fluorescence anisotropy decays were analyzed with the classical exponential model function for a spherical emitter, Eq. (2), where r_0 is the maximum anisotropy at $t = 0$, and θ is the rotational correlation time of the sphere.

$$r(t) = r_0 \exp(-t/\theta) \quad (2)$$

All fluorescence measurements were performed under air-saturated conditions and controlled temperature at ($T \pm 0.1$°C) using an external thermostat (Haake F3, Germany).

Dynamic Light Scattering Measurements

Dynamic light scattering (DLS) experiments were carried out on a Particle Analyzer SZ100 (Horiba) with a backscattering detection at 90°, using 5 × 5 mm quartz cuvettes. BlsA solutions were left equilibrating for 10 min at each temperature before measurements were performed. The hydrodynamic diameter value (HD) was calculated from a set of 3 measurements (∼40 runs each). The HD of the sample was obtained from the peak with the highest scattered light intensity (i.e., the mode) in number intensity distributions after averaging all runs using the instruments software (SZ-100, Horiba) (Su et al., 2008).

Working buffer solution was filtered with HV (Durapore) PVDF (polyvinylidene difluoride) membranes, 0.45 μm pore size. Purified BlsA was desalted against filtered buffer using a PD-minitrap column pre-equilibrated with 20 volumes of filtered buffer. Last elution of equilibration was used as blank to determine artifacts present in the solution with DLS. Controls

with air and buffer-only were performed to detect any possible artifacts. BlsA in working buffer (10 mM phosphate, 10 mM NaCl, pH 7) was used for all the determinations at a protein concentration of 10 μM as calculated using the absorbance at 460 with an ε = 11300 M^{-1} cm^{-1}.

RESULTS

Acinetobacter baumannii Motility Is Regulated by Light Within a Low to Moderate Temperature Range

To determine the critical temperature of photoregulation of motility in *A. baumannii*, i.e., the temperature at which photoregulation is lost, we monitored motility at different temperatures from 18 to 35°C. **Figures 1A,B** show representative motility assays for ATCC 17978 at different temperatures from 18 to 35°C under both blue light illumination and dark conditions. It can be observed that bacterial motility was only inhibited between 18 and 24°C under blue light illumination, while photoregulation was lost above 24°C and the bacteria moved throughout the plates at this condition. In the dark, the bacteria spread throughout the plates at all temperatures. Hence, the above results indicate a dramatic change in *A. baumannii* photoregulation with temperature, with a sharp threshold between 24 and 25°C. It is noteworthy that below 18°C, we were not able to test motility at this condition, as bacterial growth was inhibited.

We also studied motility in different illumination and temperature conditions for the Δ*blsA* mutant. Contrary to the wild type, this strain moved covering the whole plates both under blue light and darkness at all temperatures assayed, with the exception of 21°C under blue light, a condition at which the cells showed a slight decrease in motility compared to darkness (**Figure 1C**).

blsA Expression Levels Follow Photoregulation of Motility in ATCC 17978

blsA expression levels were analyzed in *A. baumannii* ATCC 17978 cells recovered from motility plates incubated at temperatures close to the critical values (24–25°C) under blue light or in the dark following procedures previously described (Müller et al., 2017). **Figure 2** shows that *blsA* was expressed at 21 and 23°C, while its expression was almost negligible at 26 and 30°C. Moreover, at 21 and 23°C, *blsA* expression levels were higher in the dark than under blue light, in agreement with previous results (Mussi et al., 2010; Abatedaga et al., 2017). Globally, *blsA* expression levels followed the same photoregulation pattern observed for motility, with significant *blsA* levels at temperatures at which

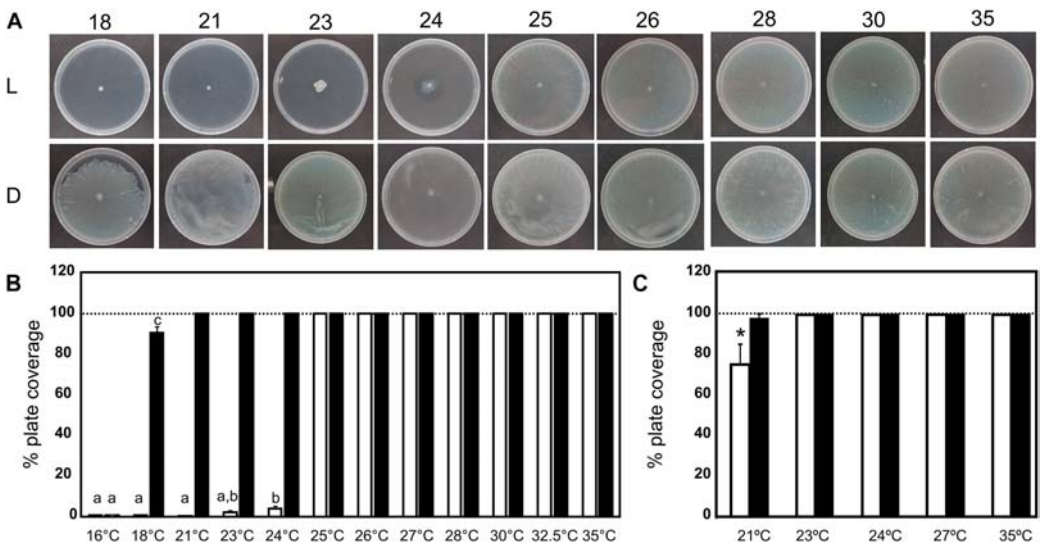

FIGURE 1 | Effects of blue light and temperature on *A. baumannii* motility. **(A)** Cells of the parental strain ATCC 17978 were inoculated on the surface of motility plates and incubated at the indicated temperatures. Plates were inspected and photographed after incubation in darkness (D) or in the presence of blue light (L) at the indicated temperatures. **(B)** Quantification of cell motility estimated as the percentage of plate coverage, i.e., the percentage of the Petri plate area covered with bacteria, in motility plates inoculated with ATCC 17978 wild type and incubated at the indicated temperatures. Three independent experiments were performed in each case. The area of plates covered with bacteria was measured with ImageJ (NIH), and then the percentage of plate coverage was calculated. The mean ± SEM is informed. Different letters indicate significant differences as determined by ANOVA followed by Tukey's multiple comparison test ($p < 0.05$). For those conditions at which the bacteria just reached the edge of the plate a value of 100% is informed. **(C)** Quantification of cell motility estimated as the percentage of plate coverage, i.e., the percentage of the Petri plate area covered with bacteria, in motility plates inoculated with the Δ*blsA* mutant and incubated at the indicated temperatures. Three independent experiments were performed in each case. The area of plates covered with bacteria was measured with ImageJ (NIH), and then the percentage of plate coverage was calculated. The mean ± SEM is informed. Asterisks indicate significant differences in light compared to dark conditions, as indicated by *t*-test ($p < 0.01$).

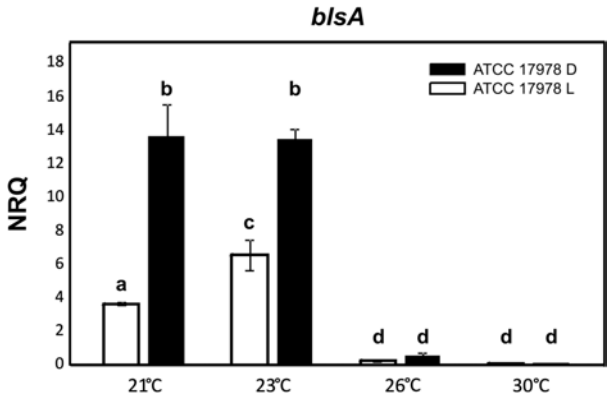

FIGURE 2 | *blsA* expression levels follow photoregulation patterns. Estimation by RT-qPCR of the *blsA* expression levels in ATCC 17978 wild-type genetic background at different temperatures analyzed indicated in the *x*-axis, under blue light (L) or in the dark (D). The data shown are mean ± SD of normalized relative quantities (NRQ) obtained from transcript levels of *blsA* from cells recovered from motility plates incubated at the indicated temperatures under blue light or in the dark, measured in three biological replicates. Different letters indicate significant differences as determined by ANOVA followed by Tukey's multiple comparison tests ($p < 0.01$).

photoregulation occurred, while negligible levels were detected at non-photoregulatory temperatures.

blsA Expression Levels Rapidly Respond to Illumination or Temperature Changes

Next, we studied the short-term response of the photoreceptor expression levels to light or temperature changes. As it can be observed in **Figure 3**, *blsA* expression levels significantly reduced when exponentially growing ATCC 17978 cultures adapted to dark conditions at 24°C were suddenly changed to illumination conditions (**Figure 3A**). In fact, after 60 min of illumination, *blsA* expression levels were half of those registered at zero time, consistent with the previous observations that *blsA* levels are higher in the dark than under blue light (**Figure 2**). Moreover, when cultures adapted to dark conditions at 24°C were shifted to 37°C, *blsA* expression levels were more efficiently reduced, since the half-time was reached after approximately 30 min (**Figure 3B**). Overall, these results show that the *blsA* photoreceptor expression system responds to illumination and temperature conditions rapidly at the physiological level.

Photoreceptor Levels Are Negligible Above the Critical Temperature

Western blot analyses directed against BlsA (**Figure 4**) were in agreement with expression analyses at the RNA level. BlsA protein levels were detected at 21 and 23°C, being much higher in the dark than under blue light. Interestingly, BlsA levels were not detectable at 26°C both under blue light and in the dark. As controls, we have included the His-tagged recombinant BlsA (Mussi et al., 2010), as well as an extract of the Δ*blsA* mutant harboring plasmid pWHBlsA, which expresses a wild type copy of *blsA* directed by its own promoter.

BlsA Photocycle Efficiency Is Compromised at 25°C and Practically Absent Above 28°C

To understand how temperature affects BlsA photoactivity, we analyzed the temperature-dependency of the BlsA photoactivation quantum yield (Φ_{lBlsA}), since this value reflects the impact of temperature in the photoreceptor integrating all structural and local protein changes. Φ_{lBlsA}, defined as the ratio of the light-adapted state of BlsA (lBlsA) concentration relative to the number of photons absorbed, was determined between 14 and 37°C by measuring the time-dependent UV-vis absorbance changes elicited on the dark-adapted BlsA (dBlsA) after blue light illumination to form the lBlsA state (**Figures 5A,B**; Abatedaga et al., 2017). **Figure 5C** shows the sigmoidal-like variation of Φ_{lBlsA} with temperature, with a maximum value of 0.24 ± 0.01 below 22°C. By increasing temperature above 22°C, Φ_{lBlsA} decreases significantly reaching non-detectable photoactivation at $T > 28$°C, suggesting that dBlsA is not active above this temperature. A sigmoidal fit of the data using a Boltzmann function indicates an inflection point at 25 ± 1°C. This value may represent the critical temperature for the dBlsA state, in which the sum of all conformational changes in the protein become important enough to alter its response to light (measured as photoactivation efficiency), leading to a complete loss of function above 28°C.

Chromophore Binding Site Evidences Structural Instability With Temperature Increments

Figure 6A compares the steady-state fluorescence emission and anisotropy spectra observed by excitation at 460 nm of dBlsA at 19 and 27°C with those of free FAD in the same buffer at 25°C. At 19°C, the vibrational structure of the emission fluorescence spectrum of dBlsA shows a maximum at 513 nm and a shoulder at 535 nm. This feature is gradually lost by a discrete red shift of the maximum when temperature increases, while shoulder disappearance mostly due to a decrease in its intensity without changes in its position. The variation of the ratio F_{535}/F_{513} evidences this effect. Also, the steady-state anisotropy of the cofactor in dBlsA solutions is strongly decreased (**Figure 6B**). Moreover, the emission anisotropy was dependent on wavelength, being larger at the blue edge of the fluorescence spectrum. These results indicate an inhomogeneous population of emitters. However, for free FAD in the buffer solution, no dependence with temperature was observed, either in emission spectral shape or anisotropy, and the constant values are indicated with arrows at the respective *y*-axis of **Figure 6B**. The anisotropy decay monitored at 510 nm was also analyzed as a function of temperature, and in all cases they were fitted accordingly to the first-order Eq. (2) (**Figure 6C**), usually related to the depolarization of a spherical rotor (Lakowicz, 2006). It was observed that the increment of temperature decreases in the same proportion both for the initial anisotropy r_0 and the rotational correlation time θ (**Figure 6D**). In fact, the trend is that at high

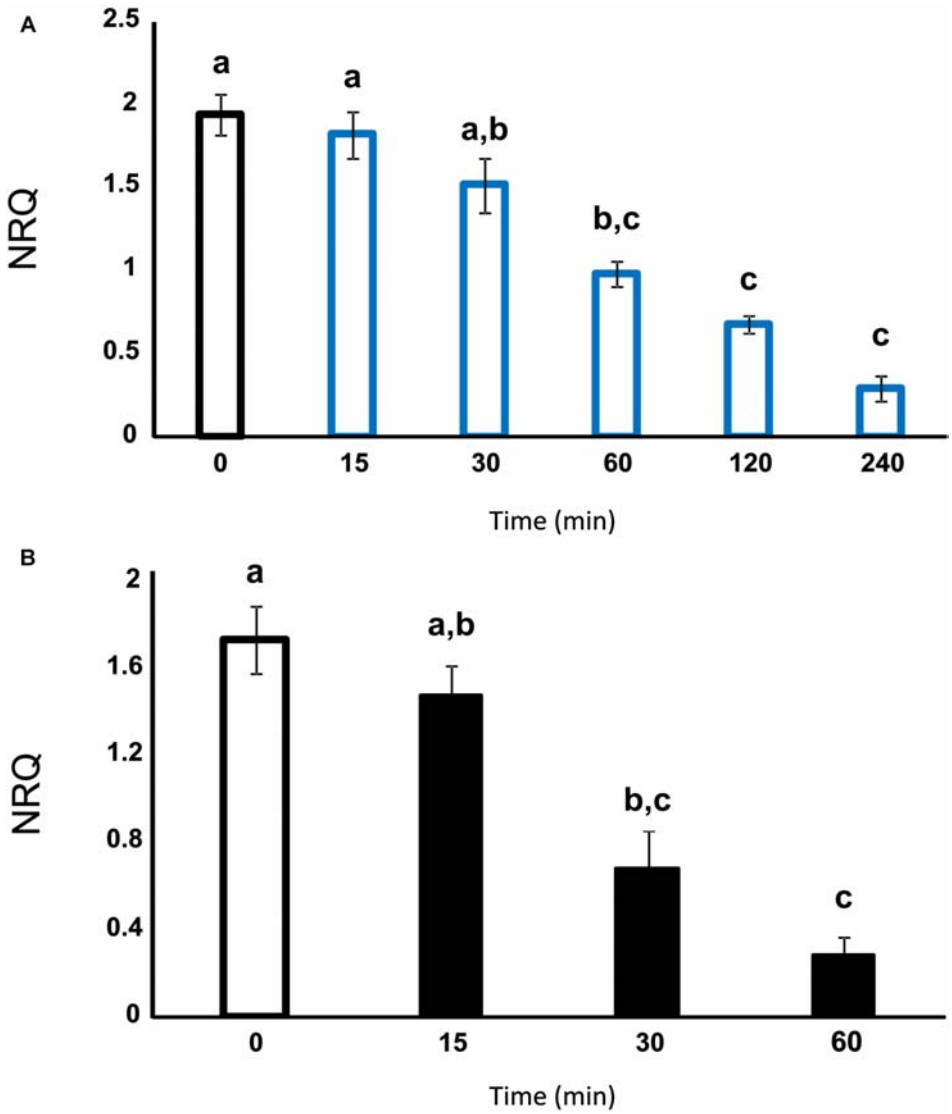

FIGURE 3 | *blsA* expression levels rapidly respond to illumination or temperature changes. **(A)** Estimation by RT-qPCR of the *blsA* expression levels in ATCC 17978 cells grown until DO = 0.5 in LB at 24°C in the dark (D) (t = 0), and then switched to light conditions. **(B)** Estimation by RT-qPCR of the *blsA* expression levels in ATCC 17978 cells grown until DO = 0.5 in LB in the dark (D) at 24°C (t = 0), and then switched to 37°C. Samples were taken at the indicated times. The data shown are mean ± SD of normalized relative quantities (NRQ) obtained from transcript levels of *blsA* from cells incubated at the indicated temperatures under blue light or in the dark, measured in three biological replicates. Different letters indicate significant differences as determined by ANOVA followed by Tukey's multiple comparison tests ($p < 0.05$).

temperatures, e.g., 37°C, both $r_{0,BlsA}$ and θ_{BlsA} are similar to the values for FAD.

Intrinsic Fluorescence of BlsA Is Not Affected by Temperature

In order to further explore temperature-dependent conformational modifications in the secondary and tertiary structure of dBlsA, the intrinsic steady-state fluorescence of dBlsA was also studied by excitation at 295 nm, since dBlsA contains two Trp residues, i.e., Trp78 and Trp92 (**Supplementary Figures S1A,B**).

The intrinsic fluorescence spectrum of the protein was then practically constant in the temperature range studies (**Supplementary Figure S1**), with a blue-shifted emission maximum and narrower full width half-maximum (FWHM) than those for free Trp in buffer solution, respectively. This indicates that the nano-environment surrounding the Trp residues of BlsA did not change with the temperature. These results indicate that both Trp residues are partially buried in the protein regardless of the temperature, sensing at all times a less polar environment than in the aqueous buffer, as confirmed by the BlsA homology model (pdb template: 2HFN), where both Trp78 and Trp92 are

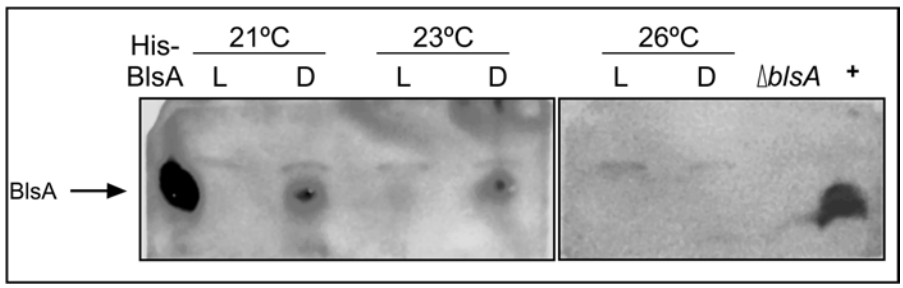

FIGURE 4 | Effects of light and temperature on BlsA protein levels. Immunoblot analysis of protein samples from ATCC 17978 cells grown overnight in motility plates at 21, 23 or 26°C, in the presence of blue light (L) or in darkness (D), using purified antibodies directed against BlsA. Crude extracts corresponding to 350 μg of total proteins were loaded in each lane. His-BlsA refers to the purified recombinant BlsA protein, expressed as a His-tag fusion. (+) corresponds to the Δ*blsA* strain harboring plasmid pWHBlsA, which overexpresses a wild type copy of *blsA* directed by its own promoter.

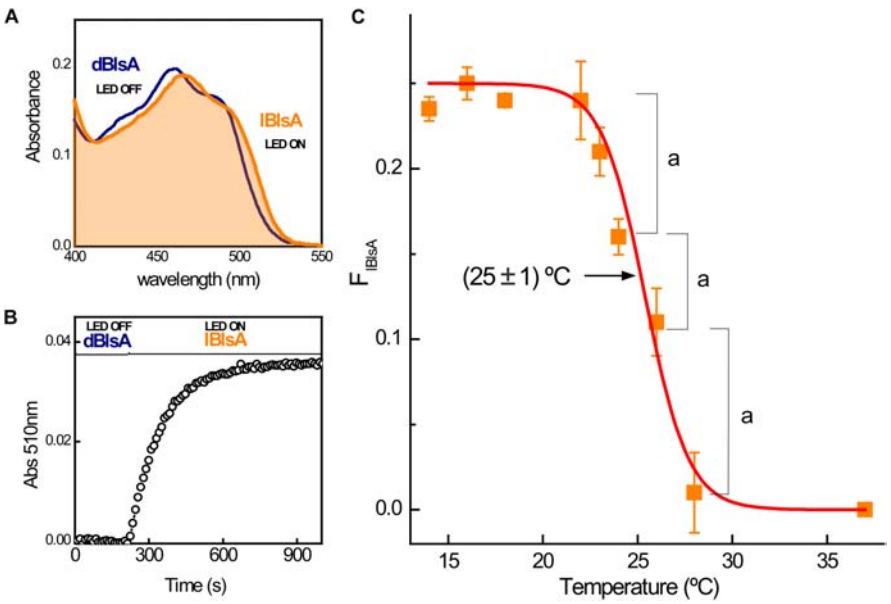

FIGURE 5 | BlsA photoactivation efficiency (Φ_{lBlsA}) versus temperature showing an inflection point at 25°C. **(A)** UV-vis absorbance changes produced for the dark-adapted BlsA, dBlsA turns into the light-adapted state, lBlsA by blue light illumination (Led Royal Blue, see Methods) at 14°C. **(B)** Kinetic profile for the lBlsA formation registered at 510 nm. **(C)** Variation of Φ_{lBlsA} with temperature, showing an inflection point at 25 ± 1°C. The data shown are mean ± SD of two independent measurements from two different protein productions. Letter (a) represents significant difference ($p < 0.05$) between the indicated temperature points.

partially protected from the solvent by nearby residues (**Supplementary Figure S1B**).

Hence, it can be concluded that the overall tertiary structure of the protein is conserved despite increments in temperature, in contrast to the spectroscopic changes observed with temperature for the cofactor due to discrete changes in the FAD-BlsA specific interaction in the active site.

Size Particle Distributions Confirm the Formation of BlsA Aggregates With Temperature

Particle size distributions (PSD) determined by DLS measurements were followed during the incubation of dBlsA solutions during 40 min at each of the following temperatures: 22, 28, 30, 33, and 37°C (**Figure 7**). As temperature increases, there is a stepwise particle size increment, e.g., 20 ± 15 nm, 45 ± 10 nm; and 71 ± 24 nm at 22, 28, and 30°C, respectively. At 33 and 37°C the aggregation process is accelerated during the incubation period and much larger polydisperse aggregates are detected, e.g., 336 ± 65 nm and 1150 ± 150 nm, respectively. In fact, at 37°C a fraction of low size particles of 88 ± 40 nm was also detected. These results confirm the existence of protein aggregation effects concomitant with solution instability and the light inactivation of dBlsA.

DISCUSSION

Blue light exerts a global influence on *A. baumannii* through the BlsA photoreceptor. Disclosing the mechanism of BlsA functioning is therefore essential to understand an important

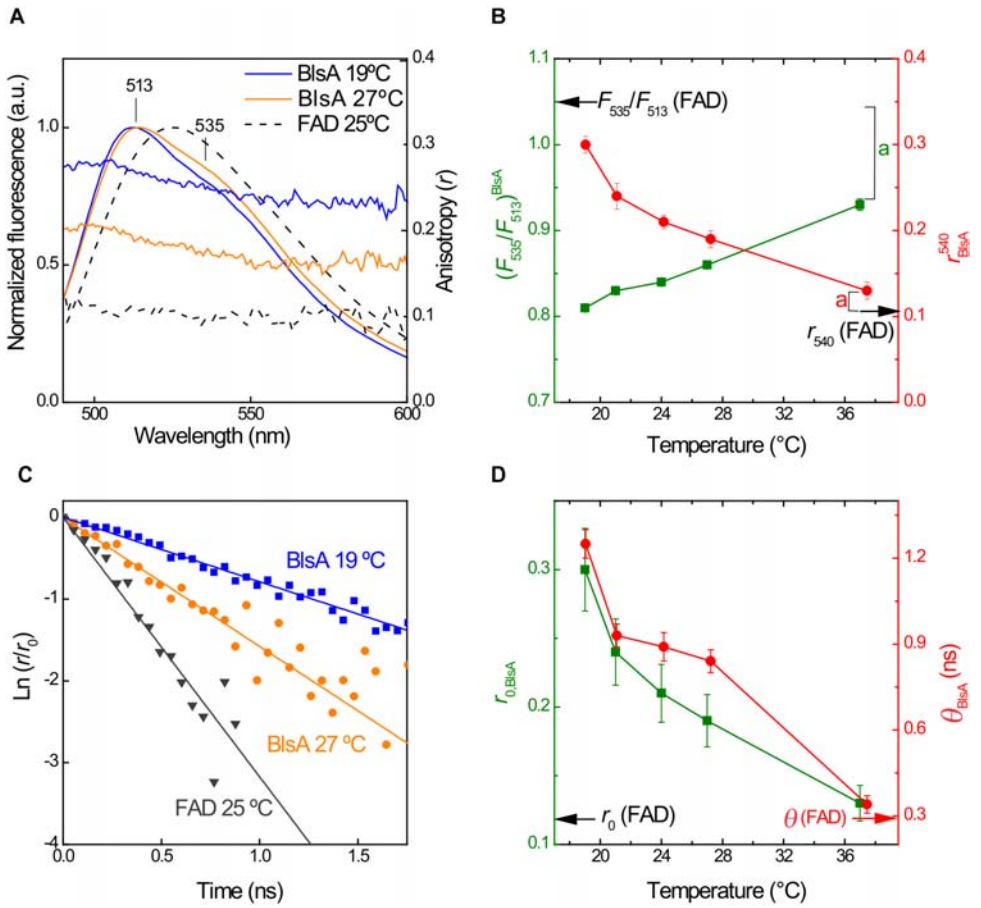

FIGURE 6 | Temperature affects rigidity of the environment surrounding FAD in dBlsA. **(A)** Normalized fluorescence emission spectra of dBlsA at 19 and 27°C and FAD at 25°C in air-saturated buffer solution obtained by excitation at 460 nm. **(B)** Temperature dependence of the fluorescence intensity ratio between 535 nm and 513 nm (F_{535}/F_{513}) and steady-state anisotropy at 540 ± 20 nm (r_{540}) for dBlsA. Arrows indicate the respective values for FAD and the respective steady state anisotropy. **(C)** Logarithmic first-order plots of the fluorescence anisotropy decays of dBlsA at 19 and 27°C monitored at 510 nm and FAD at 25°C monitored at 525 nm. **(D)** Temperature dependence of the initial anisotropy (r_0) and the rotational correlation time (θ) for the cofactor in dBlsA. The data shown are mean ± SD of two independent measurements from two different protein productions. Letter (a) represents significant difference ($p < 0.05$) between dBlsA and free FAD at the indicated temperature points **(B,D)**.

aspect of this pathogen's physiology. The evidence accumulated in this work, including physiological, gene expression and protein analysis, indicates that *blsA* expression and the corresponding photoreceptor levels fall above 24°C, reaching negligible levels. This is consistent with the lack of the photo-regulation observed for motility at these temperatures. It has been recently reported that motility depends on the pilus assembly system PrpABCD at 24°C, with differential expression of *prpA* in response to light in a BlsA-dependent manner in *A. baumannii* ATCC 17978 (Wood et al., 2018), confirming our previous results showing dependence on BlsA of this phenotype (Mussi et al., 2010). On the contrary, no photoregulation of motility was observed in the wild type cells at 37°C, while *prpA* expression showed no dependence on light at this temperature (Wood et al., 2018). Whether other yet unknown systems could also eventually contribute to motility at higher temperatures, the *prpABCD* system coding for type I pili governs motility and the response to light observed through BlsA in *A. baumannii* ATCC 17978 wild type cells (Wood et al., 2018). This notion is further supported by our data using the Δ*blsA* mutant, which show that this photoreceptor is the main responsible for the photoregulation of motility observed. Whether the reduction of motility perceived under blue light at 21°C corresponds to an uspecific effect of light on the motility machinery, or rather there exists another photosensory system operating, the data still show that BlsA is the major photoreceptor involved in the response. The overall data indicate that BlsA is a photoreceptor governing the response to blue light at low-moderate temperatures, i.e., $T < 24$°C, and the main line of control of its functioning is the regulation of its expression levels in the cell.

Previous work regarding BlsA functioning are in agreement with this notion. In this sense, BlsA has been shown to interact with transcriptional regulators such as Fur in a light dependent manner at 24°C but not at 30°C, and photoregulation of iron uptake itself occurs at 24°C but not at 30 or 37°C in *A. baumannii* ATCC 19606 (Tuttobene et al., 2018).

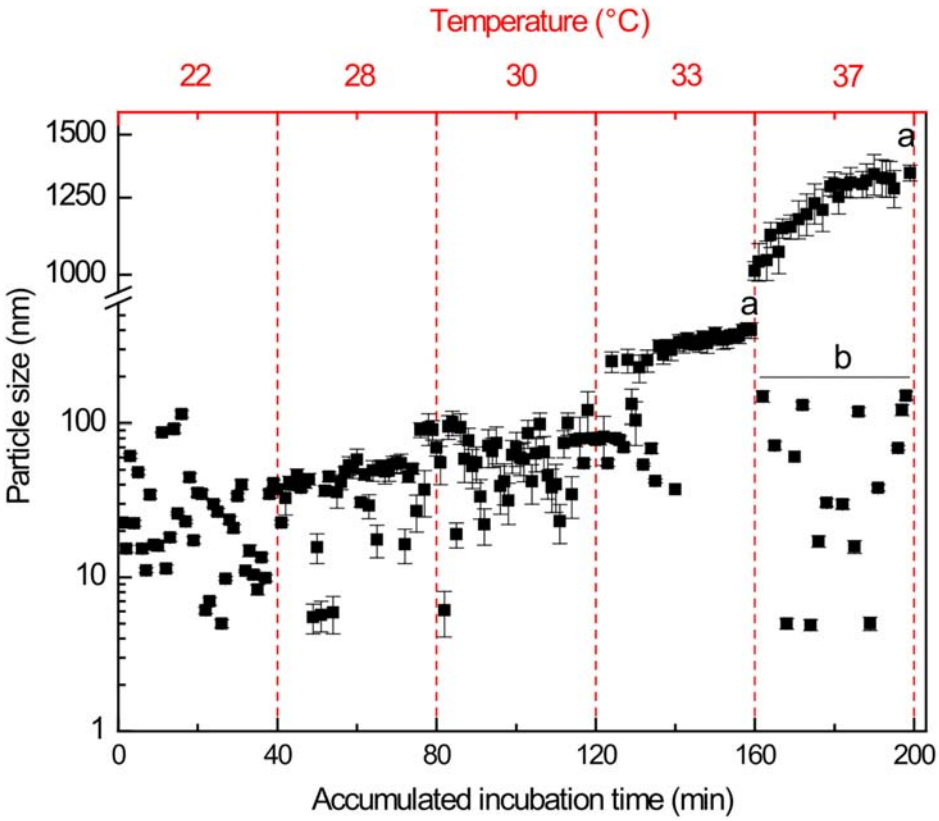

FIGURE 7 | Particle size distribution of oligomeric states of dBlsA determined by DLS. The data shown are mean ± SD of two independent measurements from two different protein productions. Letter (a) represents significant difference ($p < 0.05$) between the first and last timepoint at any given temperature. Letter (b) represents significant difference ($p < 0.05$) between the mean of all values at the upper and the lower particle population (line).

Similar temperature-dependent modulation by light of acetoin catabolism has also been described for BlsA and the repressor AcoN in *A. baumannii* ATCC 17978 (Tuttobene et al., 2019b).

In our previous work, we demonstrated by monitoring the UV-vis absorbance changes at the red-edge of the flavin absorption band (see **Figures 5A,B**) that the efficacy of the photoconversion of the dark adapted dBlsA to form the lBlsA state was dependent on the displacement of FAD from its correct position inside the nanocavity active site (Abatedaga et al., 2017). In this condition, the conserved Tyr7 is very close to the isoalloxazine ring of the flavin to produce the ultrafast electron-transfer and subsequent proton-transfer processes between the cofactor to the residue generating the reduced semiquinone radical of FAD ($FADH^{\cdot}$). The efficiency of this process is measured by the quantum yield of photoconversion of the lBlsA state (Φ_{lBlsA}), which falls from 0.22 to zero as the temperature increases above 22°C (**Figure 5C**). This result was accompanied with the progressive loss of anisotropy and red-shifting of the fluorescence of the cofactor in dBlsA with the temperature (**Figure 6**), linking the photo-regulation of BlsA with the environmental properties of the active site. In fact, the relatively low value of the rotational correlation time θ_{BlsA} = 1.25 ns at 19°C indicates that the light induced formation of $FADH^{\cdot}$ produces an efficient depolarization channel of the cofactor, since a 10-times larger value of θ can be expected for a globular protein of approximately 20 kDa as dBlsA (Lakowicz, 2006). It is interesting to note that as the nanoenvironment of FAD is changed with temperature, the intrinsic fluorescence of dBlsA reported by the Trp78 and Trp92 residues (**Supplementary Figure S1A**) indicated that no significant changes of the protein structure occurred. From the BlsA homology model both Trp residues are located in opposite sides of the molecule and outside the FAD binding site (**Supplementary Figure S1B**). This suggests that the BlsA side-containing FAD is more sensitive to increments in temperature than any other region of BlsA.

Moreover, besides the environmental rearrangement around the cofactor, temperatures above 30°C play a role on the protein aggregation process (**Figure 7**). Precipitation of BlsA above 30°C, which can be seen after centrifugation as a white pellet (Abatedaga et al., 2017) correlates with the presence of macroaggregates (HD > 80 nm) as determined with DLS. This aggregation process appears to be dependent on temperature. Interestingly, from DLS data at 37°C, soluble microaggregates corresponding to non-functional low oligomeric forms (HD ∼80 nm) are present and may well confirm that the protein remaining in solution regenerates the functional oligomeric

forms, once the temperature is restored to 24°C or lower temperatures, recovering the photocycling activity, as previously shown (Abatedaga et al., 2017). All these data suggest that the conformational changes are somewhat reversible but limited by the temperature exposure time, the longer the exposure time at temperatures > 30°C, the higher amounts of aggregates are formed and the larger the particle sizes. This behavior has been described for other proteins such as bovine serum albumin (BSA) (Su et al., 2008).

It should be noted that all the evidence gathered indicates that BlsA is a photoreceptor that functions both in the dark and under blue light, and therefore "the signaling state" frequently referred to as the state acquired by photoreceptors upon illumination does not apply here. Indeed, it has been recently shown that BlsA binds to and likely captures transcriptional repressors such as Fur in the dark at 23°C (Tuttobene et al., 2018), but also other set of transcriptional repressors, such as AcoN, under blue light (Tuttobene et al., 2019a). This differential ability to bind several transcriptional regulators, both under blue light or in the dark in a temperature dependent manner, is probably related to the differential oligomerization states acquired by BlsA under blue light/dark or induced by different temperatures. We are currently working on this matter to provide more insights in the future.

In summary, BlsA modulation by temperature occurs on two levels: one at cellular level, controlling the photoreceptor expression and production in the cells, which is drastically reduced above the critical temperature. The second modulation point is at the protein level, involving a deleterious effect of temperature above the critical point in the interaction of FAD and the residues surrounding it in its nanocavity with a concomitant loss of photoactivity, and general conformational changes that lead to protein aggregation.

DATA AVAILABILITY

All datasets generated for this study are included in the manuscript and/or the **Supplementary Files**.

AUTHOR CONTRIBUTIONS

AG, LV, IA, CÁ, PJ, and CP performed the experiments. LV collaborated in writing the manuscript. CÁ analyzed the experiments. MM, IA, LV, and CB designed the experiments and wrote the manuscript. MM and CB provided funding.

FUNDING

This work was supported by grants from Agencia Nacional de Promoción Científica y Tecnológica PICT 2014-1161 and PICT-2015-0828 to MM and CB, respectively. CÁ, CB, and IA are career investigators of CONICET. AG and PJ are fellows from the same institution.

SUPPLEMENTARY MATERIAL

The Supplementary Material for this article can be found online at: https://www.frontiersin.org/articles/10.3389/fmicb.2019.01925/full#supplementary-material

FIGURE S1 | Intrinsic fluorescence emission is not affected by temperature. **(A)** Normalized emission spectra of dBlsA, from 19 and 37°C by excitation at 295 nm. Inset: dBlsA Full Width at Half Maximum (FWHM) and maximum emission wavelength (λ_{max}) versus temperature. **(B)** Detail of BlsA homology model (template:2HFN) showing relative positions of Tyr7, Gln51, Trp78 and Trp92 to the FAD molecule.

REFERENCES

Abatedaga, I., Valle, L., Golic, A. E., Müller, G. L., Cabruja, M., Morán Vieyra, F. E., et al. (2017). Integration of temperature and blue-light sensing in *Acinetobacter baumannii* through the BlsA sensor. *Photochem. Photobiol.* 93, 805–814. doi: 10.1111/php.12760

Brust, R., Haigney, A., Lukacs, A., Gil, A., Hossain, S., Addison, K., et al. (2014). Ultrafast structural dynamics of BlsA, a photoreceptor from the pathogenic bacterium *Acinetobacter baumannii*. *J. Phys. Chem. Lett.* 5, 220–224. doi: 10.1021/jz4023738

Dragnea, V., Waegele, M., Balascuta, S., Bauer, C., and Dragnea, B. (2005). Time-resolved spectroscopic studies of the AppA blue-light receptor BLUF domain from *Rhodobacter sphaeroides*. *Biochemistry* 44, 15978–15985. doi: 10.1021/bi050839x

Fujisawa, T., and Masuda, S. (2018). Light-induced chromophore and protein responses and mechanical signal transduction of BLUF proteins. *Biophys. Rev.* 10, 327–337. doi: 10.1007/s12551-017-0355-6

Fukushima, Y., Okajima, K., Shibata, Y., Ikeuchi, M., and Itoh, S. (2005). Primary intermediate in the photocycle of a blue-light sensory BLUF FAD-protein, Tl0078, of *Thermosynechococcus elongatus* BP-1. *Biochemistry* 44, 5149–5158. doi: 10.1021/bi048044y

Gauden, M., van Stokkum, S. I., Key, J. M., Lührs, D. C. H., van Grondelle, R., Hegemann, P., et al. (2006). Hydrogen-bond switching through a radical pair mechanism in a flavin-binding photoreceptor. *PNAS* 103, 10895–10900. doi: 10.1073/pnas.0600720103

Golic, A., Vaneechoutte, M., Names, A., Viale, A. M., Actis, L. A., and Mussi, M. A. (2013). Staring at the cold sun: blue light regulation is distributed within the genus *Acinetobacter*. *PLoS One* 8:e55059. doi: 10.1371/journal.pone.0055059

Gomelsky, M., and Hoff, W. D. (2011). Light helps bacteria make important lifestyle decisions. *Trends Microbiol.* 19, 441–448. doi: 10.1016/j.tim.2011.05.002

Hasegawa, K., Masuda, S., and Ono, T. A. (2006). Light induced structural changes of a full-length protein and its BLUF domain in YcgF(Blrp), a blue-light sensing protein that uses FAD (BLUF). *Biochemistry* 45, 3785–3793. doi: 10.1021/bi051820x

Hellemans, J., Mortier, G., De Paepe, A., Speleman, F., and Vandesompele, J. (2007). qBase relative quantification framework and software for management and automated analysis of real-time quantitative PCR data. *Genome Biol.* 8:R19.

Lakowicz, R. (2006). *Principles of Fluorescence Spectroscopy*. Singapore: Springer Science+Business Media.

Mathes, T., van Stokkum, S. I., Stierl, M., and Kennis, J. T. (2012). Redox modulation of flavin and tyrosine determines photoinduced proton-coupled electron transfer and photoactivation of BLUF photoreceptors. *J Biol Chem.* 287, 31725–31738. doi: 10.1074/jbc.M112.391896

Müller, G. L., Altilio, T. M., Martínez Amezaga, M., Nguyen, M., Cribb, M., and Cybulski, P. (2017). Light modulates metabolic pathways and other novel physiological traits in the human pathogen *Acinetobacter baumannii*. *J. Bacteriol.* 199:e00011–17. doi: 10.1128/JB.00011-17

Mussi, M. A., Gaddy, J. A., Cabruja, M., Arivett, B. A., Viale, A. M., Rasia, R., et al. (2010). The opportunistic human pathogen *Acinetobacter baumannii*

senses and responds to light. *J. Bacteriol.* 192, 6336–6345. doi: 10.1128/JB.00917-10

Nakasone, Y., Ono, T. A., Ishii, A., Masuda, S., and Terazima, M. (2007). Transient dimerization and conformational change of a BLUF protein: YcgF. *J. Am. Chem. Soc.* 129, 7028–7035. doi: 10.1021/ja065682q

Nakasone, Y., Ono, T. A., Ishii, A., Masuda, S., and Terazima, M. (2010). Temperature-sensitive reaction of a photosensor protein YcgF: possibility of a role of temperature sensor. *Biochemistry* 49, 2288–2296. doi: 10.1021/bi902121z

Pandey, R., Flockerzi, D., Hauser, M. J., and Straube, R. (2011). Modeling the light- and redox-dependent interaction of PpsR/AppA in *Rhodobacter sphaeroides*. *Biophys. J.* 100, 2347–2355. doi: 10.1016/j.bpj.2011.04.017

Sambrook, J. F., and Russell, D. W. (2001). *Molecular Cloning: a Laboratory Manual*, 3rd Edn. New York, NY: Cold Spring Harbor Laboratory Press.

Su, R., Qi, W., He, Z., Zhang, Y., and Jin, F. (2008). Multilevel structural nature and interactions of bovine serum albumin during heat-induced aggregation process. *Food Hydrocoll.* 22, 995–1005. doi: 10.1016/j.foodhyd.2007.05.021

Tschowri, N., Busse, S., and Hengge, R. (2009). The BLUF-EAL protein YcgF acts as a direct anti-repressor in a blue-light response of *Escherichia coli*. *Genes Dev.* 23, 522–534. doi: 10.1101/gad.499409

Tuttobene, M. R., Cribb, P., and Mussi, M. A. (2018). BlsA integrates light and temperature signals into iron metabolism through fur in the human pathogen *Acinetobacter baumannii*. *Sci. Rep.* 8:7728. doi: 10.1038/s41598-018-26127-8

Tuttobene, M. R., Fernandez-García, L., Blasco, L., Cribb, P., and Müller, G. L. (2019a). Quorum and light signals modulate acetoin/butanediol catabolism in *Acinetobacter* spp. *Front. Microbiol.* 10:1376. doi: 10.3389/fmicb.2019.01376

Tuttobene, M. R., Laura, F.-G., Blasco, L., Cribb, P., Ambroa, A., Müller, G. L., et al. (2019b). Quorum and light signals modulate acetoin/butanediol catabolism in *Acinetobacter* spp. *Front. Microbio.* 10:1376. doi: 10.3389/fmicb.2019.01376

Valle, L., Abatedaga, I., Morán Vieyra, F. E., Bortolotti, A., Cortez, N., and Borsarelli, C. D. (2015). Enhancement of photophysical and photosensitizing properties of flavin adenine dinucleotide by mutagenesis of the C-terminal extension of a bacterial flavodoxin reductase. *Chem. Phys. Chem.* 16, 872–883. doi: 10.1002/cphc.201402774

van der Horst, K. M., and Hellingwerf, K. (2007). Photosensing in chemotrophic, non-phototrophic bacteria: let there be light sensing too. *Trends Microbiol.* 15, 554–562. doi: 10.1016/j.tim.2007.09.009

Villegas, J. M., Valle, L., Moran Vieyra, F. E., Rintoul, M. R., Borsarelli, C. D., and Rapisarda, V. A. (2014). FAD binding properties of a cytosolic version of *Escherichia coli* NADH deshydrogenase-2. *Biochim. Biophys. Acta* 1844, 576–584. doi: 10.1016/j.bbapap.2013.12.021

Wood, C. R., Ohneck, E. J., Edelmann, R. E., and Actis, L. A. (2018). A Light-regulated type I pilus contributes to *Acinetobacter baumannii* biofilm, motility, and virulence functions. *Infect. Immun.* 86:e00442–18. doi: 10.1128/IAI.00442-18

Conflict of Interest Statement: The authors declare that the research was conducted in the absence of any commercial or financial relationships that could be construed as a potential conflict of interest.

frontiers in Microbiology

ORIGINAL RESEARCH
published: 01 November 2019
doi: 10.3389/fmicb.2019.02519

Bioinformatic Analysis of the Type VI Secretion System and Its Potential Toxins in the *Acinetobacter* Genus

Guillermo D. Repizo[1], Martín Espariz[1], Joana L. Seravalle[1] and Suzana P. Salcedo[2]*

[1] Departamento de Microbiologia, Facultad de Ciencias Bioquimicas y Farmaceuticas, Instituto de Biologia Molecular y Celular de Rosario (IBR, CONICET), Universidad Nacional de Rosario, Rosario, Argentina, [2] Laboratory of Molecular Microbiology and Structural Biochemistry, CNRS UMR 5086, University of Lyon, Lyon, France

Several *Acinetobacter* strains are important nosocomial pathogens, with *Acinetobacter baumannii* as the species of greatest concern worldwide due to its multi-drug resistance and recent appearance of hyper-virulent strains in the clinical setting. *Acinetobacter* colonization of the environment and the host is associated with a multitude of factors which remain poorly characterized. Among them, the secretion systems (SS) encoded by *Acinetobacter* species confer adaptive advantages depending on the niche occupied. Different SS have been characterized in this group of microorganisms, including T6SS used by several *Acinetobacter* species to outcompete other bacteria and in some *A. baumannii* strains for *Galleria mellonella* colonization. Therefore, to better understand the distribution of the T6SS in this genus we carried out an in-depth comparative genomic analysis of the T6SS in 191 sequenced strains. To this end, we analyzed the gene content, sequence similarity, synteny and operon structure of each T6SS loci. The presence of a single conserved T6SS-main cluster (T6SS-1), with two different genetic organizations, was detected in the genomes of several ecologically diverse species. Furthermore, a second main cluster (T6SS-2) was detected in a subgroup of 3 species of environmental origin. Detailed analysis also showed an impressive genetic versatility in T6SS-associated islands, carrying VgrG, PAAR and putative toxin-encoding genes. This *in silico* study represents the first detailed intra-species comparative analysis of T6SS-associated genes in the *Acinetobacter* genus, that should contribute to the future experimental characterization of T6SS proteins and effectors.

Keywords: comparative genomics, toxins, PAAR proteins, VgrG, type 6 secretion system, *Acinetobacter*

OPEN ACCESS

Edited by:
Maria Alejandra Mussi, National Council for Scientific and Technical Research (CONICET), Argentina

Reviewed by:
Peng Luo, South China Sea Institute of Oceanology (CAS), China
German Matias Traglia, University of the Republic, Uruguay

****Correspondence:***
Guillermo D. Repizo
repizo@ibr-conicet.gov.ar

Specialty section:
This article was submitted to Infectious Diseases, a section of the journal Frontiers in Microbiology

Received: *28 February 2019*
Accepted: *18 October 2019*
Published: *01 November 2019*

Citation:
Repizo GD, Espariz M, Seravalle JL and Salcedo SP (2019) Bioinformatic Analysis of the Type VI Secretion System and Its Potential Toxins in the Acinetobacter Genus. Front. Microbiol. 10:2519. doi: 10.3389/fmicb.2019.02519

INTRODUCTION

The *Acinetobacter* genus comprises a heterogeneous group of strictly aerobic Gram-negative bacterial organisms endowed with great metabolic versatility. This genus includes numerous non-pathogenic environmental species as well as some with significant pathogenic potential, notably *Acinetobacter baumannii,* frequently associated with disease in the context of hospital-acquired infections (McConnell et al., 2013). Although infections due to multi-drug resistant (MDR) *Acinetobacter* species are a serious health threat worldwide, the knowledge about the mechanisms that enable them to colonize the host and hospital environments is still scarce (Antunes et al., 2014; Harding et al., 2018).

Bacteria use several secretory mechanisms to export effector proteins into the environment or straight into target cells (Costa et al., 2015; Galán and Waksman, 2018). Among them, the multicomponent type VI secretion system (T6SS), which is structurally related to the cell-puncturing device of the T4 bacteriophage, was described in Gram-negative bacteria, including *Acinetobacter* (Weber et al., 2017; Elhosseiny and Attia, 2018). The T6SS dynamic machinery permits the injection of toxic effector proteins into prey cells in a contact-dependent manner. The concomitant expression of cognate immunity proteins prevents self-intoxication (Benz and Meinhart, 2014; Alcoforado et al., 2015). T6SS effectors with diverse enzymatic activities have been identified, including the membrane-, cell wall-, or nucleic acid-targeting antibacterial effectors and the heterogenous group of eukaryote-targeting effectors (Lien and Lai, 2017).

The T6SS apparatus is assembled from a set of core components proteins (Boyer et al., 2009), which comprise the minimal machinery necessary for its functionality. The genes coding for the core components (*tss*) are frequently organized within one genetic cluster. Most T6SS gene clusters contain additional genes (T6SS-associated genes; *tag*), the function of most remains unknown. Previous studies using a limited number of *Acinetobacter* species predicted the presence of a conserved T6SS gene cluster with two different genetic organizations (Weber et al., 2013). This locus, hereafter referred as T6SS main cluster (T6MC; **Figure 1A** and **Table 1**), is described to encompass 18 genes (Carruthers et al., 2013; Weber et al., 2013). Fourteen genes showed a significant homology at the protein level with T6SS components present in other bacteria, and were thus initially named following the nomenclature proposed by Shalom et al. (2007), namely *tss* and *tag* genes. The only gene that does not follow this nomenclature is that encoding a PAAR-domain protein, which has been accordingly dubbed just as PAAR gene (Weber et al., 2016). It was recently shown in *A. baylyi* ADP1 that one of the four genes with non-attributable function (ACIAD2699) coded for a peptidoglycan hydrolase (TagX), facilitating the passage of the T6SS apparatus through the cell wall (Weber et al., 2016). Despite the high levels of homology observed between most T6MCs, the genes encoding the VgrG and PAAR-repeat domain proteins (usually more than 1 of each per genome) are scattered throughout the genomes and conservation between *Acinetobacter* strains is low (Eijkelkamp et al., 2014). The regions flanking these genes are known as VgrG and PAAR islands (De Maayer et al., 2011) and represent evolutionary hot spots for genes that encode effector proteins. Genes encoding the cognate immunity proteins are usually present in these regions as well. These regions account for strain specificity regarding T6SS-related components (Unterweger et al., 2014).

A number of VgrG proteins have been characterized in *A. baumannii* (Weber et al., 2016; Fitzsimons et al., 2018). They all share a common domain structure (**Figure 2A**), with the typical N-terminal part constituted by domains commonly found in the bacteriophagic components gp44 and gp5, which altogether compose the VgrG domain (COG3501) defining the VgrG superfamily (cl27827). This domain is followed by a DUF2345 domain (pfam10106, superfamily cl27827) close to the C-terminus, responsible for the binding of the effector (Flaugnatti et al., 2016), and a C-terminal stretch of variable aminoacidic composition and length, which could even be totally absent. In *Vibrio cholerae*, the C-terminal portion of a number of these proteins, known as evolved VgrGs, displays an additional domain that functions itself as an effector (Pukatzki et al., 2007; Ma and Mekalanos, 2010).

Accessory proteins such as the PAAR-repeat domain protein are also part of most T6SS and have been shown to play a significant role in T6SS-mediated bacterial competition in *A. baylyi* (Shneider et al., 2013). The PAAR-repeat domain was found to dock onto the terminus of the pilus-like structure formed by VgrG and have been shown to interact with VgrGs and effector proteins, thus functioning as adaptors (Bondage et al., 2016).

The PAAR_like domain superfamily (cl21497; NCBI conserved domains database, CDD) includes proteins bearing PAAR motifs (pfam05488) or the DUF4150 domain (pfam13665). Tandemly repeated PAAR motifs constitute a PAAR domain (cd14671), which has been subclassified in 8 subgroups (cd14737–cd14744), according to the presence of additional N- and C-terminal domains with various predicted functions. Shneider et al. (2013) have classified PAAR-domain containing proteins in 7 classes according to their domain architecture. Following this scheme, Eijkelkamp et al. (2014) have previously detected the presence of PAAR proteins belonging to classes 1 (PAAR-1, N-terminal PAAR domain and no additional domains), 2 (PAAR-2, N-terminal PAAR domain and C-terminal extension of variable length) and 5 (PAAR-5, central PAAR domain) in a group of 8 *A. baumannii* strains (**Figure 2B**). As described for VgrG proteins, some PAAR proteins have evolved to contain virulence activity in their C-termini ("evolved PAAR"; Shneider et al., 2013).

T6SS involvement in eliminating competitors has been reported in a number of *Acinetobacter* species. *A. nosocomialis* M2 and *A. baylyi* ADP1 were found to utilize the T6SS for dueling against *Escherichia coli* (Carruthers et al., 2013; Shneider et al., 2013). In particular, *A. baylyi* ADP1 encodes 5 different effectors that provoke different degrees of *E. coli* cells lysis (Ringel et al., 2017), namely a putative metallopeptidase (Tpe1), a peptidoglycan-hydrolyzing amidase (Tae1), a phospholipase (Tle1), and two effectors (Tse1, and Tse2) representing new classes of effectors for which no enzymatic activity could be predicted or deduced from the lysis phenotype. Subsequent prey-DNA uptake has been detected, providing a competitive advantage to those strains expressing the T6SS (Ringel et al., 2017), and opening the possibility for the acquisition, among others, of antimicrobial resistance genes (Cooper et al., 2017). Moreover, *A. baumannii* strains DSM30011, ATCC17978 and AB307-0294 were able to outcompete other *A. baumannii* species as well as *E. coli* and *P. aeruginosa*, a bacterial pathogen relevant in mixed nosocomial infections (Weber et al., 2013; Repizo et al., 2015; Fitzsimons et al., 2018). Recently, toxins acting as peptidoglycan hydrolases (LysM), amidases (Tse4), nucleases (Rhs2 and Tse2), lipases (Tse1) and two with unknown function (Tse3 and Rhs1) have been characterized in *A. baumannii* (Weber et al., 2016; Fitzsimons et al., 2018),

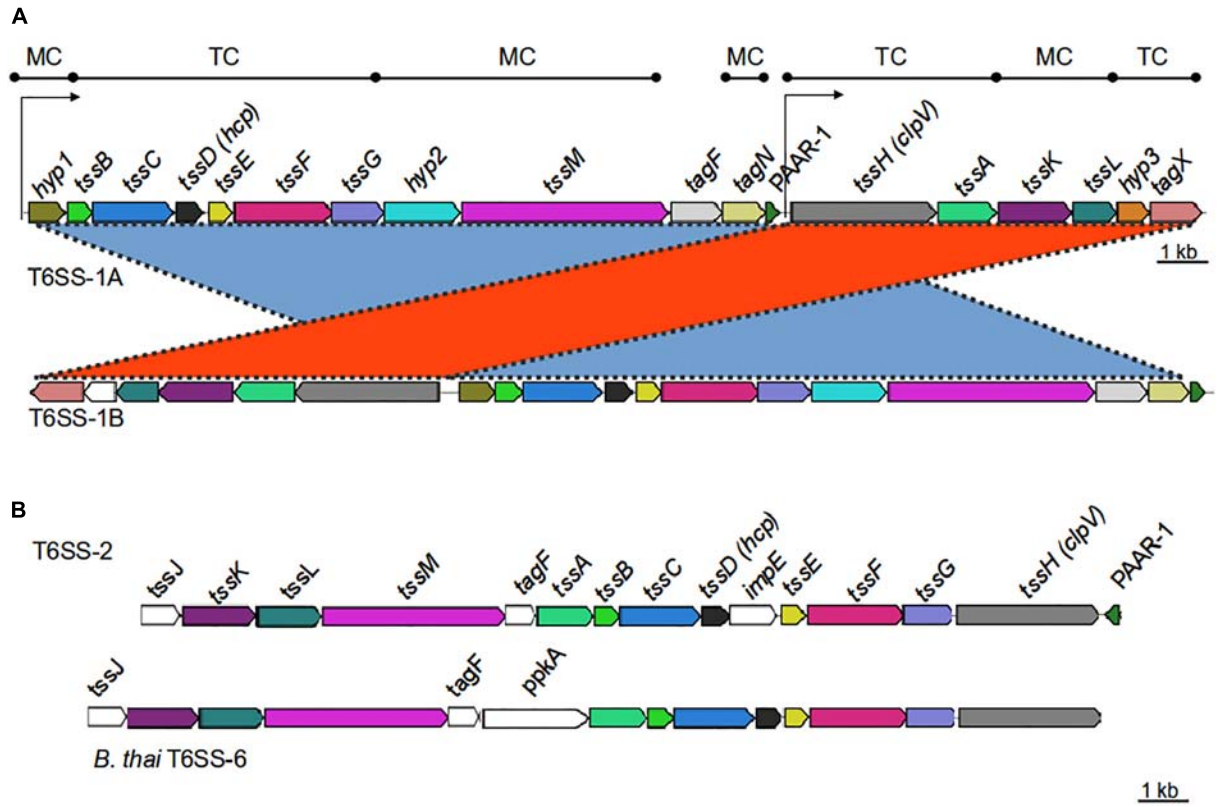

FIGURE 1 | Genetic organization of T6SS-main loci in the *Acinetobacter* genus. **(A)** T6SS-1-main gene cluster (for details refer to **Table 1**). Gene products are classified according to their participation in the membrane complex (MC) or tail complex (TC) of the T6SS apparatus. Thin arrows represent putative promoter regions. **(B)** T6SS-2-main gene cluster (for details refer to **Table 4**). *B. thailandiensis* T6SS-6 main cluster is shown for comparison. Genes encoding proteins with amino acidic identity > 25% and query coverage > 50% were represented with the same color.

TABLE 1 | T6SS-1-main locus genes in *Acinetobacter* spp.

		***A. baumannii* DSM30011 (T6SS-1A)**		***A. baylyi*. ADP1 (T6SS-1B)**		
Protein	**COG**	**Locus (DSM30011_)**	**Length (AA)**	**Locus[a] (ACIAD)**	**Length (AA)**	**% AA identity/similarity with Ab DSM30011**
Hyp1		11500	229	**2693**	218	52/70
TssB	3516	11495	167	**2691**	169	87/95
TssC	3517	11490	493	**2690**	498	94/96
TssD/Hcp	3157	11485	167	**2689**	167	97/98
TssE	3518	11480	158	**2688**	157	86/94
TssF	3519	11475	603	**2687**	602	73/86
TssG	3520	11470	332	**2686**	332	64/78
Hyp2		11465	470	**2685**	476	43/64
TssM	3523	11460	1274	**2684**	1273	84/92
TagF	3913	11455	319	2683	319	75/86
TagN	2885	11450	255	2682	254	75/86
PAAR	4104	11445	87	2681	88	70/81
TssH/ClpV	0542	11440	892	**2694**	894	80/87
TssA	3515	11435	364	**2695**	367	67/80
TssK	3522	11430	454	**2696**	455	81/91
TssL	3455	11425	268	**2697**	267	81/91
Hyp3		11420	200	2698	193	-
TagX		11415	317	**2699**	287	78/89

[a]*Essential components described by Weber et al. (2016) and Ringel et al. (2017) are shown in bold.*

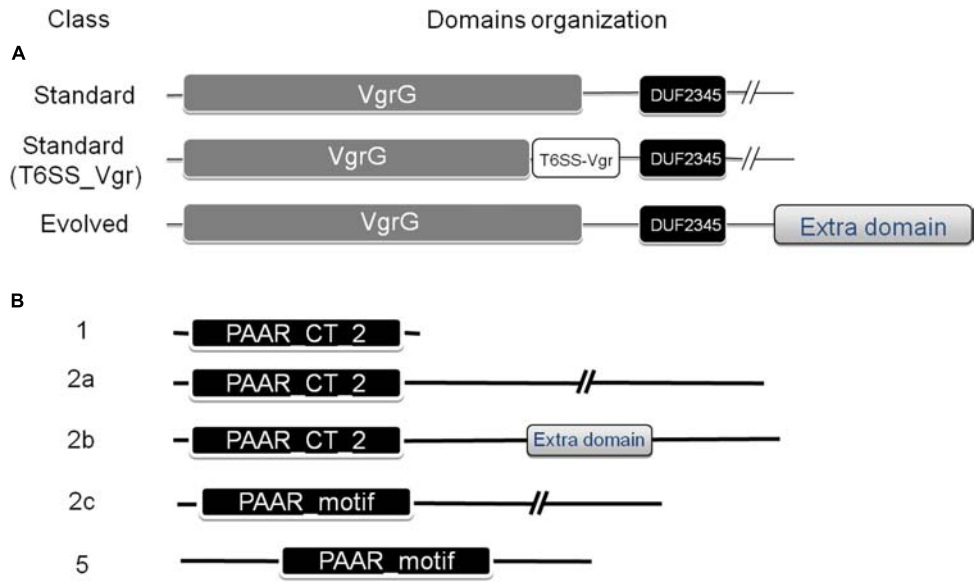

FIGURE 2 | Domain architecture of VgrG **(A)** and PAAR repeat proteins **(B)** found in the *Acinetobacter* genus. The NCBI-CDD (Marchler-Bauer et al., 2015) was used for the domain search. The classification defined by Shneider et al. (2013), which categorized PAAR proteins into seven classes based on domain architecture, was used. Additional subclasses were defined for PAAR-2 proteins (see text for details).

and many other effectors predicted using bioinformatics (Repizo et al., 2015; Fitzsimons et al., 2018), suggesting these microorganisms possess a significant arsenal of secreted toxins and immunity proteins.

In addition to an established role of the T6SS in bacterial competition, that could be advantageous in *Acinetobacter* colonization of specific environments such as the hospital setting, for some strains the T6SS seems to participate in host colonization, according to assays performed with the insect infection model *Galleria mellonella* (Gebhardt et al., 2015; Repizo et al., 2015). A recent report suggests that the presence of a functional T6SS contributes to infections in immune-compromised patients and those with implanted medical devices (Kim et al., 2017). In this work, the prevalence of the T6SS on 162 *A. baumannii* clinical isolates obtained from patients with bacteremia was also analyzed (Kim et al., 2017). The *hcp* gene was detected in 31.5% of the isolates and its presence showed a clear affiliation to particular STs. This observation is in agreement with genomic comparative analysis of phylogenetically- and epidemiologically-related *A. baumannii* MDR strains showing that the T6MC is only present in particular populations (Wright et al., 2014; Jones et al., 2015). Also, it suggests that this system is not critical in the conditions prevailing in the nosocomial environment. Indeed, the T6SS in *A. baumannii* is clearly tightly regulated, often repressed to promote conjugation and dissemination of MDR-carrying plasmids within a bacterial population (Di Venanzio et al., 2019).

In this study, we aimed at extending the present knowledge on T6SS core and accessory genes and toxins in the *Acinetobacter* genus. Therefore, we carried out an in-depth *in silico* comparative analysis of these clusters in different *Acinetobacter* species to better understand the composition and distribution of T6SS loci in this genus.

MATERIALS AND METHODS

In silico Identification of the T6SS Loci

We conducted a comparative genomic analysis including *Acinetobacter* strains available the NCBI-GenBank database. Those strains with a complete genome sequence were included in this analysis. In order to have a full representation of the genus, for those *Acinetobacter* species with no complete genome we decided to work with draft genomes (**Supplementary Table S1**). We then extracted genomic and proteomic data corresponding to 191 strains and a local database was constructed. Of note, 110 genomes corresponded to *A. baumannii* strains and 81 to non-*baumannii* species, totalizing 42 accepted species and 9 strains so far not assigned to any known species. The proteins encoded within the T6MC from *A. baumannii* DSM30011 (**Table 1**) which carries a functional T6SS (Repizo et al., 2015) were used as query to perform BlastP-sequence similarity searches (Altschul et al., 1990) against the local database. With these data the corresponding T6SS loci were identified. Furthermore, each of the clusters was manually inspected to corroborate its genetic integrity, and those strains showing incomplete/non-functional clusters were accordingly informed (**Supplementary Table S1**). Visual representation of the alignments using nucleotide similarities (tblastx) of the T6SS loci were carried out with MultiGeneBlast (default parameters; Medema et al., 2013). Calculations of GC content[1] and Codon adaptation index (CAI;

[1]http://www.endmemo.com/bio/gc.php

coRdon) were performed in order to infer if studied regions were acquired by horizontal gene transfer. The CAI of each T6SS gene was normalized using the average CAI of all genes encoded in the corresponding genome. These values were compared with the CAIs obtained for those genes encoding ribosomal proteins in each case, generally accepted as highly adapted to the set of codons available in a particular genome. Statistical analysis (unpaired *t*-test) indicated for each of these genomes a significant difference between both data sets ($p < 0.0001$).

VgrG, PAAR, and Toxin-Proteins Search

A. baumannii DSM30011 encodes 4 VgrG proteins of variable length. However, they all share the basic domain architecture, with a conserved N-terminal VgrG domain. Therefore, the VgrG domain of the protein encoded by DSM30011_13325 (amino acids 23–631) was used as query for a bioinformatic search of homologous proteins in *Acinetobacter* strains contained in our local database. Regarding PAAR-proteins, a homology search was performed using as queries the PAAR-1 and PAAR-2 encoded by *A. baumannii* DSM30011 (DSM30011_11445 and DSM30011_14800), and the PAAR-5 encoded by *A. baylyi* ADP1 (ACIAD0051). Besides, representative proteins found at the NCBI-CDD were used as query in a BlastP-homology search for DUF4150-domain containing proteins. Finally, proteins acting as putative toxins in the *vgrG* and PAAR gene islands were searched with BlastP ($e < 0.0001$), using as query T6SS-reported toxins identified in *Acinetobacter* spp. (Weber et al., 2016; Ringel et al., 2017; Fitzsimons et al., 2018) and in other bacteria (Lien and Lai, 2017; Ma et al., 2018), both targeting prokaryotic and eukaryotic cells.

Annotation of Proteins With Unknown Function

A number of bioinformatic analyses were conducted in order to infer the role of T6SS-main components and proteins encoded in the *hcp* and *vgrG* islands with unknown function. A search for conserved domains was done by means of the Batch Web-CD search tool (Marchler-Bauer et al., 2015). SignalP 4.0 (Petersen et al., 2011) and TMHMM Server v.2.0[2] were used to predict signal peptides and trans-membrane helices, respectively.

Analysis of Genetic Context of PAAR and *vgrG* Islands

In order to analyze the genetic context of the PAAR (not located within T6MCs) and *vgrG* genes, the accession numbers of the 5 downstream and upstream genes were parsed using an R script designed *ad hoc* and the feature table files of the strains under analysis. Then, a search for conserved domains carried by proteins encoded in the PAAR and *vgrG* islands was done using the Batch Web-CD search tool (Marchler-Bauer et al., 2015), and each of them was assigned to a superfamily. Then, the presence or absence of a particular domain superfamily was used as a binary score (present = 1, absent = 0) to perform a hierarchical clustering of PAAR or *vgrG* islands using "pvcluster" R package (Suzuki and Shimodaira, 2006), with binary distance and average agglomerative clustering. Only genetic islands encoding proteins with conserved superfamily domains found at least 3 times in our database were considered. Clustering reliability was assessed by bootstrapping with 1,000 repetitions. The resulting dendrogram was displayed using iTOL (Letunic and Bork, 2011). Those gene islands sharing a similar genetic context were grouped in PAAR or VgrG gene neighborhoods (PGNs and VGNs, respectively).

[2]http://www.cbs.dtu.dk/services/TMHMM/

RESULTS AND DISCUSSION

T6SS Activity in *Acinetobacter* Strains

T6SS activity has been previously explored in a limited number of *Acinetobacter* spp. (see Introduction). In order to further investigate its function in a larger set of strains, a total number of 20 strains (**Table 2**) that were available in our laboratory collection were grown and tested. The ability of each *Acinetobacter* strain to eliminate *E. coli* was used as a proxy for an operative T6SS, as previously reported (Carruthers et al., 2013; Shneider et al., 2013; Weber et al., 2013; Repizo et al., 2015; Fitzsimons et al., 2018). Obtained results indicated that 11 out of 20 strains were able to outcompete *E. coli* (**Table 2**), of which *A. guillouiae* and *A. oleivorans* have never been reported as T6SS-positive strains. T6SS involvement in the observed killing was corroborated by Hcp-secretion assays (**Supplementary Figure S1**). In view of the observed variability in the killing capacity of different *Acinetobacter* spp. we decided to conduct a bioinformatic search that could shed light on the observed differences.

Identification and Prevalence of Orthologous T6SS Loci in the *Acinetobacter* Genus

Bioinformatic analysis exerted on a local database including 191 *Acinetobacter* genomes (**Supplementary Table S1**) revealed the presence of genes encoding a T6SS in most *Acinetobacter* species (33 out of 42; **Table 3**). In some cases, such as *A. lwoffi* and *A. haemoly*ticus, we were not able to detect a T6SS loci for those strains included in our local database. However, when performing a broader search against the complete NCBI-Protein database, some strains encoded a T6MC. Therefore, we decided to include these species in **Table 3** as well.

It is worth noting the particular case of *A. towneri* DSM 14962 = CIP 107472, the only strain of this species which genome is available at the non-redundant protein database (NCBI). It encodes a complete T6SS-main cluster, but the *tssH* gene is interrupted by an insertion sequence (IS). No orphan copy of the *tssH* gene was detected, and thus *A. towneri* was thereby considered as a T6SS-deficient strain. Sequencing of other strains is needed to determine if this is the rule for this species. A number of *Acinetobacter* species (8 out of 42), namely *A. brisouii, A. defluvii, A. marinus, A. nectaris, A. parvus, A. puyangensis, A. qingfengensis,* and *A. ursingii* do not encode a T6MC (**Supplementary Table S1**). Lack of T6SS main genes was

TABLE 2 | *Acinetobacter* strains tested for T6SS activity.

Strain	Killing (fold change)[a]	Hcp secretion[b]
Acinetobacter baumannii DSM 30011	Complete	+
Acinetobacter bereziniae HPC 229	Partial (1.7)	NA
Acinetobacter bereziniae LMG 1003	None	NA
Acinetobacter brisouii ANC 4119	None	NA
Acinetobacter calcoaceticus NIPH 2245	None	NA
Acinetobacter guillouiae LMG 988	Partial (3.3)	+
Acinetobacter gyllenbergii LUH 4712	Partial (1.9)	NA
Acinetobacter indicus ANC 4215	Complete	–
Acinetobacter johnsonii DSM 6963	Partial (1.6)	NA
Acinetobacter junii SH 205	None	NA
Acinetobacter lwoffii DSM 2403	None	NA
Acinetobacter lwoffii LMG 985	Partial (7.4)	–
Acinetobacter nosocomialis M2	Complete	+
Acinetobacter nosocomialis NIPH 2119	Complete	–
Acinetobacter oleivorans DR1	Complete	+
Acinetobacter pittii LMG 1035	None	NA
Acinetobacter schindleri NIPH 1034	None	NA
Acinetobacter ursingii NIPH 137	None	NA
Acinetobacter venetianus LMG19082	Partial (1.6)	NA
Acinetobacter sp. Ver3	None	NA

[a]Killing was calculated by dividing the recovered CFU/ml of E. coli used as prey with respect to a control culture not mixed with any other Acinetobacter strain (see Repizo et al., 2015 for experimental details). [b]Only strains showing killing-fold changes > 2 were analyzed. NA: not assayed.

TABLE 3 | Classification of T6SS main clusters present in the *Acinetobacter* genus[a].

T6SS	Subclass	Type	Species[b]
1	A		*A. baumannii, A. calcoaceticus, A. lactucae, A. nosocomialis, A. oleivorans, A. pitti, A. seifertii*
	B	a	*A. baylyi, A. beijerinckii, A. bereziniae, A. colistinresistens, A. equi, A. guillouiae, A. gyllenbergii, A. haemolyticus, A. junii, A. larvae, A. lwoffii, A. proteolyticus, A. radioresistens, A. soli, Acinetobacter* sp. TGL-Y2
		b	*A. apis, A. bohemicus, A. bouvetii, A. celticus, A. gerneri, A. indicus, A. johnsonii, A. pragensis, A. schindleri, A. tandoii, Acinetobacter* sp. LOGeW2-3, ACNIH1
2			*A. gerneri, A. populi, A. rudis*
Negative			*A. brisouii, A. defluvii, A. marinus, A. nectaris, A. parvus, A. puyangensis, A. qingfengensis, A. ursingii, A. twoneri, Acinetobacter* sp. ACNIH2, DUT-2, Ncu2D-2, SWBY1, TTH0-4, and WCHA45

*[a]A given species was included in this classification when at least one of its strains contained a complete T6SS loci. [b]Strains correspond to those present in **Supplementary Table S1**, with the exception of particular cases hereafter indicated. A. haemolyticus strains HW-2A (NZ_CP030880.1) and KCRI-348C (NZ_OVCN01000011.1); A. lwoffi NCTC 5866 = CIP 64.10 = NIPH 512 (APQS01000022.1), NIPH 478 (APQU01000010.1).*

also observed for 6 out of 9 *Acinetobacter* spp. (ACNIH2, DUT-2, Ncu2D-2, SWBY1, TTH0-4, and WCHA45).

Regarding the prevalence of the T6MCs in *A. baumannii*, 27 out of 110 strains showed a complete deletion of the T6SS-main cluster, while 15 contained gene frameshifts, partial deletions or insertions resulting in an abnormal T6MC (**Supplementary Table S1**), very likely conducting to a non-functional apparatus. T6SS genes loss has been already documented in MDR *A. baumannii* clinical strains (Wright et al., 2014; Jones et al., 2015; Kim et al., 2017), suggesting that this system is not critical for survival in the nosocomial environment. Possible hypotheses favoring this genetic loss are higher chances of evasion from the host immune system and/or the lower requirement for interbacterial competition over the course of antibiotic therapy (Repizo, 2017). Furthermore, silencing of the T6SS was recently shown to be critical for horizontal gene transfer through conjugation, which is crucial for antimicrobial resistance spread (Di Venanzio et al., 2019).

Classification of the T6SS-Main Clusters in *Acinetobacter* Species

Bioinformatic analyses revealed the presence of two types of T6MC in *Acinetobacter* species, here designated as T6SS-1 and T6SS-2 (**Figure 1** and **Supplementary Figure S2**, and **Tables 1**, **4**). Different bacterial species encoding more than one T6MC have been previously reported (Boyer et al., 2009). These two loci differ in genetic composition but both encode the essential components of the T6SS apparatus. The TSS6-1 is the more ubiquitous T6MC in the *Acinetobacter* genus (30 out of 32 T6SS-proficient species; **Table 3**) and its gene composition is coincident with that reported for *A. baumannii* by Boyer et al. (2009). We established that the main characteristics that define the *Acinetobacter* T6SS-1 are: (1) No *hcp* genes are encoded outside the core cluster; (2) None of its genes code for evolved-Hcp proteins, as previously reported in other bacterial species (Blondel et al., 2009; Ma et al., 2017a); (3) no *vgrG* genes are encoded within the main cluster, in contrast to many other bacteria (Boyer et al., 2009).

A search for T6SS-1-core proteins in non-*Acinetobacter* species, using as query *A. baumannii* DSM30011 conserved components (TssB, TssC, TssK, TssL) indicated the presence of homologous proteins (identity > 45%) in members of several genera, namely *Alkanindiges, Psychrobacter, Achromobacter, Chitinimonas,* and *Cupriavidus,* and as previously noticed with those which are frequently associated to plants such as *Ralstonia, Burkholderia,* and *Xanthomonas* (Boyer et al., 2009; Spiewak et al., 2019). However, it is important to notice that the genetic architecture of T6SS-core clusters in these species is diverse. It has already been demonstrated that the T6SS mediates bacterial interactions with host plants, through the secretion of

TABLE 4 | T6SS-2-main locus genes in *Acinetobacter* spp.

			A. garneri DSM14967			
Protein[a]	**COG**	**Locus**	**Length (AA)**	**% AA Id/Sim with *A. rudis* CIP 110305**	**% AA Id/Sim with *A. populi* PBJ7**	**% AA Id/Sim with *B. thailandensis* E264[b,c]**
TssJ	3521	F960_01894	218	60/82	50//73	34/56 (41)
TssK	3522	F960_01893	446	70/85	60/81	36/54 (99)
TssL	3455	F960_01892	415	77/87	71/81	37/59 (90)
TssM	3523	F960_01891	1176	69/83	61/78	25/45 (99)
TagF	3913	F960_01890	182	58/78	38/63	24/35 (48)
TssA	3515	F960_01889	349	62/80	59/76	34/52 (96)
TssB	3516	F960_01888	170	85/93	81/94	65/83 (90)
TssC	3517	F960_01887	494	93/98	89/96	72/87 (96)
TssD/Hcp	3157	F960_01886	161	95/98	88/97	48/66 (97)
ImpE	4455	F960_01885	255	49/65	38/62	–
TssE	3518	F960_01884	159	74/86	67/82	33/57 (91)
TssF	3519	F960_01883	623	70/86	58/76	24/43 (99)
TssG	3520	F960_01882	328	70/85	60/79	– (Pseudogene)
TssH/ClpV	0542	F960_01881	879	80/89	72/85	53/71 (99)
PAAR	4104	F960_01880	88	82/92	52/74	–
VgrG	3501	F960_01907	894	29/47		37/55 (61)

[a]Core components described by Boyer et al. (2009) are shown in bold. [b]Sequence homology with proteins encoded in the T6SS-6. [c]Query coverage is indicated in parenthesis.

effectors which act in symbiosis, biofilm formation, virulence, and interbacterial competition (Ryu, 2015). Given the fact that several *Acinetobacter* species have been isolated from plants, including the enviromental isolate *A. baumannii* DSM30011 (Repizo et al., 2017), it is not surprising that they might have originally acquired T6SS-core genes from other plant associated bacteria and subsequently modeled these clusters to the actual genetic organization.

The T6SS loci encoded by most bacteria are organized in operons, suggesting a coregulated expression (Bernard et al., 2010). Therefore, we investigated the presence of putative transcriptional units in the *A. baumannii* T6SS-1 main cluster. According to bioinformatic predictions available at ProOpDb (Taboada et al., 2012), two transcriptional blocks might be present in these loci, the first encompassing *hyp1*-PAAR genes and the second including *tssH-tagX* genes (**Figure 1A**). The separation of this locus into two transcriptional units might explain the existence of two different genetic arrangements among T6SS-1 gene clusters (**Figure 1A**):

(i) T6SS-1A: In this case, all the T6MC genes are encoded in the same DNA strand. This genetic architecture is conserved in *Acinetobacter* species belonging or phylogenetically related to the *calcoaceticus-baumannii* complex (**Table 3**).

(ii) T6SS-1B: In this T6MC the *tssH-tagZ* gene block is divergently located to the *hyp1*-PAAR gene block (**Figure 1A**). This is the more ubiquitous organization (23 out of 32 species; **Table 3**) and for clarity, we further classified it in two types depending on the presence (T6SS-1Ba) or not (T6SS-1Bb) of the gene encoding a PAAR domain containing-protein within the locus. In line with this observation, the PAAR domain-protein encoded in the main cluster is not essential for T6SS functioning in *A. baylyi* (Weber et al., 2016). This is not surprising since more than one gene is usually present per *Acinetobacter* genome (see below).

We observed a strain clustering that was in line with the proposed sub-classification (**Supplementary Figure S2** heat map), with some exceptions mostly corresponding to ACB complex species carrying T6SS-1A loci that did not group with the larger block of T6SS-1A ACB strains. This might be an indication of gene acquisition by horizontal gene transfer. Furthermore, ST affiliation of each *A. baumannii* strain was included in this same figure, showing a sub-clustering, which correlated with the ST classification (Pasteur Scheme).

The role played by three of the genes present in the *Acinetobacter* T6SS-1 encoding cluster is still unknown (ACIAD2693, ACIAD2685, and ACIAD2698), although deletion of any of the former two, coding for hypothetical proteins 1 (Hyp1) and 2 (Hyp2), affects the functionality of the system (Weber et al., 2016; Ringel et al., 2017). We therefore decided to investigate if we could infer putative functions based on bioinformatic predictions carried out with the DSM30011 homologous proteins. We observed that Hyp1 (DMS30011_11500) bears no putative transmembrane segments and was predicted to carry a signal peptide which might direct it to the periplasm (**Supplementary Figure S3A**). Interestingly, we were able to identify in DSM30011 Hyp1 several features of its signal peptide sequence, which are characteristic of lipoproteins. It possesses a C23 residue which is part of a lipobox motif (PROSITE pattern PS51257), a positively charged K5 residue and a stretch of hydrophobic and uncharged amino acids residues

between position 7 and 22 (Zückert, 2014). These structural characteristics resemble those of TssJ, which has been proposed to anchor the membrane complex (MC) to the inner membrane (IM) through its interaction with TssM (Felisberto-Rodrigues et al., 2011). Moreover, TssJ bears a lipobox motif which is critical for the association of the mature protein with the outer membrane through acylation of the N-terminal cysteine residue (Aschtgen et al., 2008). However, no protein showing homology with TssJ could be identified (Weber et al., 2013). Therefore, we propose that Hyp1 encoded within the *A. baumannii* T6MC could fulfill a role similar to that played by TssJ.

In enteroaggregative *E. coli* and in several other bacteria, TagL associates with the TssJLM membrane complex (Aschtgen et al., 2010). TagL is embedded in the IM through 3 transmembrane regions. It also bears a central cytoplasmic loop and a C-terminal periplasmic domain with a functional peptidoglycan-binding motif (Aschtgen et al., 2010), which tethers the T6SS to the cell wall. The peptidoglycan binding motif may also be encoded in a separate subunit, TagN. We and others (Ringel et al., 2017) observed that this is the case in *Acinetobacter* species. *A. baumannii* DSM300011 TagN bears an OmpA_C-like peptidoglycan binding-domain (152–254; cd07185; **Supplementary Figure S4A**) and a putative exportation signal (cleavage site between positions 27 and 28: ALA-QP). The obvious question is which *Acinetobacter* protein fulfills the role played by the N-terminal portion of *E. coli* TagL. Topology predictions performed on Hyp2 (DSM30011_11465) indicates that this could be a good candidate to play this role, since it contains two putative transmembrane domains in the N-terminal followed by a long periplasmic region (**Supplementary Figure S3B**). Recent predictions consistent with this hypothesis have been made when analyzing the topology of a homologous protein (TagZ) encoded by *Burkholderia*, *Paraburkholderia* and related species (Spiewak et al., 2019), which share a T6SS-1 main cluster with a similar gene composition but with a different arrangement with respect to *Acinetobacter* spp.

Hyp3 (DSM30011_11420) contains a C-terminal domain (PRK03427) found in the *E. coli* cell division protein ZipA, which is tied to the membrane through a short N-terminal membrane-anchored domain. Correspondingly, Hyp3 bears a putative transmembrane domain in its N-terminal region (residues 21–43; **Supplementary Figure S3C**) with the rest of the protein protruding toward the periplasm. Despite the fact that this protein shows low conservation in the *Acinetobacter* genus, its predicted topology is conserved. Weber et al. (2016) have suggested that TagX interaction with other components of the T6SS apparatus may control its enzymatic activity, allowing for precise spatial regulation of PG degradation. It is therefore possible that Hyp3 fulfils this role but experimental work needs to be carried out to test this hypothesis.

VgrG Protein Diversity in *Acinetobacter* spp.

Varying numbers of genes located outside the *Acinetobacter* T6MC encode putative VgrG proteins (Weber et al., 2013). These T6SS-associated regions additionally encode a variable number of accessory and hypothetical proteins that act as effectors and immunity proteins (see Toxins section). VgrG proteins encoded in *Acinetobacter* genomes under study were investigated (see section Materials and Methods). As result, 534 homologous proteins were detected (average *vgrG* genes per genome = 2.79; **Supplementary Table S2**) throughout the *Acinetobacter* genus. In correlation with the lack of T6SS structural components, 7 out of 8 T6SS- *Acinetobacter* species (with *A. ursingii* as the exception; **Table 3**) do not encode *vgrG* genes. Lack of *vgrG* genes was also observed for the aforementioned T6SS-deficient *Acinetobacter* sp. Ncu2D-2, TTH0-4 and WCHA45 (**Supplementary Table S1**). Interestingly, species such as *A. celticus*, *A. equi*, *A. pragensis,* and *A. radioresistens* encode only 1 *vgrG* gene, whereas *A. bereziniae* carries 13 (**Supplementary Table S2**). *A. baumannii* T6SS-proficient strains usually contain between 2 and 4 copies. Interestingly, some *Acinetobacter* strains, show a split *vgrG* locus encoding separate N-terminal and C-terminal VgrG domains. This split among VgrG domains resembled the case of the bacteriophage spike proteins, and supported the proposed common evolutionary origin of these two membrane-penetrating devices (Pukatzki et al., 2007; Zoued et al., 2014). In addition, 3 of the identified VgrG sequences in our database contain putative effector domains in their C-termini (**Supplementary Tables S2, S3**). These evolved-VgrGs, which were identified in *A. bereziniae* and *A. proteolyticus*, encode both LysM and Het-C domains (**Table 5**). While the former (cd00118) is responsible for protein binding to peptidoglycan (Buist et al., 2008), the latter (pfam07217, cl20332 superfamily) is found in proteins regulating self/non-self-recognition in filamentous fungi (Wu et al., 1998). Antifungal effectors dependent on the T6SS have been recently described in *Serratia marcescens* (Trunk et al., 2018), therefore it is possible that those *Acinetobacter* VgrG proteins bearing a Het-C domain fulfill a similar function. In sum, these predictions suggest that some of these VgrGs may have additional functions, adding further levels of complexity to the *Acinetobacter* T6SS toxins repertoire.

The Newly Identified T6SS-2 Is Present in Three Environmental *Acinetobacter* Species

As previously mentioned, a T6MC with a different gene composition (T6SS-2) was also detected. We identified the T6SS-2 locus in *A. gerneri* DSM 14967 (also encoding a T6SS-1Bb cluster), isolated from activated sludge (Carr et al., 2003); in *A. rudis* CIP 110305 isolated from raw milk, and in *A. populi* PBJ7, isolated from a bark canker of *Populus euramericana* (**Table 4** and **Supplementary Table S1**). It is composed of 15 genes, including the 13 T6SS-core genes described by Boyer et al. (2009); **Figure 1B** and **Table 4**). It shares 13 orthologous genes with the T6SS-1 main cluster, with *tssJ* and *impE* as genes specific of the T6SS-2 cluster. Key components (TssB, TssC, TssK, TssL) are highly conserved (aminoacidic identity > 60%) among the three aforementioned *Acinetobacter* species (**Table 4**). Remarkably, the PAAR gene is encoded in the complementary strand in *A. gerneri* and *A. rudis*, whereas in *A. populi* it is located in the same strand

TABLE 5 | VgrG-evolved proteins in *A. bereziniae*.

VgrG-evolved proteins in *Acinetobacter* species						
Organism	**Protein accession no.**	**Length (AA)**	**Start**	**End**	**Extra domain[a]**	
					Domain	**Domain accession no.**
A. bereziniae	ATZ63530.1	1738	995	1037	LysM	cd00118
A. bereziniae	ATZ63530.1	1738	1320	1688	Het-C superfamily	c120332
A. bereziniae	ATZ63848.1	1737	991	1034	LysM	cd00118
A. bereziniae	ATZ63848.1	1737	1313	1678	Het-C superfamily	c120332

[a] *Obtained from the NCBI-CDD (Marchler-Bauer et al., 2015).*

as the rest of the cluster. This observation is in line with the documented variability of PAAR genes location in the *Acinetobacter* T6SS-1 core clusters.

T6SS-2 organization resembles that of the gene cluster encoding the T6SS-6 described in *Burkholderia* species (**Figure 1B** and **Table 4**; Schwarz et al., 2014) with genes encoding VgrG proteins, putative toxins and cognate immunity proteins all located in the proximity of the main cluster in these three *Acinetobacter* strains. Still, important differences in genetic composition of the main cluster are observed between them such as the presence of the *impE* gene in the *Acinetobacter* T6SS-2, which is part of the T6MC in *Rhizobium leguminosarum* (Bladergroen et al., 2003), and the absence of the *ppkA* gene, encoding a kinase involved in post-translational regulation of the system in *P. aeruginosa* (Basler et al., 2013). Interestingly, the *A. gerneri* T6SS-2 specific components (meaning those for which no homologous proteins are encoded in the T6SS-1 cluster also encoded in its genome), namely TssJ, TssL and ImpE, show the highest identity percentages (between 35 and 50%) with proteins present in members of the *Moraxella* and *Neisseria* genera, which carry an unreported T6SS cluster with a different genetic structure. Analysis of G + C% of the T6SS-2 region in each of the three above mentioned *Acinetobacter* strains shows a significant deviation from the genomic average (35.8% vs. 37.9% for *A. gerneri* DSM14967; 33.3% vs. 39.2% for *A. rudis* CIP110305; and 32.6% vs. 40.2% for *A. populi* PBJ7). Moreover, average codon adaptation index calculations for each of these T6SS-2 clusters indicate a significant deviation ($p < 0.0001$) from the results obtained with the corresponding ribosomal proteins of each organism. Overall, these predictions imply a recent acquisition of this cluster by horizontal gene transfer from an unknown bacterial donor, thereby suggesting that the T6SS-1 and T6SS-2 clusters are evolutionarily distinct.

Remarkably, *Acinetobacter* species carrying the T6SS-2-core cluster encode several VgrG proteins with an additional domain (T6SS_Vgr; **Supplementary Table S3**) not frequently detected in VgrG present in other members of this genus (**Figure 2A**). The T6SS_Vgr domain (pfam13296) overlaps with the C-terminal part of the VgrG domain and is usually located before the start of the DUF2345 domain. Of note, *A. populi,* which is the only *Acinetobacter* species under study carrying uniquely a T6SS-2 main cluster, solely encodes VgrG proteins (total number = 3) with this domain architecture in its genome (**Supplementary Table S2**). On the other hand, *A. gerneri* (T6SS-1 and -2 clusters; total number = 9) and *A. rudis* (incomplete T6SS-1 and complete T6SS-2 clusters; total number = 8) inspected strains encode VgrG proteins falling into both domains architectures (**Figure 2A** and **Supplementary Tables S2, S3**). Furthermore, we detected that these types of VgrGs are encoded by genes which are usually in close proximity to the T6SS-2 main cluster. It is tempting to speculate that VgrGs bearing the T6SS_Vgr domain are somehow related to the apparatus encoded by T6SS-2-main cluster. An additional evidence supporting this hypothesis is that the most similar VgrG proteins outside the *Acinetobacter* genus are encoded by members of the *Moraxella* genus (40% average identity), in agreement with what has been observed for proteins encoded in the T6SS-2 main cluster (see above). This suggests that the complete system (T6MC plus VgrG proteins) has been acquired from species of the *Moraxella* genus.

Overall, these observations suggest that the *Acinetobacter* T6SS-2 cluster has a unique genetic organization and composition so far not described in other bacteria. Future work needs to be directed toward understanding the role that this T6SS plays in the biology of these *Acinetobacter* spp.

Three Major Classes of PAAR Domain Containing-Proteins Are Found in *Acinetobacter* spp.

A bioinformatic search for PAAR proteins in members of the *Acinetobacter* genus was conducted (see section Materials and Methods). As result, 377 homologous proteins were detected (average PAAR genes per genome = 1.97; **Supplementary Table S4**) throughout the *Acinetobacter* genus. An interesting case is that of *A. baumannii* SDF which carries 10 PAAR genes (Eijkelkamp et al., 2014), namely 1 PAAR-1, 7 PAAR-2, and 2 PAAR-5. Remarkably, one of the PAAR-2 proteins (CAP02972) is encoded in a plasmid (p2ABSDF, CU468232) as part of a locus carrying two *vgrG* genes and several putative toxins, such as a potential amidase (CAP02973). Plasmid-borne T6SS genes have been described in other bacteria such as *Pantoea ananatis* (Shyntum et al., 2014), but so far not in *Acinetobacter* species. On the other hand, 7 out of 8 T6SS$^-$ *Acinetobacter* species (with *A. ursingii* as the exception; **Table 3**) do not encode any PAAR gene, in correlation with the lack of the structural components of the T6SS. Lack of PAAR genes was also observed for all the

aforementioned T6SS$^-$ *Acinetobacter* members still not assigned to any species (**Supplementary Table S1**).

By means of this analysis we also determined that the majority of *Acinetobacter* PAAR proteins (**Figure 2B** and **Table 6**) belong to Shneider's classes 1 (PAAR_CT_2 domain, cd14744 of NCBI-CDD), 2 (PAAR_CT_2 domain or PAAR_motif), and 5 (PAAR_motif; **Supplementary Table S5**). Interestingly, the PAAR proteins encoded within the T6SS-main clusters all belong to class 1, with the exception of *A. colistinresistens* NIPH 1859 which encodes a PAAR-2 protein (ENX34299) of 176 amino acids (**Table 5** and **Supplementary Table S4**) and no other PAAR-1 elsewhere in its genome. Through this analysis we also observed that all *Acinetobacter* species bearing a T6SS-1Bb cluster (lacking a PAAR gene in the main cluster), encode an orphan PAAR-1 elsewhere in the genome. With the exception of *A. indicus* SGAir0564 (3 PAAR genes in total) and *A. gerneri* DSM 14967 = CIP 107464 (6 PAAR genes in total; also encoding a T6SS-2 main cluster) this is the only PAAR gene copy they carry in their genomes. This suggests that the PAAR-1 proteins are the T6SS-apparatus dedicated proteins in *Acinetobacter* species.

We also noticed that PAAR-2 proteins could be sub-classified into 3 classes (2a to 2c) according to their domain organization (**Figure 2B**), with those belonging to class 2b bearing additional domains (evolved-PAAR proteins; **Table 6**). Some of the latter carry a DUF2345 domain (pfam10106), usually part of VgrG proteins, suggesting it could fulfill an adapter role. Others bear domains probably acting as toxins, such as those belonging to the Lysozyme-like superfamily (cl00222). However, only 9 PAAR-2b proteins were detected and according to predictions in most cases the additional domain is not complete (**Supplementary Table S5**). Another aspect that is worth-commenting is that PAAR-2c proteins were mostly encoded by *A. baumannii* strains (25 out of 26; **Supplementary Table S4**).

With respect to PAAR-5 proteins, they are the less represented with only 29 members among *Acinetobacter* strains under study (**Table 6**). This is coincident with previous analysis performed on 1,353 bacterial PAAR proteins (24 occurrences, Shneider et al., 2013). Another aspect that is interesting to mention, is that PAAR-5 genes are usually located in tandem with a PAAR-2 gene (**Supplementary Table S4**) as has been described for *A. baylyi* ADP1 (CAG67033 and CAG67034; Shneider et al., 2013) and that these regions usually encode toxin genes (see below).

The genetic variability within each PAAR class was lastly investigated, based on the identity percentage of PAAR proteins under study with respect to *A. baumannii* DSM30011 PAAR-1 (**Supplementary Table S4**). We observed a significant level of conservation among PAAR-1 proteins encoded within the T6MC-1A and 1Ba (%Id 64–100), which was also evidenced from the heatmap (**Supplementary Figure S2**). These levels of conservation were also detected for 12 out of 15 PAAR-1 proteins present in the genomes of strains carrying the T6MC-1Bb (%Id 66–82; with respect to *Acinetobacter* sp. ACNIH1 PAAR-1). High conservation levels were also observed for PAAR-2c proteins (%Id 83–87), mainly encoded in *A. baumannii* strains. In turn, other groups showed an important variability, such as PAAR-2a (Id% 30–88) and PAAR-5 (Id% 40–100; with respect to *A. baylyi* ADP1

TABLE 6 | PAAR-domain proteins in *Acinetobacter* spp.

Classification of PAAR-domain proteins in the *Acinetobacter* genus				
Organism	**Location**	**Length (AA)**	**Classification[a]**	**Occurrence**
Several species (T6SS-1A, T6SS-1Ba, T6SS-2)	Main cluster	86–88	1	119
Several species (T6SS-1Bb)	Orphan PAAR gene	86–88	1	16
A. colistiniresistens NIPH 1859	T6SS-1Ba (main cluster)	176	2a	1
Several species	Orphan PAAR gene	96–368	2a	177
Several species	Orphan PAAR gene	171–399	2b	9
A. baumannii, A. oleivorans	Orphan PAAR gene	125–257	2c	26
Several species	Orphan PAAR gene	133–161	5	29
PAAR-2b proteins in the *Acinetobacter* genus				
Organism	**Accession number**	**Length (AA)**	**Extra domain[b]**	
A. lactucae OTEC-02	ARD27797	178	DUF2345 superfamily	
A. gyllenbergii NIPH 230	ESK35400	172	DUF2345 superfamily	
A. indicus SGAir0564	AVH13769	284	Pox_polyA_pol_C superfamily	
A. gyllenbergii FMP01	OBY73915	171	SdrD_B superfamily	
A. proteolyticus 2P01AA	PKF32710	171	SdrD_B superfamily	
A. guillouiae NIPH 991	ENV17008	183	DUF2345 superfamily	
A. colistiniresistens NIPH 2036	EPG34566	181	HP superfamily	
A. guillouiae CIP 63.46	ENU60235	399	Lysozyme_like superfamily	
A. baumannii SDF	CAP02689	183	YbbN superfamily	

[a]*Adapted from Shneider et al. (2013).* [b]*Obtained from the NCBI-CDD (Marchler-Bauer et al., 2015).*

TABLE 7 | Putative toxins identified in the PAAR and *vgrG* gene neighborhoods[a].

PGN[b]	Anchor gene function (gene name)	PGN occurrence	PAAR length range	PAAR class	Toxin			
					Domain	**Domain superfamily**	**Function**	***Acinetobacter* spp.**
1	Outer membrane porin, OprD family	9	181 (8)	2a (9)				
2	NUDIX hydrolase	9	Variable	2a (9)	T6SS amidase effector protein 4 (6)	cl16625	Amidase	*A. gyllenbergii* (3), *A. colistiniresistens* (2), *A. baumannii* (1), A. *proteolyticus* (1), *A. towneri* (1), *A*. sp. TGL-Y2 (1)
3	Uncharacterized protein (NlpC/P60 superfamily domain)	46	256–280 (42)	2a (41)/2c (5)				
4[c]	Pimeloyl-ACP methyl ester carboxylesterase	12	88 (12)	1 (88)				
5	SDR family NAD(P)-dependent oxidoreductase	61	279 (45)/256 (16)	2a (45)/2c (16)				
6	SDR family NAD(P)-dependent oxidoreductase	6	272 (4)/249 (2)	2a (4)/2c (2)				
VGN[b]	**Anchor gene function**	**VGN occurrence**	**VgrG length range**	**Other associated proteins**	**Toxin**			
					Domain	**Domain superfamily**	**Function**	***Acinetobacter* spp.**
1 (Tse4[d])	Disulfide bond formation protein (*dsbB*)	120	1093–1133 (106)		Lysozyme_like (5)	cl00222	Beta-1,4- linked polysaccharides hydrolysis	*A. baumannii* (94), *A. beijerinckii* (2), *A. calcoaceticus* (2), *A. colistiniresistens* (2), *A. gerneri* (1), *A. gyllenbergii* (1), *A. haemolyticus* (1), *A. junii* (1), *A. lactucae* (1), *A. nosocomialis* (4), *A. oleivorans* (1), *A. pittii* (4), *A. populi* (1), *A. proteolyticus* (1), *A. seifertii* (3), *A*. sp. DUT-2

(Continued)

TABLE 7 | Continued

VGN[b]	Anchor gene function	VGN occurrence	VgrG length range	Other associated proteins	Toxin			
					Domain	**Domain superfamily**	**Function**	***Acinetobacter* spp.**
					LysM (30)	cl28306/cl21525	Peptidoglycan binding in bacteria and chitin in eukaryotes	
					Peptidase_M23 (23)	cl27539	Zinc-dependent metallopeptidase (Gly-Gly endopeptidases)	
					LysM + Amidase_5 (12)	cl28306/ cl21525 + cl21534 (NlpC/P60)	N-acetylmuramoyl-L-alanine amidase	
					Lysozyme_like + LysM (12)	cl00222 + cl28306/ cl21525	see above	
					LysM + Peptidase_M23 (32)	cl28306/cl21525 + cl27539	see above	
2	Patatin-like phospholipase	4	878–879 (4)	DUF4123-containing protein	Metallo-peptidase family M12 (4)	cl00064	Zinc-dependent metalloprotease	*A. guillouiae* (3), *A. bereziniae* (1)
3	Methionine aminotransferase	9	variable		lysozyme_like (1)	cl00222	See above	*A*. sp. (1)
					LysM (3)	cl28306/cl21525	See above	*A. bohemicus* (1), *A. celticus* (1), *A. pragensis* (1)
					LysM + Peptidase_M23 (1)	cl28306/ cl21525 + cl27539	See above	*A. schindleri* (1)
4 (Tae1[e])	Malate dehydrogenase	16	1095–1129 (13)		lysozyme_like (1)	cl00222	see above	*A. soli* (1)
					LysM (4)	cl28306/cl21525	see above	*A. baylyi* (2), *A. radioresistens* (1), *A. guillouiae* (1)
					Peptidase_M23 (1)	cl27539	See above	*A. guillouiae* (1)
					lysozyme_like + LysM (1)	cl00222 + cl21525	See above	*A. ursingii* (1)
					LysM + Peptidase_M23 (2)	cl28306/ cl21525 + cl27539	See above	*A. ursingii* (1), *A. johnsonii* (1)
5 (Tse2[e])	Enoyl-[acyl-carrier-protein] reductase	4	Variable		Undetermined (3)			*A. baylyi* (1), *A. guillouiae* (1)
6	SDR family NAD(P)-dependent oxidoreductase	27	920–948 (27)	Sel1 repeat containing protein (cl27881), DUF3396 (cl13337)	Undetermined (2)		Putative lipase	*A. baumannii* (25), *A. pittii* (1), *A. nosocomialis* (1)

(Continued)

TABLE 7 | Continued

VGN[b]	Anchor gene function	VGN occurrence	VgrG length range	Other associated proteins	Toxin			
					Domain	**Domain superfamily**	**Function**	***Acinetobacter* spp.**
7	Uncharacterized protein (NTF2_lilke superfamily domain)	14	876 (13)	DUF4123-containing protein	Undetermined			*A. baumannii* (12)
8 (Tse3[d])	T6SS-1a main cluster	5	926–928 (5)		Undetermined		Amidase	*A. pittii* (2), *A. baumannii* (2)
					RhsA + NUC (1)	cl27255/ cl04135 + cl00089	DNA/RNA non-specific endonuclease	*A. pittii* (1)
					RhsA + Tox-ART-HYD1 (1)	cl27255/ cl04135 + cl21425	Toxin of the ADP-ribosyltransferase superfamily	*A. pittii* (1)
9 (Tse2[d])	DNA-binding transcriptional regulator, AcrR family	10	94–947 (6)		Ntox15 (6)	cl21405	Predicted RNase toxin	*A. baumannii* (4), *A. pittii* (1), *A. bereziniae* (1)
					DUF2235 (1)	cl01480	Alpha/beta hydrolase	*A. pittii* (1)
10	5-carboxymethyl-2-hydroxymuconate Delta-isomerase	6	Variable	Sel1 repeat containing protein (cl27881)	LysM (2)	cl28306	See above	*A. gyllenbergii* (1), *A. colistiniresistens* (1)
11	LysR-family transciptional regulator	7	875–913 (7)	DUF4123-containing protein	DUF2235 (5)	cl01480	Alpha/beta hydrolase	*A. pittii* (2), *A. baumannii* (1), *A. seifertii* (1)
					Ab_hydrolase (2)	cl21494	Alpha/beta hydrolase	*A. guillouiae* (1), *A. bereziniae* (1)
12 (Rhs-2[f])	Beta-lactamase class A *(penP)*	88	1048–1060 (84)		RhsA + Tox-GHH (57)	cl27255/ cl04135 + cl21428	Toxin of the HNH/Endonuclease VII fold superfamily (sG[HQ]H motif)	*A. baumannii* (74)
					RhsA + AHH (11)	cl27255/ cl04135 + cl16862	Nuclease of the HNH/ENDO VII superfamily (AHH motif)	
					RhsA + YwqJ-deaminase (6)	cl27255/ cl04135 + cl24268	Toxin of the nucleic acid/nucleotide deaminase superfamily	
					RhsA + undetermined (9)	cl27255/ cl04135		

(Continued)

TABLE 7 | Continued

VGN[b]	Anchor gene function	VGN occurrence	VgrG length range	Other associated proteins	Toxin			
					Domain	Domain superfamily	Function	*Acinetobacter* spp.
13 (Tse1[d])	3-oxoacyl-(acyl carrier protein) synthase I	8	918–952 (8)	Sel1 repeat containing protein (cl27881)	Undetermined (5)		Putative lipase	*A. baumannii* (5)
14 (Rhs-1[f])	DNA-binding transcriptional regulator, AcrR family	67	1039–1164 (61)	Sel1 repeat containing protein (cl27881)	RhsA + YwqJ-deaminase (1)	cl27255/ cl04135 + cl24268	See above	*A. tandoii* (1)
					RhsA + Bacuni_01323_like (1)	cl25912	Uncharacterized protein conserved in Bacteroidetes	*A. guillouiae* (1)
					RhsA + undetermined (63)	cl27255/ cl04135		*A. baumannii* (58)

[a]*Numbers in parenthesis indicate the occurrence of the given feature.* [b]*Characterized toxins belonging to a specific PGN/VGN are indicated in parenthesis.* [c]*This PGN nucleates PAAR-proteins present in Acinetobacter spp. bearing a T6SS-1Bb main cluster.* [d]*Weber et al. (2016).* [e]*Ringel et al. (2017).* [f]*Fitzsimons et al. (2018).*

PAAR-5), and as expected PAAR-2b (%Id 31–85), since they carry an extra domain. It is tempting to speculate that those PAAR proteins fulfilling a structural role tend to be more conserved than those probably acting as toxin-chaperones (see below).

Two Undescribed PAAR-Rhs Proteins Probably Acting as Toxins

Since none of the PAAR proteins identified through this analysis bore a DUF4150 domain, also found in proteins belonging to the PAAR_like domain superfamily, a search for proteins carrying this domain was conducted. By this means, two proteins present in *A. gerneri* DSM 14967 = CIP 107464 (ENV33198) and *A. equi* (ALH95481) with significant homology were detected. These proteins additionally carried RhsA domains (cl27255; **Supplementary Figure S4B**) and thus could be categorized as PAAR-3 proteins according to a previous classification (Shneider et al., 2013). A predicted toxin domain (pfam15633) of the ADP-ribosyltransferase superfamily was detected in ENV33198. PAAR-3 proteins carrying this toxin domain (categorized as "protein-modifying") have been identified in 16 bacterial species (Ma et al., 2017b). The genes encoding these PAAR-3 proteins, are preceded by genes coding for a protein carrying a DUF2169 domain and a "short" VgrG (<750 aa, lacking a DUF2345 domain). We found that these clusters are also present in bacteria belonging to diverse genera such as *Bordetella*, *Burkholderia*, *Variovorax*, *Alcalinovorax,* and *Pseudomonas*. Furthermore, a DUF2169 domain-carrying protein fulfill an adapter role specific for the Tde2 toxin (AAK89757; carrying a DUF4150 and a Ntox15 DNase domain) in *Agrobacterium tumefaciens* (Bondage et al., 2016). Interestingly, the gene encoding for the DUF2169-domain–containing protein is always located between the *vgrG2* and *tde2* genes. Conservation in gene cluster organization across diverse Proteobacterial lineages has also been reported. All these data are on favor of the hypothesis that the Tde effector is stabilized and carried by its cognate adaptor/chaperone, which loads the effector onto the C terminus of VgrG for secretion across bacterial membranes (Bondage et al., 2016). It is thus tempting to speculate that the DUF2169 domain-carrying protein present in *Acinetobacter* strains is involved in the loading of PAAR-3 partners.

T6SS-Associated Toxin Repertoire in *Acinetobacter* spp.

In order to search for putative toxin encoding genes in the proximity of *vgrG* and PAAR identified genes, a homology search using as query T6SS-reported toxins was performed (see section Materials and Methods and **Supplementary Table S6**). Gene neighborhoods of PAAR and *vgrG* genes were further investigated in order to analyze the existence of specific genomic spots where PAAR and *vgrG* islands are located, the *Acinetobacter* species encoding specific islands, the presence of different classes of PAAR or VgrG proteins linked to these neighborhoods and finally, the toxins associated to each of them. With all this information, a clustering approach was followed

in order to distinguish either PAAR or VgrG proteins sharing common genetic environments (**Supplementary Figures S5, S6**). According to this analysis 6 PAAR- and 14 VgrG-gene neighborhoods (PGN and VGN, respectively) were defined (**Supplementary Table S7**), which are summarized in **Table 7**. We observed that a gene encoding for a SDR family NAD(P)-dependent oxidoreductase is part of several of these gene neighborhoods (PGN5, PGN6, and VGN6), suggesting this genome region might be a conserved spot for PAAR and *vgrG* islands. Moreover, 12 out of 15 PAAR-1 genes present in the genomes encoding a T6SS1-Bb-core cluster grouped in PGN4, whereas the remaining 3 (ENV70927, SNQ29620, and ENV33195) were located within mixed PAAR-*vgrG* islands not associated to any particular PGN/VGN (**Supplementary Figure S5**). The conservation of PGN4 reinforces the idea that the PAAR-1 proteins encoded in these clusters are devoted to the T6SS.

In correlation with toxin genes, we initially observed that *vgrG* islands were particularly enriched in genes encoding different classes of previously reported toxins whereas in PAAR islands mostly Tpe1 and Tae4 toxins were detected (**Supplementary Table S6**). In *A. baylyi* ADP1 the *tpe1* gene is located downstream a PAAR-2 encoding gene (Ringel et al., 2017). In agreement with this data, our analysis detected only 1 *tpe1* orthologous gene next to a *vgrG* gene whereas 20 were in close proximity to a PAAR gene (**Supplementary Table S6**). Furthermore, we observed that in 11 out of these 20 loci, there is a PAAR-5 gene upstream the PAAR-2 gene (**Supplementary Table S6**). This information suggests that these toxins are usually genetically linked to PAAR genes in *Acinetobacter* spp. Interestingly, *A. colistineresistens* encodes a Tpe1 toxin (ENX34300) in the T6MC next to an unusual PAAR-2a gene. While Tpe1 proteins are not particularly associated to any PGN, putative Tae4 proteins are encoded in the PGN2 (**Supplementary Figure S5**). We noticed that 6 out of the 9 clusters included in PGN2 encoded Tae4-amidase effectors accompanied by their immunity proteins (Tai4; **Table 7**). Of note, the Tae4-Tai4 pair (CAP02973-CAP02974) is encoded in *A. baumannii* SDF p2ABSDF. Furthermore, 5 PAAR genes (ATZ62304, ESK36633, OBY73307, ATZ64949, AMW78666; **Supplementary Figure S5**) were found to be accompanied by a gene encoding a protein with a VRR_Nuclease domain (cl22959) and followed by 1 to 4 genes bearing a DUF3396 domain (cl13337). These PAAR proteins all belong to class 2a and are between 176 and 179 aa long (**Supplementary Table S4**). It would be interesting to determine if they are responsible for the secretion of the putative nuclease effector and if the DUF3396-proteins are involved in this task as well.

When analyzing the different VGNs, we observed that VGN1 (the most prevalent), 3, 4, and 10 encoded peptidoglycan hydrolases, M12 and M23 domain peptidases, LysM-domain containing proteins and numerous proteins of unknown function. This is in agreement with a previous report including 23 *Acinetobacter* genomes (Fitzsimons et al., 2018). We also detected the presence of proteins with significant homology with toxins previously reported in *Acinetobacter* spp. (Weber et al., 2016; Ringel et al., 2017; Fitzsimons et al., 2018), associated to specific VGNs (**Table 7**). Several DUF4123 proteins were found in VGN2, 7 and 11, accompanied by a "short VgrG" (875–883 aa) and associated to Tle1 toxins (DUF2235) or proteins carrying a M12 metallo-peptidase family domain (pfam13688). The presence of DUF4123 proteins in VGNs has already been pinpointed by Fitzsimons et al. (2018). Ringel et al. (2017) identified in *A. baylyi* the Tap-1 chaperone (carrying a DUF4123 domain) necessary for the putative Tse2 toxin delivery. Therefore, it is possible that these proteins might play a role as chaperones for different toxin partners.

In this analysis we were also able to identify a vast repertoire of Rhs-domain containing proteins, which were found to be present in *vgrG* islands of 13 out of the 33 *Acinetobacter* T6SS-proficient species under study (**Supplementary Table S6**). Moreover, they are clearly conserved in *A. baumannii* strains (90 out of 110). Rhs-encoding genes were particularly grouped in the VGN8, 12, and 14 (**Table 7**), of which 174 showed homology at the protein level with Rhs1 and Rhs2 identified in *A. baumannii* AB307-0294 (**Supplementary Table S6**; Fitzsimons et al., 2018). We observed that while a group of 20 of these proteins belonging to the VGN14 showed an identity > 94% with the Rhs1 toxin of unknown function, 11 proteins (VGN12) were identical to the Rhs2 effector which carries an AHH nuclease domain (cl16862). This prompted us to analyze the variety of effector domains carried by the remaining Rhs-domain containing proteins (**Supplementary Table S8**). Remarkably, 59 candidates contained a Tox-GHH superfamily nuclease domain (cl21428) and 8 a YwqJ-deaminase superfamily domain (cl24268). Importantly, with the exception of the aforementioned PAAR-3 protein (ALH95481), none of these Rhs proteins bears a PAAR domain or a chaperone gene nearby, and thus their delivery mechanism remains unknown.

Diverse functions have been attributed to Rhs proteins in other bacteria such as motility, cellular toxicity, virulence in mice and insecticidal activity (Lien and Lai, 2017; Yang et al., 2018), and contact-dependent killing of other bacteria species in *A. baumannii* (Fitzsimons et al., 2018). Rhs proteins are capable of replacing the C-terminal end with a non-homologous alternative. By this means, they can switch between different toxin domains and thereby they have been included within the bacterial polymorphic toxin systems (Jamet and Nassif, 2015). Our findings indicate that the *rhs* genes associated with the *Acinetobacter vgrG* islands encode different C-terminal domains which might play different roles as toxins. To date none of these proteins have been implicated in *A. baumannii* virulence.

CONCLUSION

The T6SS fulfills critical roles in bacterial competition, bacterium–host interaction and other functions associated with bacterial physiology. We therefore conducted a genomic comparative analyses of 191 *Acinetobacter* strains which let us identify two putative gene clusters responsible for the synthesis of a functional T6SS. The T6SS-1 was widespread in the genome of most species, while the T6SS-2 was restricted to three environmental species. In this respect, it will be interesting to

determine whether the T6SS-2 is active and the roles it plays. Future work will certainly focus on the identification and characterization of the secreted components of this system.

The finding that the T6SS-1 gene cluster was present in both pathogenic and non-pathogenic species raises the hypothesis that the T6SS may have evolved to play different roles in the *Acinetobacter* lifestyle. In this respect, the variable regions associated with PAAR and *vgrG* genes could account for specialization of the T6SS based on the needs of each species. A plethora of toxin-encoding genes was detected in these genomic regions, with those encoding Rhs-domain containing proteins clearly overrepresented. Although no proteins showing significant homology to previously characterized effectors targeting eukaryotic cells (Lien and Lai, 2017) were detected, these regions also encode an impressive number of proteins of unknown function. Hence, we cannot rule out the existence of novel effector functions still to be discovered.

The overall observations described above not only highlight both the high diversity and potential plasticity of the *Acinetobacter* T6SS genes at the species level, but also support the notion that this system could have evolved differential and even strain-specific roles related to the interaction with other cells in particular environments. We hope the results obtained in this work can provide a foundation for future characterization of the *Acinetobacter* T6SSs and its effectors.

DATA AVAILABILITY STATEMENT

Publicly available datasets were analyzed in this study. This data can be found here: https://www.ncbi.nlm.nih.gov.

AUTHOR CONTRIBUTIONS

GR and SS conceived and designed the work. JS conducted the experimental work. GR and ME conducted the bioinformatic analysis. GR, ME, and SS analyzed the data and wrote the manuscript. All authors read and approved the final manuscript.

FUNDING

This work was supported by a FINOVI Young Researcher Grant awarded to SS and by grants from Agencia Nacional de Promoción Científica y Tecnológica (ANPCyT PICT-2017-3536) to GR. SS is a staff scientist of INSERM. GR and ME are staff members of CONICET.

SUPPLEMENTARY MATERIAL

The Supplementary Material for this article can be found online at: https://www.frontiersin.org/articles/10.3389/fmicb.2019.02519/full#supplementary-material

FIGURE S1 | Hcp secretion assay. The presence of Hcp (indicative of a functional T6SS) in concentrated culture supernatants of the indicated *Acinetobacter* strains grown up to stationary phase in L-Broth was determined by 18% SDS-PAGE and Coomasie Blue staining (see Repizo et al., 2015 for experimental details). MM, molecular markers.

FIGURE S2 | Clustering of T6MC-proteins in 191 *Acinetobacter* strains. *A. baumannii* DSM30011 was used as reference. Strain subclustering according to T6MC classification is indicated. For *A. baumannii* strains, ST-classification according to the Pasteur scheme is also shown.

FIGURE S3 | (A–C) Putative transmembrane domains present in *Acinetobacter* T6SS proteins with unknown function (Hyp1-3). TMHMM Server v.2.0 (http://www.cbs.dtu.dk/services/TMHMM) was used for predictions.

FIGURE S4 | (A) TagN domain structure. The NCBI-CDD was used for the domain search (Marchler-Bauer et al., 2015). **(B)** Domain architecture of PAAR-3 proteins found in *Acinetobacter* spp. The NCBI-CDD database was used for the domain search (Marchler-Bauer et al., 2015).

FIGURE S5 | Clustering of PAAR islands based on gene context. Conserved superfamily domains of proteins encoded within PAAR islands were used to define similar genetic contexts by clustering. Those gene islands sharing a similar genetic context were grouped in PAAR gene neighborhoods (PGN1-6, see **Table 7** for detail). PAAR islands encoding putative toxins are indicated. Accession numbers corresponding to PAAR proteins encoded by *A. baylyi* ADP1 are boxed.

FIGURE S6 | Clustering of VgrG islands based on gene context. Conserved superfamily domains of proteins encoded within VgrG islands were used to define similar genetic contexts by clustering. Those gene islands sharing a similar genetic context were grouped in VgrG gene neighborhoods (VGN1-14, see **Table 7** for detail). PAAR islands encoding putative toxins are indicated. Accession numbers corresponding to VgrG proteins encoded by *A. baylyi* ADP1 are boxed.

TABLE S1 | Strain under study.

TABLE S2 | BlastP-homology search for VgrG domain-containing proteins in *Acinetobacter* spp.

TABLE S3 | NCBI web-Conserved domains search tool results for *Acinetobacter* VgrG proteins.

TABLE S4 | BlastP-homology search for PAAR proteins in the *Acinetobacter* genus.

TABLE S5 | NCBI web-Conserved domains search tool results for *Acinetobacter* PAAR proteins.

TABLE S6 | BlastP-homology search for toxins in PAAR and *vgrG* genetic islands in *Acinetobacter* spp.

TABLE S7 | List of PAAR and *vgrG* proteins grouped into the gene neighborhoods defined in this study.

TABLE S8 | NCBI web-Conserved domains search tool results for *Acinetobacter* Rhs proteins.

REFERENCES

Alcoforado, D. J., Liu, Y. C., and Coulthurst, S. J. (2015). Molecular weaponry: diverse effectors delivered by the type VI secretion system. *Cell. Microbiol.* 17, 1742–1751. doi: 10.1111/cmi.12532

Altschul, S. F., Gish, W., Miller, W., Myers, E. W., and Lipman, D. J. (1990). Basic local alignment search tool. *J. Mol. Biol.* 215, 403–410. doi: 10.1016/S0022-2836(05)80360-2

Antunes, L. C. S., Visca, P., and Towner, K. J. (2014). *Acinetobacter baumannii*: evolution of a global pathogen. *Pathog. Dis.* 71, 292–301. doi: 10.1111/2049-632X.12125

Aschtgen, M. S., Bernard, C. S., De Bentzmann, S., Lloubès, R., and Cascales, E. (2008). SciN is an outer membrane lipoprotein required for type VI secretion in enteroaggregative *Escherichia coli*. *J. Bacteriol.* 190, 7523–7531. doi: 10.1128/JB.00945-08

Aschtgen, M. S., Thomas, M. S., and Cascales, E. (2010). Anchoring the type VI secretion system to the peptidoglycan TssL, TagL, TagP, what else? *Virulence* 1, 535–540. doi: 10.4161/viru.1.6.13732

Basler, M., Ho, B. T., and Mekalanos, J. J. (2013). Tit-for-tat: type VI secretion system counterattack during bacterial cell-cell interactions. *Cell* 152, 884–894. doi: 10.1016/j.cell.2013.01.042

Benz, J., and Meinhart, A. (2014). Antibacterial effector/immunity systems: It's just the tip of the iceberg. *Curr. Opin. Microbiol.* 17, 1–10. doi: 10.1016/j.mib.2013.11.002

Bernard, C. S., Brunet, Y. R., Gueguen, E., and Cascales, E. (2010). Nooks and crannies in type VI secretion regulation. *J. Bacteriol.* 192, 3850–3860. doi: 10.1128/JB.00370-10

Bladergroen, M. R., Badelt, K., and Spaink, H. P. (2003). Infection-blocking genes of a symbiotic rhizobium leguminosarum strain that are involved in temperature-dependent protein secretion. *Mol. Plant Microbe Interact.* 16, 53–64. doi: 10.1094/mpmi.2003.16.1.53

Blondel, C. J., Jiménez, J. C., Contreras, I., and Santiviago, C. A. (2009). Comparative genomic analysis uncovers 3 novel loci encoding type six secretion systems differentially distributed in *Salmonella* serotypes. *BMC Genomics* 10:354. doi: 10.1186/1471-2164-10-354

Bondage, D. D., Lin, J.-S., Ma, L.-S., Kuo, C.-H., and Lai, E.-M. (2016). VgrG C terminus confers the type VI effector transport specificity and is required for binding with PAAR and adaptor-effector complex. *Proc. Natl. Acad. Sci. U.S.A.* 113, E3931–E3940. doi: 10.1073/pnas.1600428113

Boyer, F., Fichant, G., Berthod, J., Vandenbrouck, Y., and Attree, I. (2009). Dissecting the bacterial type VI secretion system by a genome wide in silico analysis: what can be learned from available microbial genomic resources? *BMC Genomics* 10:104. doi: 10.1186/1471-2164-10-104

Buist, G., Steen, A., Kok, J., and Kuipers, O. P. (2008). LysM, a widely distributed protein motif for binding to (peptido)glycans. *Mol. Microbiol.* 68, 838–847. doi: 10.1111/j.1365-2958.2008.06211.x

Carr, E. L., Kämpfer, P., Patel, B. K. C., Gürtler, V., and Seviour, R. J. (2003). Seven novel species of Acinetobacter isolated from activated sludge. *Int. J. Syst. Evol. Microbiol.* 53(Pt 4), 953–963. doi: 10.1099/ijs.0.02486-0

Carruthers, M. D., Nicholson, P. A., Tracy, E. N., and Munson, R. S. (2013). *Acinetobacter baumannii* utilizes a type VI secretion system for bacterial competition. *PLoS One* 8:e59388. doi: 10.1371/journal.pone.0059388

Cooper, R. M., Tsimring, L., and Hasty, J. (2017). Inter-species population dynamics enhance microbial horizontal gene transfer and spread of antibiotic resistance. *eLife* 6:e25950. doi: 10.7554/elife.25950

Costa, T. R. D., Felisberto-Rodrigues, C., Meir, A., Prevost, M. S., Redzej, A., Trokter, M., et al. (2015). Secretion systems in gram-negative bacteria: structural and mechanistic insights. *Nat. Rev. Microbiol.* 13, 343–359. doi: 10.1038/nrmicro3456

De Maayer, P., Venter, S. N., Kamber, T., Duffy, B., Coutinho, T. A., and Smits, T. H. M. (2011). Comparative genomics of the type VI secretion systems of pantoea and erwinia species reveals the presence of putative effector islands that may be translocated by the VgrG and Hcp proteins. *BMC Genomics* 12:576. doi: 10.1186/1471-2164-12-576

Di Venanzio, G., Moon, K. H., Weber, B. S., Lopez, J., Ly, P. M., Potter, R. F., et al. (2019). Multidrug-resistant plasmids repress chromosomally encoded T6SS to enable their dissemination. *Proc. Natl. Acad. Sci. U.S.A.* 116, 1378–1383. doi: 10.1073/pnas.1812557116

Eijkelkamp, B. A., Stroeher, U. H., Hassan, K. A., Paulsen, I. T., and Brown, M. H. (2014). Comparative analysis of surface-exposed virulence factors of *Acinetobacter baumannii*. *BMC Genomics* 15:1020. doi: 10.1186/1471-2164-15-1020

Elhosseiny, N. M., and Attia, A. S. (2018). Acinetobacter: an emerging pathogen with a versatile secretome review-article. *Emerg. Microbes Infect.* 7:33. doi: 10.1038/s41426-018-0030-4

Felisberto-Rodrigues, C., Durand, E., Aschtgen, M. S., Blangy, S., Ortiz-Lombardia, M., Douzi, B., et al. (2011). Towards a structural comprehension of bacterial type vi secretion systems: characterization of the TssJ-TssM complex of an *Escherichia coli* pathovar. *PLoS Pathog.* 7:e1002386. doi: 10.1371/journal.ppat.1002386

Fitzsimons, T. C., Lewis, J. M., Wright, A., Kleifeld, O., Schittenhelm, R. B., Powell, D., et al. (2018). Identification of novel *Acinetobacter baumannii* type VI secretion system antibacterial effector and immunity pairs. *Infect. Immun.* 86:e297-18. doi: 10.1128/IAI.00297-18

Flaugnatti, N., Le, T. T. H., Canaan, S., Aschtgen, M. S., Nguyen, V. S., Blangy, S., et al. (2016). A phospholipase A1 antibacterial Type VI secretion effector interacts directly with the C-terminal domain of the VgrG spike protein for delivery. *Mol. Microbiol.* 99, 1099–1118. doi: 10.1111/mmi.13292

Galán, J. E., and Waksman, G. (2018). Protein-injection machines in Bacteria. *Cell* 172, 1306–1318. doi: 10.1016/j.cell.2018.01.034

Gebhardt, M. J., Gallagher, L. A., Jacobson, R. K., Usacheva, E. A., Peterson, L. R., Zurawski, D. V., et al. (2015). Joint transcriptional control of virulence and resistance to antibiotic and environmental stress in *acinetobacter baumannii*. *mBio* 6, 1–12. doi: 10.1128/mBio.01660-15

Harding, C. M., Hennon, S. W., and Feldman, M. F. (2018). Uncovering the mechanisms of *Acinetobacter baumannii* virulence. *Nat. Rev. Microbiol.* 16, 91–102. doi: 10.1038/nrmicro.2017.148

Jamet, A., and Nassif, X. (2015). New players in the toxin field: polymorphic toxin systems in bacteria. *mBio* 27, 897–905. doi: 10.1128/mbio.00285-15

Jones, C. L., Clancy, M., Honnold, C., Singh, S., Snesrud, E., Onmus-Leone, F., et al. (2015). fatal outbreak of an emerging clone of extensively drug-resistant *Acinetobacter baumannii* with enhanced virulence. *Clin. Infect. Dis.* 61, 145–154. doi: 10.1093/cid/civ225

Kim, J., Lee, J. Y., Lee, H., Choi, J. Y., Kim, D. H., Wi, Y. M., et al. (2017). Microbiological features and clinical impact of the type VI secretion system (T6SS) in *Acinetobacter baumannii* isolates causing bacteremia. *Virulence* 8, 1378–1389. doi: 10.1080/21505594.2017.1323164

Letunic, I., and Bork, P. (2011). Interactive tree of Life v2: online annotation and display of phylogenetic trees made easy. *Nucleic Acids Res.* 39, W475–W478. doi: 10.1093/nar/gkr201

Lien, Y.-W., and Lai, E.-M. (2017). Type VI secretion effectors: methodologies and biology. *Front. Cell. Infect. Microbiol.* 7:254. doi: 10.3389/fcimb.2017.00254

Ma, A. T., and Mekalanos, J. J. (2010). In vivo actin cross-linking induced by *Vibrio cholerae* type VI secretion system is associated with intestinal inflammation. *Proc. Natl. Acad. Sci. U.S.A.* 107, 4365–4370. doi: 10.1073/pnas.0915156107

Ma, J., Pan, Z., Huang, J., Sun, M., Lu, C., and Yao, H. (2017a). The Hcp proteins fused with diverse extended-toxin domains represent a novel pattern of antibacterial effectors in type VI secretion systems. *Virulence* 8, 1189–1202. doi: 10.1080/21505594.2017.1279374

Ma, J., Sun, M., Dong, W., Pan, Z., Lu, C., and Yao, H. (2017b). PAAR-Rhs proteins harbor various C-terminal toxins to diversify the antibacterial pathways of type VI secretion systems. *Environ. Microbiol.* 19, 345–360. doi: 10.1111/1462-2920.13621

Ma, J., Sun, M., Pan, Z., Lu, C., and Yao, H. (2018). Diverse toxic effectors are harbored by vgrG islands for interbacterial antagonism in type VI secretion system. *Biochim. Biophys. Acta Gen. Subj.* 1862, 1635–1643. doi: 10.1016/j.bbagen.2018.04.010

Marchler-Bauer, A., Derbyshire, M. K., Gonzales, N. R., Lu, S., Chitsaz, F., Geer, L. Y., et al. (2015). CDD: NCBI's conserved domain database. *Nucleic Acids Res.* 43, D222–D226. doi: 10.1093/nar/gku1221

McConnell, M. J., Actis, L., and Pachón, J. (2013). *Acinetobacter baumannii*: Human infections, factors contributing to pathogenesis and animal models. *FEMS Microbiol. Rev.* 37, 130–155. doi: 10.1111/j.1574-6976.2012.00344.x

Medema, M. H., Takano, E., and Breitling, R. (2013). Detecting sequence homology at the gene cluster level with multigeneblast. *Mol. Biol. Evol.* 30, 1218–1223. doi: 10.1093/molbev/mst025

Petersen, T. N., Brunak, S., von Heijne, G., and Nielsen, H. (2011). SignalP 4.0: discriminating signal peptides from transmembrane regions. *Nat. Methods* 8, 785–786. doi: 10.1038/nmeth.1701

Pukatzki, S., Ma, A. T., Sturtevant, D., Revel, A. T., and Mekalanos, J. J. (2007). Type VI secretion system translocates a phage tail spike-like protein into target cells where it cross-links actin. *Proc. Natl. Acad. Sci. U.S.A.* 104, 15508–15513. doi: 10.1073/pnas.0706532104

Repizo, G. D. (2017). Prevalence of *Acinetobacter baumannii* strains expressing the type 6 secretion system in patients with bacteremia. *Virulence* 8, 1099–1101. doi: 10.1080/21505594.2017.1346768

Repizo, G. D., Gagné, S., Foucault-Grunenwald, M. L., Borges, V., Charpentier, X., Limansky, A. S., et al. (2015). Differential role of the T6SS in *acinetobacter baumannii* virulence. *PLoS One* 10:e0138265. doi: 10.1371/journal.pone.0138265

Repizo, G. D., Viale, A. M., Borges, V., Cameranesi, M. M., Taib, N., Espariz, M., et al. (2017). The environmental *Acinetobacter baumannii* isolate DSM30011 reveals clues into the preantibiotic era genome diversity, virulence potential, and niche range of a predominant nosocomial pathogen. *Genome Biol. Evol.* 9, 2292–2307. doi: 10.1093/gbe/evx162

Ringel, P. D., Hu, D., and Basler, M. (2017). The role of type VI secretion system effectors in target cell lysis and subsequent horizontal gene transfer. *Cell Rep.* 21, 3927–3940. doi: 10.1016/j.celrep.2017.12.020

Ryu, C. M. (2015). Against friend and foe: type 6 effectors in plant-associated bacteria. *J. Microbiol.* 53, 201–208. doi: 10.1007/s12275-015-5055-y

Schwarz, S., Singh, P., Robertson, J. D., LeRoux, M., Skerrett, S. J., Goodlett, D. R., et al. (2014). VgrG-5 is a Burkholderia type VI secretion system-exported protein required for multinucleated giant cell formation and virulence. *Infect. Immun.* 82, 1445–1452. doi: 10.1128/IAI.01368-13

Shalom, G., Shaw, J. G., and Thomas, M. S. (2007). In vivo expression technology identifies a type VI secretion system locus in *Burkholderia pseudomallei* that is induced upon invasion of macrophages. *Microbiology* 153, 2689–2699. doi: 10.1099/mic.0.2007/006585-0

Shneider, M. M., Buth, S. A., Ho, B. T., Basler, M., Mekalanos, J. J., and Leiman, P. G. (2013). PAAR-repeat proteins sharpen and diversify the type VI secretion system spike. *Nature* 500, 350–353. doi: 10.1038/nature12453

Shyntum, D. Y., Venter, S. N., Moleleki, L. N., Toth, I., and Coutinho, T. A. (2014). Comparative genomics of type VI secretion systems in strains of *Pantoea ananatis* from different environments. *BMC Genomics* 15:163. doi: 10.1186/1471-2164-15-163

Spiewak, H. L., Eberl, L., Shastri, S., Zhang, L., Schwager, S., Thomas, M. S., et al. (2019). Burkholderia cenocepacia utilizes a type VI secretion system for bacterial competition. *Microbiologyopen* 9:e774. doi: 10.1002/mbo3.774

Suzuki, R., and Shimodaira, H. (2006). Pvclust: an R package for assessing the uncertainty in hierarchical clustering. *Bioinformatics* 22, 1540–1542. doi: 10.1093/bioinformatics/btl117

Taboada, B., Ciria, R., Martinez-Guerrero, C. E., and Merino, E. (2012). ProOpDB: prokaryotic operon database. *Nucleic Acids Res.* 40, D627–D631. doi: 10.1093/nar/gkr1020

Trunk, K., Peltier, J., Liu, Y. C., Dill, B. D., Walker, L., Gow, N. A. R., et al. (2018). The type VI secretion system deploys antifungal effectors against microbial competitors. *Nat. Microbiol.* 3, 920–931. doi: 10.1038/s41564-018-0191-x

Unterweger, D., Miyata, S. T., Bachmann, V., Brooks, T. M., Mullins, T., Kostiuk, B., et al. (2014). The *vibrio cholerae* type VI secretion system employs diverse effector modules for intraspecific competition. *Nat. Commun.* 20, 130–137. doi: 10.1038/ncomms4549

Weber, B. S., Hennon, S. W., Wright, M. S., Scott, N. E., de Berardinis, V., Foster, L. J., et al. (2016). Genetic dissection of the type VI secretion system in *Acinetobacter* and identification of a novel peptidoglycan hydrolase, TagX, required for its biogenesis. *mBio.* 7:e01253-16. doi: 10.1128/mBio.01253-16

Weber, B. S., Kinsella, R. L., Harding, C. M., and Feldman, M. F. (2017). The secrets of acinetobacter secretion. *Trends Microbiol.* 25, 532–545. doi: 10.1016/j.tim.2017.01.005

Weber, B. S., Miyata, S. T., Iwashkiw, J. A., Mortensen, B. L., Skaar, E. P., Pukatzki, S., et al. (2013). Genomic and functional analysis of the Type VI secretion system in acinetobacter. *PLoS One* 8:e55142. doi: 10.1371/journal.pone.0055142

Wright, M. S., Haft, D. H., Harkins, D. M., Perez, F., Hujer, K. M., Bajaksouzian, S., et al. (2014). New insights into dissemination and variation of the health care- associated pathogen *Acinetobacter baumannii* from genomic analysis. *mBio*. 5:e00963-13. doi: 10.1128/mBio.00963-13

Wu, J., Saupe, S. J., and Glass, N. L. (1998). Evidence for balancing selection operating at the het-c heterokaryon incompatibility locus in a group of filamentous fungi. *Proc. Natl. Acad. Sci. U.S.A.* 95, 12398–12403. doi: 10.1073/pnas.95.21.12398

Yang, X., Long, M., and Shen, X. (2018). Effector–immunity pairs provide the T6SS nanomachine its offensive and defensive capabilities. *Molecules* 23:1009. doi: 10.3390/molecules23051009

Zoued, A., Brunet, Y. R., Durand, E., Aschtgen, M. S., Logger, L., Douzi, B., et al. (2014). Architecture and assembly of the Type VI secretion system. *Biochim. Biophys. Acta Mol. Cell Res.* 1843, 1664–1673. doi: 10.1016/j.bbamcr.2014.03.018

Zückert, W. R. (2014). Secretion of bacterial lipoproteins: through the cytoplasmic membrane, the periplasm and beyond. *Biochim. Biophys. Acta Mol. Cell Res.* 1843, 1509–1516. doi: 10.1016/j.bbamcr.2014.04.022

Conflict of Interest: The authors declare that the research was conducted in the absence of any commercial or financial relationships that could be construed as a potential conflict of interest.

frontiers in Microbiology

ORIGINAL RESEARCH
published: 18 March 2020
doi: 10.3389/fmicb.2020.00342

Crucial Role of the Accessory Genome in the Evolutionary Trajectory of *Acinetobacter baumannii* Global Clone 1

*Verónica Elizabeth Álvarez[1†], María Paula Quiroga[1†], Angélica Viviana Galán[1], Elisabet Vilacoba[1‡], Cecilia Quiroga[2], María Soledad Ramírez[3] and Daniela Centrón[1]**

[1] Laboratorio de Investigaciones en Mecanismos de Resistencia a Antibióticos, Instituto de Investigaciones en Microbiología y Parasitología Médica, Facultad de Medicina, Universidad de Buenos Aires - Consejo Nacional de Investigaciones Científicas y Tecnológicas (IMPaM, UBA-CONICET), Buenos Aires, Argentina, [2] Instituto de Investigaciones en Microbiología y Parasitología Médica, Facultad de Medicina, Universidad de Buenos Aires - Consejo Nacional de Investigaciones Científicas y Tecnológicas (IMPaM, UBA-CONICET), Buenos Aires, Argentina, [3] Center for Applied Biotechnology Studies, Department of Biological Science, California State University Fullerton, Fullerton, CA, United States

Acinetobacter baumannii is one of the most important nosocomial pathogens able to rapidly develop extensive drug resistance. Here, we study the role of accessory genome in the success of the globally disseminated clone 1 (GC1) with functional and genomic approaches. Comparative genomics was performed with available GC1 genomes (n = 106) against other *A. baumannii* high-risk and sporadic clones. Genetic traits related to accessory genome were found common and conserved along time as two novel regions of genome plasticity, and a CRISPR-Cas system acquired before clonal diversification located at the same loci as "sedentary" modules. Although identified within hotspot for recombination, other block of accessory genome was also "sedentary" in lineage 1 of GC1 with signs of microevolution as the AbaR0-type genomic island (GI) identified in A144 and in A155 strains which were maintained one month in independent experiments without antimicrobial pressure. The prophage YMC/09/02/B1251_ABA_BP was found to be "mobile" since, although it was shared by all GC1 genomes, it showed high intrinsic microevolution as well as mobility to different insertion sites. Interestingly, a wide variety of Insertion Sequences (IS), probably acquired by the flow of plasmids related to Rep_3 superfamily was found. These IS showed dissimilar genomic location amongst GC1 genomes presumably associated with promptly niche adaptation. On the other hand, a type VI secretion system and three efflux pumps were subjected to deep processes of genomic loss in *A. baumannii* but not in GC1. As a whole, these findings suggest that preservation of some genetic modules of accessory genome harbored by strains from different continents in combination with great plasticity of IS and varied flow of plasmids, may be central features of the genomic structure of GC1. Competition of A144 and A155

OPEN ACCESS

Edited by:
Yuji Morita,
Meiji Pharmaceutical University, Japan

Reviewed by:
Raffaele Zarrilli,
University of Naples Federico II, Italy
Guillermo Daniel Repizo,
CONICET Instituto de Biología Molecular y Celular de Rosario (IBR), Argentina

***Correspondence:**
Daniela Centrón
dcentron@gmail.com

[†]*These authors have contributed equally to this work*

[‡]***Present address:***
Elisabet Vilacoba, División Ornitología, Museo Argentino de Ciencias Naturales "Bernardino Rivadavia", Buenos Aires, Argentina

Specialty section:
This article was submitted to Infectious Diseases, a section of the journal Frontiers in Microbiology

Received: *12 April 2019*
Accepted: *17 February 2020*
Published: *18 March 2020*

Citation:
Álvarez VE, Quiroga MP, Galán AV, Vilacoba E, Quiroga C, Ramírez MS and Centrón D (2020) Crucial Role of the Accessory Genome in the Evolutionary Trajectory of Acinetobacter baumannii Global Clone 1. Front. Microbiol. 11:342. doi: 10.3389/fmicb.2020.00342

versus A118 (ST 404/ND) without antimicrobial pressure suggested a higher ability of GC1 to grow over a clone with sporadic behavior which explains, from an ecological perspective, the global achievement of this successful pandemic clone in the hospital habitat. Together, these data suggest an essential role of still unknown properties of "mobile" and "sedentary" accessory genome that is preserved over time under different antibiotic or stress conditions.

Keywords: *A. baumannii*, international clone 1 (GC1), accessory genome, genomic plasticity, high-risk clone

INTRODUCTION

The broad diversification of species among the genus *Acinetobacter* occurred mostly due to Lateral Genetic Transfer (LGT) events, and to some allelic recombination at specific hotspots (Touchon et al., 2014; Holt et al., 2016). The size of the pangenome of *A. baumannii* has larger values than the rest of species within the genus, evidencing also a high biochemical diversity (Touchon et al., 2014; Chan et al., 2015). *A. baumannii* is well known as an opportunistic pathogen mainly implicated in ventilator-associated pneumonia, catheter-related bloodstream, urinary tract, and wound infections (Falagas et al., 2006; Peleg et al., 2008; Roca et al., 2012; Park et al., 2013; Inchai et al., 2015). This species has a highly plastic genome evidenced by the amount of insertions, deletions, inversions and SNPs reported (Peleg et al., 2008; Imperi et al., 2011; Antunes et al., 2014), which may contribute to its adaptation to several niches and the evolution to extensive (XDR) and pandrug resistance (PDR) phenotypes (Adams et al., 2008; Vallenet et al., 2008; Arduino et al., 2012; Ou et al., 2015; Holt et al., 2019), harboring a pangenome of over 9000 gene families (Antunes et al., 2011; Touchon et al., 2014).

Comparative typing of European outbreak strains of *A. baumannii* demonstrated the occurrence of three successful clones identified as "International Clones I–III" (IC1-3), or also known as Global Clones (GC) (Diancourt et al., 2010). Homologous recombination near the origin of replication was the mechanism associated with the diversification of these GC (Snitkin et al., 2013).

Global Clone 1 has been showed to have a broad international distribution in more than 30 countries from all continents (Karah et al., 2012). Regarding to the evolutionary trajectory of GC1, genomic studies showed that the most recent common ancestor emerged in the 1960s and then diverged into two phylogenetically distinct lineages (Holt et al., 2016; Hamidian et al., 2019). In the 1970s, the main lineage acquired an AbaR0-type GI where the resistance mechanisms to the older antibiotics usually are found (Holt et al., 2016). This epidemic clone has diversified into multiple successful extensively antibiotic-resistant subclones that differ in their surface structures (Holt et al., 2016). Concerning the genomic topology of GC1, four hotspots of recombination non-related to the accessory genome were identified within GC1 (Holt et al., 2016). From those, two hotspots of recombination are associated with biosynthesis of exopolysaccharides via the K locus and OC locus, the third is the gene encoding the outer membrane protein CarO, and the fourth introduces resistance to third-generation cephalosporins via the insertion sequence-enhanced expression of the intrinsic AmpC β-lactamase (Holt et al., 2016). Also, two CRISPR-Cas systems have been identified in some strains of *A. baumannii* (Di Nocera et al., 2011; Hauck et al., 2012). The AYE strain, whose genome is taken in many studies as the basis for GC1 studies (Touchon et al., 2014; Karah et al., 2015), and other *A. baumannii* clones were identified to harbor the subtype I-Fb, indicating potential inter-strain horizontal transfer of this CRISPR-Cas system (Di Nocera et al., 2011; Karah et al., 2015). Based on distinct assortment of spacers harbored by each strain, a CRISPR-based sequence type (Schouls et al., 2003) identified a subclone of *A. baumannii* GC1 that it is likely it has been originated in Iraq and spread later to the United States and Europe (Karah et al., 2015). Holt et al. (2016) reported the existence of two lineages within GC1. Lineage 1 genomes carried an AbaR0-type island with a Tn*6019*–like element inserted within the *comM* gene (Hamidian et al., 2014; Holt et al., 2016). In turn, a deletion in *intI1* defines AbaR3-type GI (Holt et al., 2016). Successive microevolution of AbaR0 and AbaR3-types includes acquisition and loss of Antimicrobial Resistance Genes (ARG), which gave rise to the different island scaffolds (Post and Hall, 2009; Post et al., 2010, 2012; Krizova et al., 2011; Nigro et al., 2011; Holt et al., 2016). Lineage 2 genomes either lack a transposon in *comM* or had acquired the transposon Tn*6022* or its variants which may lead to the formation of AbaR4 GI (Hamidian and Hall, 2011; Holt et al., 2016).

Concerning our local epidemiology, recent studies of Carbapenem Resistant *A. baumannii* (CRAB) isolates, revealed that GC1 is the most widespread and common clone of CRAB in Argentina (Rodríguez et al., 2018).

Previously, we reported the genome of A144 (CC1/CC231) and A155 (CC1/CC231) *A. baumannii* strains from Argentina which belonged to GC1 (Vilacoba et al., 2014; Arivett et al., 2015). These strains were isolated in the 1990s when carbapenems were recently introduced in Argentina (Vilacoba et al., 2014). Since at that time clonal complex CC113 was predominant (Stietz et al., 2013), A155 (CC1/CC231) was considered among the first GC1 isolates in Argentina (Ramírez et al., 2013).

The aim of this work was to examine the role of the accessory genome of the high-risk clone GC1 across time and continents from genomic and functional approaches. Although previous comparative genomic studies evidenced genetic variability across all *A. baumannii* strains (Adams et al., 2008; Vallenet et al., 2008; Di Nocera et al., 2011; Sahl et al., 2013; Touchon et al., 2014;

Holt et al., 2019; Meumann et al., 2019), no data, excluding evolution to antimicrobial resistance (Karah et al., 2017; Hamidian and Hall, 2018b; Holt et al., 2019), is focused on the features of the accessory genome of prevalent clones. Interestingly, two patterns of preservation of the accessory genome within GC1 strains regardless their site or time of isolation were found: (i) "sedentary" modules such as two novel regions of genome plasticity, the AbaR GI in lineage 1, and even a CRISPR-Cas type-If system located in the same loci; and (ii) a "mobile" module as the case of the putative prophage YMC/09/02/B1251_ABA_BP shared by all 106 GC1 genomes which showed high genomic plasticity evidenced by intrinsic microevolution as well as mobility to different insertion sites amongst GC1's chromosomes. Because AbaR GI is widespread among *A. baumannii* clinical samples, particularly in GC1, this GI was used as a biological model for comparative genomics and experimental studies of maintenance. We found that AbaR0-type GI from A144 (CC1/CC231) as well as in A155 (CC1/CC231) was maintained at least over one month in three independent experiments without antimicrobial pressure, while *in silico* analysis revealed AbaR0-type GI were all different including AbaR0-type GI from A144 (CC1/CC231) which showed signs of microevolution events compared to A155 (CC1/CC231). On the other hand, a Type VI Secretion System (T6SS) and three efflux pumps showed to be subjected to deep processes of genomic loss in *A. baumannii* but not in GC1. As a whole, these studies highlighted that the conservation of genetic elements of the accessory genome may play a still unknown role in the success of this high-risk clone.

MATERIALS AND METHODS

Bacterial Strains Used for Experimental Assays

The multidrug resistant GC1 *A. baumannii* A144 and A155 strains (CC1/CC231), and A118 (ST 404/ND) which belongs to an sporadic clone were isolated from the same hospital H1 from Argentina in 1997 (Vilacoba et al., 2014), 1994 (Arivett et al., 2015), and 1995 (Traglia et al., 2014), respectively. These strains that were available in our laboratory were used to perform experimental investigation concerning maintenance of accessory genome along time as well as clone competition assays (see below).

Previous DNA Sequencing of H1 Strains

Strains from H1 Hospital from Argentina, *A. baumannii* A144 and A155 (CC1/CC231), and the sporadic clone A118 (ST 404/ND) that were the basis of this study, were previously sequenced (Traglia et al., 2014; Vilacoba et al., 2014; Arivett et al., 2015). Briefly, Whole-Genome Shotgun (WGS) sequencing was performed using Illumina MiSeq-I, using Nextera XT libraries for sample preparation. Reads were assembled with Ray assembler[1]. The draft genome sequence of A144 (CC1/CC231) consist of 92 contigs (length > 500 bp), a total sequence of 4,312,914 bp with an N_{50} contig size of 89,819. The GC% average was 39.2. Using RAST (Aziz et al., 2008) we identified 4,151 possible ORFs, 74 copies of 16S-23S-5S rRNA operons and 69 tRNA genes (Vilacoba et al., 2014). The WGS project has been deposited at DDBJ/EMBL/GenBank under the Accession Number (AN) JQSF00000000. The *de novo* assembly of A155 (CC1/CC231) resulted in a 3,933,455 bp genome encoding 55 tRNAs and 3,760 genes with 3,704 proposed CDSs (Arivett et al., 2015). The first version of the *de novo* whole-genome assembly of A155 (CC1/CC231) was deposited into GenBank under Bioproject ID PRJNA261239 with the accession number JXSV00000000, version JXSV01000000 with 53 contigs (Arivett et al., 2015). The draft genome of A118 (ST 404/ND) (AN: AEOW00000000) consist of 156 scaffolds with a total length of 3,730,023 bp (Ramirez et al., 2011). The genome has an average GC content of 38.4%, 88 tRNA genes and 3,520 coding sequences were identified, of which 93.64% was annotated and manually curated using blastn results (Traglia et al., 2014).

Data Collections for Comparative Genomics

In order to perform accurate comparative genomics in combination with experimental assays, we identified four groups of genomes that were clustered to do our analysis (see below).

Global Clone 1 Group 1 (CC1/CC231) was composed by 18 genomes as follows: (i) A144 and A155 from Argentina (Vilacoba et al., 2014; Arivett et al., 2015); (ii) 14 GC1 complete genomes retrieved from GenBank which correspond to strains AYE (AN: NC_010410.1), D36 (AN: CP012952.1), A1 (AN: CP010781.1), AB307-0294 (AN: CP001172.2), AB5075-UW (AN: CP008706.1), AB0057 (AN: CP001182.1), USA15 (AN: NZ_CP020595.1), A85 (AN: NZ_CP021782.1), A388 (AN: NZ_CP024418.1), AR_0083 (AN: NZ_CP027528.1), DA33382 (AN: NZ_CP030106.1), 9102 (AN: NZ_CP023029.1), 11W359501 (AN: CP041035.1), NCTC13421 (AN: NZ_LS483472.1); and (iii) two highly quality genomes available for GC1, strains NIPH 527 and NIPH 290, isolated in 1984 and 1994, respectively (APQW00000000.1 and APRD00000000.1) (**Table 1**). Both GC1 strains, A144 and A155, were relevant for our country since they were isolated in the 1990s when at that time clonal complex CC113 was predominant (Stietz et al., 2013). Therefore, A155 was considered among the first GC1 isolates emerging in Argentina (Ramírez et al., 2013) which is in agreement with the introduction of carbapenems in our country (Vilacoba et al., 2014). This GC1 Group 1 of genomes include all GC1 complete genomes till July, 2019 and they were used to perform the comparative genomics for RGP, prophages, plasmids, CRISPR-Cas system, Insertion Sequences (IS), Transposons, AbaR-types GI, and genes encoding AdeABC, AdeIJK, and AdeFGH efflux pumps, among others. The site of insertion of RGP, prophages, CRISPR-Cas system, IS and AbaR-types GI, were identified for this group, since most of these are complete genomes and allow accurate identification.

Global Clone 1 Group 2 (CC1/CC231) was composed by 27 genomes as scaffolds and 61 genomes as contigs from GenBank

[1]http://denovoassembler.sourceforge.net

TABLE 1 | General features of GC1 Group 1 and Outgroup Group 3 genomes.

Group	Strain	Country	Year	MLST[a]	GC	GC1 lineage	AbaR type	*intI1* in AbaR	CRISPR
GC1 Group 1	A144	Argentina	1997	CC1/CC231	1	1	AbaR0-type	Complete	Yes
	A155	Argentina	1994	CC1/CC231	1	1	AbaR0-type	Complete	Yes
	A1	United Kingdom	1982	CC1/CC231	1	1	AbaR24	Complete	Yes
	AB307-0294	United States	1997	CC1/CC231	1	1	–	–	Yes
	AYE	France	2001	CC1/CC231	1	1	AbaR1	Complete	Yes
	AB0057	United States	2004	CC1/CC231	1	1	AbaR3	Deleted	Yes
	AB5075-UW	United States	2008	CC1/CC231	1	1	AbaR11	–	Yes
	D36	Australia	2008	CC1/CC231	1	2	AbaR4	–	Yes
	USA15	South Korea	2013	CC1/CC231	1	1	AbaR10	–	Yes
	A85	Australia	2003	CC1/CC231	1	1	AbaR3	Complete	Yes
	A388	Greece	2002	CC1/CC231	1	1	AbaR28	Complete	Yes
	AR_0083	United States	Unknown	CC1/CC231	1	1	AbaR0-type	Complete	Yes
	DA33382	Germany	Unknown	CC1/CC231	1	1	AbaR0-type	Complete	Yes
	9102	Mexico	2010	CC1/CC231	1	1	–	–	Yes
	11W359501	United Kingdom	2015	CC1/CC231	1	1	AbaR0-type	Complete	Yes
	NCTC13421	United Kingdom	2004	CC1/CC231	1	1	AbaR0-type	Complete	Yes
	NIPH 527	Netherlands	1984	CC1/CC231	1	1	AbaR21	Complete	Yes
	NIPH 290	Czechia	1994	CC1/CC231	1	1	AbaR0-type	Complete	Yes
Outgroup Group 3	ACICU	Italy	2005	CC2/CC208	2	–	AbaR2	Complete	No
	Naval-13	United States	2006	ST3/CC928	3	–	AbaR4	–	No
	A118	Argentina	1995	ST404/*	–	–	–	–	No
	AB33405	Argentina	2013	CC79/CC113	–	–	AbaR4	–	No
	ATCC 17978	United States	1951	ST437/ST112	–	–	AbaR4	–	No

[a]*Pasteur's/Oxford's MLST schemes; Clonal complexes (CCs) are numbered according to the most prevalent clone. STs are indicated when singletons. *The sequence type (ST) was not found in Oxford's MLST database.*

(until July, 2019) that were identified as GC1 using the program mlst[2] which scans genome files against traditional PubMLST typing schemes (**Supplementary Table 1**). The 88 genomes of this GC1 Group 2 were used for searching RGP, genes encoding AdeABC, AdeIJK, and AdeFGH efflux pumps, CRISPR-Cas system as well as identification of K and OC locus in combination with GC1 Group 1.

In summary, all GC1 genomes deposited in GenBank till July, 2019 were included in our analysis.

In order to identify exclusive accessory genome of GC1, we clustered in the Outgroup Group 3 five genomes belonging to other high-risk epidemic clones such as ACICU (AN: CP000863.1) as representative of GC2, Naval-13 (AN: AMDR01000001.1) as representative of GC3, AB33405 (NZ_JPXZ00000000.1;[3]) as representative of local epidemic clone CC113 and both ATCC 17978 (AN: CP018664.1), and A118 (AN: AEOW01000000) as sporadic clones (**Table 1**).

The Outgroup Group 4 was composed by 2407 genomes as contigs and 549 genomes as scaffolds of *A. baumannii* that were identified as non-GC1 using the program mlst[2] (**Supplementary Table 1**). The 2956 genomes of this group were downloaded from GenBank (until August, 2019). The Outgroup Group 4 was used to analyze if the CRISPR-Cas system identified in GC1 Group 1 and 2 was also present in this group.

[2]https://github.com/tseemann/mlst#mlst

[3]http://www.higiene.edu.uy/ddbp/Andres/gtraglia_et_al_2018b_data.html

Antibiotic Susceptibility Assays

Disk diffusion antibiotic susceptibility and/or minimal inhibitory concentration tests were performed following the procedures recommended by the CLSI (CLSI, 2018) with antimicrobial commercial disks of ampicillin-sulbactam, sulbactam, ceftazidime, cefepime, cefotaxime, imipenem, meropenem, colistin, gentamicin, amikacin, minocycline, tetracycline, ciprofloxacin, levofloxacin, trimethoprim-sulfamethoxazole, rifampin, and chloramphenicol from Britania (**Table 2**). When clinical breakpoints were not available from CLSI, only the values obtained were shown. For sulbactam we used a provisional susceptibility breakpoint of $\leq$4 μg/ml derived from the CLSI breakpoint for ampicillin/sulbactam ($\leq$8/4 μg/ml; Krizova et al., 2013).

Comparison of AbaR Genomic Islands

Software ACT was used to compare AbaR islands (Carver et al., 2005).

Phylogenetic Analysis

The core genome of the 18 genomes from GC1 Group 1 was calculated with GET_HOMOLOGUES software (Contreras-Moreira and Vinuesa, 2013). Core genome SNPs were detected using SNP-sites (Keane et al., 2016). SNP likely to have been introduced together via a homologous recombination event were detected and analyzed using Gubbins with default parameters (Croucher et al., 2015). Phylogenetic tree was built using Gubbins

TABLE 2 | Antimicrobial susceptibility profiles of strains under study.

Strain	Susceptibility profiles Disk diffusion (mm)/MIC (μg/ml)																
	AMS	SUL	CAZ	FEP	CTX	IPM	MEM	CL	GEN	AMK	MIN	TET	CIP	LEV	SXT	RIF	CHL
A144	R	–/16	R/32	I	R/ ≥ 64	S	S/2	–/S < 2	R/ ≥ 16	S/16	S	R	R/32	R	R	(12)/4	–/8
A155	R	–/16	R/32	I	R/ ≥ 64	S	S/2	–/S < 2	R/ ≥ 16	S/16	S	R	R/32	R	R	(16)/4	–/8
A118	–	–/4	–	–	–	S	S/1	–	S/ ≤ 2	S	–	–	S	S	–	4	–
ATCC 17978	–	–/2	–	–	–	–	–	–	–	–	–	–	–	–	–	8	–

AMS, ampicillin-sulbactam; SUL, sulbactam; CAZ, ceftazidime; FEP, cefepime; CTX, cefotaxime; IPM, imipenem; MEM, meropenem; CL, colistin; GEN, gentamicin; AMK, amikacin; MIN, minocycline; TET, tetracycline; CIP, ciprofloxacin; LEV, levofloxacin; SXT, trimethoprim-sulfamethoxazole; RIF, rifampicin; CHL, chloramphenicol; R, resistant; I, intermediate; S, susceptible. –, not determined. In the absence of CLSI 2018 interpretive breakpoint, the zone diameters are shown.

based on the alignment of the non-recombinant SNP obtained and using a maximum-likelihood (ML) phylogeny inferred from the alignment of these SNP. The five genomes from Outgroup Group 3 were used as outgroup. The figure of the phylogenetic tree was obtained using Evolview v3 (Subramanian et al., 2019).

Maintenance Studies of the AbaR Genomic Islands

Strains A144 and A155 were grown each at 37°C overnight in 2 ml LB broth. Subcultures were carried out for 30 days (Moffatt et al., 2010). At 1st, 7th, and 30th day, 30 colonies were tested for presence of AbaR GI by PCR using two pairs of specific primers that detect the disruption of the gene *comM*, which target the junction with the 3′ATPase (4R: 5′-AATCGATGCGGTCGAGTAAC-3′ and 4F: 5′-TATCAGCAGCAAAACGATGG-3′) and the junction with the 5′ATPase (2R: 5′-TTGGGGATTCTGTCCGTAAG-3′ and 2F: 5′-TCCATTTTACCGCCACTTTC-3′) (Shaikh et al., 2009; Ramírez et al., 2013). The experiments were performed in triplicates.

In vitro Competition and Fitness Measurements

A144 or A155 and A118 isolates were diluted to 1.6×10^8 (OD_{600} 0.2) colony-forming units (CFU)/ml, equal volumes were combined, thus the initial ratio of the isolate pairs was close to 1:1, then 10 μl of the mixture was added to 20 ml LB broth and grown at 37°C with agitation at 200 rpm. At 24-h intervals, 10 μl of bacterial subcultures were transferred to fresh LB broth; meanwhile, 10 μl was inoculated on MH agar plates, and 10 μl on MH agar plates containing 16 μg/ml gentamicin. CFU of A144 (resistant to gentamicin, **Table 2**) and A118 (susceptible to gentamicin, **Table 2**) were counted, and after 96 h, adaptive difference of each pair (A144/A118) was calculated as $S = \ln\left[\left(\frac{\frac{r_t}{s_t}}{\frac{r_{t-1}}{s_{t-1}}}\right)^{\left(\frac{1}{y}\right)}\right]$ relative adaptive fitness as $F = 1 + S$, and the fitness cost as $C = (1 - F)\,x100\%$, where S is the selection coefficient and show the difference in fitness between two competing strains at time t, r_t = number of drug-resistant colonies and s_t = number of drug-susceptible colonies, r_{t-1} and s_{t-1} are the number of drug-resistant and drug-susceptible colonies at the preceding time point, respectively, and the quotient of the ratios of the cell numbers was standardized with 1/y, where "y" is the number of bacterial generations during the assay (Sander et al., 2002; Guo et al., 2012; Li et al., 2018). Here the exponent was 1/8 because cell numbers were determined every eight generations. The terms *rt*/*rt*_1 and *st*/*st*_1 give the growth rates for drug-resistant and drug-susceptible strains, respectively. Hence, *S* is the natural logarithm of the quotient of the growth rates of the competing strains. *S* is positive if resistance increases bacterial fitness compared to that of the drug-susceptible competitor strain (Sander et al., 2002).

Statistical Analysis

Statistical analysis was performed with the software GraphPad Prism version 8 using one-way analysis of variance (ANOVA). $P < 0.05$ was considered to be statistically significant (Li et al., 2018).

Detection of Regions of Genomic Plasticity

As defined by Mathee et al. (2008) the minimum size of a region of genomic plasticity (RGP) is defined as a block of at least four contiguous ORFs that are not conserved in all strains from a species. RGP were identified in GC1 Group 1 using RAST (Aziz et al., 2008), in combination with Prokka (Seemann, 2014), ISFinder (Siguier, 2006), PHASTER (Arndt et al., 2016), and IslandViewer4 (Bertelli et al., 2017).

Mobilome and Resistome Analysis

Search of IS and transposons was done using ISFinder (Siguier, 2006) and blastn (Altschul et al., 1990) with a cut-off *E*-value of E^{-10}; genomic islands were predicted with IslandViewer4 (Bertelli et al., 2017) and phages with PHASTER (Arndt et al., 2016). ARG were identified using RESfinder (Zankari et al., 2012) and blastn (Altschul et al., 1990) with a cut-off *E*-value of E^{-10}. The ARG content previously reported was also included, when required (Holt et al., 2016). BM4587 (AN: KR297239.1) was taken as reference to compare the 7,591 bp comprising the *adeL*, *adeF*, *adeG*, and *adeH* genes of the *adeFGH* efflux pump and its regulator with a wild type expression level (Coyne et al., 2010). The *bla*OXA-51-like genes were identified by Single-Locus-Sequence-Based Typing (SBT) analyzing 825 bp (forward primer,

5′-ATGAACATTAAAGCACTCTTAC-3′; reverse primer, 5′-CTATAAAATACCTAATTGTTCT-3′) by blastn (Pournaras et al., 2014). The *ampC* alleles were assigned using the database hosted at the pubmlst platform for *A. baumannii*[4] (Karah et al., 2017). The bla_{TEM} promoters were identified by blastn (Lartigue et al., 2002). Mutations in *rpoB* were analyzed by the comparison of the nucleotide sequences with the deduced amino acid sequence of *rpoB* from *Escherichia coli* strain ATCC 8739 (ACA79637.1) and ACICU (YP_001844962.1) using blastn (Giannouli et al., 2012). To determine the Quinolone Resistance-Determining Regions (QRDR), the wild-type *A. baumannii* GyrA (X82165) and ParC (X95819), QRDR GyrA81, ParC84, and ParC88 were compared with those of *E. coli* at positions Ser-83, Ser-84, and Glu-88, respectively (Ostrer et al., 2019).

Pangenome Calculation

The pangenome, the soft-core genome, and the core genome were identified using the GET_HOMOLOGUES software (Contreras-Moreira and Vinuesa, 2013) based on the GC1, GC2, GC3, CC113, and sporadic clones genomes analyzed using a minimal identity value of 70% and a minimal query coverage of 80% sequence identity in blastn query/subject pairs.

Plasmid Recognition

Genes related to plasmids were identified mapping the A144 and A155 contigs using the AYE strain genome as reference (AN: CU459141.1) with MAUVE version 2.4.0 (Darling et al., 2004). Contigs not mapping with AYE genome where blasted against the non-redundant (nr) GenBank database with a cut-off *E*-value of E^{-10} and analyzed for plasmid replicons.

Detection of Recombination Hotspots

Recombination hotspots (HS) are regions in a genome that exhibit elevated rates of recombination relative to a neutral expectation. Hotspots in the present study are associated with both an increase in mutations in a region of the genome and incorporation of accessory DNA. HS were identified using the same methodology as in Touchon et al., 2014. The GC1 Group 1 core genome was used to identify and locate large integration/deletion (indel) regions. All regions including more than ten genes between two consecutive core genes of the genomes were considered as large indel regions. The relative positions of these regions were defined by the order of the core genes in *A. baumannii* AYE. This strain was used as a reference to assemble the GC1 Group 1 genes.

Identification of K and OC Loci

The exopolysaccharide loci were identified by blastn search for the flanking genes (K: *fkpA*, *lldP*; OC: *ilvE*, *aspS*) as described previously (Holt et al., 2016). Each locus was matched against a set of known K loci or OC loci (Kenyon and Hall, 2013; Holt et al., 2016).

[4]http://pubmlst.org/abaumannii/

CRISPR-Cas System Predictions

CRISPR were predicted using CRISPRfinder[5] and CRISPRone[6] using the default parameters.

RESULTS

Genomic Analysis of GC1 Strains From H1 Hospital

Comparative genomics was carried out for A144 and A155 strains from H1 Hospital with all GC1 Group 1 which were isolated from four different continents (America, Oceania, Asia and Europe) and with other epidemic and sporadic clones of the Outgroup Group 3 genomes (**Table 1**). We found that A144 genome has 99% Average Nucleotide Identity (ANI) with A155 isolated from the same hospital. Both A144 and A155 have 97% ANI with GC1 Group 1 strains (**Table 1**). A144 and A155 exhibited 81% ANI with ACICU (IC2), 83% with Naval-13 (IC3), and 79% with AB33405 (GC113), A118 (sporadic clone), and also with ATCC 17978 (sporadic clone) of Outgroup Group 3 (**Table 1**).

We found that 2,840 genes were part of the core genome comprising the 18 GC1 complete genomes under scrutiny. The phylogenetic tree obtained with the non-recombinant SNPs found in the core genes of the GC1 Group 1 genomes reflected the two lineages previously reported (Holt et al., 2016), evidencing that A144 and A155 genomes belonged to lineage 1 and they were closely related to the strain AYE (**Figure 1**).

A difference of one order of magnitude was found when analyzing the number of unique genes within the chromosomes of GC1 (from 15 to 74 unique genes) when compared to GC2, GC3, CC113, and sporadic clones (from 362 to 626 unique genes). A144 contained 37 unique genes when we compared its chromosome with GC1 Group 1 (**Supplementary Table 2**); most of them were coding sequences of unknown function. Only ten unique genes out of 37 had an assigned function, such as two phage-related proteins, a copper resistance system oxidase (*copA*), a zinc transporter (*zitB*), a cobalt transporter (*czcD*), and two transcriptional regulatory proteins (*qseB_2* and *qseB_3*) that probably belong to a novel heavy metal resistance GI (Data not shown). A155 contained sixteen unique genes not related to pathogenicity or antimicrobial resistance (**Supplementary Table 2**). The emergence of *aac(6′)-Ian* gene cassette was found unique in AYE strain [94.13% *aac(6′)-Ian* allele (CP023420.1)].

The GC1 Group 1 possessed 39 unique genes compared to Outgroup Group 3 that most of them were scattered in the topology of the chromosome (**Supplementary Table 2**). For example the array of the 6 *cas* genes (*cas1-cas3-cas8f-cas5f-cas7f-cas6f*) from the type IF-b CRISPR-Cas system that we found in all GC1 genomes (GC1 Group 1 and 2) located in the same loci in GC1 Group 1, a LysR_substrate_binding domain related to LysR family of transcriptional regulators (ABAYE2346) that have been identified that regulate a diverse set of genes, including those involved in virulence, metabolism, quorum sensing and motility (Maddocks and Oyston, 2008), three genes related to the lipid

[5]http://crispr.i2bc.paris-saclay.fr/Server/

[6]http://omics.informatics.indiana.edu/CRISPRone/

metabolic process [coenzyme A (CoA) transferase (ABAYE2345), acyl-CoA desaturase (ABAYE1343), and hydroxymethylglutaryl CoA reductase (ABAYE2344)] among other genes that coded for transferases, reductases, hydrolases and hypothetical proteins (**Supplementary Table 2**).

Otherwise, we found that the Outgroup Group 3 ACICU, A118, Naval-13, AB33405, and ATCC 17978 chromosomes had 358, 595, 412, 311, and 395 unique genes, respectively, when we compared them with the pangenome of the GC1 Group 1, most of them coding sequences of unknown function. The smaller number of unique genes in GC1 could be related to the need of balance among new genes putatively acquired by events of the LGT and the genes of the core genome that may be necessary to preserve synteny and/or functionality. Interestingly, in the case of ATCC 17978, the previously described Tn*6171* transposon of 49.9 kb length carrying a potential siderophore synthesis gene cluster and transposition genes related to Tn*7* (Hamidian et al., 2015) without the typical invasion of a class 2 integron (Ramírez et al., 2010) was found amongst the unique genes, evidencing its independent acquisition by LGT events.

Comparative analysis between A144 and A155 chromosomes revealed as expected that they had high degree of synteny between them (**Supplementary Figure 1**). Besides, a high degree of synteny among all GC1 Group 1 genomes was found including D36, which belongs to another lineage within GC1 epidemic clone (**Supplementary Figure 1**). Four regions related to hotspots (HS) (see below) disrupted synteny among GC1 chromosomes; at loci ABAYE1410 to ABAYE1438, ABAYE2053 to ABAYE2054, ABAYE2822 to ABAYE3048 and ABAYE3550 to ABAYE3552 in AYE genome; these regions also showed signs of microevolution identified as Regions of Genomic Plasticity (RGP) RGP2/HS8, RGP3/HS12, RGP5 and RGP6 with HS15 and HS16, and RGP7/HS18 that corresponded to AbaR genomic island, respectively (**Figure 2**) (see below).

Comparative Analysis of the Resistome of GC1 Genomes

The resistome analysis was carried out in detail for A144 and A155 strains compared with GC1 Group 1 and with the epidemic and sporadic clones of the Outgroup Group 3 genomes (**Figure 1**, **Table 1**, and **Supplementary Table 3**). We found that A144 and A155 showed a multidrug resistant phenotype as defined by Magiorakos et al. (2012) that was in concordance with the findings of antimicrobial resistance determinants by bioinformatics tools (**Table 2**, and **Supplementary Table 3**).

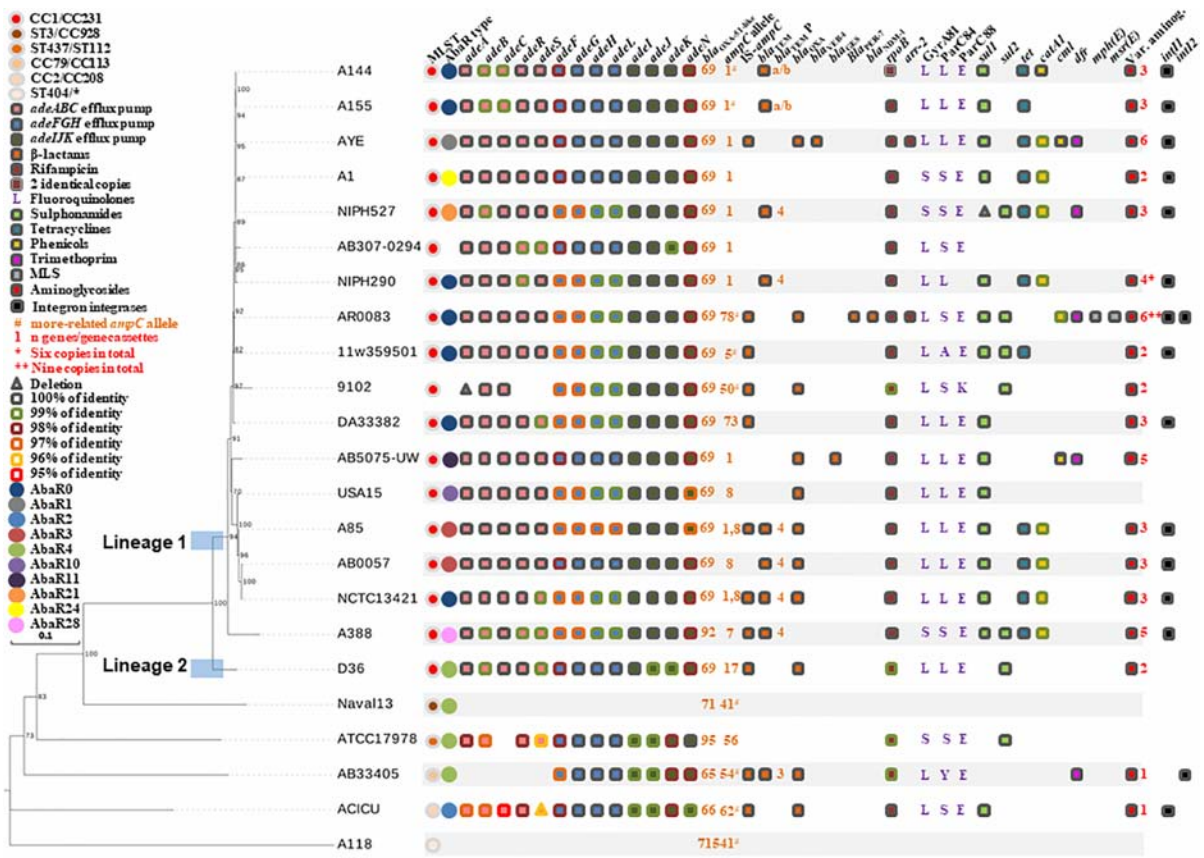

FIGURE 1 | Molecular phylogenetic analysis and antimicrobial resistance determinants of GC1 Group 1 and Outgroup Group 3. The evolutionary history was inferred by using the Maximum Likelihood method based on the General Time Reversible model. The inset legend indicates the genetic determinants highlighted. When required, blastn was used with a cut-off *E*-value of E^{-10}.

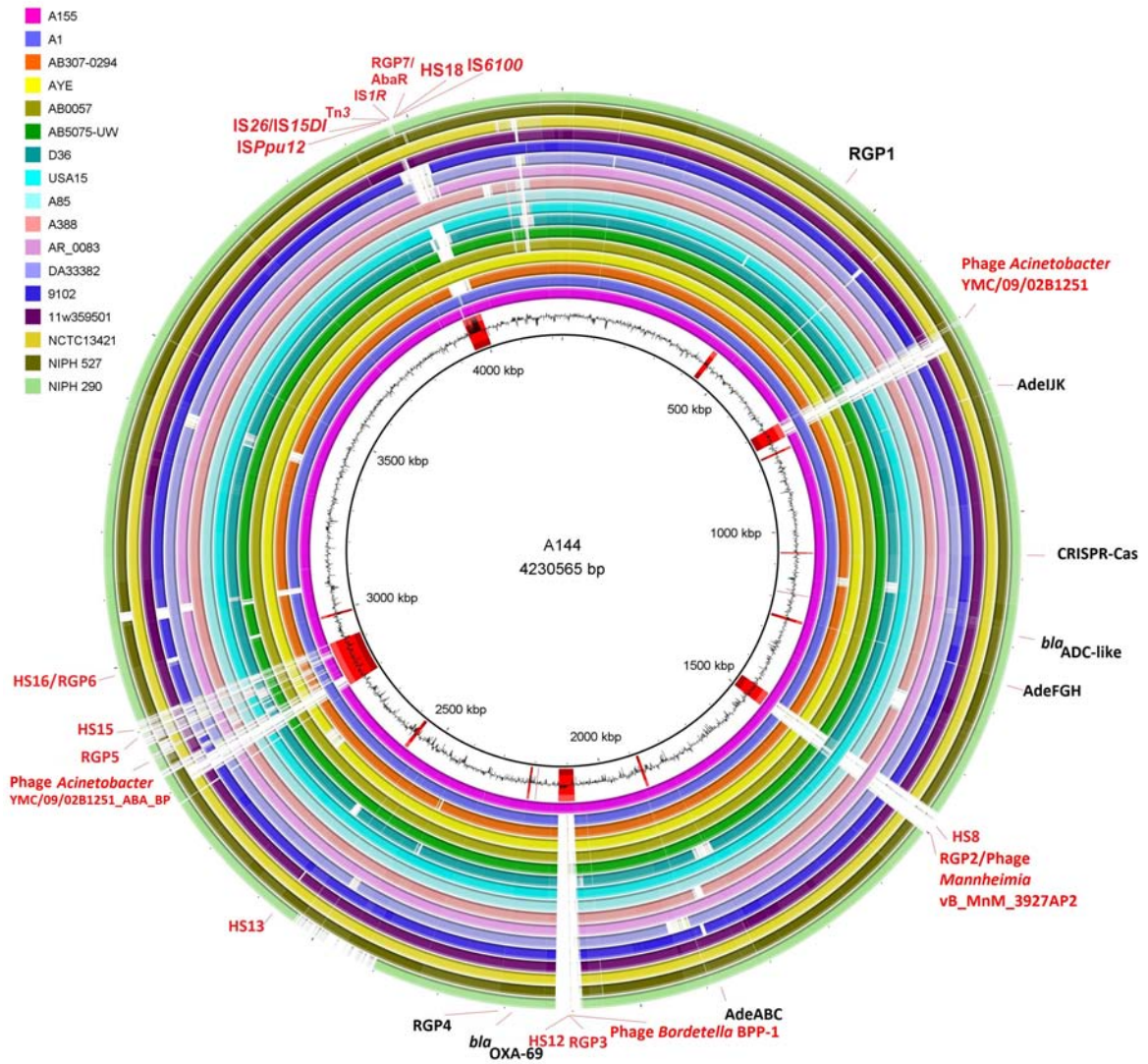

FIGURE 2 | Prediction of elements of the accessory genomes identified in GC1 Group 1 genomes from this study. Genetic and physical map of GC1 chromosomes. The inner black circle belongs to A144 chromosome and the inset legend indicates the remaining GC1 Group1 chromosomes. The outer legend corresponds to RGP, *bla* genes, the three efflux pumps and CRIPSR/Cas found in the eighteen GC1 Group 1 genomes in the same loci, indicated with black letters and lines is also shown in the outer circle. The hot spots (HS), RGP, and prophages found in A144 are shown in red letters and lines. Black histogram represents CG content of A144 strain. Regions related to some hotspots (HS) disrupted synteny among GC1 chromosomes which also corresponded to RGP in A144 as follows, RGP2/HS8 (JQSF01000083.1: 1-33700 and JQSF01000082.1: 24920-27366), RGP3/HS12 (JQSF01000043.1: 1 -38248 and JQSF01000071.1: 12398-14538), RGP5/HS15 together with RGP6/HS16 (JQSF01000080.1: 153-15902, JQSF01000022.1, JQSF01000055.1, JQSF01000037.1, JQSF01000003.1, QSF01000040.1, JQSF01000042.1, JQSF01000065.1 and JQSF01000041.1: 1-20291), and RGP7/HS18 that corresponded to AbaR GI (JQSF01000053.1: 1-8092, JQSF01000058.1, JQSF01000063.1: 797-1612, JQSF01000054.1: 253-2358, JQSF01000030.1: 448-21672, and JQSF01000084.1: 23-13490).

Both strains harbored almost the same ARG usually associated with the core genome (i.e., $bla_{\mathrm{OXA-51-like}}$ and *ampC*) as well as those acquired by LGT events, but A144 had two copies instead of one of the rifampicin resistance *rpoB* gene as well as for the tetracycline resistance *tet*(A) gene, and one copy of the chloramphenicol resistance *catA1* gene (**Supplementary Table 3**). The only phenotypic difference related to the presence of these extra genes was a reduced zone diameter for rifampicin in A144 but maintaining the same low MIC (**Table 2**). Neither A144 nor A155 showed acquired ARG for colistin, fluoroquinolones, trimethoprim, fosfomycin, fusidic acid, glycopeptides, nor rifampicin (**Supplementary Table 3**).

In regard to the β-lactams resistance genes, the naturally harbored $bla_{\mathrm{OXA-51-like}}$ and *ampC* alleles identified in the GC1 Group 1 genomes were different from those found in the other clones from Outgroup Group 3 (**Supplementary Table 3**). The $bla_{\mathrm{OXA-69}}$ allele (AY458016) was conserved in 17/18 GC1 Group 1 genomes and the remaining strain A388 contained $bla_{\mathrm{OXA-92}}$ (WP_059262713.1), in agreement with previous finding of Pournaras et al. (2014). In AYE, $bla_{\mathrm{OXA-69}}$ was downstream of

IS*Aba1*, which was related to increase β-lactam resistance (Chen et al., 2010). It was not the case for A144 nor A155 which could be in part related to their susceptibility to carbapemens. Analysis of *ampC* showed that A144 and A155 harbored a same novel allele with no IS upstream. A wide variety of *ampC* alleles were in the GC1 Group 1 (mostly alleles 1 and 8) and Outgroup Group 3. The IS*Aba1* and IS*Aba125* were upstream of *ampC* in both groups, with no apparent preference for any allele (**Supplementary Table 3**).

We found four bla_{TEM} alleles in 8/18 GC1 Group 1 genomes and only one $bla_{\mathrm{TEM-1-like}}$ allele with the P3 promoter in the Outgroup Group 3. We identified that A144 and A155 are resistant to sulbactam and harbored $bla_{\mathrm{TEM-1}}$ with the Pa/Pb promoters (**Table 2**, and **Supplementary Table 3**), which had been shown to exhibit higher strength when compared to P3 (Lartigue et al., 2002; Krizova et al., 2013). Our results suggest that $bla_{\mathrm{TEM-1}}$ in A144 and A155 with the Pa/Pb promoters could be involved in the increase of the sulbactam MIC (**Table 2**). The other three different alleles in GC1 Group 1 genomes were $bla_{\mathrm{TEM-19-like}}$ with P3, which is the weakest promoter and was related to sulbactam susceptibility (Lartigue et al., 2002; Krizova et al., 2013). The other β-lactams resistance genes that we detected in GC1 Group 1 genomes were $bla_{\mathrm{OXA-10}}$ (1/18), $bla_{\mathrm{OXA-23}}$ (7/18), $bla_{\mathrm{OXA-235}}$ (1/18 with 5 copies), $bla_{\mathrm{VEB-1}}$ (1/18), bla_{GES} (1/18), $bla_{\mathrm{PER-7}}$ (1/18), and $bla_{\mathrm{NDM-1}}$ (1/18). Of those, we also found $bla_{\mathrm{OXA-23}}$ in Outgroup Group 3.

Regarding rifampicin resistance genes, we detected the acquired ARG *arr-2* in two (2/18) GC1 Group 1 genomes and it was absent in Outgroup Group 3 (**Supplementary Table 3**). A144 was the only strain studied that harbored two copies of the most common *rpoB* allele (Giannouli et al., 2012). Two other GC1 Group 1 genomes and two from Outgroup Group 3 had different alleles of *rpoB* (**Supplementary Table 3**). Concerning the fluoroquinolone resistance, we found that the Plasmid Mediated Quinolone Resistance genes (PMQR) were absent in the GC1 Group 1 genomes and the Outgroup Group 3. Noteworthy, we detected the mutations in the QRDR of *gyrA* and *parC* enough to predict fluoroquinolone resistance (Ostrer et al., 2019), specifically for ciprofloxacin resistance (GyrA81) in 15 (15/18) and for ciprofloxacin plus levofloxacin (GyrA81-ParC84) in A144 and A155 together with others (11/18) in GC1 Group 1, but only in two and one genomes of Outgroup Group 3 (**Supplementary Table 3**).

The acquired aminoglycoside resistance genes that we identified in A144 and A155 were the *aac(6′)-Ib3* gene cassette located in a class 1 integron within the AbaR GI, and Δ*aac(3)-IIa* and *aph(3′)-Ia* located in transposons (Vliegenthart et al., 1989; Arduino et al., 2012) (AN: X60321, X51534, X62115, respectively; **Supplementary Table 3**). The respective Δ*aac(3)-IIa* genes from A144 and A155 lacked the last 59 bp of the 3′ end of the gene, and they were adjacent to $bla_{\mathrm{TEM-1}}$ surrounded by IS*26* as previously described in plasmid pAB35063_a (MK323042.1) (**Supplementary Table 4**). In total, 14 (14/18) GC1 Group 1 genomes and two in Outgroup Group 3 showed at least one acquired aminoglycoside resistance gene (**Supplementary Table 3**). A deeper analysis of *aph(3′)-Ia* revealed that the same variant surrounded by IS*26* and IS*15DI* was also found in AYE, AB0057, A85, A388, AR_0083, DA33382, NCTC 13421 and NIPH527 GC1 Group 1 genomes at the same locus in A144 and A155 genomes.

Regarding sulfonamide resistance, we detected *sul1* in 15 (15/18) and *sul2* in 4/18 GC1 Group 1 genomes (**Supplementary Table 3**). In A144 and A155, *sul1* was within a class 1 integron.

The tetracycline resistance genes *tet*(A) (11/18) and *tet*(G) (1/18) were identified only in GC1 Group 1 genomes.

The phenicol resistance gene *catA1* was found in eight GC1 Group genomes with 99.85% of identity compared to the one identified in A144 (**Supplementary Table 3**).

The *cmlA*, *dfr* and genes related to macrolides, lincosamides and streptogramines resistance (MLS), the *mph(E)* and *msr(E)* genes were found in some GC1 Group 1 and Outgroup Group 3 while they were not detected in A144 nor in A155 (**Supplementary Table 3**).

Moreover, the presence of class 1 and class 2 integrons was analyzed. The *intI1* gene was identified in 13 out of 18 GC1 Group 1 genomes and in a total of 56 from the 106 genomes of GC1 Groups 1 and 2 (**Figure 1**, and **Supplementary Tables 3, 5**). The *intI2* gene was found in seven out of the 106 genomes of GC1 Groups 1 and 2, of which only strain AR_0083 was from GC1 Group 1 (**Figure 1**, and **Supplementary Tables 3, 5**).

The relevance of three resistance-nodulation-cell division-type efflux pumps (AdeABC, AdeIJK, and AdeFGH; **Figure 3**) in antimicrobial resistance in *A. baumannii* has been highlighted (Marchand et al., 2004; Fournier et al., 2006; Coyne et al., 2010, 2011; Rosenfeld et al., 2012). Here, we investigated their variability in GC1. We found that A144 and A155 shared the same alleles for the three efflux pumps and that all GC1 Group 1 and Group 2 genomes contained these three efflux pumps with different levels of identity for each gene (**Figure 1**, and **Supplementary Tables 3, 6**). The complete AdeABC efflux pump genetic structure includes the *adeA*, *adeB*, *adeC* and their regulatory genes, which encode the two-component system

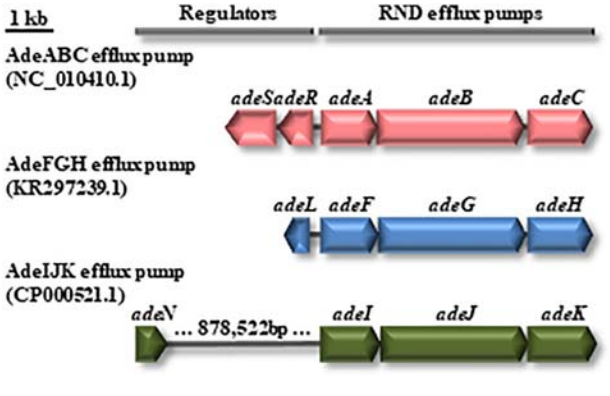

FIGURE 3 | Genetic organization of the AdeFGH, AdeFGH and AdeIJK RND efflux pumps and their regulatory genes. Reference sequences: *adeABC* and *adeRS*, NC_010410.1 (coordinates 1883328-1891105); *adeFGH* and *adeL*, KR297239.1; *adeIJK* and *adeN*, CP000521.1 (coordinates 3171871-3177761 to 2292697-2293350).

AdeRS (*adeR* and *adeS*) (Coyne et al., 2010). None of the *adeR* or *adeS* alleles exhibited the T153M or P116L mutations previously associated with an MDR phenotype in the 106 GC1 genomes (Marchand et al., 2004; Fournier et al., 2006). The *adeABC* and *adeRS* genes were surrounded by ABAYE1818 and ABAYE1824 which encoded hypothetical proteins in AYE. This genetic context was in 17 out of the 18 GC1 Group 1 genomes, except in strain 9102, where ABAYE1818 was also lost together with part of the efflux pump genes described above. Apart from the difference in this last strain, the other GC1 Group 1 genomes contained these genes in the same location as a module; in the case of D36 invasion of IS*Aba1* was identified between *adeR* and *adeA* suggesting a recent acquisition. Interestingly, from the Outgroup Group 4 comprising 2956 non-GC1 draft genomes, *adeC* was absent in 615 draft genomes; even 64 draft genomes lacked the complete *adeABCRS* genes (**Supplementary Table 6**). Concerning the *adeFGH* efflux pump genes and the *adeL* regulator (Coyne et al., 2010), we found they were within the same loci surrounded by ABAYE1169 and ABAYE1178 which encoded a putative exported protein and a histidine transport system permease protein, respectively. The four genes related to this efflux pump were present in the 106 G1 Group 1 and 2 and also in Outgroup Group 3 genomes, except for Naval-13 and A118 (**Figure 1**, and **Supplementary Tables 3, 6**). From the 2956 non-GC1 draft genomes of the GC1 Outgroup Group 4, *adeFGHL* genes were absent in 2 genomes (**Supplementary Table 6**). The third efflux pump analyzed in this study was the *adeIJK* efflux system which is controlled by a TetR regulator namely *adeN* (Coyne et al., 2010, 2011). GC1 Group 1 genomes showed the *adeN* gene without insertions, and they shared the same allele with 11SNP compared to CP000521.1 except both A144 and A155 which had an extra point mutation (**Supplementary Table 3**). It was reported previously that the IS*Aba1* disruption of *adeN* in *A. baumannii* PKAB07 eliminated the *adeN* repression of AdeIJK triggering uncontrolled expression of genes of the *adeIJK* operon (Rosenfeld et al., 2012); this event was not found in GC1 Group 1 and 2 genomes. We also observed that in GC1 Group 1 the *adeIJK* efflux pump module was located in the same genetic context flanked by ABAYE0745 and ABAYE0749, as well as the *adeN* regulator gene surrounded by ABAYE1571 and ABAYE1573. Amongst the 2956 non-GC1 draft genomes of the GC1 Outgroup Group 4, the *adeIJK* genes were not complete in 3 genomes, while its regulator gene, *adeN*, was not identified in ten genomes (**Supplementary Table 6**).

Noteworthy, *adeA* and *adeI* were the only genes that showed 100% identity in GC1 Group 1 and 2, with the exception for *adeA* and *adeRS* genes that were deleted or lost in strain 9102, respectively, probably due to genetic rearrangements (**Figure 1**, and **Supplementary Tables 3, 6**). Unlike the other genomes studied here from GC1 Group 1 and 2 and Outgroup Group 3, Naval-13 and A118 lacked the 3 major resistance-nodulation-cell division-type efflux pumps of *A. baumannii* as well as their regulators (**Figure 1**, and **Supplementary Tables 3, 6**). Most non-GC1 from Outgroup Group 3 suffered the loss of different *ade* features (**Figure 1**, and **Supplementary Table 3**).

The 106 GC1 genomes from Groups 1 and 2 maintained intact the three efflux pumps, except for the partial deletion of *adeABC* efflux pump in strain 9102 (**Supplementary Tables 3, 6**). As a whole the deep analysis of the three resistance-nodulation-cell division-type efflux pumps in *A. baumannii* revealed that the deletion and loss of some genes affected non-GC1 genomes at different extents, evidencing events of genomic loss mostly in the *adeABC* efflux pump.

Mobile Genetic Elements Found in GC1 Strains

A wide variety of mobile genetic elements (MGE) associated with the mobilome were identified in GC1 Group 1. We found that the type and the copy number of the IS varied among all the genomes of GC1 Group 1. A144 and A155 shared IS*1R*, IS*6100*, IS*Ppu12*, IS*26* or IS*15DI* (not possible to specify with the sequence available data), and Tn*3*; in A144 we also identified ten IS*Aba125*, five IS*26*, while in A155 we detected three IS*Aba125*, and one IS*Aba125*-related (**Supplementary Table 7**). It is interesting to note that in A144 we identified a deletion of 1,521 bp within the AbaR GI compared to AYE and AB0057 which resulted in the loss of the 5′ end of a transposase (ABAYE3582) adjacent to an IS*26*, rendering a structure compatible to IS26/IS*15DI-tnpR*-Δtnp-IS*26* (AN: JQSF01000054.1). This arrangement was absent in other genomes of the GC1 Groups 1 and 2. A144, A155, AYE, A1, AB0057, A85, NIPH 527, and NIPH 290 shared four IS (IS*1R*, IS*26*, IS*6100* and IS*Ppu12*-related) with different degree of identity among the genomes (from 97 to 100%), which belong to the IS families IS*1*, IS*6*, and IS*L3*, respectively. Most IS copies were found at different loci (**Supplementary Table 7**).

The IS*6100* found in A144, A155, AYE, A1, AB0057, A85, A388, 11W359501, NIPH 527, and NIPH 290 genomes was located within the same loci in the AbaR GI close to a *mer* module (*merA*, *merC*, *merD*, *merE*, *merP*, *merR*, *merT* genes) between ABAYE3607 and ABAYE3610. In addition, this IS was found related to indels from one side and different insertions or inversions on the other side. IS*6100* was found inverted in A144 and A155 when compared to AYE, evidencing events of microevolution.

As expected, IS*26* and IS*Ppu12*-related that are usually find within the AbaR0-type GI were detected in 14 and 15 out of 18 of GC1 genomes, respectively, evidencing that their absence in some strains was related to genomic reduction or to the absence of the AbaR0-type GI (see below) (**Supplementary Table 7**).

While six IS (IS*Aba125*, IS*Aba1*, IS*Aba2*, IS*Aba12*, IS*26*, and IS*Ppu12*) were shared by GC1 Group 1 and Outgroup Group 3, 16 IS (IS*1R*, IS*aba10*, IS*Aba26*, IS*Aba14*, IS*10A*, IS*18*, IS*aba13*, IS*15DI*, IS*15DII*, IS*6100*, IS*1396*, Tn*3*, IS*1006*, IS*Vsa3*, IS*Ec29*, and IS*Ec28*) were detected solely in GC1 Group 1 isolates (**Supplementary Table 7**). On the contrary, three IS identified in Outgroup Group 3 (IS*Aba18*, IS*17* and IS*Aba11*) were not detected in GC1 Group 1 nor in Group 2 draft genomes, while IS*Vsa3* was the only identified in Outgroup Group 3 which was not detected in GC1 Group 1 but in Group 2 draft genomes (7/106). It was curious that AB307-0294 (GC1,

Lineage 1) and A118 (sporadic clone) did not harbor any IS (**Supplementary Tables 7, 8**). These results suggest that although IS may be relevant in most strains, they are not essential for *A. baumannii* survival.

With our set of genomes, prophage analysis showed that the strains from GC1 Group 1 had 11 different putative prophages (**Table 3**, and **Supplementary Figure 2**). Interestingly, one of these prophages, the putative prophage YMC/09/02/B1251_ABA_BP (AN: NC_019541.1) was found complete in A144 and with variable lengths in the remaining 17 GC1 genomes assessed including A155 (**Table 3**). A144 contained a second deleted copy of this prophage (**Table 3**). We searched for this prophage in GC1 Group 2 and Outgroup Group 3. We found several complete and incomplete copies in every genome of the 88 *A. baumannii* strains from GC1 Group 2 (Data not shown). Four out of five genomes from the Outgroup Group 3 has at least one copy of this prophage (**Table 3**), evidencing its wide dissemination not only in GC1 but also in several clones of *A. baumannii*. When we investigated the sites of insertion of the prophage YMC/09/02/B1251_ABA_BP in GC1 Group 1, we found several locations except three patterns for some genomes. In AYE, D36, AR_0083, and 9102 the prophage was flanked by the same genes, a cell division gene *zapA* (ABAYE2682) and the 23S rRNA (ABAYE2761) gene (**Supplementary Table 9**). In one of the prophages found in A155, as well as in AB307-0294, the prophage was flanked by the same cell division gene *zapA* (ABAYE2682) and gdhA_2 gene (ABBFA_02560 locus from AB307-0294) (**Supplementary Table 9**). Thirdly, in A1, AB0057 and A85 the prophage was flanked by the same genes *aroP* (ABA1_03000) and chaperone *hsp31* gene (ABA1_03077) (**Supplementary Table 9**). In the case of A144, the prophage was flanked by a putative signal peptide (ABAYE2757) and the same chaperone *hsp31* gene (ABA1_03077). Interestingly both copies of the prophage in A144 and A155 have different insertion sites (**Supplementary Table X9**), evidencing a trade-off between maintenance of this prophage probably acquired before diversification of GC1, and great processes of microevolution, deletions and insertions. Previously, it has been described the dissemination of *Acinetobacter* ACICU prophage 3 in 151 genomes of *A. baumannii* (Chan et al., 2015). When we searched for prophage 3 in GC1 Group 1 and 3, we found that it was not detected in A144 nor in A155 but present with different lengths in D36, AB0057, A85, A388, DA33382, 11W359501, NCTC13421, and NIPH 290 genomes (**Table 3**).

Also, a total of 27 plasmids were found in thirteen out of the eighteen GC1 Group 1 genomes (**Supplementary Table 4**). AB307-0294, 11W359501, NCTC13421, NIPH 527 and NIPH 290 strains did not harbor any plasmid or replicon. The search of replication initiation proteins previously described (Carattoli et al., 2014; Hamidian and Hall, 2018a; Salto et al., 2018), revealed the predominance of the Rep_3 superfamily (17/27) in the GC1 Group 1 genomes (**Supplementary Table 4**). It was not possible to identify any replicases in eight replicons, suggesting that they may have other replication mechanisms as previously found in other *A. baumannii* isolates (Salto et al., 2018). The putative plasmids from A144 and A155 had 100%

TABLE 3 | Prophages found in GC1 Group 1 and outgroup group 3 genomes.

Phage	Strain	Size (bp)
Acinetobacter YMC/09/02/B1251_ABA_BP (NC_019541.1)	A144	41,400; 123,300
	A155	17,800; 68,000
	AYE	56,900
	D36	60,000
	A1	42,800
	AB307-0294	22,500
	AB5075-UW	22,600
	AB0057	27,100; 52,800
	USA15	57,891
	A85	22,275; 57,891; 52,826
	A388	56,058; 23,332
	AR_0083	53,135; 56,637
	DA33382	27,147; 58,967; 49,779
	9102	56,197
	11W359501	91,575; 22,641; 50,064
	NCTC13421	22,641; 33,306
	NIPH 527	44,365
	NIPH 290	49,616
	ACICU	24,700; 53,600
	A118	21,000
	AB33405	62,500; 86,200
	ATCC 17978	64,500
Mannheimia vB_MhM_3927AP2 (NC_028766.1)	A144	39,100
	A155	39,100
	D36	36,200
	AR_0083	39,265
Bordetella BPP-1 (NC_005357.1)	A144	44,100
	A155	43,700
Pseudomonas phi CTX (NC_003278.1)	AYE	34,100
	AB5075-UW	36,900
	USA15	34,024
	A388	20,962
	A85	34,024
	DA33382	34,025
	NIPH 290	33,497
Pelagibacter HTVC010P (NC_020481.1)	AYE	35,400
Psychrobacter Psymv2 (NC_023734.1)	D36	36,400; 57,800
	Naval-13	54,100
	AR_0083	30,576
Cronobacter ENT39118 (NC_019934.1)	D36	20,500
	11W359501	22,507
Acinetobacter AP22 (NC_017984.1)	AB5075-UW	27,100
	AB0057	34,600
	NCTC13421	34,689
Staphylococcus SPbeta-like (NC_029119.1)	AB0057	43,200
Pseudomonas F116 (NC_006552.1)	AB0057	16,000
Salmonella vB_SosS_Oslo (NC_018279.1)	AB0057	22,200
	A85	22,274
	DA33382	22,274
	NCTC13421	33,306

(Continued)

TABLE 3 | Continued

Phage	Strain	Size (bp)
Acinetobacter ACICU prophage 3 (CP000863.1: ACICU_02140-ACICU_02234)	D36	62,720
	AB0057	68,945
	A85	68,984
	A388	69,231
	DA33382	69,628
	11W359501	62,780
	NCTC13421	69,538
	NIPH 290	70,118
Acinetobacter vB_AbaS_TRS1 (NC_031098.1)	Naval-13	54,000
	A118	40,749
	AB33405	48,400
	ATCC_17978	34,900
Enterobacteria phage mEp235 (NC_019708.1)	AB33405	44,800
Erwinia vB_EamM_ChrisDB (NC_031126.1)	AB33405	7,300

of query cover and 100% identity with *rep_3* from pIH18, which has been recently identified in nosocomial *A. baumannii* isolates from Argentina (Salto et al., 2018). The rep_3 replicase related genes were also spreading in GC1 Group 3 genomes. The RepAci1 that also belongs to Rep_3 Superfamily (ALJ89812.1) was identified in several GC1 plasmids around the world but not in A144 and A155 nor in a previous study from Argentina (Salto et al., 2018) evidencing a different pattern of plasmid dissemination.

Plasmids or putative extrachromosomal replicons ranged from 1,967 bp (p3AB5075, NZ_CP008709.1) to 98,301 bp (pUSA15_1, NZ_CP020594.1). Ten out of the 27 plasmids or putative extra chromosomal replicons carried ARG, whereas p1AB5075 (NZ_CP008707.1) and pD36-2 (NZ_CP012954.1) possessed class 1 integrons with different gene cassettes arrays (**Supplementary Table 4**). Several IS such as IS*Aba125*, IS*Aba2*, IS*Aba3*, IS*Aba5*, IS*1*, IS*6*, IS*30*, IS*L3*, Tn*4352*:IS*Aba1*, Tn*501*/Tn*1696*, and IS*Aba32* were found in eight plasmids which have related sequences to *rep_3* gene (**Supplementary Table 4**), evidencing the important role of this family of replicases for the acquisition of IS due to the flux of plasmids by events of LGT by GC1 strains.

Genomic Analysis and Maintenance Along Time of the AbaR0-Type Genomic Island Identified in A144 and A155 Strains

Sixteen out of eighteen GC1 genomes harbored an AbaR GI inserted in the *comM* gene, except AB307-0294 (Holt et al., 2016) and 9102 that possessed a complete *comM* gene. A144 and A155 genomes contained an AbaR0-type backbone GI, with the typical complete *intI1* gene (Hamidian et al., 2016). The remaining GC1 Group 1 strains from lineage 1 carried AbaR0 or AbaR3-types GIs (Hamidian et al., 2014; Holt et al., 2016; Hamidian and Hall, 2018b). Many of them showed deletions in their structure caused by IS*26* (Data not shown), probably due to either recombination events between duplicate copies of *sul1* or Tn*6018*, or by gene cassette addition or replacement as previously described (Holt et al., 2016; Hamidian and Hall, 2018b).

The AbaR0-type GI from A144 contained all the core modules, including Tn*1721*/Tn*21*, Tn*1000*-like, Tn*5393*, Tn*6020* and Tn*21* (**Figure 4**). In addition, it harbored the transposon Tn*2760* found in AbaR3, but lacked transposon Tn*2*. We also found a variant of multidrug-resistance regions described previously with a change in the module of the Tn*1696* transposon, which presented two copies of *mer* genes flanking the IS*6100* sequence (**Figure 4**). The class 1 integron found in A144 and A155 had the genetic platform IS*26*-Tn*21*-*intI1*-*aac(6′)-Ib*-*qacE*Δ1-*sul1*-orf5. The presence of *aac(6′)-Ib* within the variable region of a class 1 integron in an AbaR0-type GI is unusual since it commonly contains the array *aacC1*-orfP-orfP-orfQ-*aadA1* (Kochar et al., 2012; Hamidian and Hall, 2018b). Downstream of orf5 we found the genes *resX* and *trbI*, as previously described (Kochar et al., 2012). As a difference with A144, the AbaR0-type GI from A155 lacked the module carrying both *mer* operons and Tn*6018*-R (**Figure 4**). The maintenance of the AbaR0-type GI from A144 and A155 strains in the absence of antibiotic pressure was evaluated in three independent experiments after serial subcultures for 30 days by PCR using specific primers for detecting an invasion at the *comM* gene. No loss of the AbaR0-type GI from A144 nor A155 genomes was observed. This experiment evidenced that this GI was stable throughout time at least over one month.

We further analyzed the *attI1* sites of the class 1 integrons found in the GI of A144 (JQSF01000046.1, contig 2 coordinates 1992-2068) and A155 (JXSV01000033.1, contig 33 coordinates 1933-1857). Both recombination sites were identical to each other and surprisingly to only one *attI1* site when compared to those found in AYE. Three complete class 1 integrons in the AbaR1-type GI had been described in AYE strain (Fournier et al., 2006). When doing this study, we identified a fourth *attI1* site with a deleted *intI1* gene (see below). Interestingly, the four *attI1* sites harbored different variants (**Figure 5**). We found the typical *attI1* site, that we referred here as variant 1 in the class 1 integron that harbored the *dfrA1* gene cassette in the variable region. The variant 2 was found in the *attI1* site associated to the gene encoding a fusion protein *GroEL/intI1*, with the bla_{VEB-1}–*aadB*-*arr-2*-*cmlA5*-bla_{OXA-10}-*aadA1* gene cassette array. This *attI1* variant was invaded by the IS*1999*, which additionally generated a 9 bp duplication. The third class 1 integron contained the variant 3 of the *attI1* site and the *aacC1*-orfP-orfP-orfQ-*aadA1* gene cassette array; this variant showed 100% identity with that found in the GI of A144 and A155. This variant contained the insertion of 19 bp in tandem (Wohlleben et al., 1989) at positions -24 and -23 of the typical *attI1* site and it was also found in 11 out of 18 GC1 Group 1 genomes (A144, A155, AYE, A1, AB0057, A85, A388, DA33382, 11W359501, NCTC13421, and NIPH 290) and in 59 genomes from GC1 Group 2, showing that it was present in at least 66% genomes of this clone (70/106). The GCF_003325575.1_ASM332557v1 genome was the only one from GC1 with two copies of this variant. Also, this *attI1* variant was present in ACICU from Outgroup Group 3 genomes (1/5) and in 1,104 genomes (1,104/2956, 31 of which harbored up to three copies of this variant) in Outgroup Group 4 (data not shown). Finally, the fourth *attI1* site in AYE that we identified

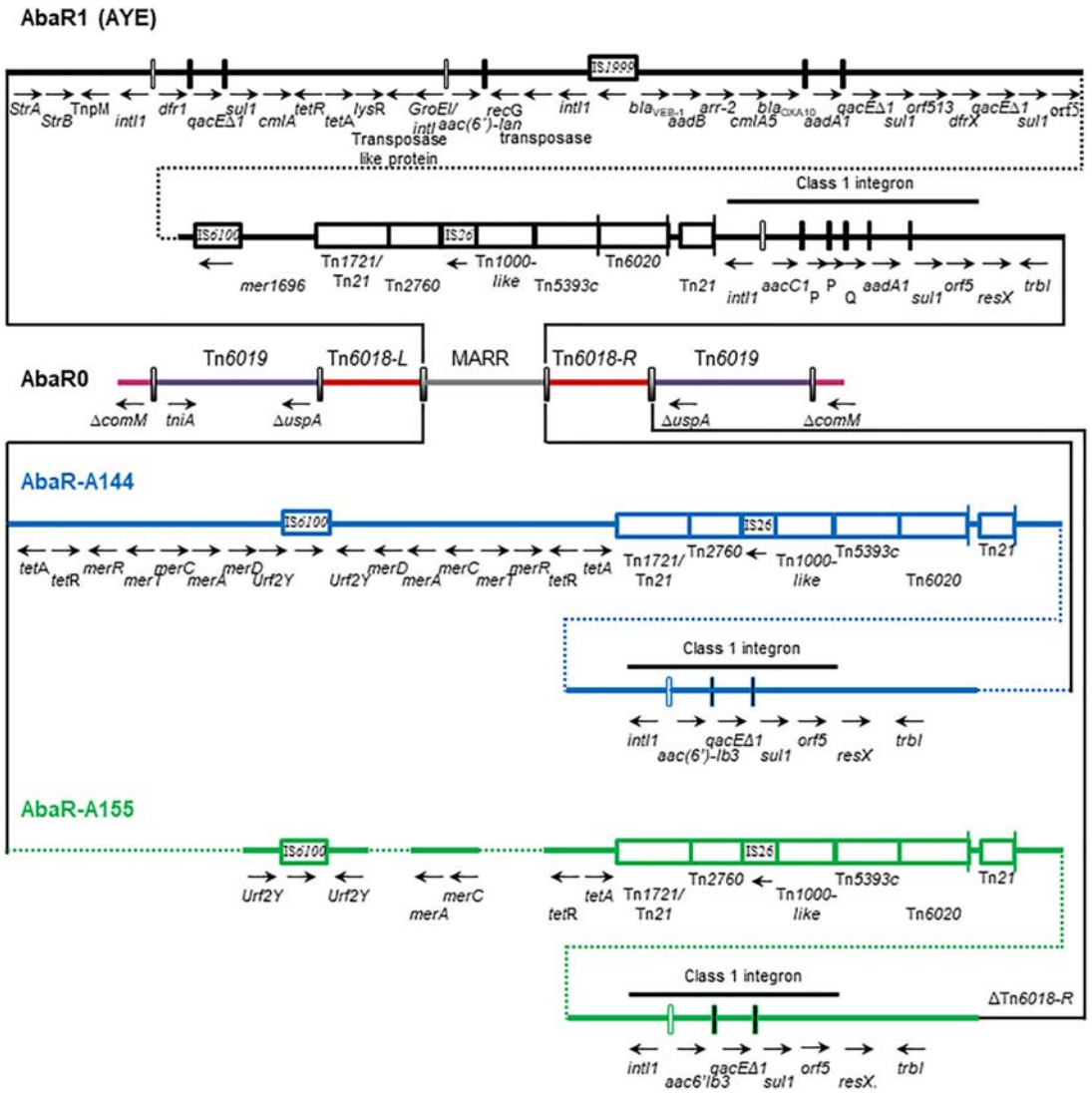

FIGURE 4 | Representation of the AbaR0-like GI found in *Acinetobacter baumannii* AYE, A144 and A155 strains. The *comM* gene is interrupted by the insertion of the AbaR0-like GI. The region of multidrug resistance (MARR) is detailed, in this area we found variations in relation with the AbaR type GI previously reported.

in this work was the variant 4, which showed a deletion at the 3′ end of the *attI1* site, from position-16 to the end of the site (**Figure 5**) linked to a second *GroEL/intI1* fusion that contains the first 301 bp of the *intI1* gene. This deleted class 1 integron possesses the *aac(6′)-Ian* gene cassette in the variable region that we have previously found as unique gene in AYE compared to other GC1 Group 1 and 2 genomes. It is likely that the novel gene cassette *aac(6′)-Ian* has been acquired by variant 4 of the *attI1* site due to an active IntI1 provided *in trans* by other complete *intI1* genes.

Genomic Diversification by LGT of GC1 Strains

Since *A. baumannii* has a large pangenome with diverse gene traits that suggests frequent LGT events, we evaluated the presence of RGP including GI, and their potential association with hotspots of recombination (HS) as defined previously (see Materials and Methods). Seven RGP were identified in A144. Two of them, the RGP1 and RGP4 were detected in the 106 GC1 Group 1 and 2 genomes but the Outgroup Group 3 (**Table 4**, and **Supplementary Table 6**). Interestingly, six of them were found in A155 (RGP1, 2, 3, 4, 6, and 7) and four of them were found in AYE (RGP1, 4, 6, and 7).

The RGP1 harbored a block of 29 genes related to LSU and SSU ribosome proteins (ABAYE0406-ABAYE0434) and its G + C content (43%) differed from the average content of *A. baumannii* GC1 strains (39%). GC1 Groups 1 and 2 harbored the RGP1 with 100% of query cover and most of them with more than 99.96% identity (**Table 4**, and **Supplementary Table 6**). The RGP4 contained 8 genes (ABAYE2146-ABAYE2153); one of them was related to a phage integrase gene, and another was a putative

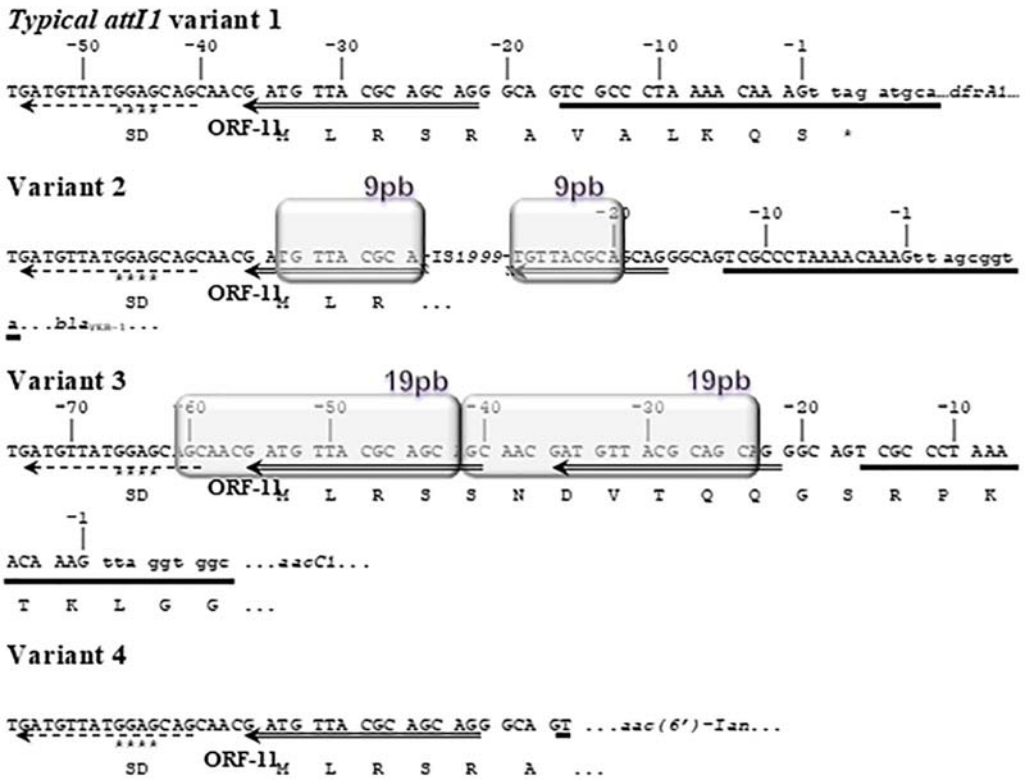

FIGURE 5 | Comparison of the *attI1* recombination sites found in the GI of A144, A155 and AYE. The variant 1 is the typical *attI1* site. Variant 2 shows the insertion of the IS*1999* and a 9 bp duplication of a portion of the *attI1* site. Variant 3 found in the three genomes, shows a 19 bp duplication. Variant 4 has a deletion of the 3′ end of the *attI1* site. The characteristic regions of the *attI1* site are marked as follows: Direct Repeat 2 (DR2), broken-line arrow; Direct Repeat 1 (DR1), double-line arrow; simple site, horizontal line; Shine-Dalgarno (SD) sequence identified for the orf-11, stars. The predicted sequence of the orf-11 is shown. The duplications are depicted in boxes. The gene cassette next to each *attI1* variant is indicated and the corresponding initial nucleotides are shown in lower case. The sequences of the variants 1 to 4 of the *attI1* site found in AYE correspond to the following coordinates in CU459141.1: 3.677.401-3.677.465 bp, 3.661.663-3.663.064 bp, 3.624.336-3.624.419 bp and 3.668.061-3.68.101 bp, respectively.

repressor related to the TetR family (TetR) which are genes that code for proteins playing an important role in the regulation of tetracycline resistance and other functions (**Supplementary Table 10**; Ramos et al., 2005; Saranathan et al., 2017). The 106 GC1 genomes harbored the RGP4 usually with more than 97.25% of query cover and most of them with more than 99.98% identity, evidencing as well as RGP1 a high nucleotide conservation among GC1 members (**Supplementary Table 6**). Twenty-seven RGP1 and 34 RGP4 were also found in other non-GC1 genomes from *A. baumannii* Outgroup Group 4 with 100% query cover and identity (**Supplementary Table 6**).

Besides the previously described AbaR0-type GI, which corresponded to RGP7, three out of seven RGPs were detected as GI by bioinformatics analysis (RGP2, RGP3, and RGP5) (**Table 4**). These three RGP also contained putative phages denoting a potential DNA mobilization to other strains. RGP2 was identified in A144, A155, USA15 and AR_0083 strains while RGP3 was identified only in A144 and A155 (**Figure 2**). A144 and A155 contained phage *Mannheimia* vB_MhM_3927AP2 (AN: NC_028766.1) in RGP2 and phage *Bordetella* BPP-1 (AN: NC_005357.1) was identified in RGP3. A144 and D36 also shared RGP5 (**Table 4**), which contained phage *Acinetobacter* YMC/09/02/B1251_ABA_BP (AN: NC_019541.1). Lastly, RGP6 in A144 contained six genes including two coding for Phage T7 exclusion proteins.

On the other hand, it has been previously identified 78 hotspots of recombination (HS) in *A. baumannii* genomes belonging to several lineages (Touchon et al., 2014). Here, we identified 19 HS of recombination along the core-genome of GC1 Group 1 strains using AYE as reference (**Figure 6**). As previously reported, a concentration of hotspots closer to the terminus of replication and symmetrically distributed around this position (Bobay et al., 2013; Touchon et al., 2014), was also observed in GC1 Group 1 genomes from our study (**Figure 6**). At the same time, GC1 chromosomes have regions with no signs of genome plasticity suggesting that they are less plastic (**Figure 6**). Interestingly, some hotspots were related to RGP such as the case of RGP6 (ABAYE2883-ABAYE2888) which contained a 3′-5′ ssDNA/RNA exonuclease gene, a queC_2 7-cyano-7-deazaguanine synthase gene and four hypothetical proteins in A144 corresponding to HS16, and RGP7 which harbors the AbaR0-type GI, corresponding to HS18, evidencing association with LGT events (**Figure 6**). HS1 in AYE and AB5075-UW was also associated with LGT events since phage related

TABLE 4 | RGP found in A144 when compared with the CG1 Group 1 genomes.

RGP	Description	# Genes	A144	AYE	A155	AB307-0294	AB0057	D36	A1	AB5075-UW	USA15
RGP1	Mostly ribosomal genes	29	A144_00407-A144_00435	ABAYE0406-ABAYE0434	A155_00395-A155_00423	CTY05_00431-CTY05_00459	AB57_RS17820-AB57_RS17695	AN415_RS02430-AN415_RS02570	ABA1_03327-ABA1_03355	ABUW_RS01985-ABUW_RS02125	B7L41_RS18650-B7L41_RS18790
RGP2	Mostly genes enconding hypotetical proteins, except for TraR and a DNA-binding protein	49	A144_01401-A144_01449	Not found	A155_01316-A155_01365	Not found	Not found	Not found	Not found	Not found	B7L41_RS13320-B7L41_RS13560
RGP3	Mostly genes enconding hypotetical proteins, except XerC and a HTH regulator	45	A144_01998-A144_02042	Not found	A155_01909-A155_01952	Not found	Not found	Not found	Not found	Not found	Not found
RGP4	Includes HTH regulators	8	A144_02125-A144_02132	ABAYE2146-ABAYE2153	A155_02036-A155_02043	CTY05_01956-CTY05_01963	AB57_RS08870-AB57_RS08840	AN415_RS10955-AN415_RS10985	ABA1_01650-ABA1_01657	ABUW_RS11280-ABUW_RS11310	B7L41_RS09985-B7L41_RS10015
RGP5	All genes encodng hypoteticaproteins	11	A144_02806-A144_02816	Not found	Not found	Not found	Not found	AN415_RS13755-AN415_RS13805	Not found	Not found	B7L41_RS14855-B7L41_RS14890
RGP6	Includes a gene encoding an ssDNA/RNA exonuclease	6	A144_02920-A144_02925	ABAYE2883-ABAYE2888	A155_02774-A155_02779	CTY05_02675-CTY05_02680	AB57_RS05065-AB57_RS05040	AN415_RS14490-AN415_RS14520	ABA1_00933-ABA1_00938	Not found	B7L41_RS06615-B7L41_RS06640
RGP7	AbaR GI	52	A144_03814-A144_03865	ABAYE3551-ABAYE3668	A155_03417-A155_03461	Not found	AB57_RS01660-AB57_RS01230	AN415_03722-AN415_03739	ABA1_00237-ABA1_00296	ABUW_3658-ABUW_3678	B7L41_RS03100-B7L41_RS03305

RGP	Description	# Genes	A85	A388	AR_0083	DA33382	9102	11W359501	NCTC13421	Phage found in RGP
RGP1	Mostly ribosomal genes	29	CBI29_RS17600-CBI29_RS17740	A388_00462-A388_00490	AM462_RS17415-AM462_RS17555	DPV67_RS00005-DPV67_RS19215	Aba9102_12825-Aba9102_12965	FIM01_02220-FIM01_02360	DQM71_RS02060-DQM71_RS02200	
RGP2	Mostly genes enconding hypotetical proteins, except for TraR and a DNA-binding protein	49	Not found	Not found	AM462_02365-AM462_RS02605	Not found	Not found	Not found	Not found	*Mannheimia* vB_MhM_3927AP2 (NC_028766.1)
RGP3	Mostly genes enconding hypotetical proteins, except XerC and a HTH regulator	45	Not found	Not found	Not found	Not found	Not found	Not found	Not found	*Bordetella* BPP-1 (NC_005357.1)
RGP4	Includes HTH regulators	8	CBI29_RS08770-CBI29_RS08800	A388_02216-A388_02224	AM462_RS06010-AM462_RS06040	DPV67_RS02970-DPV67_RS03000	Aba9102_01795-Aba9102_01825	FIM01_11750-FIM01_11780	DQM71_RS10890-DQM71_RS10920	
RGP5	All genes encodng hypoteticaproteins	11	CBI29_RS13420-CBI29_RS13455	A388_01316-A388_01322	AM462_RS09115-AM462_RS09155	DPV67_RS07705-DPV67_RS07740	Aba9102_04210-Aba9102_04225	FIM01_06560-FIM01_06625	DQM71_RS06140-DQM71_RS06175	*Acinetobacter* YMC/09/02/B1251_ABA_BP (NC_019541.1)
RGP6	Includes a gene encoding an ssDNA/RNA exonuclease	6	CBI29_RS04950-CBI29_RS04975	A388_02963-A388_02968	AM462_RS09990-AM462_RS10095	DPV67_RS18455-DPV67_RS18480	Not found	FIM01_15120-FIM01_15145	DQM71_RS14685-DQM71_RS14710	
RGP7	AbaR GI	52	CBI29_RS01230-CBI29_RS01660	A388_00226-A388_03612	AM462_RS13330-AM462_RS15430	DPV67_RS15110-DPV67_RS15295	Not found	FIM01_18920-FIM01_19280	DQM71_RS18135-DQM71_RS18565	

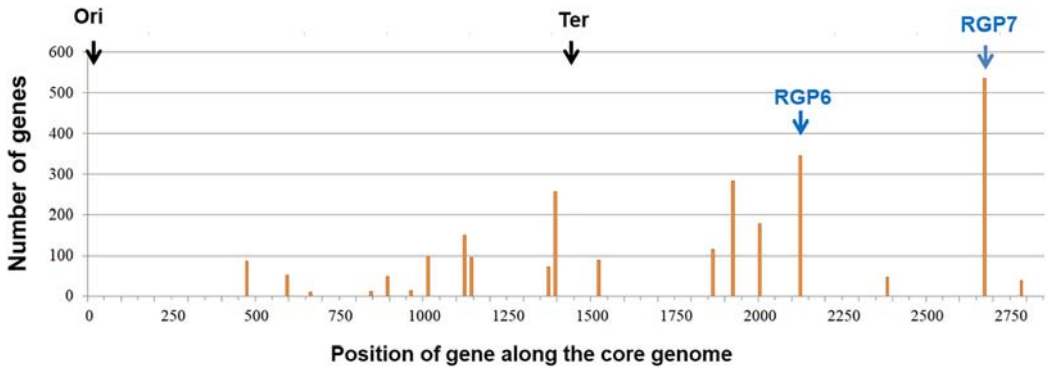

FIGURE 6 | Distribution of hotspots along the core-genome of *Acinetobacter baumannii* GC1 Group 1 genomes. The gene order of *A. baumannii* AYE strain was used as a reference (see section "Materials and Methods"). The bars represent the number of different gene families in all the genomes found between two consecutive genes of the core-genome of GC1 genomes.

genes were found inserted within the two core genes. HS2 also encoded phage related proteins in D36 and was inserted within two core genes. HS3 to HS6, HS14 and HS15 possessed genes coding for hypothetical proteins; HS7 in AB5075-UW encoded a site-specific integrase, one IS*256* and also a phage-related protein; HS10 in AYE had the transposase IS*Aba1*; HS11 and HS13 had phage-related genes; and HS17 in AYE had *copC* and *copD* genes that belong to a diverse group of periplasmic copper binding proteins. Lastly, as previously detected by Holt et al. (2016), HS19 was found within genes coding for the biosynthesis of exopolysaccharides via the K locus. When we investigated deeply the variability in K locus in our set of 106 genomes from GC1 Group 1 and 2, we found ten gene clusters of K locus (KL1, KL4, KL9, KL12, KL15, KL17, KL20, KL25, KL40 and KL42) with 100% of query cover and more than 97% of identity, and five gene clusters for OC locus (OCL1, OCL2, OCL3, OCL4 and OCL5) which were already described by Holt et al. (2016, **Supplementary Table 8**). The KL1 locus (31/106) was prevalent amongst GC1 genomes in both lineages (**Supplementary Table 11**). The OC locus was absent in 9102 (NZ_CP023029.1) complete genome (**Supplementary Table 11**).

Identification of Adaptive Immune Systems in GC1 Genomes

We also looked for Clustered Regularly Interspaced Short Palindromic Repeats and their associated Cas proteins (CRISPR-Cas systems). These elements can provide host immunity against bacteriophages and plasmids (Shmakov et al., 2017), which are commonly associated to LGT events (Di Nocera et al., 2011; Touchon et al., 2014). Previously it has been reported that most CRISPR-Cas systems found in the genus *Acinetobacter* corresponded to type I-Fa or Fb elements, where type I-Fb was highly spread in different clonal complexes with a significant vertical evolution including GC1 (Hauck et al., 2012; Touchon et al., 2014; Karah et al., 2015).

In silico prediction and analysis showed that A144 and A155 genomes had the identical type I-Fb system found in strain AYE, which consist of 6 *cas* genes (*cas1-cas3-cas8f-cas5f-cas7f-cas6f*). A144 and A155 systems contained each an identical CRISPR array consisting of 53 spacers and repeat sequences (**Table 5**). This finding supports the clonal relationship between both strains. All 106 GC1 genomes from GC1 Group 1 and 2 had the same *cas* operon (100% of query cover and 99.97%), and their respective CRISPR arrays contained between 45 and 81 spacers adjacent to the same repeat sequence (**Table 5**). We then analyzed all the spacer sequences from A144 and AYE and we found that most of them had a low degree of complementation to phage related sequences from *Staphylococcus aureus*, *S. epidermidis*, *Klebsiella* spp., *Escherichia* ssp., and other species usually found in nosocomial niches (**Supplementary Table 12**).

TABLE 5 | Analysis of CRISPR-Cas system in GC1 genomes.

Strain	Number of spacers
A144	52
A155	52
A1	50
AB307-0294	45
AYE	59
AB0057	52
AB5075-UW	52
D36	81
USA15	49
A85	34
A388	52
AR_0083	47
DA33382	15
9102	50
11W359501	46
NCTC13421	46
NIPH 527	18
NIPH 290	18

The 6 cas1-cas3-cas8f-cas5f-cas7f-cas6f genes were identified in the eighteen GC1 genomes of this study. All the repeats had the same sequence (5′-GTTCATGGCGGCATACGCCATTTAGAAA-3′).

Last, we investigated the dissemination of *cas1-cas3-cas8f-cas5f-cas7f-cas6f* (8103 bp) in Outgroup Group 3, Outgroup Group 4 and other genomes from GenBank. Blastn search revealed that the locus was present in 121 out of 2956 *A. baumannii* non-GC1 genomes belonging to different sequence types from Outgroup Group 4 with a nt identity that ranged from 97.42 to 99.89% as previously described (**Supplementary Table 6**; Karah et al., 2015). Also, the locus was present in isolates from other *Acinetobacter* species such as *A. haemolyticus* TG19602, *A. gyllenbergii* NIPH 230 and in *A. parvus* as previously reported (Touchon et al., 2014; Karah et al., 2015).

In vitro Competition of A144 and A155

To understand the success of GC1 in the nosocomial niche with experimental data, we also investigated both the clonal competition between A144 or A155 versus A118 (sporadic clone) in the absence of antimicrobial pressure.

A144 and A118 showed slight differences in the growth rate. The growth rate of A144 was $r = 0.015$ OD/min with a doubling time Dt = 46.18 min. For A118, the growth rate was $r = 0.015$ OD/min with a doubling time Dt = 46.98 min. Conversely, A155 showed a faster growth in the conditions assayed, with values of $r = 0.017$ OD/min, and a doubling time Dt = 40.98 min.

A144 showed a fitness advantage with an *S*-value $S = 0.333 \pm 0.069$ in the fitness assays for the clonal competition between A144 and A118 carried out for 124 generations; with a relative adaptive fitness $F = 1.333$ (133.318%) and a fitness cost $C = -33.318\%$. As expected, the clonal competition between A155 and A118 carried out for 140 generations also showed a fitness advantage ($C < 15.574\%$) with an *S*-value $S = -0.156 \pm 0.018$, $F = 1.156$ (115.574%) and $C = -15.574\%$. The clonal competition assay showed a competitive advantage of the GC1 strains over the sporadic clone in the two pairs (A144/A118 and A155/A118) with the fitness cost $C > 10\%$ and a statistically significant difference ($P = 0.00001$, $P < 0.05$). Previous reports described that the greater the difference in growth rate between two strains, the greater is the bacterial burden difference over time (Guo et al., 2012); nevertheless, differences i.e., in antimicrobial resistance and virulence factors should be under consideration altogether. Here, the difference between this two pairs of strains (A144/A118 and A155/A118) showed the relevance of even small genomic modifications in the fitness of a strain (A144 and A155) when competes with another.

Regarding virulence factors, *A. baumannii* usually encodes a type VI secretion system (T6SS), which can be used to kill competitors (Weber et al., 2013). It is likely that the presence of this system may be associated to the survival in the nosocomial niche (Fitzsimons et al., 2018). Here, we searched the genes coding for the proteins critical for T6SS operation (Weber et al., 2016; Repizo et al., 2019) in Groups 1, 2, 3 and 4, as well as *tetR1* and *tetR2* repressors in Groups 1, 2 and 3 (**Supplementary Table 13**). The genes coding for the core proteins of this system were present in A144 and A155 and in all genomes from GC1 Group 1 and 2 but NIPH290, GCF_000369185.1, GCF_000369325.1, GCF_004347305.1_ASM434730v1 and GCF_006494215.1_ASM649421v1 where the T6SS was partially lost (101/106) (**Supplementary Table 13**). The *tetR1* and *tetR2* repressor genes were not detected in GC1 Group 1 and 2 but GCF_001512215.1_9179_4_6 and GCF_006492525.1_ASM649252v1 genomes that harbored *tetR2* (*tetR2* = 2/106). When we searched in the Outgroup Group 3, we identified the complete T6SS in epidemic clones and partially deleted in A118 which belongs to a sporadic clone (**Supplementary Table 13**). Interestingly, both repressor genes *tetR1* and *tetR2* were only present in Naval-13. In Outgroup Group 4, which includes *A. baumannii* non-GC1 strains, we found that the 17.46% of draft genomes had partially or complete lost components of the T6SS (2440/2956) (**Supplementary Table 13**).

Taken together, the fitness of A144 and A155 over sporadic clones, and the finding of complete T6SS in almost all GC1 strains compared to non-GC1 genomes, suggests that these features can be related to the epidemic behavior of the so-called clones that can rapidly displaced sporadic clones or strains lacking the T6SS.

DISCUSSION

Genomic studies in combination with biological analysis led us to identify maintenance along time of genes usually subjected to LGT that may have a crucial role during the evolutionary trajectory of the high-risk clone GC1. The genes from the accessory genome acquired by GC1 strains were mostly grouped in modules along the chromosome and preserved by two adaptation pathways over time. On the one hand, the paradigmatic AbaR GI, the CRISPR-Cas type I-Fb system, as well as two novel regions of genome plasticity (RGP1 and 4), were located within the same loci as "sedentary" modules (**Figure 2**). In turn, the AbaR GI showed high plasticity evidenced by several signs of microevolution including deletions, inversions and duplications as previously described (Hamidian et al., 2016). We found that even the AbaR0-type GI from our two strains A144 and A155 isolated from the same hospital H1, presented signs of microevolution since A144 isolated 3 years later than A155 had acquired a duplicated *mer* operon and a Tn*6018*-R (**Figure 4**). In concordance with these results, this region was identified as a hotspot for recombination, corresponding to HS18 in our study (**Figure 6**). This is in agreement with the fact that, to the best of our knowledge, there are no reports of AbaR GI harboring identical genetic structure in *A. baumannii* strains (Ramírez et al., 2013; Hamidian and Hall, 2018b). Otherwise, our experimental studies revealed that AbaR GI is maintained over time in A144 as well as in A155 without antimicrobial pressure for at least one month. We can assume that there is a balance between conservation and plasticity of particular regions of the accessory genome, as previously described for the core genome regions of *A. baumannii* (Touchon et al., 2014; Hamidian et al., 2016). The other remaining "sedentary" modules, the *cas* genes from the type IF-b CRISPR-Cas system, RGP1, and RGP4, did not show signs of microevolution.

We confirmed the preliminary data reported by Karah et al. (2015), since we found that the *cas* operon from AYE was conserved in all the 106 GC1 genomes, supporting that its acquisition occurred before GC1 clonal diversification (**Supplementary Tables 6, 12**) but after speciation of *A. baumannii*. It is particularly intriguing the complete identity

found between the CRISPR-Cas systems, including the order and identity of 53 spacers of both A144 and A155 strains from the same hospital, considering that they were isolated at distant time points (**Table 5**). It is highly probable that each strain was exposed to different phages and plasmids; however, there is no evidence of new invasions. Since the same *cas* genes from the type IF-b CRISPR-Cas system were found in other GC1 chromosomes and also in other species of the genus *Acinetobacter* carrying different spacers (Karah et al., 2015; **Supplementary Table 12**), it is likely that they are functional systems. Thus, it is possible to assume that a tight regulation of these systems may have led to a stable array for A144 and A155. In this regard, it has been reported that phages can encode proteins with anti-CRISPR activity that may inhibit their function (Pawluk et al., 2014; Bondy-Denomy et al., 2015). Further studies are necessary to confirm this hypothesis. This finding and the closeness observed in the phylogenetic tree (**Figure 1**) suggest that A144 and A155 strains may share a common ancestor from which they adapted and evolved within the H1 nosocomial niche.

Concerning the regions of genomic plasticity, we found that RGP1 and RGP4 were highly conserved in the 106 GC1 genomes and absent in almost all other lineages of *A. baumannii*. Ortholog genes of the RGP1 harboring 29 genes related to LSU and SSU ribosome proteins were previously described as an unusual multisequence alignment block structure with important evolutionary implications (Vishwanath et al., 2004). The implication of the RGP4 that includes a putative repressor protein related to the TetR family which can act on various genes with diverse functions such as biosynthesis, metabolism, bacterial pathogenesis, and response to cell stress (Ramos et al., 2005; Saranathan et al., 2017) remains unclear. The functional role of both RGP1 and RGP4 in GC1 lineage would be an interesting challenge to further investigate.

On the other hand, another module of the accessory genome showed to be "mobile" though present in the 106 GC1 genomes (**Table 3**). This is the case of the YMC/09/02/B1251_ABA_BP putative prophage which showed to vary in length structure across GC1 genomes (**Table 3**) and it was located in diverse insertion sites as we identified in this study (**Supplementary Table 9**). Ten additional prophages were detected in the GC1 Group 1 genomes. The biodiversity of prophages as well as the rearrangements they promote within each genome reflects frequent events of successful phage invasion. Since phages may acquire ORFs named morons (Hendrix et al., 2000), the presence and the mobility of prophage *Acinetobacter* YMC/09/02/B1251_ABA_BP in all 106 GC1 strains denotes it may have an important role in acquisition of accessory genome by LGT in this pandemic clone. In agreement with this, we found also a process of deep microevolution for prophage 3 that is widespread in *A. baumannii* strains (Chan et al., 2015), suggesting that prophages may play an important role for genomic plasticity not only in GC1 but in all the species.

Interestingly, a particular genetic behavior was identified for the IS. They showed a great variability in terms of IS families and copy number, having each GC1 strain different amount of IS in different chromosomal locations. There was no evidence of a sequential acquisition of the IS in the distribution observed among the 18 GC1 Group 1 genomes, indicating that the presence of these genetic elements is likely to be related to the rapid adaptation of the strains to the environment they are exposed to. Hence, they may be involved in niche adaptation in GC1 strains. IS analysis also showed that A144 and A155 shared some IS as a main difference with other GC1 Group 1 strains (**Figure 2**), reinforcing our phylogeny data (**Figure 1**) that they share a common ancestor. Other IS, such as IS*26* and IS*Aba1* were frequent in GC1 Group 1 strains and they were identified in both GC1 lineages. Remarkably, the GC1 Group 1 genomes did not share a common IS (**Supplementary Table 7**). The fact that no IS were detected in AB307-0294 genome supports the hypothesis that IS may have been acquired after the diversification of this clone and/or that IS are easily acquired and lost by GC1 strains. Besides, a great variety of IS were identified in plasmids from GC1 Group 1 genomes suggesting that extrachromosomal replicons, especially plasmids harboring Rep_3 replicases, may contribute to the capture and flux of IS that later could invade the chromosome. The relevance of Rep_3 replicases in the acquisition of IS by the chromosome is reinforced by the fact that this family of replicases were found in different species, families and even phyla as well as in environmental or clinical strains (Salto et al., 2018), which enhances the set of IS diversity that can be captured by GC1 strains.

Concerning our genomic analysis related to antimicrobial resistance, we found that the bioinformatic results matched the multidrug resistant phenotype of A144 and A155 with only slight differences in the ARG content (**Tables 2**, and **Supplementary Table 3**). An interesting feature was found by analyzing the naturally harbored β-lactamase genes *ampC* and $bla_{\mathrm{OXA-51-like}}$ in GC1. Both β-lactamase genes are ubiquitous in *A. baumannii* strains (Merkier and Centrón, 2006; Karah et al., 2017). Previously, several alleles of *ampC* were identified (Karah et al., 2017). We found nine *ampC* alleles in the eighteen genomes from our GC1 Group 1. Conversely, $bla_{\mathrm{OXA-51-like}}$ was identified as $bla_{\mathrm{OXA-69}}$ in 17/18 GC1 Group 1 genomes except A388 which contained $bla_{\mathrm{OXA-92}}$ as previously described (Pournaras et al., 2014). These results suggest different degrees of genomic plasticity for each β-lactam resistance gene. This feature is also supported by the identification of a hotspot of recombination in the *ampC* flanking regions (Holt et al., 2016). It is likely that different genetic behaviors of each β-lactamase gene within the same cell may be a powerful tool to a more successful response to antimicrobial selection in the nosocomial niche. The sulbactam resistance in A144 and A155 may be explained by the presence of the $bla_{\mathrm{TEM-1}}$ gene with the Pa/Pb promoters since our results indicated that this gene/promoter combination could be involved in the increase of the sulbactam MIC (**Tables 2**, and **Supplementary Table 3**). Additional studies to effectively quantify the level of increase in the MIC for sulbactam remain to be done, but the evidence showed here correlates perfectly with the results from other authors, which showed that that the Pa/Pb promoters were stronger than the promoter P3 (Lartigue et al., 2002; Krizova et al., 2013).

The fluoroquinolone resistance in A144 and A155 and of the GC1 Group 1 (15/18 GC1 Group 1) correlated with the results of Ostrer et al., which stated that it could be predicted based solely on target gene quinolone-resistance mutations for *A. baumannii* and that the primary mutation is followed

by either of two mutations in the alternate target in this species ParC88 ← **GyrA81** → ParC84 (Ostrer et al., 2019). Even when most of the GC1 Group 1 genomes showed a predicted fluoroquinolone resistance due to mutation in QRDR, it is remarkable the absence of PMQR genes in the isolates analyzed here.

By focusing in the antimicrobial resistance adaptation of GC1 to XDR phenotypes, our data evidenced that class 1 integrons were identified in 13 out of 18 GC1 genomes suggesting they may play an essential role for acquisition of mobile antimicrobial resistance. We identified one additional deleted *attI1* site, which may have arisen from deletions and rearrangements of previous complete class 1 integrons within the AbaR GI of AYE. It is likely that this fourth deleted *attI1* was recognized as a secondary site and at the same time it was related to the acquisition of the novel allele *aac(6′)-Ian* which has not been found in other isolates. It is likely that ARG cassettes could be captured by a type 1 integron integrase from a complete class 1 integron and inserted in the respective *attI1* site or in secondary sites, which may act as hotspots for active acquisition of mobile antimicrobial resistance in nosocomial niches. In agreement with previous results from our laboratory (Ramírez et al., 2015), only seven class 2 integrons were identified in GC1 Group 1 and 2 strains ($n = 106$), confirming that the prevalence of *intI2* in *A. baumannii* strains from Argentina is related to the emergence of novel singletons and to the abundance of CC113/CC79, which has been the local dominant lineage for several decades (Stietz et al., 2013). On the other hand, the fact that 56 out of 106 GC1 strains harbored an *intI1* gene, suggests a wide dissemination of class 1 integrons in this pandemic clone. Taking together, these results evidence a different epidemiology of multidrug resistant integrons among *A. baumannii* lineages.

Regarding the investigation about the variability of three resistance-nodulation-cell division-type efflux pumps in GC1, we found that the 106 GC1 genomes contained all the genes encoding the AdeABC, AdeFGH and the AdeIJK efflux pumps altogether with their regulators with different levels of identity for each gene, except for the partial deletion of AdeABC in strain 9102 (**Supplementary Tables 3, 6**). Meanwhile, our study showed that the three efflux pumps are subjected of processes of genomic loss in non-GC1 strains, particularly those related to *adeABC* genes (**Supplementary Table 6**). In this regard, it has been previously suggested that *adeABC* was subjected to loss and acquisition along time, while the *adeFGH* system is intrinsic to the *A. baumannii* species (Coyne et al., 2010, 2011). Concerning the molecular epidemiology of the *adeABC* genes, it has been shown that this operon is present in ca. 80% (from 53% to 97%) of *A. baumannii* strains and it is associated mainly with clinical isolates since it has not been found in 32 environmental strains (Huys et al., 2005; Chu et al., 2006; Hujer et al., 2006; Nemec et al., 2007; Bratu et al., 2008; Chen et al., 2009; Lin et al., 2009; Srinivasan et al., 2009). Moreover, Ab421 HEIGH-2010 strain as well as other 10 clinical strains of *A. baumannii* belonging to clone ST79/ST924 lacked these genes and were found to display increased invasiveness (Rumbo et al., 2013; López et al., 2017). Taking together the evidence, the *adeABC* genes from *A. baumannii* may be suffering genomic losses resulting in its presence in less than the 90% of the total genomes of the species as also seen in our study (**Supplementary Tables 3, 6**), suggesting that the *adeABC* efflux pump as part of the core genome could be under consideration. We also have detected a deep process of genomic loss of the T6SS in non-GC1 strains. It is likely that the maintenance along time and continents of complete AdeABC, AdeFGH and the AdeIJK efflux pumps related to antimicrobial resistance as well as the T6SS which is associated to kill competitors (Weber et al., 2013) may contribute to the survival of GC1 in the nosocomial niche. Although the huge pangenome of *A. baumannii* (Touchon et al., 2014; Chan et al., 2015) evidences dynamic processes of loss and gain of genes, the maintenance of some blocks of accessory genome within a lineage suggests that the general idea that all genes acquired by LGT are easily lost, should be analyzed more deeply in biological models.

We identified an essential role of still unknown properties of "mobile" and "sedentary" accessory genome that is preserved over time under different antibiotic conditions and nosocomial habitats having a decisive role in the adaptive success of the pandemic GC1. In fact, it may be associated with the survival under stress conditions of GC1, which is reflected in its perpetuation along time in strains from different continents. At the same time, our data suggests that GC1 is constantly evolving and adapting to novel niches by exposure to a continuous acquisition of IS which may contribute to the instantly adaptation to the changing stresses suffered by the trajectory of GC1 strains. In these processes, plasmids harboring *rep_3* replicases might have an important role for the flux of IS and antimicrobial resistance determinants. Not only genomic plasticity in *A. baumannii* is evidenced by hotspots for recombination, gene duplications, deletions and/or insertions (Touchon et al., 2014; Holt et al., 2016), but also for the maintenance of several modules of accessory genome, such as RGP1 and RGP4, CRISPR-Cas system, AbaR GI as previously found (Holt et al., 2016), mobile prophage YMC/09/02/B1251_ABA_BP as well as the preservation of synteny of genomes belonging to GC1, being these traits pivotal for the success of this high-risk clone. Competition assay of A144 as well as A155 versus A118 without antimicrobial pressure suggested a greater ability of GC1 to thrive over the clones with sporadic behavior, which in conjunction with the presence of a complete T6SS and efflux pumps in almost all GC1 genomes can explain from an ecological perspective the success of this pandemic clone to spread and survive in hospital environments.

AUTHOR'S NOTE

DC, MQ, and CQ are members of the Carrera del Investigador Científico, CONICET, Argentina. VA and AG are recipients of a CONICET postdoctoral and doctoral and fellowships, respectively. EV received a CONICET doctoral fellowship.

DATA AVAILABILITY STATEMENT

The raw data supporting the conclusions of this article will be made available by the authors, without undue reservation, to any qualified researcher.

AUTHOR CONTRIBUTIONS

DC and MQ contributed to the conception and design of the study. VA, MQ, AG, MR, and EV performed the experimental and/or bioinformatic assays. DC structured the work, wrote and coordinated the drafts of the manuscript and did the final edition. VA, MQ, CQ, and DC wrote sections of the result's section. All the authors contributed to the analysis of the data, manuscript revision, read, and approved the submitted version.

FUNDING

The authors' work was supported by the grant PUE 2522 from the CONICET given to IMPAM; Fundación Alberto J. Roemmers Grant 2017, UBACYT Programación Científica 2018 20020170100387BA from Universidad de Buenos Aires and PICT 1881 2014 from the Agencia Nacional de Promoción Científica y Tecnológica (ANPCYT) given to DC; and grants UBACYT Programación Científica 2018 20020170200189BA from Universidad de Buenos Aires and ANPCyT PICT2015-3610 from the Agencia Nacional de Promoción Científica y Tecnológica (ANPCYT) given to MQ.

SUPPLEMENTARY MATERIAL

The Supplementary Material for this article can be found online at: https://www.frontiersin.org/articles/10.3389/fmicb.2020.00342/full#supplementary-material

REFERENCES

Adams, M. D., Goglin, K., Molyneaux, N., Hujer, K. M., Lavender, H., Jamison, J. J., et al. (2008). Comparative genome sequence analysis of multidrug-resistant *Acinetobacter baumannii*. *J. Bacteriol.* 190, 8053–8064.

Altschul, S. F., Gish, W., Miller, W., Myers, E. W., and Lipman, D. J. (1990). Basic local alignment search tool. *J. Mol. Biol.* 215, 403–410.

Antunes, L. C. S., Imperi, F., Towner, K. J., and Visca, P. (2011). Genome-assisted identification of putative iron-utilization genes in *Acinetobacter baumannii* and their distribution among a genotypically diverse collection of clinical isolates. *Res. Microbiol.* 162, 279–284. doi: 10.1016/j.resmic.2010.10.010

Antunes, L. C. S., Visca, P., and Towner, K. J. (2014). *Acinetobacter baumannii*: evolution of a global pathogen. *Pathog. Dis.* 71, 292–301. doi: 10.1111/2049-632X.12125

Arduino, S. M., Quiroga, M. P., Ramírez, M. S., Merkier, A. K., Errecalde, L., Di Martino, A., et al. (2012). Transposons and integrons in colistin-resistant clones of *Klebsiella pneumoniae* and *Acinetobacter baumannii* with epidemic or sporadic behaviour. *J. Med. Microbiol.* 61, 1417–1420. doi: 10.1099/jmm.0.038968-0

Arivett, B. A., Fiester, S. E., Ream, D. C., Centrón, D., Ramírez, M. S., Tolmasky, M. E., et al. (2015). Draft genome of the multidrug-resistant *Acinetobacter baumannii* strain A155 clinical isolate. *Genome Announc.* 3, e212–e215.

Arndt, D., Grant, J. R., Marcu, A., Sajed, T., Pon, A., Liang, Y., et al. (2016). PHASTER: a better, faster version of the PHAST phage search tool. *Nucleic Acids Res.* 44, W16–W21. doi: 10.1093/nar/gkw387

Aziz, R. K., Bartels, D., Best, A., DeJongh, M., Disz, T., Edwards, R. A., et al. (2008). The RAST Server: rapid annotations using subsystems technology. *BMC Genomics* 9:75. doi: 10.1186/1471-2164-9-75

Bertelli, C., Laird, M. R., Williams, K. P., Lau, B. Y., Hoad, G., Winsor, G. L., et al. (2017). IslandViewer 4: expanded prediction of genomic islands for larger-scale datasets. *Nucleic Acids Res.* 45, W30–W35. doi: 10.1093/nar/gkx343

Bobay, L.-M., Rocha, E. P. C., and Touchon, M. (2013). The adaptation of temperate bacteriophages to their host genomes. *Mol. Biol. Evol.* 30, 737–751. doi: 10.1093/molbev/mss279

Bondy-Denomy, J., Garcia, B., Strum, S., Du, M., Rollins, M. F., Hidalgo-Reyes, Y., et al. (2015). Multiple mechanisms for CRISPR-cas inhibition by anti-CRISPR proteins. *Nature* 526, 136–139. doi: 10.1038/nature15254

Bratu, S., Landman, D., Martin, D. A., Georgescu, C., and Quale, J. (2008). Correlation of antimicrobial resistance with -lactamases, the ompa-like porin, and efflux pumps in clinical isolates of *Acinetobacter baumannii* endemic to New York City. *Antimicrob. Agents Chemother.* 52, 2999–3005. doi: 10.1128/aac.01684-07

Carattoli, A., Zankari, E., García-Fernández, A., Voldby Larsen, M., Lund, O., Villa, L., et al. (2014). In silico detection and typing of plasmids using plasmidfinder and plasmid multilocus sequence typing. *Antimicrob. Agents Chemother.* 58, 3895–3903. doi: 10.1128/aac.02412-14

Carver, T. J., Rutherford, K. M., Berriman, M., Rajandream, M.-A., Barrell, B. G., and Parkhill, J. (2005). ACT: the Artemis comparison tool. *Bioinformatics* 21, 3422–3423. doi: 10.1093/bioinformatics/bti553

Chan, A. P., Sutton, G., DePew, J., Krishnakumar, R., Choi, Y., Huang, X.-Z., et al. (2015). A novel method of consensus pan-chromosome assembly and large-scale comparative analysis reveal the highly flexible pan-genome of *Acinetobacter baumannii*. *Genome Biol.* 16:143.

Chen, T.-L., Lee, Y.-T., Kuo, S.-C., Hsueh, P.-R., Chang, F.-Y., Siu, L.-K., et al. (2010). Emergence and distribution of plasmids bearing the blaOXA-51-like gene with an upstream ISAba1 in carbapenem-resistant *Acinetobacter baumannii* isolates in Taiwan. *Antimicrob. Agents Chemother.* 54, 4575–4581. doi: 10.1128/aac.00764-10

Chen, Y., Pi, B., Zhou, H., Yu, Y., and Li, L. (2009). Triclosan resistance in clinical isolates of *Acinetobacter baumannii*. *J. Med. Microbiol.* 58, 1086–1091. doi: 10.1099/jmm.0.008524-0

Chu, Y. W., Chau, S. L., and Houang, E. T. S. (2006). Presence of active efflux systems AdeABC, AdeDE and AdeXYZ in different *Acinetobacter* genomic DNA groups. *J. Med. Microbiol.* 55, 477–478. doi: 10.1099/jmm.0.46433-0

CLSI, (2018). *Performance Standards for Antimicrobial Susceptibility Testing: 28th Informational Supplement*. Dallas, TX: CLSI.

Contreras-Moreira, B., and Vinuesa, P. (2013). GET_HOMOLOGUES, a versatile software package for scalable and robust microbial pangenome analysis. *Appl. Environ. Microbiol.* 79, 7696–7701. doi: 10.1128/aem.02411-13

Coyne, S., Courvalin, P., and Périchon, B. (2011). Efflux-mediated antibiotic resistance in *Acinetobacter* spp. *Antimicrob. Agents Chemother.* 55, 947–953. doi: 10.1128/aac.01388-10

Coyne, S., Rosenfeld, N., Lambert, T., Courvalin, P., and Perichon, B. (2010). Overexpression of resistance-nodulation-cell division pump AdeFGH confers multidrug resistance in *Acinetobacter baumannii*. *Antimicrob. Agents Chemother.* 54, 4389–4393. doi: 10.1128/aac.00155-10

Croucher, N. J., Page, A. J., Connor, T. R., Delaney, A. J., Keane, J. A., Bentley, S. D., et al. (2015). Rapid phylogenetic analysis of large samples of recombinant bacterial whole genome sequences using Gubbins. *Nucleic Acids Res.* 43:e15. doi: 10.1093/nar/gku1196

Darling, A. C. E., Mau, B., Blattner, F. R., and Perna, N. T. (2004). Mauve: multiple alignment of conserved genomic sequence with rearrangements. *Genome Res.* 14, 1394–1403. doi: 10.1101/gr.2289704

Di Nocera, P., Rocco, F., Giannouli, M., Triassi, M., and Zarrilli, R. (2011). Genome organization of epidemic *Acinetobacter baumannii* strains. *BMC Microbiol.* 11:224. doi: 10.1186/1471-2180-11-224

Diancourt, L., Passet, V., Nemec, A., Dijkshoorn, L., and Brisse, S. (2010). The population structure of *Acinetobacter baumannii*: expanding multiresistant clones from an ancestral susceptible genetic pool. *PLoS ONE* 5:e10034. doi: 10.1371/journal.pone.0010034

Falagas, M. E., Kopterides, P., and Siempos, I. I. (2006). Attributable mortality of *Acinetobacter baumannii* infection among critically ill patients. *Clin. Infect. Dis.* 43:389.

Fitzsimons, T. C., Lewis, J. M., Wright, A., Kleifeld, O., Schittenhelm, R. B., Powell, D., et al. (2018). Identification of novel *Acinetobacter* baumannii type VI secretion system antibacterial effector and immunity pairs. *Infect. Immun.* 86:e00297-18. doi: 10.1128/IAI.00297-18

Fournier, P.-E., Vallenet, D., Barbe, V., Audic, S., Ogata, H., Poirel, L., et al. (2006). Comparative genomics of multidrug resistance in *Acinetobacter baumannii*. *PLoS Genet.* 2:e7. doi: 10.1371/journal.pgen.0020007

Giannouli, M., Di Popolo, A., Durante-Mangoni, E., Bernardo, M., Cuccurullo, S., Amato, G., et al. (2012). Molecular epidemiology and mechanisms of rifampicin resistance in *Acinetobacter baumannii* isolates from Italy. *Int. J. Antimicrob. Agents* 39, 58–63. doi: 10.1016/j.ijantimicag.2011.09.016

Guo, B., Abdelraouf, K., Ledesma, K. R., Nikolaou, M., and Tam, V. H. (2012). Predicting bacterial fitness cost associated with drug resistance. *J. Antimicrob. Chemother.* 67, 928–932. doi: 10.1093/jac/dkr560

Hamidian, M., Ambrose, S. J., and Hall, R. M. (2016). A large conjugative *Acinetobacter baumannii* plasmid carrying the sul2 sulphonamide and strAB streptomycin resistance genes. *Plasmid* 8, 43–50. doi: 10.1016/j.plasmid.2016.09.001

Hamidian, M., and Hall, R. M. (2011). AbaR4 replaces AbaR3 in a carbapenem-resistant *Acinetobacter baumannii* isolate belonging to global clone 1 from an Australian hospital. *J. Antimicrob. Chemother.* 66, 2484–2491. doi: 10.1093/jac/dkr356

Hamidian, M., and Hall, R. M. (2018a). Genetic structure of four plasmids found in *Acinetobacter baumannii* isolate D36 belonging to lineage 2 of global clone 1. *PLoS One* 13:e0204357. doi: 10.1371/journal.pone.0204357

Hamidian, M., and Hall, R. M. (2018b). The AbaR antibiotic resistance islands found in *Acinetobacter baumannii* global clone 1 – Structure, origin and evolution. *Drug Resist. Updat.* 41, 26–39. doi: 10.1016/j.drup.2018.10.003

Hamidian, M., Hawkey, J., Holt, K. E., and Hall, R. M. (2015). Genome sequence of *Acinetobacter baumannii* strain D36, an antibiotic-resistant isolate from lineage 2 of global clone 1. *Genome Announc.* 3, e1478–e1415. doi: 10.1128/genomeA.01478-15

Hamidian, M., Hawkey, J., Wick, R., Holt, K. E., and Hall, R. M. (2019). Evolution of a clade of *Acinetobacter baumannii* global clone 1, lineage 1 via acquisition of carbapenem- and aminoglycoside-resistance genes and dispersion of ISAba1. *Microb. Genom.* 5:e000242. doi: 10.1099/mgen.0.000242

Hamidian, M., Wynn, M., Holt, K. E., Pickard, D., Dougan, G., and Hall, R. M. (2014). Identification of a marker for two lineages within the GC1 clone of *Acinetobacter baumannii*. *J. Antimicrob. Chemother.* 69, 557–558. doi: 10.1093/jac/dkt379

Hauck, Y., Soler, C., Jault, P., Mérens, A., Gérome, P., Nab, C. M., et al. (2012). Diversity of *Acinetobacter baumannii* in four french military hospitals, as assessed by multiple locus variable number of tandem repeats analysis. *PLoS ONE* 7:e44597. doi: 10.1371/journal.pone.0044597

Hendrix, R. W., Lawrence, J. G., Hatfull, G. F., and Casjens, S. (2000). The origins and ongoing evolution of viruses. *Trends Microbiol.* 8, 504–508. doi: 10.1016/s0966-842x(00)01863-1

Holt, K., Kenyon, J. J., Hamidian, M., Schultz, M. B., Pickard, D. J., Dougan, G., et al. (2016). Five decades of genome evolution in the globally distributed, extensively antibiotic-resistant *Acinetobacter baumannii* global clone 1. *Microb. Genomics* 2:e000052. doi: 10.1099/mgen.0.000052

Holt, K. E., Kenyon, J. J., Hamidian, M., Schultz, M. B., Pickard, D. J., Dougan, G., et al. (2019). Corrigendum: five decades of genome evolution in the globally distributed, extensively antibiotic-resistant *Acinetobacter baumannii* global clone 1. *Microb. Genomics* 5:e000280. doi: 10.1099/mgen.0.000280

Hujer, K. M., Hujer, A. M., Hulten, E. A., Bajaksouzian, S., Adams, J. M., Donskey, C. J., et al. (2006). Analysis of antibiotic resistance genes in multidrug-resistant *Acinetobacter* sp. isolates from military and civilian patients treated at the Walter Reed Army Medical Center. *Antimicrob. Agents Chemother.* 50, 4114–4123. doi: 10.1128/aac.00778-06

Huys, G., Cnockaert, M., Nemec, A., and Swings, J. (2005). Sequence-based typing of ade B as a potential tool to identify intraspecific groups among clinical strains of multidrug-resistant *Acinetobacter baumannii*. *J. Clin. Microbiol.* 43, 5327–5331. doi: 10.1128/JCM.43.10.5327-5331.2005

Imperi, F., Antunes, L. C. S., Blom, J., Villa, L., Iacono, M., Visca, P., et al. (2011). The genomics of *Acinetobacter baumannii*: insights into genome plasticity, antimicrobial resistance and pathogenicity. *IUBMB Life* 63, 1068–1074. doi: 10.1002/iub.531

Inchai, J., Pothirat, C., Bumroongkit, C., Limsukon, A., Khositsakulchai, W., and Liwsrisakun, C. (2015). Prognostic factors associated with mortality of drug-resistant *Acinetobacter baumannii* ventilator-associated pneumonia. *J. Intensive Care* 3:9. doi: 10.1186/s40560-015-0077-4

Karah, N., Jolley, K. A., Hall, R. M., and Uhlin, B. E. (2017). Database for the ampC alleles in *Acinetobacter baumannii*. *PLoS ONE* 12:e0176695. doi: 10.1371/journal.pone.0176695

Karah, N., Samuelsen, Ø, Zarrilli, R., Sahl, J. W., Wai, S. N., and Uhlin, B. E. (2015). CRISPR-cas subtype I-Fb in *Acinetobacter baumannii*: evolution and utilization for strain subtyping. *PLoS ONE* 10:e0118205. doi: 10.1371/journal.pone.0118205

Karah, N., Sundsfjord, A., Towner, K., and Samuelsen, O. (2012). Insights into the global molecular epidemiology of carbapenem non-susceptible clones of *Acinetobacter baumannii*. *Drug Resist. Updat.* 15, 237–247. doi: 10.1016/j.drup.2012.06.001

Keane, J. A., Page, A. J., Delaney, A. J., Taylor, B., Seemann, T., Harris, S. R., et al. (2016). SNP-sites: rapid efficient extraction of SNPs from multi-FASTA alignments. *Microb. Genomics* 2:e000056. doi: 10.1099/mgen.0.000056

Kenyon, J. J., and Hall, R. M. (2013). Variation in the complex carbohydrate biosynthesis loci of *Acinetobacter baumannii* genomes. *PLoS ONE* 8:e62160. doi: 10.1371/journal.pone.0062160

Kochar, M., Crosatti, M., Harrison, E. M., Rieck, B., Chan, J., Constantinidou, C., et al. (2012). Deletion of Tn AbaR23 results in both expected and unexpected antibiogram changes in a multidrug-resistant *Acinetobacter baumannii* strain. *Antimicrob. Agents Chemother.* 56, 1845–1853. doi: 10.1128/aac.05334-11

Krizova, L., Dijkshoorn, L., and Nemec, A. (2011). Diversity and evolution of AbaR genomic resistance islands in *Acinetobacter baumannii* strains of European clone I. *Antimicrob. Agents Chemother.* 55, 3201–3206. doi: 10.1128/aac.00221-11

Krizova, L., Poirel, L., Nordmann, P., and Nemec, A. (2013). TEM-1 β-lactamase as a source of resistance to sulbactam in clinical strains of *Acinetobacter baumannii*. *J. Antimicrob. Chemother.* 68, 2786–2791. doi: 10.1093/jac/dkt275

Lartigue, M. F., Leflon-Guibout, V., Poirel, L., Nordmann, P., and Nicolas-Chanoine, M.-H. (2002). Promoters P3, Pa/Pb, P4, and P5 upstream from bla(TEM) genes and their relationship to beta-lactam resistance. *Antimicrob. Agents Chemother.* 46, 4035–4037. doi: 10.1128/aac.46.12.4035-4037.2002

Li, S., Sun, S., Yang, C., Chen, H., Yin, Y., Li, H., et al. (2018). The changing pattern of population structure of *Staphylococcus aureus* from bacteremia in China from 2013 to 2016: ST239-030-MRSA replaced by ST59-t437. *Front. Microbiol.* 9:332. doi: 10.3389/fmicb.2018.00332

Lin, L., Ling, B.-D., and Li, X.-Z. (2009). Distribution of the multidrug efflux pump genes, adeABC, adeDE and adeIJK, and class 1 integron genes in multiple-antimicrobial-resistant clinical isolates of *Acinetobacter baumannii-Acinetobacter calcoaceticus* complex. *Int. J. Antimicrob. Agents* 33, 27–32. doi: 10.1016/j.ijantimicag.2008.06.027

López, M., Blasco, L., Gato, E., Perez, A., Fernández-Garcia, L., Martínez-Martinez, L., et al. (2017). Response to bile salts in clinical strains of *Acinetobacter baumannii* lacking the AdeABC efflux pump: virulence associated with quorum sensing. *Front. Cell. Infect. Microbiol.* 7:143. doi: 10.3389/fcimb.2017.00143

Maddocks, S. E., and Oyston, P. C. F. (2008). Structure and function of the LysR-type transcriptional regulator (LTTR) family proteins. *Microbiology* 154, 3609–3623. doi: 10.1099/mic.0.2008/022772-0

Magiorakos, A.-P., Srinivasan, A., Carey, R. B., Carmeli, Y., Falagas, M. E., Giske, C. G., et al. (2012). Multidrug-resistant, extensively drug-resistant and pandrug-resistant bacteria: an international expert proposal for interim standard definitions for acquired resistance. *Clin. Microbiol. Infect.* 18, 268–281. doi: 10.1111/j.1469-0691.2011.03570.x

Marchand, I., Damier-Piolle, L., Courvalin, P., and Lambert, T. (2004). Expression of the RND-type efflux pump AdeABC in *Acinetobacter baumannii* is regulated by the AdeRS two-component system. *Antimicrob. Agents Chemother.* 48, 3298–3304. doi: 10.1128/AAC.48.9.3298-3304.2004

Mathee, K., Narasimhan, G., Valdes, C., Qiu, X., Matewish, J. M., Koehrsen, M., et al. (2008). Dynamics of *Pseudomonas aeruginosa* genome evolution. *Proc. Natl. Acad. Sci. U.S.A.* 105, 3100–3105. doi: 10.1073/pnas.0711982105

Merkier, A. K., and Centrón, D. (2006). blaOXA-51-type β-lactamase genes are ubiquitous and vary within a strain in *Acinetobacter baumannii*. *Int. J. Antimicrob. Agents* 28, 110–113. doi: 10.1016/j.ijantimicag.2006.03.023

Meumann, E. M., Anstey, N. M., Currie, B. J., Piera, K. A., Kenyon, J. J., Hall, R. M., et al. (2019). Genomic epidemiology of severe community-onset *Acinetobacter baumannii* infection. *Microb. Genomics* 5:e000258. doi: 10.1099/mgen.0.000258

Moffatt, J. H., Harper, M., Harrison, P., Hale, J. D. F., Vinogradov, E., Seemann, T., et al. (2010). Colistin resistance in *Acinetobacter baumannii* is mediated by complete loss of lipopolysaccharide production. *Antimicrob. Agents Chemother.* 54, 4971–4977. doi: 10.1128/aac.00834-10

Nemec, A., Maixnerová, M., van der Reijden, T. J. K., van den Broek, P. J., and Dijkshoorn, L. (2007). Relationship between the AdeABC efflux system gene content, netilmicin susceptibility and multidrug resistance in a genotypically diverse collection of *Acinetobacter baumannii* strains. *J. Antimicrob. Chemother.* 60, 483–489. doi: 10.1093/jac/dkm231

Nigro, S. J., Post, V., and Hall, R. M. (2011). The multiresistant *Acinetobacter baumannii* European clone I type strain RUH875 (A297) carries a genomic antibiotic resistance island AbaR21, plasmid pRAY and a cluster containing ISAba1-sul2-CR2-strB-strA. *J. Antimicrob. Chemother.* 66, 1928–1930. doi: 10.1093/jac/dkr213

Ostrer, L., Khodursky, R. F., Johnson, J. R., Hiasa, H., and Khodursky, A. (2019). Analysis of mutational patterns in quinolone resistance-determining regions of GyrA and ParC of clinical isolates. *Int. J. Antimicrob. Agents* 53, 318–324. doi: 10.1016/j.ijantimicag.2018.12.004

Ou, H.-Y., Kuang, S. N., He, X., Molgora, B. M., Ewing, P. J., Deng, Z., et al. (2015). Complete genome sequence of hypervirulent and outbreak-associated *Acinetobacter baumannii* strain LAC-4: epidemiology, resistance genetic determinants and potential virulence factors. *Sci. Rep.* 5:8643. doi: 10.1038/srep08643

Park, S. Y., Choo, J. W., Kwon, S. H., Yu, S. N., Lee, E. J., Kim, T. H., et al. (2013). Risk factors for mortality in patients with *Acinetobacter baumannii* bacteremia. *Infect. Chemother.* 45, 325–330. doi: 10.3947/ic.2013.45.3.325

Pawluk, A., Bondy-Denomy, J., Cheung, V. H. W., Maxwell, K. L., and Davidson, A. R. (2014). A new group of phage anti-CRISPR genes inhibits the type I-E CRISPR-cas system of *Pseudomonas aeruginosa*. *MBio* 5, e896–e814.

Peleg, A. Y., Seifert, H., and Paterson, D. L. (2008). *Acinetobacter baumannii*: emergence of a successful pathogen. *Clin. Microbiol. Rev.* 21, 538–582. doi: 10.1128/cmr.00058-07

Post, V., and Hall, R. M. (2009). AbaR5, a large multiple-antibiotic resistance region found in *Acinetobacter baumannii*. *Antimicrob. Agents Chemother.* 53, 2667–2671. doi: 10.1128/aac.01407-08

Post, V., Hamidian, M., and Hall, R. M. (2012). Antibiotic-resistant *Acinetobacter baumannii* variants belonging to global clone 1. *J. Antimicrob. Chemother.* 67, 1039–1040. doi: 10.1093/jac/dkr586

Post, V., White, P. A., and Hall, R. M. (2010). Evolution of AbaR-type genomic resistance islands in multiply antibiotic-resistant *Acinetobacter baumannii*. *J. Antimicrob. Chemother.* 65, 1162–1170. doi: 10.1093/jac/dkq095

Pournaras, S., Gogou, V., Giannouli, M., Dimitroulia, E., Dafopoulou, K., Tsakris, A., et al. (2014). Single-locus-sequence-based typing of blaOXA-51-like genes for rapid assignment of *Acinetobacter baumannii* clinical isolates to international clonal lineages. *J. Clin. Microbiol.* 52, 1653–1657. doi: 10.1128/jcm.03565-13

Ramirez, M. S., Adams, M. D., Bonomo, R. A., Centrón, D., and Tolmasky, M. E. (2011). Genomic analysis of *Acinetobacter baumannii* A118 by comparison of optical maps: identification of structures related to its susceptibility phenotype. *Antimicrob. Agents Chemother.* 55, 1520–1526. doi: 10.1128/aac.01595-10

Ramírez, M. S., Montaña, S., Cassini, M., and Centrón, D. (2015). Preferential carriage of class 2 integrons in *Acinetobacter baumannii* CC113 and novel singletons. *Epidemiol. Infect.* 143, 3118–3121. doi: 10.1017/S0950268815000060

Ramírez, M. S., Piñeiro, S., Argentinian Integron, Study Group, D., and Centrón, D. (2010). Novel insights about class 2 integrons from experimental and genomic epidemiology. *Antimicrob. Agents Chemother.* 54, 699–706. doi: 10.1128/aac.01392-08

Ramírez, M. S., Vilacoba, E., Stietz, M. S., Merkier, A. K., Jeric, P., Limansky, A. S., et al. (2013). Spreading of AbaR-type genomic islands in multidrug resistance *Acinetobacter baumannii* strains belonging to different clonal complexes. *Curr. Microbiol.* 67, 9–14. doi: 10.1007/s00284-013-0326-5

Ramos, J. L., Martinez-Bueno, M., Molina-Henares, A. J., Teran, W., Watanabe, K., Zhang, X., et al. (2005). The TetR family of transcriptional repressors. *Microbiol. Mol. Biol. Rev.* 69, 326–356. doi: 10.1128/mmbr.69.2.326-356.2005

Repizo, G. D., Espariz, M., Seravalle, J. L., and Salcedo, S. P. (2019). Bioinformatic analysis of the type VI secretion system and its potential toxins in the *Acinetobacter* genus. *Front. Microbiol.* 10:2519. doi: 10.3389/fmicb.2019.02519

Roca, I., Espinal, P., Vila-Farrés, X., and Vila, J. (2012). The *Acinetobacter baumannii* oxymoron: commensal hospital dweller turned pan-drug-resistant menace. *Front. Microbiol.* 3:148. doi: 10.3389/fmicb.2012.00148

Rodríguez, C., Nastro, M., Flores, S. A., Rodriguez, M., Spinozzi, M., Bruni, G., et al. (2018). Epidemiología molecular de aislados de *Acinetobacter baumannii* resistentes a carbapenems en Argentina. *Rev. Argent. Microbiol.* 51, 247–250. doi: 10.1016/j.ram.2017.12.004

Rosenfeld, N., Bouchier, C., Courvalin, P., and Périchon, B. (2012). Expression of the resistance-nodulation-cell division pump AdeIJK in *Acinetobacter baumannii* is regulated by AdeN, a TetR-type regulator. *Antimicrob. Agents Chemother.* 56, 2504–2510. doi: 10.1128/aac.06422-11

Rumbo, C., Gato, E., López, M., Ruiz, de Alegría, C., Fernández-Cuenca, F., et al. (2013). Contribution of efflux pumps, porins, and β-lactamases to multidrug resistance in clinical isolates of *Acinetobacter baumannii*. *Antimicrob. Agents Chemother.* 57, 5247–5257. doi: 10.1128/aac.00730-13

Sahl, J. W., Gillece, J. D., Schupp, J. M., Waddell, V. G., Driebe, E. M., Engelthaler, D. M., et al. (2013). Evolution of a pathogen: a comparative genomics analysis identifies a genetic pathway to pathogenesis in *Acinetobacter*. *PLoS ONE* 8:e54287. doi: 10.1371/journal.pone.0054287

Salto, I. P., Torres Tejerizo, G., Wibberg, D., Pühler, A., Schlüter, A., and Pistorio, M. (2018). Comparative genomic analysis of Acinetobacter spp. plasmids originating from clinical settings and environmental habitats. *Sci. Rep.* 8:7783.

Sander, P., Springer, B., Prammananan, T., Sturmfels, A., Kappler, M., Pletschette, M., et al. (2002). Fitness cost of chromosomal drug resistance-conferring mutations. *Antimicrob. Agents Chemother.* 46, 1204–1211. doi: 10.1128/aac.46.5.1204-1211.2002

Saranathan, R., Pagal, S., Sawant, A. R., Tomar, A., Madhangi, M., Sah, S., et al. (2017). Disruption of tetR type regulator adeN by mobile genetic element confers elevated virulence in *Acinetobacter baumannii*. *Virulence* 8, 1316–1334. doi: 10.1080/21505594.2017.1322240

Schouls, L. M., Reulen, S., Duim, B., Wagenaar, J. A., Willems, R. J. L., Dingle, K. E., et al. (2003). Comparative genotyping of *Campylobacter jejuni* by amplified fragment length polymorphism, multilocus sequence typing, and short repeat sequencing: strain diversity, host range, and recombination. *J. Clin. Microbiol.* 41, 15–26. doi: 10.1128/jcm.41.1.15-26.2003

Seemann, T. (2014). Prokka: rapid prokaryotic genome annotation. *Bioinformatics* 30, 2068–2069. doi: 10.1093/bioinformatics/btu153

Shaikh, F., Spence, R. P., Levi, K., Ou, H.-Y., Deng, Z., Towner, K. J., et al. (2009). ATPase genes of diverse multidrug-resistant *Acinetobacter baumannii* isolates frequently harbour integrated DNA. *J. Antimicrob. Chemother.* 63, 260–264. doi: 10.1093/jac/dkn481

Shmakov, S. A., Sitnik, V., Makarova, K. S., Wolf, Y. I., Severinov, K. V., and Koonin, E. V. (2017). The CRISPR spacer space is dominated by sequences from species-specific mobilomes. *MBio* 8, e1397–e1317.

Siguier, P. (2006). ISfinder: the reference centre for bacterial insertion sequences. *Nucleic Acids Res.* 34, D32–D36. doi: 10.1093/nar/gkj014

Snitkin, E. S., Zelazny, A. M., Gupta, J., Comparative, N., Program, S., Palmore, T. N., et al. (2013). Genomic insights into the fate of colistin resistance and *Acinetobacter baumannii* during patient treatment. *Genome Res.* 23, 1155–1162. doi: 10.1101/gr.154328.112.Park

Srinivasan, V. B., Rajamohan, G., and Gebreyes, W. A. (2009). Role of AbeS, a novel efflux pump of the SMR family of transporters, in resistance to antimicrobial agents in *Acinetobacter baumannii*. *Antimicrob. Agents Chemother.* 53, 5312–5316. doi: 10.1128/aac.00748-09

Stietz, M. S., Ramírez, M. S., Vilacoba, E., Merkier, A. K., Limansky, A. S., Centrón, D., et al. (2013). *Acinetobacter baumannii* extensively drug resistant lineages in buenos aires hospitals differ from the international clones I–III. *Infect. Genet. Evol.* 14, 294–301. doi: 10.1016/j.meegid.2012.12.020

Subramanian, B., Gao, S., Lercher, M. J., Hu, S., and Chen, W.-H. (2019). Evolview v3: a webserver for visualization, annotation, and management of phylogenetic trees. *Nucleic Acids Res.* 47, W270–W275. doi: 10.1093/nar/gkz357

Touchon, M., Cury, J., Yoon, E. J., Krizova, L., Cerqueira, G. C., Murphy, C., et al. (2014). The genomic diversification of the whole *Acinetobacter* genus:

origins, mechanisms, and consequences. *Genome Biol. Evol.* 6, 2866–2882. doi: 10.1093/gbe/evu225

Traglia, G. M., Chua, K., Centron, D., Tolmasky, M. E., and Ramírez, M. S. (2014). Whole-genome sequence analysis of the naturally competent *Acinetobacter baumannii* clinical isolate A118. *Genome Biol. Evol.* 6, 2235–2239. doi: 10.1093/gbe/evu176

Vallenet, D., Nordmann, P., Barbe, V., Poirel, L., Mangenot, S., Bataille, E., et al. (2008). Comparative analysis of *Acinetobacters*: three genomes for three lifestyles. *PLoS ONE* 3:e1805. doi: 10.1371/journal.pone.0001805

Vilacoba, E., Déraspe, M., Traglia, G. M., Roy, P. H., and Ramírez, S. (2014). Draft genome sequence of an international clonal lineage 1 *Acinetobacter baumannii* strain from Argentina. *Genome Announc.* 2, 13–14. doi: 10.1128/genomeA.01190-14.Copyright

Vishwanath, P., Favaretto, P., Hartman, H., Mohr, S. C., and Smith, T. F. (2004). Ribosomal protein-sequence block structure suggests complex prokaryotic evolution with implications for the origin of eukaryotes. *Mol. Phylogenet. Evol.* 33, 615–625. doi: 10.1016/j.ympev.2004.07.003

Vliegenthart, J. S., Ketelaar-van Gaalen, P. A., and van de Klundert, J. A. (1989). Nucleotide sequence of the aacC2 gene, a gentamicin resistance determinant involved in a hospital epidemic of multiply resistant members of the family *Enterobacteriaceae*. *Antimicrob. Agents Chemother.* 33, 1153–1159. doi: 10.1128/aac.33.8.1153

Weber, B. S., Hennon, S. W., Wright, M. S., Scott, N. E., de Berardinis, V., Foster, L. J., et al. (2016). Genetic dissection of the type vi secretion system in *Acinetobacter* and identification of a novel peptidoglycan hydrolase, TagX, required for its biogenesis. *MBio* 7, e1253–e1216.

Weber, B. S., Miyata, S. T., Iwashkiw, J. A., Mortensen, B. L., Skaar, E. P., Pukatzki, S., et al. (2013). Genomic and functional analysis of the type VI secretion system in *Acinetobacter*. *PLoS One.* 8:e55142. doi: 10.1371/journal.pone.0055142

Wohlleben, W., Arnold, W., Bissonnette, L., Pelletier, A., Tanguay, A., Roy, P. H., et al. (1989). On the evolution of Tn21-like multiresistance transposons: sequence analysis of the gene (aacC1) for gentamicin acetyltransferase-3-I(AAC(3)-I), another member of the Tn21-based expression cassette. *Mol. Gen. Genet.* 217, 202–208. doi: 10.1007/bf02464882

Zankari, E., Hasman, H., Cosentino, S., Vestergaard, M., Rasmussen, S., Lund, O., et al. (2012). Identification of acquired antimicrobial resistance genes. *J. Antimicrob. Chemother.* 67, 2640–2644. doi: 10.1093/jac/dks261

Conflict of Interest: The authors declare that the research was conducted in the absence of any commercial or financial relationships that could be construed as a potential conflict of interest.

The reviewer GR declared a shared affiliation with no collaboration, with the authors, to the handling Editor at the time of review.

Advantages of publishing in Frontiers

OPEN ACCESS
Articles are free to read for greatest visibility and readership

FAST PUBLICATION
Around 90 days from submission to decision

HIGH QUALITY PEER-REVIEW
Rigorous, collaborative, and constructive peer-review

TRANSPARENT PEER-REVIEW
Editors and reviewers acknowledged by name on published articles

Frontiers
Avenue du Tribunal-Fédéral 34
1005 Lausanne | Switzerland

Visit us: www.frontiersin.org
Contact us: info@frontiersin.org | +41 21 510 17 00

REPRODUCIBILITY OF RESEARCH
Support open data and methods to enhance research reproducibility

DIGITAL PUBLISHING
Articles designed for optimal readership across devices

FOLLOW US
@frontiersin

IMPACT METRICS
Advanced article metrics track visibility across digital media

EXTENSIVE PROMOTION
Marketing and promotion of impactful research

LOOP RESEARCH NETWORK
Our network increases your article's readership